EMERGING INFECTIOUS DISEASES®

U.S. CENTERS FOR DISEASE CONTROL AND PREVENTION

Parasitic Infections

September 2025

Giulio Aristide Sartorio (1860–1932), *Malaria*, official title *Dum Romae consulitur, morbos imperat* (1883). Oil on canvas. 125 cm × 223 cm. Museo Nacional de Bellas Artes, Buenos Aires, Argentina.
Public domain digital image from Wikipedia Commons.

EMERGING INFECTIOUS DISEASES®

Emerging Infectious Diseases is published monthly by the Centers for Disease Control and Prevention, 1600 Clifton Rd NE, Mailstop H16-2, Atlanta, GA 30329-4018, USA. Telephone 404-639-1960; email eideditor@cdc.gov

EMERGING INFECTIOUS DISEASES®

Parasitic Infections **September 2025**

On the Cover

Giulio Aristide Sartorio (1860–1932), *Malaria*, official title *Dum Romae consulitur, morbos imperat* (1883). Oil on canvas. 125 cm × 223 cm. Museo Nacional de Bellas Artes, Buenos Aires, Argentina. Public domain digital image from Wikipedia Commons.

About the Cover p. 1876

Perspective

Research

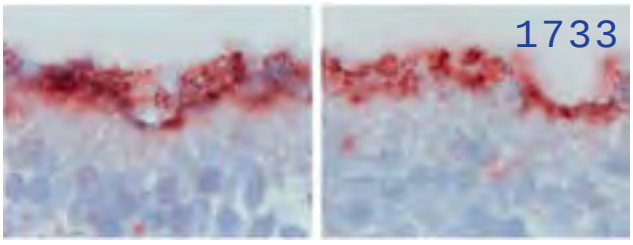

Dispatches

EMERGING INFECTIOUS DISEASES®
September 2025

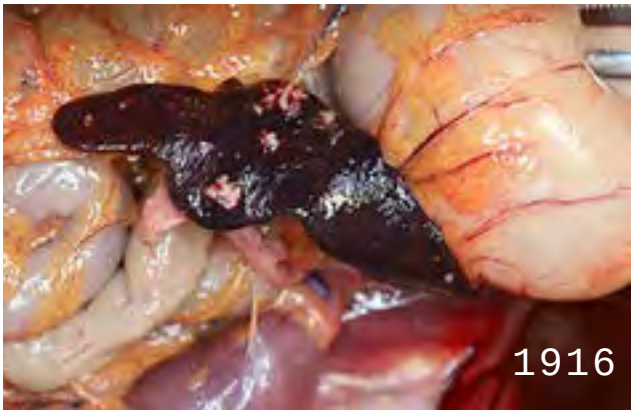

EMERGING INFECTIOUS DISEASES
September 2025

Research Letters

Comment Letter

About the Cover

Etymologia

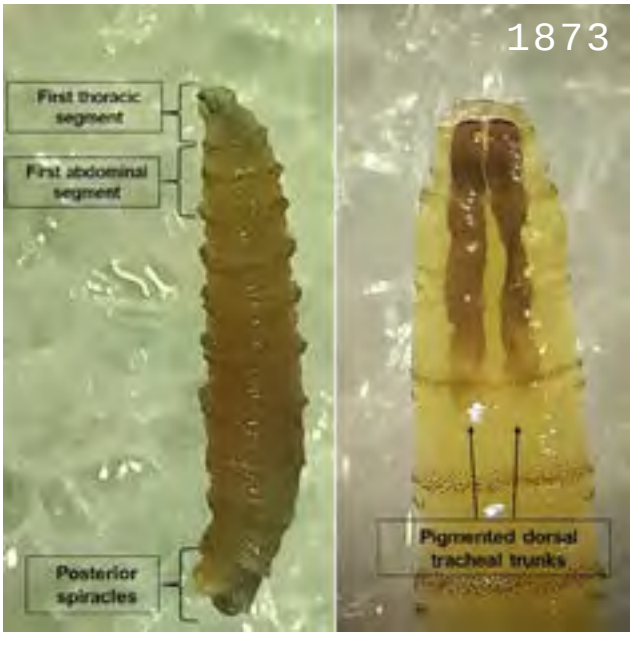

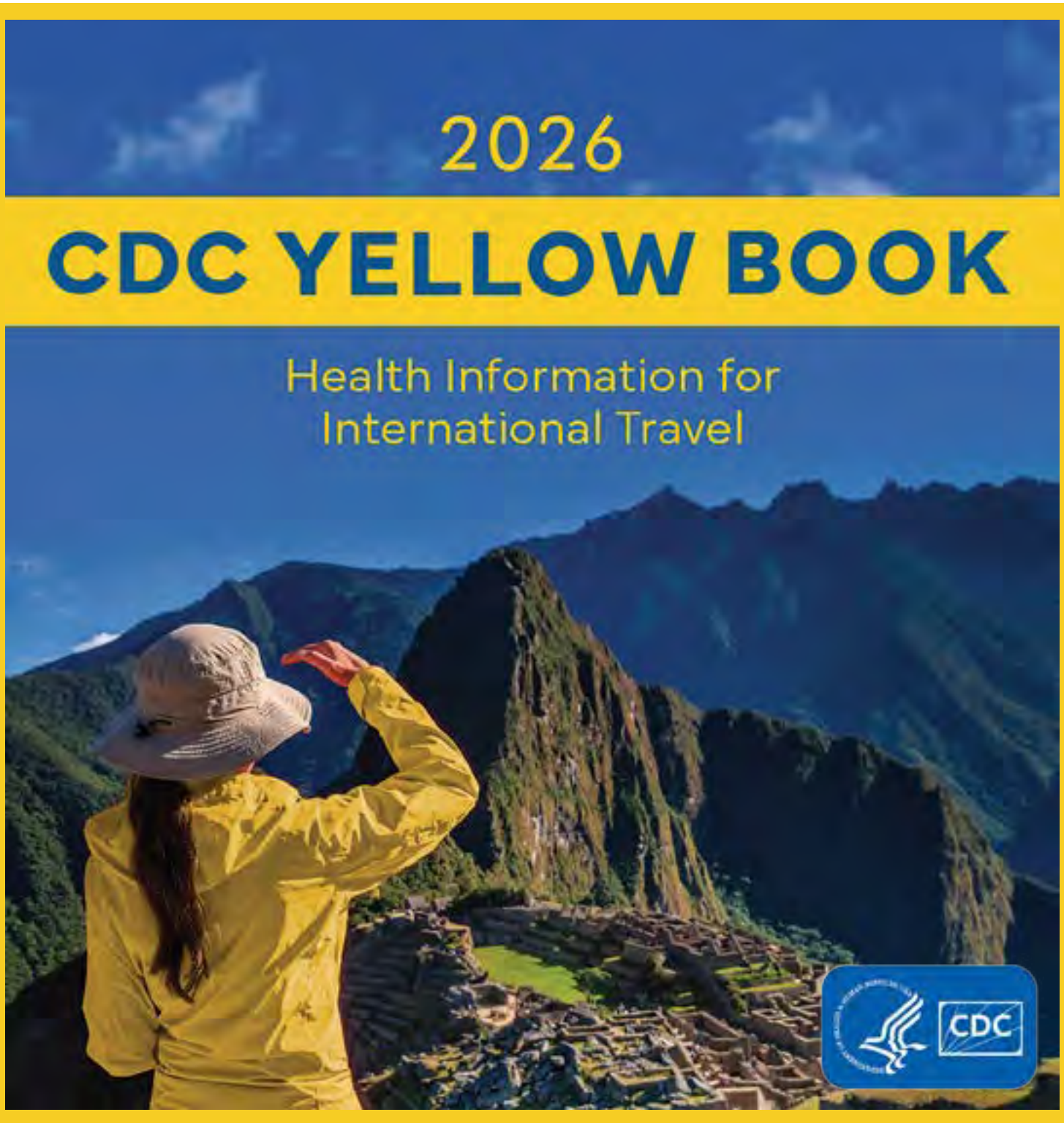

Launch of CDC Yellow Book 2026– A Trusted Travel Medicine Resource

CDC is pleased to announce the launch of the **CDC Yellow Book 2026**. The CDC Yellow Book is a resource containing the U.S. government's travel medicine recommendations and has been trusted by the travel medicine community for over 50 years. Healthcare professionals can use the print and digital versions to find the most up-to-date travel medicine information to better serve their patients' healthcare needs.

The CDC Yellow Book is available online now at www.cdc.gov/yellowbook and in print starting in June 2025 through Oxford University Press and other major online booksellers.

Chagas Disease, an Endemic Disease in the United States

Norman L. Beatty, Gabriel L. Hamer, Bernardo Moreno-Peniche, Bonny Mayes, Sarah A. Hamer[1]

Chagas disease, caused by *Trypanosoma cruzi* parasites, is considered endemic to 21 countries in the Americas, excluding the United States. However, increasing evidence of *T. cruzi* parasites in the United States in triatomine insects, domestic animals, wildlife, and humans challenges that nonendemic label. Several triatomine species are common in the southern United States, where they transmit *T. cruzi* and invade human dwellings. Wildlife, captive animals, and companion animals, especially dogs, are commonly infected with *T. cruzi* parasites in this region and serve as reservoirs. Autochthonous human cases have been reported in 8 states, most notably in Texas. Labeling the United States as non–Chagas disease–endemic perpetuates low awareness and underreporting. Classification of Chagas disease as endemic, in particular as hypoendemic, to the United States could improve surveillance, research, and public health responses. Acknowledging the endemicity of Chagas disease in the United States is crucial for achieving global health goals.

Chagas disease, or American trypanosomiasis, is caused by the parasitic protozoan *Trypanosoma cruzi*, which is transmitted through congenital, oral, and vectorborne routes; vectorborne infections result from contact with the feces of infected triatomine insects (kissing bugs). The World Health Organization (WHO) and Pan American Health Organization highlight 21 countries in the Americas to which Chagas disease is endemic (https://www.who.int/publications/i/item/9789240010352; https://www.paho.org/en/topics/chagas-disease), excluding the United States. As a result, the United States is often labeled as nonendemic, and this designation permeates the scientific literature (*1*,*2*), the Centers for Disease Control and Prevention (CDC) website (https://www.cdc.gov/chagas/index.html), the media, pest professional websites, and the general community of researchers and physicians (*3*,*4*). In this article, we review a body of evidence establishing the robust presence of *T. cruzi* parasites in the United States, not only among insect vectors, wildlife, and domestic animals but also among humans without travel histories who are assumed to be locally infected. Through revisiting definitions of endemicity, we conclude that sufficient evidence exists to support the inclusion of the United States as an endemic country for Chagas disease.

Robust Sylvatic Cycles of *T. cruzi* Parasites in the United States

In the United States, triatomines are commonly known as kissing bugs. The blood-sucking insects occur naturally in the southern half of the country and have been identified in 32 states (https://www.cdc.gov/chagas/index.html) (*5*) (Figure 1). Although available data are inadequate to prove that triatomines are increasing in geographic distribution or abundance, largely owing to a lack of standardized surveillance over time, triatomines are increasingly recognized because of frequent encounters with humans in the domestic and peridomestic habitat and increased research attention (*6*). Invasion into homes, human bites, subsequent allergic reactions or exposure to *T. cruzi* parasites, and increasing frequency of canine diagnoses have led to growing public awareness (*7*–*10*). Of all 11 triatomine species found in the United States, 9 have been found to be naturally infected with *T. cruzi* (*9*,*11*). Of those, 4 species (*Triatoma sanguisuga*, *T. gerstaeckeri*, *T. protracta*, and *T. rubida*) are commonly found in human dwellings, raising concern for increased opportunity for vectorborne transmission to humans (*7*,*8*,*12*,*13*). Although

Author affiliations: University of Florida College of Medicine, Gainesville, Florida, USA (N.L. Beatty); Emerging Pathogens Institute, University of Florida, Gainesville (N.L. Beatty); Texas A&M University College of Agriculture and Life Sciences, College Station, Texas, USA (G.L. Hamer); University of California, Berkeley, California, USA (B. Moreno-Peniche); Texas Department of State Health Services, Austin, Texas, USA (B. Mayes); Texas A&M University College of Veterinary Medicine and Biomedical Sciences, College Station (S.A. Hamer)

DOI: https://doi.org/10.3201/eid3109.241700

[1]All authors contributed equally to this article.

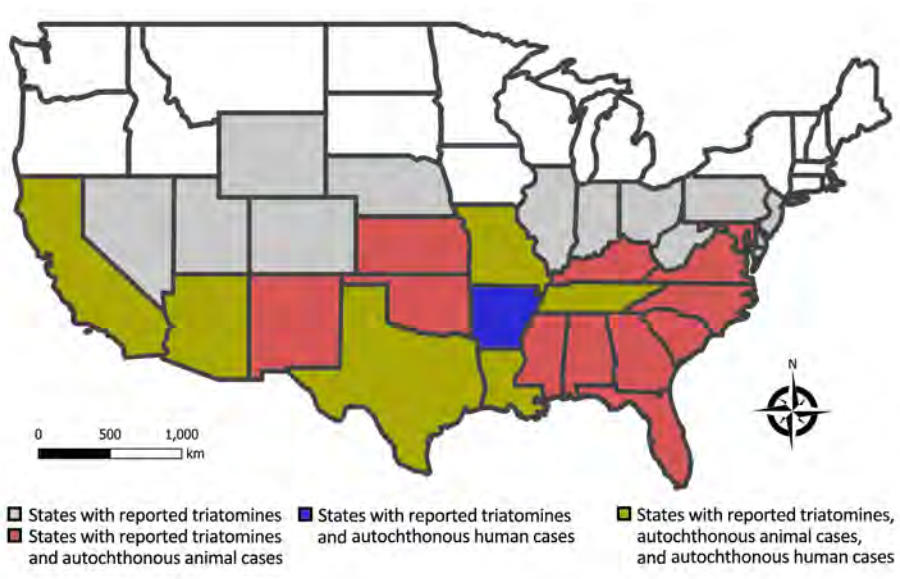

Figure 1. US states with reported wild, domestic, or captive animals exposed to *Trypanosoma cruzi* locally; states with reported autochthonous human Chagas disease; and all states with reported triatomines in assessment of Chagas disease as endemic to the United States.

triatomine colonization (defined as the presence of flightless immature nymphal stages in the domicile) occurs in the United States (*12*,*14*), metrics of colonization are lower than those observed in Chagas disease–endemic communities in rural Latin America. Numerous investigations of triatomines in the United States have revealed they harbor *T. cruzi* parasites; infection prevalence ranges from 30% to >50% (*15*,*16*). *Triatoma sanguisuga* and *T. protracta* kissing bugs have the largest overall distribution within the United States, but the *T. gerstaeckeri* kissing bug appears to be the most common species in domestic settings in Texas and is likely responsible for transmission resulting in locally acquired *T. cruzi* infection in dogs and humans (*9*).

T. cruzi infections among sylvatic and peridomestic mammalian reservoirs have been documented in ≥17 states in the southern United States (Figure 1) (Appendix, https://wwwnc.cdc.gov/EID/article/31/9/24-1700-App1.pdf) and include species such as woodrat (*Neotoma* spp.), Virginia opossum (*Didelphis virginiana),* raccoon (*Procyon lotor),* nine-banded armadillo (*Dasypus novemcinctus*), striped skunk (*Mephitis mephitis*), and coyote (*Canis latrans*) (*6*). Infection prevalence among some wild mammal populations can be as high as >50%, and parasitemias are considered high enough to infect triatomines, thus these mammals function as reservoir hosts (*6*,*17*). *T. cruzi* discrete typing units I and IV have been consistently identified in wild and domestic reservoir species (*6*,*9*,*18*); additional discrete typing units have been detected using deep-sequencing methods (*19*). Among wildlife reservoirs in the United States, Virginia opossums can possess the unique feature of harboring *T. cruzi* parasites within the anal gland and anal gland secretions, and vertical transmission from infected mother opossum to joey has been shown (*19*,*20*); those observations suggest alternative parasite transmission pathways within wildlife.

Infection among companion animals, such as domestic and working canines and felines, has also been demonstrated throughout the United States (*6*). Dogs exposed to *T. cruzi* have been found in 23 states, as well as in Washington, DC, and the US Virgin Islands, although dogs infected in northern states likely reflect travel from regions where vectors are present (*16*,*20*). In Texas, the only state where Chagas disease in animals has been a reportable condition, 431 canine cases were reported during 2013–2015 (in addition to cases in 2 cats, 1 horse, 1 rat, 3 chimpanzees, and 1 walrus) (https://www.dshs.texas.gov/notifiable-conditions/zoonosis-control/zoonosis-control-diseases-and-conditions/chagas-disease/chagas-disease-data). After that period of widespread documenting of canine infections, the reporting requirement ceased, in part because of the substantial resources required to collate reports. Canine Chagas disease has been most studied in Texas, where cross-sectional and cohort studies have shown a prevalence ranging from ≈10% to >50% and a study across several large dog kennels showed an incidence of 30.7 new infections/100 dogs/year (e.g., *21*,*22*). Canines are a major domestic reservoir of *T. cruzi* parasites among communities in Latin America where human infection is routinely demonstrated (*23*). That link has also been shown in Texas communities located along the Rio Grande River, where infected canines and humans have been documented, raising

additional concerns regarding ongoing domestic *T. cruzi* transmission (*24*–*27*).

T. cruzi infection among zoo-housed, exotic mammals has been recognized in states known to have triatomines, including Georgia, Alabama, Kansas, and Texas (*6*). In addition, infections occur in nonhuman primates at biomedical research facilities across the southern United States, posing challenges for research with those animal models (*28*). Exact transmission routes to these animals are hard to determine, but transmission likely occurs by ingesting the triatomine bug (*29*). Although many exotic animals have extensive travel histories, local infections are possible when triatomine are present on the premises.

Autochthonous Human Chagas Disease in the United States

Autochthonous human *T. cruzi* infections have been identified in 8 states: California, Arizona, Texas, Tennessee, Louisiana, Missouri, Mississippi, and Arkansas (*8*). A systematic literature review found 29 confirmed and 47 suspected cases of locally acquired Chagas disease during 2000–2018; shared risk factors included rural residence, history of hunting or camping, and agricultural or outdoor work (*30*). Those numbers likely greatly underrepresent underlying human infections. The Council of State and Territorial Epidemiologists created a surveillance case definition for *T. cruzi* infection and Chagas disease in June 2024 (*31*); however, human Chagas disease is not a nationally notifiable disease, and thus the true prevalence or incidence of autochthonous Chagas disease remains unknown. Human Chagas disease is a notifiable disease in 8 states (Arizona, Arkansas, Louisiana, Mississippi, Tennessee, Texas, Utah, and Washington) and 2 California health jurisdictions (San Diego County and Los Angeles County).

Texas has undertaken extensive efforts to document human Chagas disease; cases were first made reportable in the state in 2013 (https://www.dshs.texas.gov/notifiable-conditions/zoonosis-control/zoonosis-control-diseases-and-conditions/chagas-disease/chagas-disease-data). The first known autochthonous case of human Chagas disease in the United States occurred in an infant in 1955 in Corpus Christi, Texas, in a home known to be infested with triatomines (*32*). However, parasite transmission to humans in the region has occurred since prehistoric times, given, for example, a paleoparasitology study that recovered *T. cruzi* DNA in a mummified body (dated to 1,150 BP) of a man from western Texas with signs of megacolon (*33*). During 2013–2023, the Texas Department of State Health Services documented 50 probable and confirmed cases that were considered autochthonous, either because the area of vector exposure was known or because of a lack of travel to or previous residence in Chagas disease–endemic areas of Latin America (https://www.dshs.texas.gov/notifiable-conditions/zoonosis-control/zoonosis-control-diseases-and-conditions/chagas-disease/chagas-disease-data) (Figure 2; Appendix). Of those 50 cases, 3 were diagnosed at the acute stage, 44 at the chronic asymptomatic (indeterminate) stage, and 3 at the chronic symptomatic (determinate) stage. Based on CDC guidelines, diagnosis of chronic Chagas disease requires positive results by $\geq$2 tests that detect antibodies to different antigens, because no single test is sufficiently sensitive and specific for diagnosis (https://www.cdc.gov/chagas/index.html). Of the 47 reported chronic cases, 31 (66%) were confirmed with serologic testing at CDC. Of the 3 acute cases, 2 were acquired in central Texas (Austin–Round Rock metropolitan area); the third case was acquired in the Rio Grande Valley region of South Texas. A Spearman correlation test indicated that there was no temporal trend in the reported cases by year (z-score −1.0004; p = 0.31), underscoring that locally acquired cases are a stable threat in the state.

Triatomine species from the southwestern United States have been shown to have a longer postfeeding defecation behavior than more efficient triatomine vectors in Latin America (*34*); that behavior has been posed to reduce the risk for contact between infectious *T. cruzi* and the host. That narrative has contributed to the perception that triatomine species in the United States are not capable of stercorarian transmission. However, a study of *T. gerstaeckeri* and *T. sanguisuga* bugs documented simultaneous feeding and defecation by the 2 key North American vectors, although the measured postfeeding defecation indices were longer than those of the *Rhodnius Prolixus* kissing bug, a highly competent triatomine from South America (*35*). Although many of the autochthonous Chagas disease cases in the United States involve persons exposed to triatomines, additional case-patients report no exposure to triatomines (*36*,*37*), underscoring the cryptic nature of the vectors and suggesting alternative transmission routes should be considered (*8*).

Oral transmission has been documented in certain regions of Latin America where fruit-based food or drink products have been contaminated with *T. cruzi* from triatomines living on trees (*38*). Triatomines in the United States have not been reported to inhabit fruit trees, and oral transmission is likely less relevant for explaining human cases acquired in the United States; nonetheless, oral parasite transmission

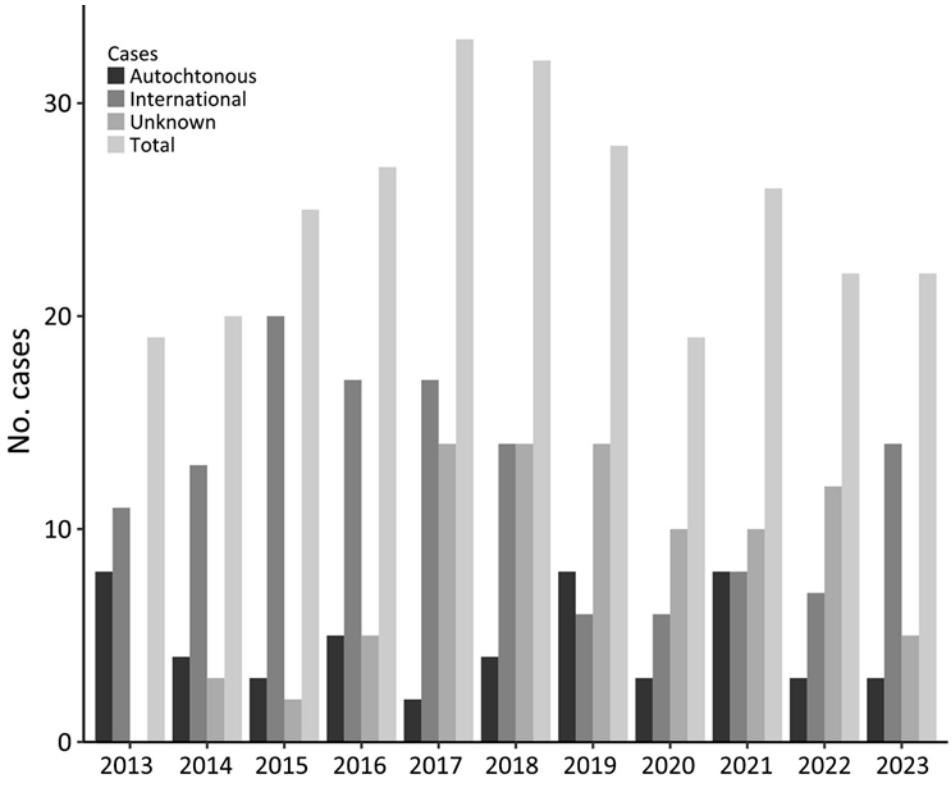

Figure 2. Yearly reported cases of autochthonous human Chagas disease in Texas in assessment of Chagas disease as endemic to the United States. Cases have been continuously reported with no apparent temporal trend (z-score −1.0004; p = 0.31), 2013–2023.

through consumption of infected triatomines is speculated to be the primary mode of transmission to dogs (*39*). In addition, screening programs to detect potential congenital *T. cruzi* transmission in the United States are critical for preventing long-term sequelae of the disease (*40*).

Definitions of Endemicity

The CDC defines endemic as the constant presence/usual prevalence of a disease or infectious agent in a population within a geographic area (*41*). In its characterization of infectious disease occurrence patterns, Clay's Handbook of Environmental Health identifies an endemic pattern as "when an infection is always present at low or moderate levels within a given geographic area or defined population" (*42*). A "hyperendemic pattern," the authors add, "is observed when infection occurs at high levels and affects all age groups equally" (*42*). WHO provides a more nuanced definition of specific terminology for malaria, such as endemic being "an area in which there is an ongoing, measurable incidence of malaria infection and mosquito-borne transmission over a succession of years"; the organization also includes specific subcategories for the percent of the population with malaria: "hypoendemic (0–10%), mesoendemic (10–50%), hyperendemic (constantly >50%), and holoendemic (constantly ≥75%)" (*43*). Such an operative scale for Chagas disease has not yet been developed, but acknowledging the nuanced nature of endemicity (as stated by WHO terminology) and the unique characteristics of Chagas disease occurrence in different regions will be crucial when considering the endemicity status of Chagas disease in the United States. The context in the southern United States presents well-established enzootic cycles and sporadic albeit constant locally acquired human cases (Figure 2), supporting a Chagas disease–endemic disease status.

Consequences of Nonendemic Label

The current classification of the United States as nonendemic for Chagas disease has led to critical issues such as low physician and veterinary awareness of possible human and animal exposure to *T. cruzi* (*4*,*44*,*45*), which prevents appropriate differential diagnosis and could subsequently contribute to potential underreporting. The nonendemic label is coupled with the portrayal of Chagas disease as an essentially foreign or an exclusively travel-related issue in the media. Such misrecognition impedes effective disease management and underscores the need to reevaluate Chagas disease's endemic status.

We propose that Chagas disease in the United States be classified as endemic and, more specifically, hypoendemic, acknowledging its presence and

effects while emphasizing the need for heightened awareness and surveillance. We recognize the burden of locally acquired human disease in the United States does not approach the levels seen in some regions of Latin America but hope that labeling the United States as Chagas disease–endemic will also raise awareness for this neglected disease across its endemic range. This reclassification reflects a broader understanding of epidemiology that aligns with a One Health approach, recognizing the interconnectedness of human, animal, and environmental health. It also acknowledges the United States' foundational and ongoing dependence on the highly variable modes of human migration and settlement. By incorporating ecologic, social, and geographic relationships, this shift paves the way for expanding research and intervention strategies. The United States contributes 23.3% of the world's scientific research on Chagas disease, but most of it is focused on pharmacological and diagnostics development and immunology (*46*). Social and epidemiologic research, which should focus on populations that are disproportionately affected (*46*), is lacking. Recognizing Chagas disease as endemic to the United States would ideally help increase funding agencies' investment in research toward improved diagnostics and treatment and, perhaps more critically, would support local public health agencies in obtaining resources needed to educate communities, report cases, and prevent new infections. Last, from a global health perspective, without recognizing stable transmission within its borders, the United States will be unable to reach its Sustainable Development Goals outlined in the WHO initiative Ending the Neglect to Attain Sustainable Development Goals: A Road Map for Neglected Tropical Disease 2021–2030; specifically, the third foundational pillar that centers on changing "operating models and culture to facilitate country ownership" would be unattainable (https://www.paho.org/en/topics/chagas-disease).

Conclusions

T. cruzi and the ecologic conditions that sustain its transmission cycles are naturally occurring throughout the southern half of the United States. Infection has been consistently demonstrated in wildlife reservoirs, companion animals, zoo and exotic mammals, and humans. At least 4 triatomine species are frequently encountered in homes and found to be harboring *T. cruzi* parasites. Canine Chagas disease is a concern in many working and companion dog populations in the southern United States but is likely underrecognized in many areas. The exposure of nonhuman primates to *T. cruzi*–infected triatomines poses a challenge to medical research. Moreover, the lack of reporting requirements for human Chagas disease adds complexity to the documentation of autochthonous cases. The number of documented autochthonous cases is higher in Texas than in other states, and cases are consistently documented each year.

This body of evidence justifies recognizing that Chagas disease is endemic to the United States, and not just from a veterinary perspective. Updating Chagas disease endemicity status as hypoendemic is a crucial step toward a more effective management model, one that addresses the unique challenges and complexities of this country regarding vectorborne diseases. Such a shift will help reform curriculum in professional schools to enable the next generation of practitioners to be competent in recognizing the low but present risk for locally acquired *T. cruzi* infections and better serve those who acquire the parasite elsewhere and require diagnosis in the United States. There is an opportunity to learn from the public health experiences in Mexico and other regions of Latin America that have long faced a high burden of human Chagas disease; those experiences call for increased understanding and disease management that integrates biomedical, sociocultural and policy perspectives (*47*). Managing endemic Chagas disease in the United States will require overcoming systemic, structural, clinical, and psychosocial healthcare barriers (*48*). Case investigations would ideally have standardized data collection and case classification, to include travel history, triatomine encounters, and proximity to suitable triatomine habitat, all of which are useful in assessing local transmission risk (*49*). In the meantime, solutions for Chagas disease can be advanced through the study of the unfortunate abundance of naturally infected animals across the southern United States (*50*). To achieve the Sustainable Development Goals for the 2030 Neglected Tropical Disease roadmap, recognizing Chagas disease endemicity in the United States as a regional issue will be imperative to begin implementing local, state, and national strategic plans to tackle this neglected disease that, as has been demonstrated, has never been exclusively tropical.

Acknowledgments

We thank all scientists, clinicians, community health workers, and colleagues who have studied and offered data and perspective about Chagas disease in the United States. We thank Amanda Brock-Morales for assisting with the creation of Figure 1.

About the Author

Dr. Beatty is an associate professor of medicine at the University of Florida College of Medicine, Department of Medicine, Division of Infectious Diseases and Global Medicine. His primary research interests are triatomine biology, *Trypanosoma cruzi* pathogenesis, and clinical Chagas disease.

References

1. Miranda-Arboleda AF, Zaidel EJ, Marcus R, Pinazo MJ, Echeverría LE, Saldarriaga C, et al.; Neglected Tropical Diseases and other Infectious Diseases affecting the Heart (NET-Heart) project. Roadblocks in Chagas disease care in endemic and nonendemic countries: Argentina, Colombia, Spain, and the United States. The NET-Heart project. PLoS Negl Trop Dis. 2021;15:e0009954. https://doi.org/10.1371/journal.pntd.0009954
2. Gascon J, Bern C, Pinazo MJ. Chagas disease in Spain, the United States and other non-endemic countries. Acta Trop. 2010;115:22–7. https://doi.org/10.1016/j.actatropica.2009.07.019
3. Tan MM, Matthews KRW. Misconceptions and limited awareness of Chagas disease in Texas among surveyed Houston physicians. 2018 [cited 2024 Oct 15]. https://www.bakerinstitute.org/sites/default/files/2018-12/import/chb-pub-chagas-121818.pdf
4. Stimpert KK, Montgomery SP. Physician awareness of Chagas disease, USA. Emerg Infect Dis. 2010;16:871–2. https://doi.org/10.3201/eid1605.091440
5. Reeves WK, Miller MM. A new state record for *Triatoma sanguisuga* (Leconte) (Hemiptera: Reduviidae) from Wyoming, U.S.A. Comp Parasitol. 2020;87:118–20. https://doi.org/10.1654/1525-2647-87.1.118
6. Busselman RE, Hamer SA. Chagas disease ecology in the United States: recent advances in understanding *Trypanosoma cruzi* transmission among triatomines, wildlife, and domestic animals and a quantitative synthesis of vector-host interactions. Annu Rev Anim Biosci. 2022;10:325–48. https://doi.org/10.1146/annurev-animal-013120-043949
7. Beatty NL, White ZS, Bhosale CR, Wilson K, Cannella AP, Stenn T, et al. Anaphylactic reactions due to *Triatoma protracta* (Hemiptera, Reduviidae, Triatominae) and invasion into a home in northern California, USA. Insects. 2021;12:1018. https://doi.org/10.3390/insects12111018
8. Beatty NL, Klotz SA. Autochthonous Chagas disease in the United States: how are people getting infected? Am J Trop Med Hyg. 2020;103:967–9. https://doi.org/10.4269/ajtmh.19-0733
9. Bern C, Messenger LA, Whitman JD, Maguire JH. Chagas disease in the United States: a public health approach. Clin Microbiol Rev. 2019;33:e00023–19. https://doi.org/10.1128/CMR.00023-19
10. Curtis-Robles R, Wozniak EJ, Auckland LD, Hamer GL, Hamer SA. Combining public health education and disease ecology research: using citizen science to assess Chagas disease entomological risk in Texas. PLoS Negl Trop Dis. 2015;9:e0004235. https://doi.org/10.1371/journal.pntd.0004235
11. Beard CB, Young DG, Butler JF, Evans DA. First isolation of *Trypanosoma cruzi* from a wild-caught *Triatoma sanguisuga* (LeConte) (Hemiptera: Triatominae) in Florida, U.S.A. J Parasitol. 1988;74:343–4. https://doi.org/10.2307/3282467
12. Curtis-Robles R, Hamer SA, Lane S, Levy MZ, Hamer GL. Bionomics and spatial distribution of Triatomine vectors of *Trypanosoma cruzi* in Texas and other southern states, USA. Am J Trop Med Hyg. 2018;98:113–21. https://doi.org/10.4269/ajtmh.17-0526
13. Dumonteil E, Tu W, Jiménez FA, Herrera C. Ecological interactions of *Triatoma sanguisuga* (Hemiptera: Reduviidae) and risk for human infection with *Trypanosoma cruzi* (Kinetoplastida: Trypanosomatidae) in Illinois and Louisiana. J Med Entomol. 2024;61:1282–9. https://doi.org/10.1093/jme/tjae017
14. Klotz SA, Smith SL, Schmidt JO. Kissing bug intrusions into homes in the Southwest United States. Insects. 2021;12:654. https://doi.org/10.3390/insects12070654
15. Mehringer PJ Jr, Wood SF. A resampling of wood rat houses and human habitations in Griffith Park, Los Angeles, for *Triatoma protracta* and *Trypanosoma cruzi*. Bull South Calif Acad Sci. 2022;57:39–46.
16. Zeledon R, Beard CB, Pinto Dias JC, Leiby DA, Dorn PL, Rodrigues Coura J. An appraisal of the status of Chagas disease in the United States. Amsterdam: Elsevier; 2012.
17. Hodo CL, Hamer SA. Toward an ecological framework for assessing reservoirs of vector-borne pathogens: wildlife reservoirs of *Trypanosoma cruzi* across the southern United States. ILAR J. 2017;58:379–92. https://doi.org/10.1093/ilar/ilx020
18. Torhorst CW, White ZS, Bhosale CR, Beatty NL, Wisely SM. Identification of the parasite, *Trypanosoma cruzi*, in multiple tissues of epidemiological significance in the Virginia opossum (*Didelphis virginiana*): implications for environmental and vertical transmission routes. PLoS Negl Trop Dis. 2022;16:e0010974. https://doi.org/10.1371/journal.pntd.0010974
19. Majeau A, Cloherty E, Anderson AN, Straif-Bourgeois SC, Dumonteil E, Herrera C. Genetic diversity of *Trypanosoma cruzi* infecting raccoons (*Procyon lotor*) in 2 metropolitan areas of southern Louisiana: implications for parasite transmission networks. Parasitology. 2023;150:374–81. https://doi.org/10.1017/S0031182023000070
20. Meyers AC, Purnell JC, Ellis MM, Auckland LD, Meinders M, Hamer SA. Nationwide exposure of U.S. working dogs to the Chagas disease parasite, *Trypanosoma cruzi*. Am J Trop Med Hyg. 2020;102:1078–85. https://doi.org/10.4269/ajtmh.19-0582
21. Busselman RE, Meyers AC, Zecca IB, Auckland LD, Castro AH, Dowd RE, et al. High incidence of *Trypanosoma cruzi* infections in dogs directly detected through longitudinal tracking at 10 multi-dog kennels, Texas, USA. PLoS Negl Trop Dis. 2021;15:e0009935. https://doi.org/10.1371/journal.pntd.0009935
22. Curtis-Robles R, Snowden KF, Dominguez B, Dinges L, Rodgers S, Mays G, et al. Epidemiology and molecular typing of *Trypanosoma cruzi* in naturally-infected hound dogs and associated triatomine vectors in Texas, USA. PLoS Negl Trop Dis. 2017;11:e0005298. https://doi.org/10.1371/journal.pntd.0005298
23. Gürtler RE, Cardinal MV. Dogs and their role in the eco-epidemiology of Chagas disease. In: Strube C, Mehlhorn H, editors. Dog parasites endangering human health. Cham: Springer International Publishing; 2021. p. 73–106.
24. Curtis-Robles R, Zecca IB, Roman-Cruz V, Carbajal ES, Auckland LD, Flores I, et al. *Trypanosoma cruzi* (agent of Chagas disease) in sympatric human and dog populations in "colonias" of the Lower Rio Grande Valley of Texas. Am J Trop Med Hyg. 2017;96:805–14. https://doi.org/10.4269/ajtmh.16-0789

25. Garcia MN, O'Day S, Fisher-Hoch S, Gorchakov R, Patino R, Feria Arroyo TP, et al. One health interactions of Chagas disease vectors, canid hosts, and human residents along the Texas-Mexico border. PLoS Negl Trop Dis. 2016;10:e0005074. https://doi.org/10.1371/journal.pntd.0005074
26. Beard CB, Pye G, Steurer FJ, Rodriguez R, Campman R, Peterson AT, et al. Chagas disease in a domestic transmission cycle, southern Texas, USA. Emerg Infect Dis. 2003;9:103–5. https://doi.org/10.3201/eid0901.020217
27. Burkholder JE, Allison TC, Kelly VP. Tr*ypanosoma cruzi* (Chagas) (Protozoa: Kinetoplastida) in invertebrate, reservoir, and human hosts of the lower Rio Grande valley of Texas. J Parasitol. 1980;66:305–11. https://doi.org/10.2307/3280824
28. Dorn PL, Daigle ME, Combe CL, Tate AH, Stevens L, Phillippi-Falkenstein KM. Low prevalence of Chagas parasite infection in a nonhuman primate colony in Louisiana. J Am Assoc Lab Anim Sci. 2012;51:443–7.
29. Kiehl WM, Hodo CL, Hamer GL, Hamer SA, Wilkerson GK. Exclusion of horizontal and vertical transmission as major sources of *Trypanosoma cruzi* infections in a breeding colony of rhesus macaques (*Macaca Mulatta*). Comp Med. 2023;73:229–41. https://doi.org/10.30802/AALAS-CM-23-000005
30. Lynn MK, Bossak BH, Sandifer PA, Watson A, Nolan MS. Contemporary autochthonous human Chagas disease in the USA. Acta Trop. 2020;205:105361. https://doi.org/10.1016/j.actatropica.2020.105361
31. Council of State and Territorial Epidemiologists. Standardized surveillance case definition for acute, congenital, and chronic trypanosoma cruzi infection or Chagas disease. 2024 [cited May 2025]. https://cdn.ymaws.com/www.cste.org/resource/resmgr/position_statements_files_2023/24-ID-04_Chagas_disease.pdf
32. Woody NC, Woody HB. American trypanosomiasis (Chagas' disease); first indigenous case in the United States. J Am Med Assoc. 1955;159:676–7. https://doi.org/10.1001/jama.1955.02960240042010a
33. Dittmar KJA, Araujo A, Reinhard KJ, Ferreira LF, Whiting A. Molecular diagnosis of prehistoric *Trypanosoma cruzi* in the Texas-Coahuila border region. Presented at: 13th Annual Meeting of the Paleopathology Association; Tempe, Arizona, USA; April 23–26, 2003.
34. Klotz SA, Dorn PL, Klotz JH, Pinnas JL, Weirauch C, Kurtz JR, et al. Feeding behavior of triatomines from the southwestern United States: an update on potential risk for transmission of Chagas disease. Acta Trop. 2009;111:114–8. https://doi.org/10.1016/j.actatropica.2009.03.003
35. Killets KC, Wormington J, Zecca I, Chaves LF, Hamer GL, Hamer SA. Comparative feeding and defecation behaviors of *Trypanosoma cruzi*-infected and uninfected triatomines (Hemiptera: Reduviidae) from the Americas. Insects. 2025;16:188. https://doi.org/10.3390/insects16020188
36. Hudson FP, Homer N, Epstein A, Mondy K. Acute Chagas disease manifesting as orbital cellulitis, Texas, USA. Emerg Infect Dis. 2021;27:2937–9. https://doi.org/10.3201/eid2711.203698
37. Turabelidze G, Vasudevan A, Rojas-Moreno C, Montgomery SP, Baker M, Pratt D, et al. Autochthonous Chagas disease—Missouri, 2018. MMWR Morb Mortal Wkly Rep. 2020;69:193–5. https://doi.org/10.15585/mmwr.mm6907a4
38. Franco-Paredes C, Villamil-Gómez WE, Schultz J, Henao-Martínez AF, Parra-Henao G, Rassi A Jr, et al. A deadly feast: elucidating the burden of orally acquired acute Chagas disease in Latin America—public health and travel medicine importance. Travel Med Infect Dis. 2020;36:101565. https://doi.org/10.1016/j.tmaid.2020.101565
39. Barr SC. Canine Chagas' disease (American trypanosomiasis) in North America.[[v–vi.]. Vet Clin North Am Small Anim Pract. 2009;39:1055–64. https://doi.org/10.1016/j.cvsm.2009.06.004
40. Reifler K, Campbell JI, Barnett ED, Bourque DL, Hamer DH, Samra H, et al. Diagnosing Chagas in pregnancy and childhood: what's old and new. Clin Lab Med. 2025;45:73–86. https://doi.org/10.1016/j.cll.2024.10.004
41. Dicker RC, Coronado F, Koo D, Parrish RG. Principles of epidemiology in public health practice; an introduction to applied epidemiology and biostatistics. 3rd ed. 2006 [cited 2024 Oct 15]. https://stacks.cdc.gov/view/cdc/6914
42. Phalkey R, Bradley N, Dobney A, Murray V, O'Hagan J, Ahmad M, et al. Human physiology, hazards and health risks. In: Battersby S, editor. Clay's handbook of environmental health. New York: Routledge; 2022. p. 190–207.
43. World Health Organization (WHO). WHO malaria terminology, 2021 update [cited 2024 Oct 15]. https://www.who.int/publications/i/item/9789240038400
44. Gavic EA, Achen SE, Fox PR, Benjamin EJ, Goodwin J, Gunasekaran T, et al. *Trypanosoma cruzi* infection diagnosed in dogs in nonendemic areas and results from a survey suggest a need for increased Chagas disease awareness in North America. J Am Vet Med Assoc. 2023;261:705–12. https://doi.org/10.2460/javma.22.10.0445
45. Stigler Granados P, Pacheco GJ, Núñez Patlán E, Betancourt J, Fulton L. Assessing the effectiveness of Chagas disease education for healthcare providers in the United States. BMC Infect Dis. 2020;20:743. https://doi.org/10.1186/s12879-020-05474-w
46. Levin LG, Kreimer PR, Jensen P. Chagas Disease across contexts: scientific knowledge in a globalized world. Med Anthropol. 2021;40:572–89. https://doi.org/10.1080/01459740.2021.1946805
47. Aké-Chan M, Sanmartino M, Castillo-Burguete MT, González-Martínez A, Ibarra-Cerdeña CN. (In)coherence between Chagas disease policy and the experiences of those affected in Mexico: the need for a transdisciplinary approach. PLoS Negl Trop Dis. 2025;19:e0013052. https://doi.org/10.1371/journal.pntd.0013052
48. Forsyth C, Meymandi S, Moss I, Cone J, Cohen R, Batista C. Proposed multidimensional framework for understanding Chagas disease healthcare barriers in the United States. PLoS Negl Trop Dis. 2019;13:e0007447. https://doi.org/10.1371/journal.pntd.0007447
49. Lund AJ, Metzger ME, Kramer VL, Kjemtrup AM. Low risk for locally acquired Chagas disease in California: a review of human cases and triatomine submissions, 2013–2023. PLoS Negl Trop Dis. 2025;19:e0013036. https://doi.org/10.1371/journal.pntd.0013036
50. Tarleton RLSA, Lococo B, Alvarez Gianni MG, Laucella S, Hodo CL, Wilkerson GK, et al. The unfortunate abundance of *Trypanosoma cruzi* in naturally infected dogs and monkeys provides unique opportunities to advance solutions for Chagas disease. Zoonoses Public Health. 2024;4. https://doi.org/10.15212/ZOONOSES-2024-0005

Address for correspondence: Sarah A. Hamer, Department of Veterinary Integrative Biosciences, 667 Raymond Stotzer Ave, Texas A&M University, College Station, TX 77843, USA; email: SHamer@cvm.tamu.edu

Severe Group A *Streptococcus* Infection among Children, France, 2022–2024

Montserrat Sierra Colomina, Alix Flamant, Guillaume Le Balle, Jérémie F. Cohen, Lionel Berthomieu, Stéphane Leteurtre, Yves Gillet, Etienne Javouhey, Stéphane Bechet, Corinne Levy, Robert Cohen, Agnès Ferroni, Damien Dubois, Miguel Angel Hernandez Martinez, Céline Plainvert, Asmaa Tazi, ISAI Study Group,[1] Camille Brehin

Medscape CME Activity

In support of improving patient care, this activity has been planned and implemented by Medscape, LLC and Emerging Infectious Diseases. Medscape, LLC is jointly accredited with commendation by the Accreditation Council for Continuing Medical Education (ACCME), the Accreditation Council for Pharmacy Education (ACPE), and the American Nurses Credentialing Center (ANCC), to provide continuing education for the healthcare team.

Medscape, LLC designates this Journal-based CME activity for a maximum of 1.00 ***AMA PRA Category 1 Credit(s)™***. Physicians should claim only the credit commensurate with the extent of their participation in the activity.

Successful completion of this CME activity, which includes participation in the evaluation component, enables the participant to earn up to 1.0 MOC points in the American Board of Internal Medicine's (ABIM) Maintenance of Certification (MOC) program. Participants will earn MOC points equivalent to the amount of CME credits claimed for the activity. It is the CME activity provider's responsibility to submit participant completion information to ACCME for the purpose of granting ABIM MOC credit.

All other clinicians completing this activity will be issued a certificate of participation. To participate in this journal CME activity: (1) review the learning objectives and author disclosures; (2) study the education content; (3) take the post-test with a 75% minimum passing score and complete the evaluation at https://www.medscape.org/qna/processor/75090?showStandAlone=true&src=prt_jcme_eid_mscpedu; and (4) view/print certificate. For CME questions, see page 1880.

NOTE: It is the policy of Medscape Education to avoid the mention of brand names or specific manufacturers in accredited educational activities. However, trade and manufacturer names in this activity are provided in an effort to provide clarity. The use of brand or manufacturer names should not be viewed as an endorsement by Medscape of any specific product or manufacturer.

Release date: August 21, 2025; Expiration date: August 21, 2026

Learning Objectives

Upon completion of this activity, participants will be able to:

- Assess the initial presentation and management of children with severe group A *Streptococcus* (GAS) infections
- Analyze the accuracy of testing for GAS in cases of severe pediatric infection
- Distinguish the most common *emm* genotype of GAS in the current study
- Evaluate risk factors for severe sequelae of GAS infection among children

CME Editor

Jill Russell, BA, Technical Writer/Editor, Emerging Infectious Diseases. *Disclosure: Jill Russell, BA, has no relevant financial relationships.*

CME Author

Charles P. Vega, MD, Health Sciences Clinical Professor of Family Medicine, University of California, Irvine School of Medicine, Irvine, California. *Disclosure: Charles P. Vega, MD, has the following relevant financial relationships: served as a consultant or advisor for Boehringer Ingelheim Pharmaceuticals, Inc.; Exact Sciences Corporation.*

Authors

Montserrat Sierra Colomina, MD, PhD; Alix Flamant, MD; Guillaume Le Balle, MD, MSc; Jérémie F. Cohen, MD, PhD; Lionel Berthomieu, MD; Stéphane Leteurtre, MD, PhD; Yves Gillet, MD, PhD; Etienne Javouhey, MD, PhD; Stéphane Bechet, MSc; Corinne Levy, MD; Robert Cohen, MD; Agnès Ferroni, PharmD; Damien Dubois, PharmD, PhD; Miguel Angel Hernandez Martinez, MSc; Céline Plainvert, PharmD, PhD; Asmaa Tazi, PharmD, PhD; Camille Brehin, MD, PhD.

Group A *Streptococcus* infections have increased in Europe since September 2022. The French Pediatric Intensive Care and French Pediatric Infectious Diseases expert groups conducted a retrospective and prospective study of children who had severe group A *Streptococcus* infections during September 1, 2022–April 1, 2024, across 34 hospitals in France. A total of 402 pediatric patients (median age 4 [interquartile range 2–7.5] years; 42% girls, 58% boys) were enrolled. Cases were characterized by a low proportion of severe skin and soft tissue infections (16%), predominance of severe upper and lower respiratory tract infections (55%), and a 3.5% case-fatality rate. In multivariate analysis, hydrocortisone, corticosteroid, and vasopressor therapies were significantly associated with major sequelae or death. Molecular analysis revealed *emm1* (73.0%) and *emm12* (10.8%) strains; the $M1_{UK}$ clone represented 50% of *emm1* strains. Clinicians, researchers, and public health authorities must collaborate to mitigate the effects of GAS on child health.

Streptococcus pyogenes, also known as group A *Streptococcus* (GAS), presents a wide spectrum of manifestations, ranging from mild infections (e.g., pharyngitis) to severe and life-threatening conditions (e.g., necrotizing fasciitis). Globally, invasive *S. pyogenes* infections (iGAS) account for nearly 2 million cases per year worldwide; the effects of those infections on young children and older adults are substantial, including a case-fatality rate of up to 20%. In late 2022 and early 2023, a surge in pediatric GAS infections garnered international attention, prompting public health agencies to issue alerts. This rise extended beyond benign cases, also encompassing a notable increase in iGAS cases (*1*–*14*).

In France, during the last 2 weeks of November 2022, pediatric clinicians and intensivists reported a higher than usual number of pediatric cases of iGAS to the French Public Health (Santé publique France) and the Regional Healthcare Agencies (Agences Régionales de Santé). The National Reference Center for Streptococci also observed an increase in the number of GAS strains received since the summer of 2022 compared with previous years, particularly involving strains isolated from severe pediatric cases as of the end of October 2022. Those GAS infections occurred in different regions in France and mainly in children <10 years of age. In response, Santé publique France and its partners (the Groupe de Pathologie Infectieuse Pédiatrique, Association Clinique et Thérapeutique du Val de Marne, and the Groupe Francophone de Réanimation et Urgences Pédiatriques) have set up surveillance of these infections.

The question of the emergence of a hypervirulent GAS clone immediately arose, as did the search for risk factors associated with the most severe forms. The primary objective of this study was to describe the clinical, biological, and microbiological characteristics of pediatric severe GAS cases that occurred in France during the 2022–2023 epidemic. Our secondary objectives were to identify risk factors associated with the most severe clinical forms, describe complications and short-term outcomes, and describe the treatment and short-term management of severe pediatric GAS cases.

Materials and Methods

Study Population and Data Collection

We conducted a retrospective (September 1, 2022–December 31, 2022) and prospective (January 1, 2023–April 30, 2024) national, multicenter cohort study in 34 hospitals in France. We included all hospitalized pediatric case-patients <18 years of age.

We included all cases of severe GAS infections, which included proven and probable iGAS cases. Proven iGAS was defined as per international criteria: cases in which GAS was isolated from a normally sterile site (by culture, PCR, or rapid antigen detection testing), such as blood, cerebrospinal fluid, pleural fluid, peritoneal fluid, pericardial fluid, bone, joint/synovial fluid, or internal body site (e.g., lymph node, brain); or GAS isolated from a nonsterile site (such as a wound) and accompanied by necrotizing fasciitis or streptococcal toxic shock syndrome (*15*). We also included probable iGAS, defined as GAS isolated from a nonsterile site such as sputum or otorhinolaryngology surgical specimens (mastoiditis, ethmoiditis, pharyngeal abscess) accompanied by ≥1 of the following severity criteria: intravenous (IV) antibiotic drugs, surgery, or admission to the pediatric

Author affiliations: CHU Toulouse, Toulouse, France (M. Sierra Colomina, G. Le Balle, L. Berthomieu, D. Dubois, C. Brehin); Necker-Enfants Malades Hospital, Assistance Publique-Hôpitaux de Paris, Paris, France (A. Flamant, J.F. Cohen, A. Ferroni); Lille University, CHU Lille, Lille, France (S. Leteurtre); Groupe Francophone de Réanimation et Urgences Pédiatriques, Lille (S. Leteurtre); CHU Lyon, Lyon, France (Y. Gillet, E. Javouhey); Association Clinique et Thérapeutique du Val de Marne, Créteil, France (S. Bechet, C. Levy); Groupe de Pathologie Infectieuse Pédiatrique, Créteil (R. Cohen); National Reference Centre for Streptococci, Assistance Publique-Hôpitaux de Paris, Paris Centre, Hôpital Cochin, Paris (M.A. Hernandez Martinez, C. Plainvert, A. Tazi)

DOI: https://doi.org/10.3201/eid3109.250245

[1]Additional members who contributed data are listed at the end of this article.

intensive care unit (PICU). Clinical data collected were demographic information (age, sex, town of residence, number of siblings, comorbidities, vaccination status, and allergies), mode of onset of illness (fever, history of viral infection within the previous 15 days), clinical manifestations, clinical evaluation upon admission, biologic and microbiological data, drug therapy, in-hospital evolution, and patient outcomes (Appendix, https://wwwnc.cdc.gov/EID/article/31/9/25-0245-App1.pdf).

Microbiological Workup

We performed local microbiological documentation at each participating center using culture, GAS-specific PCR, 16S rDNA PCR, and antigen detection testing, as part of usual care. After inclusion of a case in the study, we sent GAS isolates to the National Reference Center for Streptococci for further characterization. Isolates were confirmed as GAS on the basis of colony morphology on horse blood agar and by matrix-assisted laser desorption/ionization time-of-flight mass spectrometry (Bruker Daltonics). We determined the *emm* genotype of each strain by sequencing the variable 5′ end of the *emm* gene and comparing sequences with the database of the US Centers for Disease Control and Prevention (http://www2.cdc.gov/vaccines/biotech/strepblast.asp). We also identified the toxin profile, particularly for superantigenic toxins. We performed antibiotic susceptibility testing by disc diffusion according to the European Committee on Antimicrobial Susceptibility Testing (http://www.eucast.org). We performed a double-disc diffusion test to detect inducible resistance to clindamycin. We used PCR to detected genetic determinants of resistance to aminoglycosides; macrolides, lincosamides, and synergistins; and tetracycline, as previously described (*16*).

We performed whole-genome sequencing on a sample of randomly selected GAS strains. We extracted genomic DNA from overnight cultures using the MasterPure Gram Positive DNA Purification kit (LGC Biosearch Technologies) according to the manufacturer's recommendations. We sequenced the DNA using the Illumina MiSeq system. Bioinformatical analyses included identification of the $M1_{UK}$ clone, by recognizing its specific 27 single-nucleotide polymorphisms (*17*).

Statistical Analysis

First, we described included cases using standard statistics. We expressed qualitative variables as frequencies and percentages and quantitative variables using the median and interquartile range (if not normally distributed). For the comparisons between groups (i.e., group without sequelae or minor sequelae vs. group with major sequelae or death; group with hospitalization in Pediatric Intermediate Care Unit [PIMCU]/PICU vs. group without hospitalization in PIMCU/PICU), we compared percentages using the χ^2 or Fisher exact test, depending on the number of patients. We compared quantitative variables using a Mann-Whitney test. We conducted all tests with a significance threshold of $p<0.05$.

Second, to identify risk factors for the most severe cases, we performed multivariate analysis using logistic regression models. A first model aimed to identify risk factors for admission in PIMCU/PICU, and a second model focused on identifying risk factors for major sequelae or death. We included all variables with a p value <0.20 on univariate analysis in the multivariable models and removed them one by one using a stepwise backward elimination approach, with a threshold of $p<0.05$, to obtain the final models. We conducted the analyses using Stata 18 (StataCorp).

Ethics Statement

In accordance with France's ethics law, patients were informed that their encoded data would be used for the study and for publication. Their nonopposition to the use of their data and publication was collected. Patients were not involved in the design of this study. This study is registered in ClinicalTrials.gov as NCT05788861 and has been approved by the ethics review board of the Créteil Hospital Center (Créteil, France).

Results

Study Population

We enrolled a total of 402 pediatric patients with severe GAS infections. Median age was 4 (interquartile range [IQR] 2–7.5) years; 42% were girls and 58% boys (Table 1; Figures 1 and 2). The most frequent comorbidities were chronic pulmonary diseases (2.2%; 9/402), notably asthma (7/9 cases). Approximately 2% of the cohort (7/402) were immunocompromised children (3 with primary immunodeficiency and 4 receiving immunosuppressive drugs). Regarding drug exposure within 7 days before admission, 8% (34/402) had recently received nonsteroidal antiinflammatory drugs (NSAIDs), 4% (17/402) had received steroids, and 25% (100/402) had received antibiotic drugs. Most GAS infections were isolated cases (81%, 326/402); 5 (1%) cases were identified as associated with collective settings, and 27 (7%) cases were linked to household clusters. A substantial

percentage of children (44%) were admitted to general pediatric wards, 23% required admission to the PICU, 7% were managed in PIMCUs, and 29% were hospitalized in other specialized wards, such as neurology and surgery departments.

A total of 140 patients were <3 years of age, and the most frequent clinical manifestation was ear-nose-throat (ENT) damage (Table 2; Figure 3). One patient experienced out-of-hospital cardiac arrest, and 3% (12/402) of patients had acute respiratory distress syndrome. Acute respiratory distress was prevalent in 27% (108/402) of cases; 78% (84/108) of those were categorized as mild and 22% (24/108) as severe. During hospital stay, 3% (12/402) of patients experienced a cardio-respiratory arrest. Median C-reactive protein level at admission was 161 (IQR 76–254) mg/L (reference range 0–5 mg/L).

Nearly half of patients (44% [177/402]) required surgical intervention during their hospital stay; causes consisted of ENT drainage in 41% (73/177), osteoarticular drainage in 24% (43/402), and deep tissue abscess drainage in 6% (23/177) of cases (Table 2). Surgical intervention within the first 24 hours was necessary in 29% (117/402) of cases, primarily for procedures such as deep tissue pus drainage and joint drainage. Median duration of hospital stay was 7 (IQR 3–12) days.

Table 1. Clinical features of severe group A *Streptococcus* infections among 402 children, France, 2022–2024*

Clinical features	Value
Median age (IQR), y	4 (2–7.5)
Sex	
M	234 (58)
F	168 (42)
Comorbidities	52 (13)
Immunosuppression	7 (2)
Viral infection in the previous 15 d	109 (27)
Influenza	28/112 (25)
Respiratory syncytial virus	7/112 (6)
Chicken pox	37/112 (33)
SARS-CoV-2	5/112 (4)
Other	37/112 (33)
Isolated case	326 (81)
Isolated fever	18 (4)
Site of infection	
Multiple	146 (36)
Ear-nose-throat	135 (34)
Skin and soft tissue	63 (16)
Bone and joint	57 (14)
Lower respiratory	84 (21)
Pleuro-pneumonia	69 (17)
Others†	34 (8)
Septic shock‡	34 (8)
Toxic rash	37 (9)

*Values are no. (%) except as indicated.
†Meningitis, endocarditis, peritonitis, dental cellulitis.
‡Defined as persistence of several organ failures or acute circulatory failure, failure to correct arterial hypotension despite vascular filling of ≥40 mL/kg, or both.

Bacterial Data

Rapid antigen detection tests showed high positivity rates when performed; results were positive for 79% (110/139) of throat samples, 70% (48/69) of pleural effusion samples, and 39% (13/33) of cutaneous samples. PCR testing identified GAS DNA in 14% of cases, predominantly in pleural effusion fluid (38%, 22/58), followed by deep tissue abscesses (especially from ear, nose, and throat area) (32%, 19/58). GAS culture yielded positive results in 71% (285/402) of cases; GAS was isolated from blood cultures in 21% (84/402) of cases.

A total of 149 GAS isolates were sent to the National Reference Center for Streptococci (Table 3), of which 148 underwent *emm* typing. The *emm1* (73.0%, 108/148) and *emm12* (10.8%; 16/148) genotypes represented most strains. Resistance to macrolides (defined by erythromycin resistance) was found in 3% (5/148) of GAS strains. All macrolide-resistant isolates were also resistant to clindamycin.

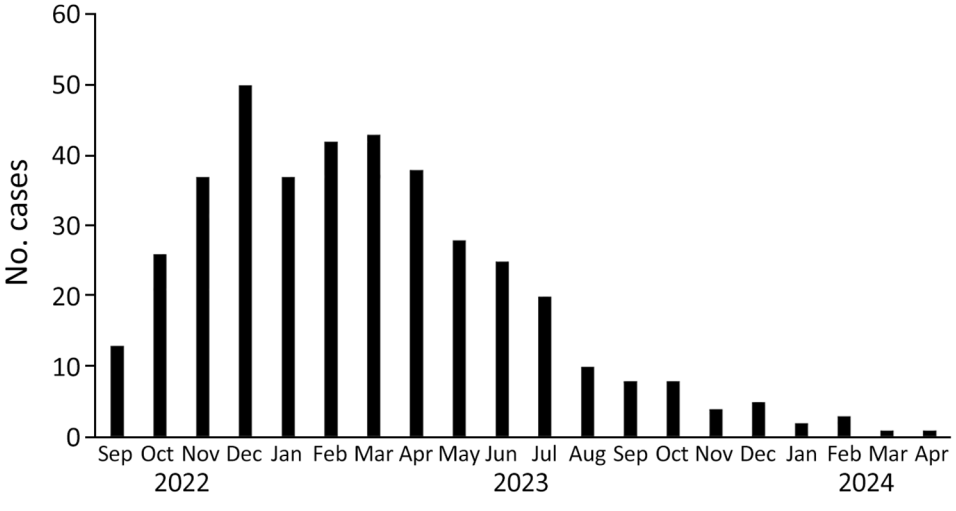

Figure 1. Trends in the number of hospital admissions for severe group A *Streptococcus* infection among 402 children, by month, France, 2022–2024.

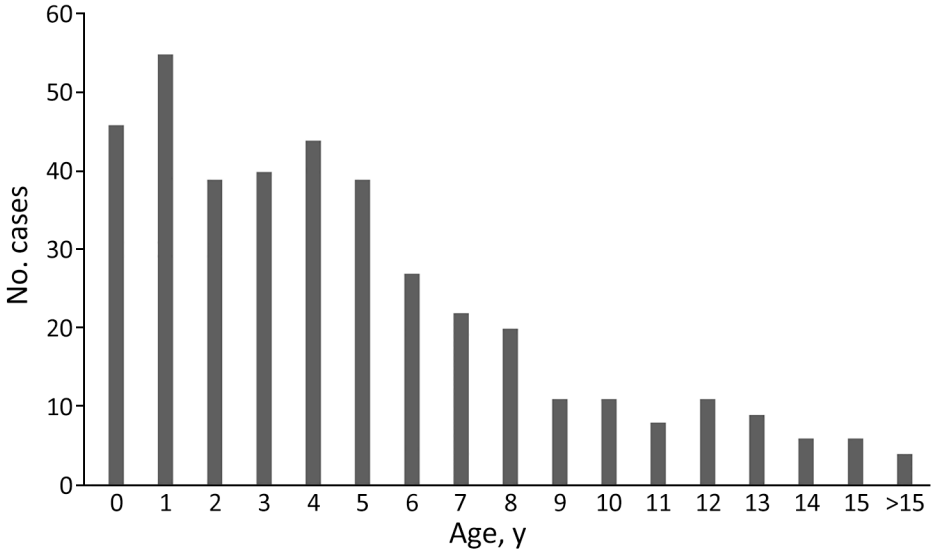

Figure 2. Severe group A *Streptococcus* infection distribution in 402 children by age, France, 2022–2024.

We performed whole-genome sequencing on 25 of the 149 isolates received at the National Reference Center for Streptococci, including 20 *emm1* isolates. The $M1_{UK}$ clone represented 50.0% (10/20) of the *emm1* isolates.

Outcomes and Sequelae

Most (77%, 311/402) patients affected by severe GAS infections were discharged with a favorable outcome, devoid of sequelae. However, 17 (4%) patients had major sequelae (amputation/cutaneous necrosis/orthopedic sequelae [n = 7], impaired respiratory function [n = 6], or neurologic deficit [n = 4]), and 14 deaths were recorded, resulting in a case-fatality rate of 3.5%.

Initial clinical factors significantly associated with hospitalization in the PICU or PIMCU in univariate analysis included age <3 years, exposure to corticosteroids in the days before hospitalization, viral infection within 15 days before symptom onset, type of disease, and presence of a toxic rash (Table 4). In multivariate analysis (n = 399), factors significantly associated with hospitalization in the PICU or PIMCU consisted of viral infection within the 15 days before symptom onset (adjusted odds ratio [aOR] 2.0 [95% CI 1.2–3.4]; p = 0.007) and type of disease (bone and joint damage, aOR 0.3 [95% CI 0.1–0.8], p = 0.013; pulmonary damage, aOR 2.1 [95% CI 1.04–4.3], p = 0.037) (Table 4).

Factors significantly associated with major sequelae or death in univariate analysis were a viral infection within 15 days before symptom onset, hospitalization in PIMCU or PICU, antibiotic therapy with a β-lactam combined with clindamycin, receipt of IV immunoglobulins, receipt of hydrocortisone, and receipt of vasopressor therapy (Table 5). In multivariate analysis (n = 395), only hydrocortisone, use of corticosteroids during hospitalization, and vasopressor therapy remained significantly associated with major sequelae or death (Table 4).

Genotypes *emm1* and *emm12* were not significantly associated with the risk for admission to PIMCU/PICU or the risk for persistent sequelae. Genotype *emm1* was significantly associated with respiratory damage (upper and lower) compared with other types of damage (p = 0.01).

Table 2. Management of severe group A *Streptococcus* infections among 402 children, France, 2022–2024

Treatment	No. (%)
Oxygen therapy	120 (30)
Conventional	45 (11)
High-flow	27 (7)
Noninvasive ventilation	11 (3)
Invasive ventilation	32 (8)
Extracorporeal membrane oxygenation	5 (1)
Hemodynamic therapy	97 (24)
Fluid resuscitation	97 (24)
Vasopressor treatment	50 (12)
First-line antibiotic treatment	
Amoxicillin/clavulanate	138 (34)
Third generation cephalosporin	141 (35)
β-lactam + clindamycin	173 (43)
Adjunctive therapies	
Intravenous Immunoglobulins	17 (4)
Hydrocortisone hemisuccinate for shock	19 (4)

Discussion

This study provides detailed characterization of severe GAS infections in pediatric patients in France. It covers a wide range of clinical data, including demographic characteristics, clinical manifestations, laboratory findings, treatment modalities, and outcomes, thereby providing a thorough understanding of the disease spectrum and its implications. Key findings

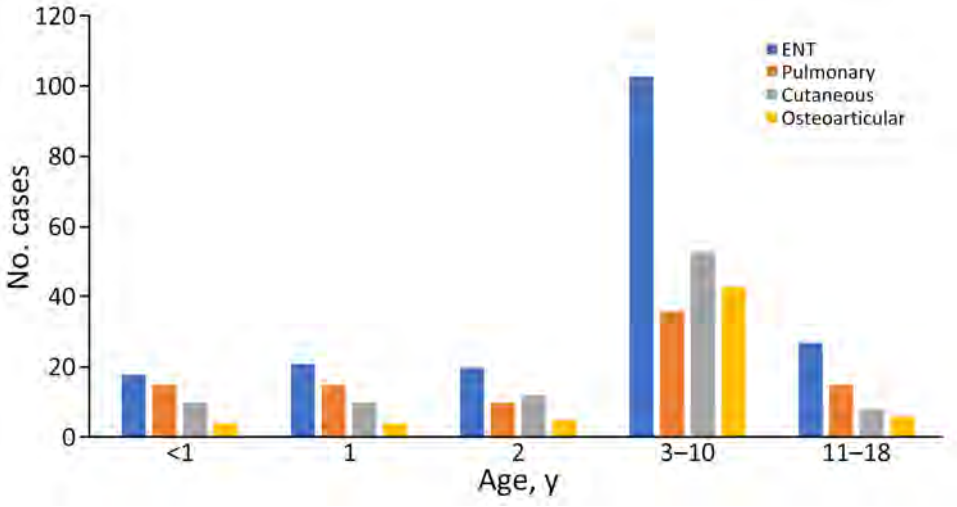

Figure 3. Distribution of severe group A *Streptococcus* infection in 402 children, by type of infection and age, France, 2022–2024. ENT, ear-nose-throat.

include the absence of emerging GAS clones, a predominance of *emm1* and *emm12* genotypes, a case-fatality rate of 3.5%, and a predominance of upper and lower respiratory tract infections. We were also able to identify several risk factors associated with the most severe forms of GAS disease.

One third of severe infections occurred in children <3 years of age, an age group in which benign GAS infections (mainly ENT-related) are considered rare, underlining the challenges of early diagnosis in this age group. The frequency of acute GAS infections peaks in childhood, but invasive infections are observed in the extreme age groups (<1 and >65 years of age) (*18*). This pattern could be explained by immune system naivety in young children and immunosenescence in the elderly. The strongest evidence for the existence of protective immune responses against GAS is the observed decrease in susceptibility to infection with increasing age. The incidence of symptomatic throat infections, including scarlet fever, increases dramatically around the age of 4 (*19*). This increase could be caused by the expansion of tonsil tissue, which enables better access to GAS; entry into school communities, with increased exposure to GAS; or simply by the ability of children of that age to verbalize sore throats. Toward the end of childhood, the frequency of streptococcal pharyngitis decreases substantially. GAS skin infections exhibit a similar peak and fall in incidence but at a slightly earlier age than throat infections, perhaps linked to a greater frequency of skin lesions in young children (*20*).

In our cohort, clinical manifestations consisted predominately of ENT and lung infections, consistent with findings from other studies (*7*). The 2022–23 winter in France saw exceptionally intense viral epidemics, including respiratory syncytial virus, influenza, and SARS-CoV-2, compared with previous years. Such respiratory viral infections have been associated with increased susceptibility to severe GAS infections and related ENT and pulmonary complications, suggesting a potential interplay between viruses and bacteria (*21*,*22*). Varicella zoster virus has also been implicated in both cutaneous and articular manifestations of iGAS infections, further supporting a potential synergistic relationship that might exacerbate disease severity (*23*,*24*). Those findings highlight the importance of monitoring viral coinfections and their potential role in the pathogenesis of iGAS.

The concept of an immunity debt because of reduced exposure and heightened hygiene measures

Table 3. Molecular characterization of 149 *Streptococcus pyogenes* isolates analyzed at the French National Reference Center for Streptococci in study of children with severe group A *Streptococcus* infections, France, 2022–2024

Variable	No. (%)
Superantigen genes	148
SpeA	110 (74.3)
SpeB	148 (100)
SpeC	76 (51.3)
SmeZ	146 (98.6)
Sic*	108 (73.0)
ssa	11 (7.4)
emm genotypes	148
emm1	108 (73.0)
emm4	4 (2.7)
emm12	16 (10.8)
emm77	4 (2.7)
emm87	4 (2.7)
emm89	4 (2.7)
Others†	8 (5.4)
Not done	1
Whole-genome sequencing	25
emm1	20
$M1_{UK}$ clone among *emm1* strains	10

*Sic-like genes were not analyzed.
†Others: 1 strain of each of *emm2*, *emm3*, *emm11*, *emm22*, *emm44*, *emm75*, *emm169*, and *emm209*.

Table 4. Univariate and multivariate analysis of factors associated with PIMCU or PICU hospitalization in children with severe group A *Streptococcus* infections, France, 2022–2024*

Category	PIMCU/PICU hospitalization	No PIMCU/PICU hospitalization	p value
Univariate analysis			
Age group, y			
<1	18/117 (15.4)	33/284 (11.6)	**0.031**
1	11/117 (9.4)	39/284 (13.7)	
2	19/117 (16.2)	20/284 (7)	
3–10	55/117 (47)	159/284 (56)	
11–18	14/117 (12)	33/284 (11.6)	
Immunosuppression	3/115 (2.6)	4/282 (1.4)	0.414
Comorbidities	16/116 (13.8)	36/283 (12.7)	0.773
Exposure to nonsteroidal antiinflammatory drug	13/112 (11.6)	21/272 (7.7)	0.223
Exposure to steroidal antiinflammatory drug	14/112 (12.5)	3/275 (1)	**<0.001**
Viral infection in the 15 days before hospitalization	47/109 (28.9)	62/268 (23.1)	**<0.001**
Type of infection			
ENT	31/117 (26.5)	104/284 (36.6)	**<0.001**
Pulmonary	44/117 (37.6)	40/284 (14.1)	
Bone and joint	7/117 (6)	50/284 (17.6)	
Cutaneous	16/117 (13.7)	47/284 (16.5)	
Other	19/117 (16.2)	43/284 (15.1)	
Multiple damage	50/117 (42.7)	96/284 (33.8)	0.091
Toxic rash	17/117 (14.5)	20/284 (7)	**0.019**
Multivariate analysis, adjusted odds ratio (95% CI)			
Viral infection in the 15 days before hospitalization	2.02 (1.21–3.37)		0.07
Osteoarticular damage	0.29 (0.11–0.77)		**0.013**
Pulmonary damage	2.11 (1.04–4.29)		**0.037**

*Values are no. (%) except as indicated. Boldface indicates significance. ENT, ear-nose-throat; PICU, pediatric intensive care unit; PIMCU, pediatric intermediate care unit.

during COVID-19 lockdowns has been proposed to explain the resurgence in 2022–2023 of invasive bacterial infections in children, including pneumococcal, meningococcal, and pertussis infections (*2*,*25*,*26*). Similarly, a rise in mild GAS infections in outpatient settings was reported in France before the 2022–2023 surge in severe cases (*2*). However, our study cannot confirm this hypothesis for iGAS infections, given the absence of pre-2022 data (Appendix) and the uncertainty regarding a potential continuum between noninvasive and severe forms of the disease, despite the high incidence of severe ENT infections and pneumonia observed in our cohort (*23*). Those considerations underscore the need for robust outpatient surveillance and appropriate use of diagnostic tools to guide GAS management. In addition, considering COVID-19 infection itself as a potential predisposing factor for iGAS is critical, as previously discussed.

The case-fatality rate of 3.5%, the elevated surgical intervention rate (44%), and the long median of hospital stay (7 days) illustrate the burden of severe

Table 5. Univariate and multivariate analysis of factors associated with major sequelae/death in children with severe group A streptococcus infections, France, 2022–2024*

Category	Major sequelae/death	No major sequelae/death	p value
Univariate analysis			
Female sex	14/31 (45)	150/365 (41)	0.668
Viral infection in the 15 days before hospitalization	16/31 (52)	88/365 (24.1)	**0.004**
Clinical damage			0.094
ENT	8/31 (25.8)	127/365 (34.8)	
Pulmonary	11/48 (35.5)	69/365 (18.9)	
Osteoarticular	3/31 (9.7)	54/365 (14.8)	
Cutaneous	2/31 (6.5)	60/365 (16.4)	
Other	7/31 (22.6)	55/365 (15)	
PIMCU/PICU admission	22/31 (71)	90/365 (24.7)	**<0.001**
Clindamycin therapy	21/31 (67.7)	148/365 (40.5)	**0.003**
Intravenous immunoglobulins	6/31 (19.3)	10/355 (2.8)	**<0.001**
Corticosteroidal therapy	5/28 (17.9)	36/356 (10.1)	0.201
Hydrocortisone hemisuccinate for shock	12/29 (41.4)	7/353 (1.9)	**<0.001**
Vasopressive drug	19/30 (63.3)	25/343 (7.3)	**<0.001**
Multivariate analysis, odds ratio (95% CI)			
Corticosteroidal therapy	4.18 (1.27–13.75)		**0.018**
Hydrocortisone hemisuccinate for shock	6.25 (1.53–25.50)		**0.011**
Vasopressive drug	11.27 (3.54–35.89)		**<0.001**

*Values are no. (%) except as indicated. Boldface indicates significance. ENT, ear-nose-throat; PICU, pediatric intensive care unit; PIMCU, pediatric intermediate care unit.

GAS infections on patients, their families, and the healthcare system. Although GAS is often considered a minor pathogen responsible for mostly mild infections, the 2022–2023 worldwide epidemic reminds us that GAS possesses a full range of virulence factors that are capable of causing severe damage and must not be overlooked. In low- and-middle income settings, rheumatic fever is an additional concern. Those challenges have prompted clinicians to diagnose and treat noninvasive infections, such as pharyngitis, and has prompted researchers to develop vaccines against them. Of note, the promising 30-valent M protein–based vaccine described by Finn et al. (*27*) includes almost all the *emm* types identified in our study. It covers the predominant *emm* types circulating in temperate regions, highlighting its potential for broad epidemiologic coverage.

Further research is needed to establish the most effective therapeutic strategies for managing iGAS infections. The role of adjunctive treatments such as clindamycin, which might help reduce GAS toxin production, and IV immunoglobulin, which might neutralize toxin activity, remains a subject of debate. A recent observational study from Japan found no significant effect of those therapies on in-hospital mortality (*22*). In our own multivariate analysis, only the use of hydrocortisone, corticosteroids, and vasopressor therapy during hospitalization was significantly associated with major sequelae or death. However, those findings likely reflect their use in the most severely ill patients, rather than indicating a direct causal effect.

The most frequent genotypes identified in our pediatric cohort were *emm1* and *emm12*, similar to those reported in other countries during the 2022–2023 epidemic and in earlier prepandemic cohorts (*24*,*28*). However, the proportion of *emm1* strains in our series was higher than in other studies (e.g., Spain, United Kingdom, Portugal series) (*5*,*29*–*31*). Of note, a recent population-based study conducted in 10 US states that included 21,312 patients (1,272 children) with invasive GAS infections during 2013–2022 documented a decline in pharyngeal strains (such as *emm1* and *emm12*) during the COVID-19 pandemic, alongside an increase in skin-associated *emm* types (*24*). The epidemic in France confirmed the continued expansion of the $M1_{UK}$ clone, which has been progressively spreading since its first detection in the United Kingdom in 2008 (*17*).

The first limitation of our study is that, despite our thorough description of the severe GAS infections observed during the 2022–2023 outbreak, the lack of a control period from the pre–COVID-19 era prevents us from drawing precise epidemiologic conclusions about changes in incidence rates over time (Appendix). Second, the relatively small number of isolates and the limited subset analyzed by whole-genome sequencing further restrict our ability to detect the emergence of specific strains. Finally, although this study relies on a large and nationwide network of 34 hospitals, we cannot guarantee the exhaustiveness or full representativeness of our case series.

Future research endeavors should focus on elucidating the underlying mechanisms driving the surge in pediatric severe GAS infections and the interplay between viral co-infections and bacterial complications. Comprehensive surveillance programs targeting both viral and bacterial pathogens, including GAS, are essential for early detection, timely intervention, and prevention of severe GAS disease outcomes. Furthermore, enhanced understanding of host–pathogen interactions, immune responses, genetic predispositions, and pathogen virulence that influence susceptibility to severe GAS infections is needed. Such knowledge can inform the development of targeted therapeutic approaches, including immunomodulatory strategies and vaccine development, to mitigate the burden of iGAS infections in pediatric populations.

In conclusion, pediatric severe GAS infections represent a substantial clinical and public health challenge, characterized by a high number of cases and associated illnesses and deaths during the winter of 2022–23 in several countries. This cohort in France demonstrated a high rate of respiratory diagnoses and a significant need for procedural intervention, mainly driven by *emm1* and *emm12* genotypes and the $M1_{UK}$ strain. Advances in diagnostic modalities, antibiotic therapy, and supportive care have improved outcomes of severe GAS infections, but continued research efforts are needed to unravel the complexities of these infections and inform evidence-based strategies for prevention, management, and surveillance. Collaboration between clinicians, researchers, and public health authorities is essential to address the evolving landscape of pediatric severe GAS infections and mitigate their effects on child health.

Additional ISAI Study Group members who contributed data: Charlotte Borocco, Gerald Boussicault, Samar Armouche, Ulrike Frey, Agnes Rey, Bertrand Soto, Charlotte Pons, Marion Favier, Letitia Pantalone, Amandine Poinot, Edwige Da Zoclanclounon, Isabelle Grimal, Etienne Bizot, Etienne Merlin, Didier Chognot, Guy Ngalula, Isabelle Hau, Blandine Desse, Annie Sfez, Cyrielle Fouquerel, Eskander Eleonore, Timé Muller, Cecile Bost-Bru, Marie-Aliette Dommergues, Justine De

Larminat, Delphine Penel, François Dubos, Jean Gaschinard, Aurelie Morand, Noemie Vanel, Olivier Vignaud, Marie Lamant, Julien Baleine, Constance Bridonneau, Julien Jegard, Nathalie Blot, Sandrine Baron-Joly, Anne Filleron, Marion Ashman, Ferrandiz Charlène, Naim Ouldali, Lea Lenglart, Pauline Meslin, Laura Labro, Didier Pinquier, Tiffany Trollet, Marie-Caroline Ploton, and Anais Chosidow.

Acknowledgments

We thank the bacteriology laboratories and the ISAI study group for supporting this project.

About the Author

Dr. Sierra Colomina is a senior pediatric critical care physician and researcher at Toulouse University Hospital, France. Her research focuses on emerging severe infectious diseases in children and their critical care management.

References

1. Alcolea-Medina A, Snell LB, Alder C, Charalampous T, Williams TGS, Tan MKI, et al.; Synnovis Microbiology Laboratory Group. The ongoing *Streptococcus pyogenes* (Group A *Streptococcus*) outbreak in London, United Kingdom, in December 2022: a molecular epidemiology study. Clin Microbiol Infect. 2023;29:887–90. https://doi.org/10.1016/j.cmi.2023.03.001
2. Cohen JF, Rybak A, Werner A, Kochert F, Cahn-Sellem F, Gelbert N, et al. Surveillance of noninvasive group A *Streptococcus* infections in French ambulatory pediatrics before and during the COVID-19 pandemic: a prospective multicenter study from 2018–2022. Int J Infect Dis. 2023;134:135–41. https://doi.org/10.1016/j.ijid.2023.06.003
3. van der Putten BCL, Bril-Keijzers WCM, Rumke LW, Vestjens SMT, Koster LAM, Willemsen M, et al. Novel *emm* 4 lineage associated with an upsurge in invasive group A streptococcal disease in the Netherlands, 2022. Microb Genom. 2023;9:mgen001026. PMID:37261428 https://doi.org/10.1099/mgen.0.001026
4. Johannesen TB, Munkstrup C, Edslev SM, Baig S, Nielsen S, Funk T, et al. Increase in invasive group A streptococcal infections and emergence of novel, rapidly expanding sub-lineage of the virulent *Streptococcus pyogenes* M1 clone, Denmark, 2023. Euro Surveill. 2023;28:2300291. https://doi.org/10.2807/1560-7917.ES.2023.28.26.2300291
5. Guy R, Henderson KL, Coelho J, Hughes H, Mason EL, Gerver SM, et al. Increase in invasive group A streptococcal infection notifications, England, 2022. Euro Surveill. 2023;28:2200942. https://doi.org/10.2807/1560-7917.ES.2023.28.1.2200942
6. de Gier B, Marchal N, de Beer-Schuurman I, Te Wierik M, Hooiveld M, de Melker HE, et al.; ISIS-AR Study Group. GAS Study group; Members of the GAS study group; Members of the ISIS-AR study group. Increase in invasive group A streptococcal (*Streptococcus pyogenes*) infections (iGAS) in young children in the Netherlands, 2022. Euro Surveill. 2023;28:2200941. https://doi.org/10.2807/1560-7917.ES.2023.28.1.2200941
7. Boeddha NP, Atkins L, de Groot R, Driessen G, Hazelzet J, Zenz W, et al.; EUCLIDS consortium. Group A streptococcal disease in paediatric inpatients: a European perspective. Eur J Pediatr. 2023;182:697–706. https://doi.org/10.1007/s00431-022-04718-y
8. Santé Publique France. Infection invasive à streptocoque du Groupe A (IISGA): point de situation au 6 décembre 2022 [cited 2025 Feb 12]. https://www.santepubliquefrance.fr/les-actualites/2022/infection-invasive-a-streptocoque-du-groupe-a-iisga-point-de-situation-au-6-decembre-2022
9. World Health Organization. Increase in invasive Group A streptococcal infections among children in Europe, including fatalities [cited 2025 Feb 12]. https://www.who.int/europe/news-room/12-12-2022-increase-in-invasive-group-a-streptococcal-infections-among-children-in-europe–including-fatalities
10. Jain N, Lansiaux E, Reinis A. Group A streptococcal (GAS) infections amongst children in Europe: taming the rising tide. New Microbes New Infect. 2022;51:101071. https://doi.org/10.1016/j.nmni.2022.101071
11. Ferretti JJ, Stevens DL, Fischetti VA, editors. *Streptococcus pyogenes*: basic biology to clinical manifestations. 2nd ed. Oklahoma City (OK): University of Oklahoma Health Sciences Center; 2022.
12. Zachariadou L, Stathi A, Tassios PT, Pangalis A, Legakis NJ, Papaparaskevas J; Hellenic Strep-Euro Study Group. Differences in the epidemiology between paediatric and adult invasive *Streptococcus pyogenes* infections. Epidemiol Infect. 2014;142:512–9. https://doi.org/10.1017/S0950268813001386
13. Floret D. Clinical aspects of streptococcal and staphylococcal toxinic diseases [in French]. Arch Pediatr. 2001;8(Suppl 4):762s–8s. PMID:11582925 https://doi.org/10.1016/S0929-693X(01)80194-9
14. Deniskin R, Shah B, Muñoz FM, Flores AR. Clinical manifestations and bacterial genomic analysis of group A *Streptococcus* strains that cause pediatric toxic shock syndrome. J Pediatric Infect Dis Soc. 2019;8:265–8. https://doi.org/10.1093/jpids/piy069
15. Miller KM, Lamagni T, Cherian T, Cannon JW, Parks T, Adegbola RA, et al. Standardization of epidemiological surveillance of invasive group A streptococcal infections. Open Forum Infect Dis. 2022;9(Suppl 1):S31–40. https://doi.org/10.1093/ofid/ofac281
16. Malhotra-Kumar S, Lammens C, Piessens J, Goossens H. Multiplex PCR for simultaneous detection of macrolide and tetracycline resistance determinants in streptococci. Antimicrob Agents Chemother. 2005;49:4798–800. https://doi.org/10.1128/AAC.49.11.4798-4800.2005
17. Lynskey NN, Jauneikaite E, Li HK, Zhi X, Turner CE, Mosavie M, et al. Emergence of dominant toxigenic M1T1 *Streptococcus pyogenes* clone during increased scarlet fever activity in England: a population-based molecular epidemiological study. Lancet Infect Dis. 2019;19:1209–18. https://doi.org/10.1016/S1473-3099(19)30446-3
18. Steer AC, Lamagni T, Curtis N, Carapetis JR. Invasive group A streptococcal disease: epidemiology, pathogenesis and management. Drugs. 2012;72:1213–27. https://doi.org/10.2165/11634180-000000000-00000
19. Lamagni TL, Darenberg J, Luca-Harari B, Siljander T, Efstratiou A, Henriques-Normark B, et al.; Strep-EURO Study Group. Epidemiology of severe *Streptococcus pyogenes* disease in Europe. J Clin Microbiol. 2008;46:2359–67. https://doi.org/10.1128/JCM.00422-08
20. Tsoi SK, Smeesters PR, Frost HRC, Licciardi P, Steer AC. Correlates of protection for M protein-based vaccines against group A Streptococcus. J Immunol Res. 2015;2015:167089. https://doi.org/10.1155/2015/167089
21. Lassoued Y, Assad Z, Ouldali N, Caseris M, Mariani P, Birgy A, et al. Unexpected increase in invasive group A

streptococcal infections in children after respiratory viruses outbreak in France: a 15-year time-series analysis. Open Forum Infect Dis. 2023;10:ofad188. https://doi.org/10.1093/ofid/ofad188
22. de Gier B, Vlaminckx BJM, Woudt SHS, van Sorge NM, van Asten L. Associations between common respiratory viruses and invasive group A streptococcal infection: a time-series analysis. Influenza Other Respir Viruses. 2019;13:453–8. https://doi.org/10.1111/irv.12658
23. Mariani F, Gentili C, Pulcinelli V, Martino L, Valentini P, Buonsenso D. State of the art of invasive group A streptococcus infection in children: a scoping review of the literature with a focus on predictors of invasive infection. Children (Basel). 2023;10:1472. https://doi.org/10.3390/children10091472
24. Gregory CJ, Okaro JO, Reingold A, Chai S, Herlihy R, Petit S, et al. Invasive group A streptococcal infections in 10 US states. JAMA. 2025;333:1498–507. https://doi.org/10.1001/jama.2025.0910
25. McMillan DJ, Drèze PA, Vu T, Bessen DE, Guglielmini J, Steer AC, et al. Updated model of group A *Streptococcus* M proteins based on a comprehensive worldwide study. Clin Microbiol Infect. 2013;19:E222–9. https://doi.org/10.1111/1469-0691.12134
26. Cohen R, Ashman M, Taha MK, Varon E, Angoulvant F, Levy C, et al. Pediatric Infectious Disease Group (GPIP) position paper on the immune debt of the COVID-19 pandemic in childhood, how can we fill the immunity gap? Infect Dis Now. 2021;51:418–23. https://doi.org/10.1016/j.idnow.2021.05.004
27. Finn MB, Penfound TA, Salehi S, Ogega CO, Dold C, Plante O, et al. Immunogenicity of a 30-valent M protein mRNA group A *Streptococcus* vaccine. Vaccine. 2024;42:126205. https://doi.org/10.1016/j.vaccine.2024.126205
28. Shulman ST, Tanz RR, Dale JB, Beall B, Kabat W, Kabat K, et al.; North American Streptococcal Pharyngitis Surveillance Group. Seven-year surveillance of North American pediatric group A streptococcal pharyngitis isolates. Clin Infect Dis. 2009;49:78–84. https://doi.org/10.1086/599344
29. Ramírez de Arellano E, Saavedra-Lozano J, Villalón P, Jové-Blanco A, Grandioso D, Sotelo J, et al. Spanish PedGAS-Net/CIBERINFEC GAS Study Group. Clinical, microbiological, and molecular characterization of pediatric invasive infections by *Streptococcus pyogenes* in Spain in a context of global outbreak. MSphere. 2024;9:e0072923. https://doi.org/10.1128/msphere.00729-23
30. Gouveia C, Bajanca-Lavado MP, Mamede R, Araújo Carvalho A, Rodrigues F, Melo-Cristino J, et al.; Portuguese Group for the Study of Streptococcal Infections. Portuguese Study Group of Pediatric Invasive Streptococcal Disease; Portuguese Study Group of Paediatric Invasive Streptococcal Disease. Sustained increase of paediatric invasive *Streptococcus pyogenes* infections dominated by $M1_{UK}$ and diverse *emm*12 isolates, Portugal, September 2022 to May 2023. Euro Surveill. 2023;28:2300427.
31. Abo YN, Oliver J, McMinn A, Osowicki J, Baker C, Clark JE, et al. Increase in invasive group A streptococcal disease among Australian children coinciding with northern hemisphere surges. Lancet Reg Health West Pac. 2023;41:100873. https://doi.org/10.1016/j.lanwpc.2023.100873

Address for correspondence: Montserrat Sierra Colomina, Réanimation Pédiatrique Hôpital des Enfants, 330 Avenue de Grande-Bretagne, TSA 70034, 31059 Toulouse CEDEX 09, France; email: sierracolomina.m@chu-toulouse.fr

Rickettsioses as Underrecognized Cause of Hospitalization for Febrile Illness, Uganda

Paul W. Blair, Sultanah Alharthi, Andrés F. Londoño, Abdullah Wailagala, Yukari C. Manabe, J. Stephen Dumler, the Acute Febrile Illness and Sepsis in Uganda Study Teams[1]

In support of improving patient care, this activity has been planned and implemented by Medscape, LLC and Emerging Infectious Diseases. Medscape, LLC is jointly accredited with commendation by the Accreditation Council for Continuing Medical Education (ACCME), the Accreditation Council for Pharmacy Education (ACPE), and the American Nurses Credentialing Center (ANCC), to provide continuing education for the healthcare team.

Medscape, LLC designates this Journal-based CME activity for a maximum of 1.00 ***AMA PRA Category 1 Credit(s)™***. Physicians should claim only the credit commensurate with the extent of their participation in the activity.

Successful completion of this CME activity, which includes participation in the evaluation component, enables the participant to earn up to 1.0 MOC points in the American Board of Internal Medicine's (ABIM) Maintenance of Certification (MOC) program. Participants will earn MOC points equivalent to the amount of CME credits claimed for the activity. It is the CME activity provider's responsibility to submit participant completion information to ACCME for the purpose of granting ABIM MOC credit.

All other clinicians completing this activity will be issued a certificate of participation. To participate in this journal CME activity: (1) review the learning objectives and author disclosures; (2) study the education content; (3) take the post-test with a 75% minimum passing score and complete the evaluation at https://www.medscape.org/qna/processor/ 75091?show StandAlone=true&src=prt_jcme_eid_mscpedu; and (4) view/print certificate. For CME questions, see page 1881.

NOTE: It is the policy of Medscape Education to avoid the mention of brand names or specific manufacturers in accredited educational activities. However, trade and manufacturer names in this activity are provided in an effort to provide clarity. The use of brand or manufacturer names should not be viewed as an endorsement by Medscape of any specific product or manufacturer.

Release date: August 22, 2025; Expiration date: August 22, 2026

Learning Objectives

Upon completion of this activity, participants will be able to:

- Assess characteristics of rickettsial disease in sub-Saharan Africa
- Analyze the accuracy of serum rRNA RT-PCR for rickettsial disease in the current study
- Compare the accuracy of RT-PCR of rickettsial rRNA vs mRNA
- Evaluate clinical characteristics and outcomes of rickettsial disease cases in the current study

CME Editor

Bryce Simons, MPH, Technical Writer/Editor, Emerging Infectious Diseases. *Disclosure: Bryce Simons, MPH, has no relevant financial relationships.*

CME Author

Charles P. Vega, MD, Health Sciences Clinical Professor of Family Medicine, University of California, Irvine School of Medicine, Irvine, California. *Disclosure: Charles P. Vega, MD, has the following relevant financial relationships: served as a consultant or advisor for Boehringer Ingelheim Pharmaceuticals, Inc.; Exact Sciences Corporation.*

Authors

Paul W. Blair, MD; Sultanah Alharthi, MS; Andrés F. Londoño, PhD; Abdullah Wailagala, MD; Yukari C. Manabe, MD; J. Stephen Dumler, MD.

The complexity of rickettsial serodiagnostics during acute illness has limited clinical characterization in Africa. We used archived samples from sepsis (n = 259) and acute febrile illness (n = 70) cohorts in Uganda to identify spotted fever and typhus group rickettsiae by using immunofluorescence assay and clinically validated rRNA reverse transcription PCR (RT-PCR). Among 329 participants, 10.0% had rickettsial infections (n = 33; n = 20 identified with immunofluorescence assay and n = 13 by RT-PCR). Serum rRNA RT-PCR was 75.0% (95% CI 42.8–94.5%) sensitive and 91.2% (95% CI 85.8–95.1%) specific. Thrombocytopenia was more common among patients with rickettsial infections than with other nonmalarial infections (adjusted odds ratio 3.7; p = 0.003). No participants were on a tetracycline antimicrobial drug at admission. rRNA RT-PCR is a promising diagnostic strategy for identifying acute rickettsial infections. Doxycycline should be included in empiric antimicrobial drug regimens for nonmalarial febrile illness in this region.

Rickettsial infections are challenging to clinically distinguish from other causes of febrile illness. Clinical, operational, and technical factors increase the difficulty of identifying rickettsioses in sub-Saharan Africa (*1*). Rickettsial infections in sub-Saharan Africa are of international importance; among returning travelers from the region, rickettsioses are common causes of nonmalarial fever (*2*–*5*). Many patients do not have an obvious eschar (*5*–*7*), and clinical signs and symptoms are not well-characterized among those hospitalized in the region (*5*,*8*). Characteristic laboratory abnormalities of thrombocytopenia, leukopenia, and elevated transaminase activities are commonly observed clinical manifestations of the most prevalent tropical infections, including malaria, typhoid fever, arboviruses, or generalized sepsis (*9*).

Clinicians do not have reliable diagnostics for acute rickettsioses (*10*,*11*). Empiric antimicrobial drug regimens rarely include antimicrobial drugs active against rickettsioses (e.g., tetracyclines) (*11*–*13*). Diagnostics are generally limited to acute- and convalescent-phase serology despite flaws in performance, sparse point-of-care availability, and almost absent acute care clinical utility (*10*). Because of the low organism concentration within the bloodstream in acute infection, serum or whole blood PCR is generally insensitive at 18% (*10*). rRNA, on the other hand, is highly abundant, conserved, and stable. Targeting rRNA with reverse transcription PCR (RT-PCR) is an approach that has been used to optimize analytical sensitivity in PCRs for rickettsial (*14*) and other low bacterial burden infections (*15*). Evaluations using archived samples from patients with rickettsioses and nonrickettsial diseases demonstrate real promise for improved detection sensitivity of rickettsial infections but have yet to be evaluated in samples from prospectively identified acute febrile illnesses in a comprehensive clinical study (*14*,*16*). To confirm the improved sensitivity of this approach, we developed and evaluated new primers targeting rRNA. We describe the performance of an rRNA-targeting RT-PCR to detect spotted fever group (SFG) rickettsiae and typhus group (TG) rickettsiae, compared with acute- and convalescent-phase immunofluorescence assays (IFA), among acute febrile hospitalized participants in 3 hospitals in rural Uganda. We used the results from those identified rickettsial infections to describe the features of hospitalized rickettsial infections and address a clinical epidemiology knowledge gap in this region.

Materials and Methods

According to internal review board–approved parent cohort protocols, participants were enrolled upon hospitalization. We collected demographic, symptom, examination finding, and laboratory data on standardized forms during hospitalization and at 1 month after enrollment (Appendix, http://wwwnc.cdc.gov/EID/article/31/9/25-0479-App1.pdf) (*13*,*17*; P.W. Blair et al., unpub. data, https://www.medrxiv.org/content/10.1101/2023.09.14.23295526v1). We collected acute blood samples at enrollment and convalescent samples at 1 month. We determined survival during in-person visits or telephone calls during a 1–3-month period after hospitalization in the acute febrile illness (AFI) cohort and a 12-month period in the sepsis cohort.

We used acute-phase serology from archived samples collected at parent study enrollment to determine seroprevalence in the sepsis (n = 311) and AFI (n = 122) cohorts. We conducted IgG IFA by using commercial slides (spotted fever group rickettsia, *Rickettsia conorii* Malish 7 strain; typhus group rickettsia, *Rickettsia typhi* Wilmington strain) (Biocell Diagnostics Inc.). We screened serum samples collected at time of hospitalization (acute phase) and at 1-month follow-up (convalescent phase) at a dilution of 1:64

Author affiliations: Vanderbilt University Medical Center, Nashville, Tennessee, USA (P.W. Blair, S. Alharthi); Uniformed Services University, Bethesda, Maryland, USA (A.F. Londoño, J.S. Dumler); Makerere University, Kampala, Uganda (A. Wailagala); Johns Hopkins University School of Medicine, Baltimore, Maryland, USA (Y.C. Manabe)

DOI: https://doi.org/10.3201/eid3109.250479

[1]Members are listed at the end of this article.

and titrated to 1:65,536 (*17*). We considered a sample seropositive at a threshold titer of ≥128. We used a titer of 32 for fold-change calculations if the screen was negative. We defined a confirmed case as a seroconversion with a ≥4-fold increase in titer from the acute to convalescent sample, in which the convalescent titer was ≥128. If a participant had a seroconversion to both SFG and TG rickettsiae, we determined the group designation by the higher convalescent titer and then the higher acute titer. We excluded rickettsial infections with an alternative nonrickettsial positive microbiological result on the basis of our protocolized testing (malaria antigen positive, tuberculosis PCR positive or urine lipoarabinomannan positive, positive blood cultures, or positive whole blood Biofire panel) from this analysis to decrease the risk for misclassification (Appendix Figure 1).

For RT-PCR, we extracted RNA (targeting mRNA and rRNA to optimize sensitivity) (*10*) from 200 μL acute serum and 200 μL acute whole blood by using QIAamp RNA Mini Kits (QIAGEN). We conducted RT-PCR by using previously published methods (*18*) targeting SFG rickettsia *sca0* and TG rickettsia 17-kDa outer membrane lipoprotein mRNA. We only considered samples positive if in duplicate. To develop the 16S rRNA primers and probes, we aligned genes across 41 rickettsial species and 17 clinically relevant nonrickettsial bacterial species downloaded from GenBank by using the MEGAX platform (*19*). We identified a conserved region that was disparate from nonrickettsial species, including the forward primer 5′-gcgggtaatgccgggaactataag-3′, reverse primer 5′-ccgaactgagatgtcttttaggg-3′, and probe 5′-/56-FAM/gccggagga/zen/aggtggggacgacgtc/3IABkFQ/-3′. To determine primer species specificity or exclusivity compared with off-target organisms, we compared detection and SYBR Green melting curves by using 14 rickettsial and 4 nonrickettsial DNA controls. We used a 175-bp target sequence cloned into the pCR2.1 vector as a plasmid for quantification with a quantitative PCR master mix (Bio-Rad Laboratories). We identified a cutoff for rRNA RT-PCR by using the lowest threshold with ≥90% detection among serially diluted whole blood samples and in serum samples from healthy donors spiked with cell-free *R. parkeri*. To determine RT-PCR clinical sensitivity and specificity, we used IFA seroconversions as the index comparator. We prioritized samples with limited volume for IFA and then 16S RT-PCR, *sca0*, and 17-kDa RT-PCR. The rRNA RT-PCR performance calculations were limited to those with sample availability for both complete paired IFA and RT-PCR testing for serum and whole blood (n = 172 participants).

Case–Control Analysis

To evaluate for differences in clinical parameters, groups included samples with a follow-up serologic test and we then divided them into groups of rickettsial infections (IFA seroconversion or acute RT-PCR positive [*sca0*, 17-kDa, or whole blood 16S rRNA]), malarial infections (on the basis of a rapid diagnostic test), and nonmalarial infections (no rickettsial seroconversion and a negative malaria test). We performed summary statistics for baseline characteristics and microbiology results. We used Kruskal-Wallis testing for continuous parameters, Fisher exact test for observations <5, and χ^2 test for categorical parameters. We assessed groups for balance of age, female sex, and a ≥2 quick sequential organ failure assessment (qSOFA) score by using Fisher exact test. We compared rash and clinical laboratory parameters (white blood cell count, platelet count, aspartate transaminase, alanine transaminase, and creatinine) between the rickettsial group and the malarial group and between the rickettsial group and the nonmalarial group. The sample size was insufficient for clinical comparisons of total participants with discordant PCR and IFA serology results. Because of performance limitations of the index IFA comparator, we also determined the performance when limiting negative cases to those with microbiologically confirmed nonrickettsial infections as a secondary analysis.

To determine the discrimination accuracy for identifying rickettsial infection from nonmalarial illness, we conducted multivariable logistic regression among covariates with a significant ($p<0.05$) result from analyses for rickettsial compared with nonmalarial illness (ultimately limited to platelet count) adjusted for age, sex, and parent cohort. We obtained receiver operating characteristic curve estimates by using 3,000-fold cross-validation. We did not perform a multiple comparisons correction because of sample size. We estimated an effect size of an odds ratio of 2.6 to be detectable with a statistical power of 80% with a 1-sided $\alpha < 0.05$ comparing 33 rickettsial infections with 8:1 matching. We conducted analyses by using Stata version 16.0 (StataCorp, LLC), and created figures by using Stata or R version 4.0.1 (The R Project for Statistical Computing).

Results

Serology

In the SFG, the median time from acute-phase sample collection to convalescent-phase sample collection was 28 days (interquartile range [IQR] 24–30

days). We found that 49.7% (215/433) of acute samples and 58.5% (196/335) of convalescent samples were seropositive (≥128) for SFG rickettsia. Among acute samples, 43.2% (187/433) were positive at ≥256 and 40.0% (173/433) were positive at ≥512 (Figure 1, panel A). Among samples with a positive screen (titer ≥64), the median acute titer was 1,024 (up to 131,072; IQR 128–4,096) and median convalescent titer was 2,048 (up to 131,072; IQR 512–8,192). Baseline acute-phase sample seropositivity was highest in the city of Arua (acute 66.7% [22/33]), followed by Fort Portal (acute 54.3% [169/311]) and Mubende (acute 27.0% [24/89]). Among samples with a positive screen, the acute geometric mean titer (GMT) was 1,137.6 (95% CI 877.0–1,475.5) and the convalescent GMT was 1,990.5 (95% CI 1,508.1–2,627.2).

In the TG, we found that 10.6% (46/433) of acute-phase samples and 13.4% (45/335) of convalescent-phase samples were seropositive (≥128) for TG rickettsia. Among acute samples, 9.0% (39/433) were positive at ≥256 and 8.3% (36/433) were positive at ≥512 (Figure 1, panel B). Among samples with a positive screen, the median acute titer was 512 (up to 65,536; IQR 128–4,096) and median convalescent titer was 2,048 (up to 131,072; IQR 512–8,192). Compared with SFG rickettsia serology, baseline acute phase sample TG seropositivity varied less across sites, with the highest prevalence of seropositive results in Arua (acute: 15.2% [5/33]), followed by Fort Portal (acute 11.6% [36/311]), and Mubende (acute: 5.6% [5/89]). Among positive screens, the acute GMT was 873.4 (95% CI 486.3–1,568.6) and convalescent GMT was 1,915.9 (95% CI 1,030.6–3,561.8). After excluding samples with multiple positive nonrickettsial and rickettsial results (n = 14) (Appendix Figure 1), we observed SFG seroconversions (≥4-fold rise in titers) among 4.4% (14 participants) and TG seroconversions among 1.9% (6 participants) of participants.

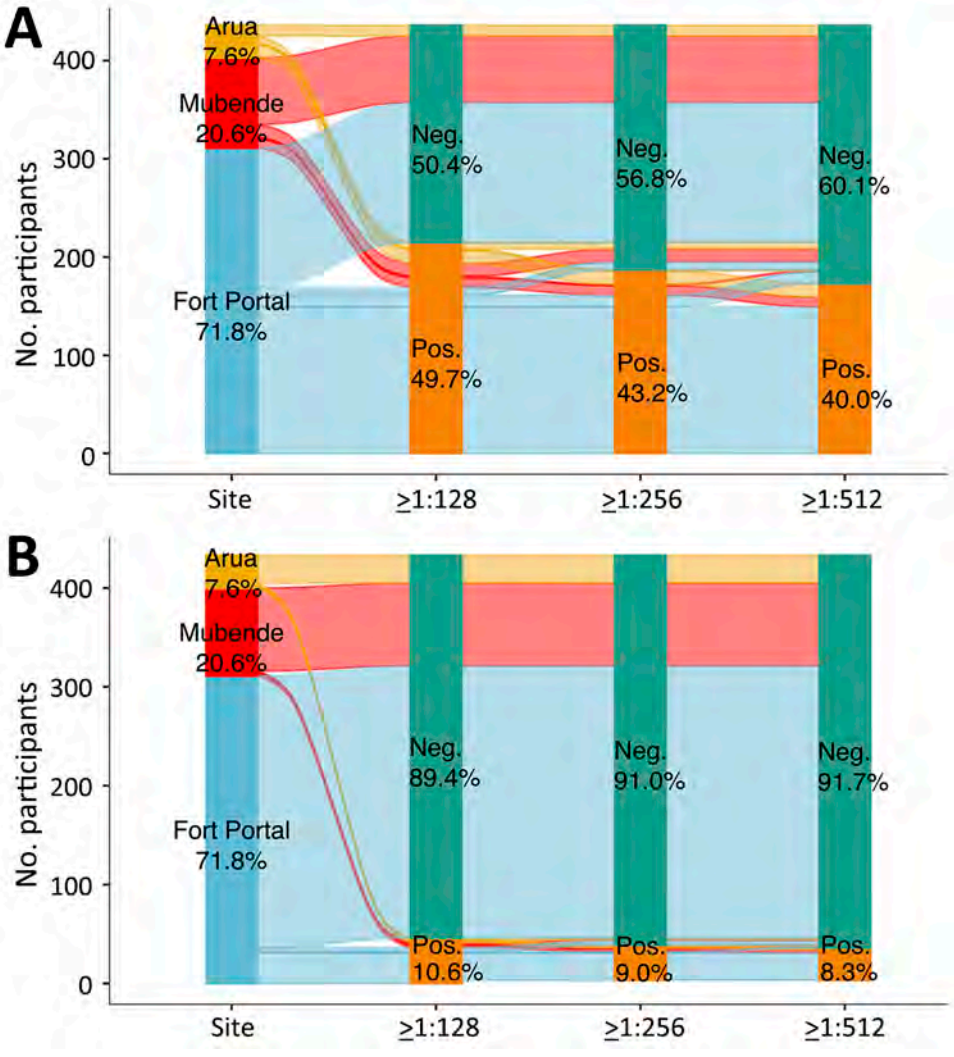

Figure 1. Alluvial plots of baseline acute serum samples from study of rickettsioses as an underrecognized cause of hospitalization for febrile illness, Uganda. A) Spotted fever group rickettsiae; B) typhus group rickettsiae. Immunofluorescence assay IgG seroprevalence is shown for different sites and different titer cutoffs. Participant samples were from referral hospital clinical study sites in Arua (in yellow; 7.6% of participants), Mubende (in red, 20.6% of participants), and in Fort Portal (in blue, 71.8%). Distribution of the colored lines across the graph shows a comparison of positive or negative samples among the sites. Green is the total percentage of negative samples. Orange is the total percentage of positive samples. Neg, negative; pos, positive.

rRNA RT-PCR Analytical Validation

To determine primer species specificity compared with off-target organisms, we conducted SYBR Green melting curves that were positive among 8 SFG species and *R. typhi* archived DNA controls and negative for 4 nonrickettsial DNA controls, 2 *Anaplasma* spp., and 2 *Ehrlichia* spp. (Appendix Table 1). We identified a16S rRNA RT-PCR cycle threshold (Ct) cutoff of 35.0 as the lowest threshold to detect ≥90% of serially diluted *R. parkeri* spiked samples in both whole blood and serum. This threshold equated to a lower limit of detection of 61 genomic equivalents/mL in whole blood and 3.8 genomic equivalents/mL in serum (Appendix Table 2). Healthy control (n = 6) samples were negative.

rRNA RT-PCR Compared with IFA Seroconversion Cases

Among participants with complete IFA testing and sufficient volume, acute-phase whole blood and serum were available for nucleic acid extraction and RT-PCR from 172 participants (including 12 with seroconversion). Compared with IFA seroconversion as the index test, rRNA RT-PCR was 33.3% sensitive (95% CI 33.3–65.1%; 4 of 12 cases) by using whole blood and 75.0% sensitive (95% CI 42.8– 94.5%; 9 of 12 cases) by using serum. Among rickettsial rRNA RT-PCR positive seroconversion positive cases, serum Ct values were 30.2–34.4 for serum and 29.8–31.9 for whole blood.

Discrepant Cases

Among cases without IFA seroconversion, 4/160 whole blood samples were rRNA RT-PCR positive (97.5% specific [95% CI 93.7%–99.3%]; Ct range 31.7–34.8) and 14/160 serum samples were rRNA RT-PCR positive (91.2% specific [95% CI 85.8%–95.1%]; Ct range 29.9–34.5) (Appendix Figure 2). Half or more (7 of 14 serum and 3 of 4 of whole blood) of the discrepant cases had an acute titer higher than the 95% CI of the GMT mean for the cohort. The time between the acute-phase and convalescent-phase sample collection was 23–49 days among positive serum cases and 23–29 days among positive whole blood cases. If restricting the nonrickettsial case definition to microbiologically confirmed diagnoses (n = 62), whole blood 16S rRNA was 100% specific (95% CI 94.2%–100.0%; 0 positive nonrickettsial cases) and serum 16S rRNA was 96.8% specific (95% CI 88.8%–99.6%). Two cases without ≥4-fold change in IFA under this definition were rRNA RT-PCR positive and were infected with malaria. One had acute and convalescent SFG IgG titers of 65,636 (seroconversion was not observable because of the titration upper limit).

Rickettsia mRNA RT-PCR Compared with IFA Seroconversion Cases

Among participants with both acute and convalescent serum samples, 1 was *Rickettsia* mRNA RT-PCR (17-kDa) positive. This case was also rRNA positive. On the basis of this single case, *sca0* and 17-kD protein gene transcript RT-PCR targets combined (positive with either target) were 14.3% sensitive (95% CI 0.4%–57.9%; 1 of 7 IFA cases) and 100.0% specific (95% CI 97.7%–100.0%). All samples were negative for 17-kDa or *sca0* targets when using PCR on whole blood with or without reverse transcription or on serum without reverse transcription.

Clinical Case–Control Rickettsial Comparisons

Participants used in the case-control comparison (n = 329) were a median of 39.0 (IQR 27–54) years of age at enrollment; 62% were female and 38% male (Table 1). Empiric tetracycline antimicrobial drugs were started across cohorts among 5.8% participants. Infection groups had similar distributions of age (p = 0.39), sex (p = 0.72) and a positive qSOFA score (p = 0.77).

On the basis of the high specificity of whole blood rRNA, serum *sca0*, and serum 17-kDa RT-PCR, we expanded our serologic case definition for a case–control comparison to include those assays (Appendix Figure 1). Among patients with acute-phase samples with or without convalescent serum samples, 8.0% (33/412; 20 patients identified with a ≥4-fold change in IFA) had rickettsial infections. To evaluate for differences in clinical parameters, we made comparisons among groups of rickettsial infections, malarial infections on the basis of a rapid diagnostic test (n = 59), and nonmalarial infections (no rickettsial seroconversion and a negative malaria test, n = 237).

Among those with confirmed rickettsial infections, severity was similar to nonrickettsial infections; 22% had a qSOFA of ≥2 (Table 2). No participants with rickettsial infections were on tetracycline treatments, and a minority (36%) had received a potentially active antimicrobial drug (i.e., macrolide, quinolone, or chloramphenicol) against rickettsial infections. Rash (including maculopapular because of *R. conorii* infection) (*7*) was observed in only 6% of participants.

Among patients with rickettsial illness, median leukocyte count was 6.2 × 10^3 cells/μL (IQR 4.6–8.1 × 10^3 cells/μL), aspartate transaminase 38 U/L (IQR 26.0–92.0 U/L), and platelet count 168.0 × 10^3/μL (IQR 116.9–264.5 × 10^3/μL) (Table 3). Among SFG seroconversions, the median acute titer was 384 (IQR 128–2,048) and median convalescent titer was 1,536 (IQR 1,024–16,384). Among TG cases, the median acute titer

Table 1. Baseline demographics for case–control comparison in study of rickettsioses as an underrecognized cause of hospitalization for febrile illness, Uganda*

Characteristic	Sepsis cohort, n = 259	AFI cohort, n = 70	Total, n = 329
Age, y, median (IQR)	30.5 (24.0–47.0)	30.5 (24.0–47.0)	39.0 (27.0–54.0)
Sex, no. (%)			
F	160 (62)	43 (61)	203 (62)
M	99 (38)	27 (39)	126 (38)
HIV-positive, no. (%)	95 (37)	23 (33)	118 (36)
Physiologic parameters, median (IQR)			
Heart rate, beats/min	101.0 (90.0–112.0)	109.0 (93.0–116.0)	101.0 (90.0–114.0)
Temperature, °C	37.5 (36.9–38.1)	38.1 (38.0–38.8)	37.6 (36.9–38.3)
Breaths/min	28.0 (24.0–32.0)	20.0 (18.0–24.0)	26.0 (22.0–32.0)
Oxygen saturation	95.0 (92.0–97.0)	98.0 (97.0–99.0)	95.0 (93.0–98.0)
qSOFA ≥2, no. (%)	53 (21)	12 (17)	65 (20)
Tetracycline treatment, no. (%)	18 (6.9)	1 (1.4)	19 (5.8)
Rickettsial† treatment, no. (%)	126 (49)	18 (26)	144 (44)

*AFI, acute febrile illness; IQR, interquartile range; qSOFA, quick sepsis organ failure assessment.
†Antimicrobial drugs with potential rickettsial activity: tetracyclines, macrolides, or quinolones.

was 64 (IQR 32–8,192) and median convalescent titer was 4,096 (IQR 1,024–65,536). Thrombocytopenia was more common among those with rickettsial infections compared with other nonmalarial infections (adjusted odds ratio 3.7; p = 0.003), but diagnostic performance was limited (sensitivity 45.5%, 95% CI 24.4–67.8%; specificity 83.6%, 95% CI 78.1–88.1%; positive likelihood ratio 2.8, 95% CI 1.6–4.8; negative likelihood ratio 0.7, 95% CI 0.4–1.0). The cross-validated area under the receiver operating characteristic curve was 0.68 (95% CI 0.46–0.74). In addition, the platelet count was lower among patients with malarial illness than rickettsial illness (p = 0.007) (Table 3; Figure 2). Leukocyte count was higher among patients with rickettsial infections than malarial illness (median 4.7 × 10^3 cells/μL, IQR 3.3–6.6 × 10^3 cells/μL; p = 0.013). Other parameters were not significantly different. Of participants with rickettsial infections, 3 of 33 died within 90 days.

Discussion

Our study found that rickettsioses were a common cause of hospitalized illness across multiple sites in Uganda, consistent with a high observed seroprevalence. Rickettsial illness manifested similarly to nonmalarial illness on the basis of well-described clinical parameters. Clinical factors (including platelet count) were neither sensitive nor specific for identifying rickettsial infections. Rashes were infrequently reported or seen on physical examination, and no eschars were observed. Specific rickettsial treatments were uncommonly used. rRNA RT-PCR sensitivity in serum samples was considerably higher than targeting rickettsial mRNAs, although the use of rRNA RT-PCR has the potential benefit as a diagnostic strategy for identifying acute cases that otherwise would not be treated. Our findings highlight the need for continued diagnostic development. Clinicians should also have a high level of suspicion and low threshold for empiric doxycycline use in this region for nonmalarial illness among hospitalized adults.

Among prior cohorts in Sub-Saharan Africa, clinical descriptions of rickettsial infections have largely been limited to returning travelers, and the course of hospitalized illness is not prospectively well

Table 2. Clinical characteristics among those with rickettsial, malarial, and nonmalarial illness in study of rickettsioses as an underrecognized cause of hospitalization for febrile illness, Uganda*

Characteristic	Rickettsial, n = 33	Malarial, n = 59	p value, rickettsial vs. malarial†	Nonmalarial, n = 237	p value, rickettsial vs. nonmalarial†
Age, y, median (IQR)	37.0 (28.0–47.0)	35.0 (24.0–51.0)	0.794	40.0 (28.0–55.0)	0.393
Sex					
F	21/33 (64)	39/59 (66)	0.812	143/237 (60)	0.716
M	12 (36)	20 (34)	0.812	94 (40)	0.716
HIV-positive	10/33 (30)	17/59 (29)	0.880	91/237 (38)	0.368
Physiologic parameters, median (IQR)					
Heart rate, beats/min	102.0 (91.0–110.0)	102.0 (92.0–113.0)	0.782	101.0 (89.0–114.0)	0.696
Temperature °C	38.0 (37.1–38.8)	38.0 (37.0–38.8)	0.964	37.5 (36.9–38.1)	0.083
Breaths/min	24.0 (20.0–29.0)	24.0 (20.0–32.0)	0.954	28.0 (24.0–32.0)	0.057
Oxygen saturation	95.0 (93.0–98.0)	97.0 (94.0–98.0)	0.134	95.0 (92.0–97.0)	0.535
qSOFA ≥2, no. (%)‡	7/33 (21)	13/59 (22)	0.927	45/236 (19)	0.770
Tetracycline treatment	0/33 (0)	0/59 (0)	>0.999	19/237 (8.0)	0.142
Rickettsial treatment	12/33 (36)	14/59 (24)	0.197	118/237 (50)	0.148

*Values are no. positive/no. tested (%) except as indicated. IQR, interquartile range; qSOFA, quick sepsis organ failure assessment.
†Fisher exact test, Wilcoxon rank-sum test, or Pearson χ^2 test.
‡Missing for 1 of 328 participants.

Table 3. Clinical examination and laboratory features among diagnostic classes in a study of rickettsioses as an underrecognized cause of hospitalization for febrile illness, Uganda*

Characteristic	Total, n = 329	Malarial, n = 59	Rickettsial, n = 33	p value, rickettsial vs. malarial†	Nonmalarial, n = 237	p value, rickettsial vs. nonmalarial†
Rash on examination, no. (%)‡	21/328 (6.4)	2/59 (3.4)	2/33 (6.1)	0.616	17/236 (7.2)	>0.999
Leukocytes, × 10^3 cells/μL§	5.5 (3.9–8.4)	4.7 (3.3–6.6)	6.2 (4.6–8.1)	0.012	5.6 (4.1–9.4)	0.900
Platelets, × 10^3/μL¶	205.0 (134.7–289.0)	104.1 (64.2–179.0)	168.0 (116.9–264.5)	0.007	227.0 (171.0–311.0)	0.013
AST, U/L#	35.0 (26.0–59.0)	32.0 (24.0–42.0)	38.0 (26.0–92.0)	0.081	36.0 (26.0–61.0)	0.524
ALT, U/L	23.0 (18.0–36.0)	21.0 (17.0–28.0)	25.0 (19.0–44.0)	0.119	24.0 (18.0–37.0)	0.596
Creatinine, mg/dL**	0.8 (0.5–1.0)	0.8 (0.0–1.0)	0.8 (0.0–1.1)	0.204	0.8 (0.6–1.0)	0.541

*Values are median (interquartile range) except as indicated. ALT, alanine transaminase; AST, aspartate transaminase; qSOFA, quick sepsis organ failure assessment.
†Fisher exact test, Wilcoxon rank-sum test, or Pearson χ^2 test.
‡No. positive/no. tested (%). Missing for 1 of 329 participants.
§Missing for 18 of 328 participants.
¶Missing for 19 of 328 participants.
#Missing for 1 of 329 participants.
**Missing for 2 of 322 participants.

characterized. The high rates of seroprevalence observed and common identification of seroconversions indicate that rickettsial infections are circulating widely in this region. A high number of rickettsial infections is supported by a recent study that identified SFG rickettsia in ticks throughout Uganda (*20*). We found rickettsial infections were common (8%) among patients with acute febrile illness or sepsis manifestations. This result is similar to an estimate from 2012–2014 among pediatric and adult febrile participants in Tanzania in which 8.9% had SFG rickettsia seroconversions (*21*). Our findings greatly strengthen the evidence that rickettsial infections frequently cause hospitalization in this region.

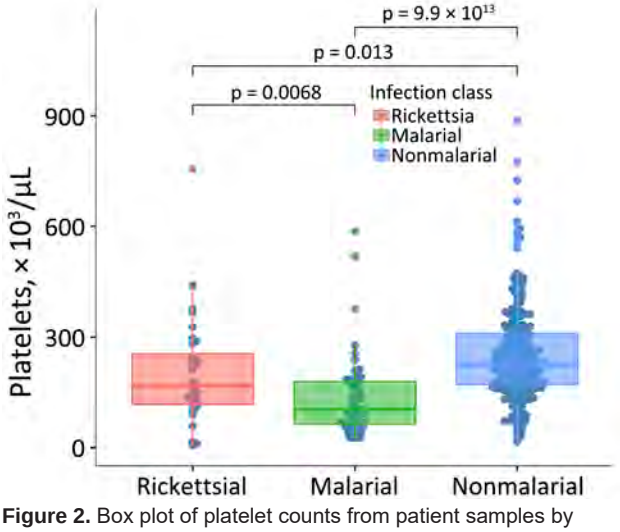

Figure 2. Box plot of platelet counts from patient samples by infection type in study of rickettsioses as an underrecognized cause of hospitalization for febrile illness, Uganda. Horizontal lines within boxes indicate median; box tops and bottoms indicate interquartile ranges; error bar above is 1.5x the IQR to the highest value and the error bar below is 1.5x the IQR to the lowest value.

Novel acute diagnostics are needed to identify rickettsioses. Diagnostic delays for rickettsial infections often result in prolonged hospital stays and increased death because rickettsial infections are not susceptible to standard empiric antimicrobial drugs used in many worldwide settings (*2*,*22*,*23*). The current diagnostic standard, indirect IFA, relies on referral acute and convalescent serum sample confirmation testing, which is only available 3–6 weeks after symptom onset and has performance limitations (*9*). Our observations of rRNA RT-PCR–positive IFA-negative participants highlighted challenges with using a 4-fold IFA titer increase. In addition to logistical barriers, IFA interpretation could be affected by blood collection timing (*24*), early receipt of antimicrobial drugs (*25*), and immunocompromising conditions (*26*). Characteristics of rickettsial infection were not reliable as clues for initiating empiric treatment, further demonstrating the diagnostic gap and need to consider empiric treatment without fully relying on clinical laboratory results in the absence of a sensitive rapid diagnostic test.

We demonstrated potential improvement in sensitivity by using RT-PCR rather than PCR and by using highly abundant and stable rickettsial rRNA targets rather than membrane protein gene DNA or mRNA targets. Molecular amplification typically has low sensitivity (≈7%–43%) for rickettsioses because of low organism burden; sensitivity can be improved by extracting nucleic acid from the buffy coat, which requires additional processing (*10*,*18*). By using multiple singleplex RT-PCR primers (targeting membrane protein gene DNA or mRNA) we were able to detect cases not identified with DNA PCR. However, sensitivity remains limited with either RT-PCR or PCR by using traditional targets present in either

low numbers or that are labile. We anticipated whole blood would contain more rickettsial organisms and improve sensitivity compared with serum across PCR targets. Instead, we found that whole blood was less sensitive than serum, potentially because of inhibitors in whole blood (*27*). rRNA RT-PCR improved sensitivity of PCR over membrane protein gene DNA and mRNA targets and demonstrated promise as an acute detection diagnostic modality that detected rickettsial cases missed by DNA, but mRNA detection was not higher than anticipated when compared with previous studies using DNA (*18*).

Our results are supported by prior efforts that showed improved performance by using 23S rRNA targets (*14*,*16*). The stability and abundance of protein-associated rickettsial rRNA targets are promising for use in remote settings where sample handling and storage can be more vulnerable to unstable conditions. However, rRNA still lacks sensitivity compared with paired serologic testing. Scalable methods to improve specificity and potentially sensitivity such as digital droplet PCR or concentrating target templates in each reaction are needed before broad clinical use (*18*). However, because RT-PCR is now widely available, potentially with increased capacity after the COVID-19 pandemic, and doxycycline is generally well tolerated, laboratory-validated rRNA RT-PCR could be used to initiate standard of care treatment with doxycycline and then serologic confirmation. Rickettsial rRNA genes are abundant stable targets that could be leveraged for furthering clinical rickettsial diagnostics, but implementation and validation studies are needed at clinical sites. Although performance could be optimized, rickettsial rRNA RT-PCR might be the best option for clinical use in highly endemic regions in the absence of a reliable acute diagnostic alternative.

The first limitation of our study is that it relied on availability of convalescent-phase serologic testing to identify approximately half of the infected patients. Therefore, the severity of each group is not anticipated to be representative of the population because participants lost to follow-up or who had died before 28 days were not included. Second, in emphasizing sample availability for multimodal case identification, our study was not designed to determine differences in deaths or duration of hospital stay. Third, sample collection, handling and storing conditions at resource-limited clinical sites might have decreased PCR sensitivity. rRNA RT-PCR performance could be improved with direct testing after collection, although rRNA is likely less vulnerable to degradation than mRNA. Last, conserved rRNA targets afford broad detection of rickettsioses but are intrinsically less phylogenetically or taxonomically informative, prohibiting the possibility for species level identification of SFG rickettsiae.

In conclusion, we found rickettsial infections to be common across 2 severe infectious illness cohorts in Uganda. Our case–control study identified that commonly suggested clinical factors for identifying rickettsial infections in sub-Saharan Africa are nonspecific or are generally absent. rRNA RT-PCR improved sensitivity over previously used membrane protein gene DNA PCR and mRNA RT-PCR and requires further clinical validation to ensure specificity when using conserved stable rRNA targets. Until acute diagnostics are widely available for rickettsial infections, empiric doxycycline should be considered for nonmalarial fever of unknown cause in this region.

Members of the Acute Febrile Illness and Sepsis in Uganda Study Team: Danielle V. Clark, Emily Clemens, Melissa Gregory, Francis Kakooza, Willy Kayondo, Mubaraka Kayiira, Hannah Kibuuka, Kenneth Kobba, Abraham Khandathil, Mohammed Lamorde, Prossy Naluyima, Edgar C. Ndawula, Stephen Okello, Matt L. Robinson, and Peter Waitt.

This project was supported by the Congressionally Directed Medical Research Programs Tickborne Diseases Related Program Career Development Award. Pathogen testing was supported by the Naval Medical Logistics Command (cooperative agreement no. N626451920001) within the parent protocol.

The sepsis protocol and informed consent were approved by the US Army Medical Research and Development Command Institutional Review (approval no. M-10573) and Makerere University School of Public Health (internal review board approval no. 490). The acute febrile illness study and informed consent process were reviewed and approved by the Joint Clinical Research Centre Research Ethics Committee (approval no. JC1518) and the Uganda National Council for Science and Technology (approval no. HS 371ES), and Johns Hopkins University School of Medicine (internal review board no. IRB00176961). All participants signed written informed consent forms before study procedures. All participants were provided written consent that was in either English or their local language. All procedures were conducted in accordance with the ethical standards of the Helsinki Declaration of the World Medical Association. The investigators have adhered to the policies for protection of human subjects as prescribed in 45 code of federal regulations 46.

Y.C.M. receives research funding from Becton Dickinson, Quanterix, and Hologic, and receives funding support from miDiagnostics to Johns Hopkins University. M.L. receives research funding support from Pfizer Inc. to the Infectious Diseases Institute.

About the Author

Dr. Blair is an infectious disease physician and scientist at Vanderbilt University Medical Center, Nashville, Tennessee, USA. His research interests include molecular and imaging approaches to clinically detect acute and emerging infectious diseases.

References

1. Hercik C, Cosmas L, Mogeni OD, Wamola N, Kohi W, Houpt E, et al. A combined syndromic approach to examine viral, bacterial, and parasitic agents among febrile patients: a pilot study in Kilombero, Tanzania. Am J Trop Med Hyg. 2018;98:625–32. https://doi.org/10.4269/ajtmh.17-0421
2. Freedman DO, Weld LH, Kozarsky PE, Fisk T, Robins R, von Sonnenburg F, et al.; GeoSentinel Surveillance Network. Spectrum of disease and relation to place of exposure among ill returned travelers. N Engl J Med. 2006;354:119–30. https://doi.org/10.1056/NEJMoa051331
3. Mendelson M, Davis XM, Jensenius M, Keystone JS, von Sonnenburg F, Hale DC, et al.; GeoSentinel Surveillance Network. Health risks in travelers to South Africa: the GeoSentinel experience and implications for the 2010 FIFA World Cup. Am J Trop Med Hyg. 2010;82:991–5. https://doi.org/10.4269/ajtmh.2010.10-0198
4. Bogovic P, Lotric-Furlan S, Korva M, Avsic-Zupanc T. African tick-bite fever in traveler returning to Slovenia from Uganda. Emerg Infect Dis. 2016;22:1848–9. https://doi.org/10.3201/eid2210.160650
5. de Vries SG, van Eekeren LE, van der Linden H, Visser BJ, Grobusch MP, Wagenaar JFP, et al. Searching and finding the hidden treasure: a retrospective analysis of rickettsial disease among Dutch international travelers. Clin Infect Dis. 2021;72:1171–8. https://doi.org/10.1093/cid/ciaa091
6. Raoult D, Fournier PE, Fenollar F, Jensenius M, Prioe T, de Pina JJ, et al. *Rickettsia africae*, a tick-borne pathogen in travelers to sub-Saharan Africa. N Engl J Med. 2001;344:1504–10. https://doi.org/10.1056/NEJM200105173442003
7. Kandathil AJ, Blair PW, Lu J, Anantharam R, Kobba K, Robinson ML, et al. Metagenomic next generation sequencing of plasma RNA for diagnosis of unexplained, acute febrile illness in Uganda. PLoS Negl Trop Dis. 2024;18:e0012451. https://doi.org/10.1371/journal.pntd.0012451
8. Parola P. Rickettsioses in sub-Saharan Africa. Ann N Y Acad Sci. 2006;1078:42–7. https://doi.org/10.1196/annals.1374.005
9. Biggs HM, Behravesh CB, Bradley KK, Dahlgren FS, Drexler NA, Dumler JS, et al. Diagnosis and management of tickborne rickettsial diseases: Rocky Mountain Spotted Fever and other spotted fever group rickettsioses, ehrlichioses, and anaplasmosis—United States. MMWR Recomm Rep. 2016;65:1–44. https://doi.org/10.15585/mmwr.rr6502a1
10. Paris DH, Dumler JS. State of the art of diagnosis of rickettsial diseases: the use of blood specimens for diagnosis of scrub typhus, spotted fever group rickettsiosis, and murine typhus. Curr Opin Infect Dis. 2016;29:433–9. https://doi.org/10.1097/QCO.0000000000000298
11. Blair PW, Lamorde M, Dumler JS. Rickettsioses and Q fever in Tanzania: estimating the burden of pervasive and neglected causes of severe febrile illness in sub-Saharan Africa. Am J Trop Med Hyg. 2021;106:371–2. https://doi.org/10.4269/ajtmh.21-0963
12. Jacob ST, Moore CC, Banura P, Pinkerton R, Meya D, Opendi P, et al.; Promoting Resource-Limited Interventions for Sepsis Management in Uganda (PRISM-U) Study Group. Severe sepsis in two Ugandan hospitals: a prospective observational study of management and outcomes in a predominantly HIV-1 infected population. PLoS One. 2009;4:e7782. https://doi.org/10.1371/journal.pone.0007782
13. Blair PW, Kobba K, Kakooza F, Robinson ML, Candia E, Mayito J, et al. Aetiology of hospitalized fever and risk of death at Arua and Mubende tertiary care hospitals in Uganda from August 2019 to August 2020. BMC Infect Dis. 2022;22:869. https://doi.org/10.1186/s12879-022-07877-3
14. Chung IH, Robinson LK, Stewart-Juba JJ, Dasch GA, Kato CY. Analytically sensitive *Rickettsia* species detection for laboratory diagnosis. Am J Trop Med Hyg. 2022;106:1352–7. https://doi.org/10.4269/ajtmh.21-0757
15. Backstedt BT, Buyuktanir O, Lindow J, Wunder EA Jr, Reis MG, Usmani-Brown S, et al. Efficient detection of pathogenic leptospires using 16s ribosomal RNA. PLoS One. 2015;10:e0128913. https://doi.org/10.1371/journal.pone.0128913
16. Kato CY, Chung IH, Robinson LK, Austin AL, Dasch GA, Massung RF. Assessment of real-time PCR assay for detection of *Rickettsia* spp. and *Rickettsia rickettsii* in banked clinical samples. J Clin Microbiol. 2013;51:314–7. https://doi.org/10.1128/JCM.01723-12
17. Blair PW, Kobba K, Okello S, Alharthi S, Naluyima P, Clemens E, et al.; Sepsis in Uganda study teams. Evidence of *Orientia* spp. endemicity among severe infectious disease cohorts, Uganda. Emerg Infect Dis. 2024;30:1442–6. https://doi.org/10.3201/eid3007.231040
18. Reller ME, Dumler JS. Optimization and evaluation of a multiplex quantitative PCR assay for detection of nucleic acids in human blood samples from patients with spotted fever rickettsiosis, typhus rickettsiosis, scrub typhus, monocytic ehrlichiosis, and granulocytic anaplasmosis. J Clin Microbiol. 2020;58:e01802–19. https://doi.org/10.1128/JCM.01802-19
19. Kumar S, Stecher G, Li M, Knyaz C, Tamura K. MEGA X: molecular evolutionary genetics analysis across computing platforms. Mol Biol Evol. 2018;35:1547–9. https://doi.org/10.1093/molbev/msy096
20. Eneku W, Erima B, Byaruhanga AM, Atim G, Tugume T, Ukuli QA, et al. Wide distribution of Mediterranean and African spotted fever agents and the first identification of Israeli spotted fever agent in ticks in Uganda. PLoS Negl Trop Dis. 2023;17:e0011273. https://doi.org/10.1371/journal.pntd.0011273
21. Pisharody S, Rubach MP, Carugati M, Nicholson WL, Perniciaro JL, Biggs HM, et al. Incidence estimates of acute Q fever and spotted fever group rickettsioses, Kilimanjaro, Tanzania, from 2007 to 2008 and from 2012 to 2014. Am J Trop Med Hyg. 2021;106:494–503. https://doi.org/10.4269/ajtmh.20-1036
22. Jensenius M, Han PV, Schlagenhauf P, Schwartz E, Parola P, Castelli F, et al.; GeoSentinel Surveillance Network. Acute and potentially life-threatening tropical diseases in Western travelers—a Geosentinel Multicenter study, 1996-2011. Am

J Trop Med Hyg. 2013;88:397–404. https://doi.org/10.4269/ajtmh.12-0551
23. Leder K, Torresi J, Libman MD, Cramer JP, Castelli F, Schlagenhauf P, et al.; GeoSentinel Surveillance Network. GeoSentinel surveillance of illness in returned travelers, 2007–2011. Ann Intern Med. 2013;158:456–68. https://doi.org/10.7326/0003-4819-158-6-201303190-00005
24. Fournier PE, Jensenius M, Laferl H, Vene S, Raoult D. Kinetics of antibody responses in *Rickettsia africae* and *Rickettsia conorii* infections. Clin Diagn Lab Immunol. 2002;9:324–8.
25. Philip RN, Casper EA, MacCormack JN, Sexton D, Thomas LA, Anacker RL, et al. A comparison of serologic methods for diagnosis of Rocky Mountain spotted fever. Am J Epidemiol. 1977;105:56–67. https://doi.org/10.1093/oxfordjournals.aje.a112356
26. Garrido HMG, Schnyder JL, Tanck MWT, Vollaard A, Spijker R, Grobusch MP, et al. Immunogenicity of pneumococcal vaccination in HIV infected individuals: a systematic review and meta-analysis. EClinicalMedicine. 2020; 29-30:100576. https://doi.org/10.1016/j.eclinm.2020.100576
27. Al-Soud WA, Rådström P. Purification and characterization of PCR-inhibitory components in blood cells. J Clin Microbiol. 2001;39:485–93. https://doi.org/10.1128/JCM.39.2.485-493.2001

Address for correspondence: Paul W. Blair, Vanderbilt University Medical Center, Division of Infectious Diseases, 1161 21st Avenue S, A-2200 Medical Center N, Nashville, TN 37232, USA; email: paul.blair@vumc.org

Epidemiology of Chikungunya Hospitalizations, Brazil, 2014–2024

Vaneide Daciane Pedí, Denise Lopes Porto, Wagner de Jesus Martins, Giovanny Vinícius Araújo de França

We describe 7,421 chikungunya hospitalizations in Brazil covered by the country's unified health system during 2014–2024. Most (43.2%) hospitalizations occurred in 2016 and 2017, reaching 0.72 (95% CI 0.69–0.76) hospitalizations/100,000 population in 2016. Hospitalizations were more frequent among persons who were female (55.8%), identifying as brown or black (63.5%), and 1–19 years of age (31.4%). Intensive care unit admissions occurred in 1.4% of cases, predominantly among children <5 and adults ≥85 years of age. The overall in-hospital case-fatality rate was 1.1%, which increased substantially with age, reaching 11.5% among patients ≥90 years of age and 14.1% among men 85–89 years of age. Patients admitted to the intensive care unit had a case-fatality rate of 21.1%. The total cost of chikungunya hospitalizations was US $560,746 (US $76.26 per patient). Our findings provide insights for surveillance of the most severe chikungunya cases.

Chikungunya virus (CHIKV), an alphavirus of the Togaviridae family, is transmitted to humans by *Aedes* spp. mosquitoes, primarily *Ae. aegypti* and *Ae. albopictus* mosquitoes, and causes chikungunya in humans, commonly in tropical and subtropical regions worldwide (*1*). Phylogenetic analyses have categorized CHIKV into 3 main lineages: the East/Central/South African (ECSA) lineage, the West African lineage, and the Asian lineage (*2*,*3*).

By December 2022, CHIKV had been detected in >110 countries in Asia, Africa, Europe, and the Americas, and all regions with established *Ae. aegypti* or *Ae. albopictus* mosquito populations have reported local transmission of the virus (*4*). Since 2016, Brazil has been the epicenter of chikungunya epidemics in the Americas, and 1,700,762 suspected cases were reported nationwide during 2017–2024 (*5*). The country has a sizeable susceptible population, a favorable climate, and abundant populations of *Ae. aegypti* mosquitoes, which could contribute to the occurrence of rapid and localized chikungunya outbreaks, and high CHIKV infection rates are followed by periods of lower chikungunya incidence (*5*). In addition, seropositivity is highly heterogeneous in Brazil, and estimates range from 7.4% to 51% (*6*,*7*).

Chikungunya fever refers to the acute illness caused by CHIKV. Most (75%–95%) infected persons develop symptoms, which usually begin within 4 to 8 days after the bite of a CHIKV-infected mosquito. Symptoms can include fever, myalgia, and arthralgia, and CHIKV infection can cause decompensation of underlying conditions (*8*). Although chikungunya illness is generally self-limited, some patients—especially infants; older adults; and persons with underlying conditions, co-infections, or certain genetic traits—can develop atypical or severe forms. Those forms can involve neurologic disturbances, cardiovascular complications, hemorrhagic signs, or Guillain-Barré syndrome (*9*–*11*). The reported frequency of such manifestations varies across outbreaks and populations, from 0.3% during the 2005–2006 Réunion Island epidemic to 9.8% among hospitalized patients in French Guiana during 2014–2015 (*12*,*13*).

In 30%–40% of patients, chikungunya becomes chronic, persisting for >3 months and causing arthritis, fatigue, sleep disorders, myalgia, skin lesions, depression, and digestive disorders (*1*,*14*,*15*). Among the severe manifestations of CHIKV infection, cases of meningoencephalitis, bullous skin lesions, multiple organ failure with hemorrhage, and sepsis have been reported (*16*,*17*). Furthermore, CHIKV infection increasingly has been associated with substantial mortality rates, particularly because of complications, such as heart or cerebrovascular disease, renal

Author affiliations: Programa de Pós-Graduação em Medicina Tropical da Faculdade de Medicina da Universidade de Brasília, Brasília, Brazil (V.D. Pedí); Fundação Oswaldo Cruz, Brasília, (V.D. Pedí, W.J. Martins); Ministério da Saúde, Brasília (D.L. Porto, G.V.A. de França)

DOI: https://doi.org/10.3201/eid3109.250554

impairment, cardiogenic or septic shock, or decompensated diabetes (*18*–*20*).

Data from outbreaks in different countries show that 0.6%–13.0% of patients with confirmed chikungunya are hospitalized (*1*,*8*,*10*,*21*). In Brazil, the unified health system, Sistema Único de Saúde (SUS), provides universal access to healthcare, and in 2019, SUS covered almost 65% of all hospitalizations in the country (*22*). The SUS hospital information system, Sistema de Informação Hospitalar/SUS (SIH/SUS), is the country's only source of information on hospitalizations. The system is mainly used to define the values for payment of medium- and high-complexity services provided by healthcare establishments throughout the country (*23*). We used SIH/SUS data to explore the epidemiology of chikungunya hospitalizations in Brazil during 2014–2024, focusing on patient demographic characteristics, spatiotemporal dynamics, and costs covered by SUS.

Materials and Methods

We conducted a cross-sectional descriptive study of chikungunya hospitalizations in Brazil, its 5 regions, and 26 states and the Federal District (Figure 1), using publicly available SIH/SUS data from Datasus (https://datasus.saude.gov.br/transferencia-de-arquivos). The SIH/SUS data reflect only hospitalizations covered by the public healthcare system and do not capture costs from private sector hospitalizations or out-of-pocket expenses.

We used data on chikungunya hospitalizations financed by SUS and registered in the SIH/SUS during January 1, 2014–December 31, 2024. We selected all hospitalizations that had chikungunya as the primary diagnosis and were registered with code A92.0 from the International Classification of Diseases, 10th Revision (ICD-10), as adopted by the Ministry of Health (*24*). Secondary diagnoses (i.e., conditions that coexisted at the time of admission) were only available in SIH/SUS dataset for 2014, and chikungunya was not reported as a secondary diagnosis during 2015–2024; therefore, our analysis was limited to chikungunya as the primary diagnosis.

We used the following variables in our analyses: year and month of hospitalization; sex; age in years, estimated from the patient's date of birth and the date of hospitalization, classified into 5-year age groups; race/skin color, according to patients' self-declarations and classified into white, black, brown, Asian, and Indigenous (*25*); and intensive care unit (ICU) admission and death, when applicable. We calculated

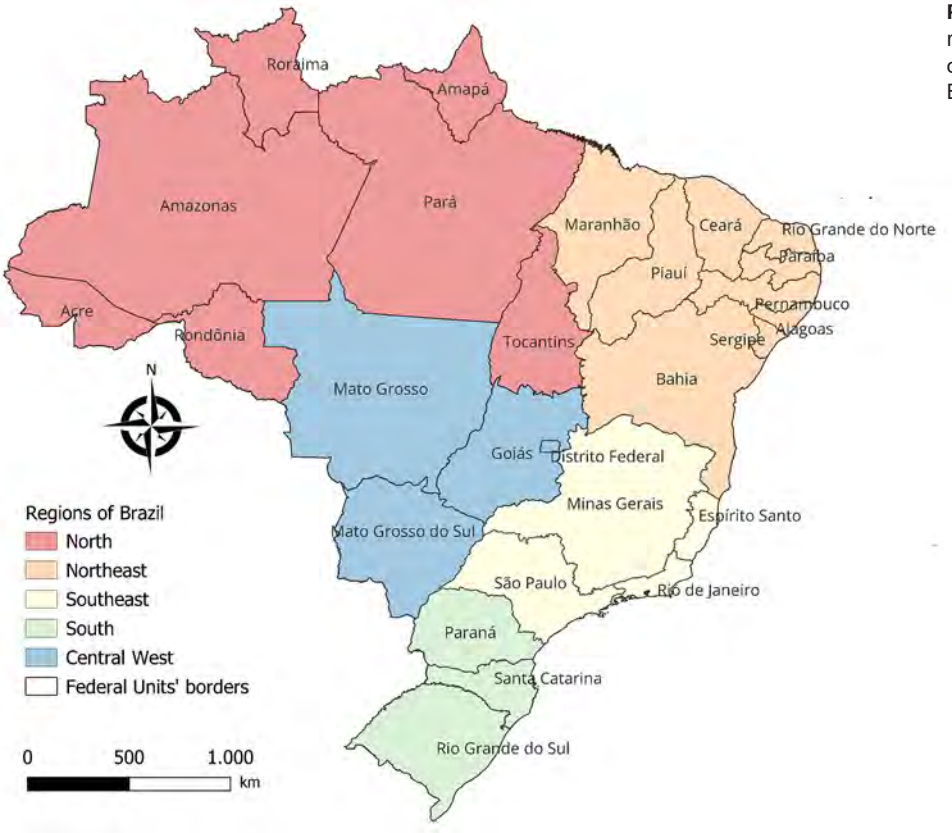

Figure 1. Regions and federal units referenced in study of epidemiology of chikungunya hospitalizations, Brazil, 2014–2024.

length of hospital stay in daily rates, considering the patient's stay in a hospital institution for an indivisible period of ≤24 hours and assuming midnight as the reference time for the start and end of the period for the daily rate, as defined by SIH/SUS.

We estimated case-fatality rates (CFRs) by dividing the number of deaths resulting from chikungunya by the number of chikungunya hospitalizations for each year. To calculate crude hospitalization rates, we used the annual population estimates based on the 2022 demographic census for Brazil (*26*). Thus, we defined crude hospitalization rates by region and state as the ratio between the number of chikungunya hospitalizations and the total population in the year, multiplied by 100,000 population. We calculated crude chikungunya hospitalization rates by year, region, state, sex, and age group.

We standardized annual hospitalization rates by age through the direct method, using the World Health Organization global standard population (*27*). We initially calculated the annual age-adjusted rate by multiplying each age-specific hospitalization rate times the world standard population in the corresponding age group. We summed the products across all age groups and divided by the total standard population to estimate the overall annual age-standardized hospitalization rate. We used R version 4.4.1 (The R Project for Statistical Computing, https://www.r-project.org) and the dsr package (https://cran.r-project.org/src/contrib/Archive/dsr) to calculate standardized hospitalization rates and 95% CIs by applying a method based on gamma distribution.

To describe the chikungunya-related hospitalization costs covered by the government of Brazil through SUS that were recorded in the SIH/SUS database, we considered the total hospitalization cost and its 2 components: professional services, which comprise doctors' and dentists' fees; and hospital services, which include daily rates, room rates, food, and other services. We also assessed costs of daily rates for patients admitted to the ICU.

We described quantitative data by using absolute and relative frequencies and quantitative variables through measures of central tendency (mean and median) and dispersion (SD and interquartile range [IQR]). We converted cost estimates from Brazilian real (BRL) to US dollars (USD) by using annual exchange rates on July 1 of each year. We also provide the annual cost estimates in BRL adjusted for inflation to July 1, 2024, values by using the Consumer Price Index for Brazil, and we converted to USD by using the exchange rate on July 1, 2014.

We analyzed chikungunya hospitalizations registered in SIH/SUS compared with the total number of suspected and confirmed chikungunya cases notified in the Notifiable Diseases Information System (SINAN), applying the case definition adopted by the Ministry of Health (*28*) and using aggregated data available in Tabnet (*5*). Although publicly available data are restricted to chikungunya cases notified from 2017 onward, the SINAN system allows retroactive case registration and records both notification and symptom onset dates. Thus, we included all cases notified from 2017 onward that had symptom onset from January 2014 onward.

We performed data analysis by using TabWin version 4.1.5 (http://www.portalsinan.saude.gov.br/sistemas-auxiliares/tabwin), Stata version 13.0 (StataCorp LLC, https://www.stata.com), R version 4.4.1, and Microsoft Office 2024 (https://www.microsoft.com). Because we used anonymized and publicly available data, we were not required to submit the project for evaluation by a research ethics committee, as established by Resolution CNS/MS no. 510/2016.

Results

During 2014–2024, Brazil recorded 7,421 chikungunya hospitalizations in SIH/SUS, which corresponded to 0.4% of 1,698,976 suspected cases and 0.9% of 830,386 cases confirmed by laboratory or clinical-epidemiologic findings that were recorded in SINAN during the same timeframe and considering date of symptom onset. Hospitalizations followed the pattern of suspected and confirmed case curves during 2017–2024 (Appendix Figure 1, https://wwwnc.cdc.gov/EID/article/31/9/25-0554-App1.pdf).

Most (43.2%) hospitalizations occurred in 2016 and 2017, and we noted peaks in June 2016 (272 hospitalizations), February 2017 (254 hospitalizations), June 2017 (272 hospitalizations), May 2019 (147 hospitalizations), May 2022 (163 hospitalizations), March 2023 (153 hospitalizations), and April 2024 (114 hospitalizations) (Figure 2, panel A). Cases in the Northeast region accounted for peaks in June 2016 (253/272 cases) and June 2017 (240/272), comprising 93.0% of hospitalizations in June 2016 and 88.2% in June 2017. In addition, 88.3% of hospitalizations in May 2022 occurred in the Northeast region. In February 2017, the North region accounted for 53.5% of hospitalizations. In the Southeast region, peaks occurred in May 2019 (95 cases), March 2023 (95 cases), and April 2024 (67 cases) (Figure 2, panel B).

In Brazil, the highest crude hospitalization rates were in 2017 at 0.84 (95% CI 0.80–0.88)/100,000 population, and 2016 at 0.72 (95% CI 0.69–0.76)/100,000 population; we observed a smaller peak of 0.49 (95% CI 0.46–0.52)/100,000 population in 2022.

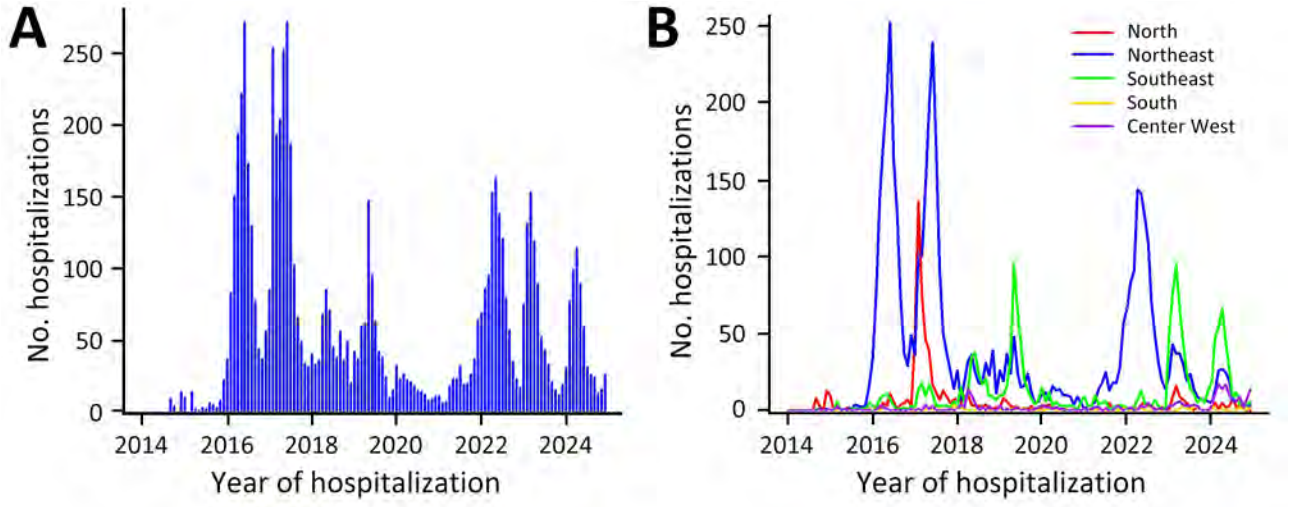

Figure 2. Number of hospitalizations per year in study of epidemiology of chikungunya hospitalizations, Brazil, 2014–2024. A) Total number of hospitalizations per year; B) number of hospitalizations per year by region.

Standardized rates closely mirrored crude rates, with minor decimal differences; therefore, we decided to focus on the crude hospitalization rates (Table 1).

Among regions, the Northeast had the highest hospitalization rate in 6 of the 11 years analyzed, reaching the highest rate in 2016 (2.46 hospitalizations/100,000 population), and the states of Maranhão (9.05/100,000 population) and Rio Grande do Norte (2.66/100,000 population) had the highest rates that year (Table 2). Maranhão had the highest hospitalization rates in 2018 (2.86/100,000 population) and 2022 (4.6/100,000 population) (Figure 3; Appendix Figure 2).

Overall, most (55.8%) hospitalized chikungunya patients were female, and 63.5% of chikungunya hospitalizations were among persons who identified as brown or black, a pattern observed throughout the evaluated years. The median age of hospitalized patients was 34 (IQR 12–58) years and ranged from 27 years in 2015 (IQR 6–48 years) and 2021 (IQR 9–49 years) to 43 (IQR 13–65) years in 2024. Cases were concentrated among persons 1–19 years of age, who comprised 31.4% of overall hospitalizations. In 2017, the year with the highest number of hospitalizations, the predominant age groups were 1–9 years (236 [23%] hospitalizations), 10–19 years (205 [13.9%]), and 30–39 years (157 [10.6%]) (Table 3; Appendix Tables 1, 2).

When we stratified annual crude hospitalization rates by sex and age group, we observed similar patterns for male and female sex in age groups from 0 to 79 years, with few exceptions (Appendix Figures 3, 4). However, we observed notable differences in the 80–84, 85–89, and ≥90 age groups. For 2016, 2018, 2022, and 2023, we observed higher hospitalization rates among men 80–84 years of age compared with women in the same age group, and the largest difference was in 2019, when the hospitalization rate in men was 4 times higher than that observed among women (1.29 vs. 0.29/100,000 population) (Appendix Figures 3, 4). For persons 85–89 years of age, we observed the highest hospitalization rate in 2016, when the rate for men was nearly twice that of women (4.25 vs. 2.5/100,000 population). Persons ≥90 years of age had the highest recorded hospitalization rates during the study period, reaching 9.22/100,000 population among men

Table 1. Annual crude and age-standardized hospitalization rates from a study of epidemiology of chikungunya hospitalizations, Brazil, 2014–2024

Year	No. hospitalizations	Population	Crude hospitalization rate (95% CI)	Age-standardized hospitalization rate (95% CI)
2014	27	200,811,131	0.013 (0.009–0.020)	0.013 (0.009–0.019)
2015	76	202,403,642	0.038 (0.030–0.047)	0.039 (0.030–0.049)
2016	1,476	203,871,925	0.724 (0.688–0.762)	0.730 (0.693–0.769)
2017	1,729	205,211,557	0.843 (0.803–0.883)	0.868 (0.827–0.910)
2018	577	206,529,038	0.279 (0.257–0.303)	0.279 (0.257–0.303)
2019	635	207,900,099	0.305 (0.282–0.330)	0.307 (0.284–0.332)
2020	211	209,164,889	0.101 (0.088–0.115)	0.101 (0.088–0.116)
2021	286	210,103,642	0.136 (0.121–0.153)	0.142 (0.126–0.160)
2022	1,037	210,862,983	0.492 (0.462–0.523)	0.482 (0.452–0.513)
2023	762	211,695,158	0.360 (0.335–0.386)	0.351 (0.326–0.377)
2024	605	212,583,750	0.285 (0.262–0.308)	0.281 (0.258–0.305)

in 2016, nearly 4 times higher than among women (2.66/100,000 population) (Appendix Figure 4).

Overall, the average length of hospital stay for chikungunya patients was 3.8 ± 0.1 days, and the median stay was 3 (IQR 2–4) days, without substantial variations by sex or age during the study period (Appendix Table 1). Of note, patients admitted to the ICU had longer stays of 13.1 ± 1.1 days than those not admitted to the ICU (3.6 ± 0.1 days). In addition, patients who died during hospitalization also had longer average stays (8.0 ± 1.5 days) than patients who survived (3.7 ± 0.1 days).

Table 2. Crude hospitalization rates by region and state in study of epidemiology of chikungunya hospitalizations, Brazil, 2014–2024*

Region, state	No. hospitalizations (rate/100,000 population)										
	2014	2015	2016	2017	2018	2019	2020	2021	2022	2023	2024
North											
Acre	0	0	0	1 (0.12)	0	0	1 (0.12)	1 (0.12)	1 (0.11)	2 (0.23)	4 (0.45)
Amapá	24 (3.26)	18 (2.41)	1 (0.13)	4 (0.52)	3 (0.39)	0	0	1 (0.13)	1 (0.13)	1 (0.13)	1 (0.12)
Amazonas	0	0	2 (0.05)	0	0	0	3 (0.07)	0	0	0	1 (0.02)
Pará	0	1 (0.01)	38 (0.46)	330 (3.99)	35 (0.42)	26 (0.31)	3 (0.04)	9 (0.11)	13 (0.15)	7 (0.08)	15 (0.17)
Rondônia	0	0	7 (0.42)	4 (0.42)	1 (0.06)	2 (0.12)	0	1 (0.06)	0	2 (0.11)	2 (0.11)
Roraima	0	0	0	29 (5.14)	7 (1.19)	1 (0.16)	0	0	0	0	0
Tocantins	0	0	1 (0.07)	45 (3)	6 (0.4)	1 (0.07)	4 (0.26)	2 (0.13)	6 (0.39)	38 (2.42)	8 (0.51)
Total	24 (0.14)	19 (0.11)	49 (0.28)	413 (2.35)	52 (0.29)	30 (0.17)	11 (0.06)	14 (0.08)	21 (0.11)	50 (0.27)	31 (0.17)
Northeast											
Alagoas	0	7 (0.22)	43 (1.35)	4 (0.13)	9 (0.28)	6 (0.19)	0	4 (0.12)	3 (0.09)	3 (0.09)	3 (0.09)
Bahia	2 (0.01)	9 (0.06)	112 (0.77)	124 (0.85)	8 (0.05)	17 (0.12)	38 (0.26)	22 (0.15)	57 (0.38)	41 (0.28)	25 (0.17)
Ceará	0	0	201 (2.27)	484 (5.42)	39 (0.43)	16 (0.18)	5 (0.06)	2 (0.02)	273 (2.98)	31 (0.34)	28 (0.3)
Maranhão	0	4 (0.06)	621 (9.05)	497 (7.21)	198 (2.86)	127 (1.83)	47 (0.67)	47 (0.67)	366 (3.2)	93 (1.33)	12 (0.17)
Paraíba	0	1 (0.03)	77 (1.95)	13 (0.33)	12 (0.3)	50 (1.24)	9 (0.22)	43 (1.05)	148 (3.6)	45 (1.09)	32 (0.77)
Pernambuco	0	14 (0.15)	192 (2.07)	8 (0.09)	8 (0.09)	11 (0.12)	14 (0.15)	59 (0.62)	20 (0.21)	4 (0.04)	14 (0.15)
Piauí	0	0	7 (0.21)	71 (2.16)	8 (0.24)	12 (0.36)	0	1 (0.03)	59 (1.76)	31 (0.92)	30 (0.89)
Rio Grande do Norte	0	0	89 (2.66)	5 (0.15)	2 (0.06)	16 (0.47)	5 (0.15)	5 (0.15)	8 (0.23)	5 (0.15)	2 (0.06)
Sergipe	0	0	22 (1)	1 (0.05)	0	2 (0.09)	2 (0.09)	21 (0.93)	54 (2.38)	3 (0.13)	1 (0.04)
Total	2 (0.01)	35 (0.06)	1,364 (2.46)	1,207 (2.17)	284 (0.51)	257 (0.46)	120 (0.21)	204 (0.36)	944 (1.66)	256 (0.45)	147 (0.26)
Southeast											
Espírito Santo	0	0	2 (0.05)	3 (0.08)	6 (0.15)	15 (0.38)	9 (0.22)	7 (0.17)	2 (0.05)	10 (0.25)	17 (0.41)
Minas Gerais	0	2 (0.01)	7 (0.03)	59 (0.29)	30 (0.14)	37 (0.18)	20 (0.1)	28 (0.13)	32 (0.15)	376 (1.77)	223 (1.05)
Rio de Janeiro	0	4 (0.02)	27 (0.16)	15 (0.09)	147 (0.86)	256 (1.49)	22 (0.13)	4 (0.02)	6 (0.03)	9 (0.05)	31 (0.18)
São Paulo	1 (0)	10 (0.02)	16 (0.04)	14 (0.03)	13 (0.03)	21 (0.05)	12 (0.03)	13 (0.03)	11 (0.02)	15 (0.03)	29 (0.06)
Total	1 (0)	16 (0.02)	52 (0.06)	91 (0.11)	196 (0.23)	329 (0.38)	63 (0.07)	52 (0.06)	51 (0.06)	410 (0.46)	300 (0.34)
South											
Paraná	0	0	2 (0.02)	2 (0.02)	2 (0.02)	1 (0.01)	1 (0.01)	2 (0.02)	0	12 (0.1)	9 (0.08)
Rio Grande do Sul	0	0	0	5 (0.04)	1 (0.01)	2 (0.02)	0	2 (0.02)	1 (0.01)	0	1 (0.01)
Santa Catarina	0	1 (0.01)	2 (0.03)	1 (0.01)	1 (0.01)	5 (0.07)	3 (0.04)	0	2 (0.03)	0	0
Total	0	1 (0)	4 (0.01)	8 (0.03)	4 (0.01)	8 (0.03)	4 (0.01)	4 (0.01)	3 (0.01)	12 (0.04)	10 (0.03)
Center West											
Distrito Federal	0	2 (0.07)	5 (0.18)	1 (0.04)	0	1 (0.03)	0	0	1 (0.03)	10 (0.34)	2 (0.07)
Goiás	0	3 (0.05)	0	4 (0.06)	3 (0.04)	4 (0.06)	2 (0.03)	9 (0.13)	7 (0.1)	6 (0.08)	27 (0.37)
Mato Grosso	0	0	2 (0.06)	4 (0.14)	36 (1.03)	4 (0.11)	9 (0.25)	2 (0.05)	6 (0.16)	9 (0.24)	85 (2.22)
Mato Grosso do Sul	0	0	0	1 (0.04)	2 (0.07)	2 (0.07)	2 (0.07)	1 (0.04)	4 (0.14)	9 (0.31)	3 (0.21)
Total	0	5 (0.03)	7 (0.04)	10 (0.06)	41 (0.26)	11 (0.07)	13 (0.08)	12 (0.07)	18 (0.11)	34 (0.2)	117 (0.69)
Brazil total	27 (0.01)	76 (0.04)	1,476 (0.72)	1,729 (0.84)	577 (0.28)	635 (0.31)	211 (0.1)	286 (0.14)	1,037 (0.49)	762 (0.36)	605 (0.28)

*Information obtained from the Brazil Ministry of Health Datasus (https://datasus.saude.gov.br/transferencia-de-arquivos).

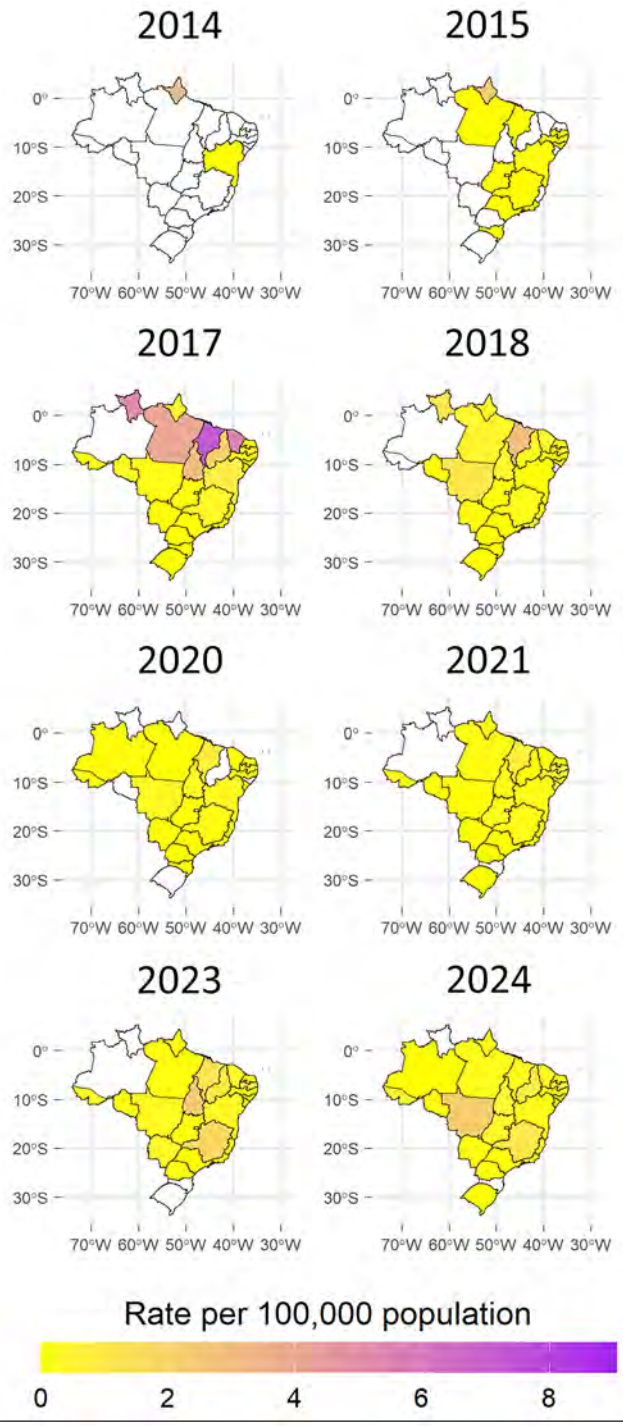

Figure 3. Annual hospitalization rates per region from study of epidemiology of chikungunya hospitalizations, Brazil, 2014–2024.

Among all 7,421 chikungunya hospitalizations, 104 (1.4%) patients were admitted to the ICU, and that population was equally divided by male and female patients, 52 (50.0%) in each group. The age groups with the highest ICU admissions were adults ≥85 years of age (3.3%) and children <5 years of age (2.7%). The ages of patients admitted to the ICU varied greatly; the mean was 38.6 ± 31.3 years, and the median was 37.5 (IQR 7.5–69) years. The highest percentages of ICU admissions were recorded in 2024 (3.5%) and 2023 (2.1%); admissions were more frequent in children <5 years of age (2.7%), but rates were similar among boys (2.7%) and girls (2.6%). Among persons ≥60 years of age, 1.9% were admitted to the ICU, predominantly men (2.3% vs. 1.6% women) (Table 3; Appendix Table 2).

Table 3. Patient characteristics from 7,421 chikungunya hospitalizations covered by the unified health system, Brazil, 2014–2024*

Characteristics	Total	Year, no. (%)										
		2014	2015	2016	2017	2018	2019	2020	2021	2022	2023	2024
Sex												
M	3,282 (44.2)	10 (37)	34 (44.7)	620 (42)	787 (45.5)	266 (46.1)	285 (44.9)	104 (49.3)	130 (45.5)	441 (42.5)	340 (44.6)	265 (43.8)
F	4,139 (55.8)	17 (63)	42 (55.3)	856 (58)	942 (54.5)	311 (53.9)	350 (55.1)	107 (50.7)	156 (54.5)	596 (57.5)	422 (55.4)	340 (56.2)
Race, ethnicity												
White	1,009 (13.6)	2 (7.4)	18 (23.7)	160 (10.8)	140 (8.1)	90 (15.6)	164 (25.8)	30 (14.2)	37 (12.9)	77 (7.4)	139 (18.2)	152 (25.1)
Black	182 (2.5)	0	3 (3.9)	19 (1.3)	33 (1.9)	20 (3.5)	32 (5)	8 (3.8)	2 (0.7)	6 (0.6)	35 (4.6)	24 (4.0)
Brown	4,526 (61)	5 (18.5)	20 (26.3)	815 (55.2)	1,099 (63.6)	337 (58.4)	293 (46.1)	133 (63)	153 (53.5)	742 (71.6)	533 (69.9)	396 (65.5)
Asian	360 (4.9)	0	1 (1.3)	148 (10)	104 (6)	29 (5)	34 (5.4)	3 (1.4)	2 (0.7)	2 (0.2)	9 (1.2)	28 (4.6)
Indigenous	9 (0.1)	0	0	1 (0.1)	0	2 (0.3)	1 (0.2)	0	0	0	0	5 (0.8)
Not reported	1,335 (18)	20 (74.1)	34 (44.7)	333 (22.6)	353 (20.4)	99 (17.2)	111 (17.5)	37 (17.5)	92 (32.2)	210 (20.3)	46 (6)	0
Age group, y												
<1	228 (3.1)	2 (7.4)	10 (13.2)	56 (3.8)	59 (3.4)	10 (1.7)	17 (2.7)	3 (1.4)	22 (7.7)	26 (2.5)	8 (1)	15 (2.5)
1–9	1,262 (17.0)	1 (3.7)	15 (19.7)	236 (16)	386 (22.3)	71 (12.3)	89 (14)	35 (16.6)	56 (19.6)	147 (14.2)	119 (15.6)	107 (17.7)
10–19	1,072 (14.4)	4 (14.8)	10 (13.2)	205 (13.9)	297 (17.2)	88 (15.3)	110 (17.3)	23 (10.9)	46 (16.1)	120 (11.6)	96 (12.6)	73 (12.1)
20–29	796 (10.7)	6 (22.2)	5 (6.6)	154 (10.4)	154 (8.9)	93 (16.1)	73 (11.5)	40 (19)	32 (11.2)	115 (11.1)	75 (9.8)	49 (8.1)
30–39	799 (10.8)	6 (22.2)	8 (10.5)	157 (10.6)	183 (10.6)	95 (16.5)	76 (12)	31 (14.7)	33 (11.5)	99 (9.5)	71 (9.3)	40 (6.6)
40–49	770 (10.4)	3 (11.1)	10 (13.2)	151 (10.2)	157 (9.1)	90 (15.6)	71 (11.2)	21 (10)	26 (9.1)	112 (10.8)	75 (9.8)	54 (8.9)
50–59	734 (9.9)	2 (7.4)	10 (13.2)	126 (8.5)	152 (8.8)	53 (9.2)	76 (12)	16 (7.6)	26 (9.1)	124 (12)	75 (9.8)	74 (12.2)
60–69	657 (8.9)	1 (3.7)	2 (2.6)	125 (8.5)	122 (7.1)	36 (6.2)	64 (10.1)	17 (8.1)	19 (6.6)	117 (11.3)	74 (9.7)	80 (13.2)
70–79	578 (7.8)	1 (3.7)	3 (3.9)	133 (9)	120 (6.9)	22 (3.8)	35 (5.5)	17 (8.1)	18 (6.3)	97 (9.4)	72 (9.4)	60 (9.9)
80–89	412 (5.6)	1 (3.7)	2 (2.6)	105 (7.1)	77 (4.5)	16 (2.8)	21 (3.3)	7 (3.3)	4 (1.4)	64 (6.2)	73 (9.6)	42 (6.9)
≥90	113 (1.5)	0	1 (1.3)	28 (1.9)	22 (1.3)	3 (0.5)	3 (0.5)	1 (0.5)	4 (1.4)	16 (1.5)	24 (3.1)	11 (1.8)
ICU admission												
N	7,317 (98.6)	27 (100)	74 (97.4)	1,466 (99.3)	1,715 (99.2)	571 (99)	624 (98.3)	206 (97.6)	281 (98.3)	1,023 (98.6)	746 (97.9)	584 (96.5)
Y	104 (1.4)	0	2 (2.6)	10 (0.7)	14 (0.8)	6 (1)	11 (1.7)	5 (2.4)	5 (1.7)	14 (1.4)	16 (2.1)	21 (3.5)
Death												
N	7,337 (98.9)	27 (100)	75 (98.7)	1,449 (98.2)	1,709 (98.8)	576 (99.8)	631 (99.4)	206 (97.6)	286 (100)	1,028 (99.1)	754 (99)	596 (98.5)
Y	84 (1.1)	0	1 (1.3)	27 (1.8)	20 (1.2)	1 (0.2)	4 (0.6)	5 (2.4)	0	9 (0.9)	8 (1)	9 (1.5)

*Information obtained from the Brazil Ministry of Health Datasus (https://datasus.saude.gov.br/transferencia-de-arquivos). ICU, intensive care unit.

Among the 84 hospitalized patients who died, 54.8% were male, 45.2% were female, and 26.4% were ≥80 years of age (mean 69.4 ± 25.8 years; median 79.0, IQR 62–86 years). The highest CFRs were recorded in 2020 (2.4%) and 2016 (1.8%) and substantially increased among persons ≥60 years of age, reaching 10.3% among persons 85–89 years of age and 11.5% among persons ≥90 years of age. Estimated rates were higher among men than women for the 85–89 age group (14.1% vs. 6.41%) and the ≥90 age group (13.7% vs. 9.7%). In addition, the CFR was higher among persons admitted to the ICU than those who were not (21.1% vs. 0.8%) (Table 3; Appendix Table 3).

During 2014–2024, the total cost of chikungunya hospitalizations covered by SUS was ≈US $560,746 and the average cost per patient was ≈US $76.26 (median $47.38) (Appendix Tables 4, 5). After adjusting for inflation to 2024 values, total hospitalization costs for chikungunya in BRL increased by 26.7%, from BRL $2.28 million to BRL $2.89 million. However, when we used the 2024 exchange rate (1 BRL = US $0.179036) to convert inflation-adjusted values to USD, the total cost decreased to US $516,921.61, reflecting the cumulative depreciation of the BRL relative to the USD over the study period (Appendix Table 6).

The highest total hospitalization costs were recorded in 2017 (US $120,960.10) and 2016 (US

$120,336.60). In contrast, the highest average costs per patient were observed in 2024 (US $85.69) and 2020 (US $84.24). Across the study period, hospital services accounted for 84.2% of the total chikungunya-related hospitalization costs, ranging from 79.5% in 2014 to 85.8% in 2020. ICU costs corresponded to 19.6% of the total hospitalization expenses during 2014–2024, reaching 42.1% in 2020 (Appendix Table 4).

Discussion

This study examined chikungunya-related hospitalizations in Brazil since 2014, the year when the first autochthonous cases were reported in Oiapoque (Amapá state) and in Feira de Santana (Bahia state) (*29*). SIH/SUS data show ≈0.4% of suspected and ≈0.9% of confirmed chikungunya cases required hospitalization during 2014–2024, consistent with previous estimates of 0.6%–13.0% reported during outbreaks in various countries (*1*,*10*,*21*). Moreover, the pattern of chikungunya-related hospitalizations followed epidemic peaks in Brazil, particularly in the Northeast (2016, 2017, and 2022), North (2017), and Southeast (2019, 2023, and 2024) regions; we also noted an increase in the Central West region in 2024. Throughout the study period, publications documented chikungunya outbreaks in Northeast states, including in Maranhão (*30*), Bahia (*31*), and Alagoas (*32*,*33*), as well as in the North (*34*) and Southeast regions (*35*,*36*). Although cases have been reported in the South, most were likely imported from other regions (*37*). The increase in suspected and confirmed chikungunya cases since 2022 reflects multiple factors, including increased transmission in several states, particularly in the Southeast and Central West regions, and improved diagnostic capacity and clinical awareness. During the COVID-19 pandemic, disruptions in surveillance and healthcare services, combined with the prioritization of hospital resources for COVID-19 patients, likely contributed to underreporting of arboviral diseases and lower chikungunya hospitalization rates during 2020–2021.

We observed higher hospitalization rates among men ≥80 years of age compared with women in the same age groups, consistent with a study in Martinique and Guadeloupe from 2013–2015, where older adults, particularly persons ≥75 years of age, had increased hospitalization rates and ICU admissions (*10*). That study also reported an ICU admission rate of 7.4% among hospitalized patients, which is substantially higher than the 1.4% rate observed in Brazil during 2014–2024.

We observed an overall CFR of 1.1%, and CFR peaked at 2.4% in 2020. In another study that used data linked between the SINAN and Brazil's mortality information system (SIM) for 2016 and 2017 (*38*), estimated CFR was 0.08% (0.8 death/1,000 cases) based solely on SINAN data. After adjusting for underreporting using SIM data, the corrected CFR increased to 0.57% (5.7 deaths/1,000 cases) (*38*). Our higher rate reflects the focus on hospitalized cases, which represent more severe clinical presentations.

In our study, CFR was substantially higher in men ≥85 years of age, and ICU admission correlated with CFR, which supports the hypothesis that those patients experienced more severe illness. During the 2014–2015 chikungunya outbreak in French Polynesia, 64 patients with confirmed chikungunya infection were admitted to ICUs, of whom 21 (32.8%) had severe sepsis or septic shock develop and 18 (28.1%) died (*39*). A 2025 meta-analysis also identified male sex, age ≥60 years, and chronic diseases, particularly diabetes mellitus, hypertension, and chronic kidney disease, as risk factors for chikungunya-related death (*20*). In our study, lack of data on underlying conditions in SIH/SUS precluded further risk assessment.

Among our cohort, 62 deaths occurred without ICU admission, which might indicate a lack of available ICU beds in the healthcare network or challenges in case management and referral processes. Furthermore, no deaths were recorded among persons 5–19 years of age, but ICU admissions among children <5 years reached 2.3% and CFR was 0.6% in that age group. Those findings are consistent with a previous study (*40*) that indicated that children, particularly children <6 months of age, are more susceptible to severe chikungunya complications, including neurologic and cardiac involvement, often leading to hospitalization (*40*).

Overall, the actual mortality burden of chikungunya is likely underreported because of limited clinical suspicion and co-circulating arboviruses, such as dengue. The extent of underreporting has been estimated to reach as high as 98% in some settings. For instance, in Minas Gerais, Brazil, the number of excess deaths was estimated to be 60 times higher than confirmed chikungunya deaths in 2023 (*41*); Pernambuco, Brazil, recorded 4,505 excess deaths in 2016 compared with 94 deaths officially attributed to chikungunya (*42*); and Puerto Rico identified 1,310 excess chikungunya deaths in 2014, but only 31 were confirmed through routine surveillance (*43*).

Another study analyzed hospitalizations from all causes in the SIH/SUS database from July 2018–

June 2019 (*44*). That study reported 9.3 million hospitalizations and a total cost of BRL $183 billion (US $47.1 billion), ≈BRL $2,000 (US $515.30) per hospitalization, and an average length of stay of 6.9 days (*44*). Infectious diseases accounted for 9% of bed days and 21% of ICU days. In our study, we found ICU expenses comprised 19.6% of chikungunya-related hospitalization costs.

In another study of hospitalization costs (*45*), the authors estimated the cost of 256 chikungunya hospitalizations in Rio de Janeiro in 2019 and found costs totaled BRL $88,926.72 (US $23,235.39), a small share of the BRL $279.8 million (US $73.1 million) in total direct and indirect chikungunya-related costs. In our study, the cost of chikungunya-related hospitalizations is modest compared with the total estimated SUS hospitalization costs described by others (*44*). Indeed, the literature indicates that indirect costs account for the largest part of the total chikungunya-related cost, particularly during the chronic phase, which can be up to 5 times higher than the direct costs (*46*).

Some limitations of our study are inherent to secondary data sources, such as the quality of data entry and the absence of relevant variables for analyzing the topic of interest. The variables of sex and date of birth had no missing or inconsistent values. However, race/skin color was missing in 18% of chikungunya-related hospitalizations; this category was previously documented (*47*) and can distort observed differences between racial groups. Moreover, we could not identify whether the same patient was hospitalized ≥1 time during the study period or was admitted to private healthcare facilities. In addition, data on underlying conditions were not available, so we were unable to assess their role in the risk of hospitalization or death. We were not able to differentiate whether the hospitalizations for chikungunya occurred during the acute, post-acute, or chronic phase of the disease; thus, we were unable to investigate at which stage of chikungunya the risk of hospitalization is highest. Because we focused on chikungunya as the primary diagnosis at admission, this study might not have captured cases admitted during the postacute or chronic phases, particularly when hospitalizations result from the decompensation of underlying conditions. In addition, SIH/SUS lacks data on cause of death, possibly underestimating death related to complications of chikungunya; thus, our analysis was limited to reporting deaths among patients hospitalized due to chikungunya, which likely underestimates the overall mortality rate associated with the disease. Finally, SIH/SUS publicly available data do not include disaggregated cost components, which prevented assessment of the relative contribution of specific services to overall hospitalization costs.

In conclusion, although the SIH/SUS is an administratively collected database primarily intended for recording hospitalizations funded by the SUS and for reimbursing healthcare facilities for services provided, the system serves as a vital source of information on hospitalizations in Brazil, where most hospitalizations occur in SUS-affiliated facilities (*22*). Although chikungunya-related hospitalization costs for SUS are not substantial, SIH/SUS records provide insights into the profile of the most severe cases of the disease, including ICU admissions and CFR. Those data are particularly valuable for supporting the planning and organization of healthcare facilities to provide appropriate care according to the severity of each case, which will be especially vital in outbreak and epidemic scenarios.

About the Author

Dr. Pedi is a veterinarian with the Brazilian Ministry of Health and serves at the Oswaldo Cruz Foundation, where she is a member of the Research Group on Science, Technology, and Innovation for Governance and Territorial Development. Her primary research interests include arbovirus diseases, public health emergencies, and the One Health framework.

References

1. Bartholomeeusen K, Daniel M, LaBeaud DA, Gasque P, Peeling RW, Stephenson KE, et al. Chikungunya fever. Nat Rev Dis Primers. 2023;9:17. https://doi.org/10.1038/s41572-023-00429-2
2. Krambrich J, Mihalič F, Gaunt MW, Bohlin J, Hesson JC, Lundkvist Å, et al. The evolutionary and molecular history of a chikungunya virus outbreak lineage. PLoS Negl Trop Dis. 2024;18:e0012349. https://doi.org/10.1371/journal.pntd.0012349
3. Volk SM, Chen R, Tsetsarkin KA, Adams AP, Garcia TI, Sall AA, et al. Genome-scale phylogenetic analyses of chikungunya virus reveal independent emergences of recent epidemics and various evolutionary rates. J Virol. 2010;84:6497–504. https://doi.org/10.1128/JVI.01603-09
4. World Health Organization. Chikungunya [cited 2025 Mar 23]. https://www.who.int/news-room/fact-sheets/detail/chikungunya
5. Brazil Ministry of Health. Chikungunya fever—notifications recorded in the Notifiable Diseases Information System [in Portuguese] [cited 2025 Mar 23]. http://tabnet.datasus.gov.br/cgi/tabcgi.exe?sinannet/cnv/chikunbr.def
6. Skalinski LM, Santos AES, Paixão E, Itaparica M, Barreto F, da Conceição Nascimento Costa M, et al. Chikungunya seroprevalence in population-based studies: a systematic review and meta-analysis. Arch Public Health. 2023;81:80. https://doi.org/10.1186/s13690-023-01081-8
7. de Souza WM, Ribeiro GS, de Lima STS, de Jesus R, Moreira FRR, Whittaker C, et al. Chikungunya: a

decade of burden in the Americas. Lancet Reg Health Am. 2024;30:100673. https://doi.org/10.1016/j.lana.2023.100673
8. Rama K, de Roo AM, Louwsma T, Hofstra HS, Gurgel do Amaral GS, Vondeling GT, et al. Clinical outcomes of chikungunya: a systematic literature review and meta-analysis. PLoS Negl Trop Dis. 2024;18:e0012254. https://doi.org/10.1371/journal.pntd.0012254
9. Cerbino-Neto J, Mesquita EC, Amancio RT, Brasil PEAAD. Events preceding death among chikungunya virus infected patients: a systematic review. Rev Soc Bras Med Trop. 2020; 53:e04312019. https://doi.org/10.1590/0037-8682-0431-2019
10. Dorléans F, Hoen B, Najioullah F, Herrmann-Storck C, Schepers KM, Abel S, et al. Outbreak of chikungunya in the French Caribbean islands of Martinique and Guadeloupe: findings from a hospital-based surveillance system (2013–2015). Am J Trop Med Hyg. 2018;98:1819–25. https://doi.org/10.4269/ajtmh.16-0719
11. Rajapakse S, Rodrigo C, Rajapakse A. Atypical manifestations of chikungunya infection. Trans R Soc Trop Med Hyg. 2010;104:89–96. https://doi.org/10.1016/j.trstmh.2009.07.031
12. Economopoulou A, Dominguez M, Helynck B, Sissoko D, Wichmann O, Quenel P, et al. Atypical chikungunya virus infections: clinical manifestations, mortality and risk factors for severe disease during the 2005–2006 outbreak on Réunion. Epidemiol Infect. 2009;137:534–41. https://doi.org/10.1017/S0950268808001167
13. Bonifay T, Prince C, Neyra C, Demar M, Rousset D, Kallel H, et al.; Char Chik Working group. Atypical and severe manifestations of chikungunya virus infection in French Guiana: a hospital-based study. PLoS One. 2018;13:e0207406. https://doi.org/10.1371/journal.pone.0207406
14. Santiago RA, Bavaresco SPP, Citrangulo SG, Medronho RA, Sampaio V, Costa AJL. Clinical manifestations associated with the chronic phase of chikungunya fever: a systematic review of prevalence. PLoS Negl Trop Dis. 2025;19:e0012810. https://doi.org/10.1371/journal.pntd.0012810
15. Paixão ES, Rodrigues LC, Costa MDCN, Itaparica M, Barreto F, Gérardin P, et al. Chikungunya chronic disease: a systematic review and meta-analysis. Trans R Soc Trop Med Hyg. 2018;112:301–16. https://doi.org/10.1093/trstmh/try063
16. Hsu CH, Cruz-Lopez F, Vargas Torres D, Perez-Padilla J, Lorenzi OD, Rivera A, et al. Risk factors for hospitalization of patients with chikungunya virus infection at sentinel hospitals in Puerto Rico. PLoS Negl Trop Dis. 2019; 13:e0007084. https://doi.org/10.1371/journal.pntd.0007084
17. Crosby L, Perreau C, Madeux B, Cossic J, Armand C, Herrmann-Storke C, et al. Severe manifestations of chikungunya virus in critically ill patients during the 2013–2014 Caribbean outbreak. Int J Infect Dis. 2016;48:78–80. https://doi.org/10.1016/j.ijid.2016.05.010
18. Brito C, Falcão MB, de Albuquerque MFPM, Cerqueira-Silva T, Teixeira MG, Franca RFO. Chikungunya: from hypothesis to evidence of increased severe disease and fatalities. Viruses. 2025;17:62. https://doi.org/10.3390/v17010062
19. Cerqueira-Silva T, Pescarini JM, Cardim LL, Leyrat C, Whitaker H, Antunes de Brito CA, et al. Risk of death following chikungunya virus disease in the 100 Million Brazilian Cohort, 2015–18: a matched cohort study and self-controlled case series. Lancet Infect Dis. 2024;24:504–13. https://doi.org/10.1016/S1473-3099(23)00739-9
20. Micheleto JPC, Melo KA, Veloso FCS, Kassar SB, Oliveira MJC. Risk factors for mortality in patients with chikungunya: a systematic review and meta-analysis. Trop Med Int Health. 2025;30:235–45. https://doi.org/10.1111/tmi.14088
21. Silva Junior GBD, Pinto JR, Mota RMS, Pires Neto RDJ, Daher EF. Impact of chronic kidney disease on chikungunya virus infection clinical manifestations and outcome: highlights during an outbreak in northeastern Brazil. Am J Trop Med Hyg. 2018;99:1327–30. https://doi.org/10.4269/ajtmh.18-0531
22. Brazilian Institute of Geography and Statistics. 2019 National Health Survey: information on households, access to, and use of health services. Brazil, major regions, and states [in Portuguese]. Rio de Janeiro: The Institute; 2020.
23. Bittencourt SA, Camacho LA, Leal MC. Hospital information systems and their application in public health. Cad Saude Publica. 2006;22:19–30. https://doi.org/10.1590/S0102-311X2006000100003
24. Brazil Ministry of Health, Secretariat of Health Care. SIH–SUS Hospital Information System: technical operational manual of the system [in Portuguese]. Brasília: The Ministry; 2017.
25. Government of Brazil. Official Diary of the Union: GM/MS Ordinance No. 344, of February 1, 2017. Provides for filling out the race/color question in health information system forms [in Portuguese]. Brasília: The Government; 2017.
26. Brazilian Institute of Geography and Statistics. Methodological notes 01/2024: population projections, Brazil and federation units, estimates and projections, 2024 review [in Portuguese]. Rio de Janeiro: The Institute; 2024.
27. Ahmad OB, Boschi-Pinto C, Lopez AD, Murray CJ, Lozano R, Inoue M. Age standardization of rates: a new WHO standard. Geneva: World Health Organization; 2001.
28. Brazil Ministry of Health, Secretariat of Health and Environmental Surveillance, Department of Strategic Actions in Epidemiology and Health and Environmental Surveillance. Health surveillance guide, 6th edition [in Portuguese]. Brasília: The Ministry; 2024.
29. Nunes MR, Faria NR, de Vasconcelos JM, Golding N, Kraemer MU, de Oliveira LF, et al. Emergence and potential for spread of chikungunya virus in Brazil. BMC Med. 2015;13:102. https://doi.org/10.1186/s12916-015-0348-x
30. Aragão CF, Cruz ACR, Nunes Neto JP, Monteiro HAO, da Silva EVP, da Silva SP, et al. Circulation of chikungunya virus in *Aedes aegypti* in Maranhão, northeast Brazil. Acta Trop. 2018;186:1–4. https://doi.org/10.1016/j.actatropica.2018.06.022
31. Tauro LB, Cardoso CW, Souza RL, Nascimento LC, Santos DRD, Campos GS, et al. A localized outbreak of chikungunya virus in Salvador, Bahia, Brazil. Mem Inst Oswaldo Cruz. 2019;114:e180597. https://doi.org/10.1590/0074-02760180597
32. Tanabe ELL, Tanabe ISB, Santos ECD, Marques JPDS, Borges AA, Lima MC, et al. Report of East-Central South African chikungunya virus genotype during the 2016 outbreak in the Alagoas State, Brazil. Rev Inst Med Trop São Paulo. 2018;60:e19. https://doi.org/10.1590/s1678-9946201860019
33. Charlys da Costa A, Thézé J, Komninakis SCV, Sanz-Duro RL, Felinto MRL, Moura LCC, et al. Spread of chikungunya virus East/Central/South African genotype in northeast Brazil. Emerg Infect Dis. 2017;23:1742–4. https://doi.org/10.3201/eid2310.170307
34. Naveca FG, Claro I, Giovanetti M, de Jesus JG, Xavier J, Iani FCM, et al. Genomic, epidemiological and digital surveillance of chikungunya virus in the Brazilian Amazon. PLoS Negl Trop Dis. 2019;13:e0007065. https://doi.org/10.1371/journal.pntd.0007065
35. Lessa-Aquino C, Trinta KS, Pestana CP, Ribeiro MO, Sucupira MVF, Boia MN, et al. Detection of East/Central/South African genotype chikungunya virus during an outbreak in a southeastern state of Brazil.

Epidemiol Infect. 2018;146:2056–8. https://doi.org/10.1017/S0950268818002467
36. Souza TM, Azeredo EL, Badolato-Corrêa J, Damasco PV, Santos C, Petitinga-Paiva F, et al. First report of the East-Central South African genotype of chikungunya virus in Rio de Janeiro, Brazil. PLoS Curr. 2017;9:9. https://doi.org/10.1371/currents.outbreaks.4200119978d62ccaa454599cd2735727
37. Resck MEB, Câmara DCP, Dos Santos FB, Dos Santos JPC, Alto BW, Honório NA. Spatial-temporal distribution of chikungunya virus in Brazil: a review on the circulating viral genotypes and *Aedes* (*Stegomyia*) *albopictus* as a potential vector. Front Public Health. 2024;12:1496021. https://doi.org/10.3389/fpubh.2024.1496021
38. Frutuoso LCV, Freitas ARR, Cavalcanti LPG, Duarte EC. Estimated mortality rate and leading causes of death among individuals with chikungunya in 2016 and 2017 in Brazil. Rev Soc Bras Med Trop. 2020;53:e20190580. https://doi.org/10.1590/0037-8682-0580-2019
39. Koeltz A, Lastere S, Jean-Baptiste S. Intensive care admissions for severe chikungunya virus infection, French Polynesia. Emerg Infect Dis. 2018;24:794–6. https://doi.org/10.3201/eid2404.161536
40. Ernould S, Walters H, Alessandri JL, Llanas B, Jaffar MC, Robin S, et al. Chikungunya in paediatrics: epidemic of 2005–2006 in Saint-Denis, Reunion Island. Arch Pediatr. 2008;15:253–62. https://doi.org/10.1016/j.arcped.2007.10.019
41. Ribas-Freitas AR, Neto ASL, Rodrigues R, Oliveira EAd, Andrade-Jr JS, Cavalcanti LPG. Excess mortality associated with chikungunya epidemic in southeast Brazil, 2023. Front Trop Dis. 2024;5:1466207. https://doi.org/10.3389/fitd.2024.1466207
42. Freitas ARR, Cavalcanti L, Von Zuben AP, Donalisio MR. Excess mortality related to chikungunya epidemics in the context of co-circulation of other arboviruses in Brazil. PLoS Curr. 2017;9:22–3. https://doi.org/10.1371/currents.outbreaks.14608e586cd321d8d5088652d7a0d884
43. Freitas ARR, Donalisio MR, Alarcón-Elbal PM. Excess mortality and causes associated with chikungunya, Puerto Rico, 2014–2015. Emerg Infect Dis. 2018;24:2352–5. https://doi.org/10.3201/eid2412.170639
44. Finkelstein BJ, Borges-Junior LH. Hospital beds in Brazil, SUS inpatients, demographic migration and procedure costs. J Bras Econ Saúde. 2020;12:273–80.
45. Gonçalves TS, Carmo CND, Marinho DS. Estimated annual costs of chikungunya fever in the municipality of Rio de Janeiro, Brazil. Rev Bras Epidemiol. 2024;27:e240026. https://doi.org/10.1590/1980-549720240026
46. Tiozzo G, de Roo AM, Gurgel do Amaral GS, Hofstra H, Vondeling GT, Postma MJ. Assessing chikungunya's economic burden and impact on health-related quality of life: two systematic literature reviews. PLoS Negl Trop Dis. 2025;19:e0012990. https://doi.org/10.1371/journal.pntd.0012990
47. Santos HLPCD, Trindade ES, Oliveira ERA, Cordeiro MVDS, Oliveira RS, Lima EC, et al. Trend of incompleteness of the race/color variable in hospitalizations due to COVID-19 whose outcome was death in Brazil, 2020–2022. Rev Saude Publica. 2024;58:37. https://doi.org/10.11606/s1518-8787.2024058006032

Address for correspondence: Giovanny V.A. França, Ministério da Saúde, Setor de Rádio e TV Norte, 701 Norte, Via W5 Norte, lote D, Brasília, Federal District 70058-900, Brazil; email: nutrigio@gmail.com

Attachment Patterns of Avian Influenza H5 Clade 2.3.4.4b Virus in Respiratory Tracts of Marine Mammals, North Atlantic Ocean

Syriam Sooksawasdi Na Ayudhya,[1] Lonneke Leijten, Willemijn F. Rijnink, Monique I. Spronken, Thijs Kuiken, Lisa Bauer,[2] Debby van Riel[2]

Highly pathogenic avian influenza A(H5N1) clade 2.3.4.4b virus infections have caused substantial mortality events in marine mammals in recent years. We hypothesized that the high number of infections and disease severity could be related to cell tropism in respiratory tracts. Therefore, we examined the attachment pattern of an H5N1 clade 2.3.4.4b virus ($H5^{2022}$) as a measure for cell tropism in the respiratory tracts of harbor seals, gray seals, harbor porpoises, and bottlenose dolphins and compared it with an H5N1 clade 2.1.3.2 virus ($H5^{2005}$) and a human seasonal H3N2 virus using virus histochemistry. Both H5 viruses attached abundantly to olfactory and respiratory mucosa in the upper respiratory tract of both seal species. $H5^{2022}$ attached more abundantly than $H5^{2005}$ to epithelial cells in the lower respiratory tract of all species. The observed attachment possibly explains the susceptibility of marine mammal species for recent H5N1 viruses and the observed development of severe disease.

Highly pathogenic avian influenza (HPAI) H5Nx virus of the A/goose/Guangdong/1/1996 lineage was first detected in domestic geese in 1996 and has since infected predominantly poultry (*1*). Since 2020, H5Nx viruses have circulated in wild birds and have spread almost worldwide (*2*). Viruses from the A/goose/Guangdong/1/1996 lineage pose a substantial threat to wild and endangered species (*3*,*4*), domestic species (*5*), and humans (*6*). H5N1 viruses of clade 2.3.4.4b are circulating in wild birds in Eurasia (*4*) North America (*7*), South America (*8*), Southern Africa (*9*), and Antarctica (*10*). Circulation has been associated with transmission to and outbreaks in marine mammals (*8*,*11*,*12*).

Historically, multiple mortality events in marine mammals have been linked to avian influenza A viruses. In different seal species, infections with H7N7 viruses in 1979–1980 (*13*), H4N5 viruses in 1982–1983 (*14*), H4N6 viruses in 1991, H3N3 viruses in 1992 (*15*), H10N7 viruses in 2014 (*16*), and H5N8 viruses in 2016, 2017 (*17*), and 2021 (*18*,*19*) have been reported. In addition, serologic evidence for infections with human 2009 pandemic influenza A(H1N1) virus was detected in northern elephant seals (*Mirounga angustirostris*), harbor seals (*Phoca vitulina*), and California sea lions (*Zalophus californianus*) (*20*). The currently circulating HPAI H5Nx clade 2.3.4.4b viruses have infected many marine mammal species from phylogenetically different families (Appendix Figure 1, https://wwwnc.cdc.gov/EID/article/31/9/25-0499-App1.pdf). HPAI H5Nx viruses have caused mortality events in different pinniped species, such as harbor seals (*21*,*22*), gray seals (*Halichoerus grypus*) (*8*,*23*,*24*), walruses (*Odobenus rosmarus*) (*4*,*25*), and elephant seals (*Mirounga leonina*) (*3*). In addition, HPAI H5N1 virus caused mass dieoffs in sea lions (*Otaria flavescens*) on the Pacific coast of South America (*8*,*11*). Cetacean species were also found to be infected with H5Nx clade 2.3.4.4b viruses; respiratory or neurologic disease has been reported in 3 common dolphins (*Delphinus delphis*) in Peru, Wales, and England (*8*); 2 harbor porpoises (*Phocoena phocoena*) in Sweden and England (*26*); an Atlantic white-sided dolphin (*Lagenorhynchus acutus*) in Canada (*27*); and a common bottlenose dolphin (*Tursiops truncatus*) in Florida, USA (*28*).

The receptor binding of influenza A virus to sialic acid moieties on glycoproteins and glycolipids, and the distribution of those receptors in a host, are critical determinants for host range and cell tropism

Author affiliation: Erasmus University Rotterdam, Erasmus Medical Center, Rotterdam, the Netherlands

DOI: https://doi.org/10.3201/eid3109.250499

[1]Current affiliation: Prince of Songkla University, Songkhla, Thailand.

[2]These authors were co–principal investigators.

(*29*). Human and avian influenza A viruses vary in their sialic acid-binding preference. Simplified, avian influenza A viruses preferentially bind to α2,3-linked sialic acids, whereas human influenza A viruses prefer α2,6-linked sialic acids (*30*,*31*). Knowledge of sialic acid expression in marine mammals is limited to harbor seals showing the presence of α2,3- and α2,6-linked sialic acids in the lower respiratory tract (*32*). Studying the direct binding of influenza A viruses to marine mammal respiratory tissues, using virus histochemistry, has revealed that human seasonal influenza H3N2 or H1N1 viruses rarely attach to the trachea and bronchi of seals and cetaceans (*33*). In contrast, low pathogenicity avian influenza A viruses H4N5 and H7N7 do attach to trachea and bronchi of harbor and gray seals but not to the trachea and bronchi of cetaceans (*33*). Both human and avian influenza A viruses attach to bronchiolar and alveolar epithelial cells in seals and cetaceans (*33*).

The ability of HPAI H5N1 clade 2.3.4.4b viruses to infect and cause severe disease in a broad range of mammal species has not been previously observed with other avian influenza A viruses (*3*,*34*). The attachment pattern in the respiratory tract of marine mammals of H5N1 clade 2.3.4.4b virus, and whether that pattern differs from the attachment pattern of previously circulating H5 viruses from different clades, is unknown. Therefore, we compared the attachment pattern of a 2022 H5N1 clade 2.3.4.4b virus, a 2005 H5N1 clade 2.1.3.2 virus, and a seasonal human H3N2 virus in the respiratory tracts of marine mammals commonly found in the North Atlantic Ocean: harbor seals, gray seals, harbor porpoises, and bottlenose dolphins.

Material and Methods

Cells

For testing, we used human epithelial kidney 293T cells and Madin-Darby canine kidney (MDCK) cells. We maintained human epithelial kidney 293T cells (ATCC accession no. ATCC-CRL-3216) in Dulbecco's Modified Eagle Medium (Capricorn Scientific, https://www.capricorn-scientific.com) supplemented with 1 mmol sodium pyruvate (Thermo Fisher Scientific, https://www.thermofisher.com), 100 IU/mL penicillin, 100 μg/μL streptomycin, 2 mmol glutamine, 1× nonessential amino acids (all Capricorn Scientific), 500 μg/mL geneticin (Thermo Fisher Scientific), and 10% fetal bovine serum at 37°C and 5% CO_2. We maintained MDCK cells in Eagle's minimum essential medium (Capricorn Scientific) supplemented with 1.5 mg/mL sodium bicarbonate (Thermo Fisher Scientific), 10 mmol HEPES buffering agent, 100 IU/mL penicillin, 100 μg/μL streptomycin, 2 mmol glutamine, 1× nonessential amino acids (all Capricorn Scientific), and 10% fetal bovine serum.

Recombinant Viruses, Virus Preparation, Inactivation, and Labeling for Virus Histochemistry

To work at Biosafety Level 2, we performed virus histochemistry with recombinant viruses that contain 7 segments of the mouse-adapted influenza A virus strain A/Puerto Rico/8/1934 (A/PR/8/34) and the hemagglutinin (HA) segment of either H5 (A/Indonesia/05/2005 [H5N1]; referred to as $H5^{\Delta MBCS2005}$) (*35*) from clade 2.1.3.2, H5 (A/Caspian gull/Netherlands/1/2022 [H5N1]; referred to as $H5^{\Delta MBCS2022}$) from clade 2.3.4.4b, or H3 (A/Netherlands/213/2003 [H3N2]; referred to as $H3^{2003}$), generated as described previously (*36*). We performed site-directed mutagenesis with the Pfu Ultra II Fusion HS DNA Polymerase (Agilent, https://www.agilent.com) and specific primers to remove the multibasic cleavage site (MBCS), which we replaced with the conserved H5 low pathogenic cleavage site, as described previously (*36*). One day before transfection, we seeded 293T cells and subsequently transfected with 5 μg of the desired HA gene segment and 5 μg of each of the remaining A/PR/8/34 gene segments. Approximately 16 hours after transfection, we removed the supernatant and washed the cells with phosphate-buffered saline (PBS) once. Three days after transfection, we harvested supernatant and passaged the virus once on a confluent layer of MDCK cells. We determined the presence of virus 3 days after inoculation with an hemagglutination assay to determine the hemagglutination units (HAU).

We inoculated MDCK cells with the described influenza A viruses at 10^{-3}, 10^{-4}, and 10^{-5} dilution. Three days after inoculation, we harvested the supernatant with the highest HAU and cleared it by low-speed centrifugation. We subsequently centrifuged cleared supernatants for 2 hours at 27,000 rpm in a SW32 rotor (Beckman Coulter, https://www.beckman.com) at 4°C on a 0.5 mL layer of 60% sucrose. We transferred the lowermost 2.5-mL virus supernatant on top of the sucrose cushion to a 60%–20% sucrose gradient and centrifuged overnight at 32,000 rpm in a SW41 rotor (Beckman Coulter,) at 4°C. We harvested the virus fraction, diluted in PBS, and centrifuged for 2 hours at 27,000 rpm in a SW32 rotor (Beckman Coulter) at 4°C to deplete leftover sucrose. We then resuspended the virus pellet in PBS and inactivated by dialyzing against 0.1% formalin for 3 days at room temperature. We labeled virus by mixing with an equal volume of

0.1 mg/mL of fluorescein isothiocyanate (FITC) (Sigma-Aldrich, https://www.sigmaaldrich.com) in 0.5 mol bicarbonate buffer (pH 9.5) for 1 hour at room temperature while constantly stirring. To lose all unbound FITC, we dialyzed labeled virus against PBS, then determined the HAU.

Hemagglutination Assay

We serially diluted viruses (1:2 dilution) in 0.1 mol PBS at pH 7.2. We mixed 50 μL of diluted virus with 50 μL of 0.5% turkey erythrocytes in a U-bottom plate and incubated for 1 hour at 4°C. We read the titer of each isolate as the reciprocal of the highest dilution in which complete hemagglutination was observed and recorded as the HAU per 25 μL.

Marine Mammal Tissue Testing

We tested formalin-fixed, paraffin-embedded (FFPE) tissues of the upper respiratory tract (nasal turbinate) from 2 harbor seals and 1 gray seal, and lower respiratory tract (trachea, bronchus, bronchiole, and alveoli) from 3 harbor seals, 3 gray seals, 3 harbor porpoises, and 3 bottlenose dolphins. The exact ages of the animals were unknown, but during necropsy, harbor and gray seals were reported as juvenile or subadult, harbor porpoises as neonate or juvenile, and bottlenose dolphins as neonate or adult. We included ≥1 slide of each tissue in every staining. Harbor seal, gray seal, and harbor porpoise FFPE tissues were derived from the Erasmus MC FFPE tissues archive, and bottlenose dolphin FFPE tissues were kindly provided by Dr. Toni Ramis. Selected tissues showed no abnormalities or histologic lesions.

Virus Histochemistry Staining on Marine Mammal Respiratory Tissues and Scoring

We deparaffinized 3-μm thick FFPE tissue sections with xylene and rehydrated using graded ethanol. We incubated slides overnight at 4°C with 100 μL FITC-labeled influenza virus (50 HAU). For visualization by light microscopy (Olympus, https://www.olympus-global.com), we detected the FITC label with a peroxidase-labeled rabbit anti-FITC antibody (Agilent). We amplified the signal with a tyramide signal amplification kit (Perkin Elmer, https://www.perkinelmer.com), according to manufacturer instructions. Peroxidase was revealed with 3-amino-9-ethylcarbazole (Sigma-Aldrich), resulting in a bright red precipitate. We counterstained tissues with hematoxylin and embedded in glycerol-gelatin (Merck, https://www.merck.com). For the negative control, we omitted the FITC-labeled virus; for the positive control, we used FFPE tissue sections of the ferret respiratory tract for H3 virus and of duck colon for H5 virus.

We scored the mean abundance of cells to which virus attached to the apical side from each individual tissue section of each marine mammal species as follows: −, no attachment; ±, attachment to rare or few cells (<10% cells positive); +, attachment to a moderate number of cells (10%–50% cells positive); and ++, attachment to many cells (>50% cells positive). Overall, we found little variation in the scores between individual animals, and we recorded the median score for each species (Table). Where possible, we recorded the predominant cell type to which virus attached: ciliated epithelial cell, goblet cell, or alveolar epithelial cell. In addition, we scored if viruses attached intracellular to epithelial cells of the submucosal gland or Bowman's gland. We took images of virus attachment from a representative tissue section of each animal species at an original magnification of ×1,000.

Phylogenetic Analysis of Marine Mammals

We obtained complete genome sequences of marine mammal species infected by H5 virus clade 2.3.4.4b, according to the list of the European Food Safety Authority report (*27*), from National Center for Biotechnology Information taxonomy database and GenBank. We aligned sequences with ClustalW (http://www.clustal.org) using MEGA version 11 (https://www.megasoftware.net) and transformed to PHYLIP in ALTER (https://phylipweb.github.io/phylip). We constructed a maximum-likelihood tree in FigTree version 1.4.4 (http://tree.bio.ed.ac.uk/software/figtree) using RAxMLHPC2 (https://www.phylo.org/tools/raxmlhpc2_tgb.html) on ACESS version 8.2.12 with rapid bootstrapping run on XSDE (*37*).

Consensus HA Sequence of H5N1 Clade 2.3.4.4.b Viruses Found in Marine Mammals

We downloaded all available influenza A H5 HA nucleotide sequences and accompanying metadata from GISAID (https://www.gisaid.org) (*38*) (Appendix). We aligned HA sequences by using Clustal Omega 22 (https://www.ebi.ac.uk/jdispatcher/msa/clustalo?stype=protein) (*39*) and trimmed the alignment to the start and stop codons of the HA sequences. After alignment, we built a consensus sequence of the influenza A H5 HA of all marine mammals and used it for alignment with other H5N1 viruses. We aligned the sequences with Clustal Omega 22 (*39*) and analyzed sequence similarities and secondary structure information with ESPRIPT version 3.023 (*40*).

Table. Attachment of 2 HPAI viruses and 1 human seasonal influenza virus in study of attachment patterns of avian influenza H5 clade 2.3.4.4b virus in respiratory tracts of marine mammals, North Atlantic Ocean*

		Seasonal $H3^{2003}$		HPAI $H5^{\Delta MBCS2005}$		HPAI $H5^{\Delta MBCS2022}$	
Tissue	Species	Score	Preferred cell type	Score	Preferred cell type	Score	Preferred cell type
Olfactory mucosa	Harbor seal	++	cil, bg	++	cil, bg	++	cil, bg
	Gray seal	+	cil, bg	++	cil, bg	++	cil, bg
Respiratory mucosa	Harbor seal	+	cil, sg	++	cil, sg	++	cil, sg
	Gray seal	+	cil	++	cil, gb	++	cil, gb
Trachea	Harbor seal	±	cil	±	cil	+	cil
	Gray seal	±	cil	±	cil, sg	++	cil, sg
	Harbor porpoise	±	cil	–	cil	±	cil, sg
	Bottlenose dolphin	+	cil, sg	–		–	
Bronchus	Harbor seal	–		±	cil sg	++	cil, sg
	Gray seal	–		++	cil sg	++	cil, sg
	Harbor porpoise	+	cil	–		+	cil
	Bottlenose dolphin	+	cil	–		–	
Bronchiole	Harbor seal	–		±	cil	+	cil
	Gray seal	–		±	cil, sg	+	cil, sg
	Harbor porpoise	++	cil	±	cil	+	cil
	Bottlenose dolphin	++	cil	±	cil	±	cil
Alveoli	Harbor seal	+	aec	±	aec	+	aec
	Gray seal	±	aec	±	aec	+	aec
	Harbor porpoise	++	aec	+	aec	++	aec
	Bottlenose dolphin	++	aec	±	aec	+	aec

*Scoring indicates attachment of viruses to the apical side of ciliated cells of the olfactory mucosa, respiratory mucosa, trachea, bronchus, bronchiole, and alveoli of marine mammal tissue sections. aec, alveolar epithelial cell; bg, Bowman's gland; cil, ciliated epithelial cell; gb, goblet cell; $H3^{2003}$, A/Netherlands/213/2003 (H3N2); $H5^{\Delta MBCS2005}$, A/Indonesia/05/2005 (H5N1); $H5^{\Delta MBCS2022}$, A/Caspian gull/Netherlands/1/2022 (H5N1); HPAI, highly pathogenic avian influenza; sg, submucosal gland; ++, abundant (>50% cells positive); +, moderate (10%–50% cells positive); ±, scarce (<10% cells positive); –, negative (no attachment).

Results

Attachment Pattern of $H5^{\Delta MBCS2022}$ and $H5^{\Delta MBCS2005}$ to Nasal Turbinate of Seals

To determine whether the HA of A/Caspian gull/Netherlands/1/2022 is similar to other H5N1 viruses from clade 2.3.4.4b detected in marine mammals, we generated a consensus sequence of all available marine mammal influenza A H5 HA sequences. An alignment of the HA of A/Caspian gull/Netherlands/1/2022 to a marine mammal consensus sequence (Appendix) showed several amino acid differences: D88G, M104L, Q115L, A210V, V510I, and M532I (H5 numbering) (Appendix Figure 2). Those amino acids are not in or close to the receptor-binding site or in amino acid residues known to affect receptor binding (*41*). Whether the amino acid changes result in differences in receptor binding properties or how they affect HA protein stability is unknown. A comparison of the HA sequence of A/Caspian Gull/Netherlands/1/2022 with H5N1 clade 2.1.3.2 virus A/Indonesia/5/2005 revealed amino acid changes known to affect receptor binding, at positions 133, 155, 156, 189 and 225 (H5 numbering) (Appendix Figure 2) (*41*,*42*; L. Bauer et al., unpub. data, https://www.biorxiv.org/content/10.1101/2024.11.27.625596v1.full).

Because of the differences in anatomy between pinnipeds and cetaceans, the nasal turbinate is absent in cetaceans (*43*). In the nasal turbinates of harbor seals and gray seals, the attachment pattern of $H5^{\Delta MBCS2022}$, $H5^{\Delta MBCS2005}$, and $H3^{2003}$ revealed that all 3 viruses attached abundantly to the apical side of the olfactory mucosa and to the Bowman's glands (Table; Figure 1). In the respiratory mucosa, all viruses attached predominantly to the apical side of ciliated epithelial cells. In general, both H5 viruses attached to the respiratory mucosa more abundantly than the human $H3^{2003}$ virus (Table; Figure 1). In addition, all viruses attached to submucosal glands in the submucosa in harbor seals and both H5 viruses to goblet cells in the gray seals. Taken together, those findings indicate that both human and avian viruses can attach to upper respiratory tract tissues in harbor and gray seals and that the attachment pattern of viruses with the $H5^{\Delta MBCS2022}$ or $H5^{\Delta MBCS2005}$ are not different.

Attachment of $H5^{\Delta MBCS2022}$ and $H5^{\Delta MBCS2005}$ to Lower Respiratory Tract Tissues

In the trachea of all animals tested, all viruses attached to ciliated epithelial cells, but to varying degrees (Table). In harbor seals, gray seals, and harbor porpoises, $H5^{\Delta MBCS2022}$ attached more abundantly than $H5^{\Delta MBCS2005}$ and $H3^{2003}$. In contrast, in bottlenose dolphins, $H3^{2003}$ attached to a moderate number of cells, whereas we observed no detectable attachment for $H5^{\Delta MBCS2022}$ and $H5^{\Delta MBCS2005}$ (Table; Figure 2). We observed attachment to submucosal glands with $H5^{\Delta MBCS2022}$ in gray seals and harbor porpoises, with $H5^{\Delta MBCS2005}$ in harbor porpoises, and with $H3^{2003}$ in bottlenose dolphins (Table).

In the bronchus of harbor and gray seals, both $H5^{\Delta MBCS2022}$ and $H5^{\Delta MBCS2005}$ attached to ciliated epithelial

cells (Table; Figure 2) and submucosal glands (Table), whereas we did not observe any attachment with $H3^{2003}$. In the bronchus of both cetaceans, $H3^{2003}$ attached to a moderate number of cells. For H5 viruses, we only observed attachment with $H5^{\Delta MBCS2022}$ in the bronchus of harbor porpoises (Table; Figure 2).

In the bronchiole of all species, both H5 viruses attached to ciliated epithelial cells. In general, the attachment of $H5^{\Delta MBCS2022}$ was more abundant than that of $H5^{\Delta MBCS2005}$. Human $H3^{2003}$ did not attach the bronchiole of harbor and gray seals, whereas it attached abundantly to the ciliated epithelial cells in the cetaceans (Table; Figure 2).

In the alveoli, all viruses attached to alveolar epithelial cells but with different abundance among different species. In harbor and gray seals, $H5^{\Delta MBCS2022}$ attached more abundantly than $H5^{\Delta MBCS2005}$ and $H3^{2003}$. In contrast, in harbor porpoises, both $H5^{\Delta MBCS2022}$ and $H3^{2003}$ attached more abundantly than $H5^{\Delta MBCS2005}$. In bottlenose dolphins, $H3^{2003}$ attached most abundantly (Table; Figure 2).

Overall, in the lower respiratory tract of seals and harbor porpoises, $H5^{\Delta MBCS2022}$ attached more abundantly than $H5^{\Delta MBCS2005}$. In bottlenose dolphins, $H3^{2003}$ attached most abundantly, with only limited attachment of $H5^{\Delta MBCS2022}$ in the bronchiole and alveoli.

Discussion

We describe the attachment patterns of HPAI H5N1 viruses in the respiratory tracts of common North Atlantic marine mammals. Our study revealed that avian H5 viruses attach abundantly to the upper respiratory tract of harbor seals and gray seals. In the lower respiratory tract of harbor seals, gray seals, and harbor porpoises, the recent H5N1 clade 2.3.4.4b virus attaches more abundantly than an H5N1 clade 2.1.3.2 virus from 2005.

The attachment pattern of HPAI H5N1 viruses to both the upper and lower respiratory tract tissues of North Atlantic marine mammals is in line with the detection of infectious virus or viral RNA in respiratory tract tissues of all included species (*21*,*23*,*24*,*26*). Unfortunately, little is known about the cell tropism of H5N1

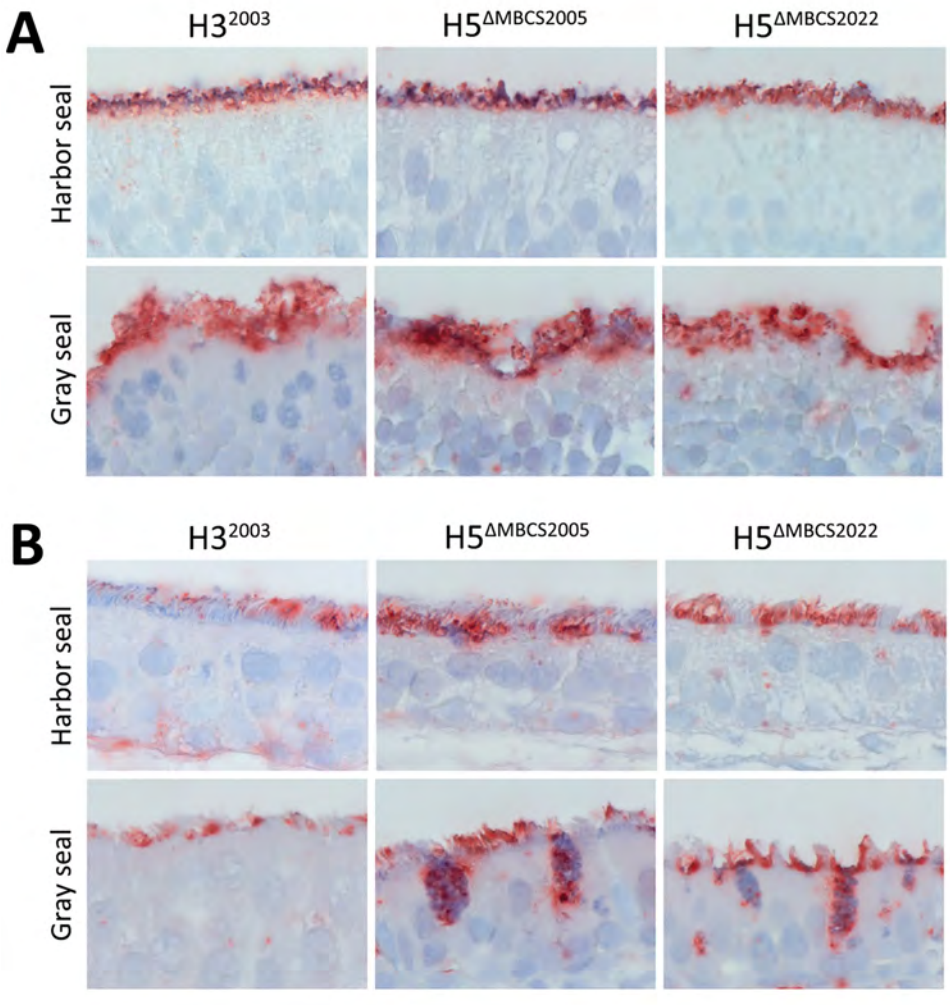

Figure 1. Attachment of influenza A viruses to the olfactory mucosa and respiratory mucosa of seals in study of attachment patterns of avian influenza H5 clade 2.3.4.4b virus in respiratory tracts of marine mammals, North Atlantic Ocean. Hematoxylin and eosin stain (red) shows attachment of human seasonal influenza A virus $H3^{2003}$ and avian influenza A viruses $H5^{\Delta MBCS2005}$ and $H5^{\Delta MBCS2022}$ to the olfactory (A) and respiratory (B) mucosa in the nasal turbinate of harbor seals (*Phoca vitulina*) and gray seals (*Halichoerus grypus*). Photos were taken at high magnification (×1,000) of the apical side of the mucosa; for this reason, Bowman's glands in the submucosa are not represented. $H3^{2003}$, A/Netherlands/213/2003 (H3N2); $H5^{\Delta MBCS2005}$, A/Indonesia/05/2005 (H5N1); $H5^{\Delta MBCS2022}$, A/Caspian gull/Netherlands/1/2022 (H5N1).

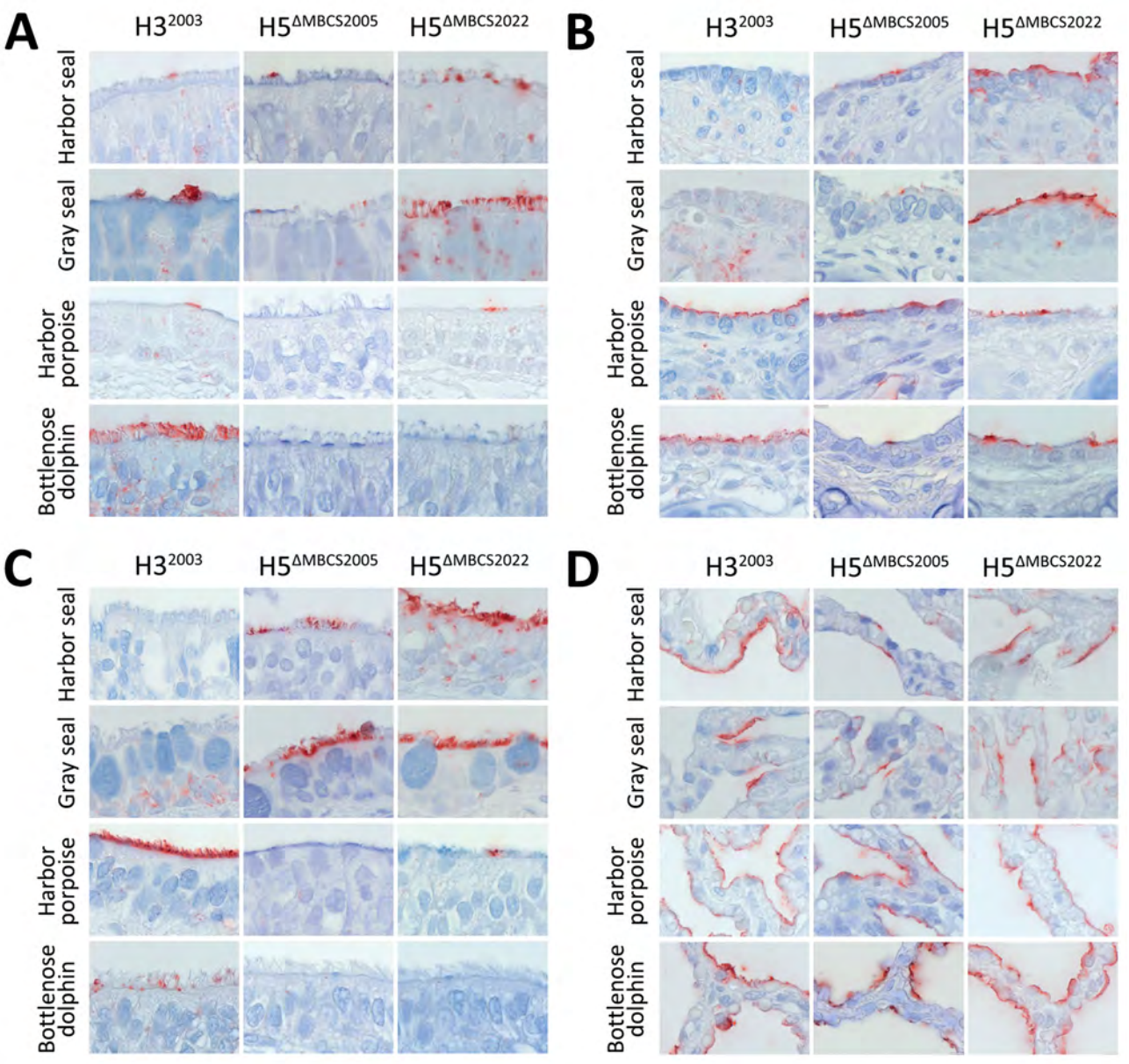

Figure 2. Attachment of influenza A viruses to epithelial cells of trachea, bronchus, bronchiole, and alveoli in study of attachment patterns of avian influenza H5 clade 2.3.4.4b virus in respiratory tracts of marine mammals, North Atlantic Ocean. Hematoxylin and eosin stain (red) shows attachment of human seasonal influenza A virus H3^{2003} and avian influenza A viruses H5$^{\Delta MBCS2005}$ and H5$^{\Delta MBCS2022}$ to the lower respiratory tracts of harbor seals (*Phoca vitulina*), gray seals (*Halichoerus grypus*), harbor porpoises (*Phocoena phocoena*), and bottlenose dolphins (*Tursiops truncatus*). A) Trachea; B) bronchiole; C) bronchus; D) alveoli. Photos were taken at high magnification (×1,000) of the apical side of the mucosa. H3^{2003}, A/Netherlands/213/2003 (H3N2); H5$^{\Delta MBCS2005}$, A/Indonesia/05/2005 (H5N1); H5$^{\Delta MBCS2022}$, A/Caspian gull/Netherlands/1/2022 (H5N1).

viruses in vivo; pathological studies on the cell tropism are scarce, and tissues from infected marine mammals are often not representative for the acute phase of infection. However, virus antigen has been detected in bronchiolar and alveolar epithelial cells in harbor seals, which fits with the ability of H5N1 virus to attach to those cells (*21*). Abundant attachment to the upper respiratory tract of pinnipeds suggests that the species are highly susceptible to infection and that viruses can be transmitted among them. In the lower respiratory tract of harbor seals and gray seals, the HA of H5N1 clade 2.3.4.4b virus had the tendency to attach more abundantly than H5N1 clade 2.1.3.2 virus. That difference could contribute to the ability of clade 2.3.4.4b viruses to cause severe lower respiratory tract disease and fits with the high mortality rates reported in harbor and gray seals

(*21*,*23*,*24*). High mortality rates associated with clade 2.3.4.4b virus infections also has been reported in sea lions and elephant seals (*3*,*12*,*44*). Whether the observed attachment pattern of clade 2.3.4.4b viruses in phylogenetically distinct pinniped species would be similar remains unknown. In both cetacean species tested, the clade 2.3.4.4b virus attached more abundantly to the respiratory tract than did clade 2.1.3.2 virus, but the attachment was overall lower than for both pinniped species. That finding is consistent with the individual cases of H5N1 virus infection in harbor porpoises, bottlenose dolphins, and other cetacean species (*8*,*26*–*28*), suggesting that cetaceans are also susceptible to infection. The ability of H5N1 viruses to attach to respiratory tissues of marine mammals is not unique; avian influenza viruses of subtypes H5N4 and H7N7 can also attach to tissues of the lower respiratory tract (*33*). However, the observed attachment pattern for HPAI H5N1 clade 2.3.4.4b viruses likely contributes to the high number of infections and the development of severe disease.

Several studies have shown that recent H5N1 clade 2.3.4.4b viruses, including bovine isolates, preferentially bind to α2,3-linked sialic acid receptors (*41*,*45*–*47*). The variability in attachment between the 2 H5N1 virus clades in our study are therefore likely not the result of a receptor switch to 2,6-linked sialic acid but potentially because of the amino acid differences in or close to the receptor-binding site, known to affect receptor specificity or affinity. However, the exact role of the individual amino acid positions remains to be investigated.

Both HPAI H5N1 viruses (either of clade 2.3.4.4b or clade 2.1.3.2) and H3N2 virus attach to olfactory mucosa in the nasal cavity of gray and harbor seals. Neurologic complications are regularly observed in marine mammals infected with H5 viruses, and virus can be detected in high titers in the brain (*19*,*21*,*23*,*24*,*28*). How H5 viruses enter the central nervous system remains unclear, but observations suggest that the viruses can enter the central nervous system via the olfactory nerve in seals, as observed in experimentally inoculated ferrets (*48*–*50*). However, HPAI H5N1 viruses can also invade the central nervous system in ceteceans, which lack a olfactory mucosa, so neuroinvasion likely could also occur via other cranial nerves or the hematogenous route (*28*).

In conclusion, our study highlights changes in the attachment pattern of a recent HPAI H5N1 clade 2.3.4.4b virus compared with H5N1 clade 2.1.3.2 virus from 2005 in the respiratory tracts of 4 marine mammal species that could lead to more efficient transmission and more severe disease. That finding, together with the recent increase in HPAI H5N1–associated deaths in marine mammals worldwide, emphasizes the need for increased avian influenza surveillance and research in such marine mammal species to limit illness and deaths and help protect both animal and human health.

Acknowledgments

We thank Ron Fouchier and Mathilde Richard for providing HA plasmids for generation of recombinant viruses.

This study is funded by the European Union under grant agreement no. 101084171 (Kappa-Flu). Views and opinions expressed are those of the author(s) only and do not necessarily reflect those of the European Union or REA. Neither the European Union nor the granting authority can be held responsible for them. This publication is part of the program NOW-XL which is (partly) financed by the Dutch Research Council (NWO) under the grant Viruses like it sweet; virus-glycan interactions as determinants of host range and pathogenesis (http://doi.org/10.61686/TOPSL61985).

About the Author

Dr. Sooksawasdi Na Ayudhya is an instructor and researcher at the Faculty of Veterinary Science, Prince of Songkla, Songkhla, Thailand. Her main interests are pathogenesis and molecular epidemiology of viral infectious diseases and viral emerging infectious diseases in humans and animals.

References

1. Xu X, Subbarao, Cox NJ, Guo Y. Genetic characterization of the pathogenic influenza A/Goose/Guangdong/1/96 (H5N1) virus: similarity of its hemagglutinin gene to those of H5N1 viruses from the 1997 outbreaks in Hong Kong. Virology. 1999;261:15–9. https://doi.org/10.1006/viro.1999.9820
2. Xie R, Edwards KM, Wille M, Wei X, Wong SS, Zanin M, et al. The episodic resurgence of highly pathogenic avian influenza H5 virus. Nature. 2023;622:810–7. https://doi.org/10.1038/s41586-023-06631-2
3. Uhart MM, Vanstreels RET, Nelson MI, Olivera V, Campagna J, Zavattieri V, et al. Epidemiological data of an influenza A/H5N1 outbreak in elephant seals in Argentina indicates mammal-to-mammal transmission. Nat Commun. 2024;15:9516. https://doi.org/10.1038/s41467-024-53766-5
4. Alexakis L, Buczkowski H, Ducatez M, Fusaro A, Gonzales JL, Kuiken T, et al.; European Food Safety Authority, European Centre for Disease Prevention and Control; European Union Reference Laboratory for Avian Influenza. Avian influenza overview September–December 2024. EFSA J. 2025;23:e9204.
5. Graziosi G, Lupini C, Catelli E, Carnaccini S. Highly pathogenic avian influenza (HPAI) H5 clade 2.3.4.4b virus infection in birds and mammals. Animals (Basel). 2024;14:1372. https://doi.org/10.3390/ani14091372
6. Garg S, Reinhart K, Couture A, Kniss K, Davis CT, Kirby MK, et al. Highly pathogenic avian influenza A(H5N1) virus infections in humans. N Engl J Med. 2025;392:843–54.

7. Caliendo V, Lewis NS, Pohlmann A, Baillie SR, Banyard AC, Beer M, et al. Transatlantic spread of highly pathogenic avian influenza H5N1 by wild birds from Europe to North America in 2021. Sci Rep. 2022;12:11729. https://doi.org/10.1038/s41598-022-13447-z
8. Leguia M, Garcia-Glaessner A, Muñoz-Saavedra B, Juarez D, Barrera P, Calvo-Mac C, et al. Highly pathogenic avian influenza A (H5N1) in marine mammals and seabirds in Peru. Nat Commun. 2023;14:5489. https://doi.org/10.1038/s41467-023-41182-0
9. Abolnik C, Phiri T, Peyrot B, de Beer R, Snyman A, Roberts D, et al. The molecular epidemiology of clade 2.3.4.4B H5N1 high pathogenicity avian influenza in southern Africa, 2021–2022. Viruses. 2023;15:1383. https://doi.org/10.3390/v15061383
10. Banyard AC, Bennison A, Byrne AMP, Reid SM, Lynton-Jenkins JG, Mollett B, et al. Detection and spread of high pathogenicity avian influenza virus H5N1 = in the Antarctic Region. Nat Commun. 2024;15:7433. https://doi.org/10.1038/s41467-024-51490-8
11. Ulloa M, Fernández A, Ariyama N, Colom-Rivero A, Rivera C, Nuñez P, et al. Mass mortality event in South American sea lions (*Otaria flavescens*) correlated to highly pathogenic avian influenza (HPAI) H5N1 outbreak in Chile. Vet Q. 2023;43:1–10. https://doi.org/10.1080/01652176.2023.2265173
12. Gamarra-Toledo V, Plaza PI, Gutiérrez R, Inga-Diaz G, Saravia-Guevara P, Pereyra-Meza O, et al. Mass mortality of sea lions caused by highly pathogenic avian influenza A(H5N1) virus. Emerg Infect Dis. 2023;29:2553–6. https://doi.org/10.3201/eid2912.230192
13. Webster RG, Hinshaw VS, Bean WJ, Van Wyke KL, Geraci JR, St Aubin DJ, et al. Characterization of an influenza A virus from seals. Virology. 1981;113:712–24. https://doi.org/10.1016/0042-6822(81)90200-2
14. Hinshaw VS, Bean WJ, Webster RG, Rehg JE, Fiorelli P, Early G, et al. Are seals frequently infected with avian influenza viruses? J Virol. 1984;51:863–5. https://doi.org/10.1128/jvi.51.3.863-865.1984
15. Callan RJ, Early G, Kida H, Hinshaw VS. The appearance of H3 influenza viruses in seals. J Gen Virol. 1995;76:199–203. https://doi.org/10.1099/0022-1317-76-1-199
16. Zohari S, Neimanis A, Härkönen T, Moraeus C, Valarcher JF. Avian influenza A(H10N7) virus involvement in mass mortality of harbour seals (*Phoca vitulina*) in Sweden, March through October 2014. Euro Surveill. 2014;19:20967. https://doi.org/10.2807/1560-7917.ES2014.19.46.20967
17. Shin DL, Siebert U, Lakemeyer J, Grilo M, Pawliczka I, Wu NH, et al. Highly pathogenic avian influenza A(H5N8) virus in gray seals, Baltic Sea. Emerg Infect Dis. 2019;25:2295–8. https://doi.org/10.3201/eid2512.181472
18. Floyd T, Banyard AC, Lean FZX, Byrne AMP, Fullick E, Whittard E, et al. Encephalitis and death in wild mammals at a rehabilitation center after infection with highly pathogenic avian influenza A(H5N8) virus, United Kingdom. Emerg Infect Dis. 2021;27:2856–63. https://doi.org/10.3201/eid2711.211225
19. Postel A, King J, Kaiser FK, Kennedy J, Lombardo MS, Reineking W, et al. Infections with highly pathogenic avian influenza A virus (HPAIV) H5N8 in harbor seals at the German North Sea coast, 2021. Emerg Microbes Infect. 2022;11:725–9. https://doi.org/10.1080/22221751.2022.2043726
20. Boyce WM, Mena I, Yochem PK, Gulland FM, García-Sastre A, Moreno N, et al. Influenza A(H1N1)pdm09 virus infection in marine mammals in California. Emerg Microbes Infect. 2013;2:e40. https://doi.org/10.1038/emi.2013.40
21. Lair S, Quesnel L, Signore AV, Delnatte P, Embury-Hyatt C, Nadeau MS, et al. Outbreak of highly pathogenic avian influenza A(H5N1) virus in seals, St. Lawrence Estuary, Quebec, Canada. Emerg Infect Dis. 2024;30:1133–43. https://doi.org/10.3201/eid3006.231033
22. Haman KH, Pearson SF, Brown J, Frisbie LA, Penhallegon S, Falghoush AM, et al. A comprehensive epidemiological approach documenting an outbreak of H5N1 highly pathogenic avian influenza virus clade 2.3.4.4b among gulls, terns, and harbor seals in the Northeastern Pacific. Front Vet Sci. 2024;11:1483922. https://doi.org/10.3389/fvets.2024.1483922
23. Puryear W, Sawatzki K, Hill N, Foss A, Stone JJ, Doughty L, et al. Highly pathogenic avian influenza A(H5N1) virus outbreak in New England seals, United States. Emerg Infect Dis. 2023;29:786–91. https://doi.org/10.3201/eid2904.221538
24. Mirolo M, Pohlmann A, Ahrens AK, Kühl B, Rubio-Garcìa A, Kramer K, et al. Highly pathogenic avian influenza A virus (HPAIV) H5N1 infection in two European grey seals (*Halichoerus grypus*) with encephalitis. Emerg Microbes Infect. 2023;12:e2257810. https://doi.org/10.1080/22221751.2023.2257810
25. Alexakis L, Fusaro A, Kuiken T, Mirinavičiūtė G, Ståhl K, Staubach C, et al.; European Food Safety Authority; European Centre for Disease Prevention and Control; European Union Reference Laboratory for Avian Influenza. Avian influenza overview March–June 2024. EFSA J. 2024;22:e8930.
26. Thorsson E, Zohari S, Roos A, Banihashem F, Bröjer C, Neimanis A. Highly pathogenic avian influenza A(H5N1) virus in a harbor porpoise, Sweden. Emerg Infect Dis. 2023;29:852–5. https://doi.org/10.3201/eid2904.221426
27. Fusaro A, Gonzales JL, Kuiken T, Mirinavičiūtė G, Niqueux É, Ståhl K, et al.; European Food Safety Authority; European Centre for Disease Prevention and Control; European Union Reference Laboratory for Avian Influenza. Avian influenza overview December 2023–March 2024. EFSA J. 2024;22:e8754.
28. Murawski A, Fabrizio T, Ossiboff R, Kackos C, Jeevan T, Jones JC, et al. Highly pathogenic avian influenza A(H5N1) virus in a common bottlenose dolphin (*Tursiops truncatus*) in Florida. Commun Biol. 2024;7:476. https://doi.org/10.1038/s42003-024-06173-x
29. de Graaf M, Fouchier RA. Role of receptor binding specificity in influenza A virus transmission and pathogenesis. EMBO J. 2014;33:823–41. https://doi.org/10.1002/embj.201387442
30. Shinya K, Ebina M, Yamada S, Ono M, Kasai N, Kawaoka Y. Influenza virus receptors in the human airway. Nature. 2006;440:435–6. https://doi.org/10.1038/440435a
31. Liu M, van Kuppeveld FJ, de Haan CA, de Vries E. Gradual adaptation of animal influenza A viruses to human-type sialic acid receptors. Curr Opin Virol. 2023;60:101314. https://doi.org/10.1016/j.coviro.2023.101314
32. Anthony SJ, St Leger JA, Pugliares K, Ip HS, Chan JM, Carpenter ZW, et al. Emergence of fatal avian influenza in New England harbor seals. MBio. 2012;3:e00166–12. https://doi.org/10.1128/mBio.00166-12
33. Ramis AJ, van Riel D, van de Bildt MW, Osterhaus A, Kuiken T. Influenza A and B virus attachment to respiratory tract in marine mammals. Emerg Infect Dis. 2012;18:817–20. https://doi.org/10.3201/eid1805.111828
34. Peacock T, Moncla L, Dudas G, VanInsberghe D, Sukhova K, Lloyd-Smith JO, et al. The global H5N1 influenza panzootic in mammals. Nature. 2025;637:304–13.
35. Chutinimitkul S, van Riel D, Munster VJ, van den Brand JM, Rimmelzwaan GF, Kuiken T, et al. In vitro assessment of attachment pattern and replication efficiency of H5N1 influenza A viruses with altered receptor specificity. J Virol. 2010;84:6825–33. https://doi.org/10.1128/JVI.02737-09
36. de Wit E, Spronken MI, Bestebroer TM, Rimmelzwaan GF, Osterhaus AD, Fouchier RA. Efficient generation and growth

of influenza virus A/PR/8/34 from eight cDNA fragments. Virus Res. 2004;103:155–61. https://doi.org/10.1016/j.virusres.2004.02.028
37. Stamatakis A, Hoover P, Rougemont J. A rapid bootstrap algorithm for the RAxML web servers. Syst Biol. 2008;57:758–71. https://doi.org/10.1080/10635150802429642
38. Elbe S, Buckland-Merrett G. Data, disease and diplomacy: GISAID's innovative contribution to global health. Glob Chall. 2017;1:33–46. https://doi.org/10.1002/gch2.1018
39. Madeira F, Madhusoodanan N, Lee J, Eusebi A, Niewielska A, Tivey ARN, et al. The EMBL-EBI Job Dispatcher sequence analysis tools framework in 2024. Nucleic Acids Res. 2024;52:W521–5. https://doi.org/10.1093/nar/gkae241
40. Robert X, Gouet P. Deciphering key features in protein structures with the new ENDscript server. Nucleic Acids Res. 2014;42:W320–4. https://doi.org/10.1093/nar/gku316
41. Song H, Hao T, Han P, Wang H, Zhang X, Li X, et al. Receptor binding, structure, and tissue tropism of cattle-infecting H5N1 avian influenza virus hemagglutinin. Cell. 2025;188:919–929.e9. https://doi.org/10.1016/j.cell.2025.01.019
42. Good MR, Suja D, Guthmiller JJ. The sweet side of H5N1 influenza virus infection. PLoS Pathog. 2025;21:e1012847. https://doi.org/10.1371/journal.ppat.1012847
43. Berta A, Ekdale EG, Cranford TW. Review of the cetacean nose: form, function, and evolution. Anat Rec (Hoboken). 2014;297:2205–15. https://doi.org/10.1002/ar.23034
44. Plaza PI, Gamarra-Toledo V, Rodríguez Euguí J, Rosciano N, Lambertucci SA. Pacific and Atlantic sea lion mortality caused by highly pathogenic avian influenza A(H5N1) in South America. Travel Med Infect Dis. 2024;59:102712. https://doi.org/10.1016/j.tmaid.2024.102712
45. Good MR, Fernández-Quintero ML, Ji W, Rodriguez AJ, Han J, Ward AB, et al. A single mutation in dairy cow-associated H5N1 viruses increases receptor binding breadth. Nat Commun. 2024;15:10768. https://doi.org/10.1038/s41467-024-54934-3
46. Chopra P, Ray SD, Page CK, Shepard JD, Kandeil A, Jeevan T, et al. Receptor-binding specificity of a bovine influenza A virus. Nature. 2025;640:E21–7. https://doi.org/10.1038/s41586-025-08822-5
47. Eisfeld AJ, Biswas A, Guan L, Gu C, Maemura T, Trifkovic S, et al. Pathogenicity and transmissibility of bovine H5N1 influenza virus. Nature. 2024;633:426–32. https://doi.org/10.1038/s41586-024-07766-6
48. Bodewes R, Kreijtz JH, van Amerongen G, Fouchier RA, Osterhaus AD, Rimmelzwaan GF, et al. Pathogenesis of influenza A/H5N1 virus infection in ferrets differs between intranasal and intratracheal routes of inoculation. Am J Pathol. 2011;179:30–6. https://doi.org/10.1016/j.ajpath.2011.03.026
49. Schrauwen EJ, Herfst S, Leijten LM, van Run P, Bestebroer TM, Linster M, et al. The multibasic cleavage site in H5N1 virus is critical for systemic spread along the olfactory and hematogenous routes in ferrets. J Virol. 2012;86:3975–84. https://doi.org/10.1128/JVI.06828-11
50. Bauer L, Benavides FFW, Veldhuis Kroeze EJB, de Wit E, van Riel D. The neuropathogenesis of highly pathogenic avian influenza H5Nx viruses in mammalian species including humans. Trends Neurosci. 2023;46:953–70. https://doi.org/10.1016/j.tins.2023.08.002

Address for correspondence: Debby van Riel, Department of Viroscience, Erasmus MC, Dr Molewaterplein 40, GD Rotterdam, the Netherlands; email: d.vanriel@erasmusmc.nl

Drivers of Crimean-Congo Hemorrhagic Fever in Natural Host and Effects of Control Measures, Bulgaria

Georgina Limon, Simona R. Tchakarova, Anna Ludi, Tsviatko Alexandrov, Iva Christova, Petya Petkova, Emmanuel Maze, Kelly Thomas, Natalie Baker, Marion England, Clare Browning, Ginette Wilsden, Sandra Belij-Rammerstorfer, Teresa Lambe, Anna Jolles, Miles Carroll, Roger Hewson, Simon Gubbins, Bryan Charleston, Nicholas A. Lyons

Crimean-Congo hemorrhagic fever (CCHF) is an emerging tickborne disease and a World Health Organization priority. Although humans are accidental hosts, infection can lead to hemorrhagic fever with a high fatality rate. Domestic animals play a critical role in disease transmission, but infected animals do not show clinical signs and viremia is short; thus, CCHF virus (CCHFV) infections can remain unobserved. During 2017–2019, we conducted 2 sequential observational studies followed by a multisite randomized controlled trial to determine spatial-temporal patterns and quantify drivers for CCHFV exposure in a natural host (sheep) in a CCHF-endemic area of Bulgaria. We found high-risk areas embedded in endemic regions. Animal characteristics were not correlated with seropositivity; however, a seasonality effect was observed, suggesting sampling time was a potential confounder. Force of infection varied across farms and over time. CCHFV transmission heterogeneity among farms is driven by preventive measures used to reduce exposure to ticks.

World Health Organization–designated priority emerging diseases are those with potential to cause severe epidemics without available or sufficient medical countermeasures (*1*). Crimean-Congo hemorrhagic fever (CCHF), a severe tickborne zoonotic disease with a high fatality rate in humans (*2*), is a priority emerging disease. Fatality rates have gradually increased in recent decades; major differences exist across geographic regions and occupations (*3*). The etiologic agent, CCHF virus (CCHFV), has a wide geographic distribution and is endemic in parts of Africa, Asia, Eastern Europe, and the Middle East. CCHFV is transmitted by ticks belonging to the Ixodidae family, mainly of the genus *Hyalomma* (*2*,*4*). Rising environmental temperatures influence CCHFV transmission to new geographic areas, in conjunction with other factors, such as travel, trade, livestock movement, and wild bird migration (*5*).

Animals, including domestic livestock, can become infected when bitten by CCHFV-infected ticks. Although animals develop a transient viremia, they do not exhibit clinical signs (*6*–*8*). Small ruminants have been suggested as good proxies to monitor the presence of CCHFV in a given region (*6*,*9*). Sheep have been epidemiologically linked to human exposure to the virus and cases (*10*–*12*). Despite many serologic studies being conducted in different settings, using various tests and a wide range of study designs (*6*,*13*–*15*), very little is known about the factors driving differences in CCHFV infection, host humoral responses, and spatial patterns of exposure in

Author affiliations: The Pirbright Institute, Pirbright, UK (G. Limon, A. Ludi, E. Maze, M. England, C. Browning, G. Wilsden, S. Gubbins, B. Charleston, N.A. Lyons); Bulgarian Food Safety Agency, Sofia, Bulgaria (S.R. Tchakarova, T. Alexandrov, P. Petkova); National Center of Infectious and Parasitic Diseases, Sofia (I. Christova); UK Health Security Agency Porton Down, Salisbury, UK (K. Thomas, N. Baker, R. Hewson); University of Oxford, Oxford, UK (S. Belij-Rammerstorfer, T. Lambe, M. Carroll); Pandemic Science Institute, Oxford (T. Lambe, M. Carroll); Oregon State University, Corvallis, Oregon, USA (A. Jolles); London School of Hygiene and Tropical Medicine, London, UK (R. Hewson)

DOI: https://doi.org/10.3201/eid3109.241952

livestock. We conducted 2 sequential observational studies followed by a multisite randomized trial to determine spatial patterns and main drivers for CCHFV exposure in sheep (a natural host) in Bulgaria. Written consent was obtained from all participating sheep farmers. Ethics approvals were obtained from the Bulgarian Food Safety Agency ethics committee and The Pirbright Institute's Animal Welfare Ethical Review Board.

Methods

Study Design

We conducted a cross-sectional study (field study 1) in October 2017 in which we recruited 120 commercial sheep farms in the CCHFV-endemic provinces of Burgas and Kardzhali, Bulgaria, after the main tick-biting season. In Europe, temperature and photoperiod are key drivers of tick seasonality; the optimum environmental temperature for tick activity is 20°C–25°C. In the Balkans, those conditions occur during March–October (*16*). We calculated the target sample size for each province to estimate the proportion of seropositive sheep with 95% confidence and 6% precision for an expected seroprevalence of 50% and 0.12 intrafarm correlation (Appendix, https://wwwnc.cdc.gov/EID/article/31/9/24-1952-App1.pdf). We selected 5 lambs (3–12 months of age) and 5 sheep (13–24 months of age) within each participating farm and collected blood samples from each selected animal. We collected animal and farm level data by using a standardized questionnaire in a mobile application (Appendix Table 1, Figure 1).

We conducted a follow-up observational study (field study 2) before the next tick-biting season (before March 2018) within the main hotspot area (northwestern part of Burgas province), identified in the cross-sectional study, to investigate the potential effects of age and seasonality on seropositivity in sheep. We visited 25 farms; 14 of those had been included during the first field study. We sampled 15 sheep at each farm, stratified by age: 5 lambs (≤12 months), 5 young adults (13–36 months), and 5 adults (>36 months). We collected blood samples from each selected animal and corresponding animal data (age, sex, breed, presence of ticks).

We then conducted a multisite, randomized, 2-arm, triple-blinded, controlled trial (field study 3) in the previously identified hotspot to determine the efficacy of a modified vaccinia virus Ankara (MVA)–vectored vaccine candidate (encoding the CCHFV envelope spike glycoprotein [GP]) in sheep during periods of expected high transmission levels (i.e., natural challenge of animals) and to estimate the force of infection (FOI) over time and across farms. In addition, we used the placebo group to better elucidate profiles for CCHFV nucleoprotein (NP) and GP Gc IgGs over time after natural exposure. The vaccine candidate has been shown to be immunogenic and 100% protective in mice (*17*) but poorly immunogenic in sheep; only a modest increase in CCHFV Gc IgG has been observed in sheep under controlled conditions (*18*). We calculated sample size by considering an incidence of 16.9% in the unvaccinated group, a between cluster variation of 0.021, and 20 animals per farm and by assuming a vaccine efficacy of 50%, 95% confidence, and 80% power (Appendix). We also assumed a 15% loss to follow-up would occur during 6 months.

We recruited 32 commercial sheep farms into field study 3. At each of those farms, we selected 20 lambs that were 2–4 months of age and already weaned. Lambs were the unit of randomization, and we allocated them in equal numbers to either the vaccine group (arm 1) or placebo (received phosphate-buffered saline) group (arm 2). We administered a vaccine booster 4 weeks after the primary dose. We conducted intention-to-treat analysis; seroconversion was the endpoint. We visited each farm and collected blood samples at 2, 4, 10, 13, 17, 21, and 27 weeks after primary dose. We gathered animal data and general information on farm characteristics, such as management practices and biosecurity, during the first visit by using an electronic standardized questionnaire. During each follow-up visit, we collected data on changes and preventive measures (deworming, tick control, and shed spraying for vector control) that had been administered between visits. We used the EpiCollect5 tool (https://five.epicollect.net) to collect the data for all studies.

Sample Storage and Laboratory Methods

We stored all field study serum samples in duplicate aliquots at −20°C. We shipped 1 aliquot per sample at the end of each field study to The Pirbright Institute (Pirbright, UK) for testing. We tested serum samples in duplicate by using an in-house indirect ELISA to detect CCHFV antigen-specific IgG responses (CCHFV NP and Gc IgGs), as previously described (*18*). We also tested serum samples from CCHFV-seropositive animals in the controlled trial for CCHFV RNA by real-time reverse transcription PCR at the Bulgarian Food Safety Agency laboratories, as previously described (*19*). We tested samples from when the animals first seroconverted

and from the previous sampling period before the sheep seroconverted.

Statistical Analysis

For field study 1, we estimated weighted sheep seroprevalence. To assess the level of clustering of seropositive sheep within farms, we estimated the intrafarm correlation coefficient for seropositive status of individual sheep by using the farm variance from a mixed effect model, considering farm as a random effect. We conducted risk factor analysis separately at both the animal and farm level.

At the animal level, we tested the extent to which animal characteristics were associated with individual serostatus (outcome variable) by using mixed effect models, including farm as a random effect. We assessed collinearity between all predictor variables for which p was $\leq$0.1 in the univariate analysis and, when collinearity was present (Pearson correlation $\geq$0.8), we kept only 1 variable in the model. We generated multivariable models by using a backward stepwise selection procedure with likelihood ratio tests to compare models with and without the variable of interest.

At the farm level, we recategorized farm and management practices after data exploration (Appendix Table 1). We used data reduction techniques to identify farm typologies on the basis of management practices and farm characteristics (Appendix Tables 2, 3, Figure 2). To assess the extent to which environmental factors affect the risk for CCHFV exposure of sheep on a farm, we used land cover (shrub, cultivated, or arboreal), mean normalized difference vegetation index (NDVI), and NDVI spring slope (*20*) as proxies to capture environmental traits that shape the distribution of *Hyalomma* spp. mosquito activity and seasonal dynamics. We tested the extent to which farm typologies and environmental variables were associated with the number of seropositive animals in the farm by using Poisson regression; we used the number of animals sampled as an offset. We selected final multivariable models by using a backward selection process with 1 variable removed each time. We then used a likelihood ratio test to assess which model best fit the data.

We generated choropleth maps of empirical Bayes smoothed rate at the municipality level to explore potential spatial clustering of CCHFV seropositive animals. We explored spatial autocorrelation of the smoothed Bayes risk at a global scale by using the Moran's *I* statistic and at a local scale by using the Getis-Ord GI* statistic.

For field study 2, we only considered farms that were visited during both field studies 1 and 2 (n = 14) and animals having the same age range (3–24 months) to capture farm-level dynamics of CCHFV NP and Gc seropositivity at key seasonal timepoints (October 2017 and March 2018). We used multivariable mixed effect models to assess differences in seropositive animals between the 2 sampling periods and age groups, including farm as a random effect.

For field study 3, we determined the number of unvaccinated and vaccinated lambs seroconverting during each sampling period for each farm. We assumed a lamb seroconverted during the first sampling period when its CCHFV NP IgG status changed from negative to positive. We used the pattern of seroconversion to estimate FOI for each lamb (Appendix Figure 3). FOI varied among farms and among sampling periods and incorporated the effects of control measures (vaccination, deworming, spraying, and tick control), enabling their efficacy to be quantified. In particular, vaccine efficacy was calculated by the formula $1-\lambda_1/\lambda_0$, where λ_1 is the FOI in vaccinated lambs and λ_0 is the FOI in unvaccinated lambs (*21*).

We used descriptive statistics to characterize CCHFV NP and GP Gc profiles in the placebo groups. We estimated median, interquartile range, and fold-change relative to day 0 for each sampling point. We used Spearman correlation coefficients (ρ) and 95% CIs to determine the relationship between CCHFV NP and Gc IgGs.

Table 1. Results from multivariable mixed-effect models used to assess serologic associations in study of Crimean-Congo hemorrhagic fever in sheep and effects of control measures, Bulgaria*

	CCHFV glycoprotein Gc IgG positive		CCHFV nucleoprotein IgG positive	
Characteristic	aOR (95% CI)	p value	aOR (95% CI)	p value
Study type				
Follow-up, March 2018, n = 58	Referent		Referent	
Cross-sectional, Oct 2017, n = 140	1.31 (0.64–2.75)	0.464	14.49 (5.54–46.93)	<0.001
Age category				
13–24 mo., young adult sheep, n = 115	Referent		Referent	
3–12 mo., lambs, n = 83	1.44 (0.74–2.82)	0.283	1.8 (0.94–3.68)	0.073

*Associations between CCHFV glycoprotein Gc or nucleoprotein seropositivity and time of sampling (study type) and age; only farms visited during both field studies 1 and 2 (n = 14) and sheep of the same age (3–24 mo) (total no. = 198) were considered. Models had farm as a random effect. Results from univariate analysis are in the Appendix (Appendix Tables 1, 2, https://wwwnc.cdc.gov/EID/article/31/9/24-1952-App1.pdf). aOR, adjusted odds ratio; CCHFV, Crimean-Congo hemorrhagic fever virus.

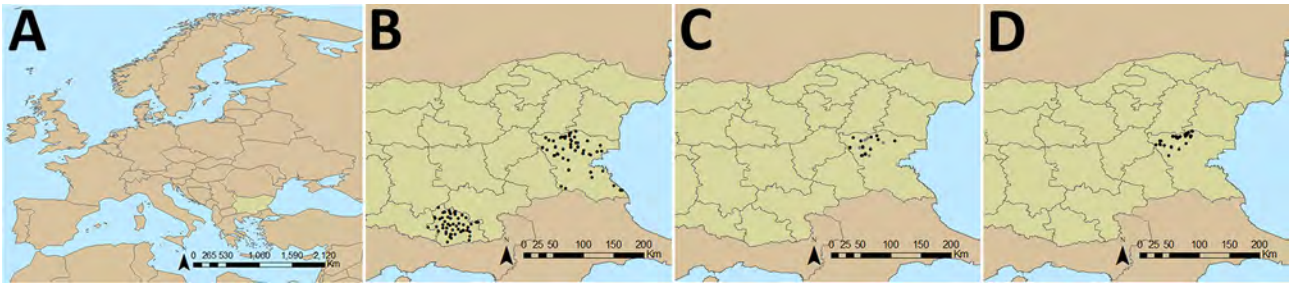

Figure 1. Geographic locations of sheep farms in study of drivers of Crimean-Congo hemorrhagic fever in natural host and effects of control measures, Bulgaria. A) Location of Bulgaria within Europe. B) Location of sheep farms that were part of cross-sectional field study 1 (n = 120). Black dots indicate sheep farms in Kardzhali Province, located in the southern part of Bulgaria, and Burgas Province, located in the southeastern part of the country. C) Location of sheep farms that were part of the follow-up field study 2 during March 2018 in Burgas Province (n = 25). Black dots indicate farms that were part of both field studies 1 and 2 (n = 14). D) Location of farms that were part of the multisite randomized control trial (field study 3) in Burgas Province (n = 32). Black dots indicate sheep farm locations.

Results

To explore the potential effect of seasonality, we assessed the difference in the number of seropositive animals between sampling periods (October 2017 and March 2018) considering only farms that were visited on both field studies 1 and 2 (n = 14) and animals from the same age groups (3–24 months). Sampled animals were not the same in both studies but came from the same farms; therefore, we expected the same management practices and levels of exposure. All farms were dairy farms, all but 1 farm reported deworming their animals regularly, and all but 1 farm reported performing regular tick control. On the 14 farms, 55/140 (39.3%) sheep were CCHFV Gc IgG seropositive in October 2017 and 22/58 (37.9%) sheep were seropositive in March 2018, whereas 75/140 (53.6%) sheep were CCHFV NP IgG seropositive in October and 5/58 (8.6%) sheep were NP IgG seropositive in March. We observed a strong seasonality effect ($p<0.001$) after adjusting for age group. Sheep were more likely to be NP IgG seropositive at the end of the tick biting period (October sampling), when CCHFV transmission is expected to be higher, than at the end of the winter (March sampling), when CCHFV transmission is expected to be low (Table 1; Appendix Tables 4, 5). However, we did not observe a seasonality effect for CCHFV Gc antibody levels, suggesting that CCHFV NP IgG might be a better marker of recent exposure than CCHFV Gc IgG. Therefore, we considered CCHFV NP IgG levels to be a main indicator of recent natural exposure for the cross-sectional and controlled trial studies.

We included 120 farms and 1,200 sheep in the cross-sectional study (Figure 1). The overall weighted NP IgG seroprevalence was 38.5% (95% CI 35.3%–42.0%); we observed a higher seroprevalence in Burgas Province than in Kardzhali Province (Appendix Table 6). Dairy breeds were more likely to be seropositive than mixed breeds. The province and breed type exhibited strong collinearity; most dairy breeds came from Burgas Province, where most dairy farms were located and where univariate models were used. We did not

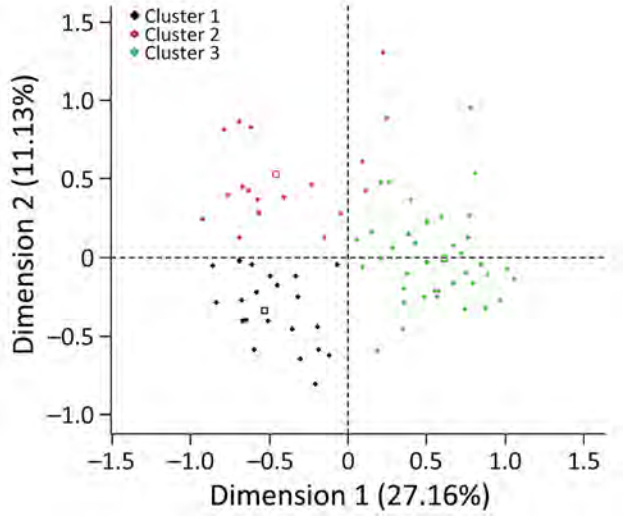

Figure 2. Farm typologies identified after hierarchical cluster analysis in study of drivers of Crimean-Congo hemorrhagic fever in natural host and effects of control measures, Bulgaria. First, multiple correspondent analysis was performed to transform correlated variables into a small number of synthetic uncorrelated factors. Hierarchical cluster analysis was then used to group farms into clusters according to their level of similarity with respect to the factors created by the multiple correspondent analysis. Data were collected during October 2017 from 120 commercial sheep farms in Burgas and Kardhzali Provinces in Bulgaria. Typology (cluster) 1 (n = 54) comprised mixed farms, most of which were located in Kardhzali Province. Lambs were kept outdoors during the day and indoors at night, and all farms reported applying tick control by spraying animals with acaracides. Typology (cluster) 2 (n = 26) comprised most of the meat farms located in either Kardhzali or Burgas Province. Most farms kept lambs outdoors during the day and indoors at night. One third of those farms did not use tick control measures for animals. Typology (cluster) 3 (n = 40) comprised most of the dairy farms; most were located in Burgas Province. Lambs were kept indoors at all times until weaning. Most farms reported applying tick control either by dipping or spraying animals with acaracides.

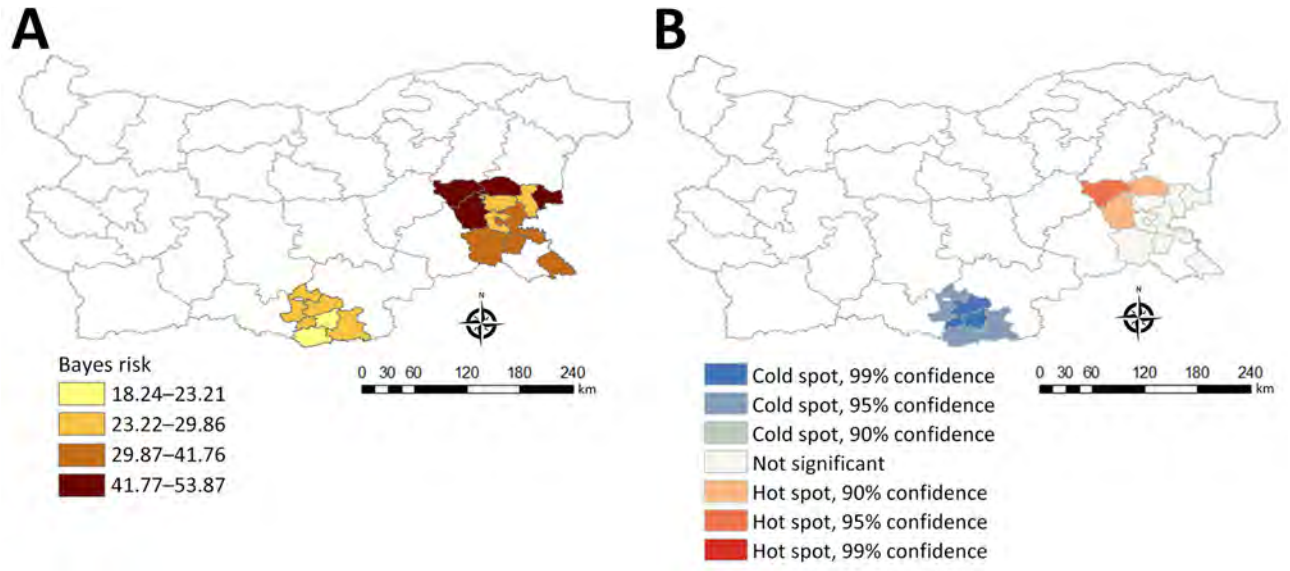

Figure 3. Choropleth maps showing Crimean-Congo hemorrhagic fever virus exposure risks in study of virus drivers in natural host and effects of control measures, Bulgaria. Bayes smoothed rate (A) and Getis-Ord Gi* hotspots (B) of Crimean-Congo hemorrhagic fever virus nucleoprotein Ig in sheep are indicated for municipalities in Burgas Province (southeastern part of the country) and Kardzhali Province (southern part of country). Data were collected during October 2017.

find statistically significant associations between serologic status and sex, age, or presence of ticks at the time of sampling (Appendix Table 7). At the farm level, 105 (87.5%) farms had ≥1 seropositive sheep. Adjusting for land cover, farms from typology (cluster) 3 were more likely to have seropositive animals than farms in typology 2 (Figure 2; Appendix Table 8). Farms within 5 km of cultivated or arboreal land cover were more likely to have seropositive animals (Appendix Table 8).

We found CCHFV seropositivity throughout both provinces studied; however, we found spatial heterogeneity at farm and municipality levels. Some level of clustering of seropositive animals occurred within farms; the overall intrafarm correlation was 0.25. Bayes smoothed rates of seropositive animals varied across municipalities. We identified higher risk for CCHFV exposure in northwestern Burgas (Figure 3). We observed a significant positive spatial autocorrelation at the municipality level (Moran's I = 0.36; p = 0.001), indicating nearby observations were more similar on average than distant ones.

The multisite randomized controlled trial comprised 32 commercial sheep farms and 640 lambs (20 per farm) (Appendix Table 9), which we followed up for 6 months. In the placebo group (n = 320), CCHFV Gc IgG was detectable at baseline but declined early during the study, consistent with waning passive immunity, whereas NP IgG levels rose during June–September, aligning with the expected peak in CCHFV transmission caused by tick activity and supporting NP IgG as a marker for recent CCHFV infection (Appendix Figure 4, panels A, B). Moreover, correlation between NP and Gc IgG responses (Spearman ρ = 0.57) was moderate at the first timepoint in early March, then declined rapidly and remained weak or inconsistent thereafter (Spearman ρ range 0.25–0.41) (Appendix Figure 4, panels C, D), indicating that CCHFV NP and Gc responses are not tightly coupled, especially over time.

FOI varied among farms and over time (Figure 4; Appendix Table 10, Figure 5). FOI was initially high (especially during weeks 2–4), declined to a minimum during weeks 4–10, then rose again and peaked during weeks 17–21. Only 2 animals tested positive for CCHFV RNA by reverse transcription PCR; both animals were from the same farm and tested positive during the sampling period at the beginning of July (week 17). Both animals were seronegative at the previous sampling timepoint (week 13), and although ELISA optical density values for both sheep increased at the following sampling timepoint (week 27), only 1 of the sheep became seropositive.

Vaccination had a limited effect on FOI at most farms; vaccine efficacy varied among farms (Figure 5; Appendix Table 10). The posterior median vaccine efficacy was >0 (median 42.7% [range 2.8%–77.1%]) for 16 farms, although the 95% lower credible limit was >0 for only 1 farm (Figure 5).

Deworming had no apparent effect on FOI (Appendix Table 11). However, tick control in animals or spraying sheds with acaricide had an effect that varied among farms. Tick control reduced FOI (i.e.,

posterior median effect <0) in 11 of 17 farms (Figure 5). Spraying reduced FOI in 4 of 23 farms. The magnitude of the effect was typically larger for tick control than for spraying (Figure 5).

Discussion

We determined epidemiologic and driver profiles for CCHFV exposure in natural hosts in a virus-endemic setting over time. Furthermore, we quantified the potential effect of different control measures on CCHFV FOI. We found spatial heterogeneity of CCHFV seropositivity at both farm and municipality levels and identified hotspots in virus-endemic areas, consistent with results in other endemic regions (*15*,*22*,*23*). In addition, we observed a critical effect of seasonality; sheep were more likely to be CCHFV NP IgG seropositive toward the end of the tick biting period, when CCHFV transmission is expected to be highest, than at the end of the winter, suggesting NP IgG is a better marker for recent CCHFV infection. Contrary to reports in previous studies (*23*–*27*), animal characteristics were not significantly associated with seropositivity. However, age was marginally associated with CCHFV NP IgG when adjusting for time of sampling, and lambs were more likely to be seropositive than were adult sheep.

Apart from nosocomial transmission, close contact with animals, farming activities, slaughtering animals, and a history of tick bites have all been reported as the main activities that can increase risks for human infection and clinical cases (*28*–*32*). In a parallel study, we took blood samples from farmers in a subset of farms that were part of the first field study (Appendix Table 12). Only 3 (6.8%) farmers were positive for CCHFV IgG. Low levels of seropositivity are to be expected in vectorborne disease–endemic areas where humans are accidental hosts.

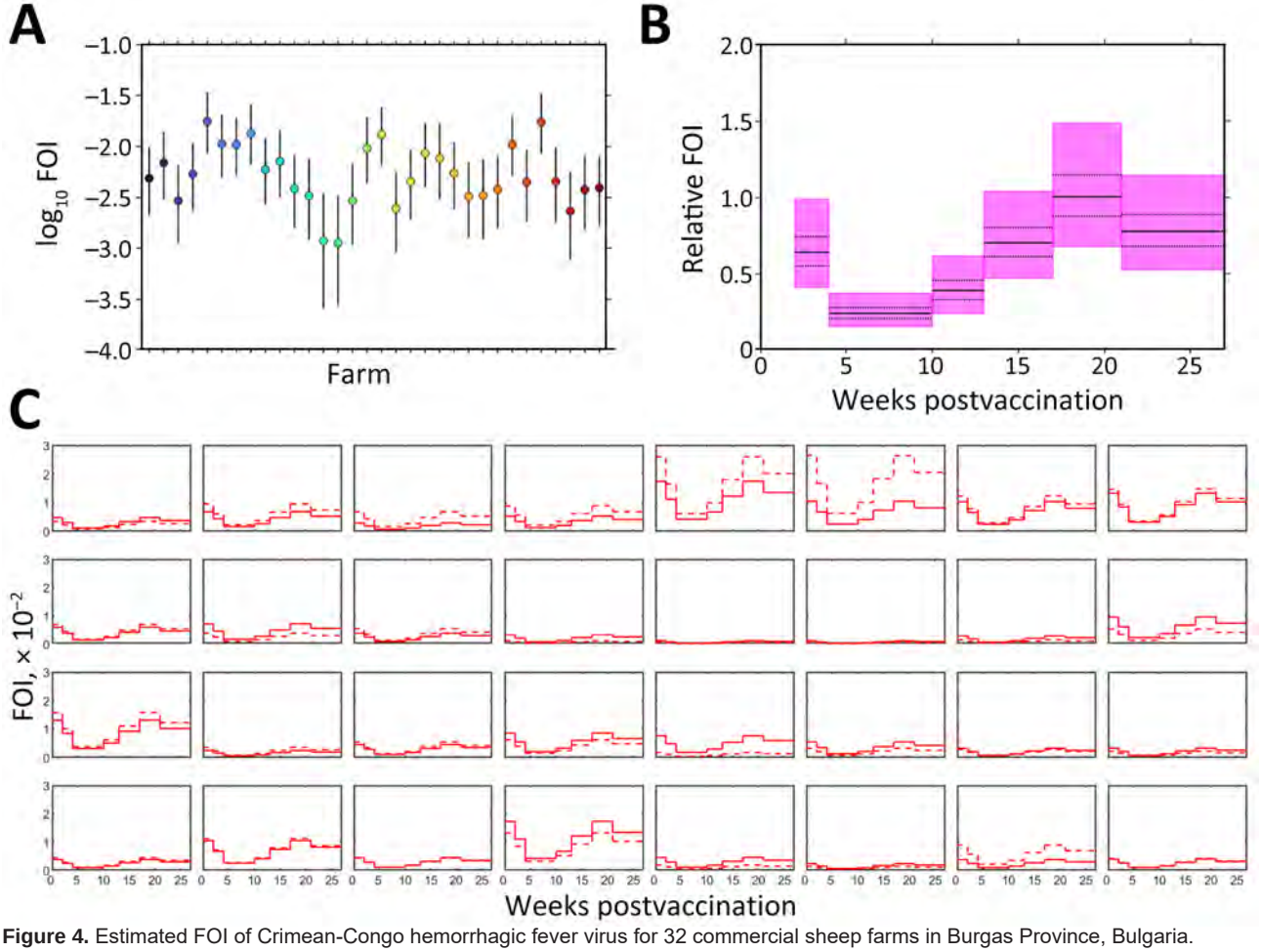

Figure 4. Estimated FOI of Crimean-Congo hemorrhagic fever virus for 32 commercial sheep farms in Burgas Province, Bulgaria. Sheep were vaccinated and tested for virus IgG over a 6-month follow-up. A) Baseline FOI for each farm. Circles indicate posterior medians; error bars indicate 95% credible intervals. B) Relative FOIs during each sampling period. Posterior median (solid black lines), interquartile range (dashed black lines), and 95% credible interval (purple shading) are indicated. C) Posterior median FOI for unvaccinated (solid lines) and vaccinated (dashed lines) animals in each farm. Each plot represents data from 1 farm. Seroconversion was determined on the basis of virus nucleoprotein IgG levels. FOI, force of infection.

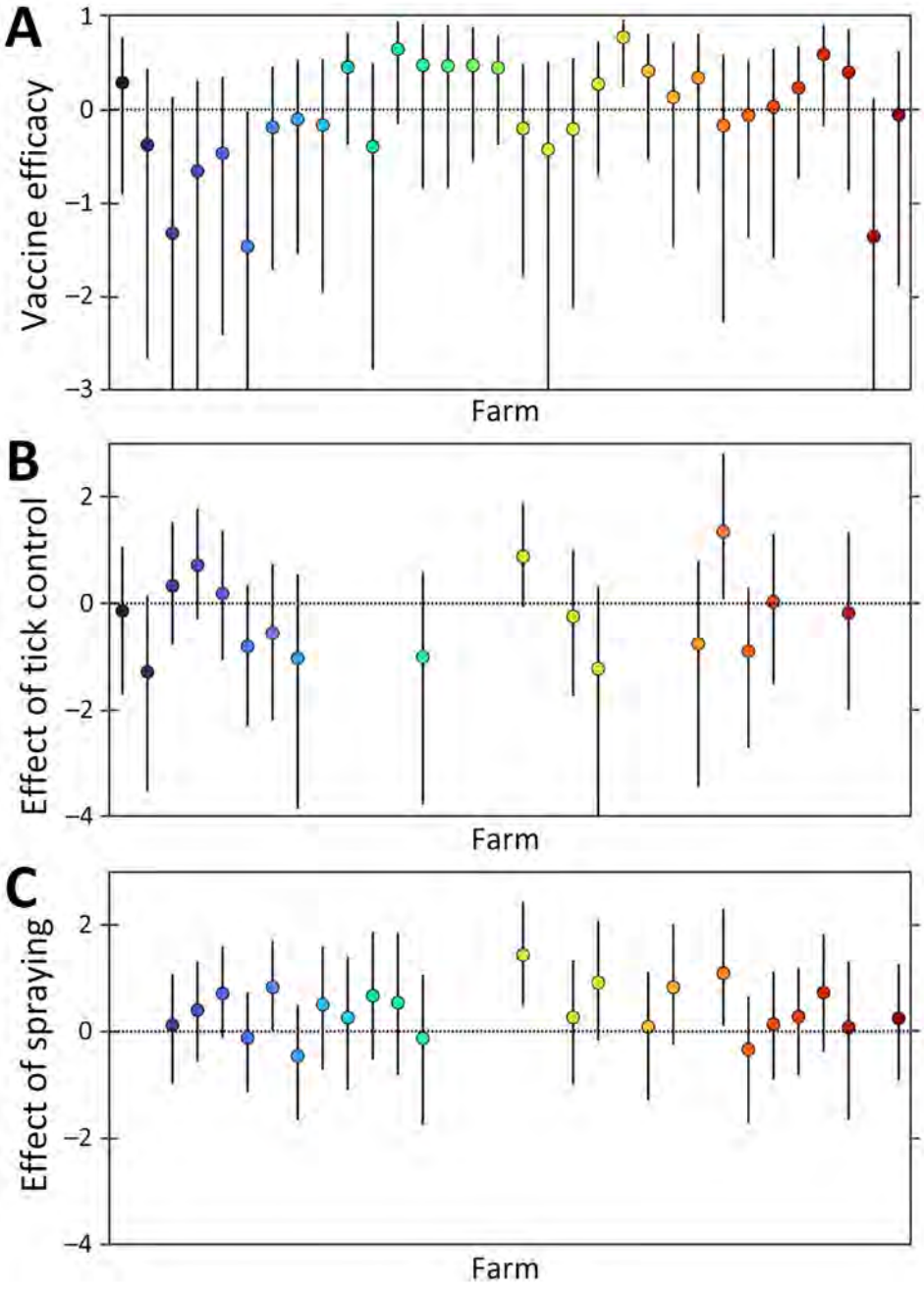

Figure 5. Effects of control measures on the force of infection for Crimean-Congo hemorrhagic fever virus at 32 sheep farms in Burgas Province, Bulgaria. A) Estimated vaccine efficacy of the Crimean-Congo hemorrhagic fever–modified vaccinia virus Ankara vaccine. B) Effect of tick control at farms. C) Effect of spraying. Circles indicate posterior medians; error bars indicate 95% credible intervals. Horizontal dotted line indicates no effect.

The proportion of seropositive farmers was slightly higher in this study than that previously reported within the general population in Bulgaria (2.8%) and Greece (4.2%) (*28*,*33*). Two of the 3 seropositive farmers lived in the high-risk area identified in northwestern Burgas Province, suggesting that CCHFV exposure is an occupational risk and not only derived from individual risk activities.

To better elucidate the dynamics of the humoral response toward CCHFV over time, we quantified temporal variation in FOI on the basis of antibody responses over a 6-month period. FOI was initially high, which might be a consequence of maternal antibodies found in lambs that were part of the study. FOI then rose again during the summer period (weeks 17–21 of the study), likely because of the higher tick activity during those months leading to increased CCHFV transmission. CCHFV NP has been shown to be highly immunogenic; NP antibodies are produced during infection in humans and mice (*34*,*35*). Further studies should be conducted to formally assess the protective role of maternal CCHFV antibodies.

FOI has been suggested to influence vaccine efficacy (*36*). Our findings indicate that FOI and vaccine efficacy varied across farms, and vaccination had a limited effect on FOI in this setting (*18*). In contrast, tick control and spraying reduced FOI, suggesting that CCHFV transmission heterogeneity among farms in high-risk areas is driven by different farm management practices and preventive measures used to reduce tick exposure. Further studies should be conducted to assess differences in tick density at the farm and animal level.

Seroepidemiologic studies have contributed to delineating transmission dynamics for various vectorborne zoonotic diseases (*37*–*40*). Our findings indicate that, given the short period of infectivity, serologic analysis is more reliable than other methods to assess CCHF dynamics in domestic animals.

In conclusion, we provide insight into the epidemiology and drivers of CCHFV transmission. As with most tickborne diseases, CCHFV dynamics are complex. We have identified key epidemiologic parameters derived from empirical data in a natural host species, in CCHFV-endemic settings, and over time. Because of the limitations in conducting controlled challenge studies with category 4 pathogens and the lack of a robust correlation of protection, natural challenge studies are a reliable approach to evaluate the efficacy of vaccine candidates and other control measures.

Acknowledgments

We thank Kim Stevens, Anthony Wilson, Agustin Estrada-Pena, and Paul Fine for helpful discussions and advice during the study design and initial data analysis stages; field veterinarians from BFSA for collecting samples and data; and participating farmers for their invaluable support.

This work was funded by the UK National Institute for Health and Care Research (grant no. 16/107/06) and the UKRI Biotechnology and Biological Science Research Council to The Pirbright Institute (grant nos. BBS/E/I/00007033, BBS/E/I/00007036, BBS/E/I/00007037, BBS/E/PI230002C, and BBS/E/PI/23NB0004 to S.G., B.C., and N.A.L.).

About the Author

Dr Limon leads the applied epidemiology group at The Pirbright Institute, United Kingdom. Her research interests focus on understanding the connections between drivers of disease transmission, spread and emergence, and their impact on people's livelihoods and health.

References

1. World Health Organization. 2018 annual review of diseases prioritized under the Research and Development Blueprint [cited 2024 Mar 10]. https://www.who.int/docs/default-source/blue-print/2018-annual-review-of-diseases-prioritized-under-the-research-and-development-blueprint.pdf
2. Bente DA, Forrester NL, Watts DM, McAuley AJ, Whitehouse CA, Bray M. Crimean-Congo hemorrhagic fever: history, epidemiology, pathogenesis, clinical syndrome and genetic diversity. Antiviral Res. 2013;100:159–89. https://doi.org/10.1016/j.antiviral.2013.07.006
3. Nasirian H. New aspects about Crimean-Congo hemorrhagic fever (CCHF) cases and associated fatality trends: a global systematic review and meta-analysis. Comp Immunol Microbiol Infect Dis. 2020;69:101429. https://doi.org/10.1016/j.cimid.2020.101429
4. Gargili A, Estrada-Peña A, Spengler JR, Lukashev A, Nuttall PA, Bente DA. The role of ticks in the maintenance and transmission of Crimean-Congo hemorrhagic fever virus: a review of published field and laboratory studies. Antiviral Res. 2017;144:93–119. https://doi.org/10.1016/j.antiviral.2017.05.010
5. Hawman DW, Feldmann H. Crimean-Congo haemorrhagic fever virus. Nat Rev Microbiol. 2023;21:463–77. https://doi.org/10.1038/s41579-023-00871-9
6. Spengler JR, Bergeron É, Rollin PE. Seroepidemiological studies of Crimean-Congo hemorrhagic fever virus in domestic and wild animals. PLoS Negl Trop Dis. 2016;10:e0004210. https://doi.org/10.1371/journal.pntd.0004210
7. Spengler JR, Estrada-Peña A, Garrison AR, Schmaljohn C, Spiropoulou CF, Bergeron É, et al. A chronological review of experimental infection studies of the role of wild animals and livestock in the maintenance and transmission of Crimean-Congo hemorrhagic fever virus. Antiviral Res. 2016;135:31–47. https://doi.org/10.1016/j.antiviral.2016.09.013
8. Li H, Pinette M, Smith G, Goolia M, Handel K, Nebroski M, et al. Distinguishing host responses, extensive viral dissemination and long-term viral RNA persistence in domestic sheep experimentally infected with Crimean-Congo haemorrhagic fever virus Kosovo Hoti. Emerg Microbes Infect. 2024;13:2302103. https://doi.org/10.1080/22221751.2024.2302103
9. Schuster I, Mertens M, Mrenoshki S, Staubach C, Mertens C, Brüning F, et al. Sheep and goats as indicator animals for the circulation of CCHFV in the environment. Exp Appl Acarol. 2016;68:337–46. https://doi.org/10.1007/s10493-015-9996-y
10. Humolli I, Dedushaj I, Zupanac TA, Mucaj S. Epidemiological, serological and herd immunity of Crimean-Congo hemorrhagic fever in Kosovo. Medical Arh. 2010;64:91–3. PubMed
11. Mostafavi E, Haghdoost A, Khakifirouz S, Chinikar S. Spatial analysis of Crimean Congo hemorrhagic fever in Iran. Am J Trop Med Hyg. 2013;89:1135–41. https://doi.org/10.4269/ajtmh.12-0509
12. Papa A, Sidira P, Kallia S, Ntouska M, Zotos N, Doumbali E, et al. Factors associated with IgG positivity to Crimean-Congo hemorrhagic fever virus in the area with the highest seroprevalence in Greece. Ticks Tick Borne Dis. 2013;4:417–20. https://doi.org/10.1016/j.ttbdis.2013.04.003
13. Atim SA, Niebel M, Ashraf S, Vudriko P, Odongo S, Balinandi S, et al. Prevalence of Crimean-Congo haemorrhagic fever in livestock following a confirmed human case in Lyantonde district, Uganda. Parasit Vectors. 2023;16:7. https://doi.org/10.1186/s13071-022-05588-x

14. Grech-Angelini S, Lancelot R, Ferraris O, Peyrefitte CN, Vachiery N, Pédarrieu A, et al. Crimean-Congo hemorrhagic fever virus antibodies among livestock on Corsica, France, 2014–2016. Emerg Infect Dis. 2020;26:1041–4. https://doi.org/10.3201/10.3201/eid2605.191465
15. Hughes EC, de Glanville W, Kibona T, Mmbaga BT, Rostal MK, Swai ES, et al. Crimean-Congo hemorrhagic fever virus seroprevalence in human and livestock populations, northern Tanzania. Emerg Infect Dis. 2024;30:836–8. https://doi.org/10.3201/eid3004.231204
16. Pavlović I, Lazarević D. Biodiversity and seasonal distribution of ticks in southeastern Serbia. Timok Medical Gazzette. 2023;48:45–8.
17. Buttigieg KR, Dowall SD, Findlay-Wilson S, Miloszewska A, Rayner E, Hewson R, et al. A novel vaccine against Crimean-Congo haemorrhagic fever protects 100% of animals against lethal challenge in a mouse model. PLoS One. 2014;9:e91516. https://doi.org/10.1371/journal.pone.0091516
18. Belij-Rammerstorfer S, Limon G, Maze EA, Hannant K, Hughes E, Tchakarova SR, et al. Development of anti–Crimean-Congo hemorrhagic fever virus Gc and NP-specific ELISA for detection of antibodies in domestic animal sera. Front Vet Sci. 2022;9:913046. https://doi.org/10.3389/fvets.2022.913046
19. Atkinson B, Chamberlain J, Logue CH, Cook N, Bruce C, Dowall SD, et al. Development of a real-time RT-PCR assay for the detection of Crimean-Congo hemorrhagic fever virus. Vector Borne Zoonotic Dis. 2012;12:786–93. https://doi.org/10.1089/vbz.2011.0770
20. Estrada-Peña A, de la Fuente J. Species interactions in occurrence data for a community of tick-transmitted pathogens. Sci Data. 2016;3:160056. PubMed https://doi.org/10.1038/sdata.2016.56
21. Halloran ME, Longini IM, Struchiner CJ. Design and analysis of vaccine studies. New York: Springer Nature; 2010.
22. Estrada-Peña A, Zatansever Z, Gargili A, Aktas M, Uzun R, Ergonul O, et al. Modeling the spatial distribution of Crimean-Congo hemorrhagic fever outbreaks in Turkey. Vector Borne Zoonotic Dis. 2007;7:667–78. https://doi.org/10.1089/vbz.2007.0134
23. Mukhaye E, Akoko JM, Nyamota R, Mwatondo A, Muturi M, Nthiwa D, et al. Exposure patterns and the risk factors of Crimean Congo hemorrhagic fever virus amongst humans, livestock and selected wild animals at the human/livestock/wildlife interface in Isiolo County, upper eastern Kenya. PLoS Negl Trop Dis. 2024;18:e0012083. https://doi.org/10.1371/journal.pntd.0012083
24. Adam IA, Mahmoud MAM, Aradaib IE. A seroepidemiological survey of Crimean Congo hemorrhagic fever among cattle in North Kordufan State, Sudan. Virol J. 2013;10:178. PubMed https://doi.org/10.1186/1743-422X-10-178
25. Barthel R, Mohareb E, Younan R, Gladnishka T, Kalvatchev N, Moemen A, et al. Seroprevalance of Crimean-Congo haemorrhagic fever in Bulgarian livestock. Biotechnol Biotechnol Equip. 2014;28:540–2. https://doi.org/10.1080/13102818.2014.931685
26. Ibrahim AM, Adam IA, Osman BT, Aradaib IE. Epidemiological survey of Crimean Congo hemorrhagic fever virus in cattle in East Darfur State, Sudan. Ticks Tick Borne Dis. 2015;6:439–44. https://doi.org/10.1016/j.ttbdis.2015.03.002
27. Swanepoel R, Shepherd AJ, Leman PA, Shepherd SP, McGillivray GM, Erasmus MJ, et al. Epidemiologic and clinical features of Crimean-Congo hemorrhagic fever in southern Africa. Am J Trop Med Hyg. 1987;36:120–32. https://doi.org/10.4269/ajtmh.1987.36.120
28. Christova I, Gladnishka T, Taseva E, Kalvatchev N, Tsergouli K, Papa A. Seroprevalence of Crimean-Congo hemorrhagic fever virus, Bulgaria. Emerg Infect Dis. 2013;19:177–9. https://doi.org/10.3201/eid1901.120299
29. Izadi S, Naieni KH, Madjdzadeh SR, Nadim A. Crimean-Congo hemorrhagic fever in Sistan and Baluchestan Province of Iran, a case-control study on epidemiological characteristics. Int J Infect Dis. 2004;8:299–306. https://doi.org/10.1016/j.ijid.2003.10.008
30. Sargianou M, Panos G, Tsatsaris A, Gogos C, Papa A. Crimean-Congo hemorrhagic fever: seroprevalence and risk factors among humans in Achaia, western Greece. Int J Infect Dis. 2013;17:e1160–5. https://doi.org/10.1016/j.ijid.2013.07.015
31. Nabeth P, Cheikh DO, Lo B, Faye O, Vall IO, Niang M, et al. Crimean-Congo hemorrhagic fever, Mauritania. Emerg Infect Dis. 2004;10:2143–9. https://doi.org/10.3201/eid1012.040535
32. Williams RJ, Al-Busaidy S, Mehta FR, Maupin GO, Wagoner KD, Al-Awaidy S, et al. Crimean-Congo haemorrhagic fever: a seroepidemiological and tick survey in the Sultanate of Oman. Trop Med Int Health. 2000;5:99–106. https://doi.org/10.1046/j.1365-3156.2000.00524.x
33. Sidira P, Maltezou HC, Haidich AB, Papa A. Seroepidemiological study of Crimean-Congo haemorrhagic fever in Greece, 2009–2010. Clin Microbiol Infect. 2012;18:E16–9. https://doi.org/10.1111/j.1469-0691.2011.03718.x
34. Garrison AR, Moresco V, Zeng X, Cline CR, Ward MD, Ricks KM, et al. Nucleocapsid protein-specific monoclonal antibodies protect mice against Crimean-Congo hemorrhagic fever virus. Nat Commun. 2024;15:1722. https://doi.org/10.1038/s41467-024-46110-4
35. Karaaslan E, Çetin NS, Kalkan-Yazıcı M, Hasanoğlu S, Karakeçili F, Özdarendeli A, et al. Immune responses in multiple hosts to nucleocapsid protein (NP) of Crimean-Congo hemorrhagic fever virus (CCHFV). PLoS Negl Trop Dis. 2021;15:e0009973. https://doi.org/10.1371/journal.pntd.0009973
36. Kaslow DC. Force of infection: a determinant of vaccine efficacy? NPJ Vaccines. 2021;6:51. https://doi.org/10.1038/s41541-021-00316-5
37. Helb DA, Tetteh KKA, Felgner PL, Skinner J, Hubbard A, Arinaitwe E, et al. Novel serologic biomarkers provide accurate estimates of recent *Plasmodium falciparum* exposure for individuals and communities. Proc Natl Acad Sci USA. 2015;112:E4438–47. https://doi.org/10.1073/pnas.1501705112
38. Katzelnick LC, Ben-Shachar R, Mercado JC, Rodriguez-Barraquer I, Elizondo D, Arguello S, et al. Dynamics and determinants of the force of infection of dengue virus from 1994 to 2015 in Managua, Nicaragua. Proc Natl Acad Sci USA. 2018;115:10762–7. https://doi.org/10.1073/pnas.1809253115
39. Lancelot R, Béral M, Rakotoharinome VM, Andriamandimby SF, Héraud JM, Coste C, et al. Drivers of Rift Valley fever epidemics in Madagascar. Proc Natl Acad Sci USA. 2017;114:938–43. https://doi.org/10.1073/pnas.1607948114
40. Salje H, Cummings DAT, Rodriguez-Barraquer I, Katzelnick LC, Lessler J, Klungthong C, et al. Reconstruction of antibody dynamics and infection histories to evaluate dengue risk. Nature. 2018;557:719–23. https://doi.org/10.1038/s41586-018-0157-4

Address for correspondence: Georgina Limon, The Pirbright Institute, Ash Road, Pirbright, Surrey GU24 0NF, UK; email: georgina.limon-vega@pirbright.ac.uk

Increased Incidence of *Candida auris* Colonization in Early COVID-19 Pandemic, Orange County, California, USA

Alissa H. Dratch, Mi Le, Matthew Zahn

Candida auris transmission surged in long-term acute-care hospitals (LTACHs) in Orange County, California, USA, during the COVID-19 pandemic. This study describes the effect of COVID-19 on *C. auris* transmission by estimating the probability of patient colonization in LTACHs across 5 epidemiologic time periods. Patients had the highest probability of developing new skin colonization during the first COVID-19 wave, with a cumulative incidence of 22.5% (95% CI 18.5–26.6) after a 30-day stay. Once the initial COVID-19 waves abated, a reduction in cumulative incidence of *C. auris* colonization was observed concurrently with persistent high prevalence, indicating that within-facility transmission can be reduced with proper infection prevention and control practices. Admission screenings and point prevalence surveys provided a wealth of data that guided public health recommendations and supported the objectives of both public health professionals and LTACHs for monitoring facility transmission dynamics and guiding decision making.

Candida auris is a multidrug-resistant yeast that can cause serious invasive infections in at-risk populations (*1*) and an emerging pathogen in the United States that can cause outbreaks in healthcare settings. Persons with extensive healthcare exposure, indwelling medical devices, or recent antimicrobial drug use are at highest risk for *C. auris* colonization or infection (*2*,*3*). Because of the high prevalence of patients with those risk factors, *C. auris* is frequently found in long-term acute-care hospital (LTACH) settings (*4*,*5*). *C. auris* is a reportable pathogen in Orange County, California, USA and all known cases are reported to the Orange County Healthcare Agency (OCHCA).

Author affiliation: Orange County Health Care Agency, Santa Ana, California, USA (A.H. Dratch, M. Le, M. Zahn)

DOI: https://doi.org/10.3201/eid3109.241342

The first outbreak in California was identified in Orange County after *C. auris* was detected in a urine specimen from an LTACH patient in February 2019. Local, state, and federal public health agencies mounted an aggressive containment response, which included active surveillance, to identify transmission in 3 LTACHs and 14 ventilator-equipped skilled nursing facilities serving adult patients in Orange County (*6*,*7*). Because of their high-risk patient populations, the 3 LTACHs in the county agreed to perform routine point prevalence surveys (PPSs) that consisted of screening all noncolonized patients at their facilities via axilla and groin swab sampling. The first PPSs at each LTACH were performed in March 2019. During March 2019–September 2020, PPS frequency varied with transmission patterns. PPSs were generally done 1–2 times per month at each LTACH, though there was variance because they were largely done in response to identification of new cases. In September 2020, the LTACHs switched to routine PPS schedules. From then on, PPSs routinely occurred 1–2 times per month regardless of the level of *C. auris* activity at individual facilities.

By November 2020, in response to widespread transmission, all 3 LTACHs implemented universal admission screening of patients not known to be *C. auris* positive. That testing enabled the rapid identification of colonized patients and early implementation of infection prevention precautions. In addition, the strategy created the opportunity to track patients longitudinally starting from their admission date. Thus, OCHCA was able to collect individual-level longitudinal screening data over 5 epidemiologically distinct time periods, which corresponded with 1 pre–COVID-19 period and 4 periods during the COVID-19 pandemic. OCHCA was able to track *C. auris* spread as the fungus became endemic to the county and while

the county's facilities were simultaneously responding to multiple COVID-19 surges. This study was conducted to objectively assess whether the suspected patterns of colonization rates across different phases of the pandemic in Orange County were supported by empirical data and to gain insights to inform future infection prevention and response activities.

Methods

This cohort study examined results from all axilla and groin surveillance swab specimens from the 3 LTACHs in Orange County during March 14, 2019–July 18, 2022 (Figure 1). We planned the study shortly after the implementation of universal admission screening, so data from November 2020 on were collected prospectively. Because of OCHCA's close working relationships with the LTACHs, we received data as the test results became available. We validated, cleaned, and prepared data for analysis on an ongoing basis as we received test results.

During sample collection, a single swab was used to swab both axilla and both inguinal creases. We tested the swabs from PPSs through the Centers for Disease Control and Prevention's Antimicrobial Resistance Laboratory Network or through Orange County's Public Health Laboratory by using PCR testing methods. If an indeterminate result was returned, the same swab specimen that was already tested was sent for culture. Admission swab specimens were tested through the LTACHs' private laboratory, where they used culture methods only.

Axilla and groin screening swab specimens that tested positive for *C. auris* indicated skin colonization, and we counted them as cases. In addition, 3

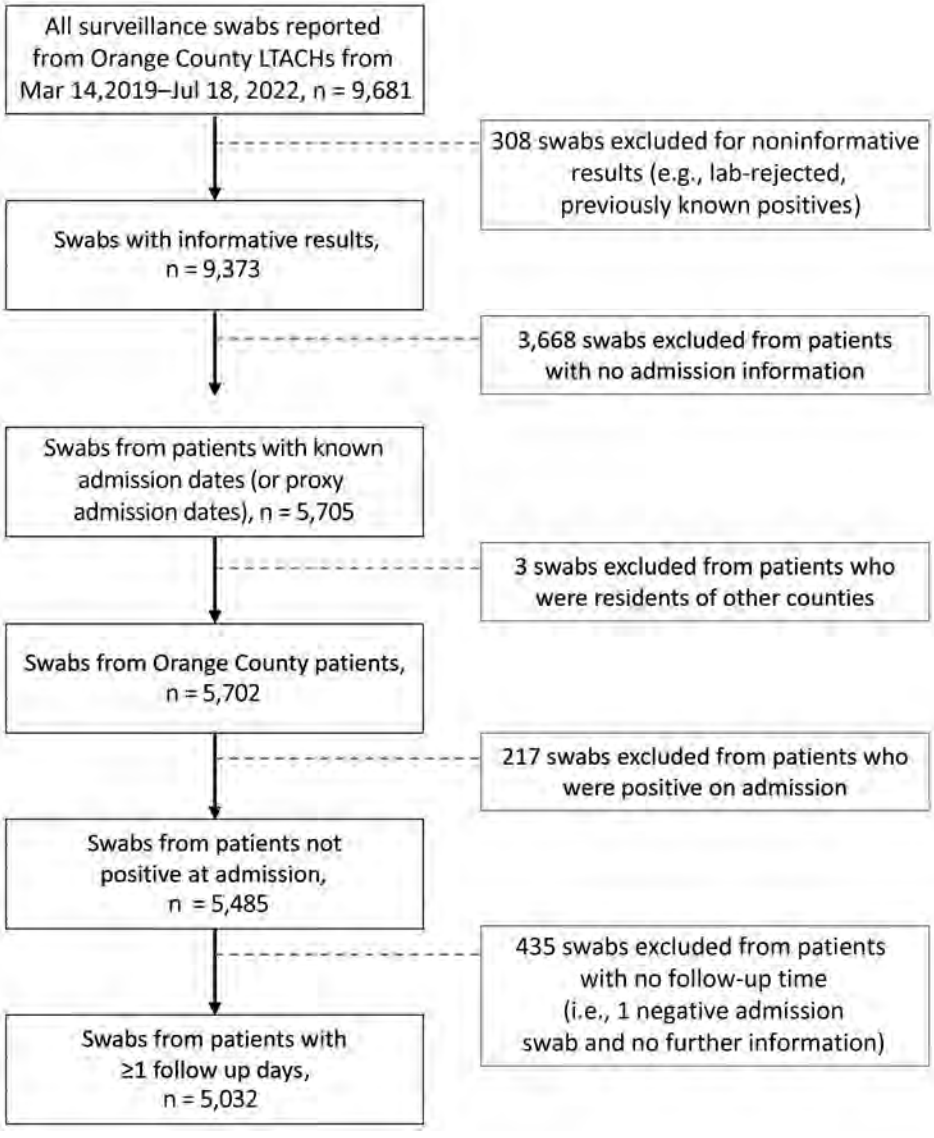

Figure 1. Flowchart showing cohort swab specimen collection and testing in study of *Candida auris* colonization early in the COVID-19 pandemic, Orange County, California, USA. LTACH, long-term acute-care hospital.

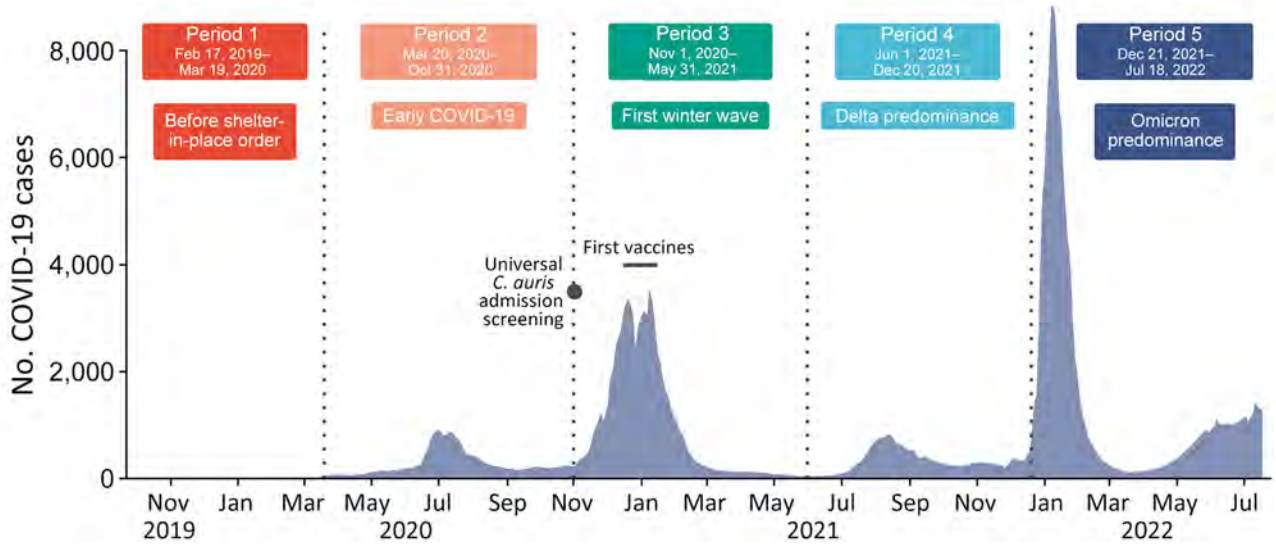

Figure 2. Seven-day moving averages of new daily COVID-19 cases in Orange County, California, USA, across 5 time periods during study of *Candida auris* colonization early in the COVID-19 pandemic. Black dot represents beginning of *C. auris* screening. Horizontal black bar represents period in which COVID vaccines first became available.

patients who had clinical cultures (such as blood or bronchoalveolar lavage samples) positive for *C. auris* before the yeast was detected via PPS screening were counted as cases. Those patients were considered positive on the collection date of the positive clinical sample. Once a patient was counted as a case, that patient was permanently considered a case and would not be rescreened.

The study duration was divided into 5 time periods for closer examination: 1 period before the initial COVID-19 shelter-in-place order and 4 periods during the COVID-19 pandemic (Figure 2). The period cut points were determined a priori on the basis of OCHCA's understanding of local COVID-19 and *C. auris* epidemiology. The cut points largely reflect COVID-19 surges and the corresponding fluctuations in infection prevention and control (IPC) resource availability. In instances where patients' exposure time straddled 2 time periods (6.4% of swab specimens), the time was assigned to the period in which most of the days were spent. We conducted a sensitivity analysis that excluded follow-up time that straddled multiple time periods, and it showed negligible effect on the results.

We ascertained death dates from Orange County's vital records data. Because the records included location of death and were well populated, we were able to verify patients were still in LTACHs on their date of death.

About the LTACHs

The average censuses among the 3 LTACHs during the 2019–2022 study period ranged from 74% to 83% of the licensed bed number, according to data from the Office of Statewide Health Planning and Development Annual Utilization Report of Hospitals (*8*,*9*,*10*,*11*). The largest facility had 109 licensed beds, and the smaller facilities had 48 and 54 licensed beds. Most rooms in the facilities served as multioccupancy rooms (typically 2–4 patients); however, if there was an infection prevention need and facility capacity, some rooms could be configured into single-occupancy rooms.

Exposure Time Calculation

We counted exposure days as the number of cumulative days a patient was admitted to an OC LTACH without a positive *C. auris* test. Exposure days were usually, but not necessarily, continuous. A patient could have exposure time from multiple admissions not temporally connected to each other.

We counted exposure time beginning at a patient's admission date (or admission screening date as proxy). For patients admitted to LTACHs before *C. auris* was first detected in the county, we imputed a start date of February 17, 2019, which is the collection date of the earliest detected *C. auris* case in Orange County. Exposure time stopped accumulating on the date of a patient's last swab or when a patient died. The 3 possible outcomes were a patient received a negative *C. auris* test and was then discharged and lost to follow-up, a patient received a positive *C. auris* test, or a patient died.

Sampling Differences During Periods 1 and 2

To avoid left-censoring, we excluded 3,668 swabs belonging to 1,732 patients, almost entirely from time

Table 1. *Candida auris* colonization frequency counts in 3 LTACHs, by time period of cases, surveillance swabs, and exposure time, during early COVID-19 pandemic, Orange County, California, USA*

	Period					
	Before shelter-in-place order	Early COVID-19	First winter wave	Delta predominance	Omicron predominance	
Characteristic	1	2	3	4	5	Total
Cases						
Skin colonization	9	15	154	57	72	304
Clinical case	0	0	3	0	0	3
Surveillance swab specimens						
Total	355	367	1,658	1,425	1,227	5,032
At admission	16	145	674	703	628	2,166
Exposure time						
Total patient-days	4,624	2,870	15,426	13,044	13,927	49,891

*Axilla and groin surveillance swab specimens were collected from patients in the 3 LTACHs in Orange County during March 14, 2019–July 18, 2022. Date ranges for each study period are shown in Figure 2. LTACH, long-term acute-care hospital.

periods 1 and 2, before universal admission surveillance was implemented. No admission dates were recorded for those patients, so we could not determine when their exposure time began.

Statistical Analysis

We plotted the cumulative incidence function estimating the probability of *C. auris* skin colonization for up to 45 days of exposure time during each period and accounted for patient death as a competing risk. Our primary outcome of interest was a difference in subdistribution estimates of *C. auris* skin colonization across time periods. We conducted Gray's test to test for equality of cause-specific cumulative incidence functions for each pair of time periods (e.g., periods 1 and 2, periods 1 and 3, periods 1 and 4) (*12*). We then adjusted the p values for multiple comparisons by using Holm's method (*13*). Next, we extracted point estimates and 95% CIs from the cumulative incidence curves at 30 days of exposure time for descriptive analysis. We chose 30 days because it was the average patient stay length in an LTACH (*14*). We overlaid and compared the extracted estimates with median *C. auris* prevalence rates from PPSs at Orange County LTACHs during each period.

To assess the effect of the smaller sample sizes during periods 1 and 2, we conducted a second sensitivity analysis in which we imputed estimated admission dates for the left-censored patients on the basis of our knowledge of past PPS dates. We plotted cumulative incidence curves and extracted point estimates and 95% CIs at 30 days of exposure time. We did not choose this approach for the final analysis because of an inability to exclude patients who were positive for *C. auris* before LTACH admission. Although the percentage of patients positive at admission was expected to be low during periods 1 and 2, particularly because admission screening was not universal, the limited availability of admission screening data prevented us from drawing that conclusion. Only 218 (7.5%) patients tested positive at admission during the full study period (0 in period 1, 6 [3.9%] in period 2, 51 [6.6%] in period 3, 78 [8.0%] in period 4, and 83 [8.3%] in period 5). We did not conduct significance testing. We computed statistics and generated plots by using the ggsurvfit (*15*), tidycmprsk (*16*), and cmprsk (*17*) packages in R version 4.3.0 (The R Project for Statistical Computing, https://www.r-project.org).

Results

The analysis included 5,032 screening swab specimens from 1,935 patients, totaling 45,343 days of associated exposure time. We ascertained an additional 43 patient-days from 3 clinical cases and 4,511 patient-days from death data. We identified 307 total *C. auris* cases for inclusion (Table 1). Patients had median of 17 (interquartile range 8–30) days of follow up time and a median of 2 (interquartile range 2–3) surveillance swab specimens.

The plotted cumulative incidence functions for the 5 time periods show markedly different trajectories

Table 2. Number of patients at risk for *Candida auris* colonization early in the COVID-19 pandemic in 3 LTACHs, by study period, Orange County, California, USA*

Study period	No. patients at 0 days	No. patients at 15 days	No. patients at 30 days	No. patients at 45 days
Period 1	104	84	53	40
Period 2	145	65	21	9
Period 3	692	364	172	81
Period 4	612	295	128	68
Period 5	563	325	159	86

*Cohort consisted of patients in the 3 LTACHs in Orange County during March 14, 2019–July 18, 2022. Date ranges for each study period are shown in Figure 2. LTACH, long-term acute-care hospital.

(Table 2; Figure 3). After adjustment for multiple comparisons, we found the curve for period 3 to be significantly different from periods 1, 4, and 5 (each p<0.001) (Table 3). Patients in OC LTACHs during period 3 had a higher probability of skin colonization than patients in periods 1, 4, or 5. The curve for period 2 appears most visually similar to period 3, but because of the small sample size during period 2, we could not detect significant differences between period 2 and other time periods.

Patients in periods 2 and 3 had the highest probabilities of skin colonization developing after 30 days of exposure; point estimates were 19.7% (95% CI 10.7–30.7%) of patients for period 2 and 22.5% (95% CI 18.5–26.6%) of patients for period 3 (Table 4). Patients in periods 1, 4, and 5 had lower probabilities: 9.2% (95% CI 4.2–16.5%) of patients for period 1, 9.6% (95% CI 6.8–13.0%) for period 4, and 10.9% (95% CI 7.9–14.5%) for period 5. The sensitivity analysis with imputed admission dates yielded similar estimates but with smaller CIs.

The probability of skin colonization occurring after 30 days of exposure rose between periods 1 and 3 and then dropped to be similar to prepandemic levels in periods 4 and 5 (Figure 4). The median *C. auris* prevalence rates from PPSs in LTACHs did not mirror the pattern we saw with cumulative incidence. Instead, median prevalence rates rose dramatically from periods 1 to 3, then remained high during periods 4 and 5.

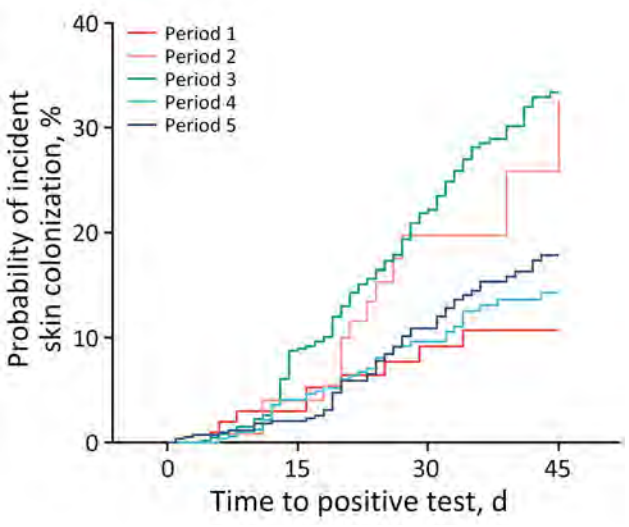

Figure 3. Cumulative incidence of *Candida auris* after 45 days of long-term acute care hospital exposure across 5 periods in study of *C. auris* colonization early in the COVID-19 pandemic, Orange County, California, USA. Date ranges for each study period are shown in Figure 2.

Discussion

Patients admitted to LTACHs in Orange County had a substantial risk of becoming colonized with *C. auris* as the pathogen emerged in the community. The risk was most pronounced during the earliest phase of the COVID-19 pandemic and during the first winter wave of COVID-19 cases (periods 2 and 3), emphasizing how pandemic-related logistical challenges faced by healthcare facilities played a pivotal role in *C. auris* transmission dynamics. Similar to other facilities nationwide, LTACHs in OC experienced critical operational challenges including shortages of personal protective equipment and disruptions to IPC practices, exacerbated by widespread concern over COVID-19 infection among both staff and patients (*18*,*19*). In response to the public health emergency, resources typically allocated to preventing the spread of pathogens such as *C. auris* were redirected to COVID-19 prevention efforts (*20*). Specifically, patient cohorting protocols prioritized COVID-19 status over *C. auris* colonization status (*21*). All those factors might have contributed to the sharp rise in *C. auris* skin colonization observed during periods 2 and 3.

After the initial COVID-19 surges abated and vaccines became more freely available, probability of *C. auris* skin colonization after 30 days of LTACH exposure decreased to approximately baseline prepandemic levels (during periods 4 and 5). The decrease occurred despite higher community prevalence of *C. auris* and the appearance of Delta- and Omicron-related COVID-19 waves. The combination of higher prevalence but lower cumulative incidence seen during those periods indicates that within-facility transmission can be reduced with close adherence to IPC. However, although transmission was mitigated, it was not eliminated. Newly colonized case-patients continued to be identified routinely across all time

Table 3. Comparison of *Candida auris* colonization rates in 3 LTACHs, by study period, during early COVID-19 pandemic, Orange County, California, USA*

Period comparison	Unadjusted Gray's test	Adjusted for multiple comparisons
1 and 2	0.032	0.224
1 and 3	**<0.001**	**<0.001**
1 and 4	0.115	0.557
1 and 5	0.038	0.229
2 and 3	0.171	0.557
2 and 4	0.111	0.557
2 and 5	0.207	0.557
3 and 4	**<0.001**	**<0.001**
3 and 5	**<0.001**	**<0.001**
4 and 5	0.423	0.557

*Bold values represent significance at p = 0.05. Cohort consisted of patients in the 3 LTACHs in Orange County during March 14, 2019–July 18, 2022. Date ranges for each study period are shown in Figure 2. LTACH, long-term acute-care hospital.

Table 4. Probability of *Candida auris* skin colonization in 3 LTACHs, by time period and cumulative exposure time, during early COVID-19 pandemic, Orange County, California, USA*

Time period	Cumulative exposure time		
	15 days	30 days	45 days
1	3.0% (0.8%–7.8%)	9.2% (4.2%–16.5%)	10.7% (5.2%–18.6%)
2	4.0% (1.3%–9.3%)	19.7% (10.7%–30.7%)	32.7% (15.1%–51.6%)
3	9.0% (6.7%–11.6%)	22.5% (18.5%–26.6%)	33.4% (28.3%–38.5%)
4	4.1% (2.5%–6.2%)	9.6% (6.8%–13.0%)	14.3% (10.4%–18.8%)
5	2.0% (1.0%–3.6%)	10.9% (7.9%–14.5%)	17.8% (13.6%–22.5%)

*Values are point estimates (95% CI). Cohort consisted of patients in the 3 LTACHs in Orange County during March 14, 2019–July 18, 2022. Date ranges for each study period are shown in Figure 2. LTACH, long-term acute-care hospital.

periods. This result is consistent with findings from previous studies showing that, once *C. auris* transmission is established in LTACHs, preventing ongoing transmission becomes exceptionally challenging because of long-term patient colonization and persistence of *C. auris* on nosocomial surfaces (*22*,*23*).

The wealth of data collected from PPSs helped guide public health recommendations and enabled OCHCA to track transmission dynamics as *C. auris* transitioned from emerging to established transmission in OC. That type of patient-level longitudinal data is highly valuable but rarely available, especially in real-time. Building infrastructure that makes data collection and use more accessible could evolve our understanding of pathogen transmission dynamics and improve public health guidance for intervention and response efforts.

As of March 2025, all 3 local LTACHs in Orange County continue to perform admission screenings through their private laboratories. OCHCA continues to support PPSs in those facilities, albeit at a more relaxed interval of approximately every 3 months. Both measures require a major resource investment from LTACHs and public health; however, both entities recognize the value and importance of those efforts. Investing in prevention can save on resources used to respond to outbreaks and can prevent potentially serious infections in at-risk patients. Future modeling efforts could distinguish the individual effects of both admission screenings and PPSs on *C. auris* transmission. By identifying the most effective applications of each approach, those models could help optimize resource use and reduce the overall investment required.

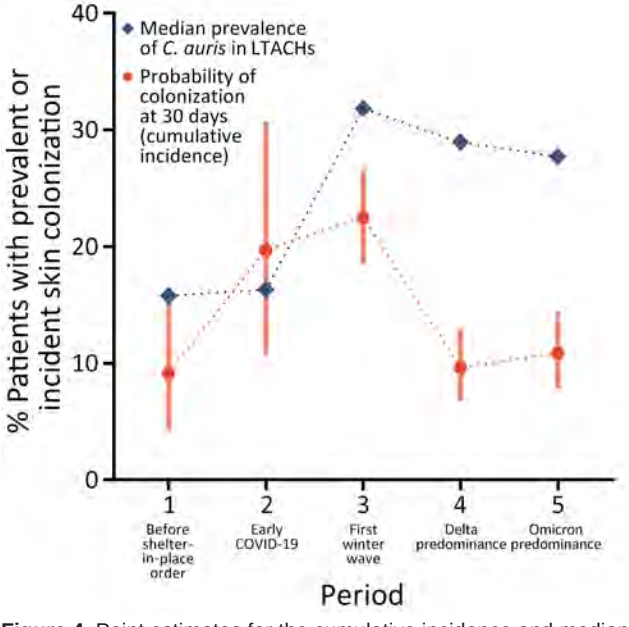

Figure 4. Point estimates for the cumulative incidence and median prevalence of *Candida auris* skin colonization in long-term acute care hospitals across 5 periods in study of *C. auris* colonization early in the COVID-19 pandemic, Orange County, California, USA. Date ranges for each study period are shown in Figure 2. LTACH, long-term acute-care hospital.

Our analysis likely missed cases in all time periods. Skin colonization has been documented to occur in as little as 4 hours after exposure (*24*); it is possible that some patients were exposed after admission but before their admission swab specimen was collected and were mistakenly counted as positive at admission and excluded from the model. Similarly, some patients may have had skin colonization develop shortly before discharge or death, and those would not always be captured. In addition, although the surveillance tests rarely produce false-positive results, they have imperfect sensitivity and can potentially produce false-negative results because of several factors (*25*–*27*).

The exclusion of swab specimens from patients without admission dates introduced sampling bias for periods 1 and 2. During those periods, patients who tested positive or who were exposed to a known *C. auris* case (i.e., had a positive roommate or resided in a room previously occupied by a positive patient) had more complete data collection because of OCHCA conducting individual-level case investigations when *C. auris* was new to Orange County. Of consequence, those patients were more likely to have recorded admission dates and be included in the analysis, potentially biasing the estimates upwards. This fact was especially true during period 2, when our resources were diverted to COVID-19 response and contact tracing efforts for *C. auris* were downsized, creating further bias as to which patients

received screenings. We handled the possible bias by taking it into consideration during interpretation of the results. We understood the probability of skin colonization to be very low during period 1 when *C. auris* was new to Orange County and believe it is likely overestimated in this study. Therefore, the finding that period 1 had a lower rate of skin colonization compared with period 3 should be considered conservative. In addition, the results of the sensitivity analysis with imputed admission dates indicate that the estimates for periods 1 and 2 are stable despite the smaller sample sizes. We expected the cumulative incidence to remain overestimated in the sensitivity analysis because PPSs were performed in response to identification of new cases during those periods, namely, when the chances of identifying new cases was highest. This understanding, combined with the smaller sample size, again makes statements about period 1 estimates being lower than those from other periods conservative.

This study is insufficient to evaluate the public health effect of PPSs and universal admission screening. To do so, we would need a model that could account for changes in the underlying patient population and transmission dynamics over time, particularly considering changes related to the first several COVID-19 surges. The model in this study does not delineate the individual contribution of admission screenings, PPSs, or other critical factors.

Our findings contribute to existing literature by quantifying the effect of IPC disruptions on *C. auris* transmission during the early stages of the COVID-19 pandemic and by highlighting the substantial risk of colonization once *C. auris* is introduced into an LTACH. Data from PPSs and admission screenings can serve as a valuable tool for monitoring facility transmission dynamics and for guiding decision making. Enhanced data collection and modeling might further clarify the role of admission screenings and PPSs in reducing the spread of *C. auris* and other hospital-acquired infections.

Acknowledgments

We thank Meghan Lyman, Malavika Rajeev, and Michelle L. Fearon Scales for their consultations and insightful guidance. We also thank Lawrence Bottorff for educating our team and providing steadfast support throughout the course of this work.

About the Author

Ms. Dratch was previously a senior epidemiologist for the Orange County Healthcare Agency and is currently a principal biostatistician with Edwards Lifesciences. Her research interests included vectorborne diseases, COVID-19 response, hospital-acquired infections, and multidrug-resistant organisms.

References

1. Tsay S, Kallen A, Jackson BR, Chiller TM, Vallabhaneni S. Approach to the investigation and management of patients with *Candida auris*, an emerging multidrug-resistant yeast. Clin Infect Dis. 2018;66:306–11. https://doi.org/10.1093/cid/cix744
2. Centers for Disease Control and Prevention. *Candida auris* (*C. auris*). Preventing the spread of *C. auris*. 2024 [cited 2025 Jan 28]. https://www.cdc.gov/candida-auris/prevention/index.html
3. Rossow J, Ostrowsky B, Adams E, Greenko J, McDonald R, Vallabhaneni S, et al.; New York Candida auris Investigation Workgroup. Factors associated with *Candida auris* colonization and transmission in skilled nursing facilities with ventilator units, New York, 2016–2018. Clin Infect Dis. 2021;72:e753–60. https://doi.org/10.1093/cid/ciaa1462
4. Adams E, Quinn M, Tsay S, Poirot E, Chaturvedi S, Southwick K, et al.; Candida auris Investigation Workgroup. *Candida auris* in healthcare facilities, New York, USA, 2013–2017. Emerg Infect Dis. 2018;24:1816–24. https://doi.org/10.3201/eid2410.180649
5. Kerins JL, Tang AS, Forsberg K, Jegede O, Ealy M, Pacilli M, et al. Rapid emergence of *Candida auris* in the Chicago region. Open Forum Infect Dis. 2018;5(suppl_1):S28. https://doi.org/10.1093/ofid/ofy209.064
6. Karmarkar EN, O'Donnell K, Prestel C, Forsberg K, Gade L, Jain S, et al. Rapid assessment and containment of *Candida auris* transmission in postacute care settings—Orange County, California, 2019. Ann Intern Med. 2021;174:1554–62. https://doi.org/10.7326/M21-2013
7. O'Donnell K, Karmarkar E, Jackson BR, Epson E, Zahn M. Public health oversight of interfacility transfers during a *Candida auris* outbreak—Orange County, California, 2019. Infect Control Hosp Epidemiol. 2020;41(S1):s76–7. https://doi.org/10.1017/ice.2020.567
8. California Office of Statewide Health Planning and Development. 2019 calendar year hospital utilization pivot table. 2019 [cited 2024 Jan 26]. https://data.chhs.ca.gov/dataset/hospital-annual-utilization-report/resource/144b3a4f-2fda-44bb-9934-bc5d17b29176
9. California Office of Statewide Health Planning and Development. 2020 calendar year hospital utilization pivot table. 2020 [cited 2024 Jan 26]. https://data.chhs.ca.gov/dataset/hospital-annual-utilization-report/resource/19a02e57-a4d1-408c-9ec9-dd3c56f7a0ca
10. California Office of Statewide Health Planning and Development. 2021 calendar year hospital utilization pivot table. 2021 [cited 2024 Jan 26]. https://data.chhs.ca.gov/dataset/hospital-annual-utilization-report/resource/c5d3b100-470b-430e-b5a4-371a33e42292
11. California Office of Statewide Health Planning and Development. 2022 calendar year hospital utilization pivot table. 2022 [cited 2024 Jan 26]. https://data.chhs.ca.gov/dataset/hospital-annual-utilization-report/resource/6af715ad-0de7-4b85-bd59-2746016ced2b
12. Gray RJ. A class of *K*-sample tests for comparing the cumulative incidence of a competing risk. Ann Stat. 1988;16:1141–54. https://doi.org/10.1214/aos/1176350951
13. Holm S. A simple sequentially rejective multiple test procedure. Scand J Stat Theory Appl. 1979;6:65–70.

14. American Speech-Language-Hearing Association. Long-term acute care hospitals [cited 2024 Feb 11]. https://www.asha.org/slp/healthcare/ltac
15. Sjoberg DD, Baillie M, Fruechtenicht C, Haesendonckx S, Treis T. ggsurvfit. Flexible time-to-event figures. 2023 [cited 2024 Feb 11]. https://cran.r-project.org/web/packages/ggsurvfit
16. Sjoberg DD, Fei T. tidycmprsk: competing risks estimation. 2023 [cited 2024 Feb 11]. https://cran.r-project.org/web/packages/tidycmprsk
17. Gray B. cmprsk: subdistribution analysis of competing risks. 2022 [cited 2024 Feb 11]. https://cran.r-project.org/web/packages/cmprsk
18. Wisckol M. Medical workers fear for their safety—and everyone else's—in coronavirus outbreak. Orange County Register. 2020 Mar 19 [cited 2024 Feb 19]. https://www.ocregister.com/2020/03/19/medical-workers-fear-for-their-safety-and-everyone-elses-in-coronavirus-outbreak
19. World Health Organization. Shortage of personal protective equipment endangering health workers worldwide [cited 2024 Feb 19]. https://www.who.int/news/item/03-03-2020-shortage-of-personal-protective-equipment-endangering-health-workers-worldwide
20. Centers for Disease Control and Prevention. COVID-19. U.S. impact on antimicrobial resistance, special report 2022 [cited 2024 Feb 19]. https://stacks.cdc.gov/view/cdc/117915
21. Mitsunaga T, Holden D, Karmarkar E, Kennedy I, Nelson T, Haridass V, et al. 169. The resurgence of *Candida auris* in California during the novel coronavirus (COVID-19) pandemic, May 2020–May 2021. Open Forum Infect Dis. 2021;8(Supplement_1):S101–2. https://doi.org/10.1093/ofid/ofab466.169
22. Vila T, Sultan AS, Montelongo-Jauregui D, Jabra-Rizk MA. *Candida auris*: a fungus with identity crisis. Pathog Dis. 2020;78:ftaa034. https://doi.org/10.1093/femspd/ftaa034
23. Forsberg K, Woodworth K, Walters M, Berkow EL, Jackson B, Chiller T, et al. *Candida auris*: the recent emergence of a multidrug-resistant fungal pathogen. Med Mycol. 2019;57:1–12. https://doi.org/10.1093/mmy/myy054
24. Schelenz S, Hagen F, Rhodes JL, Abdolrasouli A, Chowdhary A, Hall A, et al. First hospital outbreak of the globally emerging *Candida auris* in a European hospital. Antimicrob Resist Infect Control. 2016;5:35. https://doi.org/10.1186/s13756-016-0132-5
25. Pacilli M, Kerins JL, Clegg WJ, Walblay KA, Adil H, Kemble SK, et al. Regional emergence of *Candida auris* in Chicago and lessons learned from intensive follow-up at 1 ventilator-capable skilled nursing facility. Clin Infect Dis. 2020;71:e718–25. https://doi.org/10.1093/cid/ciaa435
26. Proctor DM, Dangana T, Sexton DJ, Fukuda C, Yelin RD, Stanley M, et al.; NISC Comparative Sequencing Program. Integrated genomic, epidemiologic investigation of *Candida auris* skin colonization in a skilled nursing facility. Nat Med. 2021;27:1401–9. https://doi.org/10.1038/s41591-021-01383-w
27. Arenas SP, Persad PJ, Patel S, Parekh DJ, Ferreira TBD, Farinas M, et al. Persistent colonization of *Candida auris* among inpatients rescreened as part of a weekly surveillance program. Infect Control Hosp Epidemiol. 2024;45:762–5. https://doi.org/10.1017/ice.2023.251

Address for correspondence: Matthew Zahn, Orange County Healthcare Agency Communicable Disease Control, 1719 W 17th St, Santa Ana, CA 92706, USA; email: mzahn@ochca.com

Differences in Lyme Disease Diagnosis among Medicaid and Medicare Beneficiaries, United States, 2016–2021

L. Hannah Gould, Sarah J. Willis, Christopher G. Prener, Stephanie A. Duench, Holly Yu, Luis Jodar, Jennifer C. Moïsi, James H. Stark

Lyme disease is the most common vectorborne disease in the United States. Evidence suggests that persons from racial and ethnic minority groups experience more severe disease. We used a claims-based algorithm on data from 16 jurisdictions with high Lyme disease incidence to identify cases among 4 populations: Medicaid beneficiaries ≤18 and ≥19 years of age, and Medicare fee-for-service beneficiaries <65 and ≥65 years of age. We calculated the prevalence of disseminated disease, hospitalization, and other clinical and epidemiologic parameters by race and ethnicity. We found that non-White persons were more likely than White persons to be female, hospitalized at diagnosis, diagnosed outside of primary care, diagnosed outside of the peak months for Lyme disease transmission, and have disseminated disease. Those data illustrate differences in Lyme disease by race and ethnicity and suggest possible differences across other sociodemographic characteristics. Additional prevention methods are needed to reduce differences in Lyme disease recognition and severity.

Lyme disease is the most reported vectorborne disease in the United States, and ≈476,000 cases are diagnosed and treated annually (*1*,*2*). Lyme disease is caused by infection with the bacterium *Borrelia burgdorferi* sensu lato, which is transmitted to humans by the bite of infected *Ixodes* spp. ticks. Approximately 80% of Lyme disease patients experience an erythema migrans rash at the site of the tick bite (*3*). Without recognition or treatment, the bacteria can disseminate and infect multiple organ systems, resulting in a range of disseminated manifestations that can have neurologic, cardiac, and musculoskeletal presentations (*3*). Although all manifestations are treatable with recommended antimicrobial drugs (*4*), patients with later-stage manifestations are more likely to be hospitalized and to have persistent symptoms after treatment than patients diagnosed with early, localized manifestations (*3*).

In US Lyme disease surveillance data, >90% of cases with reported race are in persons who identify as White (*5*,*6*). That demographic distribution is thought to reflect the populations residing in areas where infected ticks are most common, which tend to be more affluent and educated rural and suburban communities in northeastern and midwestern states that have predominantly White populations (*7*–*9*). However, accumulated evidence has shown that non-White persons, particularly persons who identify as Black or African American, have higher rates of disseminated manifestations of Lyme disease, such as neurologic manifestations and arthritis, than do White persons (*10*–*15*). Higher rates of disseminated manifestations among non-White persons likely are caused in part by difficulty seeing and recognizing erythema migrans rash on darker skin, which can lead to misdiagnosis or delayed or missed diagnoses.

Author affiliations: Global Vaccines Medical Affairs, Pfizer, Inc., New York, New York, USA (L.H. Gould); Global Vaccines Medical Affairs, Pfizer, Inc., Cambridge, Massachusetts, USA (S.J. Willis, J.H. Stark); RWE Platforms and Partnerships, Pfizer, Inc., New York (C.G. Prener); US Medical Affairs, Vaccines and Anti-infectives, Pfizer, Inc., Collegeville, Pennsylvania, USA (S.A. Duench); Global HTA, Value & Evidence Vaccines, Pfizer, Inc., Collegeville (H. Yu); Global Vaccines Medical Affairs, Pfizer, Inc., Collegeville (L. Jodar); Global Vaccines Medical Affairs, Inc., Pfizer, Paris, France (J.C. Moïsi)

DOI: https://doi.org/10.3201/eid3109.241653

Other factors, including differential risk behaviors and knowledge (*16*), likely create and perpetuate the differences in Lyme disease diagnoses (*10*).

Prior studies examining Lyme disease epidemiology by race and ethnicity have been too small to fully disaggregate results by group or have collected data that only enabled comparison of outcomes for White versus non-White persons. Given the heterogeneity of the non-White group, analyses using datasets sufficiently powered to generate incidence estimates and more fully describe disease characteristics and progression by race and ethnic group can improve the characterization of Lyme disease epidemiology.

Medicaid and Medicare are health insurance programs administered by the US Centers for Medicaid and Medicare Services. Medicaid provides healthcare coverage to persons with lower income, and Medicare provides coverage for adults ≥65 years of age and persons of any age with a qualifying disability, end-stage renal disease, or amyotrophic lateral sclerosis (Lou Gehrig's disease). Administrative claims data from those programs provide an opportunity to obtain a robust sample to further disaggregate disease outcomes by race and ethnicity. We used administrative claims data to investigate the demographic and clinical characteristics, disease outcomes, and healthcare utilization for Lyme disease cases among Medicaid and Medicare beneficiaries residing in US jurisdictions with high Lyme disease incidence rates.

Materials and Methods

Study Design

We conducted a retrospective cross-sectional study using Medicare and Medicaid administrative claims databases covering the period of January 1, 2016–December 31, 2021. The study population included persons residing in high-incidence jurisdictions, which are defined as states with an average Lyme disease incidence of ≥10 confirmed cases/100,000 population for a period of 3 consecutive years (*5*). The included jurisdictions were the states of Connecticut, Delaware, Massachusetts, Maryland, Maine, Minnesota, New Hampshire, New Jersey, New York, Pennsylvania, Rhode Island, Virginia, Vermont, West Virginia, and Wisconsin and the District of Columbia (*5*). We included cases recorded in Medicaid or Medicare fee-for-service administrative claims databases during the study period that met the inclusion criteria.

Data Sources

The Medicare and Medicaid databases include enrollment information and adjudicated claims for inpatient care, ambulatory care, and outpatient prescriptions. Data available for facility and professional service claims include the dates and places of service, diagnoses, procedures performed, services rendered, and number of visits for professional services. Data available for outpatient pharmacy claims were the drug dispensed, dispensing date, dose, quantity, and number of therapy days supplied.

Case Identification and Inclusion Criteria

Inclusion criteria were continuous enrollment in Medicaid or Medicare benefits for ≥183 days during the study period and residence in a jurisdiction with high Lyme disease incidence at the beginning of each eligible enrollment period; we permitted an enrollment gap of up to 45 days to allow for administrative disruptions in coverage. In addition, for Lyme disease cases, we only included patients who were enrolled for at least 183 days before their Lyme disease diagnosis date. We excluded 15% of cases among Medicaid beneficiaries and 3.4% among Medicare beneficiaries because information on self-reported race/ethnicity was missing. We also excluded beneficiaries with ≥1 Lyme disease diagnosis during the 183 days before the date they met criteria of the case identification algorithm.

We adapted Lyme disease case identification and classification algorithms from prior studies (*2*,*17*) (Appendix Table 1, https://wwwnc.cdc.gov/EID/article/31/9/24-1653-App1.pdf). In brief, we defined an outpatient Lyme disease case as ≥1 Lyme disease diagnosis code from the International Classification of Diseases, 10th Revision, Clinical Modification (ICD-10-CM), including A69.20, Lyme disease, unspecified; A69.21, meningitis due to Lyme disease; A69.22, other neurologic disorders in Lyme disease; A69.23, arthritis due to Lyme disease; or A69.29, other conditions associated with Lyme disease. Included case-patients also had ≥7 days of dispensed oral antibiotics (doxycycline, amoxicillin, azithromycin, or cefuroxime axetil), identified using National Drug Codes, or ≥1 Healthcare Common Procedure Coding System code for intravenous antibiotics (Appendix Table 2) within 30 days of diagnosis. We defined an inpatient case as a principal Lyme disease diagnosis code (ICD-10-CM, A69.2x) or a principal diagnosis code of a documented objective clinical manifestation of Lyme disease or a tickborne disease transmitted by the same vector (e.g., babesiosis) and a secondary diagnosis code for Lyme disease in the same record per the algorithm.

We further classified Lyme disease cases as localized or disseminated. For disseminated Lyme

disease, we classified cases by neurologic, cardiac, or musculoskeletal manifestations, on the basis of the ICD-10-CM codes in the administrative claims (Appendix Table 3). A person could be counted as having a Lyme disease case ≥1 time during the study period if ≥183 days had elapsed since the previous diagnosis and the subsequent case happened in the next calendar year.

Analyses

We separately conducted analyses for each data source and age group. Thus, we had 4 analytic populations: Medicaid beneficiaries ≤18 years of age, Medicaid beneficiaries ≥19 years of age, Medicare beneficiaries <65 years of age (disability group), and Medicare beneficiaries ≥65 years of age.

Beneficiaries self-identify their race and ethnicity at enrolment. We combined those variables into a single variable with mutually exclusive categories: White, Black or African American, Hispanic, Asian/Pacific Islander, Native American, and other (i.e., patients who selected other and multiracial for race). We used descriptive statistics to summarize continuous variables by mean and SD and categorical variables by frequency and percentage for the following: demographic data (age, sex, seasonality), clinical characteristics and disease outcomes (disease manifestations, hospitalization, underlying conditions), and healthcare utilization (type of provider who diagnosed Lyme disease; number of sick visits in the 30, 60, and 183 days before Lyme disease diagnosis, antibiotic prescriptions; and laboratory testing within 30 days of Lyme disease diagnosis). We defined sick visits as visits that were not billed with codes for routine health examinations or other preventive reevaluation and management codes. We assessed seasonality by calculating counts and percentage of cases by month and peak Lyme disease season (June–August vs. September–March).

We calculated Lyme disease incidence by race or ethnicity for algorithm-defined Lyme disease overall and for disseminated and localized Lyme disease. We calculated incidence across the entire study period among all patients who had ≥183 days of continuous enrollment in Medicaid or Medicare as the number of beneficiaries with algorithm-defined Lyme disease per 100,000 person-years.

Observed Person-Time at Risk for Lyme disease

We defined person-time at risk for Lyme disease from date of eligibility to the first instance of meeting the case ascertainment algorithm or end of continuous follow-up, whichever came first: end of study period, withdrawal from health insurance, or death. For beneficiaries with subsequent Lyme disease cases during the study period, we only used the first case for assessing person-time and calculating incidence rates.

We calculated prevalence ratios (PRs) and 95% CIs by using White persons as the reference group. We considered a PR statistically significant when the 95% CI did not include 1.0. We used *t*-tests to evaluate differences in means for continuous variables and χ^2 tests to compare the distribution of disseminated disease manifestations between groups and considered $p<0.05$ statistically significant. We performed all analyses and data management in SAS 9.4 (SAS Institute, Inc., https://www.sas.com) and Databricks version 15.4 (https://docs.databricks.com).

Because of sample size limitations, we summarized most analyses as White versus non-White. We disaggregated analyses of incidence, risk of developing disseminated disease, and hospitalization at the time of diagnosis by race and ethnic group. Because the study involved data that exist in anonymized structured format and contained no patient personal information, we were not required to have institutional review board approval.

Results

In Medicaid data from 2016–2021, we identified 33,776 Lyme disease cases among beneficiaries ≤18 years of age and 30,935 cases among beneficiaries ≥19 years of age. In Medicare data from 2016–2021, we identified 12,911 Lyme disease cases among beneficiaries <65 years of age and 90,913 among beneficiaries ≥65 years of age. Most cases were in persons who identified as White, ranging from 85.0% among Medicaid beneficiaries ≥19 years of age to 96.6% among Medicare beneficiaries ≥65 years of age (Table 1).

Incidence

Medicare recipients ≥65 years of age had the highest overall incidence and highest incidence of localized (209.4/100,000 person-years) and disseminated (54.5/100,000 person-years) disease; Medicare recipients <65 years of age also had high incidence of localized (118.4/100,000 person-years) and disseminated (47.6/100,000 person-years) disease. Medicaid beneficiaries ≤18 years of age had the lowest incident rates for localized (73.3/100,000 person-years) and disseminated (15.7/100,000 person-years) disease. Across all age and beneficiary groups, incidence of disease was highest among White persons; next highest rates were among persons who identified as Native American, and lowest rates were among persons who identified as Black or African American (Table 1).

Table 1. Number of cases and incidence in a study of differences in Lyme disease diagnosis among Medicaid and Medicare beneficiaries, United States, 2016–2021*

Group	Total no. (%) cases†	Localized Lyme disease			Disseminated Lyme disease		
		No. cases	Person-years	Incidence‡	No. cases	Person-years	Incidence‡
Medicaid, age ≤18 y	33,776	27,165	37,110,817	73.3	5,798	27,058,337	15.7
White	29,405 (87.1)	24,093	17,461,207	138.1	4,576	17,412,994	26.3
Black, African American	1,244 (3.7)	744	9,611,964	7.8	483	9,611,379	5.0
Asian, Pacific Islander	741 (2.2)	551	2,783,663	19.8	181	2,782,940	6.5
Hispanic	2,063 (6.1)	1,526	6,833,641	22.4	495	6,831,111	7.3
Native American	208 (0.6)	159	268,217	59.3	44	267,950	16.4
Other	115 (0.3)	92	152,126	60.5	19	151,963	12.5
Medicaid, age ≥19 y	30,935	23,663	25,536,958	92.7	5,380	25,496,013	21.1
White	26,298 (85.0)	20,456	13,156,621	155.6	4,214	13,120,278	32.1
Black, African American	1,461 (4.7)	978	6,188,543	15.8	408	6,187,289	6.6
Asian, Pacific Islander	1,082 (3.5)	813	2,745,246	29.6	212	2,743,918	7.7
Hispanic	1,867 (6.0)	1,253	3,235,335	38.8	500	3,233,589	15.5
Native American	191 (0.6)	133	168,295	79.1	40	168,080	23.8
Other	36 (0.1)	–	–	–	–	–	–
Medicare, age <65 y	12,911	8,204	6,933,720	118.4	3,293	6,923,326	47.6
White	11,845 (91.7)	7,581	5,149,098	147.3	2,930	5,139,283	57.1
Black, African American	513 (4.0)	284	1,267,371	22.4	205	1,267,135	16.2
Asian, Pacific Islander	72 (0.6)	50	105,505	47.4	16	105,440	15.2
Hispanic	293 (2.3)	181	284,434	63.7	84	284,264	29.6
Native American	53 (0.4)	32	32,348	99.0	14	32,306	43.4
Other	135 (1.0)	76	94,964	80.1	44	94,897	46.4
Medicare, age ≥65 y	90,913	65,298	31,199,802	209.4	16,938	31,087,605	54.5
White	87,831 (96.6)	63,252	27,353,152	231.4	16,201	27,243,943	59.5
Black, African American	1,172 (1.3)	753	2,299,786	32.8	324	2,298,791	14.1
Asian, Pacific Islander	591 (0.7)	410	649,660	63.2	141	649,082	21.7
Hispanic	283 (0.3)	183	357,614	51.2	76	357,380	21.3
Native American	64 (0.1)	45	30,197	149.1	14	30,127	46.5
Other	872 (1.1)	655	509,397	128.7	182	508,283	35.8

*–, sample size too small to calculate rate.
†Total cases include all cases of Lyme disease identified during the study period. For incidence rate calculations, we included only the first case during the study period for beneficiaries with subsequent Lyme disease diagnoses.
‡Incidence rate was calculated across the entire study period among all persons who had ≤183 days of continuous enrollment in Medicaid or Medicare and resided in a high incidence state as follows: incidence = [(number beneficiaries with Lyme disease algorithm-defined Lyme disease)/(observed person-time at risk for Lyme disease)] × 100,000 person-years.

Characteristics of Lyme Disease Cases

We noted marked differences in the characteristics of Lyme disease cases for White and non-White Medicaid and Medicare beneficiaries (Tables 2, 3; Appendix Tables 4–7). In all groups, disseminated disease was more prevalent among non-White persons, particularly among Medicaid beneficiaries ≤18 years of age (PR 1.77 [95% CI 1.68–1.87]) and ≥19 years of age (PR 1.57 [95% CI 1.49–1.66]). We saw the highest prevalence of disseminated disease among Black/African American Medicare beneficiaries <65 years of age (42.7%, 294/513) and Black/African American Medicaid beneficiaries ≤18 years of age (39.1%, 487/1,244) (Appendix Tables 4, 6).

Musculoskeletal disease (arthritis) was the most common disseminated manifestation among Medicaid beneficiaries of all ages and was more prevalent among non-White than White beneficiaries ≤18 years of age (941/4371 [76.3%] vs. 3,353/29,405 [71.6%]; p = 0.00006) and ≥19 years of age (704/4637 [55.9%] vs. 2,299/26,298 [50.6%]; p = 0.002) (Table 2). Among Medicare beneficiaries, neurologic manifestations were the most common disseminated manifestation, but we noted no difference in the prevalence of disseminated manifestations by race or ethnic group among Medicare beneficiaries ≥65 years of age (Table 3).

Across all age and beneficiary groups, non-White persons had a higher prevalence of hospitalization at diagnosis, particularly among Medicaid beneficiaries ≤18 years of age (PR 1.96 [95% CI 1.67–2.30]). Non-White persons with Lyme disease were more likely to be female and were more likely to be diagnosed during September–March, outside of the peak months for Lyme disease transmission.

Among Medicaid beneficiaries, we noted no difference between White and non-White persons in the prevalence of diagnosis outside of primary care. Among Medicaid beneficiaries ≥19 years of age, non-White persons had a higher mean Quan-Carlson Comorbidity Index score than did White persons (Table 2). Among Medicare beneficiaries, non-White persons were more likely to have a diagnosis outside of primary care and had higher mean Quan-Charlson Comorbidity Index scores than were White persons (Table 3).

Non-White beneficiaries also had more sick visits in the 30 and 60 days before Lyme disease diagnosis

than did White persons, except among Medicare beneficiaries <65 years of age, for whom we noted no difference. Non-White Medicaid beneficiaries ≥19 years of age also had more sick visits in the 183 days before Lyme disease diagnosis than did White beneficiaries. Among Medicare beneficiaries ≥65 years of age, White beneficiaries had more sick visits in the 183 days before Lyme disease diagnosis than did non-White beneficiaries.

Among Medicaid beneficiaries ≤18 years of age, we noted no differences in the prevalence of receiving an amoxicillin or doxycycline prescription by White versus non-White race/ethnicity. In the other 3 groups, non-White beneficiaries were more likely than White beneficiaries to receive an amoxicillin prescription and less likely to receive a doxycycline prescription.

Among Medicare beneficiaries <65 years of age, we saw no difference in the percentage of persons who received a *B. burgdorferi* antibody test by White versus non-White race/ethnicity. In the other 3 groups, non-White beneficiaries were more likely than White beneficiaries to have had antibody testing.

Disseminated Disease and Hospitalization by Disaggregated Race and Ethnic Group

Black/African American, Asian/Pacific Islander, and Hispanic Medicaid beneficiaries of all ages and Medicare beneficiaries <65 years of age were more likely than White beneficiaries to have disseminated Lyme disease manifestations (Table 4). Black/African American, Asian/Pacific Islander, and Hispanic pediatric Medicaid beneficiaries were also more likely to be hospitalized than were White beneficiaries. Compared with White Medicaid beneficiaries ≤18 years of age, Black/African American children had a PR of 2.35 (95% CI 2.15–2.56) for developing disseminated disease and PR of 2.57 (95% CI 1.96–3.36) for hospitalization.

Seasonality

Among all groups, June and July were the peak months for Lyme disease diagnosis (Appendix Figure). White persons were more likely than non-White persons to receive a Lyme disease diagnosis during the summer months. Across all groups, Black/African American persons were more likely to receive diagnoses during December–February than during peak Lyme disease months.

Discussion

Using 2 large administrative datasets that include healthcare claims for nearly 40% of children and half of older adults in the United States (*18*,*19*), this study found substantial differences in Lyme disease diagnoses across race and ethnic groups in the United States. Those differences were most pronounced for

Table 2. Clinical characteristics of cases among Medicaid beneficiaries in a study of differences in Lyme disease diagnosis among Medicaid and Medicare beneficiaries, United States, 2016–2021*

	Medicaid, age ≤18 y			Medicaid, age ≥19 y		
Characteristic	White, n = 29,405	Non-White, n = 4,371	PR (95% CI) or p value	White, n = 26,298	Non-White, n = 4,637	PR (95% CI) or p value
Disseminated disease†	4,685 (15.9)	1,234 (28.2)	1.77 (1.68–1.87)	4,542 (17.3)	1,259 (27.2)	1.57 (1.49–1.66)
Neurologic	1,248 (26.6)	265 (21.5)	0.00006	2,054 (45.2)	518 (41.1)	0.002
Musculoskeletal	3,353 (71.6)	941 (76.3)	NA	2,299 (50.6)	704 (55.9)	NA
Cardiac	84 (1.8)	28 (2.3)	NA	189 (4.2)	37 (2.9)	NA
Hospitalization at diagnosis	645 (2.2)	188 (4.3)	1.96 (1.67–2.30)	1,124 (4.3)	229 (4.9)	1.56 (1.01–1.33)
Diagnosed outside of primary care‡	4,170 (17.7)	644 (19.1)	1.08 (0.99–1.18)	4,893 (23.2)	824 (23.1)	0.99 (0.92–1.08)
Diagnosed during September–March	6,271 (21.3)	1,204 (27.5)	1.29 (1.23–1.36)	7,351 (28.0)	1,596 (34.4)	1.23 (1.18–1.29)
Sex						
M	16,227 (55.2)	2,301 (52.6)	Referent	12,067 (45.9)	1,627 (35.1)	Referent
F	13,178 (44.8)	2,070 (47.4)	1.06 (1.02–1.09)	14,231 (54.1)	3,010 (64.9)	1.20 (1.17–1.23)
Mean Quan-Charlson Comorbidity Index score (SD)	1.1 (0.3)	1.1 (0.2)	0.339	1.7 (1.3)	1.8 (1.5)	0.003
Mean no. visits before diagnosis (SD)						
≤30 d before	1.8 (2.5)	2.0 (2.5)	<0.0001	2.7 (3.4)	3.2 (3.6)	<0.0001
≤60 d before	3.2 (4.5)	3.4 (4.4)	0.006	4.9 (6.3)	5.6 (6.6)	<0.0001
≤183 d before	8.8 (12.8)	8.8 (12.3)	0.8843	13.6 (17.6)	14.3 (17.2)	0.0122
Treatment and testing						
Amoxicillin	16,989 (57.8)	2,576 (58.9)	1.02 (0.97–1.08)	4,128 (15.7)	894 (19.3)	1.22 (1.13–1.32)
Doxycycline	12,708 (43.2)	1,882 (43.1)	1.00 (0.94–1.06)	22,518 (85.6)	3,841 (82.8)	0.96 (0.92–1.00)
Antibody testing§	4,141 (14.1)	923 (21.1)	1.08 (1.07–1.11)	4,019 (15.3)	1,025 (22.1)	1.08 (1.07–1.11)

*Values are no. (%) except as indicated. Reference group = White. NA, not applicable; PR, prevalence ratio.
†We used χ^2 test to compare distribution of disseminated manifestations between White and non-White beneficiaries.
‡Calculated only among claims with known provider type.
§Current Procedural Terminology code 86618, *Borrelia burdorferi* antibody.

Table 3. Clinical characteristics of cases among Medicare beneficiaries in a study of differences in Lyme disease diagnosis among Medicaid and Medicare beneficiaries, United States, 2016–2021*

	Medicare, age <65 y			Medicare, age ≥65 y		
Characteristic	White, n = 11,845	Non-White, n = 1,066	PR (95% CI) or p value	White, n = 87,831	Non-White, n = 3,037	PR (95% CI) or p value
Disseminated disease†	3,345 (28.2)	400 (37.5)	1.33 (1.22–1.44)	18,277 (20.8)	817 (26.9)	1.29 (1.22–1.37)
Neurologic	2,155 (64.4)	242 (60.5)	NA	9,808 (53.7)	428 (52.4)	0.055
Musculoskeletal	1,101 (32.9)	–	NA	7,127 (39.0)	344 (42.1)	NA
Cardiac	89 (2.7)	–	NA	1,342 (7.3)	45 (5.5)	NA
Hospitalization at diagnosis	967 (8.2)	109 (10.2)	1.25 (1.04–1.51)	6,325 (7.2)	250 (8.2)	1.14 (1.01–1.29)
Diagnosed outside of primary care‡	4,105 (36.4)	447 (44.3)	1.22 (1.08–1.37)	27,719 (32.6)	1,275 (43.6)	1.34 (1.25–1.43)
Diagnosed during September–March	3,793 (32.0)	377 (35.4)	1.10 (1.01–1.20)	22,316 (25.4)	890 (29.3)	1.15 (1.09–1.22)
Sex						
M	5,199 (43.9)	400 (37.5)	Referent	41,438 (47.2)	1,322 (43.5)	Referent
F	6,646 (56.1)	666 (62.5)	1.11 (1.06–1.17)	46,393 (52.8)	1,715 (56.5)	1.07 (1.04–1.10)
Mean Quan-Charlson Comorbidity Index score (SD)	2.4 (2.0)	2.9 (2.3)	<0.0001	2.6 (2)	2.8 (2.2)	<0.0001
Mean no. visits before diagnosis (SD)						
≤30 d before	0.99 (1.5)	1.1 (1.6)	0.111	0.7 (1.2)	0.6 (1.1)	<0.0001
≤60 d before	1.8 (2.5)	1.9 (2.7)	0.057	1.2 (1.9)	1.0 (1.7)	<0.0001
≤183 d before	4.8 (6.2)	5.2 (6.6)	0.448	3.1 (4.4)	2.6 (4.1)	<0.0001
Treatment and testing						
Amoxicillin	2,297 (19.4)	295 (27.7)	1.43 (1.25–1.64)	13,594 (15.5)	632 (20.8)	1.32 (1.21–1.44)
Doxycycline	9,208 (77.7)	758 (71.1)	0.92 (0.83–1.01)	73,558 (83.7)	2,366 (77.9)	0.92 (0.87–0.97)
Antibody testing§	5,619 (47.4)	522 (49.0)	1.03 (0.97–1.09)	42,212 (48.1)	1,617 (53.2)	1.10 (1.06–1.13)

*Values are no. (%) except as indicated. Reference group = White. NA, not applicable; PR, prevalence ratio; –, sample size <11, thus counts suppressed from calculations.
†We used χ^2 test to compare distribution of disseminated manifestations between White and non-White beneficiaries.
‡Calculated only among claims with known provider type.
§Current Procedural Terminology code 86618, *Borrelia burdorferi* antibody.

children, particularly Black/African American children, who had more than twice the prevalence of more severe, disseminated disease than did White children. Those results expand on prior published literature by identifying group-specific differences in the clinical manifestations and demographic characteristics of persons with Lyme disease in US states with high Lyme disease incidence.

This study provides a demographic profile of Lyme disease cases in high-incidence states that is difficult to discern from US Lyme disease surveillance data, in which race and ethnicity are unknown for nearly 40% of reported cases (*5*). As observed in Lyme disease surveillance data, we saw that cases among White persons are overrepresented compared with their representation in the population. However, that observation was attenuated among Medicaid beneficiaries, likely reflecting the overall demographic distribution of persons covered by that insurance program, which is more racially and ethnically diverse than the US population, particularly among pediatric beneficiaries (*20*). Because US Lyme disease surveillance in high-incidence states is now laboratory-based (*21*), information on race and ethnicity is likely to continue to be underreported because those variables are not routinely available in laboratory reporting systems, highlighting the importance of administrative claims to supplement surveillance data.

Although detailed analyses were limited by the small sample size, we found that incidence rates among Medicaid and Medicare beneficiaries who identified as Native American were second to those of White persons; however, Native American persons did not have increased risk for disseminated disease or hospitalization. Medicaid provides health coverage to ≈30% of Native American/Alaska Native persons ≤65 years of age in the eastern United States and nationally to ≈60% of Native American/Alaska Native children (*22*,*23*). Future analyses on the epidemiology of Lyme disease in Native American populations could also include Indian Health Service data. Regardless, recognizing the seemingly high incidence of Lyme disease in that population, jurisdictions in high Lyme disease–incidence states with substantial Native American populations might consider routine analysis of Lyme disease outcomes by race and ethnic group and develop tailored Lyme disease education programs and interventions (*24*).

Diagnosis of disseminated Lyme disease might indicate that early signs and symptoms were missed or not recognized as Lyme disease (*3*). Diagnostic differences were most pronounced among persons who identified as Black or African American,

suggesting that difficulties in recognition of the erythema migrans rash on darker skin likely account for at least some of those differences, as previously suggested (*10*). However, the finding that non-White beneficiaries also had more sick visits in the 30 and 60 days before their Lyme disease diagnosis than did White beneficiaries suggests that patients, especially Medicaid beneficiaries, might have sought care frequently enough to provide opportunity to diagnose Lyme disease. Such patient journeys have been described in case reports (*25*,*26*). In addition, reports have documented that persons who identify as Black/African American or Hispanic receive lower quality healthcare for multiple diseases and conditions than do persons who identify as White, which can delay diagnosis and lead to inferior outcomes (*27*,*28*).

Musculoskeletal disease (arthritis) was the most common disseminated manifestation among Medicaid beneficiaries and was also a more prevalent disseminated manifestation among non-White Medicaid beneficiaries. Because arthritis represents the late stage of disease dissemination (*3*), that finding further suggests differences in time to disease diagnosis among persons from racial and ethnic minority groups and is consistent with our finding that fewer cases were diagnosed during the summer months among non-White persons, which also has been reported by others (*11*,*16*,*29*,*30*). Differences in the development of disseminated manifestations and seasonality of infections have also been found by age and sex (*31*,*32*). Other possible explanations for those differences include differential care-seeking behaviors and healthcare access for some groups and misdiagnosis, including possible overdiagnosis and treatment of Lyme disease in some groups.

Our findings cannot be readily explained by differences in underlying health status for certain race or ethnic groups. For example, the greatest difference in development of disseminated disease was for Black/African American children, and that population had a similar number of underlying conditions as White children. Conversely, differences in the development of disseminated disease were less pronounced for Native American beneficiaries compared with other racial and ethnic minority groups, and Native American beneficiaries had more underlying conditions than did White beneficiaries. Although limited, some evidence suggests that certain conditions, such as hypercholesterolemia (*33*), might predispose persons to Lyme disease. The higher Charlson Comorbidity Index among some groups, along with more frequent healthcare utilization before diagnosis, also might reflect misdiagnosis of Lyme disease in the face of chronic, unexplained illness.

Of note, we found a high incidence of Lyme disease among beneficiaries of the disability portion of Medicare, which represents ≈12% of total Medicare enrollment. Across all racial groups, about one third of persons with Lyme disease in the disability group had disseminated disease develop, particularly neurologic manifestations, and nearly 10% were hospitalized. That finding has implications for considering risk related to Lyme disease and tick exposure, which extends beyond rigorous outdoor activities to include risk factors around the home and yard (*34*,*35*). In addition, although the high hospitalization rates in that population could be because of a higher prevalence of underlying illness, the high percentage of disseminated manifestations suggests possible delays in diagnosing Lyme disease, because of either a missed rash or conflation with other conditions.

Although claims data are extremely valuable for the efficient and effective examination of healthcare outcomes, treatment patterns, and healthcare resource utilization, those data are collected for the purpose of payment and not research. A validation study of the claims-based algorithms for Lyme disease case identification used in this study found the positive predictive value was 93.8% (95% CI 88.1%–97.3%) for confirmed,

Table 4. Prevalence ratios for development of disseminated Lyme disease and hospitalization by race and ethnicity among Medicaid and Medicare beneficiaries, United States, 2016–2021*

Group	Prevalence ratio (95% CI)	
	Disseminated disease	Hospitalization at diagnosis
Medicaid, age ≤18 y		
Black, African American	2.35 (2.15–2.56)	2.57 (1.96–3.36)
Asian, Pacific Islander	1.57 (1.34–1.83)	1.71 (1.09–2.69)
Hispanic	1.51 (1.37–1.66)	1.59 (1.21–2.11)
Native American	1.16 (0.84–1.60)	1.14 (0.56–2.21)
Other	1.45 (0.91–2.29)	0.74 (0.11–5.20)
Medicaid, age ≥19 y		
Black, African American	1.67 (1.52–1.84)	1.58 (1.27–1.98)
Asian, Pacific Islander	1.23 (1.06–1.42)	0.87 (0.60–1.26)
Hispanic	1.73 (1.59–1.89)	0.90 (0.69–1.19)
Native American	1.19 (0.85–1.65)	0.51 (0.17–1.56)
Other	1.75 (0.77–3.95)	–
Medicare, age <65 y		
Black, African American	1.51 (1.35–1.68)	1.51 (1.17–1.94)
Asian, Pacific Islander	0.83 (0.53–1.29)	1.53 (0.80–2.93)
Hispanic	1.09 (0.90–1.31)	0.83 (0.53–1.31)
Native American	1.05 (0.68–1.64)	1.30 (0.57–2.99)
Other	1.37 (1.10–1.72)	1.11 (0.63–1.96)
Medicare, age ≥65 y		
Black, African American	1.46 (1.33–1.61)	1.17 (0.95–1.43)
Asian, Pacific Islander	1.18 (1.01–1.38)	1.06 (0.78–1.44)
Hispanic	1.48 (1.22–1.78)	1.21 (0.80–1.82)
Native American	1.11 (0.67–1.83)	1.87 (0.94–3.73)
Other	1.07 (0.94–1.22)	1.14 (0.90–1.45)

*Reference group White for all comparisons. –, sample size too small to calculate.

probable, or suspected cases and 66.4% (95% CI 57.5%–74.5%) for confirmed and probable cases (*17*). More recent efforts to evaluate the claims-based algorithm suggest that varying algorithm parameters related to the type and timing of antimicrobial therapy might further improve the identification of Lyme disease cases; however, characteristics of Lyme disease diagnoses did not differ greatly between 3 modified case definitions (*36*). On the other hand, if differences in prescribing or coding patterns related to Lyme disease by patient race and ethnicity exist, cases possibly were misclassified or missed using those algorithms. Regardless, misclassification of some Lyme disease cases remains a possibility. Similarly, our classification of disseminated versus localized disease could be incorrect for some cases. In addition, although our classification of sick visits was designed to exclude visits conducted for primary or ongoing routine care, we could not confirm the reason for individual healthcare visits.

Race and ethnicity in the Medicaid and Medicare datasets are self-reported, the standard for ascertainment of those demographic variables, and overall missingness was limited, especially in the Medicare claims database, supporting the overall robustness of the data. However, one limitation of our study is that we cannot rule out misclassification of race and ethnicity or missingness of race and ethnicity for some groups, particularly for persons of Hispanic ethnicity (*37*,*38*); thus, some groups might remain underrepresented or misclassified in our results. Second, although our goal was to disaggregate findings by race/ethnic group, sample sizes were too small to do so for some analyses. Finally, our findings cannot be generalized to populations with other types of insurance coverage.

In conclusion, the incidence of Lyme disease continues to increase in the United States. Our characterization of Lyme disease diagnoses and outcomes by race and ethnicity provides insights into populations most at risk for potential long-term outcomes and highlights imbalances in disease diagnoses. To improve Lyme disease detection and reduce severe disease, healthcare providers who see patients receiving publicly funded insurance need Lyme disease prevention and education programs.

Acknowledgments

We thank Christopher Craver, Michelle Silver, and Michelle Van Tieghem who supported the data analysis.

This analysis was supported and jointly funded by Valneva and Pfizer as part of their codevelopment of a Lyme disease vaccine.

All authors are employees of Pfizer and may hold stock or stock options.

About the Author

Dr. Gould is an epidemiologist at Pfizer working on the Lyme disease vaccine candidate. Her research interests focus on the epidemiology of vectorborne diseases and public health surveillance.

References

1. Kugeler KJ, Schwartz AM, Delorey MJ, Mead PS, Hinckley AF. Estimating the frequency of Lyme disease diagnoses, United States, 2010–2018. Emerg Infect Dis. 2021;27:616–9. https://doi.org/10.3201/eid2702.202731
2. Schwartz AM, Kugeler KJ, Nelson CA, Marx GE, Hinckley AF. Use of commercial claims data for evaluating trends in Lyme disease diagnoses, United States, 2010–2018. Emerg Infect Dis. 2021;27:499–507. https://doi.org/10.3201/eid2702.202728
3. Steere AC, Strle F, Wormser GP, Hu LT, Branda JA, Hovius JW, et al. Lyme borreliosis. Nat Rev Dis Primers. 2016;2:16090. https://doi.org/10.1038/nrdp.2016.90
4. Lantos PM, Rumbaugh J, Bockenstedt LK, Falck-Ytter YT, Aguero-Rosenfeld ME, Auwaerter PG, et al. Clinical practice guidelines by the Infectious Diseases Society of America (IDSA), American Academy of Neurology (AAN), and American College of Rheumatology (ACR): 2020 guidelines for the prevention, diagnosis and treatment of Lyme disease. Clin Infect Dis. 2021;72:e1–8. https://doi.org/10.1093/cid/ciaa1215
5. Centers for Disease Control and Prevention. Lyme disease surveillance data [cited 2024 Oct 8]. https://www.cdc.gov/lyme/data-research/facts-stats/surveillance-data-1.html
6. Schwartz AM, Hinckley AF, Mead PS, Hook SA, Kugeler KJ. Surveillance for Lyme disease—United States, 2008–2015. MMWR Surveill Summ. 2017;66:1–12. https://doi.org/10.15585/mmwr.ss6622a1
7. Springer YP, Johnson PTJ. Large-scale health disparities associated with Lyme disease and human monocytic ehrlichiosis in the United States, 2007–2013. PLoS One. 2018;13:e0204609. https://doi.org/10.1371/journal.pone.0204609
8. Moon KA, Pollak J, Hirsch AG, Aucott JN, Nordberg C, Heaney CD, et al. Epidemiology of Lyme disease in Pennsylvania 2006–2014 using electronic health records. Ticks Tick Borne Dis. 2019;10:241–50. https://doi.org/10.1016/j.ttbdis.2018.10.010
9. Greene SK, Levin-Rector A, Hadler JL, Fine AD. Disparities in reportable communicable disease incidence by Census tract–level poverty, New York City, 2006–2013. Am J Public Health. 2015;105:e27–34. https://doi.org/10.2105/AJPH.2015.302741
10. Gould LH, Fathalla A, Moïsi JC, Stark JH. Racial and ethnic disparities in Lyme disease in the United States. Zoonoses Public Health. 2024;71:469–79. https://doi.org/10.1111/zph.13137
11. Ly DP. Black–white differences in the clinical manifestations and timing of initial Lyme disease diagnoses. J Gen Intern Med. 2022;37:2597–600. https://doi.org/10.1007/s11606-021-07129-1
12. Wormser GP, McKenna D, Morgan T, Scavarda C, Cooper D, Visintainer P. A prospective study to characterize symptoms

and symptom severity in adult patients with extracutaneous manifestations of Lyme disease. Am J Med. 2023;136:702–6. https://doi.org/10.1016/j.amjmed.2023.04.001
13. Hunt KM, Michelson KA, Balamuth F, Thompson AD, Levas MN, Neville DN, et al.; for Pedi Lyme Net. Racial differences in the diagnosis of Lyme disease in children. Clin Infect Dis. 2023;76:1129–31. https://doi.org/10.1093/cid/ciac863
14. Nelson CA, Starr JA, Kugeler KJ, Mead PS. Lyme disease in Hispanics, United States, 2000–2013. Emerg Infect Dis. 2016;22:522–5. https://doi.org/10.3201/eid2203.151273
15. Fix AD, Peña CA, Strickland GT. Racial differences in reported Lyme disease incidence. Am J Epidemiol. 2000;152:756–9. https://doi.org/10.1093/aje/152.8.756
16. Shafquat M, Patel N, McFadden B, Stark JH, Gould LH. Racial differences in knowledge, attitudes toward vaccination, and risk practices around Lyme disease in the United States. Front Public Health. 2025;13:1473304. https://doi.org/10.3389/fpubh.2025.1473304
17. Cocoros NM, Kluberg SA, Willis SJ, Forrow S, Gessner BD, Nutt CT, et al. Validation of claims-based algorithm for Lyme disease, Massachusetts, USA. Emerg Infect Dis. 2023;29:1772–9. https://doi.org/10.3201/eid2909.221931
18. Centers for Medicaid and Medicare Services. Medicare.gov [cited 2024 Jun 29]. https://www.medicare.gov
19. Kaiser Family Foundation. Medicaid state fact sheets [cited 2024 Jun 26]. https://www.kff.org/interactive/medicaid-state-fact-sheets
20. Centers for Medicaid and Medicare Services. Race and ethnicity of the national Medicaid and CHIP population in 2020 [cited 2024 Jul 1]. https://www.medicaid.gov/medicaid/data-and-systems/downloads/macbis/2020-race-etncity-data-brf.pdf
21. Kugeler KJ, Earley A, Mead PS, Hinckley AF. Surveillance for Lyme disease after implementation of a revised case definition—United States, 2022. MMWR Morb Mortal Wkly Rep. 2024;73:118–23. https://doi.org/10.15585/mmwr.mm7306a1
22. Kaiser Family Foundation. Health coverage by race and ethnicity, 2010–2022 [cited 2025 Jan 9]. https://www.kff.org/racial-equity-and-health-policy/issue-brief/health-coverage-by-race-and-ethnicity
23. Kaiser Family Foundation. Health coverage among American Indian and Alaska Native and Native Hawaiian and other Pacific Islander people [2025 Jan 9]. https://www.kff.org/racial-equity-and-health-policy/issue-brief/health-coverage-among-american-indian-and-alaska-native-and-native-hawaiian-and-other-pacific-islander-people
24. Adekoya N, Truman B, Landen M; Centers for Disease Control and Prevention. Incidence of notifiable diseases among American Indians/Alaska Natives—United States, 2007–2011. MMWR Morb Mortal Wkly Rep. 2015;64:16–9.
25. Dennison R, Novak C, Rebman A, Venkatesan A, Aucott J. Lyme disease with erythema migrans and seventh nerve palsy in an African-American man. Cureus. 2019;11:e6509. https://doi.org/10.7759/cureus.6509
26. Newman JH. A case of Lyme disease in a 9-year-old black male. Arthritis Rheum. 1987;30:237. https://doi.org/10.1002/art.1780300223
27. Mays VM, Cochran SD, Barnes NW. Race, race-based discrimination, and health outcomes among African Americans. Annu Rev Psychol. 2007;58:201–25. https://doi.org/10.1146/annurev.psych.57.102904.190212
28. Fiscella K, Sanders MR. Racial and ethnic disparities in the quality of health care. Annu Rev Public Health. 2016;37:375–94. https://doi.org/10.1146/annurev-publhealth-032315-021439
29. Sundheim KM, Levas MN, Balamuth F, Thompson AD, Neville DN, Garro AC, et al. Seasonality of acute Lyme disease in children. Trop Med Infect Dis. 2021;6:196. https://doi.org/10.3390/tropicalmed6040196
30. Abul Y, Chow R, Spallone A, Luft B, Marcos L. Epidemiology of Lyme disease in Hispanics admitted to a tertiary medical center in Long Island. Open Forum Infect Dis. 2016;3:1422. https://doi.org/10.1093/ofid/ofw172.1125
31. Rebman AW, Wang L, Yang T, Marsteller JA, Murphy SME, Uriyo M, et al. Incidence of Lyme disease diagnosis in a Maryland Medicaid population, 2004–2011. Am J Epidemiol. 2018;187:2202–9. https://doi.org/10.1093/aje/kwy133
32. Kwit NA, Nelson CA, Max R, Mead PS. Risk factors for clinician-diagnosed Lyme arthritis, facial palsy, carditis, and meningitis in patients from high-incidence states. Open Forum Infect Dis. 2018;5:ofx254. https://doi.org/10.1093/ofid/ofx254
33. Forrest IS, O'Neal AJ, Pedra JHF, Do R. Cholesterol contributes to risk, severity, and machine learning–driven diagnosis of Lyme disease. Clin Infect Dis. 2023;77:839–47. https://doi.org/10.1093/cid/ciad307
34. Gould LH, Fee R, White J, Webb N, Carlyle M, Dick L, et al. Risk factors for Lyme disease among residents of rural, suburban, and urban areas in the United States: a case-control study. Am J Epidemiol. 2024;9:kwae368. https://doi.org/10.1093/aje/kwae368
35. Mead P, Hook S, Niesobecki S, Ray J, Meek J, Delorey M, et al. Risk factors for tick exposure in suburban settings in the northeastern United States. Ticks Tick Borne Dis. 2018;9:319–24. https://doi.org/10.1016/j.ttbdis.2017.11.006
36. Nawrocki CC, Earley AR, Hook SA, Hinckley AF, Kugeler KJ. Optimizing identification of Lyme disease diagnoses in commercial insurance claims data, United States, 2016–2019. BMC Infect Dis. 2024;24:1322. https://doi.org/10.1186/s12879-024-10195-5
37. Martinez RAM, Andrabi N, Goodwin AN, Wilbur RE, Smith NR, Zivich PN. Conceptualization, operationalization, and utilization of race and ethnicity in major epidemiology journals, 1995–2018: a systematic review. Am J Epidemiol. 2023;192:483–96. https://doi.org/10.1093/aje/kwac146
38. Johnson JA, Moore B, Hwang EK, Hickner A, Yeo H. The accuracy of race & ethnicity data in US based healthcare databases: a systematic review. Am J Surg. 2023;226:463–70. https://doi.org/10.1016/j.amjsurg.2023.05.011

Address for correspondence: L. Hannah Gould, Pfizer, Inc., 66 Hudson Blvd, New York, NY10001, USA; email: hannah.gould@pfizer.com

Theileria luwenshuni and Novel *Babesia* spp. Infections in Humans, Yunnan Province, China

Rong Xiang,[1] Chun-Hong Du,[1] Yi-Lin Zhao,[1] Zhi Luo, Miao Li, Dan-Ni Zeng, Fan Wang, Chao-Bo Du, Yi Sun, Qiao-Cheng Chang, Jia-Fu Jiang

Piroplasmid parasites such as *Theileria luwenshuni* protozoa pose a global threat to both animal and human health. However, human theileriosis remains underexplored compared to infections caused by *Plasmodium* and *Babesia* species parasites. We investigated potential hemoparasite infections among 1,721 persons with fever, anemia, or both in Yunnan Province, China. Molecular detection identified 13 cases positive for *T. luwenshuni* protozoa, of which 5 patients were further confirmed by Western blot antibody analysis. We also identified 6 babesiosis cases, 3 infections with *B. microti* and 3 with novel *Babesia* spp. Subsequent vector and host investigations in the vicinity of the index cases revealed *T. luwenshuni* protozoa in 1 tick and 53 livestock animals. Of note, 3.3% combined vector-host samples tested positive for genetically diverse *Babesia* species. Our findings highlight the endemic circulation of *T. luwenshuni* and *Babesia* spp. parasites in southwest China, underscoring their importance as emerging public health concerns.

Piroplasmorida, a group of tickborne hemoparasites within the phylum Apicomplexa, includes diverse protozoa species such as *Babesia* spp. and *Theileria* spp., which are responsible for causing babesiosis and theileriosis in humans and animals (*1*,*2*). Human babesiosis is a globally recognized parasitic zoonosis that primarily targets red blood cells. Parasite transmission to humans occurs predominantly through the bite of an infected tick; however, alternative transmission routes include blood transfusion, perinatal transmission, and organ transplantation (*3*). Since 1957, the number of human babesiosis cases has increased, posing a growing global public health challenge (*4*). In China, ≈317 cases of human babesiosis or asymptomatic infections had been reported by 2022 (*5*). That relatively low number is likely because of underdiagnosis and limited clinical recognition of these protozoan infections. Rare human infections with hemogregarines of the genus *Hepatozoon*, traditionally considered animal pathogens, have been also detected in immunocompromised patients in Russia, suggesting potential zoonotic spillover of diverse apicomplexan parasites (*6*).

Theileria spp. parasites primarily infect ruminants such as cattle and sheep, as well as various wild animals (*7*). Historically, *Theileria* spp. have not been considered pathogenic to humans. However, a 2014 serosurvey in Italy reported IgG reactivity against *T. equi* antigens in veterinary practitioners, indicating potential human exposure, particularly among persons at higher risk for infection (*8*,*9*). That finding has garnered attention because zoonotic *Theileria* species were widespread in livestock.

Yunnan Province, located in southwestern China, provides an ideal habitat for various tick species and their host animals because of its distinct geographic features, dense vegetation, and high biodiversity. Those characteristics make the region a hotspot for tickborne diseases (*10*,*11*). In Tengchong, along the China–Myanmar border, 8 cases of human babesiosis caused by *Babesia microti* and 2 case co-infections with *B. microti* and *Plasmodium* parasites were confirmed in 2013 (*12*). To enhance understanding of the prevalence of tickborne protozoa in China, we studied patients experiencing fever and anemia in Yunnan Province and traced potential sources of infection by examining protozoan prevalence in domestic animals, small wild animals, and ticks within the affected areas. Our

Author affiliations: State Key Laboratory of Pathogen and Biosecurity, Academy of Military Medical Sciences, Beijing, China (R. Xiang, Y.-L. Zhao, D.-N. Zeng, Y. Sun, J.-F. Jiang); Yunnan Institute of Endemic Disease Control and Prevention, Dali, China (C.-H. Du, Z. Luo, M. Li, F. Wang, C.-B. Du); School of Public Health at Shantou University, Shantou, China (Q.-C. Chang)

DOI: https://doi.org/10.3201/eid3109.241919

[1]These authors contributed equally to this article.

goal was to further characterize the epidemiologic and clinical features of piroplasmid parasite infections and identified their possible sources.

Materials and Methods

Identification of Piroplasmosis in Patients

We conducted a retrospective investigation among participants experiencing unexplained fever or anemia across 10 counties in Yunnan Province, China, during May 2017–June 2020. Demographic data, medical history, and epidemiologic exposure history had been collected through a structured questionnaire. We retrieved data on clinical manifestations, underlying medical conditions, laboratory test results, treatments, and outcomes from medical records; 2 investigators cross-validated the data. The patients' blood samples were collected at various time points during their hospital stay; a portion of each patient's blood samples were immediately processed for blood smear preparation, and the residual blood was stored at −80°C until nucleic acid extraction for batch PCR amplification and downstream analysis. The Ethics Committee of the Yunnan Provincial Institute of Endemic Disease Control approved the study (approval no. 2016-005), which was conducted in accordance with medical research regulations in China. All participants provided written informed consent before their inclusion in the study.

Source Tracing Investigation

As part of the study, we conducted retrospective testing on ticks, livestock, and small mammals from areas surrounding the participants. Wild small mammals were captured using snap traps, and aseptic tissue samples, including liver and spleen, were collected and stored at −80°C for subsequent analysis. We taxonomically identified the captured animals to the species level on the basis of external morphology, coloration, measurements, and dental characteristics. We collected whole-blood samples from livestock via jugular vein puncture using EDTA anticoagulant tubes and stored them at −20°C until DNA extraction. We manually removed ticks from livestock and collected host-seeking ticks by flag-sweeping vegetation at the same sampling sites. An entomologist identified tick species. We preserved tick samples at −80°C before DNA extraction.

PCR Amplification and Sequencing

We extracted DNA from human blood, livestock blood, small mammal tissues, and tick samples using the DNeasy Blood & Tissue Kit (QIAGEN, https://www.qiagen.com) in accordance with manufacturer's instructions. To detect *Theileria* and *Babesia* parasites, we performed nested PCR targeting the 18S rRNA gene using outer primers Piro0F/Piro6R and inner primers Piro1F/Piro5.5R (13,14), followed by agarose gel electrophoresis and Sanger sequencing. We amplified additional genetic loci, including the 5.8S rRNA (303 bp), internal transcribed spacer region (1,300 bp), P32 immunodominant protein gene (875 bp), and cytochrome oxidase subunit I (1,200 bp). We conducted concurrent testing for other potential infections with *Rickettsia* spp., *Borrelia burgdorferi*, *B. recurrentis*, and *Bartonella* spp., which could potentially be transmitted by similar transmission routes or cause similar symptoms, to exclude differential diagnoses (Appendix 1 Table 1, https://wwwnc.cdc.gov/EID/article/31/9/24-1919-App1.xlsx).

Phylogenetic Analysis

We performed phylogenetic analysis using sequences assembled with the CLC Main Workbench version5.5 (QIAGEN). We conducted comparative

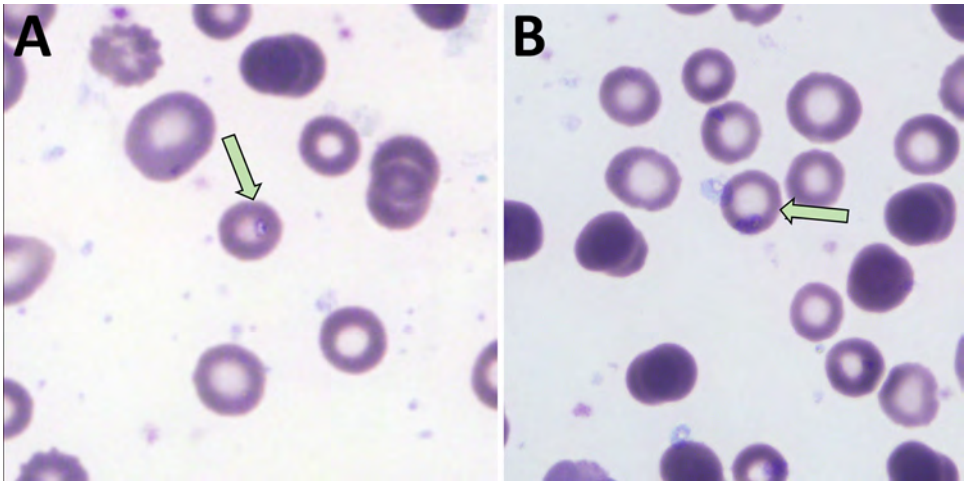

Figure 1. Photomicrographs from peripheral blood smears of a patient (patient 2) who tested positive for *Theileria luwenshuni* parasite in study of piroplasmorida in humans, southwest China, May 2017–June 2020. Arrows indicate typical ring forms; single (A) and multiple (B) parasitism was observed.

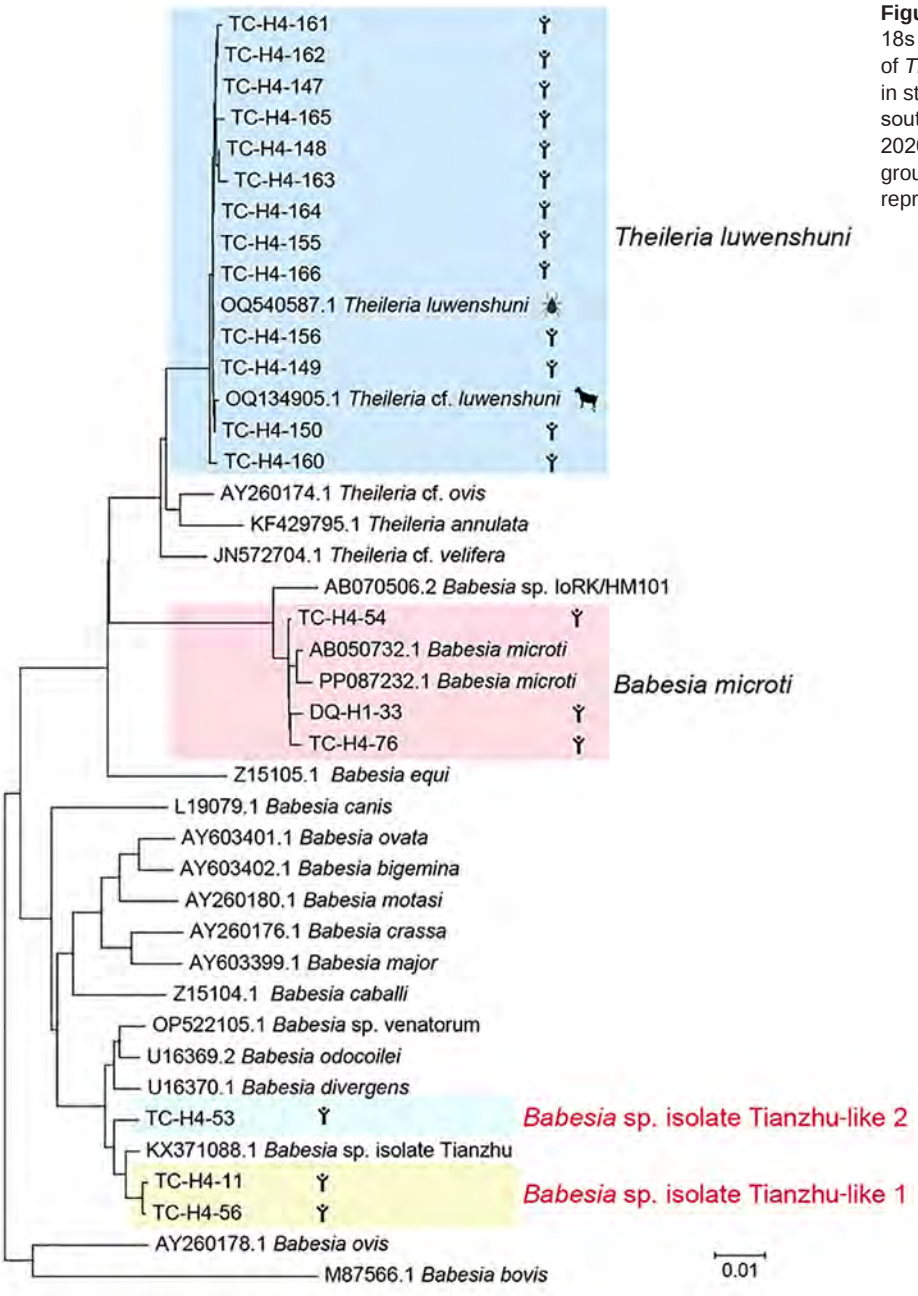

Figure 2. Phylogenetic analysis of 18s rRNA (1,600-bp) gene sequences of *Theileria* and *Babesia* spp. isolates in study of piroplasmorida in humans, southwest China, May 2017–June 2020. Colored shading represents groups of isolates by strain. Scale bar represents 0.01 substitutions per site.

analysis against sequences in GenBank using BLAST (https://blast.ncbi.nlm.nih.gov). We conducted phylogenetic analysis of all sequences using MEGA version 11.0 software (https://www.megasoftware.net). We constructed phylogenetic trees using the neighbor-joining method with the p-distance model based on 1,000 bootstrap replicates.

Morphologic and Serologic Testing

We stained thin peripheral blood smears collected from the participants with Giemsa and examined under a light microscope (Olympus, https://evidentscientific.com). We used the recombinant *T. uilenbergi* immunodominant protein (rTuIP) as the diagnostic antigen for Western blot analysis (15,16). Anhui Global Gene Technology Company (Chuzhou, China) conducted protein expression and purification using the pQE31 vector as the expression vector and BL21 (DE3) as the expression host. Tengchong People's Hospital (Tengchong County, China) provided serum samples collected for rTuIP antibody detection from some patients with suspected protozoan

infections and used serum samples from healthy persons as negative controls.

We separated recombinantly expressed TuIP protein (20 μg) using 12% sodium dodecyl sulfate-polyacrylamide gel electrophoresis and transferred it onto a polyvinylidene difluoride membrane (0.45 μm pore size). To block nonspecific binding, we incubated the membrane with 5% skimmed milk powder in Tris-buffered saline containing Tween 20 for 2 hours. We used patient serum samples diluted at various ratios (1:25–1:800) as primary antibodies; serum samples from healthy persons diluted at 1:100 served as negative controls. We then incubated the membrane overnight at 4°C. We applied horseradish peroxidase–labeled human IgG secondary antibody, diluted at 1:5,000, for a 1-hour incubation at room temperature. After washes in Tris-buffered saline containing Tween 20, we detected the signal using an enhanced chemiluminescence developing reagent.

Results

Identification of Piroplasmosis in Participants

We screened a total of 1,721 participants from 10 counties in Yunnan Province for protozoan infections; 1,362 participants were experiencing fever, and 359 had anemia, (Appendix 1 Table 2). Among those, we identified 18 inpatients and 1 outpatient to have suspected protozoan infections by 18S rRNA sequencing of blood samples; amplification for additional *T. luwenshuni* genetic loci was not successful. Meanwhile, molecular testing for *Rickettsia* spp., *B. burgdorferi* sensu lato, *B. recurrentis*, and *Bartonella* spp. yielded uniformly negative results. We examined peripheral blood smears from the 19 suspected cases for intraerythrocytic parasites using Giemsa staining; patient 2 tested positive for piroplasmosis parasites (Figure 1). No parasites were detected in the blood smears of the remaining patients.

We successfully amplified and sequenced the 18S rRNA gene of *T. luwenshuni* parasites from 13 blood samples, yielding sequences ≈1,600 bp long. Those sequences exhibited a similarity range of 99.28%–100% among the samples; we deposited them into GenBank (accession nos. PQ720759–71). Similarity analysis indicated that the *T. luwenshuni* samples shared 99.69% identity with a reference sequence isolated from a *Haemaphysalis longicornis* tick (GenBank accession no. OQ540587.1) and 98.60% identity with a *T. luwenshuni* isolate from goats (GenBank accession no. OQ134905.1), both collected in Shandong Province, China. Phylogenetic analysis further showed that the sequences clustered within the same monophyletic branch (Figure 2; Appendix 1 Table 3).

We successfully amplified and sequenced the 18S rRNA gene of *Babesia* spp. from 6 blood samples, yielding sequences ≈1,600 bp long. We submitted those sequences to GenBank (accession nos. PQ720772–5, PQ722837, PQ722838). Phylogenetic analysis demonstrated that samples DQ-H1-33, TC-H4-76, and TC-H4-54 clustered with multiple *B. microti* strains from reference sequences (GenBank

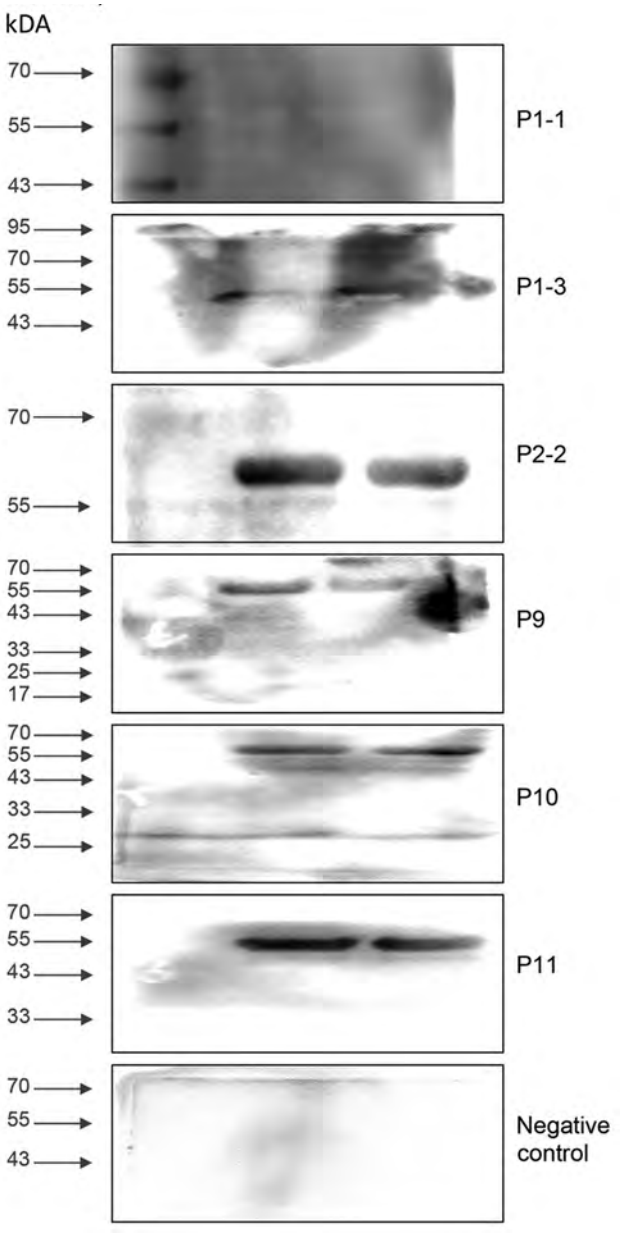

Figure 3. Western blot analysis of the target protein (55-kDa) expression in the serum samples from 5 patients with suspected protozoan infection in study of piroplasmorida in humans, southwest China, May 2017–June 2020.

accession nos. KF410825.1 and AB050732.1), exhibiting a high genetic similarity (Figure 2). In addition, samples TC-H4-11 and TC-H4-56 clustered with *Babesia* Tianzhu–like subgroups that were identified in white yaks in China (*14*). Meanwhile, sample TC-H4-53 clustered with another subgroup, which suggested that TC-H4-53 may represent an uncharacterized or novel *Babesia* variant or strain (Figure 2).

Western blot analysis confirmed the diagnostic utility of the rTuIP protein for detecting *T. luwenshuni* infections. Of 11 serum samples from participants with suspected hemoprotozoan infections, 6 samples (from 5 patients) exhibited characteristic rTuIP-specific bands at a 1:25 dilution (Figure 3). Of note, longitudinal samples from patient 1 (P1-1 and P1-3) both exhibited positive reactivity. Control samples from healthy participants showed no target protein–specific bands.

Analysis of longitudinal antibody responses also revealed dynamic seroconversion patterns over time (Appendix 2 Figure, panel A, https://wwwnc.cdc.gov/EID/article/31/9/24-1919-App2.pdf). Sample P1-1 exhibited faint reactivity at 1:25 dilution but was negative at ≥1:50. In contrast, subsequent samples from the same patient (P1-2 and P1-3) displayed strong immunoreactivity across all consecutive doubling tested dilutions (1:50–1:800) (Appendix 2 Figure, panel A), indicating the maturation of antibody titers. We saw similar consistently high-titer responses in patient 2 at 2 timepoints, with clear bands visible from 1:50–1:800 dilutions (Appendix 2 Figure, panel B).

Epidemiologic and Clinical Characteristics of the Patients

Among the 13 patients with suspected *T. luwenshuni* infection (Appendix 1 Table 4), the median age was 40 (interquartile range [IQR] 32.5–68.0) years; 10 (77%) patients were male and 13 (23%) female. The median hospital stay was 13 (IQR 7.5–17.0) days. All patients were engaged in farming. Underlying conditions

Table 1. Characteristics of 18 patients hospitalized for *Theileria luwenshuni* and *Babesia* spp. infection, China*

Characteristic	*T. luwenshuni* cases, n = 13	*Babesia* spp. cases, n = 5
Age, y (IQR)	40 (32.5–68.0)	56 (25.5–59.5)
Sex		
M	10 (77)	4 (80)
F	3 (23)	1 (20)
Length of hospital stay, d (IQR)	13 (7.5–17.0)	10 (5.5–10.5)
Occupation as farmer	13 (100)	5 (100)
Medical history and underlying disease		
Renal failure	5 (38)	1 (20)
Cancer	3 (23)	0
Upper gastrointestinal bleeding	5 (38)	3 (60)
Clinical manifestations†		
Nonspecific symptoms		
Dizziness	3 (23)	4 (80)
Malaise	5 (38)	4 (80)
Cough	1 (8)	0
Jaundice	1 (8)	0
Splenomegaly	1 (8)	0
Weight loss	1 (8)	0
Cardiovascular manifestations		
Chest discomfort	1 (8)	1 (20)
Palpitations	3 (23)	1 (20)
Dyspnea	2 (15)	1 (20)
Gastrointestinal manifestations		
Anorexia	8 (62)	2 (40)
Vomiting	4 (31)	0
Bloating	1 (8)	1 (20)
Stomachache	1 (8)	0
Hematemesis	3 (23)	0
Melena	4 (31)	3 (60)
Neurologic manifestations		
Syncope	1 (8)	1 (20)
Listlessness	8 (62)	2 (40)
Laboratory findings		
Anemia	13 (100)	5 (100)
Leukocytosis	2 (15)	1 (20)
Elevated serum AST or ALT or γ-GGT concentration	1 (8)	0

*Values are no. (%) patient except as indicated. ALT, alanine aminotransferase; AST, aspartate aminotransferase; γ-GGT, gamma-glutamyl transferase; IQR, interquartile range.
†Patients could report ≥1 symptom.

Table 2. Piroplasmorida infections by pathogen in humans, livestock, small mammals, and ticks, southwest China, May 2017–June 2020*

Pathogen	No. positive/no. tested										
	Tengchong	Puer	Jianchuan	Yunlong	Dali	Gengma	Fugong	Deqin	Weixi	SL	Total
Human with fever											
Babesia microti	0/583	0/171	0/28	0/64	0/141	0/325	0/10		1/40†		1/1,362
Total	0/583	0/171	0/28	0/64	0/141	0/325	0/10		1/40†		1/1,362
Human with anemia											
B. microti	2/174	NA	NA	0/21	0/151	0/13	NA	NA	NA	NA	2/359
B. tianzhu like	3/174	NA	NA	0/21	0/151	0/13	NA	NA	NA	NA	3/359
Theileria luwenshuni	13/174	NA	NA	0/21	0/151	0/13	NA	NA	NA	NA	13/359
Total	18/174	NA	NA	0/21	0/151	0/13	NA	NA	NA	NA	18/359
Livestock											
B. microti	1/758	0/10									1/2,100
B. tianzhu like	2/758	NA	26/175	16/212	NA	1/54	NA	NA	2/200	0/450	47/2,100
B. bigemina	20/758	NA	0/175	0/212	NA	0/54	NA	NA	8/200	5/450	33/2,100
B. bovis	7/758	NA	0/175	0/212	NA	0/54	NA	NA	2/200	4/450	13/2,100
T. luwenshuni	53/758	NA	0/175	0/212	NA	0/54	NA	NA	0/200	0/450	53/2,100
Total	82/758	0/10	26/175	16/212		1/54	0/139	0/102	12/200	9/450	147/2,100
Small mammals											
B. microti	8/299	3/10	0/212	19/177	0/126	NA	0/135	3/346	2/99	0/126	35/1,530
Babesia sp.	0/299	0/10	0/212	0/177	2/126	NA	0/135	0/346	0/99	0/126	2/1,530
Total	8/299	3/10	0/212	0/177	0/126	NA	0/135	3/346	2/99	0/126	37/1,530
Ticks											
B. microti	8/405	0/10	0/284	2/127	NA	0/187	NA	0/144	0/359	NA	10/1,516
B. bigemina	0/405	0/10	3/284	0/127	NA	0/187	NA	1/144	0/359	NA	4/1,516
B. tianzhu like	0/405	0/10	2/284	2/127	NA	0/187	NA	0/144	5/359	NA	9/1,516
B. bovis	0/405	0/10	1/284	0/127	NA	0/187	NA	0/144	0/359	NA	1/1,516
Babesia sp.	0/405	0/10	0/284	0/127	NA	0/187	NA	0/144	12/359	NA	12/1,516
T. luwenshuni	0/405	0/10	0/284	0/127	NA	0/187	NA	1/144	0/359	NA	1/1,516
Total	405	10	284	127	NA	0/187	NA	144	359	NA	37/1,516

*NA, not available; SL, Shangri-La.
†These patients are from the same autonomous prefecture, and the case records do not specify the county-level units.

noted at admission included renal failure in 5 (38%) patients, upper gastrointestinal bleeding in 5 (38%) patients, and a history of cancer in 3 (23%) patients; 1 patient reported prior blood transfusion history. The primary clinical manifestations were anorexia (8 [62%] patients), listlessness (8 [62%] patients), malaise (5 [38%] patients), and melena (4 [31%] patients). Other reported symptoms included vomiting (4 [31%] patients), dizziness (3 [23%] patients), and palpitations (3 [23%] patients); cough, jaundice, splenomegaly, and weight loss were each observed in 1 patient (8%). One patient reported neurologic symptoms (Appendix 1 Table 4). Laboratory findings revealed anemia in all 13 patients and leukocytosis in 2 (15%) patients. Elevated serum levels of aspartate aminotransferase, alanine aminotransferase, or gamma-glutamyl transferase were present in 1 patient (8%). All patients received general supportive and symptomatic treatment; 4 (31%) patients underwent blood transfusions, and 5 (38%) patients required hemodialysis (Table 1).

Among the 5 patients with suspected *Babesia* infections (Appendix 1 Table 5), median age was 56 years (IQR 25.5–59.5 years); 4 (80%) patients were male and 1 (20%) female. Similar to the *T. luwenshuni* cohort, all patients were engaged in farming. Underlying conditions were renal failure in 1 patient (20%) and a history of upper gastrointestinal bleeding in 3 patients (60%). Median hospitalization duration was relatively short at 10 days (IQR 5.5–10.5 days). Two patients (40%) had a history of blood transfusion; 1 (20%) patient had a history of gastric hemorrhage or hypertension. The most frequently reported symptoms were nonspecific. Four (80%) patients experienced dizziness and malaise, 3 (60%) patients melena, and 2 (40%) listlessness. Bloating, chest discomfort, palpitations, and dyspnea were all present in 1 (20%) patient. Of note, none of the patients in this group reported vomiting, jaundice, or splenomegaly. Laboratory tests revealed anemia in all patients and leucopenia in 1 (20%) patient. Elevated serum levels of aspartate aminotransferase, alanine aminotransferase, or gamma-glutamyl transferase were not detected in any case. In terms of treatment, 3 (60%) patients received blood transfusions, and 1 patient (20%) required hemodialysis (Table 1).

Traceability Survey

We performed PCR analyses on 2,100 livestock, 1,530 wild small mammals, and 1,516 ticks collected from 10 counties in Yunnan Province to detect Piroplasmorida infections (Table 2). We used the same protocol previously optimized for human diagnostics. Among the livestock samples, 147 (7.00%) tested positive. We

constructed a phylogenetic tree using 18S rRNA sequences (≈1,600 bp) to classify the positive samples into 5 species: *B. microti*, *Babesia* sp. Tianzhu-like, *B. bigemina*, *B. bovis*, and *T. luwenshuni* (Figures 4, 5). We detected 1 strain of *B. microti* and 2 strains of *T. luwenshuni* parasites in livestock from Tengchong County. The overall positivity rate for small mammals was 2.42%. We identified *B. microti* as the predominant species. Phylogenetic analysis identified a variant, tentatively named *Babesia* sp. YN-2, in small mammals (Figure 4). Among tick samples, 37 (2.44%) tested positive for Piroplasmorida; detected species including *B. microti*, *B. bigemina*, *Babesia* sp. Tianzhu-like, *B. bovis*, *Babesia* sp., *Colpoda* sp., and *T. luwenshuni*. Phylogenetic analysis further classified the novel *Babesia* sp. into 2 clades: *Babesia* sp. YN-2 and *Babesia* sp. YN-3.

Genetic analysis of the *Babesia* sp. Tianzhu-like isolates identified in patients, livestock, and ticks yielded 2 major clades with high homology (96.11%–98.67%) but distinct variations of 21–62 bp. We tentatively designated those clades as *Babesia* sp. isolate Tianzhu-like 1 and *Babesia* sp. isolate Tianzhu-like 2. The phylogenetic tree depicted the relationships among *Babesia* and *Theileria* species collected from various hosts and vectors. Of note, we identified *B. microti* in multiple host and vector types, indicating its high adaptability across diverse environments (Figure 5). In addition, we detected the novel *Babesia* sp. YN-2 in both small mammals and ticks, suggesting the existence of a potential transmission cycle between wildlife and arthropod vectors. The detection of *Babesia* sp. isolate Tianzhu-like parasites across humans, livestock, and ticks highlights its broad host range and geographic distribution. Similarly, the widespread occurrence of *T. luwenshuni* parasites in humans,

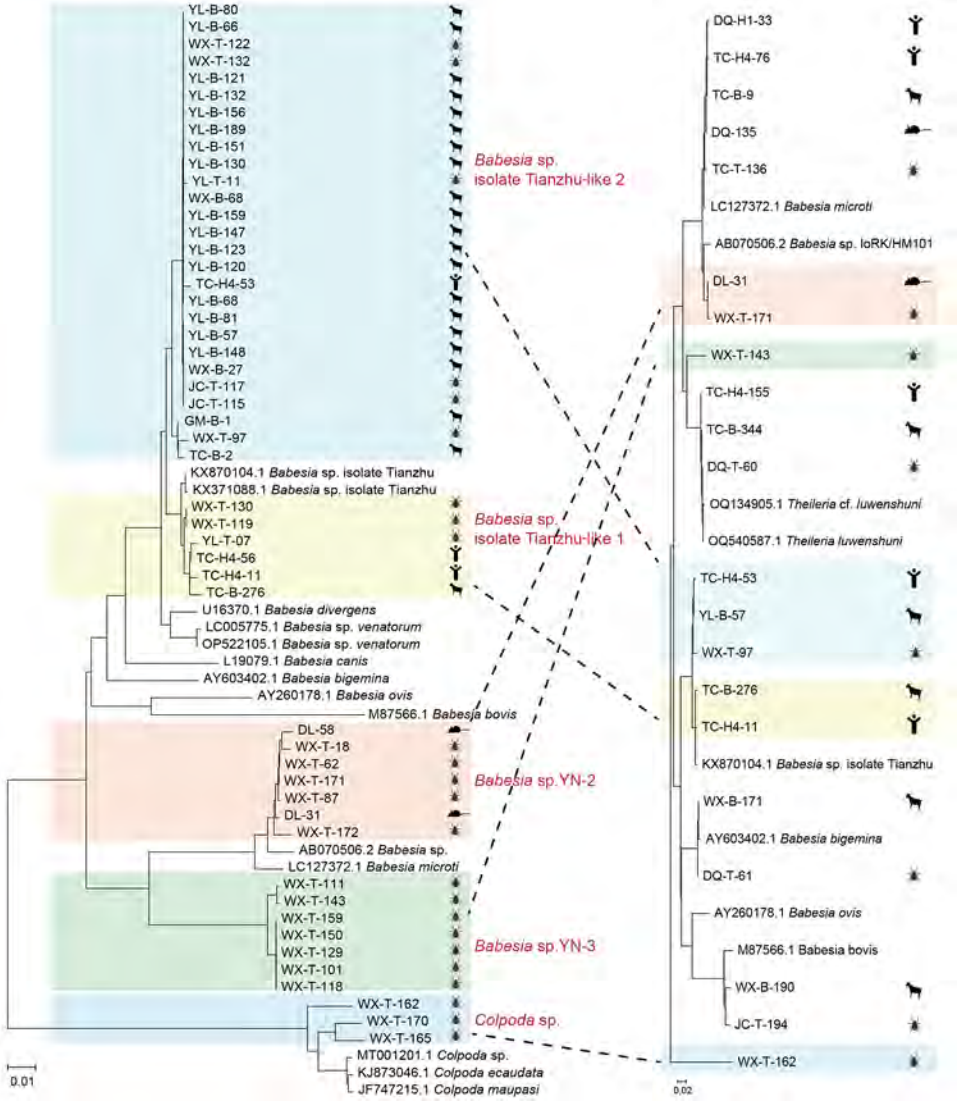

Figure 4. Phylogenetic analysis of 18s rRNA (1,600-bp) gene sequences of *Theileria* and *Babesia* spp. isolates in study of piroplasmorida in humans, southwest China, May 2017–June 2020. Tree on the left highlights the sequences of novel variants/strains (accession nos. PQ722834–6, PQ722839–82). Tree on the right shows classification and distribution of all detected organisms across various hosts and vectors. Colored shading represents groups of isolates by strain. Dotted lines indicate the correspondence between different organisms, illustrating their ecologic and evolutionary connections. Left scale bar represents 0.01 substitutions per site; right scale bar represents 0.02 substitutions per site.

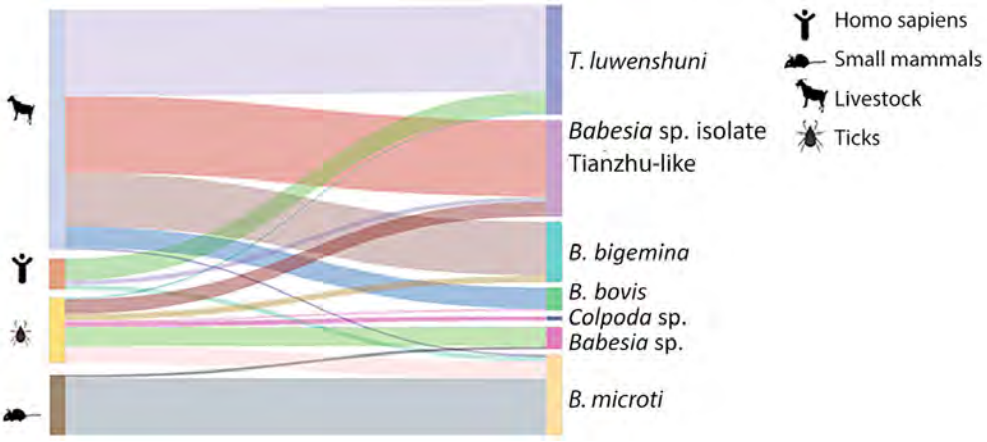

Figure 5. Characterization of host and vector associations determined from phylogenetic analysis of *Theileria* and *Babesia* spp. isolates in study of piroplasmorida in humans, southwest China, May 2017–June 2020.

livestock, and ticks underscores the species' potential for transmission among multiple hosts.

Discussion

This study identified 4 tickborne hemoparasites with human infectivity, including a zoonotic infection caused by 2 known pathogenic agents and 2 novel *Babesia* species. It characterized the diversity and complexity of tickborne protozoa in ticks, small wild animal hosts, and livestock in southwestern China. Our findings are critical for public health and the enhancement of parasitic disease surveillance systems in Yunnan Province. The study presented a clinically relevant finding of human *Theileria* infections, corroborated through molecular diagnostics and Western blot serology, which were validated previously (16) and were further confirmed by our serologic titers and longitudinal testing, with no cross-reactivity against other tickborne pathogens.

A previous serosurvey in Italy (*8*) reported IgG reactivity against *T. equi* antigens in veterinary practitioners, indicating potential human exposure to this pathogen, particularly among persons at heightened risk for infection. That result raised considerable interest because of the prevalence of zoonotic *Theileria* species in livestock. Of note, our study reported a series of human infections with *T. luwenshuni* parasites, previously recognized as primarily affecting ruminants, with less reported pathogenicity in humans.

Our study also identified potential host-vector transmission routes involving domestic animals and ticks. Genetic analysis indicated that *T. luwenshuni* isolates exhibited high similarity to vector-derived strains from Shandong Province, in the east of China. That finding indicates a widespread distribution, an emerging epidemic trend, and the potential for cross-species transmission of these organisms. Those results provide valuable insights for future epidemiologic investigations targeting affected populations, hosts, and vectors across diverse regions.

In this study, we detected ≥6 species of Piroplasmorida in livestock, small mammals, and ticks: *B. microti*, *Babesia* sp. Tianzhu-like, *B. bigemina*, *B. bovis*, *Babesia* sp., and *T. luwenshuni*. We observed genetic diversity within *Babesia* sp. Tianzhu-like; homology was 96.11%–98.67% and 21–62 bp variations. Four of those species are known or suspected to exhibit explicit pathogenicity. Of note, we identified *Babesia* sp. Tianzhu-like 1 in patients, livestock, and ticks, with homology of 99.10% –99.61%. However, the exact infection source remains uncertain for some patients who lacked a clear history of tick bites but reported previous blood transfusions. In addition, most patients were immunocompromised, raising questions about the potential for opportunistic infections. Similar to *B. venatorum* and *B. microti* (*17*), asymptomatic carriage of *T. luwenshuni* and other *Babesia* spp. parasites may occur in healthy persons. Furthermore, as the endemic regions expand, *T. luwenshuni* parasites may emerge as a more frequent complication in immunosuppressed hosts, akin to patterns observed in human babesiosis (*18*). Enhanced surveillance, particularly among blood donors in this region, is imperative (*19*).

Since the earliest report of *Theileria* parasites in Sichuan Province in 1958, ≥4 species have been documented in China: *T. luwenshuni*, *T. unilenbergi*, *T. ovis*, and *T. annulata*. Among them, *T. luwenshuni*, designated in 2007 (*20*,*21*), has been a species recognized for its high pathogenicity in sheep and goats. The presence of *T. luwenshuni* parasites has now been confirmed in multiple provinces, including Yunnan, Hubei, Henan, Gansu, Jilin, Hunan, and Shandong (*20*). Of note, the prevalence of *T. luwenshuni* parasites in goats in Shandong Province has been reported to

reach 81.5%, higher than rates previously reported in small ruminants and deer in central and northwestern China (*22*–*25*). Those findings suggest an emerging epidemic trend of *T. luwenshuni* infections in humans across multiple regions.

B. microti is the predominant species causing human babesiosis in the United States. In China, it has been associated with >100 reported human infections, most occurring in Guangxi Province (*9*). Of note, 10 *B. microti* infections were identified in a study of 449 patients with fever in Tengchong County, Yunnan Province, along the China–Myanmar border (*12*). *Babesia* sp. isolate Tianzhu was initially discovered in Tianzhu Tibetan Autonomous County, northwestern China, in 2017. In our study, we identified this agent in both ticks and water buffalo, demonstrating a close genetic relationship to isolates obtained from 2 human patients (Figure 2); that finding suggests that *Babesia* sp. isolate Tianzhu may present a public health risk.

A limitation of this study is that *T. luwenshuni* infections were identified in immunocompromised patients, and as a retrospective investigation, it was not possible to establish causal relationships between the protozoan infection and patient symptoms or clinical features. Specifically, whether the observed anemia resulted directly from protozoan-induced red blood cell damage or from comorbid conditions (e.g., bleeding disorders or renal failure) remains unclear. Future research should prioritize prospective cohort studies at in sentinel hospitals involving similar patients. Such studies should exclude anemia caused by renal failure or other underlying conditions using interventions such as erythropoietin combined with iron therapy. Those patients should receive antiprotozoal therapy with monitoring of parameters, such as reticulocyte counts and L-lactic dehydrogenase levels, to assess treatment efficacy.

In conclusion, we used molecular biology techniques, including PCR, serology, and phylogenetic analysis, to characterize the diversity and potential risks of tickborne protozoa in Yunnan Province, China. Our findings confirmed the endemic circulation of *T. luwenshuni* and multiple *Babesia* spp. parasites in southwestern China. Further investigation of *T. luwenshuni* infection will elucidate transmission dynamics, clinical impact, and targeted prevention strategies, as well as its implications for public health. Clinicians in this region should remain aware of these emerging public health concerns.

The Natural Science Foundation of China supported this study (grant no. U2002219 to J.-F. J.).

About the Author

Mrs. Xiang is a DPH candidate in State Key Laboratory of Pathogen and Biosecurity, Academy of Military Medical Sciences, Beijing. Her primary research interest is the prevention and control of vectorborne pathogens.

References

1. Almazán C, Scimeca RC, Reichard MV, Mosqueda J. Babesiosis and theileriosis in North America. Pathogens. 2022;11:168. https://doi.org/10.3390/pathogens11020168
2. Karasartova D, Gureser AS, Gokce T, Celebi B, Yapar D, Keskin A, et al. Bacterial and protozoal pathogens found in ticks collected from humans in Corum province of Turkey. PLoS Negl Trop Dis. 2018;12:e0006395. https://doi.org/10.1371/journal.pntd.0006395
3. Schnittger L, Rodriguez AE, Florin-Christensen M, Morrison DA. *Babesia*: a world emerging. Infect Genet Evol. 2012;12:1788–809. https://doi.org/10.1016/j.meegid.2012.07.004
4. Skrabalo Z, Deanovic Z. Piroplasmosis in man; report of a case. Doc Med Geogr Trop. 1957;9:11–6.
5. Chen MX, Xue JB, Ai L, Song P, Cai YC, Chen JX. Epidemic status and research progress of babesiosis in China [in Chinese]. J Trop Dis Parasitol. 2022;20:149–57. https://doi.org/10.3969/j.issn.1672-202.2022.03.005
6. Shuĭkina EE, Beĭer TV, Sergiev VP, Iastrebova RI. Detection of hemogregarin of the genus *Hepatozoon* in patients in Russia [in Russian]. Med Parazitol (Mosk). 2004; (4):3–6.
7. Sivakumar T, Hayashida K, Sugimoto C, Yokoyama N. Evolution and genetic diversity of *Theileria*. Infect Genet Evol. 2014;27:250–63. https://doi.org/10.1016/j.meegid.2014.07.013
8. Gabrielli S, Calderini P, Cassini R, Galuppi R, Tampieri MP, Pietrobelli M, et al. Human exposure to piroplasms in Central and Northern Italy. Vet Ital. 2014;50:41–7. https://doi.org/10.12834/VetIt.1302.13
9. Chen Z, Li H, Gao X, Bian A, Yan H, Kong D, et al. Human babesiosis in China: a systematic review. Parasitol Res. 2019;118:1103–12. https://doi.org/10.1007/s00436-019-06250-9
10. Madison-Antenucci S, Kramer LD, Gebhardt LL, Kauffman E. Emerging tick-borne diseases. Clin Microbiol Rev. 2020;33:e00083-18. https://doi.org/10.1128/CMR.00083-18
11. Zhao GP, Wang YX, Fan ZW, Ji Y, Liu MJ, Zhang WH, et al. Mapping ticks and tick-borne pathogens in China. Nat Commun. 2021;12:1075. https://doi.org/10.1038/s41467-021-21375-1
12. Zhou X, Li SG, Chen SB, Wang JZ, Xu B, Zhou HJ, et al. Co-infections with *Babesia microti* and *Plasmodium* parasites along the China–Myanmar border. Infect Dis Poverty. 2013;2:24. https://doi.org/10.1186/2049-9957-2-24
13. Kawabuchi T, Tsuji M, Sado A, Matoba Y, Asakawa M, Ishihara C. *Babesia microti*–like parasites detected in feral raccoons (*Procyon lotor*) captured in Hokkaido, Japan. J Vet Med Sci. 2005;67:825–7. https://doi.org/10.1292/jvms.67.825
14. Liu J, Guan G, Li Y, Liu A, Luo J, Yin H. A molecular survey of *Babesia* species and detection of a new *Babesia* species by DNA related to *B. venatorum* from white yaks in Tianzhu, China. Front Microbiol. 2017;8:419. https://doi.org/10.3389/fmicb.2017.00419
15. Liu Z, Li Y, Salih DE, Luo J, Ahmed JS, Seitzer U, et al. Validation of a recombinant protein indirect ELISA for the detection of specific antibodies against *Theileria uilenbergi*

and *Theileria luwenshuni* in small ruminants. Vet Parasitol. 2014;204:139–45. https://doi.org/10.1016/j.vetpar.2014.05.010
16. Liu Z, Wang Z, Yin H, Luo J, Zhang B, Kullmann B, et al. Identification of *Theileria uilenbergi* immunodominant protein for development of an indirect ELISA for diagnosis of ovine theileriosis. Int J Parasitol. 2010;40:591–8. https://doi.org/10.1016/j.ijpara.2009.10.011
17. Ruebush TK II, Juranek DD, Chisholm ES, Snow PC, Healy GR, Sulzer AJ. Human babesiosis on Nantucket Island—evidence for self-limited and subclinical infections. N Engl J Med. 1977;297:825–7. https://doi.org/10.1056/NEJM197710132971511
18. Heller HM. Babesiosis in immunosuppressed hosts: pathogenesis, diagnosis and management. Curr Opin Infect Dis. 2024;37:327–32. https://doi.org/10.1097/QCO.0000000000001038
19. Jiang JF, Zheng YC, Jiang RR, Li H, Huo QB, Jiang BG, et al. Epidemiological, clinical, and laboratory characteristics of 48 cases of "*Babesia venatorum*" infection in China: a descriptive study. Lancet Infect Dis. 2015;15:196–203. https://doi.org/10.1016/S1473-3099(14)71046-1
20. Yin H, Liu Z, Guan G, Liu A, Ma M, Ren Q, et al. Detection and differentiation of *Theileria luwenshuni* and *T. uilenbergi* infection in small ruminants by PCR. Transbound Emerg Dis. 2008;55:233–7. https://doi.org/10.1111/j.1865-1682.2008.01031.x
21. Yin H, Schnittger L, Luo J, Seitzer U, Ahmed JS. Ovine theileriosis in China: a new look at an old story. Parasitol Res. 2007;101(Suppl 2):191–5. https://doi.org/10.1007/s00436-007-0689-2
22. Wang BH, Du LF, Zhang MZ, Xia LY, Li C, Lin ZT, et al. Genomic characterization of *Theileria luwenshuni* strain Cheeloo. Microbiol Spectr. 2023;11:e0030123. https://doi.org/10.1128/spectrum.00301-23
23. Li Y, Chen Z, Liu Z, Liu J, Yang J, Li Q, et al. Molecular identification of *Theileria* parasites of northwestern Chinese Cervidae. Parasit Vectors. 2014;7:225. https://doi.org/10.1186/1756-3305-7-225
24. Li Y, Zhang X, Liu Z, Chen Z, Yang J, He H, et al. An epidemiological survey of *Theileria* infections in small ruminants in central China. Vet Parasitol. 2014;200:198–202. https://doi.org/10.1016/j.vetpar.2013.07.023
25. Zhang X, Liu Z, Yang J, Chen Z, Guan G, Ren Q, et al. Multiplex PCR for diagnosis of *Theileria uilenbergi*, *Theileria luwenshuni*, and *Theileria ovis* in small ruminants. Parasitol Res. 2014;113:527–31. https://doi.org/10.1007/s00436-013-3684-9

Address for correspondence: Jia-Fu Jiang and Yi Sun, State Key Laboratory of Pathogen and Biosecurity, Academy of Military Medical Sciences, 20 Dong-Da St, Fengtai District, Beijing 100071, China; email: jiangjf2008@139.com and sunyi7310@sina.com; Qiao-Cheng Chang, School of Public Health, Shantou University, 243 University St, Shantou 515063, China; email: changqiaocheng2001@163.com

etymologia revisited

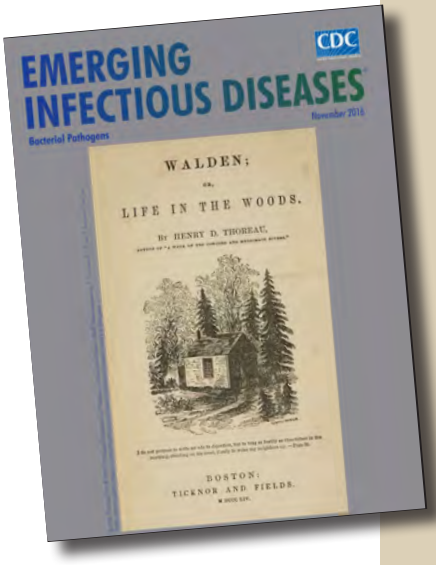

Originally published in November 2016

Streptococcus

From the Greek *streptos* ("chain") + *kokkos* ("berry"), streptococcal diseases have been known since at least the 4th century BCE when Hippocrates described erysipelas (Greek for "red skin"). The genus *Streptococcus* was named by Austrian surgeon Theodor Billroth, who in 1874 described "small organisms as found in either isolated or arranged in pairs, sometimes in chains" in cases of erysipelas or wound infections. Over subsequent decades, as microscopy and staining techniques improved, many different researchers characterized the bacteria now known as *Streptococcus pyogenes* (Lancefield group A β-hemolytic streptococcus), *S. pneumoniae*, and other species.

Reference:
Majno G, Joris I. Billroth and Penicillium. Rev Infect Dis. 1979;1:880–4. http://dx.doi.org/10.1093/clinids/1.5.880c

https://wwwnc.cdc.gov/eid/article/22/11/et-2016_article

Detection of Multiple Nosocomial *Trichosporon asahii* Transmission Events via Microsatellite Typing Assay, South America

Elaine C. Francisco, Norma B. Fernández, Mauricio Carbia, Chendo Dieleman, Andra-Cristina Bostanaru-Iliescu, Jos Houbraken, Arnaldo L. Colombo, Ferry Hagen

The fungus *Trichosporon asahii* has emerged as a cause of nosocomial infections, particularly in immunocompromised patients. Given its rising prevalence, information on its genetic diversity and transmission dynamics is urgently needed. We developed a microsatellite typing tool to investigate the genetic relatedness of *T. asahii* isolates. We selected 6 microsatellite markers from nanopore long-read sequencing of the *T. asahii* type-strain CBS 2479. We applied those markers to 111 clinical and environmental isolates; microsatellite typing showed high variability among isolates (11–37 alleles per marker) and identified 71 genotypes with strong discriminatory power (Simpson index of 0.9793). We applied the microsatellite typing method to *T. asahii* isolates from South America and identified multiple nosocomial transmission events from hospitals in Brazil, including clusters spanning more than a decade. The panel we developed offers high reproducibility and specificity, making it an effective tool for tracking outbreaks and determining the public health effects of *T. asahii* infections.

Trichosporon asahii is an emerging yeast-like fungal pathogen causing life-threatening catheter-related infections worldwide (*1*–*3*). Despite being often overlooked, the occurrence of invasive trichosporonosis has dramatically increased in recent decades, and crude mortality rates have reach up to 80% depending on patients' underlying conditions (*3*–*6*). Episodes of invasive trichosporonosis caused by *T. asahii* are primarily reported in long-term hospitalized patients with underlying hematologic malignancies and neutropenia, as well as among critically ill patients who have undergone invasive medical procedures, have indwelling medical devices, and have been exposed to broad-spectrum antimicrobial therapy (*3*,*5*). Since the 2000s, cases of invasive trichosporonosis have also been reported in immunocompetent hosts and hospitalized COVID-19 patients, posing new challenges in stratifying at-risk populations (*7*–*11*).

T. asahii exhibits a peculiar antifungal susceptibility profile, and is intrinsically resistant to echinocandins, often showing decreased in vitro susceptibility to amphotericin B (*1*,*2*,*12*,*13*), which can exert substantial selective pressure on the growth of this pathogen. Triazoles, particularly voriconazole, are recommended as first-line therapy for treating invasive trichosporonosis (*14*). However, the intraspecific diversity among clinical *T. asahii* isolates can contribute to their reduced susceptibility to triazoles, highlighting the relevance of early diagnosis for effective management of invasive trichosporonosis (*15*,*16*).

Some authors have reported clusters of nosocomial *T. asahii* infections, but epidemiologic typing tools to investigate the potential clonal spread of *T. asahii* in clinical settings are notably lacking (*11*,*17*,*18*). Sequencing of the intergenic spacer (IGS) 1 of the rDNA has been used to explore the intraspecific diversity of

Author affiliations: Westerdijk Fungal Biodiversity Institute, Utrecht, the Netherlands (E.C. Francisco, C. Dieleman, J. Houbraken, F. Hagen); Escola Paulista de Medicina-Universidade Federal de São Paulo, São Paulo, Brazil (E.C. Francisco, A.L. Colombo); Hospital de Clínicas José de San Martín, Universidad de Buenos Aires, Buenos Aires, Argentina (N.B. Fernández); Instituto de Higiene, Facultad de Medicina, Universidad de la República, Montevideo, Uruguay (M. Carbia); Iași University of Life Sciences, Iasi, Romania (A.-C. Bostanaru-Iliescu); Antimicrobial Resistance Institute of São Paulo, São Paulo (A.L. Colombo); University Medical Center Utrecht, Utrecht (F. Hagen); Institute for Biodiversity and Ecosystem Dynamics, University of Amsterdam, Amsterdam, the Netherlands (F. Hagen)

DOI: https://doi.org/10.3201/eid3109.241929

T. asahii, and 15 IGS1 genotypes have already been described (*19*). However, epidemiologic studies assessing the global distribution of those genotypes have predominantly reported high prevalence rates for IGS genotypes G1–G7. In contrast, other recently identified IGS1 genotypes, G8–G15, have been documented (*15*), underscoring the need for a robust discriminatory typing approach to investigate the intraspecific diversity of clinical *T. asahii* isolates (*15*,*16*,*20*).

Microsatellites, also known as short tandem repeat (STR) units, are widely used as a fast, highly sensitive, and cost-effective typing technique to investigate the molecular diversity within fungal populations during nosocomial outbreaks and for monitoring pathogens over time (*21*). Microsatellite-based typing has been recognized as the optimal tool for population studies and outbreak investigations in healthcare settings, particularly for *Candida auris*, *C. parapsilosis*, *Aspergillus fumigatus*, and *Cryptococcus* spp. (*22*–*27*), providing reliable evidence in the epidemiologic investigations. We developed a microsatellite-based typing tool for *T. asahii* and applied it to a large and genetically diverse collection of clinical and environmental isolates to assess its use in epidemiological investigations.

Materials and Methods

Media, Strains, and Standard DNA Extraction

To set up the microsatellite typing panel, we used the clinical *T. asahii* type-strain CBS 2479 from the CBS culture collection (https://wi.knaw.nl/fungal_table) hosted by the Westerdijk Fungal Biodiversity Institute (Utrecht, the Netherlands) as a reference and a set of 21 CBS isolates that originated from clinical (n = 5), veterinary (n = 5), and environmental (n = 11) sources. We also used a large set of unique clinical isolates from Brazil (n = 46), Argentina (n = 9), and Romania (n = 1), a set of 29 sequential isolates collected on different days from 12 patients across 6 medical centers in Brazil, and 4 isolates from 2 patients in Uruguay (Figure 1). We cultured isolates onto malt extract agar and incubated for 48 hours at 25°C. We performed DNA extraction by using previously described methods (*28*). We identified all strains as *T. asahii* on the basis of sequencing the IGS1 rDNA locus, as previously described (*15*,*20*).

Genome Sequencing

The genome of *T. asahii* type-strain CBS 2479 was published a decade ago and was generated at that time by short-read sequencing (National Center for Biotechnology Information [NCBI] BioSample no. SAMN02981437 and BioProject no. PRJNA164647). However, that draft genome was found to be highly fragmented into 78 scaffolds and 342 contigs (*29*). Hence, we resequenced the genome using long-read nanopore sequencing to cover complex genetic regions like the microsatellite loci. We prepared a fresh culture of CBS 2479 onto malt extract agar and incubated for 48 hours at 25°C, then extracted high-quality genomic DNA, as previously described by our team (*30*). In brief, we performed library preparation by using the SQK-LSK109 and EXP-NBD114 Native Barcoding DNA Kits (Oxford Nanopore Technologies, https://nanoporetech.com), following the manufacturer's instructions. We first loaded the prepared library onto a Flongle flow cell to confirm the quality, then ran the library on a MinION flow cell and basecalled raw data by using Guppy version 4.5.4 (all Oxford Nanopore Technologies) using the high-accuracy mode. That process yielded 4.8 Gbp of data with an N50 (sequence length of the shortest contig at 50% of the total assembly length) of 17 kbp and an N90 (sequence length for which the collection of all contigs contains at least 90% of the sum of the lengths of all contigs) of 3.370 bp. We performed de novo genome assembly by using Flye version 2.9 (https://github.com/mikolmogorov/Flye) and the setting –genome-size 24m–min-overlap 10000, which resulted in a genome size of 25,250,028 bp dispersed over 19 fragments with an N50 of 2,305,946 bp, and the largest fragment was 5,662,815 bp. The mean coverage was 198× for the nuclear fragment and 1,310× for the mitochondrial genome that had a length of 31,421 bp after manual curation. We deposited data in NCBI under GenBank accession nos. CP116781–99 for the genome assembly, BioProject accession no. PRJNA926907 for the project description, BioSample accession no. SAMN32886118 for the biological sources, and Sequence Read Archive accession no. SRR23205074 for the sequence reads.

Development of Microsatellite Typing Panel

We used the fasta-file of the de novo assembled CBS 2479 genome as input for the Tandem Repeat Finder software using the standard parameters (*31*), and included flanking regions for each locus to enable primer design. We detected nearly 4,800 microsatellite loci, which we subjected to the following selection criteria: >10 copies of the repeat unit; >90% of the repeat units were intact, preferentially a dinucleotide, trinucleotide, or tetranucleotide repeat unit; and selected loci were on different fragments of the de novo genome assembly of CBS 2479. That process resulted in an initial list of 26 loci for which we developed

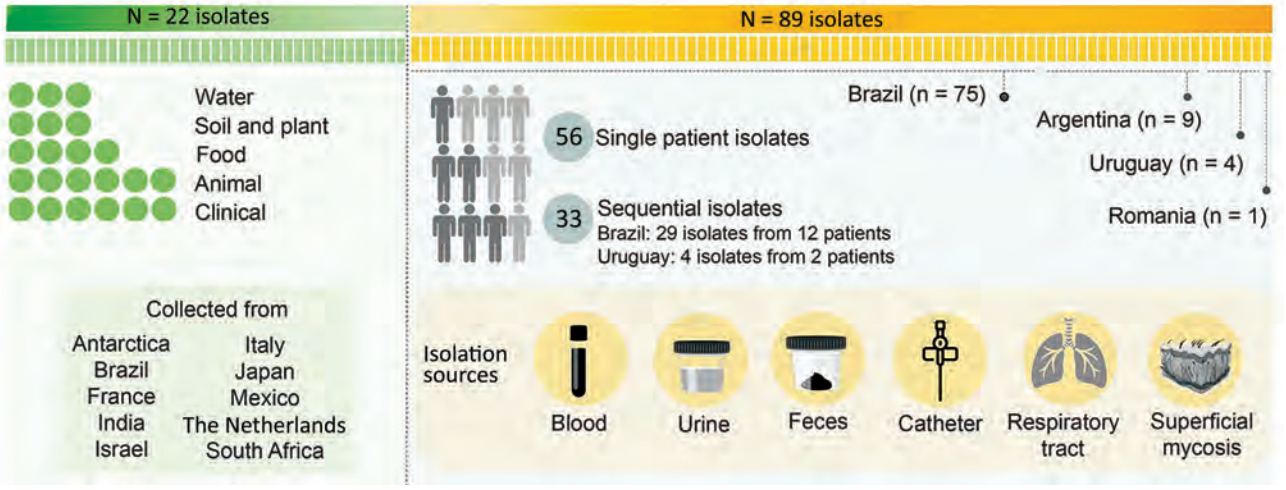

Figure 1. Graphical representation of 111 isolates evaluated in a study of multiple nosocomial *Trichosporon asahii* transmission events, South America. Reference strains are from CBS culture collection (https://wi.knaw.nl/fungal_table) hosted by the Westerdijk Fungal Biodiversity Institute.

primers by using Primer3 version 0.4.0 (*32*) with the standard settings, which we slightly adapted as follows: optimal primer T_m 60°C ± 1°C, a maximum of 3 poly-X nucleotides, and an optimal primer size of 20 bp (range 18–27 bp). The searched amplicon length was 50–200 bp, excluding the microsatellite loci.

First, we used a set of 8 *T. asahii* isolates, CBS collection nos. CBS 2479, CBS 5599, CBS 7631, CBS 8969; and isolate nos. L2122, L7918, L9206, and L920/2016 from the microorganism bank of the Special Mycology Laboratory at Universidade Federal de São Paulo (São Paulo, Brazil), as the primary test set to determine whether the designed primer sets yielded amplicons for all isolates. We performed PCR in a reaction containing 16.8 μL water, 2.5 μL 10× PCR buffer, 1.0 μL $MgCl_2$ (50 mmol), 1.0 μL 0.5 U BIOTAQ Taq polymerase, and 2.5 μL dNTP (1 mmol) (all Bioline Meridian Bioscience, https://www.bioline.com), 0.1 μL 100 pmol/μL unlabeled forward and reverse primer (Integrated DNA Technologies, https://www.idtdna.com), and 1.0 μL DNA template. We performed PCR as follows: initial denaturation at 94°C for 5 minutes, 35 cycles of 94°C for 30 seconds, 60°C for 30 seconds, and 72°C for 1 minute, a final extension for 72°C for 5 minutes, and hold at 21°C.

To check the success of the designed primer sets, we checked all amplicons by 2% agarose gel electrophoresis. We found 12 of the 26 initial primer sets yielded an amplicon for the set of 8 test isolates; we subsequently tested those 12 primer sets by using a second larger set of 16 additional *T. asahii* isolates, including clinical and environmental isolates from CBS culture collection, using the same PCR procedure. After running the second set, we identified 6 primer combinations that yielded amplicons for all 24 isolates tested and observed size differences by agarose gel electrophoresis. For each of the primer sets, we ordered a primer (Integrated DNA Technologies) with a fluorescein-label to enable detection of amplicons by capillary electrophoresis (Table).

Finally, we used a large set of 75 clinical isolates obtained from South America and Europe to check for reproducibility, stability, and specificity of the *T. asahii* microsatellite typing panel of 6 loci (Appendix 1 Table, https://wwwnc.cdc.gov/EID/article/31/9/24-1929-App1.xlsx). The isolates had been obtained from different anatomic sites, including deep-seated and superficial infections, representing the 5 most prevalent IGS1 genotypes, as previously described (*15*).

For capillary-based fragment analyses, we followed the PCR approach described by performing 6 PCRs using a fluorescein-labeled primer (Table). We checked PCR yields by using 2% agarose gel electrophoresis. Thereafter, we purified amplicons by using Sephadex (Sigma-Aldrich, https://www.sigmaaldrich.com), and arbitrarily diluted amplicons 50–200× with water. We mixed 1 μL diluted amplicon with 10× diluted Orange500 size marker (NimaGen, https://www.nimagen.com) in a 96-well plate, then incubated at 94°C for 1 minute and at 4°C for 1 minute. We obtained raw data by running the fragment analysis on an ABI3700xL Genetic Analyzer (Thermo Fisher Scientific, https://www.thermofisher.com).

Data Analysis and Discriminatory Power

We analyzed raw data and relatedness between strains by using Bionumerics version 7.6 (Applied

Maths, http://www.applied-maths.com) via the unweighted pair group method with arithmetic averages, as previously described (*24*). We determined the discriminatory power of the microsatellite panel by using the Simpson index of diversity (*D*) (*33*). A *D* value of 1 indicates that the typing method was able to discriminate between all isolates, and a value of 0 indicates that all isolates were identical (clonal).

Results

Development and Evaluation of *T. asahii* Microsatellite Typing Assay

To develop the typing assay, we selected 6 of 26 promising loci: 4 dinucleotide loci (E, G, I, and K), 1 trinucleotide (locus Q), and 1 tetranucleotide repeat loci (locus P). Loci G, P, and Q were all on the same contig, but loci E, I, and K were on different contigs (Table).

We used a total of 111 *T. asahii* isolates, including 22 CBS reference strains, 56 nonreplicated single-patient isolates, 29 sequential clinical isolates from 12 patients in Brazil, and 4 sequential isolates from 2 patients in Uruguay. The *D* values ranged from 0.6452 for locus Q (tetranucleotide repeat unit) to 0.8280 for locus E (dinucleotide repeat unit) (Table). The combination of all 6 loci yielded a *D* value of 0.9793.

Among the 111 *T. asahii* isolates tested, we identified 71 microsatellite genotypes, in which each genotype contained clusters of 1–11 isolates (Appendix 2 Figure 1, https://wwwnc.cdc.gov/EID/article/31/9/24-1929-App2.pdf). Of the 46 nonreplicated clinical isolates from Brazil, 20 (44%) exhibited unique STR markers. Among the 9 *T. asahii* isolates from Argentina evaluated, 6 displayed unique STR markers, 2 shared identical genotypes, and 1 clustered in a separate group, hitchhiking with isolates collected from both clinical and environmental sources.

Among 12 patients from Brazil who had sequential isolates, 10 exhibited identical or highly related genotypes that differed by ≤1 marker (Appendix 2 Figure 1). We observed genetically distinct genotypes in the other 2 patients: isolates from patient 8 (1199/2020 and 1200/2020) displayed varying numbers of microsatellite repeat units across all 6 loci examined, and isolates from patient 11 (L1871/2017, 1880/2017, and 1881/2017) differed at loci I and K (Appendix 2 Figure 2). Among the identified clusters, the largest consisted of 11 isolates, 7 of which were from a single hospital in the southwest of Brazil. The first isolate appeared in April 2001 (patient 4), followed by a second in July 2001 (patient 5), and others appeared in July 2014 (patient 6). The second largest cluster included 7 isolates collected from 2 patients at a hospital in the south of Brazil; the first isolate appeared in 2010 (patient 1) and the second in 2015 (patient 2). Of note, we found that 4 sequential isolates from a single hospital in Uruguay, collected from 2 different patients (patient 13, isolates nos. MC215 and MC216; and patient 14, isolate nos. MC217 and MC218), were identical. However, we could not obtain retrospective epidemiologic data for those patients (Appendix 2 Figure 1).

Comparison of IGS1 Sequence-Based Genotyping and Microsatellite Typing

The neighbor-joining method divided the 111 *T. asahii* isolates into 5 IGS1 genotypes: 47 (42.3%) G1, 17 (15.3%) G3, 12 (10.8%) G4, 20 (18%) G5, and 15 (13.5%) G7. Clinical isolates from Brazil were represented by all 5 of those IGS1 genotypes; 30 (40%) were genotype G1, 16 (21.3%) were G5, 13 (17.3%) were G7, 10 (13.3%) were G3, and 6 (8%) were G4. We observed nonconcordant results between IGS1 sequencing–based genotypes and microsatellite typing, even among isolates sharing identical IGS1 genotypes, such as the 4 G4 clinical isolates from Uruguay (Figure 2; Appendix 2 Figures 1, 2).

Table. Microsatellite typing panel used for detection of multiple nosocomial *Trichosporon asahii* transmission events via microsatellite typing assay, South America*

Accession no.	Contig; reference code†	Expected size; total fragment, bp‡	Repeat unit	*D* value; no. alleles	Forward primer, 5′ → 3′	Reverse primer, 5′ → 3′
CP116786	6; E	173; 206	CA	0.8280; 12	FLU-TCGTCTGTCATCGACCCATA	GGCTCAGCTGAAGCTCACTT
CP116785	5; G	123; 153	GA	0.7731; 11	FLU-TCCCTTTGATTTGGGTGTGT	CTCTCCCAGGTTCGTTTCAA
CP116781	1; I	183; 211	TG	0.7481; 9	FLU-AGCCTTAGTTGCCCTTGTCA	ACTCAACACTTGGGCGACTT
CP116782	2; K	139; 165	AG	0.7666; 10	GATCGAGTCCAAGGAACGAC	FLU-TTCCCGTCCACCTTTACTGA
CP116785	5; P	112; 158	TCGT	0.6600; 14	FLU-ACGAACTCCATGGCTGAGTC	TGACTGACAACACACCCGATA
CP116785	5; Q	135; 169	GTT	0.6452; 12	FLU-ATCTCGGTTGTTGCCGTTAT	GCAACAGCAACAGCAGTACC

*Isolates sourced from CBS culture collection (https://wi.knaw.nl/fungal_table) hosted by the Westerdijk Fungal Biodiversity Institute, Utrecht, the Netherlands. Discriminatory power of microsatellite typing panel assay as determined via the Simpson index of diversity (*D*). FLU, fluorescein.
†de novo assembly contig number; microsatellite panel reference code.
‡The expected fragment size without the repeat units; number of alleles refers to the total fragment size of the *T. asahii* type strain CBS 2479.

Reproducibility and Specificity of Microsatellite Typing Panel

To test the reproducibility of the developed panel, we independently amplified the first set of 8 isolates ≥4 times. In all replicate assays, the microsatellite markers showed identical profiles for all isolates evaluated, indicating reproducible results. Finally, to validate the microsatellite typing panel for *T. asahii*, we tested 20 *Trichosporon* isolates representing the 11 different non–*T. asahii* species currently recognized in the genus and added representative isolates of the correlated *Apiotrichum* and *Cutaneotrichosporon* genera. We found the PCR product amplification of the 6 selected loci did not demonstrate the highly species-specific typing toll seen for *T. asahii*.

Discussion

The *T. asahii* basidiomycete yeast-like pathogen causes a broad spectrum of human infections and has gained increasing prevalence in life-threatening infections worldwide (*3*,*5*,*12*,*14*). *T. asahii* is recognized as the second or third non–*Candida*-related yeast detected in invasive infection episodes and competes with *Cryptococcus* as leading basidiomycetous yeast pathogen (*3*,*14*). IGS1 sequence-based genotyping is the preferred approach to investigate genetic diversity among *T. asahii* isolates (*3*,*15*,*34*). Despite its relevance, the IGS1-based genotyping can lack the genetic diversity required for outbreak and epidemiologic typing tools, making it difficult to apply in nosocomial outbreak investigations (*8*,*35*). We developed a microsatellite typing panel to genotype *T. asahii*, which can be a valuable complement to IGS1 sequencing genotyping.

Microsatellites, short repetitive DNA sequences, are widely used in molecular studies to explore the genetic relatedness between isolates within fungal populations. This typing tool has greatly contributed

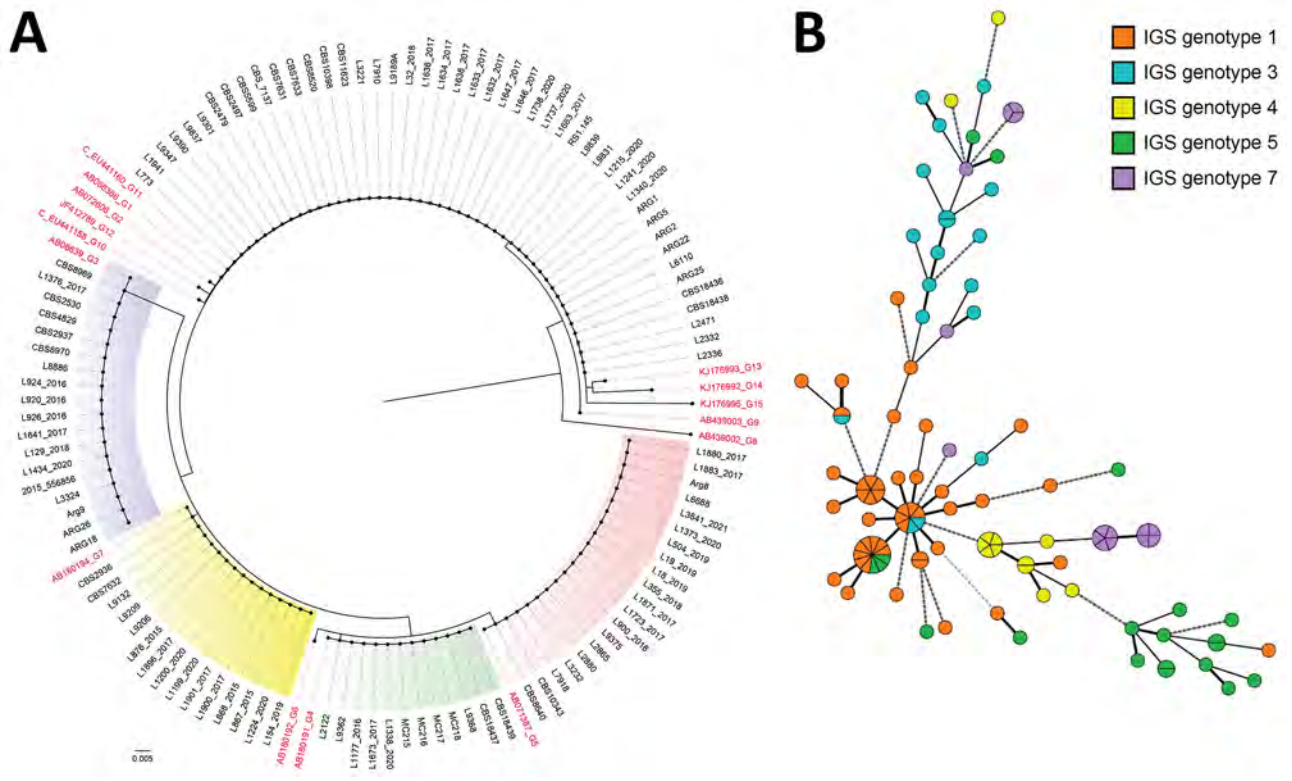

Figure 2. Phylogeny of multiple nosocomial *Trichosporon asahii* transmission events via microsatellite typing assay, South America. We compared IGS1 sequencing–based genotyping and a microsatellite panel for 111 *T. asahii* isolates. A) Neighbor-joining tree based on the rDNA sequencing target, conducted in MEGAX (https://www.megasoftware.net). Red text indicates GenBank accession numbers for reference strains of the described genotypes. Scale bar indicates nucleotide differences per site. B) Minimum spanning tree generated by 6 loci of microsatellite data showing the relationship between microsatellite typing and IGS1 genotypes. Each circle represents a unique genotype; if multiple isolates share an identical genotype, they are shown as a fraction of the circle. Lines between circles indicate the relative similarity, the shorter the line the less prominent the difference between the microsatellite genotypes. Thick lines identify genotypes with fewer differences (1 of 6 loci tested); medium thick lines identify genotypes with differences in 2 of the 6 loci; thick and medium thick dashed lines represent genotypes that share 2–3 identical loci of the 6 tested. Thin dotted lines identify genotypes sharing only 1 identical locus. IGS, intergenic spacer.

to the advancement of epidemiologic typing for a variety of human pathogens, including *C. auris*, *C. parapsilosis*, *Nakaseomyces glabratus* (syn. *C. glabrata*), *Cryptococcus neoformans*, *Cryptococcus deneoformans*, *Cryptococcus deuterogattii*, and *Aspergillus* spp. (*25*–*27*,*34*,*36*–*40*). Compared with other DNA-typing tools, such as internal transcribed spacer–based and amplified fragment length polymorphism (AFLP) profiling, microsatellites have demonstrated superior performance in epidemiologic studies (*23*,*24*,*41*,*42*).

The *T. asahii* microsatellite typing panel we describe consists of 6 loci and revealed remarkable genetic diversity among *T. asahii* isolates. This novel panel successfully distinguished 78 unique isolates (comprising 22 CBS reference isolates and 56 clinical isolates from single patients) into 58 distinct genotypes, a substantially better genetic discriminatory power than the IGS1 sequencing genotyping method, which identified only 5 IGS1 genotypes in the same isolate set. Of note, our panel effectively differentiated between isolates on the basis of their origins, anatomic sites, and year of isolation. Moreover, similar to IGS1 sequencing genotyping, we observed 100% similarity among sequential isolates obtained from 9 of the 12 patients from Brazil from whom multiple isolates were available. Sequential isolates from the 3 other patients were distributed across different microsatellite genotypes; all those sequential isolates were collected 2–7 days after the first isolate, suggesting potential coinfection of those patients by different *T. asahii* genotypes. To underscore the limitation of IGS1 genotyping, all those sequential isolates shared the same IGS1 genotype.

Most isolates we investigated clustered with their sequential counterparts on the basis of microsatellite profiles, suggesting co-infection or cocolonization by the same strain. When we applied our microsatellite assay, we uncovered several clusters spanning single or multiple hospitals. Because microsatellite typing assays are known for high resolution (*27*), the isolates with identical genotypes suggest nosocomial transmission. In the Brazil healthcare setting, the application of this microsatellite panel could provide an accessible and effective strategy to monitor the spread and evolution of *T. asahii* infections. The panel proved particularly useful in different hospital contexts, as demonstrated in 1 outbreak spanning 13 years in a hospital in the southeastern region and another outbreak cluster of 2 patients from southern Brazil. This panel offers a high-resolution intermediate solution for low- and middle-income countries and can be a valuable tool to complement IGS1 sequencing, whereas next-generation sequencing (NGS) remains costly and is not yet widely accessible. In addition, the 4 identical isolates from Uruguay suggest potential interhospital transmission.

Although the described microsatellite genotyping tool might offer a high-resolution intermediate, future studies should seek further validation of this panel in other hospitals and countries with different epidemiologic profiles. To date, no prior nosocomial *Trichosporon* transmission has been reported, which could indicate a rare event but could also be the result of a lack of genotyping investigations. Previously, potential genetic relationships among *T. asahii* clinical isolates were assessed using a multilocus sequence typing (MLST) tool, but that approach revealed a relatively low level of genetic diversity (*11*,*35*). This study highlights multiple events of nosocomial *T. asahii* transmission in hospitals in South America.

Few studies comparing different typing tools for *T. asahii* are available. IGS1 sequencing is a powerful tool and is considered the standard to discriminate the Trichosporonales genera and species in reference laboratories globally, even for the different genetic lineages within *T. asahii* (*20*). A 2019 study used ISG1 sequencing for molecular characterization of a set of locally collected *Trichosporon* species isolates in Brazil (*2*). That endeavor led to identification of a novel genetic lineage, *T. austroamericanum*, in 2024 (*43*). *T. asahii* IGS1 genotypes G1, G3, G5, and G7 have been extensively associated with *Trichosporon* spp. infections worldwide (*15*,*16*,*19*,*20*,*44*–*46*). However, the various epidemiologic studies demonstrate IGS1 sequencing genotyping lacks the resolution needed for outbreak typing (*15*,*16*,*20*,*44*,*45*,*47*). In this study, we considered isolates from those 5 genotypes at all stages of the research, highlighting their potential application in diverse clinical scenarios.

In a study of the genetic relationship between *T. asahii* isolates from elderly patients hospitalized in a single care center in Spain (*48*), one group supplemented IGS1 sequencing with the since-discontinued commercial DiversiLab typing tool (bioMérieux, https://www.biomerieux.com). However, the addition of that repetitive element PCR typing tool led to inconclusive results because the fingerprint patterns lacked sufficient discriminatory power. The genomewide-based AFLP analysis typing tool has been shown to be an informative approach for fungal outbreak investigations but has been reported only once for *Trichosporon* (*49*). Unfortunately, the selective primer combination used in that study resulted in AFLP profiles that could not distinguish potential related isolates from the unrelated ones (*49*). Moreover, AFLP genotyping has been found to be more

laborious, more costly, and less reproducible than other methods, such as microsatellite typing. Hence, microsatellite typing has gradually replaced AFLP to investigate outbreaks caused by fungal pathogens.

A 2023 study published an MLST assay consisting of sequencing from 5 nuclear loci applied to a set of 51 clinical *T. asahii* isolates from Thailand (*35*). The authors of that study concluded that their MLST was useful for population structure analysis, but it seemed to have limited genetic diversity for use in outbreak investigations because the 51 isolates were dispersed among only 5 sequence types (*35*). Another study used whole-genome sequencing (WGS) on a subset of 32 of 54 *T. asahii* isolates that were collected over ≈17 years (*46*). Initially, those isolates were typed using IGS1 sequencing; thus, the finding that short-read genome sequencing resulted in a higher discriminatory power than the former IGS1 typing approach is not surprising (*46*). Because of its high resolution, WGS could soon be used for investigating fungal nosocomial outbreaks. However, WGS is currently costly and technically demanding, making it inaccessible for many diagnostic laboratories in low- and middle-income countries (*50*). In contrast, microsatellite typing offers a more affordable, accessible, and technically simpler alternative, providing sufficient resolution for outbreak investigation at a fraction of the cost of WGS (*36*,*38*). The microsatellite approach we describe provides a middle ground, enabling effective genetic typing of *T. asahii* strains in resource-limited settings. In addition, this method can complement IGS1-based genotyping (*50*) and can be widely implemented in countries without the extensive infrastructure required for WGS.

In conclusion, we assessed intrahospital *T. asahii* transmission by using microsatellite typing, which suggested multiple events of nosocomial transmission by this pathogen in hospitals in South America. The panel we developed offers high reproducibility and specificity, positioning it as an effective epidemiologic tool for tracking *T. asahii* outbreaks and understanding the public health effects of *T. asahii* infections. Our findings highlight the need for ongoing surveillance and effective control measures in hospital settings to mitigate the public health threat of this emerging fungal pathogen.

This article was preprinted at https://www.biorxiv.org/content/10.1101/2024.11.12.623230v1.full.

This study was approved by the Research Ethics Committee of Universidade Federal de São Paulo, Brazil (approval no. CEP-UNIFESP 6183240519/2019).

This study was supported by a grant received from Fundação de Amparo à Pesquisa do Estado de São Paulo–FAPESP (project nos. 2021/10599-3, 2020/14097-0, and 2019/24960-0).

A.L.C. received educational grants from Eurofarma, Biotoscana-Knight, United Medical-Knight, Gilead, and Pfizer. The other authors report no conflicts of interest.

About the Author

Dr. Francisco is a researcher at the Special Mycology Laboratory of Universidade Federal de São Paulo and collaborates with the Medical Mycology Group at the Westerdijk Fungal Biodiversity Institute, the Netherlands. Her research interests include rare and emerging yeast infections, particularly within *Trichosporon* and *Candida*, and integrating epidemiologic, molecular, and taxonomic approaches to study the evolutionary ecology of opportunistic pathogens in Brazil and Latin America.

References

1. Colombo AL, Padovan AC, Chaves GM. Current knowledge of *Trichosporon* spp. and trichosporonosis. Clin Microbiol Rev. 2011;24:682–700. https://doi.org/10.1128/CMR.00003-11
2. Francisco EC, de Almeida Junior JN, de Queiroz Telles F, Aquino VR, Mendes AVA, de Andrade Barberino MGM, et al. Species distribution and antifungal susceptibility of 358 *Trichosporon* clinical isolates collected in 24 medical centres. Clin Microbiol Infect. 2019;25:909.e1–5. https://doi.org/10.1016/j.cmi.2019.03.026
3. Li H, Guo M, Wang C, Li Y, Fernandez AM, Ferraro TN, et al. Epidemiological study of *Trichosporon asahii* infections over the past 23 years. Epidemiol Infect. 2020;148:e169. https://doi.org/10.1017/S0950268820001624
4. Lin SY, Lu PL, Tan BH, Chakrabarti A, Wu UI, Yang JH, et al.; Asia Fungal Working Group (AFWG). The epidemiology of non-*Candida* yeast isolated from blood: the Asia Surveillance Study. Mycoses. 2019;62:112–20. https://doi.org/10.1111/myc.12852
5. Nobrega de Almeida J, Francisco EC, Holguín Ruiz A, Cuéllar LE, Rodrigues Aquino V, Verena Mendes A, et al. Epidemiology, clinical aspects, outcomes and prognostic factors associated with *Trichosporon* fungaemia: results of an international multicentre study carried out at 23 medical centres. J Antimicrob Chemother. 2021;76:1907–15. https://doi.org/10.1093/jac/dkab085
6. Xiao M, Chen SC, Kong F, Fan X, Cheng JW, Hou X, et al.; China Hospital Invasive Fungal Surveillance Net (CHIF-NET) Study Group. Five-year China Hospital Invasive Fungal Surveillance Net (CHIF-NET) study of invasive fungal infections caused by noncandidal yeasts: species distribution and azole susceptibility. Infect Drug Resist. 2018;11:1659–67. https://doi.org/10.2147/IDR.S173805
7. Ali GA, Husain A, Salah H, Goravey W. *Trichosporon asahii* fungemia and COVID-19 co-infection: an emerging fungal pathogen; case report and review of the literature. IDCases. 2021;25:e01244. https://doi.org/10.1016/j.idcr.2021.e01244
8. Benelli JL, Basso RP, Grafulha TW, Poester VR, Munhoz LS, Martins KB, et al. Fungal bloodstream co-infection by

Trichosporon asahii in a COVID-19 critical patient: case report and literature review. Mycopathologia. 2022;187:397–404. https://doi.org/10.1007/s11046-022-00637-6
9. Kruschewsky WLL, Massaroni-Peçanha P, Maifrede SB, Leite MS, Pôssa TAL, Alberto-Lei F, et al. *Trichosporon asahii* causing subcutaneous mycoses in an immunocompetent patient: case report and a minireview. Braz J Microbiol. 2022;53:1221–9. https://doi.org/10.1007/s42770-022-00737-x
10. Lopacinski A, Kim C, Khreis M. A case of fatal invasive trichosporonosis in the setting of immunosuppression and post–COVID-19 pneumonia. Cureus. 2023;15:e35079. https://doi.org/10.7759/cureus.35079
11. Nobrega de Almeida J Jr, Moreno L, Francisco EC, Noronha Marques G, Mendes AV, Barberino MG, et al. *Trichosporon asahii* superinfections in critically ill COVID-19 patients overexposed to antimicrobials and corticosteroids. Mycoses. 2021;64:817–22. https://doi.org/10.1111/myc.13333
12. Arastehfar A, de Almeida Júnior JN, Perlin DS, Ilkit M, Boekhout T, Colombo AL. Multidrug-resistant *Trichosporon* species: underestimated fungal pathogens posing imminent threats in clinical settings. Crit Rev Microbiol. 2021;47:679–98. https://doi.org/10.1080/1040841X.2021.1921695
13. Padovan ACB, Rocha WPDS, Toti ACM, Freitas de Jesus DF, Chaves GM, Colombo AL. Exploring the resistance mechanisms in *Trichosporon asahii*: triazoles as the last defense for invasive trichosporonosis. Fungal Genet Biol. 2019;133:103267. https://doi.org/10.1016/j.fgb.2019.103267
14. Chen SC, Perfect J, Colombo AL, Cornely OA, Groll AH, Seidel D, et al. Global guideline for the diagnosis and management of rare yeast infections: an initiative of the ECMM in cooperation with ISHAM and ASM. Lancet Infect Dis. 2021;21:e375–86. https://doi.org/10.1016/S1473-3099(21)00203-6
15. Francisco EC, de Almeida Junior JN, Queiroz-Telles F, Aquino VR, Mendes AVA, de Oliveira Silva M, et al. Correlation of *Trichosporon asahii* genotypes with anatomical sites and antifungal susceptibility profiles: data analyses from 284 isolates collected in the last 22 years across 24 medical centers. Antimicrob Agents Chemother. 2021;65:e01104-20. https://doi.org/10.1128/AAC.01104-20
16. Guo LN, Yu SY, Hsueh PR, Al-Hatmi AMS, Meis JF, Hagen F, et al. Invasive infections due to *Trichosporon*: species distribution, genotyping, and antifungal susceptibilities from a multicenter study in China. J Clin Microbiol. 2019;57:e01505-18. https://doi.org/10.1128/JCM.01505-18
17. Fanfair RN, Heslop O, Etienne K, Rainford L, Roy M, Gade L, et al. *Trichosporon asahii* among intensive care unit patients at a medical center in Jamaica. Infect Control Hosp Epidemiol. 2013;34:638–41. https://doi.org/10.1086/670633
18. Vashishtha VM, Mittal A, Garg A. A fatal outbreak of *Trichosporon asahii* sepsis in a neonatal intensive care unit. Indian Pediatr. 2012;49:745–7. https://doi.org/10.1007/s13312-012-0137-y
19. Almeida AA, Crispim BA, Grisolia AB, Svidzinski TI, Ortolani LG, Oliveira KM. Genotype, antifungal susceptibility, and biofilm formation of *Trichosporon asahii* isolated from the urine of hospitalized patients. Rev Argent Microbiol. 2016;48:62–6. https://doi.org/10.1016/j.ram.2015.11.005
20. Hazirolan G, Koçak N, Karagöz A. Sequence-based identification, genotyping and virulence factors of *Trichosporon asahii* strains isolated from urine samples of hospitalized patients (2011–2016). J Mycol Med. 2018;28:452–6. https://doi.org/10.1016/j.mycmed.2018.06.006
21. Liu P, Seo TS, Beyor N, Shin KJ, Scherer JR, Mathies RA. Integrated portable polymerase chain reaction-capillary electrophoresis microsystem for rapid forensic short tandem repeat typing. Anal Chem. 2007;79:1881–9. https://doi.org/10.1021/ac061961k
22. Balajee SA, de Valk HA, Lasker BA, Meis JF, Klaassen CH. Utility of a microsatellite assay for identifying clonally related outbreak isolates of *Aspergillus fumigatus*. J Microbiol Methods. 2008;73:252–6. https://doi.org/10.1016/j.mimet.2008.02.011
23. Sabino R, Sampaio P, Rosado L, Videira Z, Grenouillet F, Pais C. Analysis of clinical and environmental *Candida parapsilosis* isolates by microsatellite genotyping—a tool for hospital infection surveillance. Clin Microbiol Infect. 2015;21:954.e1–8. https://doi.org/10.1016/j.cmi.2015.06.001
24. Vatanshenassan M, Boekhout T, Mauder N, Robert V, Maier T, Meis JF, et al. Evaluation of microsatellite typing, ITS sequencing, AFLP fingerprinting, MALDI-TOF MS, and Fourier-transform infrared spectroscopy analysis of *Candida auris*. J Fungi (Basel). 2020;6:146. https://doi.org/10.3390/jof6030146
25. Hagen F, Illnait-Zaragozí MT, Meis JF, Chew WH, Curfs-Breuker I, Mouton JW, et al. Extensive genetic diversity within the Dutch clinical *Cryptococcus neoformans* population. J Clin Microbiol. 2012;50:1918–26. https://doi.org/10.1128/JCM.06750-11
26. Hagen F, Ceresini PC, Polacheck I, Ma H, van Nieuwerburgh F, Gabaldón T, et al. Ancient dispersal of the human fungal pathogen *Cryptococcus gattii* from the Amazon rainforest. PLoS One. 2013;8:e71148. https://doi.org/10.1371/journal.pone.0071148
27. Spruijtenburg B, Meis JF, Verweij PE, de Groot T, Meijer EFJ. Short tandem repeat genotyping of medically important fungi: a comprehensive review of a powerful tool with extensive future potential. Mycopathologia. 2024;189:72. https://doi.org/10.1007/s11046-024-00877-8
28. de Hoog GS, Gerrits van den Ende AH. Molecular diagnostics of clinical strains of filamentous basidiomycetes. Mycoses. 1998;41:183–9. https://doi.org/10.1111/j.1439-0507.1998.tb00321.x
29. Yang RY, Li HT, Zhu H, Zhou GP, Wang M, Wang L. Draft genome sequence of CBS 2479, the standard type strain of *Trichosporon asahii*. Eukaryot Cell. 2012;11:1415–6. https://doi.org/10.1128/EC.00237-12
30. Navarro-Muñoz JC, de Jong AW, Gerrits van den Ende B, Haas PJ, Then ER, Mohd Tap R, et al. The high-quality complete genome sequence of the opportunistic fungal pathogen *Candida vulturna* CBS 14366T. Mycopathologia. 2019;184:731–4. https://doi.org/10.1007/s11046-019-00404-0
31. Benson G. Tandem repeats finder: a program to analyze DNA sequences. Nucleic Acids Res. 1999;27:573–80. https://doi.org/10.1093/nar/27.2.573
32. Rozen S, Skaletsky H. Primer3 on the WWW for general users and for biologist programmers. Methods Mol Biol. 2000;132:365–86. https://doi.org/10.1385/1-59259-192-2:365
33. Hunter PR, Gaston MA. Numerical index of the discriminatory ability of typing systems: an application of Simpson's index of diversity. J Clin Microbiol. 1988;26:2465–6. https://doi.org/10.1128/jcm.26.11.2465-2466.1988
34. Wang Q, Cai X, Li Y, Zhao J, Liu Z, Jiang Y, et al. Molecular identification, antifungal susceptibility, and resistance mechanisms of pathogenic yeasts from the China antifungal resistance surveillance trial (CARST-fungi) study. Front Microbiol. 2022;13:1006375. https://doi.org/10.3389/fmicb.2022.1006375
35. Pumeesat P, Wongsuk T. Genetic analysis of emerging fungal pathogens: *Trichosporon asahii*. Diagn Microbiol

Infect Dis. 2023;107:116057. https://doi.org/10.1016/j.diagmicrobio.2023.116057
36. de Groot T, Puts Y, Berrio I, Chowdhary A, Meis JF. Development of *Candida auris* short tandem repeat typing and its application to a global collection of isolates. MBio. 2020;11:e02971-19. https://doi.org/10.1128/mBio.02971-19
37. de Valk HA, Meis JF, Curfs IM, Muehlethaler K, Mouton JW, Klaassen CH. Use of a novel panel of nine short tandem repeats for exact and high-resolution fingerprinting of *Aspergillus fumigatus* isolates. J Clin Microbiol. 2005;43:4112–20. https://doi.org/10.1128/JCM.43.8.4112-4120.2005
38. Spruijtenburg B, Rudramurthy SM, Meijer EFJ, van Haren MHI, Kaur H, Chakrabarti A, et al. Application of novel short tandem repeat typing for *Wickerhamomyces anomalus* reveals simultaneous outbreaks within a single hospital. Microorganisms. 2023;11:1525. https://doi.org/10.3390/microorganisms11061525
39. Sampaio P, Gusmão L, Alves C, Pina-Vaz C, Amorim A, Pais C. Highly polymorphic microsatellite for identification of *Candida albicans* strains. J Clin Microbiol. 2003;41:552–7. https://doi.org/10.1128/JCM.41.2.552-557.2003
40. Wu Y, Zhou HJ, Che J, Li WG, Bian FN, Yu SB, et al. Multilocus microsatellite markers for molecular typing of *Candida tropicalis* isolates. BMC Microbiol. 2014;14:245. https://doi.org/10.1186/s12866-014-0245-z
41. Díaz-García J, Gómez A, Machado M, Alcalá L, Reigadas E, Sánchez-Carrillo C, et al.; on behalf of the Candimad Study Group. *Candida* genotyping of blood culture isolates from patients admitted to 16 hospitals in Madrid: genotype spreading during the COVID-19 pandemic driven by fluconazole-resistant *C. parapsilosis*. J Fungi (Basel). 2022;8:1228. https://doi.org/10.3390/jof8111228
42. Ener B, Ergin Ç, Gülmez D, Ağca H, Tikveşli M, Aksoy SA, et al. Frequency of azole resistance in clinical and environmental strains of *Aspergillus fumigatus* in Turkey: a multicentre study. J Antimicrob Chemother. 2022;77:1894–8. https://doi.org/10.1093/jac/dkac125
43. Francisco EC, Desnos-Olliver M, Dieleman C, Boekhout T, Santos DW, Medina-Pestana JO, et al. Unveiling *Trichosporon austroamericanum* sp. nov.: a novel emerging opportunistic basidiomycetous yeast species. Mycopathologia. 2024;189:43. https://doi.org/10.1007/s11046-024-00851-4
44. Kuo SH, Lu PL, Chen YC, Ho MW, Lee CH, Chou CH, et al. The epidemiology, genotypes, antifungal susceptibility of *Trichosporon* species, and the impact of voriconazole on *Trichosporon* fungemia patients. J Formos Med Assoc. 2021;120:1686–94. https://doi.org/10.1016/j.jfma.2020.12.007
45. Wongsuk T, Boonsilp S, Pumeesat P, Homkaew A, Sangsri T, Chongtrakool P. Genotyping, antifungal susceptibility testing, and biofilm formation of *Trichosporon* spp. isolated from urine samples in a university hospital in Bangkok, Thailand. Acta Microbiol Immunol Hung. 2022;69:247–57. https://doi.org/10.1556/030.2022.01797
46. Desnos-Ollivier M, Maufrais C, Pihet M, Aznar C, Dromer F; French Mycoses Study Group. Epidemiological investigation for grouped cases of *Trichosporon asahii* using whole genome and IGS1 sequencing. Mycoses. 2020;63:942–51. https://doi.org/10.1111/myc.13126
47. Rodriguez-Tudela JL, Gomez-Lopez A, Alastruey-Izquierdo A, Mellado E, Bernal-Martinez L, Cuenca-Estrella M. Genotype distribution of clinical isolates of *Trichosporon asahii* based on sequencing of intergenic spacer 1. Diagn Microbiol Infect Dis. 2007;58:435–40. https://doi.org/10.1016/j.diagmicrobio.2007.03.001
48. Treviño M, García-Riestra C, Areses P, García X, Navarro D, Suárez FJ, et al. Emerging *Trichosporon asahii* in elderly patients: epidemiological and molecular analysis by the DiversiLab system. Eur J Clin Microbiol Infect Dis. 2014;33:1497–503. https://doi.org/10.1007/s10096-014-2099-6
49. Ahangarkani F, Ilkit M, Vaseghi N, Zahedi N, Zomorodian K, Khodavaisy S, et al. MALDI-TOF MS characterisation, genetic diversity and antifungal susceptibility of *Trichosporon* species from Iranian clinical samples. Mycoses. 2021;64:918–25. https://doi.org/10.1111/myc.13306
50. Sugita T, Nakajima M, Ikeda R, Matsushima T, Shinoda T. Sequence analysis of the ribosomal DNA intergenic spacer 1 regions of *Trichosporon* species. J Clin Microbiol. 2002;40:1826–30. https://doi.org/10.1128/JCM.40.5.1826-1830.2002

Address for correspondence: Ferry Hagen, Westerdijk Fungal Biodiversity Institute (WI-KNAW), Department of Medical Mycology, Uppsalalaan 8, 3584CT Utrecht, the Netherlands; email: f.hagen@wi.knaw.nl or f.hagen@gmail.com

Sporothrix brasiliensis Treatment Failure without Initial Elevated Itraconazole MICs in Felids at Border of Brazil

Carolina Melchior do Prado,[1] Bram Spruijtenburg,[1] Emanuel Razzolini, Luciana Chiyo, Carlos Santi, Caroline Amaral Martins, Gabriela Santacruz, Nancy Segovia, José Pereira Brunelli, Regielly Caroline Raimundo Cognialli, Jacques F. Meis, Vânia Aparecida Vicente, Theun de Groot, Eelco F.J. Meijer,[2] Flávio Queiroz-Telles[2]

Cat-transmitted sporotrichosis caused by *Sporothrix brasiliensis* is an emerging zoonosis in Latin America. Because treatment of feline sporotrichosis is often not effective, we sought to determine whether treatment failure results from *S. brasiliensis* strains that have existing elevated MICs for itraconazole, the primary treatment for this disease. During 2021–2023 at the triple border region of Brazil, Paraguay, and Argentina, 108 *S. brasiliensis* strains were isolated from felines before antifungal treatment. The main clinical manifestation was cutaneous disseminated sporotrichosis (61%), which was the only form resulting in sporotrichosis-induced deaths (61%). We conducted antifungal susceptibility testing for 9 antifungal compounds, evaluating for both mycelial and yeast phases. MIC levels were low for most antifungal agents but were higher in the mycelial phase than in the yeast phase, especially for voriconazole and isavuconazole. We conclude that the varying clinical manifestations of sporotrichosis and large differences in mortality rates were not caused by elevated itraconazole MICs.

Sporotrichosis is a globally neglected epizoonotic and sapronotic disease, primarily affecting the skin and subcutaneous tissues, caused by fungi of the *Sporothrix* genus, and represents the most prevalent implantation mycosis in Latin America, especially in Brazil (*1*). *Sporothrix* spp. are thermally dimorphic fungi from the order Ophiostomatales, showing filamentous forms at 25°C–30°C in the environment and yeast-like forms at temperatures of 35°C–37°C, as in mammals (*2*). The main clinical pathogenic species are *S. brasiliensis*, *S. schenckii*, *S. globosa*, and *S. luriei*. *S. schenckii* and *S. globosa* are usually transmitted via the sapronotic route, involving traumatic implantation with plant or soil debris (*3*). During the past 3 decades, zoonotic transmission of *S. brasiliensis* from infected cats to humans, other felids, and canines has resulted in multiple outbreaks in Brazil and other Latin America countries (*4*–*7*). Cat-transmitted sporotrichosis caused by *S. brasiliensis* is a major public health concern in Latin America. Infections are rapidly spreading from Brazil to other countries, and cases have been described in Brazil (*8*,*9*), Argentina (*5*,*10*), Paraguay (*4*), and Chile (*6*). In addition, imported cases in the United Kingdom (*11*) and United States (*12*) have been reported. Transmission by infected cats, via yeast form (*13*), occurs through bites, scratches, direct contact with exudate from skin lesions, and probably through respiratory droplets by

Author affiliations: Radboudumc–CWZ Center of Expertise for Mycology, Nijmegen, the Netherlands (C.M. do Prado, B. Spruijtenburg, J.F. Meis, T. de Groot, E.F.J. Meijer); Federal University of Paraná, Curitiba, Brazil (C.M. do Prado, E. Razzolini, R.C.R. Cognialli, V.A. Vicente, F. Queiroz-Telles); Canisius-Wilhelmina Hospital (CWZ)/Dicoon, Nijmegen (B. Spruijtenburg, T. de Groot, E.F.J. Meijer); Zoonosis Control Center, Foz do Iguaçu, Brazil (L. Chiyo, C. Santi, C.A. Martins); National University of the East, Minga Guazú, Paraguay (G. Santacruz, N. Segovia); Ministry of Public Health and Social Welfare, Asuncion, Paraguay (J.P. Brunelli); Institute of Translational Research, Cologne Excellence Cluster on Cellular Stress Responses in Aging-Associated Diseases, Excellence Center for Medical Mycology, University of Cologne, Cologne, Germany (J.F. Meis)

DOI: https://doi.org/10.3201/eid3109.250156

[1]These first authors contributed equally to this article.

[2]These senior authors contributed equally to this article.

cat sneezes (*2*,*14*). Cats are the primary animal hosts and main source of infection for other cats, dogs, and humans (*15*).

Cat-transmitted sporotrichosis outbreaks often involve clonal zoonotic transmission (*8*,*16*). To curb such outbreaks, one of the necessary measures is antifungal treatment of cats (*15*). The drug of choice is itraconazole, although various refractory cases have been reported (*17*,*18*). Whether treatment failure results from high antifungal MICs is unknown because that possibility has been poorly investigated (*19*). Recently, high antifungal MICs against itraconazole were reported in isolates obtained from both cats and humans (*19*–*21*). Whether strains with reduced susceptibility are also transmitted or whether reduced susceptibility only develops during treatment remain unclear. Antifungal susceptibility testing (AFST), applicable to both the yeast and mycelial form, has not been standardized in dimorphic fungi, leading to different protocols. As a consequence, published MICs are currently difficult to compare.

We investigated the spread of feline sporotrichosis in the triple border region between Brazil, Paraguay, and Argentina by molecular genotyping. In addition, we obtained MICs for common antifungal drugs using microbroth dilution methods of both the yeast and mycelial phase to determine whether cats with sporotrichosis had *S. brasiliensis* with elevated itraconazole MICs at the onset of treatment. This study was approved by the Committee for Ethics in Research of the Federal University of Paraná (approval no. CAAE 52726021.8.0000.0102) and by the Animal Use Ethics Committee of the Federal University of Paraná, Curitiba, Brazil.

Materials and Methods

Isolate and Data Collection

During July 2021–October 2023, we collected swab samples from 108 symptomatic cats that had lesions compatible with sporotrichosis. All cats lived in the triple border region between Brazil, Paraguay, and Argentina. Cats were selected through notification of the owners; health agents of the Zoonosis Control Center of Foz do Iguaçu, Brazil; veterinarians from private clinics and hospitals; and receipt at the Zoonosis Control Center of animals suspected to be infected. In Foz do Iguaçu, samples were collected at the homes of the cats or at the place indicated by the citizen in cases of stray cats. In Paraguay, samples were collected at private veterinary clinics. We obtained clinical and environmental data by using questionnaires sent to the owners of each cat.

We evaluated and classified all cats according to the types of their lesions and divided them into 3 groups: cutaneous disseminated, cats with ulcerated lesions in different parts of the body and systemic signs; fixed cutaneous, cats with single ulcerated lesion without systemic signs; and extracutaneous, cats without ulcerated lesions but with other clinical manifestations including sneezing, dyspnea, nasal discharge, and other respiratory symptoms. We used cartographic bases from the Brazilian Institute of Geography and Statistics (IBGE) for georeferencing the coordinates where cats lived and QGIS software (https://qgis.org) to assemble the maps. To determine clinical outcomes, we followed the cats for the duration of treatment, until they died, recovered, or were lost to follow-up.

Diagnosis and Molecular Investigation

We diagnosed sporotrichosis via fungal culture of swab specimens collected from the wounds, as previously described (*4*). We cultivated specimens on Sabouraud dextrose agar (KASVI, https://www.kasvi.com.br) containing chloramphenicol and incubated at 25°C–27°C for up to 10 days. We performed micromorphology of colonies to confirm *Sporothrix* growth and calmodulin sequencing for species identification, as previously described (*4*). As control isolates, we used *S. brasiliensis* CBS 133017 (GenBank accession no. KP101458.1), *S. schenckii* CBS 117440 (accession no. KP101386.1), *S. globosa* CBS 129721 (accession no. KP101478.1), *S. luriei* ATCC 18616 (accession no. KT427639.1), *S. mexicana* Ss133 (accession no. JF811341.1), *S. chilensis* Ss470 (accession no. KP711816.1), *S. humicola* CBS 118129 (accession no. KX590808.1), and *S. phasma* CBS 119721 (accession no. KX590795.1). We deposited sequences generated in this study into GenBank (accession nos. OR501574, OR501573, and PQ741608–713) (Appendix Table 1, https://wwwnc.cdc.gov/EID/article/31/9/25-0156-App1.pdf). We performed genotyping of isolates using short tandem repeats, as previously described (*16*) (Appendix).

AFST

We performed AFST for the mycelial and yeast phases of all isolates using broth microdilution as outlined in Clinical and Laboratory Standards Institute (CLSI) reference standard M38 for the mycelial phase (*22*,*23*) and CLSI reference standard M27 for the yeast phase (*24*) (Appendix). For the mycelial phase, we cultured isolates on potato dextrose agar (Sigma Aldrich, https://www.sigmaaldrich.com) plates at 30°C for 7 days and confirmed the absence of yeast cells microscopically. For the yeast phase, we cultured isolates

onto brain–heart infusion plates (Xebios Diagnostics GmbH, https://www.xebios.com) at 35°C for 7 days, then performed a second passage on brain–heart infusion plates at 35°C for 7 days. We then microscopically confirmed the absence of filamentous fungi.

Results

Clinical Epidemiology

We obtained 108 isolates of *Sporothrix* spp. originating from 88 households (Appendix Table 1). Of the animals, 100 were from Foz do Iguaçu (Brazil), 4 from Ciudad del Este (Paraguay), and 4 from Hernandarias (Paraguay). No animals had a history of travel to other regions. Sporotrichosis cases were initially only found in neighborhoods in the eastern region of Foz do Iguaçu (Figure 1, panel A), but over time, cases were found in other regions, close to the country border, especially around the international bridges (Figure 1, panels B, C). The prevalence of sporotrichosis cases was highest in the northern, southern, and eastern districts (Table 1), regions with the highest density

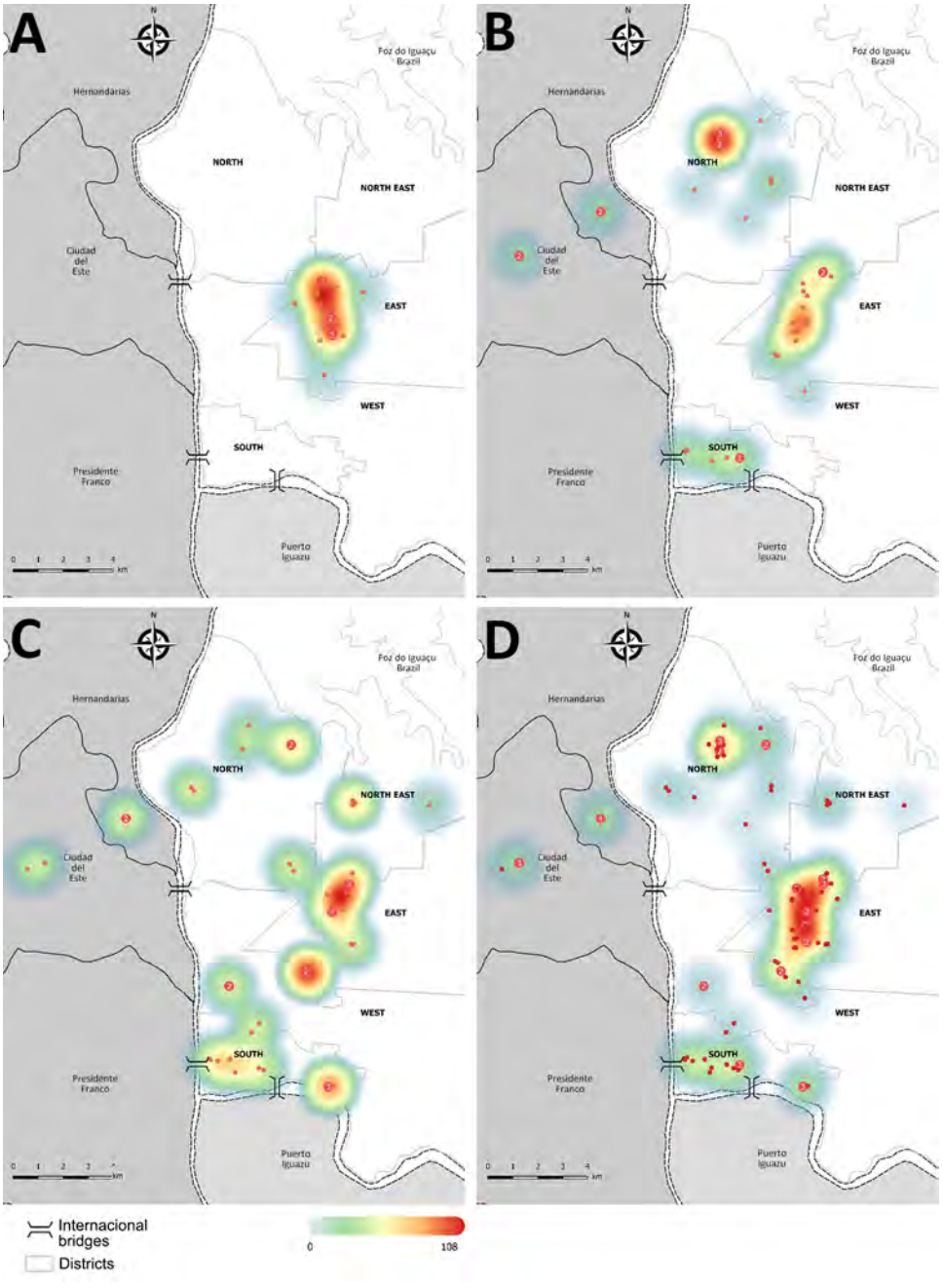

Figure 1. Heatmaps showing the spatial distribution of cats with proven sporotrichosis in the triple border region of Brazil (white), Paraguay (dark gray), and Argentina (light gray) during 2021–2023 in study of *Sporothrix brasiliensis* treatment failure without initial elevated itraconazole MICs in felids at border of Brazil. Red dots show locations of feline sporotrichosis cases during 2021 (A), 2022 (B), and 2023 (C) and for all 3 years combined (D). Numbers in red dots indicate multiple positive cats in the same house.

Table 1. Prevalence of *Sporothrix brasiliensis* among cats in study of treatment failure without initial elevated itraconazole MICs in felids at border of Brazil

District	No. residences	No. positive animals	Prevalence/1,000 residences
North	32,610	24	0.73
West	32,705	3	0.09
South	16,175	17	1.05
North East	18,804	4	0.21
East	36,315	52	1.43

of humans (Appendix Figure 1). Furthermore, most cases were found at or close to low-income urban communities and favelas (Appendix Figure 2), which are low-income, dense housing settlements, characterized by low socioeconomic status, precarious conditions, and lack of essential services, mostly found at the eastern region of Foz do Iguaçu (Appendix Figure 2). Of note, all cats had easy access to the street, other homes, backyards, and vacant lots. Feline sporotrichosis was more frequently in male cats (male:female ratio 2.8:1), adults, uncastrated cats, those not vaccinated for any disease, and those with little or no access to veterinary services; most cats did have an owner (Table 2).

The main clinical manifestation was cutaneous disseminated sporotrichosis (61%), followed by fixed cutaneous (34%) and extracutaneous (5%) sporotrichosis (Table 3). The mortality rate was 61% for cats with the disseminated form, but no cats with the fixed cutaneous or extracutaneous forms died from sporotrichosis. Ten animals were euthanized because they lived on the street without owners, hindering any possibility of treatment; 8 cats were lost to follow-up.

Table 2. Characteristics of cats tested in study of *Sporothrix brasiliensis* treatment failure without initial elevated itraconazole MICs in felids at border of Brazil

Characteristic	No. (%) cats	
	Sporotrichosis	No sporotrichosis
Total no.	108	25
Sex		
M	80 (74)	17 (68)
F	28 (26)	8 (32)
Age, mo.		
≤12	13 (12)	3 (12)
>12	95 (88)	22 (88)
Castration status		
Uncastrated	81 (75)	12 (48)
Castrated	23 (21)	12 (48)
Unknown	4 (4)	1 (4)
Vaccination status		
Never vaccinated	64 (59)	14 (56)
Full vaccination	11 (10)	4 (16)
Only primary	12 (11)	3 (12)
Occasional	4 (4)	3 (12)
Unknown	17 (16)	1 (4)
Access to veterinary care		
No access	76 (70)	22 (88)
With access	32 (30)	3 (12)
Ownership		
With an owner	95 (88)	24 (96)
Stray cat	13 (12)	1 (4)

All cats received itraconazole (25–100 mg/d), and those with disseminated and extracutaneous forms also received potassium iodide (2.5–20 mg/kg/24 h, depending on the severity of symptoms). For the clinically cured cats, treatment duration ranged from 2 to 15 months, and we observed no correlation to the clinical form (Table 4). For the cats that died, 12 never received treatment; for the others, treatment duration ranged from 1 week to 7 months.

Phylogenetic Analysis

Calmodulin sequencing identified all 104 isolates as *S. brasiliensis*, displaying no genetic variation within that gene. Short tandem repeat genotyping yielded 20 genotypes, of which 6 previously had been found in other regions (*16*) (Figure 2). All isolates from the triple border region were highly related, and all grouped within the Rio de Janeiro clade, a previously described dominant group of genotypes originating from Rio de Janeiro, Brazil (*16*). In this study, those isolates often clustered with isolates from other regions of Paraná, Rio de Janeiro, and several other states. In addition, isolates did not cluster based on clinical outcome; all clusters contained isolates from cats who were clinically cured, died, and were euthanized (Appendix Figure 3).

MIC Investigation

For AFST, on the basis of Espinel-Ingroff et al. (*23*), who proposed epidemiological cutoff values (ECVs) based on the M38 CLSI protocol (*22*), we classified all isolates as wild-type for antifungal drugs with available ECVs (Figure 3). For the mycelial phase, itraconazole and posaconazole had the highest in vitro activity, followed by amphotericin B. In contrast, fluconazole, voriconazole, and isavuconazole had low activity and high MICs. For the yeast phase, itraconazole, posaconazole, and isavuconazole showed the highest activity, followed by voriconazole and amphotericin B. Comparing susceptibility levels between both phases, isolates at the mycelial phase had higher MICs for all azoles (for example, differences in 50% MIC values were 8-fold for itraconazole, 64-fold for voriconazole, and 128-fold isavuconazole) and amphotericin B, whereas terbinafine and echinocandins had higher MICs at the yeast phase. Finally, the

geometric mean of strains isolated from cats with disseminated disease that recovered was similar to those from cats that died (Appendix Table 2).

Discussion

Epidemiologic data show that, within 3 years, *S. brasiliensis*–induced sporotrichosis spread across the triple border region of Brazil, Paraguay, and Argentina. The rapidly increasing number of cases in felids highlights the severity of sporotrichosis as a public health problem and the potential for outbreaks (*25*). The data also suggest that cat-transmitted sporotrichosis mainly affects an urban cat population in areas with a high concentration of humans and likely also cats, as compared with areas with a low density of humans (*8*,*26*). All cats in this study were free to roam outside with access to the street, other homes, backyards, and vacant lots, and although no cats had reported travel history, they were also able to roam freely across national borders in this region. We observed introduction of sporotrichosis into Paraguay near the international bridges in the area. Furthermore, based on general assumptions, cases correlate with low socioeconomic status; the eastern region of Foz do Iguaçu has a low overall standard of living. As a consequence, most cats had owners but no access to a veterinarian (*27*). In most cases, owners were not financially able to provide basic resources for their cats' health and, in cases of sporotrichosis, they were not able to provide diagnosis and treatment. Therefore, public policies that provide such tools free of charge are crucial.

Although all reported sporotrichosis cases in both the Brazil and Paraguay sides of the border were included, most isolates originated from Brazil. The population numbers for the cities at the triple border region are similar; the 2024 population of Foz do Iguaçu was 295,000 (*28*) and of Ciudad del Este was 339,000 (*29*). The numbers for the feline populations are not known for either city. The differences in sporotrichosis cases are partly the result of the river between the 2 countries, which halted spread originating from the east of Brazil. In addition, differences between the healthcare systems of the 2 countries might play a role. In Brazil, the Health Unic System (SUS) is a decentralized system, meaning that the city decides how the resources from the state and the federal government will be used (*30*). In Paraguay, a centralized health system has most action concentrated in the capital, Asunción, which is 324 km from the border (*30*). Although the Epidemiologic Laboratory in Ciudad del Este can track cases and diagnose sporotrichosis in cats and humans free of charge, not enough clinicians and veterinarians are available.

In this study, uncastrated and unvaccinated male cats represented most patients with feline sporotrichosis, as previously described (*31*). Unvaccinated cats may have comorbidities such as feline leukemia virus, calicivirus, herpes, and panleukopenia, leading to immunosuppression and rapid evolution to the disseminated form of sporotrichosis (*32*). Castration of male cats reduces production of testosterone and curbs behaviors of territory disputes and sexual intercourse between male and

Table 3. Outcomes of cats with sporotrichosis according to clinical form of disease in study of *Sporothrix brasiliensis* treatment failure without initial elevated itraconazole MICs in felids at border of Brazil*

Outcomes	No. (%) cats
Cutaneous disseminated disease, n = 66	
Death	40 (61)
Clinical cure	16 (24)
Lost to follow-up	3 (4)
Euthanized	7 (11)
Fixed cutaneous disease, n = 37	
Clinical cure	29 (78)
Lost to follow-up	5 (14)
Euthanized	3 (8)
Extracutaneous disease, n = 5†	
Clinical cure	5 (100)

*Total number of cats with sporotrichosis was 108.
†Absence of skin lesions but presence of extracutaneous signs, such as sneezing, dyspnea, and nasal discharge and other respiratory signs.

Table 4. Treatment regimen and duration among 50 clinically cured cats and 40 that died from sporotrichosis according to clinical form of disease in study of *Sporothrix brasiliensis* treatment failure without initial elevated itraconazole MICs in felids at border of Brazil

Sporotrichosis treatment	Duration	No. cats	
		Clinically cured	Died
Cutaneous disseminated disease, n = 56			
No treatment applied	Not applicable	0	12
Itraconazole + potassium iodide	1–4 wk	0	12
Itraconazole + potassium iodide	2–7 mo	3	16
Itraconazole + potassium iodide	8–12 mo	11	0
Itraconazole + potassium iodide	13–15 mo	2	0
Fixed cutaneous disease, n = 29			
Itraconazole	2–6 mo	12	0
Itraconazole	7–12 mo	17	0
Extracutaneous disease, n = 5			
Itraconazole + potassium iodide	2–6 mo	5	0

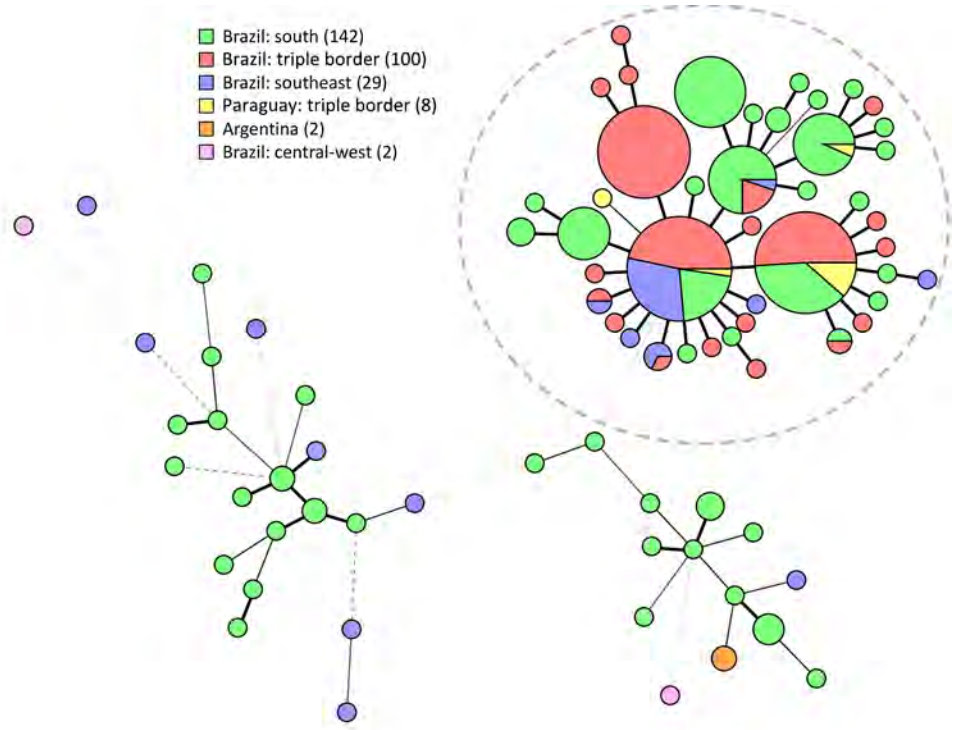

Figure 2. Minimum-spanning tree of isolates in study of *Sporothrix brasiliensis* treatment failure without initial elevated itraconazole MICs in felids at border of Brazil. Tree comprises 283 isolates, including 108 isolates based on 9 short tandem repeat markers from this study (red and yellow); green, blue, and pink indicate comparison isolates from previous studies; and numbers in the key represent the number of isolates from each location. Gray dashed circle indicates Rio de Janeiro clade. Regions of Brazil: south, Paraná, Rio Grande do Sul; southeast, Rio de Janeiro, Minas Gerais, São Paulo, Espírito Santo; central-west, Federal District.

female cats, both of which usually involves fights with injuries, so reducing those interactions decreases chances of transmission to female cats and newborn kittens (*33*). Because most cats in this study were ≥12 months of age, public interventions (vaccination and neutering programs) at <12 months of age would likely reduce the risk for transmission of sporotrichosis. Such measures are crucial to control and prevent sporotrichosis based on a One Health approach, which also reinforces the need for public health education, especially about responsible cat ownership. Furthermore, the lack of awareness about this disease among health professionals is a primary difficulty in identifying sporotrichosis in humans and animals, making searching for cases more difficult (*12*). Thus, public health education on responsible feline ownership and increasing disease awareness in health professionals are the first steps toward preventing sporotrichosis outbreaks and providing effective treatment (*34*).

To show the genetic relatedness among the *S. brasiliensis* isolates, we performed short tandem repeat analysis (*35*). All isolates clustered in the Rio de Janeiro clade and were closely related to isolates from the south and southeastern parts of Brazil. Curitiba and other cities in the Brazil state of Paraná have steadily reported *S. brasiliensis* cases since 2011, and those isolates display identical or highly related genotypes (*16*). The introduction of *S. brasiliensis* in regions could happen by the movement of sick or colonized cats (*11*). The isolates from this study were closely related to those from Curitiba, which, like Foz do Iguaçu, is in Paraná state, although the 2 regions are >600 km apart. Even though all our isolates clustered in the Rio de Janeiro clade (*16*), we identified different genotypes, so multiple introductions cannot be excluded. Whole-genome sequencing is needed to elucidate the origin of *S. brasiliensis* in this region and whether all isolates originate from the same strain. Finally, we observed different clinical manifestations and mortality rates, but those differences were not related to different genetic backgrounds of isolates.

We determined MIC values for 9 different antifungal drugs for *S. brasiliensis* isolates in both the pure yeast and mycelial phases and microscopically confirmed results. According to the interpretation of an international multicenter study for definition of tentative ECVs for mycelial *S. brasiliensis* (*23*), all isolates were susceptible to amphotericin B, itraconazole, voriconazole, posaconazole, and terbinafine (*36*). Espinel-Ingroff et al. used standard incubation of 2–3 days at 35°C, according to the CLSI reference standard M38 for filamentous fungi, whereas in our study, we used 30°C to avoid conversion of the mold form. We found that incubation at 35°C induces transition to the yeast phase, taking up to 2 weeks for full transition. Because Espinel-Ingroff et al. did not perform microscopy, the ECVs possibly were

established on a mixture of filamentous and yeast phases in that study. Moreover, many centers were excluded because of insufficient or unsuitable data, suggesting suboptimal methodology or implementation (*23*). Thus, additional studies are required to analyze the impact of yeast–mold mixtures resulting from short incubation at 35°C versus pure mold at 30°C on the MICs and to establish the ECVs. Nonetheless, the normal distribution of our MIC values indeed suggests an absence of non–wild-type isolates. Of note, we found mycelial phase MICs were overall higher than those for the yeast phase. One explanation for that difference is the higher concentration of melanin in the cell wall in the filamentous phase. Melanin is associated with a reduced susceptibility to antifungal drugs. However, it is important to note that MICs for most of the drugs in the mycelial phase were read at 100% inhibition compared with growth control, whereas at the yeast phase, inhibition was 50%. Therefore, direct comparisons of the MICs between both phases should be made with caution.

AFST results might not reflect in vivo treatment in the absence of clinical breakpoints (*34*). Nonetheless, for itraconazole, which is the first-choice drug for feline treatment (*15*,*34*), MICs of all isolates in both phases were below the tentative ECV, and similar results were reported earlier (*17*,*37*). In contrast, other studies recently found MICs of itraconazole and other azoles above the tentative ECV (*19*,*38*). Of note, the reported bimodal distribution with low and elevated MICs for itraconazole, and the identification of *cyp51* mutants (*19*) suggests that those MICs would also be well above the tentative ECV in conditions of pure mycelial and yeast phase (*23*). That discrepancy with our study might be because we included different strains. Our collection consisted of closely related genotypes only, and strains were isolated before start of treatment. Smaller MIC differences could also be explained by differences in AFST protocols, including the mixed presence of filamentous and yeast phases. Other factors, including panel preparation, media or reagents, and inoculum preparation, might influence AFST results. Finally, because the mycelial form had the least variation in our genotypically similar isolates, is easiest to use, and mycelial AFST data seemingly correspond to in vivo failure of voriconazole (*39*), the mycelial phase might be most suitable for AFST. A multicenter evaluation comparing robust AFST methodologies in a genotypically variable cohort would be needed to establish the

Antifungal		≤0.063	0.125	0.25	0.5	1	2	4	8	16	32	≥64	MIC/MEC$_{50}$
FLU	M											108	≥64
	Y					1	1	1	13	49	30	13	16
		≤0.016	0.031	0.063	0.125	0.25	0.5	1	2	4	8	≥16	
AMB	M						1	38	57	12			2
	Y				2	9	27	66	4				1
ITC	M				3	42	62	1					0.5
	Y	14	35	37	18	4							0.063
VOR	M										7	101	≥16
	Y		2	8	18	26	19	21	13	1			0.25
POS	M				2	31	65	10					0.5
	Y	11	29	36	28	4							0.063
ISA	M									31	51	26	8
	Y	20	18	29	25	10	6						0.063
		≤0.008	0.016	0.031	0.063	0.125	0.25	0.5	1	2	4	≥8	
TRB	M				53	44	9						0.063
	Y			2	14	65	29						0.125
AFG	M	101	6	1									0.008
	Y	7	9	20	34	32	6						0.063
MFG	M	101	2	5									0.008
	Y	4	21	14	40	24	5						0.063

Figure 3. Distribution of MICs for 108 clinical isolates in study of *Sporothrix brasiliensis* treatment failure without initial elevated itraconazole MICs in felids at border of Brazil. MICs were determined according to Clinical Laboratory and Standards Institute M38 (*22*) and M27 (*24*) guidelines. Red dotted lines indicate division of wild-type versus non–wild-type isolates based on ECV values proposed by Espinel-Ingroff (*23*), when available. The ECV value for voriconazole is 32 μg/mL. MICs are given in μg/mL. For AFG and MFG, the MEC$_{50}$ (filamentous phase) was determined. AFG, anidulafungin; AMB, amphotericin B; FLU, fluconazole; ISA, isavuconazole; ITC, itraconazole; M, mycelial phase; MEC$_{50}$, minimal effective concentration that inhibits 50% of isolates; MFG, micafungin; MIC$_{50}$, MIC that inhibits 50% of isolates; POS, posaconazole; TRB, terbinafine; VOR, voriconazole; Y, yeast phase.

best method to determine antifungal susceptibility for *S. brasiliensis*. Moreover, further research is needed to determine whether inoculum incubation at 35°C, in adherence with the M38 guideline for the mycelial phase, has influence on MIC outcome in comparison to incubation at 30°C.

We observed a high (61%) mortality rate in cats with the disseminated form and no sporothrichosis-related deaths in cats with the fixed cutaneous form. Other studies reported unfavorable clinical outcomes in 32%–59% of cats with the disseminated form (*40*–*42*). In our study, all cats with extracutaneous form achieved clinical cure, in contrast with previous studies, which generally considered that form to be indicative of a poor prognosis and high chances of treatment failure and death (*15*,*41*). Of note, all isolates in our study were genetically similar and displayed initially low MICs of itraconazole, used for sporothrichosis treatment in all cats. The 50% MIC levels of strains isolated from cats with the disseminated form that were cured were also not different from those that were not cured. Thus, the mortality rate in cats with the disseminated form is not because of initial elevated MICs, although we cannot exclude the development of reduced susceptibility overtime because we did not collect isolates after itraconazole treatment. The observation that transmission only involved itraconazole-susceptible isolates, because we did not find an isolate with high MIC in any cat, suggests that an increase in MICs was probably uncommon, if present at all. Moreover, some cats from the same household became infected months after each other, and in those households no elevated MICs were found, suggesting no resistance was acquired within the households despite itraconazole exposure. However, isolates collected after itraconazole exposure should be tested to formally exclude resistance development. Regarding treatment failure, other factors, such as disease progression, treatment variations, and host factors, likely were involved in treatment failure in this cohort. Besides clinical outcomes, treatment duration was different between clinical forms. Cats with the fixed cutaneous form were treated for fewer months. Disease progression is likely to play an important role, but erratic itraconazole pharmacokinetics might also be involved.

For feline sporotrichosis, the proposed itraconazole dose by the guideline for the management of feline sporotrichosis caused by *S. brasiliensis* is 100 mg/24 hours for cats >3 kg (*15*). To our knowledge, however, a robust dose-response study evaluating the efficacy of that dose is lacking. When administering the medication, guidelines recommend opening the capsules over a small amount of wet food (*15*); however, no studies have verified the absorption degree of itraconazole administered that way. In disseminated cases, whether itraconazole can reach the mucous membranes at an adequate level for cure also is unknown. Moreover, the disease in the disseminated form could be too advanced to treat with itraconazole. However, suboptimal itraconazole blood levels prolong treatment and increase risk for resistance development in other diseases (*43*,*44*). Optimal dosing to reach effective serum itraconazole concentrations in severe disease would enable the best standard of care, but that information is not available for cats. Alternative therapeutic strategies should be investigated for the disseminated feline form to reduce mortality.

In summary, our investigation of cat-transmitted sporotrichosis caused by *S. brasiliensis* at the triple border region of Brazil, Paraguay, and Argentina found that varying clinical manifestations of sporotrichosis and large differences in mortality rates were not caused by elevated itraconazole MICs. Early diagnosis and effective treatment for this infection are crucial to prevent disease progression, death, and transmission to other humans and animals.

This study was financed in part by the Coordenação de Aperfeiçoamento de Pessoal de Nível Superior–Brasil (CAPES)–Finance Code 001; the Canisius-Wilhelmina Hospital, Nijmegen, the Netherlands (grant no. CWZ_001421); and fellowships from CNPq, Brasilia, Brazil (grant no. 312811/2018-7). The work was also supported by the Araucaria Foundation (http://www.fappr.pr.gov.br; NAPI grant no. 113/2020). F.Q.-T. received a scholarship from CNPq (no. 312222/2021-1), Sporotrichosis One Health and INFOCUS LATAM–ISHAM Working Groups.

E.F.J.M. received research grants from Mundipharma and Scynexis, is on the scientific advisory board for Pfizer, and has received speaker fees from Gilead Sciences. All other authors declare no conflict of interest.

About the Author

Ms. do Prado is a PhD candidate in medical and veterinary mycology at the Federal University of Paraná, Curitiba, Brazil. Her research interests include clinical-epidemiological and diagnostic aspects of zoonotic-transmitted mycoses, characterization of antifungal resistance, and molecular mechanisms involved. Mr. Spruijtenburg is PhD candidate at the Radboudumc-CWZ Center of Expertise for Mycology, Nijmegen, the Netherlands. His primary research interests include outbreak and resistance investigation on medically important fungi.

References

1. Rossow JA, Queiroz-Telles F, Caceres DH, Beer KD, Jackson BR, Pereira JG, et al. A One Health approach to combatting *Sporothrix brasiliensis*: narrative review of an emerging zoonotic fungal pathogen in South America. J Fungi (Basel). 2020;6:247. https://doi.org/10.3390/jof6040247
2. Rodrigues AM, Della Terra PP, Gremião ID, Pereira SA, Orofino-Costa R, de Camargo ZP. The threat of emerging and re-emerging pathogenic *Sporothrix* species. Mycopathologia. 2020;185:813–42. https://doi.org/10.1007/s11046-020-00425-0
3. Rodrigues AM, Gonçalves SS, de Carvalho JA, Borba-Santos LP, Rozental S, Camargo ZP. Current progress on epidemiology, diagnosis, and treatment of sporotrichosis and their future trends. J Fungi (Basel). 2022;8:776. https://doi.org/10.3390/jof8080776
4. do Prado CM, Razzolini E, Santacruz G, Ojeda L, Geraldo MR, Segovia N, et al. First cases of feline sporotrichosis caused by *Sporothrix brasiliensis* in Paraguay. J Fungi (Basel). 2023;9:972. https://doi.org/10.3390/jof9100972
5. Etchecopaz A, Toscanini MA, Gisbert A, Mas J, Scarpa M, Iovannitti CA, et al. *Sporothrix brasiliensis*: a review of an emerging South American fungal pathogen, its related disease, presentation and spread in Argentina. J Fungi (Basel). 2021;7:170. https://doi.org/10.3390/jof7030170
6. Thomson P, González C, Blank O, Ramírez V, Río CD, Santibáñez S, et al. Sporotrichosis outbreak due to *Sporothrix brasiliensis* in domestic cats in Magallanes, Chile: a One-Health-approach study. J Fungi (Basel). 2023;9:226. https://doi.org/10.3390/jof9020226
7. Gallo S, Arias-Rodriguez C, Sánchez-Cifuentes EA, Santa-Vélez C, Larrañaga-Piñeres I, Gaviria-Barrera ME, et al. First three cases of cat-associated zoonotic cutaneous sporotrichosis in Colombia. Int J Dermatol. 2022;61:1276–9. https://doi.org/10.1111/ijd.16377
8. Cognialli RCR, Cáceres DH, Bastos FAGD, Cavassin FB, Lustosa BPR, Vicente VA, et al. Rising incidence of *Sporothrix brasiliensis* infections, Curitiba, Brazil, 2011–2022. Emerg Infect Dis. 2023;29:1330–9. https://doi.org/10.3201/eid2907.230155
9. Rabello VBS, Almeida MA, Bernardes-Engemann AR, Almeida-Paes R, de Macedo PM, Zancopé-Oliveira RM. The historical burden of sporotrichosis in Brazil: a systematic review of cases reported from 1907 to 2020. Braz J Microbiol. 2022;53:231–44. https://doi.org/10.1007/s42770-021-00658-1
10. Etchecopaz AN, Lanza N, Toscanini MA, Devoto TB, Pola SJ, Daneri GL, et al. Sporotrichosis caused by *Sporothrix brasiliensis* in Argentina: case report, molecular identification and in vitro susceptibility pattern to antifungal drugs. J Mycol Med. 2020;30:100908. https://doi.org/10.1016/j.mycmed.2019.100908
11. Barnacle JR, Chow YJ, Borman AM, Wyllie S, Dominguez V, Russell K, et al. The first three reported cases of *Sporothrix brasiliensis* cat-transmitted sporotrichosis outside South America. Med Mycol Case Rep. 2022;39:14–7. https://doi.org/10.1016/j.mmcr.2022.12.004
12. Kaadan MI, Dennis M, Desai N, Yadavalli G, Lederer P. One Health education for future physicians: a case report of cat-transmitted sporotrichosis. Open Forum Infect Dis. 2020;7:ofaa049. https://doi.org/10.1093/ofid/ofaa049
13. Queiroz-Telles F, Cognialli RC, Salvador GL, Moreira GA, Herkert PF, Hagen F. Cutaneous disseminated sporotrichosis in immunocompetent patient: case report and literature review. Med Mycol Case Rep. 2022;36:31–4. https://doi.org/10.1016/j.mmcr.2022.05.003
14. Bastos F, Farias M, Monti F, Cognialli R, Lopuch L, Gabriel A, et al. Spread of *Sporothrix brasiliensis* from the sneeze of infected cats: a potential novel route of transmission. Med Mycol. 2022;60(Supplement_1):myac072P462. https://doi.org/10.1093/mmy/myac072.P462
15. Gremião IDF, Martins da Silva da Rocha E, Montenegro H, Carneiro AJB, Xavier MO, de Farias MR, et al. Guideline for the management of feline sporotrichosis caused by *Sporothrix brasiliensis* and literature revision. Braz J Microbiol. 2021;52:107–24. https://doi.org/10.1007/s42770-020-00365-3
16. Spruijtenburg B, Bombassaro A, Meijer EFJ, Rodrigues AM, Grisolia ME, Vicente VA, et al. *Sporothrix brasiliensis* genotyping reveals numerous independent zoonotic introductions in Brazil. J Infect. 2023;86:610–3. https://doi.org/10.1016/j.jinf.2023.02.034
17. Roldán Villalobos W, Monti F, Ferreira T, Sato S, Telles F, Farias M. Therapeutic efficacy of isavuconazole and potassium iodide in a cat with refractory sporotrichosis. Vet Dermatol. 2023;34:624–8. https://doi.org/10.1111/vde.13188
18. Nakasu CCT, Waller SB, Ripoll MK, Ferreira MRA, Conceição FR, Gomes ADR, et al. Feline sporotrichosis: a case series of itraconazole-resistant *Sporothrix brasiliensis* infection. Braz J Microbiol. 2021;52:163–71. https://doi.org/10.1007/s42770-020-00290-5
19. Ribeiro Dos Santos A, Gade L, Misas E, Litvintseva AP, Nunnally NS, Parnell LA, et al. Bimodal distribution of azole susceptibility in *Sporothrix brasiliensis* isolates in Brazil. Antimicrob Agents Chemother. 2024;68:e0162023. https://doi.org/10.1128/aac.01620-23
20. Ramos MLM, Almeida-Silva F, de Souza Rabello VB, Nahal J, Figueiredo-Carvalho MHG, Bernardes-Engemann AR, et al. In vitro activity of the anthelmintic drug niclosamide against *Sporothrix* spp. strains with distinct genetic and antifungal susceptibility backgrounds. Braz J Microbiol. 2024;55:1359–68. https://doi.org/10.1007/s42770-024-01301-5
21. Waller SB, Ripoll MK, Pierobom RM, Rodrigues PRC, Costa PPC, Pinto FDCL, et al. Screening of alkaloids and withanolides isolated from Solanaceae plants for antifungal properties against non-wild type *Sporothrix brasiliensis*. J Mycol Med. 2024;34:101451. https://doi.org/10.1016/j.mycmed.2023.101451
22. Clinical and Laboratory Standards Institute. Reference method for broth dilution antifungal susceptibility testing of filamentous fungi. CLSI standard M38. 3rd edition. Wayne (PA): The Institute; 2017.
23. Espinel-Ingroff A, Abreu DPB, Almeida-Paes R, Brilhante RSN, Chakrabarti A, Chowdhary A, et al. Multicenter, international study of MIC/MEC distributions for definition of epidemiological cutoff values for *Sporothrix* species identified by molecular methods. Antimicrob Agents Chemother. 2017;61:e01057–17. https://doi.org/10.1128/AAC.01057-17
24. Clinical and Laboratory Standards Institute. Reference method for broth dilution antifungal susceptibility testing of yeasts. CLSI standard M27. 4th edition. Wayne (PA): The Institute; 2017.
25. Rodrigues AM, de Melo Teixeira M, de Hoog GS, Schubach TM, Pereira SA, Fernandes GF, et al. Phylogenetic analysis reveals a high prevalence of *Sporothrix brasiliensis* in feline sporotrichosis outbreaks. PLoS Negl Trop Dis. 2013;7:e2281. https://doi.org/10.1371/journal.pntd.0002281
26. Silva CE, Valeriano CA, Ferraz CE, Neves RP, Oliveira MM, Silva JC, et al. Epidemiological features and geographical expansion of sporotrichosis in the state of Pernambuco, northeastern Brazil. Future Microbiol. 2021;16:1371–9. https://doi.org/10.2217/fmb-2021-0142

27. Alzuguir CLC, Pereira SA, Magalhães MAFM, Almeida-Paes R, Freitas DFS, Oliveira LFA, et al. Geo-epidemiology and socioeconomic aspects of human sporotrichosis in the municipality of Duque de Caxias, Rio de Janeiro, Brazil, between 2007 and 2016. Trans R Soc Trop Med Hyg. 2020;114:99–106.
28. IBGE–Instituto Brasileiro De Geografia E Estatística. Cidades: Foz do Iguaçu. Rio de Janeiro: IBGE, 2022 [cited 2024 Nov 1]. https://cidades.ibge.gov.br/brasil/pr/foz-do-iguacu/panorama
29. World Population Review. Ciudad del Este, Paraguay population 2024 [cited 2024 Nov 1]. https://worldpopulationreview.com/cities/paraguay/ciudad-del-este
30. do Prado CM, Svoboda WK, Chiyo L, Queiroz-Telles F. Fundamentos de Saúde Única (One Health) e Planejamento Estratégico Situacional para Implementação de Política Pública de Saúde para Prevenção e Controle da Esporotricose na Região da Tríplice Fronteira (Brasil, Paraguai, Argentina). In: Zilly A, da Silva RMM, editors. Saúde Pública Na Região Da Fronteira Brasil-Paraguai-Argentina. São Carlos: Pedro & João Editores; 2022. p. 101–18.
31. Pereira SA, Gremião IDF, Kitada AAB, Boechat JS, Viana PG, Schubach TMP. The epidemiological scenario of feline sporotrichosis in Rio de Janeiro, state of Rio de Janeiro, Brazil. Rev Soc Bras Med Trop. 2014;47:392–3. https://doi.org/10.1590/0037-8682-0092-2013
32. de Miranda LHM, Meli M, Conceição-Silva F, Novacco M, Menezes RC, Pereira SA, et al. Co-infection with feline retrovirus is related to changes in immunological parameters of cats with sporotrichosis. PLoS One. 2018;13:e0207644. https://doi.org/10.1371/journal.pone.0207644
33. Araújo AA, Codeço C, F S Freitas D, M de Macedo P, A Pereira S, D F Gremião I, et al. Mathematical model of the dynamics of transmission and control of sporotrichosis in domestic cats. PLoS One. 2023;18:e0272672. https://doi.org/10.1371/journal.pone.0272672
34. Lloret A, Hartmann K, Pennisi MG, Ferrer L, Addie D, Belák S, et al. Sporotrichosis in cats: ABCD guidelines on prevention and management. J Feline Med Surg. 2013;15:619–23. https://doi.org/10.1177/1098612X13489225
35. Fernandez NB, Spruijtenburg B, Tiraboschi IN, Meis JF, Lugo A, López Joffre MC, et al. Genotyping and clonal origin of *Sporothrix brasiliensis* in human sporotrichosis cases in Argentina. Med Mycol Case Rep. 2024;43:100633. https://doi.org/10.1016/j.mmcr.2024.100633
36. Fichman V, Almeida-Silva F, Francis Saraiva Freitas D, Zancopé-Oliveira RM, Gutierrez-Galhardo MC, Almeida-Paes R. Severe sporotrichosis caused by *Sporothrix brasiliensis*: antifungal susceptibility and clinical outcomes. J Fungi (Basel). 2022;9:49. https://doi.org/10.3390/jof9010049
37. Reis EGD, Pereira SA, Miranda LHM, Oliveira RVC, Quintana MSB, Viana PG, et al. A randomized clinical trial comparing itraconazole and a combination therapy with itraconazole and potassium iodide for the treatment of feline sporotrichosis. J Fungi (Basel). 2024;10:101. https://doi.org/10.3390/jof10020101
38. Waller SB, Dalla Lana DF, Quatrin PM, Ferreira MRA, Fuentefria AM, Mezzari A. Antifungal resistance on *Sporothrix* species: an overview. Braz J Microbiol. 2021;52:73–80. https://doi.org/10.1007/s42770-020-00307-z
39. Fernández-Silva F, Capilla J, Mayayo E, Guarro J. Modest efficacy of voriconazole against murine infections by *Sporothrix schenckii* and lack of efficacy against *Sporothrix brasiliensis*. Mycoses. 2014;57:121–4. https://doi.org/10.1111/myc.12112
40. Lecca LO, Paiva MT, de Oliveira CSF, Morais MHF, de Azevedo MI, Bastos CVE, et al. Associated factors and spatial patterns of the epidemic sporotrichosis in a high density human populated area: a cross-sectional study from 2016 to 2018. Prev Vet Med. 2020;176:104939. https://doi.org/10.1016/j.prevetmed.2020.104939
41. Schubach TM, Schubach A, Okamoto T, Barros MB, Figueiredo FB, Cuzzi T, et al. Evaluation of an epidemic of sporotrichosis in cats: 347 cases (1998–2001). J Am Vet Med Assoc. 2004;224:1623–9. https://doi.org/10.2460/javma.2004.224.1623
42. Boechat JS, Oliveira MME, Almeida-Paes R, Gremião IDF, Machado ACS, Oliveira RVC, et al. Feline sporotrichosis: associations between clinical-epidemiological profiles and phenotypic-genotypic characteristics of the etiological agents in the Rio de Janeiro epizootic area. Mem Inst Oswaldo Cruz. 2018;113:185–96. https://doi.org/10.1590/0074-02760170407
43. Chen Y, Ma F, Lu T, Budha N, Jin JY, Kenny JR, et al. Development of a physiologically based pharmacokinetic model for itraconazole pharmacokinetics and drug-drug interaction prediction. Clin Pharmacokinet. 2016;55:735–49. https://doi.org/10.1007/s40262-015-0352-5
44. Prentice AG, Glasmacher A. Making sense of itraconazole pharmacokinetics. J Antimicrob Chemother. 2005;56(Suppl 1):i17–22. https://doi.org/10.1093/jac/dki220

Address for correspondence: Flávio Queiroz-Telles, Department of Public Health, Hospital de Clínicas, Federal University of Paraná, Curitiba, Brazil; email: queiroz.telles@uol.com.br

Insights into Infant Strongyloidiasis, Papua New Guinea

Huan Zhao, Juciliane Haidamak, Eva Noskova, Vladislav Ilik, Barbora Pafčo, Rebecca Ford, Geraldine Masiria, Tobias Maure, Nichola Kotale, William Pomat, Catherine Gordon, Severine Navarro, Paul F. Horwood, Constantin Constantinoiu, Andrew R. Greenhill, Richard S. Bradbury

The human-infecting parasite *Strongyloides fuelleborni* subspecies *kellyi* has been reported from the island of New Guinea. We analyzed fecal DNA extracts (n = 164) from 19 infants in Papua New Guinea by using *Strongyloides* real-time PCR and undertook metabarcoding of *cox1* and 18S rRNA hypervariable regions I and IV loci. Eight infants were infected with *Strongyloides* spp.; 7 were infected with *S. fuelleborni* subsp. *fuelleborni* and 1 with a *Strongyloides* sp. previously misattributed to *S. fuelleborni* subsp. *kellyi*. Phylogenetic and haplotyping analyses indicated *S. fuelleborni* in Papua New Guinea belongs to the Indochina subclade of *S. fuelleborni* subsp. *fuelleborni* and is not a unique subspecies. We report molecular evidence of *S. fuelleborni* subsp. *fuelleborni* infection in humans in the Pacific. Our findings also demonstrate the potential co-existence of an undescribed human-infecting *Strongyloides* sp. on the island of New Guinea, indicating a need for renewed clinical and epidemiologic investigations into infant strongyloidiasis.

New Guinea, consisting of Indonesian New Guinea in the west and Papua New Guinea in the east, is the world's largest tropical island and a biodiversity hotspot. The island is home to the widespread and well-understood human pathogen *S. stercoralis* but also to a unique and enigmatic agent of human strongyloidiasis, the nematode *Strongyloides fuelleborni* subspecies *kellyi* (*1*–*3*). This *S. fuelleborni*–like intestinal nematode of humans was first reported in western Papua New Guinea in 1971 (*4*) and later found in Indonesian New Guinea (*5*).

There was taxonomic confusion over the identity of the New Guinea *Strongyloides* and its relationship to *S. fuelleborni* from Africa. Unlike *S. stercoralis*, which is passed as rhabditiform larvae, *S. fuelleborni* subsp. *kellyi* is passed as eggs, resembling those of larvated hookworms, in feces (*1*,*6*). Viney et al. observed the adult nematodes were morphologically distinguishable by subtle differences in the peri-vulval cuticle of parasitic female specimens and the phasmidial pore position of free-living male specimens (*3*). A separate isoenzyme electrophoresis analysis revealed that the 2 worm isolates clustered closely, separate from other mammal-infecting *Strongyloides* spp. (*7*). On the basis of those findings, subspeciation of *S. fuelleborni* into 2 subspecies was proposed (*3*): *S. fuelleborni* subsp. *fuelleborni*, and *S. fuelleborni* subsp. *kellyi* for the New Guinea nematode. Of note, strains of *S. fuelleborni* from Asia were not included in that analyses (*3*,*7*).

The epidemiology of *S. fuelleborni* subsp. *kellyi* nematodes is similarly enigmatic. Infection in children has been observed within 3 weeks after birth (*6*). One study found the incidence of infection rose rapidly in the first 12 months of life and then stabilized until 5 years of age, at which age-related incidence began to drop (*8*). How infection occurs in children so young is unclear. Transmammary transmission has been suggested (*6*), although a screening of breastmilk from 40 mothers in an endemic village during the 1970s revealed no larvae (*9*). Nonhuman primates, the animal reservoir of *S. fuelleborni* subsp. *fuelleborni*, are not native to New Guinea, and attempts to find an animal reservoir for *S. fuelleborni* subsp. *kellyi* by

Author affiliations: James Cook University, Townsville, Queensland, Australia (H. Zhao, J. Haidamak, P.F. Horwood, C. Constantinoiu, R.S. Bradbury); QIMR Berghofer Medical Research Institute, Brisbane, Queensland, Australia (J. Haidamak, C. Gordon, S. Navarro); Czech Academy of Sciences, Brno, Czech Republic (E. Noskova, V. Ilik, B. Pafčo); Masaryk University, Brno (E. Noskova, V. Ilik, B. Pafčo); Papua New Guinea Institute of Medical Research, Goroka, Papua New Guinea (R. Ford, G. Masiria, T. Maure, N. Kotale, W. Pomat); University of Queensland, Brisbane (C. Gordon); Federation University Australia, Gippsland, Victoria, Australia (A.R. Greenhill).

DOI: https://doi.org/10.3201/eid3109.241923

screening domestic animals, including pigs, chickens, and dogs from villages where infections occurred at high prevalence in humans, were unsuccessful (*4*,*7*).

Heavy *S. fuelleborni* subsp. *kellyi* infection has been implicated as the cause of swollen belly syndrome (SBS), a rapidly fatal disease in infants around 2 months of age (*6*). SBS is a protein-losing enteropathy characterized by eosinophilia, distended abdomen, diarrhea, and respiratory distress (*10*). The etiology of SBS remains poorly understood. SBS was observed during 1974–1983, predominantly in 2 remote villages in mountainous regions of Papua New Guinea, Kanabea (Gulf Province, ≈1270 m above sea level) and Wanuma (Madang Province, ≈750 m above sea level). Only occasional, sporadic cases were reported elsewhere (*6*). In Kanabea, infection with an egg-producing *Strongyloides* sp. was found in 100% of infants 3–8 weeks after birth, with a mean average egg burden of 94,000 eggs/mL of feces (*9*). SBS caused 8% of infant deaths in this village until specific anthelmintic therapy was introduced (*6*). This possible correlation of *Strongyloides* sp. infection to SBS is despite reports of high burdens and prevalence of *Strongyloides* eggs, presumed to be *S. fuelleborni* subsp. *kellyi*, in infants across several other regions of Papua New Guinea, where infections were associated with nutritional deficiencies but not SBS (*11*,*12*). An unknown factor was proposed to be involved in the development of SBS (*10*).

We found only 1 *S. fuelleborni* subsp. *kellyi* DNA sequence recorded to date (*13*), a 330-bp segment of 18S (small subunit) rRNA that covers the hypervariable region (HVR) I (*14*). Phylogenetic analysis on the basis of this region placed *S. fuelleborni* subsp. *kellyi* in a clade with *S. cebus*, *S. papillosus*, and *S. venezuelensis* but distant from *S. fuelleborni* subsp. *fuelleborni*. That work prompted calls to elevate *S. fuelleborni* subsp. *kellyi* to the species rank (*2*). However, a criticism of that finding is that 18S rRNA HVR-I is a poor marker for inferring taxonomic positions of *Strongyloides* spp (*15*,*16*). That gene region did not enable the separation of *Strongyloides* spp. with spiraled and straight ovary morphotypes, whereas nearly full-length 18S rRNA and 28S rRNA sequences did (*13*,*17*). Furthermore, 1 study (*13*) found *S. fuelleborni* subsp. *fuelleborni* to be phylogenetically closer to *S. stercoralis* than to *S. papillosus*, contradicting evidence suggested by mitochondrial genome data (*18*). Molecular taxonomy of *Strongyloides* spp. determined by using markers such as mitochondrial cytochrome oxidase subunit 1 (*cox*1) and 18S rRNA HVR-IV showed considerable consistency with whole-genome and mitochondrial genome analyses (*18*,*19*). The true phylogeny and taxonomic identity of *S. fuelleborni* subsp. *kellyi* could be elucidated by using those informative markers.

Despite its public health significance, *S. fuelleborni* subsp. *kellyi* remains a neglected and underexplored human helminth. This enigmatic causative agent of strongyloidiasis in New Guinea warrants focused research to clarify its identity and epidemiology. We analyzed fecal DNA extracts from 19 infants in Papua New Guinea to explore the identity of *S. fuelleborni* subsp. *kellyi* infection.

Methods

Sampling

We obtained samples from a 1-year longitudinal study investigating gut health in infants in Eastern Highlands Province, Papua New Guinea, during 2018–2019 (Figure 1). Ethics approval was obtained from the Papua New Guinea Institute of Medical Research Institutional Review Board (approval no. 1614) and the Papua New Guinea Medical Research Advisory Committee (approval no. 17.17). Infants were enrolled into the study within the first 5 weeks after birth. Initially, parents gave consent for participation in the study during antenatal clinic visits; after birth, informed consent was obtained from ≥1 parent or legal guardian. Fecal samples were collected from participants monthly for 12 months.

For our study, we investigated the presence of *Strongyloides* spp. in fecal samples from 19 total infants, 12 boys and 7 girls. For samples used in our study, infants were 0–101 days (average 30 days) of age when their first fecal sample was collected. Clinical data on the participants was limited, but no marked gastrointestinal pathology was noted during the study.

Fresh fecal samples were transported to the Papua New Guinea Institute of Medical Research (Goroka, Papua New Guinea), where they were stored at −70°C. Samples were subsequently sent to Queensland Institute of Medical Research-Berghofer Medical Research Institute (Herston, Queensland, Australia) and James Cook University (Townsville, Queensland, Australia) for laboratory analysis. We extracted DNA from each sample by using a QIAamp DNA mini kit (QIAGEN, https://www.qiagen.com). Before extraction, we mixed fecal samples (≈200 mg) with 500 μL of rapid 1-step extraction buffer, 15 μL of proteinase K, and 500 μL of 0.5-mm silica/zirconia beads (Daintree Scientific, http://www.daintreescientific.com.au) in 2-mL screw-cap tubes (Starstedt, https://www.sarstedt.com). We homogenized the tubes at 6,500 rpm for 40 seconds by using a Precellys

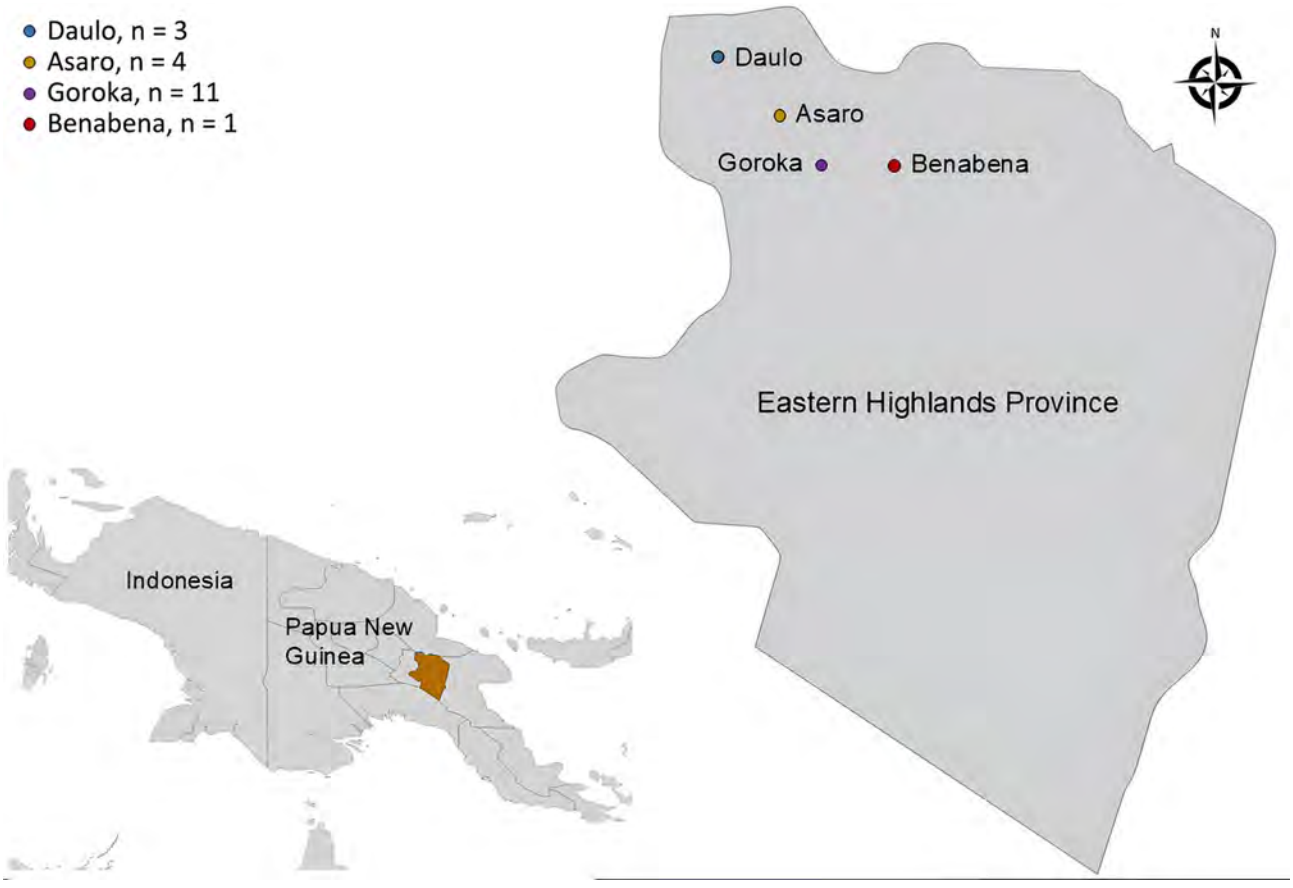

Figure 1. Sampling locations from study of infant strongyloidiasis, Eastern Highlands Province, Papua New Guinea. Participant numbers are shown for each location. Inset shows location of study area on the island of New Guinea.

homogenizer (Bertin Technologies, https://www.bertin-technologies.com). After homogenization, we incubated the samples at 95°C for 5 minutes and then centrifuged at 4,000 relative centrifugal force for 3 minutes. We transferred the supernatant to a new 1.5-mL tube and then followed the QIAGEN protocol for DNA extraction.

We assessed the extracted fecal DNA for quality and quantity by using a NanoDrop 2000 (Thermo Fisher Scientific, https://www.thermofisher.com). We used DNA samples with a concentration >10 ng/μL, and a 260/280 ratio between 1.6 and 2.10 as quantitative PCR templates. We reextracted 5 samples that did not meet those requirements; all subsequently reached the required DNA concentration. We then diluted the DNA 1:5 with Milli Q water (Thermo Fisher Scientific) and subjected it to 2 *Strongyloides* qPCRs (*20*,*21*). We confirmed positive qPCR results by triplicate testing and samples were considered positive when the cycle threshold (Ct) was <35. To tentatively infer the identity of the qPCR product, we conducted Sanger sequencing of positive amplicons from the 2 qPCRs, targeting a 471-bp region of 18S rRNA (*20*) and a 138-bp repeat sequence (*21*) by using the BigDye Direct Cycle Sequencing kit (Thermo Fisher Scientific).

We also performed a metabarcoding assay targeting 18S rRNA HVR-IV (≈252-bp) by using the Illumina MiSeq Reagent Nano Kit v2 (Illumina, https://www.illumina.com) (*16*). We then subjected positive samples to additional metabarcoding of the 18S rRNA HVR-I (≈432-bp) and partial *cox*1 (217-bp) genotyping targets (*16*) by using the same Illumina MiSeq platform. We conducted sequencing with 500 cycles (paired-end, 250-bp) for 18S rRNA products and 300 cycles (paired-end, 150-bp) for the *cox*1 products to ensure adequate sequencing coverage.

Statistical and Bioinformatic Analysis

We imported demographic and qPCR data into Excel (Microsoft, https://www.microsoft.com) for statistical analysis. We had the raw Illumina sequencing data analyzed by 3 blinded researchers at James Cook University and the Institute of Vertebrate Biology (IVB) through 2 different computational pipelines: a custom Geneious Prime (https://www.geneious.com)

workflow as previously published (*16*) at both James Cook University and IVB, and a combination of Skewer (*22*) and DADA2 (*23*) packages implemented in R software version 4.2.2 (The R Project for Statistical Computing, https://www.r-project.org) at IVB. Both pipelines incorporated read quality control, contig assembly, and haplotype assignment. We conducted maximum-likelihood phylogenetic analysis in MEGA 11 (https://www.megasoftware.net) and Bayesian inference phylogenetic analysis in MrBayes (https://nbisweden.github.io/MrBayes) on MUSCLE-aligned (https://github.com/rcedgar/muscle) *cox1* sequences by using the general time-reversible model for nucleotide substitutions. We then used Cohen's κ to assess the diagnostic agreement between different molecular methods for the detection of *Strongyloides* spp.

Results

A total of 164 fecal samples were collected from 19 infants during 5–13 occasions over the study period (Figure 1, 2). Eight (42%) of the 19 infants, comprising 6 boys and 2 girls, were found to be infected with a *Strongyloides* spp. Infections were detected at an average age of 212 days (range 94–334 days) (Figure 2). Of the 8 positive cases, fecal metabarcoding at *cox1* and 18S rRNA HVR-I and HVR-IV loci identified 6 infections as *S. fuelleborni* subsp. *fuelleborni* and 1 as a *Strongyloides* sp. previously attributed to *S. fuelleborni* subsp. *kellyi* (*13*) (Table). The remaining positive sample could only be amplified at the qPCR 18S rRNA target. That 471-bp sequence was 99.2% identical to a published *S. fuelleborni* subsp. *fuelleborni* sequence (GenBank accession no. AB272235) by BLAST analysis (https://blast.ncbi.nlm.nih.gov/).

The previously published genus-specific qPCR method (*20*) performed comparably with a previously published 18S rRNA HVR-IV metabarcoding method (*16*) in detecting *Strongyloides* infections, yielding a Cohen's κ coefficient of 0.85. The second qPCR method (*21*) did not detect *S. fuelleborni* subsp. *fuelleborni* but did detect the *Strongyloides* spp. previously considered *S. fuelleborni* subsp. *kellyi* (Figure 3).

We obtained sequences of 18S rRNA HVR-I (432-bp) and HVR-IV (≈252-bp) from 7 samples (Table). Six positive samples harbored HVR-IV haplotype S and HVR-I haplotype XIV, both genotypes previously identified in all *S. fuelleborni* subsp. *fuelleborni* isolates from Asia. The remaining positive sample was infected with 3 HVR-I haplotypes (deposited into GenBank under accession nos. PV489780–2): two with 275-bp sequences identical to the only published sequence of *S. fuelleborni* subsp. *kellyi* (GenBank accession no. AJ417029) (*13*) and the third differing by 1 single-nucleotide polymorphism (SNP) (T-C at position 28). HVR-I sequences of that *Strongyloides* sp. (432-bp) differed from those of *S. ransomi* (GenBank accession nos. LC324901, OP288111) by 2 SNPs and from *S. venezuelensis* (GenBank accession no. AB923887) by 1 SNP (Figure 4). At the HVR-IV locus, the 248-bp sequence was 100% identical to sequences of *S. ransomi* (GenBank accession nos. OP288111, KU724127) and *S. venezuelensis* (GenBank accession no. AB923887).

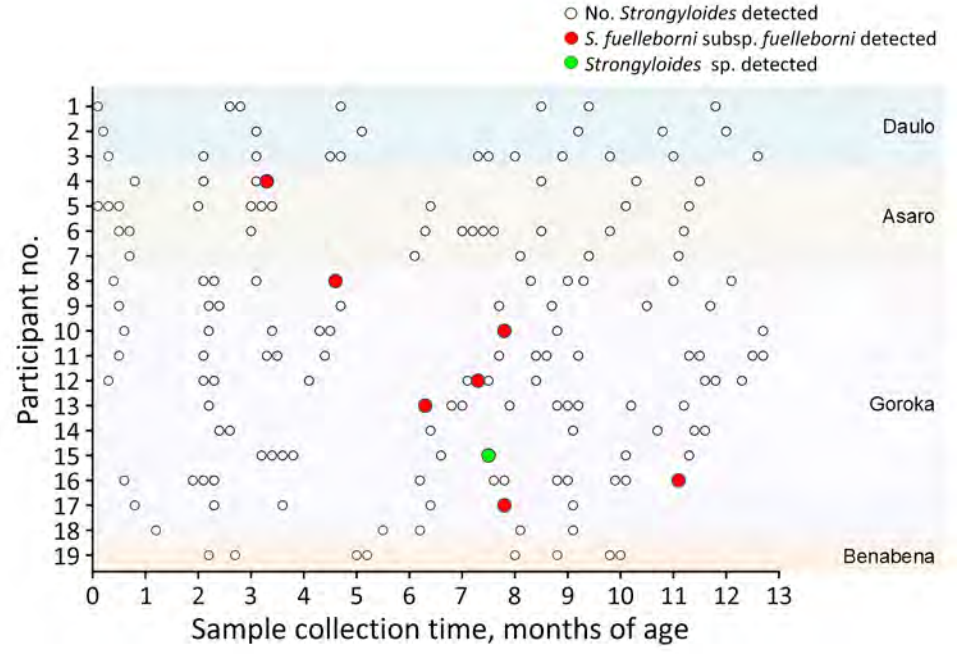

Figure 2. Sampling frequency and *Strongyloides* infection in infants from Eastern Highlands Province, Papua New Guinea. At least 5 samples were collected from each infant enrolled during the first 13 months of life. Samples that demonstrated molecular evidence of *Strongyloides* spp. infection are shown. Sample locations are indicated at right.

Table. *Strongyloides* samples analyzed and their genotypes in study of infant strongyloidiasis, Papua New Guinea*

Sample no.	Patient age, d/sex	Species detected	18S rRNA HVR-IV haplotypes	18S rRNA HVR-I haplotypes	*cox*1 haplotypes
1	205/M	*S. fuelleborni* subsp. *fuelleborni*	S (PQ774622)	XIV (PV489783)	3 OTUs (PQ774615–7)
2	94/M	*S. fuelleborni* subsp. *fuelleborni*	S (PQ774622)	XIV (PV489783)	3 OTUs (PQ774615–7)
3	140/F	*S. fuelleborni* subsp. *fuelleborni*	S (PQ774622)	XIV (PV489783)	2 OTUs (PQ774615, PQ774616)
4	234/M	*S. fuelleborni* subsp. *fuelleborni*	S (PQ774622)	XIV (PV489783)	2 OTUs (PQ774615, PQ774616)
5	227/F	*Strongyloides* spp.	1 OTU (PQ774624)	3 OTUs (PV489780–2)	NA†
6	225/M	*S. fuelleborni* subsp. *fuelleborni*	S (PQ774622)	XIV (PV489783)	2 OTUs (PQ774616, PQ774617)
7	236/M	*S. fuelleborni* subsp. *fuelleborni*	S (PQ774622)	XIV (PV489783)	2 OTUs (PQ774615, PQ774616)
8	334/M	*S. fuelleborni* subsp. *fuelleborni*	NA‡	NA‡	NA‡

*Values in parentheses are GenBank accession numbers. HVR, hypervariable region; NA, not available; OTU, operational taxonomic unit.
†*cox1* region cPCR did not amplify.
‡Metabarcoding on the 18S rRNA HVR-IV locus yielded no detectable product on agar electrophoresis.

cox1 sequences were available for 6 samples, all assigned to *S. fuelleborni* subsp. *fuelleborni* (Table). The seventh sample, containing the genetically distinct *Strongyloides* sp., did not amplify. We identified 3 separate *S. fuelleborni* subsp. *fuelleborni* haplotypes (deposited into GenBank accession nos. PQ774615–7). Maximum-likelihood and Bayesian inference phylogenetic analyses on the *cox1* locus placed *S. fuelleborni* subsp. *fuelleborni* from Papua New Guinea in a clade with *S. fuelleborni* subsp. *fuelleborni* from Myanmar *rhesus macaques* (GenBank accession no. OL672153). Those sequences also clustered closely with *S. fuelleborni* subsp. *fuelleborni* from Bangladesh (GenBank accession nos. OR805176 and OR805181) (Figure 5).

Discussion

We provide molecular evidence of human infections with *S. fuelleborni* subsp. *fuelleborni* outside of Asia and Africa. The potential existence of an undescribed human-infecting *Strongyloides* sp., previously misattributed to *S. fuelleborni* subsp. *kellyi* (*13*), is also suggested. On the basis of those findings, we hypothesize that ≥2 genetically distinct, non–*S. stercoralis Strongyloides* nematodes infect humans in Papua New Guinea and that *S. fuelleborni* subsp. *kellyi*, as previously described (*3*), is not a unique subspecies but is likely synonymous with the Asia-Pacific clade of *S. fuelleborni* subsp. *fuelleborni*.

Our phylogenetic findings corroborate a previously published study (*3*) that described very subtle morphologic distinctions between *S. fuelleborni* adult isolates from Africa and Papua New Guinea. Both strains differed markedly in morphology from *S. ransomi* in Papua New Guinea pigs. Because those analyses did not include isolates of *S. fuelleborni* subsp. *fuelleborni* from Asia, and no morphologic studies of this nematode from Asia exist, it is possible that study described the first representatives of what is now recognized as the clade of *S. fuelleborni* subsp. *fuelleborni* from Asia (*3*). Further comparative morphologic and genomic analyses of adult isolates from Africa, Asia, and the Pacific are required to test that hypothesis. If confirmed, the finding would warrant a revision of current subspecies epithets to reflect the divergence between Africa and Asia-Pacific *S. fuelleborni*.

In Africa and Asia, *S. fuelleborni* subsp. *fuelleborni* is a common infection of nonhuman primates and is considered a zoonosis originating from those animals (*24*,*25*). Multiple studies suggest human-to-human transmission of *S. fuelleborni* subsp. *fuelleborni* occurs in some regions of Africa (*25*,*26*). This suggestion is supported by genetic analysis (*27*) identifying a human-specific subpopulation among *S. fuelleborni* subsp. *fuelleborni* isolates from Africa. Because of the absence of a nonhuman primate reservoir on the island of New Guinea, it is likely that *S. fuelleborni* subsp. *fuelleborni* has adapted to exclusive human-to-human

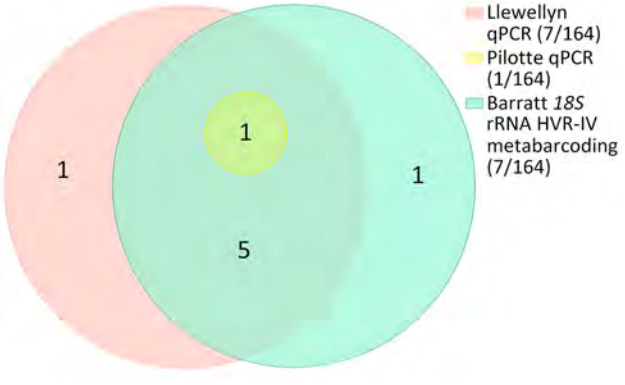

Figure 3. Euler diagram showing the performance of 2 qPCRs (*20*,*21*) and 18S rRNA HVR-IV metabarcoding (*16*) for the detection of *Strongyloides* spp. in 164 infant fecal samples from Papua New Guinea. Values in parentheses are no. positive samples/total no. tested. HVR, hypervariable region; qPCR, quantitative PCR.

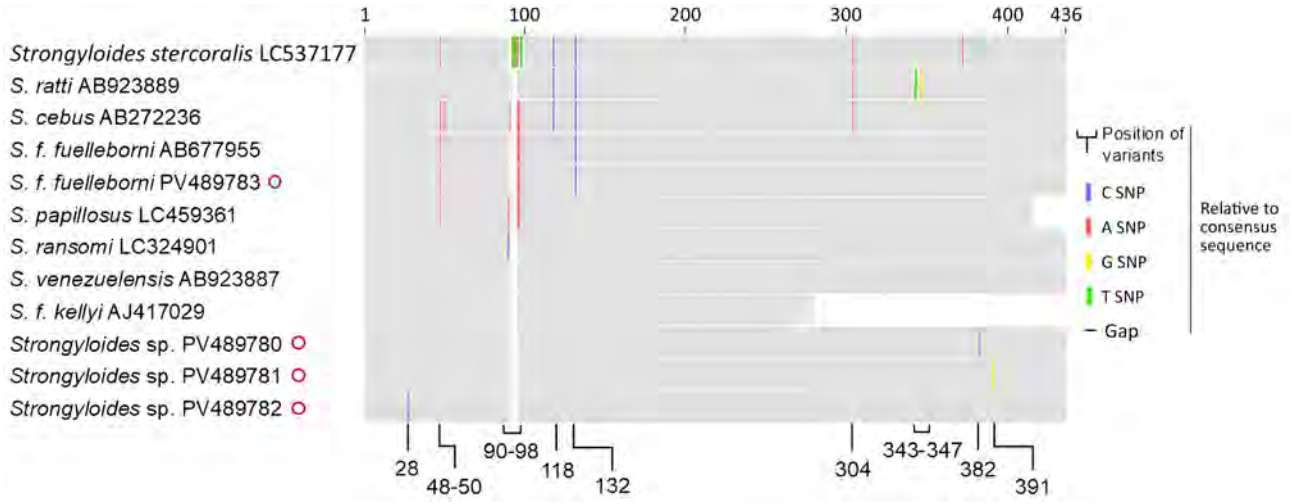

Figure 4. Schematic of MUSCLE-aligned (https://github.com/rcedgar/muscle) *Strongyloides* sp. *18S rRNA* HVR-I sequences from study on infant strongyloidiasis, Papua New Guinea. Sequences obtained are marked with red circles. Previously published sequences are annotated with their GenBank accession numbers. *S. f. fuelleborni*, *S. fuelleborni* subsp. *fuelleborni*; *S. f. kellyi*, *S. fuelleborni* subsp. *kellyi*.

transmission after being introduced to Papua New Guinea through human migration (*28*).

The distinct *Strongyloides* genospecies identified in 1 infant from this study corresponds to the genospecies previously misattributed to *S. fuelleborni subsp. kellyi* (*13*). This species was indistinguishable from *S. ransomi* and *S. venezuelensis* at the 18S rRNA HVR-IV locus and exhibited only 1–2 SNPs at the HVR-I locus, suggesting a recent common ancestry among them. An earlier isoenzyme electrophoretic analysis (*7*) found that 4 of 26 *Strongyloides* isolates recovered from persons in Papua New Guinea clustered closely with *S. ransomi* from local pigs. Although there was speculation those samples might have originated from pigs, it is plausible they represented the same distinct species identified in this and a previous study (*13*). However, caution is warranted when interpreting taxonomic placements based solely on single-locus 18S rRNA data from fecal DNA, without accompanying morphologic data, because those inferences might be artifactual. Detailed morphologic analysis of adult isolates, combined with whole-genome or mitochondrial genome sequencing, is needed to resolve the taxonomic status of this nematode.

Historical reports of *S. fuelleborni* subsp. *kellyi* predated the molecular era and relied solely on microscopic identification of *Strongyloides* eggs (*4*,*6*,*8*,*9*,*12*,*28*). Those data require reassessment because they might conflate infections with 2 co-endemic human-infecting *Strongyloides* spp. nematodes. Surveys conducted during 1976–1997 in Papua New Guinea reported *S. fuelleborni* subsp. *kellyi* prevalence of 20%–93% in children, with rates reaching 60% within the first year of life (*6*,*8*,*9*,*12*,*28*). We similarly found a high incidence of *S. fuelleborni* infection (7/19), but also 1 infection (1/19) with an undescribed *Strongyloides* sp. in Papua New Guinea infants. Future surveillance for strongyloidiasis in New Guinea should use species-specific molecular tools to differentiate those 2 agents.

Our findings provide explanation for much of the unknown epidemiology of infant strongyloidiasis in Papua New Guinea. Patent *S. fuelleborni* infections in infants as young as 18 days of age have been found in Papua New Guinea (*6*). Sampling of breastmilk from mothers in Papua New Guinea (*29*) did not identify any *Strongyloides* larvae; however, difficulties in obtaining fecal samples from those mothers left their infection status uncertain. In the same village, the prevalence of *Strongyloides* spp. in adult feces was only 14% (*12*). In a survey of 25 lactating mothers of infants with confirmed *S. fuelleborni* subsp. *fuelleborni* infection in the Democratic Republic of the Congo, *Strongyloides* spp. filariform larvae were found in the breast milk of 1 mother (*30*). That finding suggests transmammary transmission could be responsible for the high rate of infection in infants as young as 50–74 days of age in that region (*30*). Because our genetic analysis indicates the worms we identified belong to clades of the same species, it is plausible that transmammary transmission to Papua New Guinea infants might occur. That speculation warrants further investigation, and the use of molecular genotyping tools might be necessary to track transmission patterns.

The attribution of *S. fuelleborni* subsp. *kellyi* as the causative agent of infantile SBS requires further validation. Despite *S. fuelleborni* infection being widespread

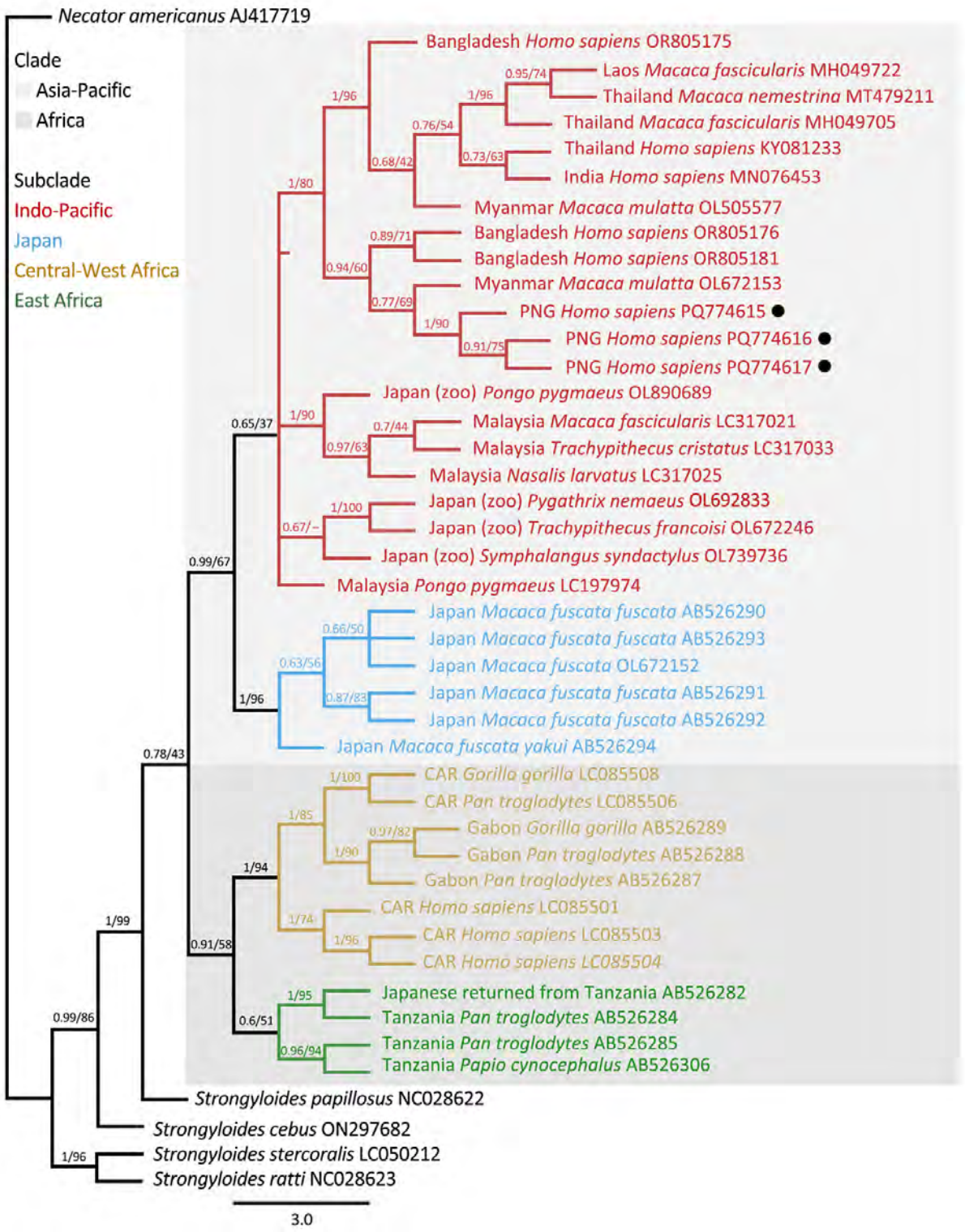

Figure 5. Phylogenetic tree of *Strongyloides fuelleborni* subsp. *fuelleborni* on the basis of *cox*1 sequences from study on infant strongyloidiasis in Papua New Guinea. Bayesian posterior probability and maximum-likelihood bootstrap support percentages (1,000 replicates) are indicated at the nodes. Black dots indicate sequences obtained in this study. Previously published sequences are annotated with their country of origin, host species, and GenBank accession numbers. Clades and subclades of *S. fuelleborni* subsp. *fuelleborni* are color-coded on the basis of geographic regions. Scale bar indicates number of substitutions per site. –, no statistics are available; CAR, Central African Republic; PNG, Papua New Guinea

in children in some parts of Africa, SBS has not been reported from that continent (*25*). Neither has SBS associated with *S. fuelleborni* infection been documented in Asia. The detection of a *Strongyloides* genospecies closely related to *S. ransomi* of pigs raises an alternative hypothesis regarding the etiology of SBS in Papua New Guinea. In newborn suckling piglets, *S. ransomi* infection causes a protein-losing enteropathy characterized by villus atrophy, malabsorption, diarrhea, progressive dehydration, hypoproteinaemia, anemia, anorexia, emaciation, sudden death (*31*,*32*), and reduced hepatic protein synthesis (*33*), a clinical picture strikingly similar to SBS in infants from Papua New Guinea (*1*,*6*). Because of the substantial genetic similarity observed between *S. ransomi* and this genospecies, a shared pathogenic mechanism is plausible. *S. ransomi* detection in only 1 of 19 infants also mirrors the rare and sporadic occurrence of SBS previously reported in this population (*6*,*9*,*10*). Further research is needed to explore this hypothesis and clarify the etiology and epidemiology of SBS.

In our study, not all diagnostic *Strongyloides* spp. qPCRs detected *S. fuelleborni* infection. The Llewelyn modification (*20*) of Verweij (*34*) qPCR appears generic and detected all except 1 *S. fuelleborni* infection. In contrast, the Pilotte *S. stercoralis* qPCR (*21*) only amplified DNA of the undescribed *Strongyloides* sp. and did not detect *S. fuelleborni* infections. That finding demonstrates that the specificity of PCR diagnostics used must be considered in future surveillance of *Strongyloides* spp. infections in humans and animals, because the choice of qPCR might markedly affect the findings of any survey.

In summary, we present molecular evidence of human infections with *S. fuelleborni* subsp. *fuelleborni* nematodes in Papua New Guinea. On the basis of this evidence and existing morphologic data on *S. fuelleborni* subsp. *kellyi*, we hypothesize that *S. fuelleborni* subsp. *kellyi* is not a unique subspecies but rather represents *S. fuelleborni* subsp. *fuelleborni* Asia-Pacific clade infections occurring in humans in New Guinea. We further molecularly identified an undescribed *Strongyloides* species in 1 infant from Papua New Guinea and raise questions about the possible role of this undescribed species in the etiology of infantile SBS. Renewed clinical, epidemiologic, and taxonomic investigations into infant strongyloidiasis in this region are needed to increase clinician awareness of such infections and guide prevention and treatment efforts.

Acknowledgments

We thank the participants and their families for providing stool samples. We thank the leadership and staff at Papua New Guinea Institute of Medical Research, particularly members of the Infection and Immunity Unit, for their collaboration on this project.

This work was partially funded by the National Health and Medical Research Council (investigator grant no. APP1194462). H.Z. and J.H. receive an Australian Government Research Training Program scholarship from James Cook University, Australia.

About the Author

Ms. Zhao is a PhD candidate at James Cook University. Her research focuses on the molecular taxonomy and epidemiology of *Strongyloides* species in humans and companion animals.

References

1. Bradbury RS. *Strongyloides fuelleborni kellyi* in New Guinea: neglected, ignored and unexplored. Microbiol Aust. 2021;42:169–72. https://doi.org/10.1071/MA21048
2. Page W, Shield J, O'Donahoo F, Miller A, Judd J, Speare R. Strongyloidiasis in Oceania. In: Hotez PT, editor. Neglected tropical diseases-Oceania. Switzerland: Springer; 2016. p. 69–99.
3. Viney M, Ashford R, Barnish G. A taxonomic study of *Strongyloides* Grassi, 1879 (nematoda) with special reference to *Strongyloides fuelleborni* von Linstow, 1905 in man in Papua New Guinea and the description of a new subspecies. Syst Parasitol. 1991;18:95–109. https://doi.org/10.1007/BF00017661
4. Kelly A, Voge M. Report of a nematode found in humans at Kiunga, Western District. P N G Med J. 1973;16:59.
5. Muller R, Lillywhite J, Bending JJ, Catford JC. Human cysticercosis and intestinal parasitism amongst the Ekari people of Irian Jaya. J Trop Med Hyg. 1987;90:291–6.
6. Ashford RW, Barnish G, Viney ME. *Strongyloides fuelleborni kellyi*: infection and disease in Papua New Guinea. Parasitol Today. 1992;8:314–8. https://doi.org/10.1016/0169-4758(92)90106-C
7. Viney ME, Ashford RW. The use of isoenzyme electrophoresis in the taxonomy of *Strongyloides*. Ann Trop Med Parasitol. 1990;84:35–47. https://doi.org/10.1080/00034983.1990.11812431
8. Barnish G, Ashford RW. *Strongyloides cf fuelleborni* in Papua New Guinea: epidemiology in an isolated community, and results of an intervention study. Ann Trop Med Parasitol. 1989;83:499–506. https://doi.org/10.1080/00034983.1989.11812378
9. Ashford RW, Vince JD, Gratten MJ, Bana-Koiri J. *Strongyloides* infection in a mid-mountain Papua New Guinea community: results of an epidemiological survey. 1979. P N G Med J. 2005;48:58–65.
10. Vince JD, Ashford RW, Gratten MJ, Bana-Koiri J. Strongyloides species infestation in young infants of Papua New Guinea: association with generalized oedema. 1979. P N G Med J. 2005;48:50–7.
11. Barnish G, Harari M. Possible effects of *Strongyloides fuelleborni*-like infections on children in the Karimui area of Simbu Province. P N G Med J. 1989;32:51–4.
12. King SE, Mascie-Taylor CGS. *Strongyloides fuelleborni kellyi* and other intestinal helminths in children from Papua New

Guinea: associations with nutritional status and socioeconomic factors. P N G Med J. 2004;47:181–91.
13. Dorris M, Viney ME, Blaxter ML. Molecular phylogenetic analysis of the genus *Strongyloides* and related nematodes. Int J Parasitol. 2002;32:1507–17. https://doi.org/10.1016/S0020-7519(02)00156-X
14. Hasegawa H, Hayashida S, Ikeda Y, Sato H. Hyper-variable regions in 18S rDNA of *Strongyloides* spp. as markers for species-specific diagnosis. Parasitol Res. 2009;104:869–74. https://doi.org/10.1007/s00436-008-1269-9
15. Aupalee K, Wijit A, Singphai K, Rödelsperger C, Zhou S, Saeung A, et al. Genomic studies on *Strongyloides stercoralis* in northern and western Thailand. Parasit Vectors. 2020;13:250. https://doi.org/10.1186/s13071-020-04115-0
16. Barratt JLN, Lane M, Talundzic E, Richins T, Robertson G, Formenti F, et al. A global genotyping survey of *Strongyloides stercoralis* and *Strongyloides fuelleborni* using deep amplicon sequencing. PLoS Negl Trop Dis. 2019;13:e0007609. https://doi.org/10.1371/journal.pntd.0007609
17. Hino A, Tanaka T, Takaishi M, Fujii Y, Palomares-Rius JE, Hasegawa K, et al. Karyotype and reproduction mode of the rodent parasite *Strongyloides venezuelensis*. Parasitology. 2014;141:1736–45. https://doi.org/10.1017/S0031182014001036
18. Ko PP, Haraguchi M, Hara T, Hieu DD, Ito A, Tanaka R, et al. Population genetics study of *Strongyloides fuelleborni* and phylogenetic considerations on primate-infecting species of *Strongyloides* based on their mitochondrial genome sequences. Parasitol Int. 2023;92:102663. https://doi.org/10.1016/j.parint.2022.102663
19. de Ree V, Nath TC, Barua P, Harbecke D, Lee D, Rödelsperger C, et al. Genomic analysis of *Strongyloides stercoralis* and *Strongyloides fuelleborni* in Bangladesh. PLoS Negl Trop Dis. 2024;18:e0012440. https://doi.org/10.1371/journal.pntd.0012440
20. Llewellyn S, Inpankaew T, Nery SV, Gray DJ, Verweij JJ, Clements AC, et al. Application of a multiplex quantitative PCR to assess prevalence and intensity of intestinal parasite infections in a controlled clinical trial. PLoS Negl Trop Dis. 2016;10:e0004380. https://doi.org/10.1371/journal.pntd.0004380
21. Pilotte N, Papaiakovou M, Grant JR, Bierwert LA, Llewellyn S, McCarthy JS, et al. Improved PCR-based detection of soil transmitted helminth infections using a next-generation sequencing approach to assay design. PLoS Negl Trop Dis. 2016;10:e0004578. https://doi.org/10.1371/journal.pntd.0004578
22. Jiang H, Lei R, Ding S-W, Zhu S. Skewer: a fast and accurate adapter trimmer for next-generation sequencing paired-end reads. BMC Bioinformatics. 2014;15:182. https://doi.org/10.1186/1471-2105-15-182
23. Callahan BJ, McMurdie PJ, Rosen MJ, Han AW, Johnson AJA, Holmes SP. DADA2: High-resolution sample inference from Illumina amplicon data. Nat Methods. 2016;13:581–3. https://doi.org/10.1038/nmeth.3869
24. Janwan P, Rodpai R, Intapan PM, Sanpool O, Tourtip S, Maleewong W, et al. Possible transmission of *Strongyloides fuelleborni* between working Southern pig-tailed macaques (*Macaca nemestrina*) and their owners in Southern Thailand: Molecular identification and diversity. Infect Genet Evol. 2020;85:104516. https://doi.org/10.1016/j.meegid.2020.104516
25. Pampiglione S, Ricciardi M. Geographic distribution of *Strongyloides fulleborni* in humans in tropical Africa. Parasitologia. 1972;14:329–38.
26. Hira PR, Patel BG. Human strongyloidiasis due to the primate species *Strongyloides fülleborni.* Trop Geogr Med. 1980;32:23–9.
27. Barratt JLN, Sapp SGH. Machine learning-based analyses support the existence of species complexes for *Strongyloides fuelleborni* and *Strongyloides stercoralis.* Parasitology. 2020;147:1184–95. https://doi.org/10.1017/S0031182020000979
28. Kelly A, Little MD, Voge M. *Strongyloides fulleborni*-like infections in man in Papua New Guinea. Am J Trop Med Hyg. 1976;25:694–9. https://doi.org/10.4269/ajtmh.1976.25.694
29. Barnish G, Ashford RW. *Strongyloides cf. fuelleborni* and hookworm in Papua New Guinea: patterns of infection within the community. Trans R Soc Trop Med Hyg. 1989;83:684–8. https://doi.org/10.1016/0035-9203(89)90398-2
30. Brown RC, Girardeau HF. Transmammary passage of *Strongyloides* sp. larvae in the human host. Am J Trop Med Hyg. 1977;26:215–9. https://doi.org/10.4269/ajtmh.1977.26.215
31. Constable P, Hinchcliff K, Done S, Grünberg W. Diseases of the alimentary tract: nonruminant. Veterinary medicine. 11th ed. St. Louis: Elsevier; 2017.
32. Uzal FA, Plattner BL, Hostetter JM. Alimentary system. In: Maxie M, editor. Jubb, Kennedy & Palmer's pathology of domestic animals. 6th ed. Philadelphia: W.B. Saunders; 2016. p. 1–257.e2.
33. Dey-Hazra A, Sallmann HP, Enigk K, Harisch G. Protein synthesis changes in the liver of piglets infected with *Strongyloides ransomi.* Vet Parasitol. 1979;5:339–51. https://doi.org/10.1016/0304-4017(79)90025-6
34. Verweij JJ, Canales M, Polman K, Ziem J, Brienen EA, Polderman AM, et al. Molecular diagnosis of *Strongyloides stercoralis* in faecal samples using real-time PCR. Trans R Soc Trop Med Hyg. 2009;103:342–6. https://doi.org/10.1016/j.trstmh.2008.12.001

Address for correspondence: Richard S. Bradbury, School of Public Health and Tropical Medicine, College of Medicine and Dentistry, Bldg 41, University Drive, James Cook University, Townsville, QLD 4811, Australia; email: richard.bradbury@jcu.edu.au

Related Melioidosis Cases with Unknown Exposure Source, Georgia, USA, 1983–2024

Skyler Brennan,[1] Julie M. Thompson,[1] Christopher A. Gulvik, Taylor K. Paisie, Mindy Glass Elrod, Jay E. Gee, Caroline A. Schrodt, Katherine M. DeBord, Brian T. Richardson, Jr., Cherie Drenzek, William A. Bower, Alex R. Hoffmaster, Zachary P. Weiner, Caitlin M. Cossaboom, Julie Gabel

We identified 4 cases of presumptive autochthonous melioidosis during 1983–2024 in Georgia, USA. Epidemiologic investigation identified no recent international travel before illness; all cases were geographically linked, and 3 patients became ill after a severe weather event. Bioinformatic analyses revealed *Burkholderia pseudomallei* genome sequences were highly related, suggesting a shared exposure.

Melioidosis is a potentially severe disease caused by the gram-negative environmental bacterium *Burkholderia pseudomallei* (*1*), which is predominantly found in tropical and subtropical regions. The median incubation is 4 days (total range 1–21 days) after exposure. Clinical manifestations vary, and infection can cause local or disseminated disease, including fulminant sepsis. Mortality ranges from <10% with early recognition and access to intensive care to ≥40% without treatment (*1*,*2*). Melioidosis does not develop from *B. pseudomallei* exposure in most persons, but comorbidities such as diabetes, which is prevalent in the southeastern United States (*3*), increase the risk (*2*).

Most melioidosis cases in the United States are associated with travel to endemic areas, but some were domestically acquired after exposure to imported household products (*4*,*5*). In 2022, three human cases were genetically linked to environmental *B. pseudomallei* isolated from the US Gulf Coast (*6*). Predictive modeling studies suggest environmental conditions in the southeastern United States are suitable for *B. pseudomallei* (*7*). In endemic regions, infections increase during the rainy season and after severe weather events such as hurricanes (*1*,*2*,*8*,*9*). The Atlantic hurricane season spans from June 1–November 30 annually (*10*).

The Study

On September 26, 2024, category 4 Hurricane Helene made landfall in Georgia, USA (Table), resulting in heavy rainfall, flooding, and windspeeds reaching 100 mph. On October 9, blood cultures from 2 patients in Georgia were presumptive positive for *B. pseudomallei*. The Georgia Department of Public Health discovered the patients shared a common worksite with exposure to mud, dust, wind, and 10 inches of rain.

Patient 1, a man in his 50s with no comorbidities, no reported international travel, and no US military service, reported working in muddy conditions on September 26, 2024. He performed routine vehicle inspections involving checking air pressure of vehicle tires, high-pressure hosing, and physical contact with mud. He became ill on September 28 and was hospitalized October 2 with fever, chills, weakness, and shortness of breath. Chest, abdominal, and pelvic imaging were unremarkable. Healthcare providers diagnosed severe sepsis. After the presumptive positive blood culture, treatment with 30 days of intravenous meropenem and oral doxycycline began on October 9, and then 3 months of oral doxycycline (*11*) was initiated. The patient was discharged on October 16.

Patient 2, a man in his 60s with no comorbidities, travel to the Bahamas in 2022, and no US military service, reported operating heavy equipment at the worksite during September 26–29, 2024, and frequent contact with soil. We could not confirm if

Author affiliations: Georgia Department of Public Health, Atlanta, Georgia, USA (S. Brennan, C. Drenzek, J. Gabel); Centers for Disease Control and Prevention, Atlanta, (J.M. Thompson, C.A. Gulvik, T.K. Paisie, M.G. Elrod, J.E. Gee, C.A. Schrodt, K.M. DeBord, B.T. Richardson, Jr., W.A. Bower, A.R. Hoffmaster, Z.P. Weiner, C.M. Cossaboom)

DOI: https://doi.org/10.3201/eid3109.250804

[1]These first authors contributed equally to this article.

Table. Characteristics, clinical findings, and timeline of events among 4 patients with related melioidosis infections, Georgia, USA, 1983–2024*

Characteristics	Patient 1	Patient 2	Patient 3	Patient 4
Preceding weather event (strength†)	Hurricane Helene (Category 4)		Hurricane Hugo (Category 4)	None
Weather event date	2024 Sep 26	2024 Sep 26	1989 Sep 22	None
Symptom onset date(s)	2024 Sep 28	2024 Sep 29	1989 Oct 5	Unknown
Hospitalization admission date	2024 Oct 2	2024 Oct 1	Unknown	Unknown
Laboratory findings at admission (reference range)				
Leukocyte count (4–11 × 10^9 cells/L)	14.98	5.92	Unknown	Unknown
Neutrophils (39.4%–72.5%)	77.8%	82.5%	Unknown	Unknown
Platelet count (140–400 × 10^9/L)	162	73	Unknown	Unknown
AST (15–37 U/L)	37	193	Unknown	Unknown
ALT (16–61 U/L)	76	79	Unknown	Unknown
Imaging findings at admission	Chest radiograph: unremarkable; persistent nodule/density in left mid-lung zone. CT abdomen and pelvis with IV contrast: unremarkable	Chest radiograph: pneumonia with nodule in left lung, suspected bronchogenic neoplasm. CT abdomen and pelvis without contrast: unremarkable	Unknown	Unknown
Comorbidities	None identified	None identified	Diabetes	None identified
Outcome	Discharged	Discharged	Died	Died
Discharge or death date	2024 Oct 16	2024 Oct 20	1989 Oct	1983 Oct
Hospital readmission date	None	2024 Nov 9	None	None
Laboratory findings at readmission (reference range)				
Leukocyte count (4–11 × 10^9 cells/L)	NA	12.5	NA	NA
AST (15–37 U/L)	NA	705	NA	NA
ALT (16–61 U/L)	NA	500	NA	NA
Imaging findings at readmission	NA	Chest radiograph: negative for consolidation. CT abdomen and pelvis without contrast: enlarged, edematous prostate, consistent with prostatitis	NA	NA
Readmission outcome	NA	Discharged	NA	NA
Readmission discharge or death date	NA	2024 Nov 15	NA	NA
International travel history (year)	NA	Bahamas (2022)	Unknown	South Korea (1950s), Vietnam (1960s)
United States military service history	NA	None	World War II	World War II, Korean War, Vietnam War

*ALT, alanine aminotransferase; AST, aspartate transferase; CT, computed tomography; IV, intravenous; NA, not applicable.
†Hurricane category according to the Saffir-Simpson Hurricane Wind Scale (*10*).

he performed high-pressure hosing. He became ill on September 29 and was hospitalized October 1 for fever, chills, weakness, confusion, and body aches. Chest imaging revealed pneumonia. Results of abdominal and pelvic imaging were unremarkable. Healthcare providers diagnosed severe sepsis without septic shock. After presumptive positive blood cultures, treatment with 30 days of intravenous ceftazidime and oral doxycycline began on October 9, and then 3 months of oral doxycycline (*11*) was initiated. The patient was discharged October 10.

Patient 2 was readmitted on November 9 for fatigue, malaise, weakness, and shortness of breath. Abdominal and pelvic imaging suggested prostatitis. The patient received 6 weeks of intravenous meropenem and oral doxycycline beginning November 15 and then 3 months of oral doxycycline. Blood and urine cultures were positive for *B. pseudomallei*. Repeat blood cultures had no growth by November 12. The patient was discharged on November 15 and was lost to follow-up.

We confirmed the patient isolates as *B. pseudomallei* by using the Centers for Disease Control and Prevention's (CDC) Laboratory Response Network algorithm. We extracted isolate DNA for whole-genome sequencing (WGS) as previously described (*6*). Multilocus sequence typing (ST) indicated all isolates were ST41, which is associated with strains of Eastern Hemisphere origin. Phylogenetic analysis indicated the new patient-derived genomes grouped with strains from East and Southeast Asia (Figure 1) (*6*).

We conducted WGS on 7 *B. pseudomallei* isolates from CDC's multidecade surveillance archive on the basis of ST or geographic proximity to the 2024 cases for higher resolution analysis (*6*). Five isolates were ST41 and clustered with the 2024 patient-derived genomes (*12*,*13*). Two isolates were from 1 person who traveled to Vietnam, 2 were from 2 retired US military members, and data were limited for 1 (Figure 2). The bacterial genomes from the 2024 patients were highly related to each other and to the 2 from the retired US military members (<20 single-nucleotide polymorphisms apart across all genomes). One publicly available ST41 genome related to this cluster was from a patient who traveled to Vietnam.

We requested medical and military service records from the National Archives and Records Administration for the 2 retired service members, who died from melioidosis in 1989 and 1983. At the time of their deaths, both lived in the same county in Georgia as the 2024 patients. Records were incomplete for patient 3, who died in October 1989. He was a US Army and Air Force Veteran who served in World War II and had no records of service in Vietnam. He was hospitalized at a Veterans Affairs facility in Georgia before his death. Patient 4, who died in October 1983, was a US Navy and Army veteran who served in World War II, the Korean War, and the Vietnam War. For 20 years, he worked on a military base located <1 mile from the

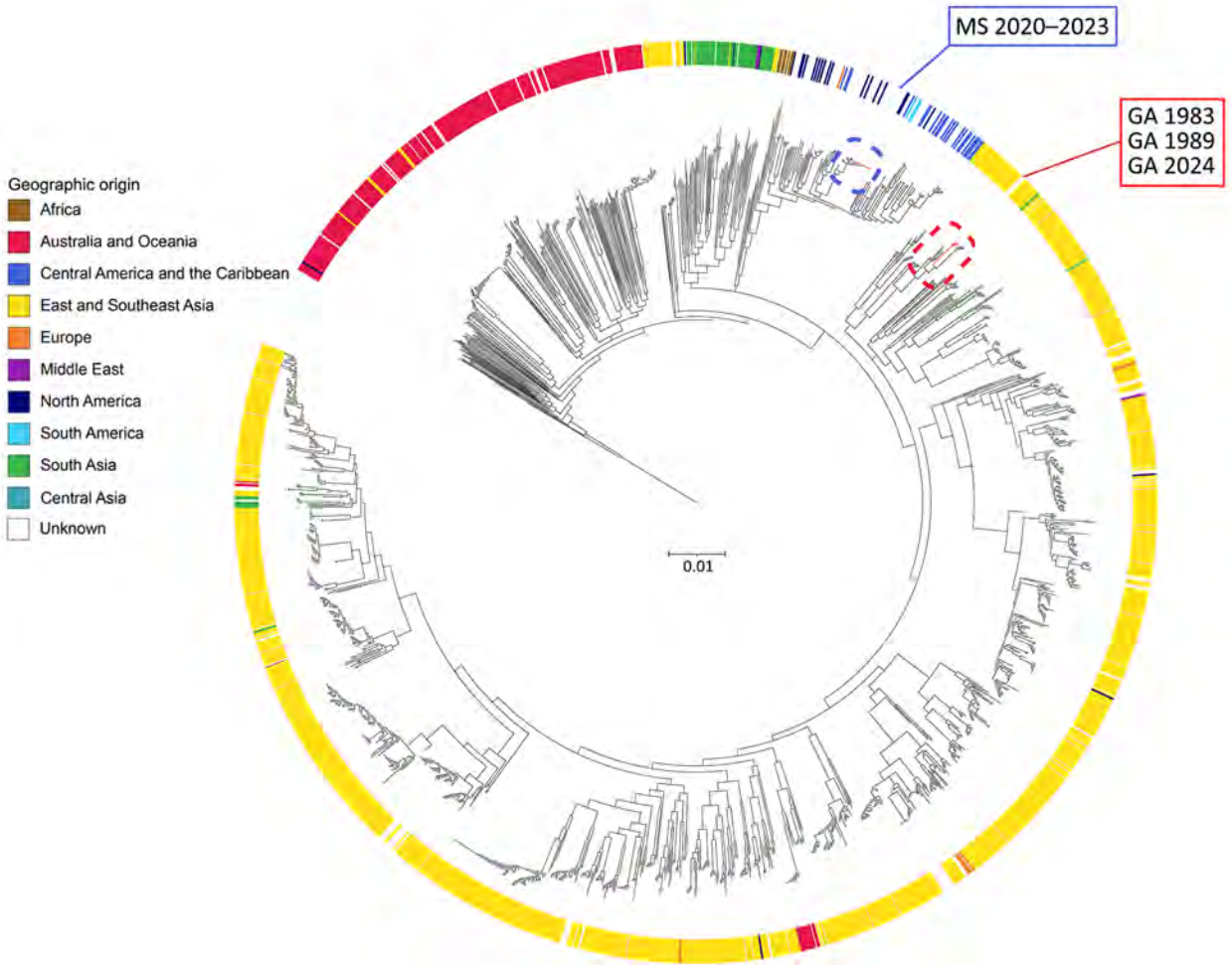

Figure 1. Global maximum-likelihood phylogenetic tree of core-genome single-nucleotide polymorphisms comparing new isolate genomes from 4 related melioidosis cases with unknown exposure source, Georgia, USA, 1983–2024 (red rectangle), with all *B. pseudomallei* genomes from the Center for Disease Control and Prevention's internal and National Center for Biotechnology Information's worldwide RefSeq databases as of August 6, 2024 (n = 1,976 genomes). Strain MSHR668 was used as an outgroup. New isolate genomes are distinct from *B. pseudomallei* genomes isolated from the environment in Mississippi (blue rectangle). Isolates with a reported geographic origin are associated with their country of origin and rings are colored according to definitions listed in The World Factbook (https://www.cia.gov/the-world-factbook). Scale bar units represent substitutions per site from a 22% core alignment against *B. pseudomallei* strain 110 (7.78 Mbp size, RefSeq accession no. GCF_001905265.1).

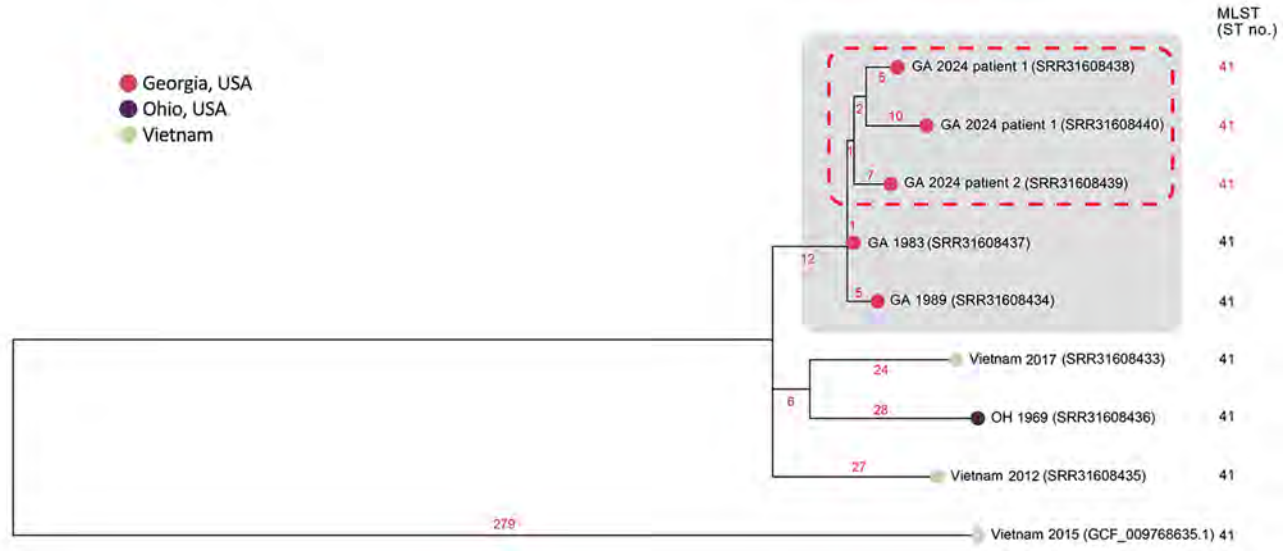

Figure 2. Subpanel maximum-likelihood phylogeny of refined mutation-only core single-nucleotide polymorphism sites of isolate genomes from 4 related melioidosis cases with unknown exposure source, Georgia, USA, 1983–2024, which includes the clinical isolates from the 2 patients from Georgia in 2024 (red dashed rectangle). *B. pseudomallei* genome sequences from the patient isolates were highly related to each other and to 2 other patients from Georgia in 1983 and 1989 (gray rectangle). Those genomes clustered most closely with genomes from Southeast Asia, particularly from Vietnam. Tree leaves contain year of isolation and National Center for Biotechnology Information sequence read archive and RefSeq accession numbers that correspond to each isolate. Branch numbers indicate the number of single nucleotide polymorphisms per site. MLST, multilocus sequence type; ST, sequence type.

shared worksite of the 2024 patients. Records indicate patient 3 retired 36 years before his death and patient 4 retired 12 years before his death. Weather records indicate no hurricanes affected the area in 1983. In September 1989, Hurricane Hugo made landfall in the United States as a Category 4 storm and affected this area of Georgia with 3–5 inches of rain.

Conclusions

This investigation identified 4 presumptive autochthonous human melioidosis cases in Georgia, USA. Without leveraging historical surveillance isolates archived at CDC, we would have concluded the 2024 cases represented a potential new local or imported exposure. However, the relatedness of patient-derived isolates and the close geographic proximity of all 4 patients in Georgia are strongly suggestive of a shared, locally acquired environmental exposure, dating back to the 1980s. Only patient 4 was known to have traveled to Southeast Asia in his lifetime. Although activation of *B. pseudomallei* from latency 2 decades after exposure during the Vietnam War is plausible, it is rare (*14*). Further, retrospective review of available medical records from patients 3 and 4 revealed no earlier illnesses or hospitalizations consistent with melioidosis, and reactivation would not explain the epidemiologic and WGS links to the other cases. Persistence of a single ST of *B. pseudomallei* in the environment over several decades has been reported (*15*). Introduction and persistence of *B. pseudomallei* in the environment from repatriation of personnel or equipment associated with the Vietnam War is possible, but other sources of environmental introduction or local exposure cannot be ruled out. Isolation of *B. pseudomallei* from the environment is needed to determine local endemicity and characterize the public health risk.

Trimethoprim/sulfamethoxazole (TMP/SMX) is the recommended first-line antimicrobial drug for *B. pseudomallei* infection; doxycycline is indicated with TMP/SMX intolerance. Relapses are more common with doxycycline compared with TMP/SMX (*11*).

All 4 patients from Georgia became ill or died in September and October. High wind speeds, rain, or flooding associated with hurricanes might have contributed to infections in 3 of the patients. Because hurricanes regularly affect the US (*10*), increased knowledge of melioidosis among healthcare providers is needed, particularly if patients have contact with floodwater, mud, or debris. Persons should wear waterproof clothing or boots, cover wounds if they cannot avoid floodwater, and follow local safety guidance during hurricanes.

Acknowledgments

We kindly thank the Georgia Department of Public Health district partners for their assistance during this investigation. We also thank Alan Lam, Tyler Sharp, and the National Archives and Records Administration for their expertise and collaboration.

Raw whole-genome sequence data generated for the 8 newly sequenced isolates are publicly available in the National Center for Biotechnology Information Sequence Read Archive (accession nos. SRR31608433–40).

About the Author

Ms. Brennan is the zoonotic disease epidemiologist at the Georgia Department of Public Health. She oversees surveillance of notifiable zoonotic diseases, including bioterrorism agents and rabies.

References

1. Meumann EM, Limmathurotsakul D, Dunachie SJ, Wiersinga WJ, Currie BJ. *Burkholderia pseudomallei* and melioidosis. Nat Rev Microbiol. 2024;22:155–69. https://doi.org/10.1038/s41579-023-00972-5
2. Currie BJ, Mayo M, Ward LM, Kaestli M, Meumann EM, Webb JR, et al. The Darwin Prospective Melioidosis Study: a 30-year prospective, observational investigation. Lancet Infect Dis. 2021;21:1737–46. https://doi.org/10.1016/S1473-3099(21)00022-0
3. Centers for Disease Control and Prevention. National diabetes statistics report 2024 [cited 2025 Jun 19]. https://www.cdc.gov/diabetes/php/data-research/index.html#cdc_report_pub_study_section_3-prevalence-of-diagnosed-diabetes
4. Petras JK, Elrod MG, Ty M, Adams P, Zahner D, Adams A, et al. Notes from the field: *Burkholderia pseudomallei* detected in a raccoon carcass linked to a multistate aromatherapy-associated melioidosis outbreak—Texas, 2022. MMWR Morb Mortal Wkly Rep. 2022;71:1597–8. https://doi.org/10.15585/mmwr.mm7150a5
5. Hall CM, Romero-Alvarez D, Martz M, Santana-Propper E, Versluis L, Jiménez L, et al. Low risk of acquiring melioidosis from the environment in the continental United States. PLoS One. 2022;17:e0270997. https://doi.org/10.1371/journal.pone.0270997
6. Petras JK, Elrod MG, Ty MC, Dawson P, O'Laughlin K, Gee JE, et al. Locally acquired melioidosis linked to environment—Mississippi, 2020–2023. N Engl J Med. 2023;389:2355–62. https://doi.org/10.1056/NEJMoa2306448
7. Limmathurotsakul D, Golding N, Dance DA, Messina JP, Pigott DM, Moyes CL, et al. Predicted global distribution of *Burkholderia pseudomallei* and burden of melioidosis. Nat Microbiol. 2016;1:15008. https://doi.org/10.1038/nmicrobiol.2015.8
8. Cheng AC, Jacups SP, Gal D, Mayo M, Currie BJ. Extreme weather events and environmental contamination are associated with case-clusters of melioidosis in the Northern Territory of Australia. Int J Epidemiol. 2006;35:323–9. https://doi.org/10.1093/ije/dyi271
9. Guendel I, Ekpo LL, Hinkle MK, Harrison CJ, Blaney DD, Gee JE, et al. Melioidosis after Hurricanes Irma and Maria, St. Thomas/St. John District, US Virgin Islands, October 2017. Emerg Infect Dis. 2019;25:1952–5. https://doi.org/10.3201/eid2510.180959
10. National Hurricane Center and Central Pacific Hurricane Center. Tropical cyclone climatology. [cited 2025 Feb 26]. https://www.nhc.noaa.gov/climo
11. Peacock SJ, Schweizer HP, Dance DA, Smith TL, Gee JE, Wuthiekanun V, et al. Management of accidental laboratory exposure to *Burkholderia pseudomallei* and *B. mallei*. Emerg Infect Dis. 2008;14:e2. https://doi.org/10.3201/eid1407.071501
12. Didelot X, Wilson DJ. ClonalFrameML: efficient inference of recombination in whole bacterial genomes. PLOS Comput Biol. 2015;11:e1004041. https://doi.org/10.1371/journal.pcbi.1004041
13. Treangen TJ, Ondov BD, Koren S, Phillippy AM. The Harvest suite for rapid core-genome alignment and visualization of thousands of intraspecific microbial genomes. Genome Biol. 2014;15:524. https://doi.org/10.1186/s13059-014-0524-x
14. Howes M, Currie BJ. Melioidosis and activation from latency: the "time bomb" has not occurred. Am J Trop Med Hyg. 2024;111:156–60. https://doi.org/10.4269/ajtmh.24-0007
15. Webb JR, Buller N, Rachlin A, Golledge C, Sarovich DS, Price EP, et al. A persisting nontropical focus of *Burkholderia pseudomallei* with limited genome evolution over five decades. mSystems. 2020;5:e00726–20. https://doi.org/10.1128/mSystems.00726-20

Address for correspondence: Julie Thompson, Centers for Disease Control and Prevention, 1600 Clifton Rd NE, Mailstop H17-2, Atlanta, GA 30329-4018, USA; email: bzb@cdc.gov

CYP2D6 Genotype and Primaquine Treatment in Patients with Malaria, Venezuela

César Pacheco, Adán Hernández-Acosta, Narviz Pulido, Yvanna Ceballos, Daniel Saavedra, Cruz Gómez, Nancy Moreno,[1] Flor Herrera[1]

We determined CYP2D6*4 and CYP2D6* genotypes and metabolizer phenotypes in 96 patients with suspected malaria in Venezuela and found intermediate or poor metabolizer phenotypes in ≈25% of cases. Nine of 44 malaria patients had *Plasmodium vivax* recurrence. Public health authorities should evaluate the benefits of increasing total doses of primaquine for treatment.

Malaria is prevalent in different tropical and subtropical regions, including those in Africa, Asia, and Latin America (*1*). In Latin America, Brazil, Colombia, and Venezuela account for 76.8% of all reported cases. Most (72.1% in 2023) cases in that region are attributed to *Plasmodium vivax* (*1*). Sucre State is a malaria-endemic region in Venezuela, where *P. vivax* is almost the only species (*2*). Treatment of *P. vivax* malaria involves a combination therapy of chloroquine and primaquine, a prodrug that requires metabolic activation to elicit its antimalarial effect against hypnozoites (*3*).

Activation of primaquine is catalyzed by the metabolic enzyme cytochrome P450 2D6 (CYP2D6), which belongs to the CYP450 superfamily, a group of enzymes responsible for metabolism of many commonly prescribed drugs (*4*). The *CYP2D6* gene is highly polymorphic and has >150 different alleles (*4*), encoding CYP2D6 isoforms with normal, decreased, increased, or no activity. In Venezuela, several CYP2D6 genotypes exhibiting the most prevalent null allele, *CYP2D6*4* (1846 G>A, rs3892097), and the less frequent *CYP2D6*6* allele (1707delT, rs5030655) have been documented (*5*,*6*). For instance, the *CYP2D6*4* allele was observed at a frequency of 14% in an urban admixed population from Aragua, a nonmalaria state, and in Amerindian populations at frequencies of 4.2%–42.5% from Zulia (nonmalaria state) and 1.7%–5.45% from Bolivar (malaria state). The *CYP2D6*6* allele was observed at frequencies ranging from 0.3% to 1.2% in 2 urban admixed populations (*5*,*6*).

Malaria patients' response to primaquine treatment is contingent on the level of CYP2D6 activity. In cases where CYP2D6 activity is low, probability of treatment failure is higher (*4*). Because CYP2D6 is necessary for primaquine metabolism, we determined the genotype of the most common *CYP2D6*4* variant and a less common *CYP2D6*6* variant with null activity and predicted the metabolizer phenotype in a sample of Mestizo persons with suspected *P. vivax* malaria from malaria-endemic Sucre state, Venezuela. We also evaluated the response to the standard treatment with primaquine.

The Study

We conducted this study by using a sample of 96 patients (60 men and 36 women) exhibiting malaria symptoms. The patients were unrelated to each other and >18 years of age. We recruited the patients in December 2022 from 4 health centers in the city of Cumaná, municipality of Sucre, Sucre state, Venezuela (Figure). We collected peripheral blood samples from

Author affiliations: Centro de Investigación y de Estudios Avanzados del Instituto Politécnico Nacional, Mexico City, Mexico (C. Pacheco); Instituto de Investigación en Ciencias de la Salud de la Secretaría de Marina, Polígono Naval de San Pablo Tepetlapa, Mexico City (A. Hernández-Acosta); Universidad de Carabobo, Sede Aragua, Facultad de Ciencias de la Salud, Instituto de Investigaciones Biomédicas "Dr. Francisco J. Triana Alonso," Estado Carabobo, Venezuela (N. Pulido, Y. Ceballos, D. Saavedra, N. Moreno, F. Herrera); FUNDASALUD Sucre, Dirección Estadal de Salud Ambiental, Sucre, Venezuela (C. Gómez)

DOI: https://doi.org/10.3201/eid3109.250316

[1]These authors were co–principal investigators.

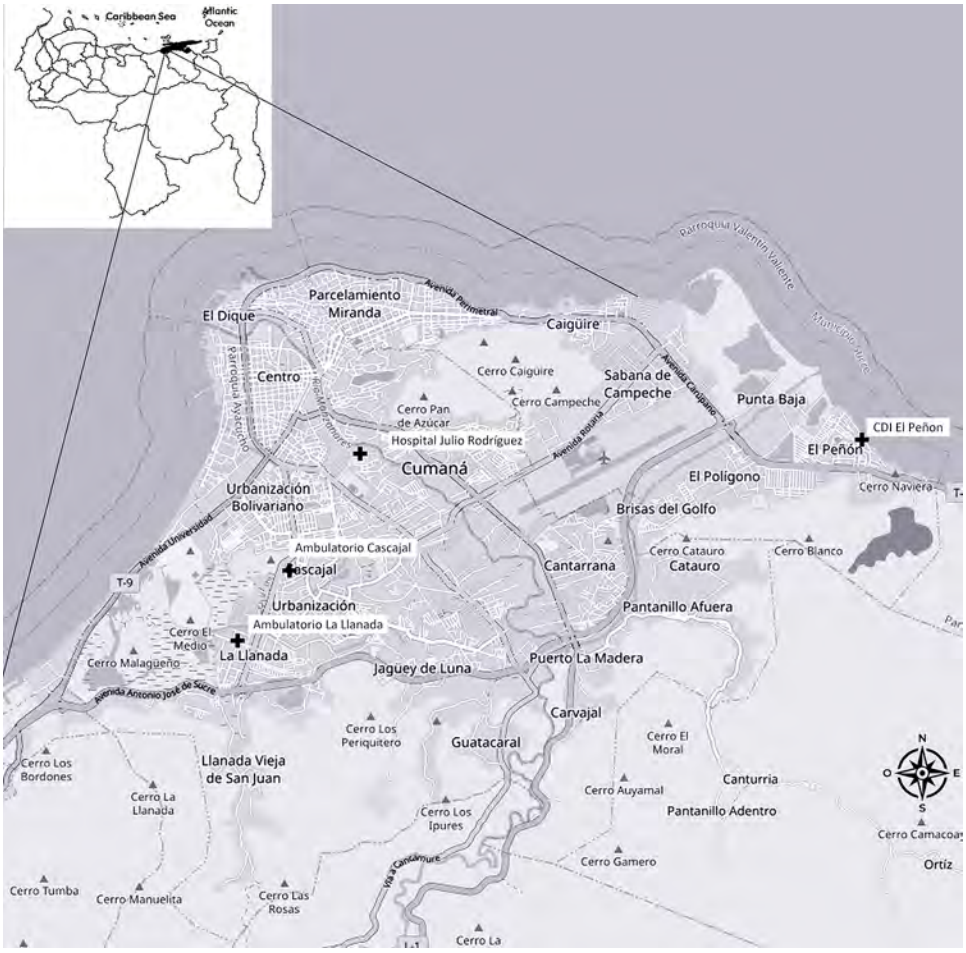

Figure. Geographic area of Sucre municipality from a study of CYP2D6 genotype and primaquine treatment in malaria, Venezuela. Crosses represent health center locations in the Sucre municipality. Inset shows map of Venezuela with Sucre state in black.

the patients after they provided informed consent as approved by the Instituto de Investigaciones Biomédicas, Universidad de Carabobo Bioethics Committee (approval no. CBIIB-UC/2022-2).

We performed microscopic malaria diagnosis and validated positive results by using PCR (*3*). We extracted genomic DNA as previously described (*7*) and conducted genotyping in accordance with previously outlined methods (*5*). If we observed no nucleotide change in the 2 allelic variants analyzed, we designated the allele as *CYP2D6*1*.

We predicted metabolizer phenotype by using the activity score (AS) system (*8*). In brief, we assigned values to the identified alleles ranging from 0 for no-function alleles (**4*, **6*) to 2 for normal-function alleles (**1*). The AS value of a given genotype is the sum of the assigned values for each allele. We designated patients with AS of 0 as poor metabolizers, AS of 1 as intermediate metabolizers, and AS of 2 as normal metabolizers (*8*,*9*).

Among 96 participants, 44 (45.83%) were malaria positive. As expected, *P. vivax* malaria was predominant; 43 (97.72%) of the 44 malaria-positive patients were infected with *P. vivax*, and 1 (2.27%) was infected with *P. falciparum*. Of the 44 malaria-positive patients, 30 (68.18%) were men and 14 (31.81%) were women, which we anticipated: men have a higher malaria risk than women because their occupations are more likely to involve outdoor work, like fishing. The patients received standard oral primaquine treatment (0.25 mg/kg/d for 14 days) (*3*). On day 28, we evaluated patients for malaria recurrence, which was characterized by fever and parasitemia (*10*).

We compared samples from the 52 malaria-negative participants and the 44 malaria-positive participants and found similar genotype profiles. CYP2D6*1*1 was the predominant genotype, which indicated a normal metabolizer phenotype. We saw a percentage of 75% in the 96 patients with the CYP2D6*1*1 genotype across both nonmalaria and malaria patients (Table). The other 25% of analyzed genotypes manifested as intermediate or poor metabolizer phenotypes, among which the CYP2D6*1*4 genotype

Table. Genotypes CYP2D6*4 and CYP2D6*6 and predicted phenotypes malaria and nonmalaria, Venezuela*

Genotype	Activity score	Predicted phenotype	Nonmalaria patients, no. (%), n = 52	Malaria patients, no. (%), n = 44
1*1	2	Normal metabolizer	39 (75)	33 (75)
1*4	1	Intermediate metabolizer	9 (17.31)	8 (18.19)
1*6	1	Intermediate metabolizer	2 (3.85)	1 (2.27)
4*4	0	Poor metabolizer	1 (1.92)	1 (2.27)
6*6	0	Poor metabolizer	0	1 (2.27)
6*4	0	Poor metabolizer	1 (1.92)	0

showed the highest frequency and had an average of 17.75% across both groups. That frequency is substantially higher than the low frequency (2.37%) of that genotype identified within the population identified in Madagascar (*11*). However, in 5 areas of Brazil, the CYP2D6*1*4 genotype exhibited a high frequency (35%–50%) (*12*). That variation can be attributed to the different ethnic origins of the genotype, which differ across regions. The ancestors of the population of Madagascar are believed to be from Asia and Africa, whereas the ancestors of the highly heterogeneous populations from Venezuela and Brazil are thought to be from Spain and Portugal. In addition, the CYP2D6*4 genotype frequency within the group from Europe is high (*13*). The metabolizer phenotype profile showed notable similarity across both groups; 75% of patients exhibited a normal metabolizer profile, 20.8% showed an intermediate metabolizer profile, and 4.19% displayed a poor metabolizer profile. Those values agree with values observed in ethnicity from Europe, thereby providing further substantiation for the initial assertion (*13*).

P. vivax recurrence was observed in 9 (20.5%) patients (6 men and 3 women); 7 exhibited an intermediate metabolizer phenotype, and 2 exhibited a poor metabolizer phenotype. That phenomenon might be attributed to a substantial correlation between the *CYP2D6* alleles with diminished activity, such as *CYP2D6*4* and *6, and the occurrence of primaquine therapeutic failure in patients infected with *P. vivax* (*4*). High rates of relapses have already been reported in Venezuela (*14*; J. Huber et al., unpub. data, https://www.medrxiv.org/content/medrxiv/early/2022/05/12/2022.04.19.22274042.full). The recurrence of *P. vivax* shown in this study might be preventable by administering a higher dose (7.0 mg/kg) of primaquine instead of the conventional dose (3.5 mg/kg) (*10*).

The first limitation of this study is the low number of patients; thus, our results might not be representative of all malaria-infected populations. Second, we only conducted patient monitoring on day 28 and thus only determined the clinical and parasitologic response and not the absence of *P. vivax* recurrence, which requires meticulous monitoring over a period of ≈6 months (*9*); thus, we might have missed recurrence that occurred after 28 days.

Conclusions

We estimated that ≈25% of malaria patients had nonfunctional alleles that would impair efficacy of primaquine. The corresponding predicted intermediate metabolizer phenotype was 20.8% and the poor metabolizer phenotype was 4.19% in a sample of malaria patients and nonmalaria patients susceptible to infection with *P. vivax* in Sucre, a malaria-endemic state of Venezuela. Those data are consistent with the 20.5% recurrence rate observed in *P. vivax* patients. To effectively treat malaria in the region, we recommend that public health authorities evaluate the potential benefits of increasing total doses of primaquine (7.0 mg/kg; 0.5 mg/kg/d) over a period of 14 days as an alternative to the current treatment regimen.

Acknowledgments

We thank all the patients who participated in the study; the staff of Ambulatorio La Llanada, Ambulatorio Cascajal, Hospital Julio Rodríguez, and Centro de Diagnóstico Integral El Peñón of the state of Sucre, Venezuela, who provided technical assistance to the authors in the collection of samples; and Juan Ernesto Ludert for support in performing some of the experiments in his laboratory at Centro de Investigación y de Estudios Avanzados del Instituto Politécnico Nacional. We used DeepL Write (https://www.deepl.com/es/write) to enhance the quality of the writing style.

This work was supported by Instituto de Investigaciones Biomédicas, Universidad de Carabobo Venezuela.

About the Author

Mr. Pacheco is a PhD student at Centro de Investigación y de Estudios Avanzados del Instituto Politécnico Nacional. His research focuses on tropical infectious diseases and facilitating appropriate control solutions for policy makers.

References

1. World Health Organization. World malaria report 2024 [cited 2025 Feb 8]. https://www.who.int/teams/global-malaria-programme/reports/world-malaria-report-2024

2. Wide A, Pabón R, De Abreu N, Bargues MD, Salcedo A, Capaldo J, et al. Prevalence of asymptomatic *Plasmodium vivax* infections in the north-eastern focus of malaria of Venezuela. Bol Mal Salud Amb. 2016;56:160–71.
3. Centers for Disease Control and Prevention. Malaria diagnosis (United States). Treatment of uncomplicated malaria 2024 [cited 2025 Feb 10]. https://www.cdc.gov/malaria/hcp/clinical-guidance/treatment-uncomplicated.html
4. Olvany JM, Williams SM, Zimmerman PA. Global perspectives on *CYP2D6* associations with primaquine metabolism and *Plasmodium vivax* radical cure. Front Pharmacol. 2022;13:752314. https://doi.org/10.3389/fphar.2022.752314
5. Flores-Angulo C, Villegas C, Mora Y, Martínez JA, Oropeza T, Moreno N. Allelic variants of the CYP2D6: *4, *6 and *10 in a sample of resident from the Aragua state, Venezuela [in Spanish]. Rev Peru Med Exp Salud Publica. 2015;32:746–51. https://doi.org/10.17843/rpmesp.2015.324.1767
6. Griman P, Moran Y, Valero G, Loreto M, Borjas L, Chiurillo MA. CYP2D6 gene variants in urban/admixed and Amerindian populations of Venezuela: pharmacogenetics and anthropological implications. Ann Hum Biol. 2012;39:137–42. https://doi.org/10.3109/03014460.2012.656703
7. Rivero J, Urdaneta L, Zoghbi N, Pernalete M, Rubio-Palis Y, Herrera F. Optimization of extraction procedure for mosquitos DNA suitable for PCR-based techniques. Int J Trop Insect Sci. 2004;24:266–9. https://doi.org/10.1079/IJT200430
8. Gaedigk A, Dinh JC, Jeong H, Prasad B, Leeder JS. Ten years' experience with the CYP2D6 activity score: a perspective on future investigations to improve clinical predictions for precision therapeutics. J Pers Med. 2018;8:15. https://doi.org/10.3390/jpm8020015
9. Nofziger C, Turner AJ, Sangkuhl K, Whirl-Carrillo M, Agúndez JAG, Black JL, et al. PharmVar GeneFocus: CYP2D6. Clin Pharmacol Ther. 2020;107:154–70. https://doi.org/10.1002/cpt.1643
10. Chamma-Siqueira NN, Negreiros SC, Ballard SB, Farias S, Silva SP, Chenet SM, et al. Higher-dose primaquine to prevent relapse of *Plasmodium vivax* malaria. N Engl J Med. 2022;386:1244–53. https://doi.org/10.1056/NEJMoa2104226
11. Mehlotra RK, Gaedigk A, Howes RE, Rakotomanga TA, Ratsimbasoa AC, Zimmerman PA. *CYP2D6* genetic variation and its implication for *vivax* malaria treatment in Madagascar. Front Pharmacol. 2021;12:654054. https://doi.org/10.3389/fphar.2021.654054
12. Salles PF, Perce-da-Silva DS, Rossi AD, Raposo LR, Ramirez Ramirez AD, Pereira Bastos OM, et al. *CYP*2D6 allele frequency in five malaria *vivax* endemic areas from Brazilian Amazon region. Front Pharmacol. 2021;12:542342. https://doi.org/10.3389/fphar.2021.542342
13. Kane M. CYP2D6 overview: allele and phenotype frequencies. In: Pratt VM, Scott SA, Pirmohamed M, Esquivel B, Kattman BL, Malheiro AJ, editors. Medical genetics summaries. Bethesda (MD): National Center for Biotechnology Information; 2012. p. 1–34.
14. Sojo-Milano M, Cáceres JL, Pizzo NN, Rojas J, Maldonado A, Rubio-Pulgar N, et al. Malaria recurrent *Plasmodium vivax*. Municipio Cajigal, Estado Sucre, Venezuela. Rev Biomed. 2008;19:3–15.

Address for correspondence: Flor Herrera, Universidad de Carabobo, Urb. San Pablo, Calle Hicelle, No 6, Turmero 2115, Venezuela; email: flormhq@gmail.com

Gastric Submucosal Tumor in Patient Infected with *Dioctophyme renale* Roundworm, South Korea, 2024

Dong-Min Kim,[1] Youngdae Kim, Jung In Lee, Jun-Won Seo, Da Young Kim, Na Ra Yun, Beomgi Lee, You Mi Lee, Choon-Mee Kim,[1] Sung-Chul Lim

We describe a case of a gastric submucosal tumor in a patient in South Korea infected with *Dioctophyme renale* roundworm. The patient had a history of consuming raw freshwater fish. Molecular and morphologic analyses confirmed *D. renale* Infection. Genetic testing should be used to diagnose rare parasitic infections with unusual clinical manifestations.

The giant kidney worm (*Dioctophyme renale*) is the largest parasitic roundworm and infects the kidneys of carnivorous mammals such as mink (family Mustelidae) (*1*). *D. renale* roundworms are found worldwide except in Africa. Female worms reach up to 103 cm long, and male worms reach up to 45 cm long (*2*). At least 49 mammal species, including humans, have been identified as definitive hosts of *D. renale* roundworms (*2*). Humans typically acquire *D. renale* infection from consuming raw or undercooked freshwater fish or frogs.

Mustelid mammals are the most common definitive hosts of *D. renale* roundworms, although infection may occur in other carnivorous mammals, including canids, raccoons, and otters. Adult male and female worms reside and sexually reproduce in the kidneys of the host. The eggs are excreted in the urine and, once reaching a freshwater environment, develop into first-stage larvae within ≈1 month. Those larvae are ingested by oligochaete worms (phylum Annelida), the intermediate hosts, in which they develop to infective third-stage (L3) larvae. Paratenic hosts, such as fish, frogs, and toads, become infected by consuming the oligochaetes, which harbor encysted L3 larvae. When a carnivorous mammal consumes an infected paratenic host, L3 larvae migrate from the gastric wall to the liver and preferentially infect the right kidney, where they mature into adult worms and complete their life cycle (*3*). We report *D. renale* roundworm infection in a woman in South Korea who had a gastric submucosal tumor.

The Study

A 53-year-old woman sought care for epigastric pain that worsened on an empty stomach and improved with eating. She had no notable medical history. Two weeks before admission, she had consumed raw smelt (*Hypomesus olidus*) and far-eastern catfish (*Silurus asotus*) stews. A gastroendoscopy 4 days before admission revealed a 2-cm mass in the stomach, prompting referral to the Department of Gastroenterology at Chosun University Hospital (Gwangju, South Korea).

Examination showed a 3 × 2 cm protruding mass in the stomach, accompanied by cheese-like exudates and edematous changes in the posterior wall of the proximal gastric antrum (Figure 1). Endoscopic ultrasound showed diffuse thickening (3.2 × 1.2 cm) and disruption of the submucosal layer (Appendix Figure 1, https://wwwnc.cdc.gov/EID/article/31/8/24-1944-App1.pdf). A biopsy showed a 1.8-cm roundworm, initially suspected to be a transmural malignancy (Appendix Figure 2). We then referred the patient to an infectious disease clinic. The worm was successfully removed during endoscopic biopsy, and follow-up revealed no additional symptoms.

Laboratory results showed a leukocyte count of 5,060 cells/mm^3 (reference range 4,000–10,800 cells/

Author affiliation: Chosun University College of Medicine, Gwangju, South Korea

DOI: https://doi.org/10.3201/eid3109.241944

[1]These authors contributed equally to this study.

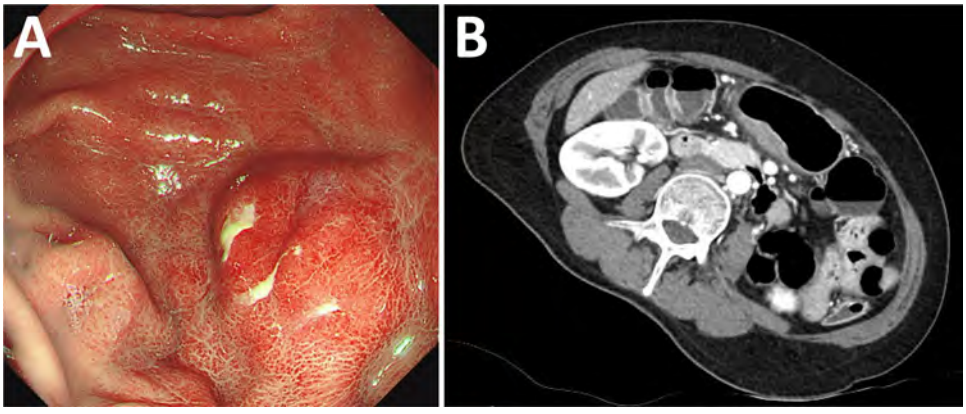

Figure 1. Gastric submucosal tumor in patient infected with *Dioctophyme renale* roundworm, South Korea, 2024. A) Gastroscopy showed a protruding mass-like lesion measuring 3 × 2 cm on the posterior gastric wall. B) Abdominal computed tomography showed enhanced wall thickening and a central low-attenuation area at the greater curvature of the gastric antrum.

mm³), eosinophil count of 230 cells/mm³ (reference range 0–500 cells/mm³), hemoglobin level of 13.2 g/dL (reference range 13–17 g/dL), and total IgE level of 52.5 IU/mL (reference range 0–358 IU/mL). ELISA revealed IgG titers of 0.328 for *Paragonimus westermani* (lung fluke) and 0.417 for *Clonorchis sinensis* (Chinese liver fluke). Results of a routine fecal examination was negative for parasites. The cross-section of the dark red roundworm showed an absence of surface spines and the presence of long polymyarian musculature and multilayered cuboidal intestinal cells with large nuclei (Figure 2).

We performed PCR by using primers designed against reference sequences of the roundworm (Appendix Table). The initial differential diagnoses included *Anisakis* spp., *Gnathostoma* spp., and *D. renale* roundworms on the basis of the patient's history and clinical manifestations. We ruled out *Anisakis* spp. infection on the basis of negative PCR results targeting the cyclooxygenase-2 gene (*4*). Next, we considered *Gnathostoma* spp. Infection but ruled it out because small subunit rRNA gene sequencing showed 100% (974/974 bp) homology with *D. renale* (GenBank accession nos. OR501903, OQ933019, and OQ918640), whereas sequence identity with *G. spinigerum* (GenBank accession no. MT879607) was only 79.05% (717/907 bp). Additional nested PCR confirmed 100% (561/561 bp) homology with *D. renale*, further excluding *Gnathostoma* (83.83% identity [337/402 bp]) with *G. spinigerum* (GenBank accession no. MT879607). We deposited the confirmed sequences in GenBank (accession nos. PP981196 and PV168478).

To confirm the diagnosis, we performed cyclooxygenase 1 gene-specific PCR, which yielded negative results for both *D. renale* and *G. spinigerum*. However, nested PCR targeting the dorylipophorin gene showed 82.59% (503/609 bp) homology with *D. renale* (GenBank accession no. MW014827.1). Phylogenetic analysis of the small subunit rRNA gene clustered the sample with *D. renale*, supporting the final diagnosis of *D. renale* infection (Figure 3). For the dorylipophorin gene, only 1 registered sequence was available in GenBank; therefore, constructing a phylogenetic tree was not possible.

Patent infections by *D. renale* roundworms in humans are rare; the infections more often manifest as larval migrans with L3 larvae (*5*). The larvae mature into adults ≈6 months after ingestion. Although humans are definitive hosts for kidney infections, the

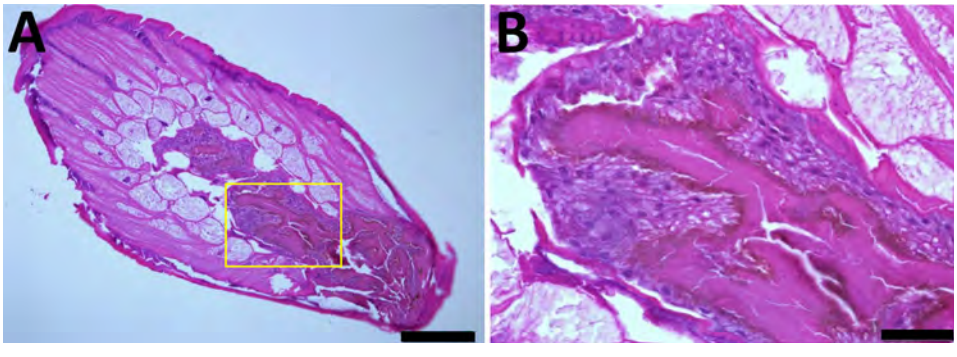

Figure 2. *Dioctophym renale* larva stained with hematoxylin and eosin in a study of gastric submucosal tumor in patient infected with *D. renale* roundworm, South Korea, 2024. A) Cross-section displays long subcuticular polymyarian musculature and characteristic intestines. Spines were not observed on the surface of the body. The intestinal epithelium consists of multilayered cuboidal cells with relatively large nuclei. Numerous dark brown granules (hematoxylin and eosin stain) are visible along the luminal border and are covered with microvilli. Scale bar indicates 200 μm. B) Higher magnification of the specimen shown in panel A (yellow box), providing a closer view of the characteristic intestine. These images suggested the presence of *D. renale* L3 larva. Scale bar indicates 2050 μm.

larvae often erratically migrate. The larvae are found in the liver, abdominal cavity, and retroperitoneal space and as subcutaneous nodules (*6*). One study reviewed 37 global human *D. renale* cases and found 32 in the kidneys and 5 within the thigh, abdominal wall, and chest wall (*7*). The main clinical manifestations of human dioctophymiasis were loin pain (59.5%) and hematuria (59.5%) (*8*).

The long subcuticular polymyarian musculature, large boxy cells with prominent nuclei, and dark brown granules in the intestine distinguish *D. renale* from *Gnathostoma* spp. and *Anisakis* spp. roundworms (*8*). Ectopic migration of *D. renale* L3 larvae might lead to tumor-like masses in other organs, particularly in humans. In cases where roundworms manifest as gastric tumors, morphologic analysis and genetic confirmation are essential for accurate diagnosis.

Conclusions

We confirmed *D. renale* giant kidney worm infection in this patient through both molecular and

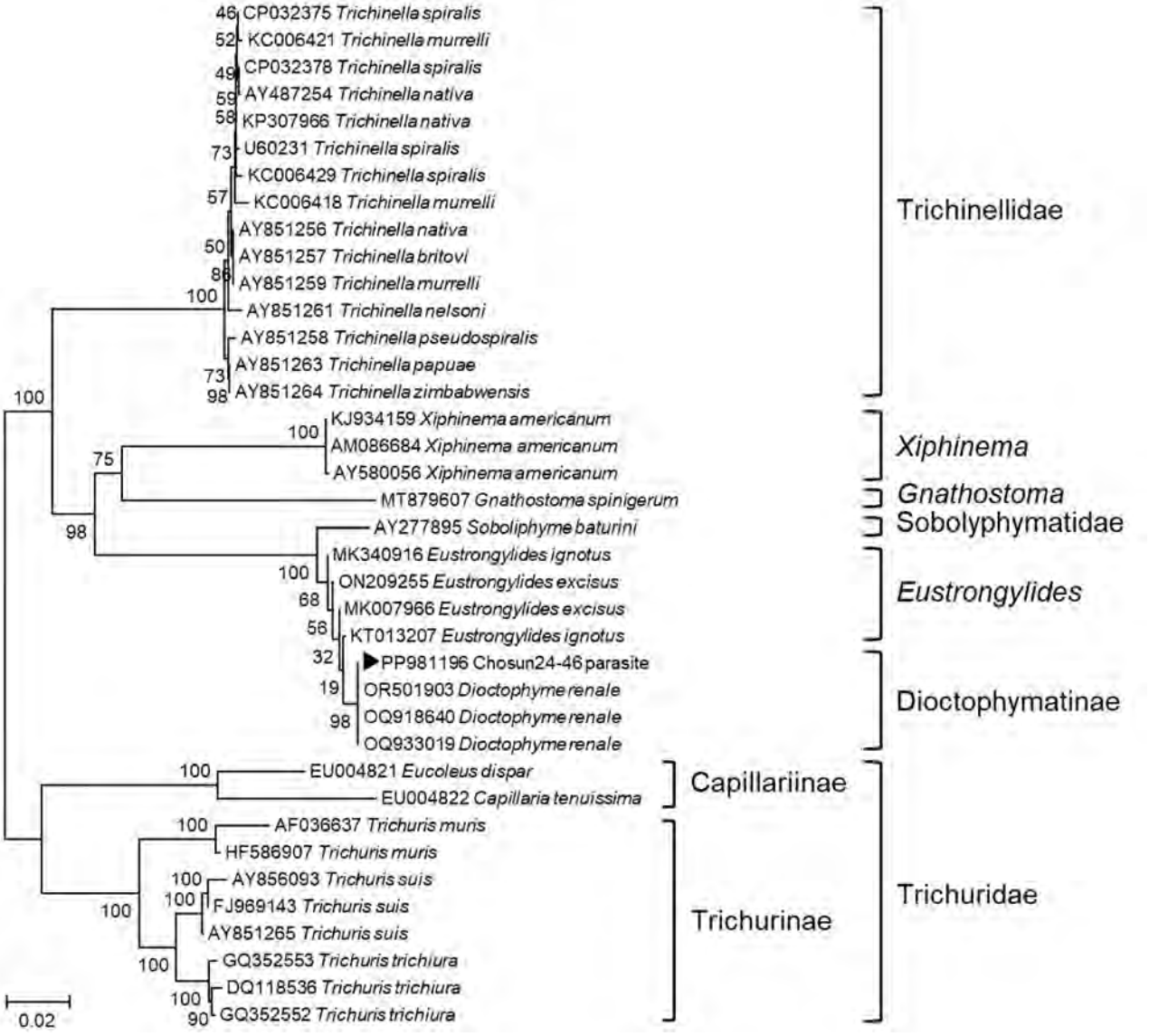

Figure 3. Phylogenetic tree for *Dioctophyme renale* roundworm showing a sequence from a patient with gastric submucosal tumor (black triangle), South Korea, 2024. Phylogenetic tree was based on the targeted 974-bp PCR amplicon sequence of *D. renale* from small subunit rRNA gene (18s RNA gene) sequences retrieved from GenBank (accession numbers shown). CLUSTAL X (http://www.clustal.org/clustal2) was used to construct phylogenetic tree by using neighbor-joining with 1,000 bootstrap replicates. We compared the *D. renale* sequence from our case with other roundworm sequences, and it aligned with 100% homology to *D. renale*. Scale bar indicates number of nucleotide substitutions per site.

morphological analyses. The patient likely contracted the infection by eating freshwater fish, specifically the far-eastern catfish (*S. asotus*) and smelt (*H. olidus*). Conversely, *Anisakis* spp. infection typically occurs in raw saltwater fish. A study in Brazil identified a 53.2% prevalence of *D. renale* L3 larvae in *Hoplosternum littorale*, a freshwater catfish (*9*). Therefore, *H. olidus* catfish may serve as an intermediate host of *D. renale* roundworms in Korea. Further research on intermediate hosts is necessary. Because *D. renale* roundworms are found worldwide, regionally investigating intermediate hosts is crucial.

A limitation of this study is that we initially considered the parasite to be *Anisakis* spp.; thus, we obtained microscopic images of the entire specimen and immediately cut it for PCR analysis, which left no specimens for systematic morphologic analyses. In addition, the 603-bp dorylipophorin gene product was only 82.59% homologous to the *D. renale* sequence in GenBank. Some PCRs, including those targeting the cyclooxygenase 1 and dorylipophorin genes, failed to produce amplicons, possibly because of low DNA quality or primer mismatch. Further studies are needed to improve PCR conditions and confirm suitable genetic targets for *D. renale*. These findings might raise awareness among clinicians that *D. renale* infection can mimic anisakiasis and that PCR for certain gene targets may fail, emphasizing the need for careful morphologic evaluation and consideration of rare parasites in differential diagnoses.

In conclusion, although parasitic infections in humans are rare, atypical clinical manifestations may lead to diagnostic confusion among clinicians. When encountering roundworms in the submucosa or extragastrointestinal lesions, especially in patients with a history of raw fish consumption, clinicians should consider genetic testing alongside morphologic diagnosis to rule out giant kidney worms, anisakiasis, or gnathostomiasis. Accurate diagnosis of rare parasitic infections through molecular methods can prevent misdiagnosis and guide appropriate treatment.

This study was supported by a research fund from the Chosun University Hospital in 2023.

About the Author

Dr. Kim is a physician in the Department of Infectious Diseases at Chosun University Hospital. His research focuses on diagnosis, treatment, and vaccine development for vectorborne and emerging infectious diseases.

References

1. Katafigiotis I, Fragkiadis E, Pournaras C, Nonni A, Stravodimos KG. A rare case of a 39-year-old male with a parasite called *Dioctophyma renale* mimicking renal cancer at the computed tomography of the right kidney. A case report. Parasitol Int. 2013;62:459–60. https://doi.org/10.1016/j.parint.2013.06.007
2. Eiras J, Zhu XQ, Yurlova N, Pedrassani D, Yoshikawa M, Nawa Y. *Dioctophyme renale* (Goeze, 1782) (Nematoda, Dioctophymidae) parasitic in mammals other than humans: a comprehensive review. Parasitol Int. 2021;81:102269. https://doi.org/10.1016/j.parint.2020.102269
3. Centers for Disease Control and Prevention. Dioctophymiasis [cited 2025 Jul 2]. https://www.cdc.gov/dpdx/dioctophymiasis/
4. Mattiucci S, Paoletti M, Colantoni A, Carbone A, Gaeta R, Proietti A, et al. Invasive anisakiasis by the parasite *Anisakis pegreffii* (Nematoda: Anisakidae): diagnosis by real-time PCR hydrolysis probe system and immunoblotting assay. BMC Infect Dis. 2017;17:530. https://doi.org/10.1186/s12879-017-2633-0
5. Tokiwa T, Ueda W, Takatsuka S, Okawa K, Onodera M, Ohta N, et al. The first genetically confirmed case of *Dioctophyme renale* (Nematoda: Dioctophymatida) in a patient with a subcutaneous nodule. Parasitol Int. 2014;63:143–7. https://doi.org/10.1016/j.parint.2013.09.015
6. Kuehn J, Lombardo L, Janda WM, Hollowell CM. Giant kidney worms in a patient with renal cell carcinoma. BMJ Case Rep. 2016;2016:bcr2015212118. https://doi.org/10.1136/bcr-2015-212118
7. Yang F, Zhang W, Gong B, Yao L, Liu A, Ling H. A human case of *Dioctophyma renale* (giant kidney worm) accompanied by renal cancer and a retrospective study of dioctophymiasis. Parasite. 2019;26:22. https://doi.org/10.1051/parasite/2019023
8. Tanaka T, Tokiwa T, Hasegawa H, Kadosaka T, Itoh M, Nagaoka F, et al. Morphologically and genetically diagnosed dermal *Dioctophyme* larva in a Chinese man: case report. SN Compr Clin Med. 2020;2:468–71. https://doi.org/10.1007/s42399-020-00256-6
9. Mascarenhas CS, Müller G, de Macedo MRP, Henzel ABD, Robaldo RB, Corrêa F. The role of freshwater fish in the life cycle of *Dioctophyme renale* in Southern Brazil. Vet Parasitol Reg Stud Reports. 2019;16:100274. https://doi.org/10.1016/j.vprsr.2019.100274

Address for correspondence: Sung-Chul Lim, Department of Pathology and Research Center for Resistant Cells, 588 Seosuk-dong, Dong-gu, Gwangju 501-717, South Korea; email: sclim@chosun.ac.kr

Rapidly Progressing Melioidosis Outbreak in City Center Zoo, Hong Kong, 2024

Christopher J. Brackman,[1] Ivan Tak-Fai Wong,[1] Allen S.L. Chan,[1] Patrick C.K. Pun, Dorothy Hong-Ting Cheung, Anne C.N. Tse, Carlton P.M. Yuen, Pierra Y.T. Law, Wing-Yin Tam, Franklin Wang-Ngai Chow, Gilman Kit-Hang Siu, Thomas Hon-Chung Sit

In October 2024, twelve primates from 4 species died of sepsis at the Hong Kong Zoological and Botanical Gardens. Postmortem examinations and microbiological analyses confirmed *Burkholderia pseudomallei* infection. Phylogenetic analysis revealed a clonal sequence type 46 strain with minimal variation, signifying a single source. This outbreak highlights melioidosis risk in zoo settings.

During October 2024, a series of sudden primate deaths occurred in the mammals section of the Hong Kong Zoological and Botanical Gardens (HKZBG), a popular city-center tourist attraction in Hong Kong, China, managed by the Leisure and Cultural Services Department. At the time of the outbreak, the facility housed 80 nonhuman primates (NHPs) across 12 species. We report the clinical course of illness and outcomes for the outbreak.

The Cases

On the morning of October 13, 2024, four monkeys at HKZBG were found dead in their enclosures: 1 cotton-top tamarin (*Saguinus oedipus*), 2 white-faced sakis (*Pithecia pithecia*), and 1 common squirrel monkey (*Saimiri sciureus*). Concurrently, another 2 cotton-top tamarins, 1 white-faced saki, and 1 De Brazza's monkey (*Cercopithecus neglectus*) with clinical signs of varying severity (e.g., lethargy, anorexia, fever) were sent to the zoo clinic for examination and emergency care; all 4 monkeys died later that day. Upon observed clinical signs, 1 additional white-faced saki and 1 De Brazza's monkey were isolated for intensive monitoring; the saki died on October 14 and the De Brazza's monkey on October 22. Another 2 common squirrel monkeys hospitalized on October 16 died on October 19 and October 20 (Table; Appendix Figure 1, https://wwwnc.cdc.gov/EID/article/31/9/25-0823-App1.pdf).

In total, 12 monkeys spanning 4 species eventually died in this outbreak. Species-specific mortality rates were high: 2 (50%) of 4 De Brazza's monkeys, 3 (75%) of 4 common squirrel monkeys, 3 (50%) of 6 cotton-top tamarins, and 4 (36.4%) of 11 white-faced saki died. Collectively, the deaths represented 15% of the zoo's NHP population and a 48% mortality rate among the 25 animals comprising the 4 species, underscoring the outbreak's severity.

To safeguard public and animal health, the mammals section of the zoo was temporarily closed starting on October 14. All enclosures were thoroughly cleaned and disinfected. The remaining animals in the section were clinically healthy. Health monitoring for staff who take care of animals was provided, and health conditions of staff were unremarkable.

A government working group conducted comprehensive follow-up actions, including postmortem examinations and diagnostic testing, to investigate the monkey deaths. On October 18, laboratory results confirmed that all tested monkeys had died from sepsis caused by *Burkholderia pseudomallei* infection. The HKZBG veterinarian performed postmortem examination and tissue sampling of the 8 monkeys that initially died on October 13. The remaining 4 monkeys were sent to the Tai Lung Veterinary Laboratory under the Agriculture, Fisheries and Conservation Department of the Government of the Hong

Author affiliations: Government of the Hong Kong Special Administrative Region, Hong Kong, China (C.J. Brackman, A.S.L. Chan, P.C.K. Pun, A.C.N. Tse, C.P.M Yuen, P.Y.T. Law, T.H.-C. Sit); Polytechnic University, Hong Kong (I.T.-F. Wong, D.H.-T. Cheung, W.-Y. Tam, F.W.-N. Chow, G.K.-H. Siu)

DOI: https://doi.org/10.3201/eid3109.250823

[1]These authors contributed equally to this article.

Table. Characteristics and laboratory findings for a rapidly progressing melioidosis outbreak in city center zoo, Hong Kong, 2024*

Case no.	Species	Age, y/sex	Onset of clinical signs	Date of death	*B. pseudomallei* isolated (source)
Case 01	White-faced saki	2/M	Found dead	2024 Oct 13	Yes (lung)
Case 02	Common squirrel monkey	18/M	Found dead	2024 Oct 13	Yes (liver, lung, spleen)
Case 03	White-faced saki	24/F	2024 Oct 12	2024 Oct 13	Yes (liver, kidney, lung, spleen)
Case 04	White-faced saki	31/F	2024 Oct 13	2024 Oct 13	Yes (liver, lung, spleen)
Case 05	Cotton-top tamarin	3/M	Found dead	2024 Oct 13	No
Case 06	Cotton-top tamarin	13/M	2024 Oct 13	2024 Oct 13	Yes (lung)
Case 07	De Brazza's monkey	11/M	2024 Oct 12	2024 Oct 13	Yes (liver, lung, spleen)
Case 08	Cotton-top tamarin	1/M	2024 Oct 13	2024 Oct 13	Yes (liver, kidney, lung, spleen)
Case 09	White-faced saki	1/F	2024 Oct 13	2024 Oct 14	Yes (lung)
Case 10	Common squirrel monkey	6/F	2024 Oct 15	2024 Oct 19	Yes (liver, lung, spleen, brain)
Case 11	Common squirrel monkey	10/F	2024 Oct 15	2024 Oct 20	Yes (spleen)
Case 12	De Brazza's monkey	13/F	2024 Oct 13	2024 Oct 22	Yes (liver, spleen)

*All animals had *Burkholderia pseudomallei* detected by real-time PCR in liver or spleen tissue.

Kong Special Administrative Region for postmortem examination, histopathology, and microbiological testing. Gross and histopathologic findings of all animals demonstrated that the liver and spleen were the most severely affected organs, characterized by acute necrotizing to necrosuppurative splenitis (Figure 1, panel A) and hepatitis (Figure 1, panel B); intralesional gram-negative bacilli were detected (Figure 1, panel C). Evidence of hematogenous spread to the lungs was also present in some monkeys, resulting in mild fibrinonecrotic interstitial pneumonia.

Bacterial cultures yielded 11 pure isolates, which were initially identified as *Burkholderia* spp. using a Biotyper matrix-assisted laser desorption/ionization time-of-flight mass spectrometry system (Bruker, https://www.bruker.com). Real-time PCR targeting a 115-bp fragment of the type III secretion system confirmed *B. pseudomallei* (*1*). Additional molecular screenings for monkeypox virus, coronavirus, SARS-CoV-2, *Leptospira* spp., and influenza A virus all produced negative results.

Initial investigations hypothesized an environmental source, including possible release from recent soil disturbances in early October. A comprehensive environmental assessment was conducted, including PCR and culture of 25 soil, 27 drinking water, 10 feed supplement, and 8 environmental samples. All samples tested negative for *B. pseudomallei* (Appendix).

B. pseudomallei was cultured from the liver, lungs, or spleen of 11 of the 12 dead animals. The isolates underwent whole-genome sequencing (Appendix), and a hybrid assembly approach using Hybracter version 0.11.0 (https://github.com/gbouras13/hybracter) generated high-quality, closed-gap complete genomes (*2*). Multilocus sequence typing (MLST) based on profiles from the PubMLST database (https://pubmlst.org) classified all isolates as sequence type (ST) 46 and core-genome MLST (cgMLST) type 1070 (*3*).

For phylogenetic context, we constructed a maximum-likelihood phylogeny comparing study isolates to 40 reference *B. pseudomallei* genomes representing ST46 and closely related sequence types from GenBank (*4*). The tree used single-nucleotide polymorphisms (SNPs) derived from 3,127 single-copy cgMLST genes (*5*) (Appendix). Results showed that the 11 Hong Kong isolates clustered together in a monophyletic clade with 100% bootstrap confidence (Appendix Figure 2), exhibiting exceptionally tight genetic relatedness of only 0–1 core-genome SNP (cgSNP) differences. In addition to core-genome phylogeny, whole-genome average nucleotide identity analysis further confirmed high genetic similarity (99.99839%–99.99954%) among the 11 isolates (Appendix Figure 3). Considering that *B. pseudomallei* can develop 8 SNPs during a 12-day acute infection period (*6*), the minimal SNP

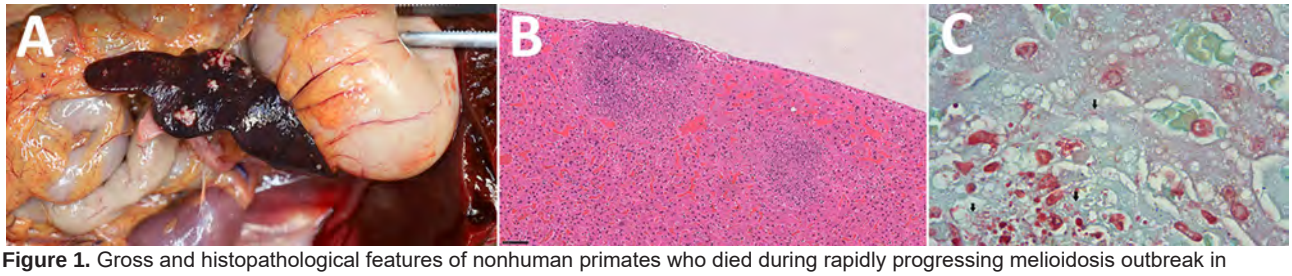

Figure 1. Gross and histopathological features of nonhuman primates who died during rapidly progressing melioidosis outbreak in city center zoo, Hong Kong, 2024. A) Gross pathology of splenic lesion in a white-faced saki (*Pithecia pithecia*). The spleen exhibits multifocal to coalescing necrosis. B) Necrotizing hepatitis of the liver in a cotton-top tamarin (*Saguinus oedipus*). Hematoxylin and eosin stain; original magnification ×200. C) Numerous gram-negative rods (black arrow) at the areas of necrosis in the liver of a cotton-top tamarin. Gram stain; original magnification ×1,000 with oil immersion objective.

variation among the HKZBG isolates suggests a single clonal infection source (*7*), likely from a singular introduction event rather than sustained transmission among the animals.

Focused comparative analysis of ST46 (Figure 2) revealed that the HKZBG clade was most closely related to a clonal cluster of 3 strains from northern Hainan Province, China, with a genetic distance of 18 cgSNPs. The next closest relatives were strains from Australia (27 cgSNP difference) and Thailand (31 cgSNP difference). Such minimal divergence underscores that ST46 is a recurring sequence type within the Asia–Oceania region. Although that ST is the third most frequently reported in the global PubMLST database and has been isolated from humans, the environment, and other animals, including monkeys (*8*,*9*), it had not been previously reported in Hong Kong. Moreover, the isolates from this outbreak are genetically distinct from the local outbreak strain ST1996 reported in 2022 (*10*) and from other local sequence types, such as ST70, ST37, and ST32 (*11*) (Figure 3). Among globally reported ST46 strains, the closest relatives to the HKZBG clade were strains isolated in 2002–2003 from northern Hainan Province, China (National Center for Biotechnology Information Assembly database accession nos. GCA_015312861.1, GCA_015312871.1, and GCA_015312851.1) (Figure 2). Those isolates share the same cgMLST type 1070 profile, suggesting that this lineage has been established in southern China for decades (*12*).

Conclusions

The rapid and nearly simultaneous deaths of multiple primates, together with the swift progression of the disease, suggest that this melioidosis outbreak was the result of a concentrated or highly virulent exposure event (*13*). Postmortem findings revealed extensive hepatic and splenic involvement in all animals. Although some animals exhibited pneumonia, pulmonary lesions were mild, and the pattern was characteristic of hematogenous spread to the lungs rather than bronchogenic. That finding is different from the lesions observed in NHP models after aerogenous infection (*14*,*15*).

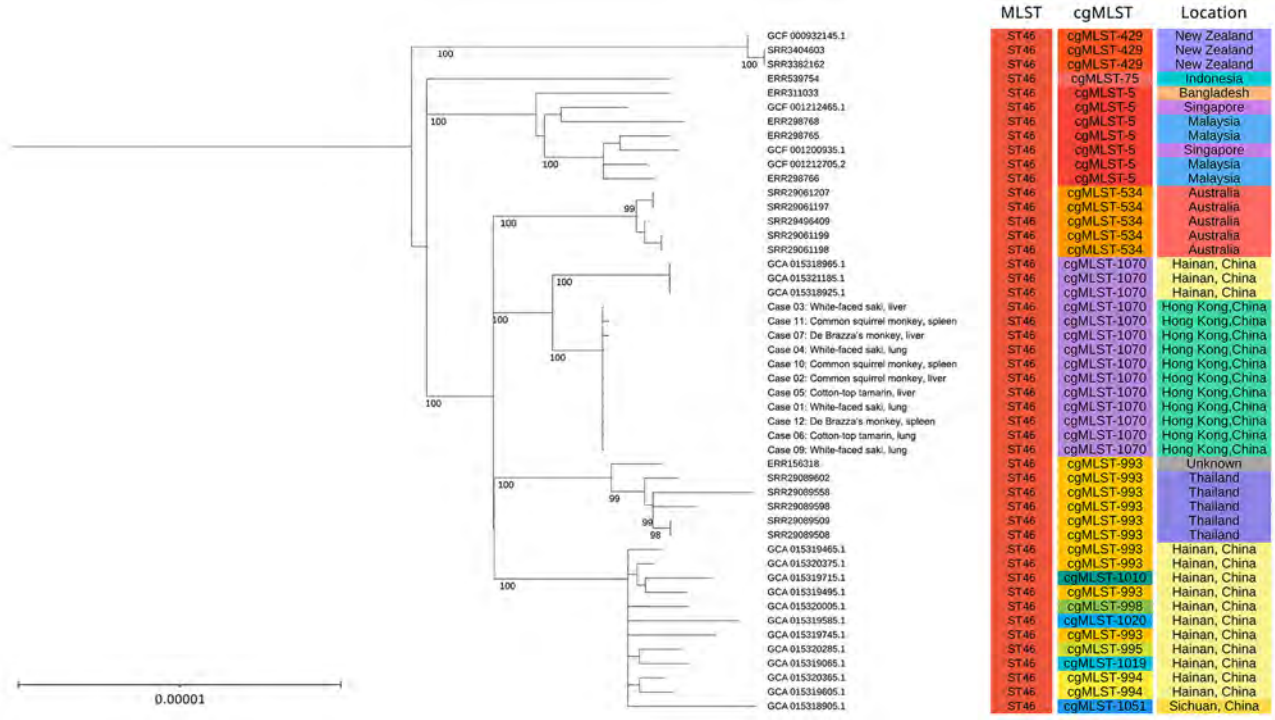

Figure 2. Phylogenetic analysis of *Burkholderia pseudomallei* ST46 genomes from nonhuman primates that died during rapidly progressing melioidosis outbreak in city center zoo, Hong Kong, 2024. Tree compares case nos. 01−11 with 40 reference genomes acquired globally from NCBI. Maximum-likelihood phylogenies of the single-nucleotide polymorphisms of the 3,127 single-copy cgMLSTs are shown. Bootstrap analysis of 1,000 replicates was performed, and bootstrap values of selected nodes are shown. The tree is midpoint rooted. The 11 monkey isolates formed a monophyletic clade with 100% bootstrap confidence. Distinct colors are used as a visual aid to group isolates by their MLST, cgMLST, and geographic location. Scale bar indicates nucleotide substitutions per site. cgMLST, core-genome MLST; MLST, multilocus sequence typing; ST, sequence type.

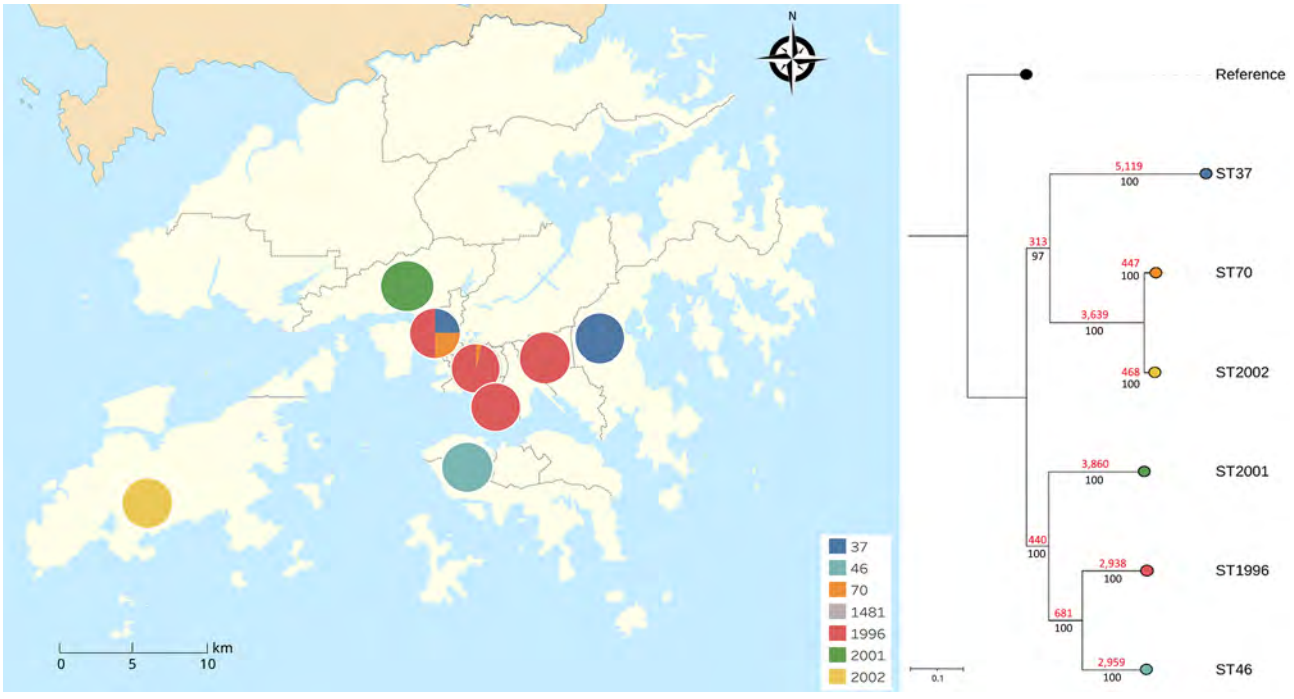

Figure 3. Spatial distribution and genetic relationships among *Burkholderia pseudomallei* STs reported in China and a rapidly progressing melioidosis outbreak in city center zoo, Hong Kong, 2024. Colored circles on map show locations where different STs were reported; sections indicate relative percentages of each ST in each location. Red numbers on the phylogenetic tree indicate core-genome single-nucleotide polymorphism differences between strains; black numbers represent bootstrap values. The tree is midpoint rooted. The reference genome used for comparison is a pseudogenome constructed by concatenating the first allele of each core-genome multilocus sequence typing gene available in the PubMLST database (https://pubmlst.org). Scale bar indicates nucleotide substitutions per site. ST, sequence type.

Despite extensive investigations, including environmental sampling and genomic analysis, the precise source of infection in this outbreak remains unidentified. The initial hypothesis that soil disturbances released environmental *B. pseudomallei* was not supported because of negative environmental results and because most affected monkeys had long-term residency at the zoo (many >6 years) with no history of melioidosis.

In reaction to this incident, the zoo implemented stringent biosecurity measures, including thorough enclosure disinfection and restricted access to affected areas. No further monkey deaths were recorded after October 22, and no cases of human melioidosis were noted during the investigation period.

This outbreak, which resulted in the loss of 12 monkeys, including critically endangered cotton-top tamarins, highlights the potential threat of melioidosis in zoologic settings. Climate change potentially could increase the incidence of *B. pseudomallei* infections, even in urban environments like Hong Kong, requiring enhanced biosecurity, vigilant health monitoring, and a high index of suspicion for melioidosis in cases of unusual illnesses and deaths in captive wildlife. Such proactive measures are critical for protecting both animal and human health.

Acknowledgments

We thank the staff of the Tai Lung Veterinary Laboratory for their technical expertise in isolating and identifying the clinical strains of *B. pseudomallei*. We are particularly indebted to the HKZBG team for their prompt implementation of stringent biosecurity measures following the initial primate mortality report and for their thorough investigation that contributed significantly to understanding the outbreak.

The whole-genome sequencing data generated for this study have been deposited in the National Center for Biotechnology Information Sequence Read Archive (BioProject accession no. PRJNA1271261; individual accession nos. SRR33822591–612).

About the Author

Dr. Brackman is a senior veterinary officer in the Agriculture, Fisheries and Conservation Department, Government of the Hong Kong Special Administrative Region, China. His research interests are focused on the field of One Health, in particular detection and characterization of zoonotic and transboundary diseases, including avian influenza and African swine fever, across wildlife and livestock.

References

1. Novak RT, Glass MB, Gee JE, Gal D, Mayo MJ, Currie BJ, et al. Development and evaluation of a real-time PCR assay targeting the type III secretion system of *Burkholderia pseudomallei*. J Clin Microbiol. 2006;44:85–90. https://doi.org/10.1128/JCM.44.1.85-90.2006
2. Bouras G, Houtak G, Wick RR, Mallawaarachchi V, Roach MJ, Papudeshi B, et al. Hybracter: enabling scalable, automated, complete and accurate bacterial genome assemblies. Microb Genom. 2024;10:001244. https://doi.org/10.1099/mgen.0.001244
3. Jolley KA, Bray JE, Maiden MCJ. Open-access bacterial population genomics: BIGSdb software, the PubMLST.org website and their applications. Wellcome Open Res. 2018;3:124. https://doi.org/10.12688/wellcomeopenres.14826.1
4. Fang Y, Hu Z, Chen H, Gu J, Hu H, Qu L, et al. Multilocus sequencing-based evolutionary analysis of 52 strains of *Burkholderia pseudomallei* in Hainan, China. Epidemiol Infect. 2018;147:e22. https://doi.org/10.1017/S0950268818002741
5. Nguyen LT, Schmidt HA, von Haeseler A, Minh BQ. IQ-TREE: a fast and effective stochastic algorithm for estimating maximum-likelihood phylogenies. Mol Biol Evol. 2015;32:268–74. https://doi.org/10.1093/molbev/msu300
6. Limmathurotsakul D, Holden MT, Coupland P, Price EP, Chantratita N, Wuthiekanun V, et al. Microevolution of *Burkholderia pseudomallei* during an acute infection. J Clin Microbiol. 2014;52:3418–21. https://doi.org/10.1128/JCM.01219-14
7. Meumann EM, Kaestli M, Mayo M, Ward L, Rachlin A, Webb JR, et al. Emergence of *Burkholderia pseudomallei* sequence type 562, northern Australia. Emerg Infect Dis. 2021;27:1057–67. https://doi.org/10.3201/eid2704.202716
8. Godoy D, Randle G, Simpson AJ, Aanensen DM, Pitt TL, Kinoshita R, et al. Multilocus sequence typing and evolutionary relationships among the causative agents of melioidosis and glanders, *Burkholderia pseudomallei* and *Burkholderia mallei*. J Clin Microbiol. 2003;41:2068–79. https://doi.org/10.1128/JCM.41.5.2068-2079.2003
9. Zhu X, Chen H, Li S, Wang LC, Wu DR, Wang XM, et al. Molecular characteristics of *Burkholderia pseudomallei* collected from humans in Hainan, China. Front Microbiol. 2020;11:778. https://doi.org/10.3389/fmicb.2020.00778
10. Wu WG, Shum MH, Wong IT, Lu KK, Lee LK, Leung JS, et al. Probable airborne transmission of *Burkholderia pseudomallei* causing an urban outbreak of melioidosis during typhoon season in Hong Kong, China. Emerg Microbes Infect. 2023;12:2204155. https://doi.org/10.1080/22221751.2023.2204155
11. Lui G, Tam A, Tso EYK, Wu AKL, Zee J, Choi KW, et al. Melioidosis in Hong Kong. Trop Med Infect Dis. 2018;3:91. https://doi.org/10.3390/tropicalmed3030091
12. Zheng H, Qin J, Chen H, Hu H, Zhang X, Yang C, et al. Genetic diversity and transmission patterns of *Burkholderia pseudomallei* on Hainan Island, China, revealed by a population genomics analysis. Microb Genom. 2021;7:000659. https://doi.org/10.1099/mgen.0.000659
13. Nelson M, Nunez A, Ngugi SA, Atkins TP. The lymphatic system as a potential mechanism of spread of melioidosis following ingestion of *Burkholderia pseudomallei*. PLoS Negl Trop Dis. 2021;15:e0009016. https://doi.org/10.1371/journal.pntd.0009016
14. Nelson M, Nunez A, Ngugi SA, Sinclair A, Atkins TP. Characterization of lesion formation in marmosets following inhalational challenge with different strains of *Burkholderia pseudomallei*. Int J Exp Pathol. 2015;96:414–26. https://doi.org/10.1111/iep.12161
15. Trevino SR, Dankmeyer JL, Fetterer DP, Klimko CP, Raymond JLW, Moreau AM, et al. Comparative virulence of three different strains of *Burkholderia pseudomallei* in an aerosol non-human primate model. PLoS Negl Trop Dis. 2021;15:e0009125. https://doi.org/10.1371/journal.pntd.0009125

Address for correspondence: Franklin Wang-Ngai Chow or Gilman Kit-Hang Sui, Hong Kong Polytechnic University, Health Technology and Informatics, Y928, 9/F, Block Y, Kowloon, Hong Kong 999077, China; email: franklin.chow@polyu.edu.hk or gilman.siu@polyu.edu.hk; Thomas Hon-Chung Sit, Agriculture, Fisheries and Conservation Department, Government of the Hong Kong Special Administrative Region, 5/F, Cheung Sha Wan Government Offices, 303 Cheung Sha Wan Rd, Kowloon, Hong Kong, China; email: thcsit@afcd.gov.hk

Genetic Characterization of *Orientia tsutsugamushi*, Bhutan, 2015

Tshokey Tshokey, John Stenos, Mythili Tadepalli, Chelsea Nguyen, Stephen R. Graves

We performed molecular characterization of *Orientia tsutsugamushi* on DNA sequences from 5 patients from Bhutan with scrub typhus. In the 56 kDa gene, all isolates aligned with those from other Asia countries, including Nepal, India, Thailand, and Taiwan. High serum IgM titers correlated with PCR positivity in acutely ill patients.

Orientia tsutsugamushi is an intracellular bacterium that causes an acute febrile illness called scrub typhus. It is transmitted through the bite of infected trombiculid larva mites (chiggers). Globally, scrub typhus is a huge public health burden, mainly in the Asian tropics; overall seroprevalence is ≈25% and is higher in male than female patients (*1*). The detection of scrub typhus in the Middle East and South America is evidence that scrub typhus may be endemic beyond the traditionally described tsutsugamushi triangle in the Asia Pacific region (*1*,*2*).

In Bhutan, scrub typhus is increasingly reported as a significant public health problem; estimated annual incidence is 62 cases/100,000 population (*3*). In 2015, ≈7% of hospitalized patients with acute febrile illnesses had scrub typhus, and a seroprevalence of ≈23% was reported in the general population (*4*). Although scrub typhus is a huge public health problem in Bhutan, data are limited to a few outbreak reports and seroepidemiologic studies with no information on genetic diversity of *O. tsutsugamushi*. This study describes the molecular characteristics of 5 *O. tsutsugamushi* sequences from Bhutan. The Bhutan Research Ethics Board of Health reviewed and approved the study. Patients provided written consent before participation.

Author affiliations: Jigme Dorji Wangchuck National Referral Hospital, Thimphu, Bhutan (T. Tshokey); Flinders University, Adelaide, South Australia, Australia (T. Tshokey); Australian Rickettsial Reference Laboratory, Geelong, Victoria, Australia (T. Tshokey, J. Stenos, M. Tadepalli, C. Nguyen, S.R. Graves)

DOI: https://doi.org/10.3201/eid3109.241763

The Study

We used 5 real-time quantitative PCR (qPCR) positive samples and their corresponding serology results for this study. In a previous study that used the same samples (*4*), blood samples were collected from a population of acute febrile patients visiting different hospitals in Bhutan and shipped to the Australian Rickettsial Reference Laboratory (ARRL) for analysis. The samples were tested for *O. tsutsugamushi*, the causal agent of scrub typhus, by qPCR and serology. For qPCR, DNA was extracted from the buffy coat sample by using a HiYield DNA Mini Kit (Real Genomics, http://www.real-biotech.com) and tested with the qPCR established in the ARRL and validated previously (*5*). Antibody testing (initial screening followed by end titration) used the microimmunofluorescence assay established and used as the routine protocol in the ARRL (*6*).

We amplified the *O. tsutsugamushi* samples that tested positive by qPCR with conventional 56 kDa PCR as described previously (*7*), with slight modification. Macrogen Inc. (Seoul, South Korea; https://dna.macrogen.com) sequenced the amplified DNA products (Figure). We submitted the 5 sequences to GenBank under accession numbers PQ206269, PQ206270, PQ206271, PQ206272, and PQ206273 for samples numbered Bhutan1, Bhutan3, Bhutan5, Bhutan6, and Bhutan7, respectively. In their corresponding antibody test by microimmunofluorescence assay, all 5 qPCR-positive samples had very high titers for *O. tsutsugamushi* IgM, IgG, or both, indicating acute illness (Table).

Conclusions

O. tsutsugamushi isolates from Bhutan appeared to be located in 2 main clusters in the phylogenetic tree (Figure) but are closely related. Samples Bhutan1, Bhutan3, Bhutan6, and Bhutan7 belonged to 1 cluster, and Bhutan 5 appeared to form a separate cluster. Bhutan1 was similar to an isolate *O. tsutsugamushi*

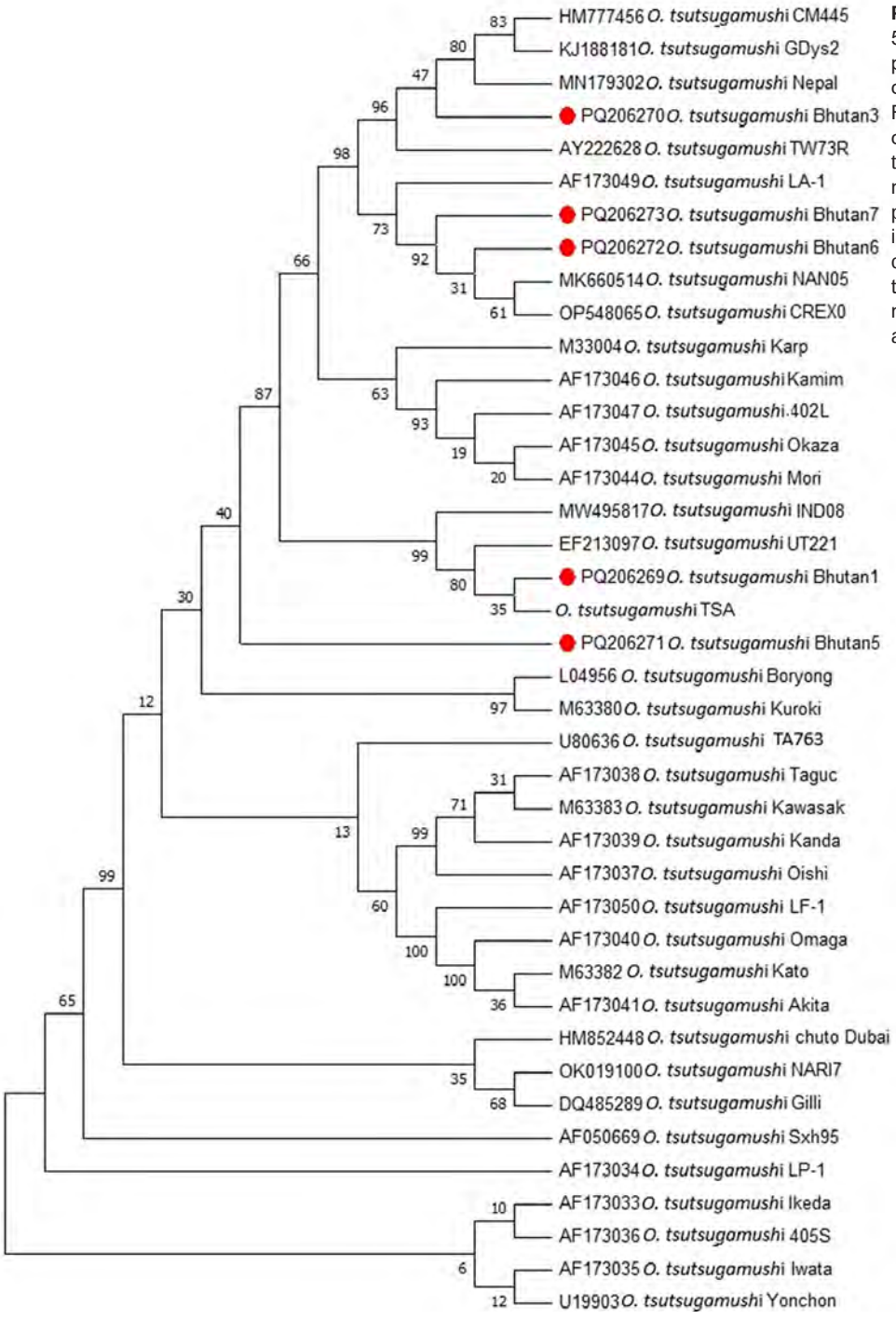

Figure. *Orientia tsutsugamushi* 56 kDa gene bootstrap consensus phylogenetic tree from genetic characterization study, Bhutan. Red dots indicate the 5 sequences characterized in this study. The tree was inferred using the neighbor-joining method. The percentages of replicate trees in which the associated taxa clustered together in the bootstrap test (1,000 replicates) are shown next to the branches. GenBank accession numbers are shown.

Table. Antibody test results of microimmunofluorescence assay screening and end titer for scrub typhus in study of *Orientia tsutsugamushi,* Bhutan, 2015*

Sample no.	Positive threshold	*Orientia tsutsugamushi* serotype test result						*Orientia chuto*	
		Gilliam		Karp		Kato			
		IgG	IgM	IgG	IgM	IgG	IgM	IgG	IgM
Bhutan1	≥1:128	1:256	1:2,048	<1:128	1:4,096	<1:128	1:4,096	<1:128	<1:128
Bhutan3	≥1:128	<1:128	1:2,048	<1:128	1:4,096	<1:128	1:4,096	<1:128	<1:128
Bhutan5	≥1:128	<1:128	1:1,024	<1:128	1:1,024	<1:128	1:1,024	<1:128	<1:128
Bhutan6	≥1:128	1:1,024	1:1,024	1:1024	1:1,024	1:1,024	1:1,024	<1:128	<1:128
Bhutan7	≥1:128	1:256	1:512	1:512	1:512	1:256	1:256	<1:128	<1:128

karp strain UT221 from northeastern Thailand (*8*). Isolates Bhutan6 and Bhutan7 were in the same phylogenetic tree as that of *O. tsutsugamushi* CREX0 found in the Maesot and Chiangrai areas of northwestern Thailand (*9*) and in China, Japan, and South Korea (*10*). Isolate Bhutan3 was at the same level as isolates from Nepal (*11*) and Taiwan (*12*) in the phylogenetic tree. Bhutan5, which appeared to be in a different cluster from the rest of the isolates, was related to isolates from the Gorakhpur area in Uttar Pradesh, India, which is geographically nearer to Nepal and the Himalayas (*13*). Overall, all 5 isolates from Bhutan align with the Asia cluster of *O. tsutsugamushi*, as expected. None of the samples was related to *O. chuto*, which, as of July 2025, had only been identified in the Middle East (*14*) and Africa (*15*). The high serum IgM titers in the 5 patients correlated well with their qPCR positivity. That finding suggests that in acute scrub typhus infection, serologic tests that detect IgM and qPCR might be useful tools for early diagnosis, which would prompt early initiation of appropriate treatment to prevent complications. We detected *O. tsutsugamushi* antibodies against Karp, Gilliam, and Kato serotypes but no *O. chuto* antibodies, indicating that *O. chuto* is not circulating in Bhutan at the time of this study.

The main limitation of this study was that 5 DNA samples were available for sequencing and only the 56 KDa gene was sequenced. That gene is the one most commonly used for phylogenetic analysis because it contains the most polymorphisms. Thus, this molecular report from Bhutan presents a preliminary genetic characterization of *O. tsutsugamushi*. Studies that include more samples and sequencing of additional gene targets will confirm characterizations.

In summary, we characterized 5 *O. tsutsugamushi* sequences from patients in Bhutan and found that they mostly align with isolates from other countries in Asia. Serologic testing for IgM and qPCR testing can provide early diagnosis of acute scrub typhus infection and timely initiation of treatment to prevent complications.

Acknowledgment

We thank the health workers in Bhutan who helped in sample collection, storage, and shipment. We also thank the patients who consented to provide their blood samples for the study.

About the Author

Dr. Tshokey is a clinical microbiologist in Bhutan, a researcher with the Australian Rickettsial Reference Laboratory, and a teaching specialist at Flinders University, South Australia. His primary research interests include infectious diseases, tropical medicine, antimicrobial resistance, public health, and medical education.

References

1. Dasgupta S, Asish PR, Rachel G, Bagepally BS, Chethrapilly Purushothaman GK. Global seroprevalence of scrub typhus: a systematic review and meta-analysis. Sci Rep. 2024;14:10895. https://doi.org/10.1038/s41598-024-61555-9
2. Weitzel T, Dittrich S, López J, Phuklia W, Martinez-Valdebenito C, Velásquez K, et al. Endemic scrub typhus in South America. N Engl J Med. 2016;375:954–61. https://doi.org/10.1056/NEJMoa1603657
3. Dorji K, Phuentshok Y, Zangpo T, Dorjee S, Dorjee C, Jolly P, et al. Clinical and epidemiological patterns of scrub typhus, an emerging disease in Bhutan. Trop Med Infect Dis. 2019;4:56. https://doi.org/10.3390/tropicalmed4020056
4. Tshokey T, Stenos J, Durrheim DN, Eastwood K, Nguyen C, Vincent G, et al. Rickettsial infections and Q fever amongst febrile patients in Bhutan. Trop Med Infect Dis. 2018;3:12. https://doi.org/10.3390/tropicalmed3010012
5. Stenos J, Graves S, Izzard L. Rickettsia. In: Schuller M, Sloots TP, James GS, Halliday CL, Carter IWJ, editors. PCR for clinical microbiology: an Australian and international perspective. Dordrecht (the Netherlands): Springer; 2010. p. 197–9.
6. Graves SR, Dwyer BW, McColl D, McDade JE. Flinders Island spotted fever: a newly recognised endemic focus of tick typhus in Bass Strait. Part 2. Serological investigations. Med J Aust. 1991;154:99–104. https://doi.org/10.5694/j.1326-5377.1991.tb120994.x
7. Unsworth NB, Stenos J, Faa AG, Graves SR. Three rickettsioses, Darnley Island, Australia. Emerg Infect Dis. 2007;13:1105–7. https://doi.org/10.3201/eid1307.050088
8. Paris DH, Aukkanit N, Jenjaroen K, Blacksell SD, Day NPJ. A highly sensitive quantitative real-time PCR assay based on the groEL gene of contemporary Thai strains of *Orientia tsutsugamushi*. Clin Microbiol Infect. 2009;15:488–95. https://doi.org/10.1111/j.1469-0691.2008.02671.x
9. Rungrojn A, Batty EM, Perrone C, Abdad MY, Wangrangsimakul T, Brummaier T, et al. Molecular diagnosis and genotyping of *Orientia tsutsugamushi* in Maesot and Chiangrai, Thailand. Front Trop Dis. 2023;4: 1146138. https://doi.org/10.3389/fitd.2023.1146138
10. Enatsu T, Urakami H, Tamura A. Phylogenetic analysis of *Orientia tsutsugamushi* strains based on the sequence homologies of 56-kDa type-specific antigen genes. FEMS Microbiol Lett. 1999;180:163–9. https://doi.org/10.1111/j.1574-6968.1999.tb08791.x
11. Gautam R, Parajuli K, Tadepalli M, Graves S, Stenos J, Sherchand JB. Scrub typhus and molecular characterization of *Orientia tsutsugamushi* from central Nepal. Pathogens. 2021;10:422. https://doi.org/10.3390/pathogens10040422
12. Qiang Y, Tamura A, Urakami H, Makisaka Y, Koyama S, Fukuhara M, et al. Phylogenetic characterization of *Orientia tsutsugamushi* isolated in Taiwan according to the sequence homologies of 56-kDa type-specific antigen genes. Microbiol Immunol. 2003;47:577–83. https://doi.org/10.1111/j.1348-0421.2003.tb03420.x
13. Nanaware N, Desai D, Banerjee A, Zaman K, Mittal M, Mittal M, et al. Genotypic characterization of *Orientia tsutsugamushi* isolated from acute encephalitis syndrome and acute febrile illness cases in the Gorakhpur Area,

Uttar Pradesh, India. Front Microbiol. 2022;13:910757. https://doi.org/10.3389/fmicb.2022.910757
14. Izzard L, Fuller A, Blacksell SD, Paris DH, Richards AL, Aukkanit N, et al. Isolation of a novel *Orientia* species (*O. chuto* sp. nov.) from a patient infected in Dubai. J Clin Microbiol. 2010;48:4404–9. https://doi.org/10.1128/JCM.01526-10
15. Masakhwe C, Linsuwanon P, Kimita G, Mutai B, Leepitakrat S, Yalwala S, et al. Identification and characterization of *Orientia chuto* in trombiculid chigger mites collected from wild rodents in Kenya. J Clin Microbiol. 2018;56:e01124-18. https://doi.org/10.1128/JCM.01124-18

Address for correspondence: Tshokey Tshokey, College of Medicine and Public Health, Flinders University, 24 Vivienne Ave, Mount Gambier, SA 5290, Australia; email: doc_tshokey@yahoo.com

Novel Henipavirus, Salt Gully Virus, Isolated from Pteropid Bats, Australia

Jennifer Barr, Sarah Caruso, Sarah J. Edwards, Shawn Todd, Ina Smith, Mary Tachedjian, Gary Crameri, Lin-Fa Wang, Glenn A. Marsh

We describe isolation and characterization of a novel henipavirus, designated Salt Gully virus, from the urine of pteropid bats in Australia. We noted the virus to be most closely related to Angavokely virus, not reliant on ephrin receptors for cell entry, and of unknown risk for human disease.

Bats of the genus *Pteropus* are natural reservoirs for zoonotic viruses, including the henipaviruses: enveloped, nonsegmented, negative-sense RNA viruses belonging to the family Paramyxoviridae (*1*). Hendra virus (HeV) and Nipah virus (NiV) represent the prototype henipaviruses and have caused fatal zoonotic spillover events from pteropid bats into animals and humans (*2*,*3*). High virulence, broad species tropism, and a lack of approved human vaccines and therapeutics classifies HeV and NiV as risk group 4 pathogens, restricting handling to Biosafety Level 4 (*4*).

Researchers first identified henipaviruses when an outbreak of HeV caused the death of 14 horses and 1 horse trainer in 1994 in Brisbane, Queensland, Australia (*2*). In total, 4 humans and >100 horses have died from HeV infection (*5*,*6*). In 2009, researchers isolated the first nonpathogenic henipavirus, Cedar virus (CedV), from pteropid bat urine collected during bat surveillance activities in Cedar Grove, Queensland, Australia (*7*).

Pteropid bats are the only natural reservoir identified within Australia for henipaviruses and, globally, detection of henipavirus relates most predominantly with pteropid bats. However, reports have noted an increasing number of novel henipa-like viruses detected in species of rodents, shrews, and opossums (*8*–*10*); such viruses have been classified by the International Committee on Taxonomy of Viruses in a new genus, *Parahenipavirus* (*11*).

We describe isolation and in vitro characterization of a novel pteropid bat–borne henipavirus in Australia. We obtained full-length sequences and assessed the virus's genetic relationship to other henipaviruses. We also compared the virus's growth, species tropism, and host cell receptor usage with HeV and CedV.

The Study

On July 11, 2011, we collected 30 pooled bat urine samples from a pteropid bat roost at Bicentennial Park, Boonah, Queensland, Australia, for an HeV surveillance project. We screened samples using quantitative real-time PCR for HeV. Ten samples were negative for HeV and inoculated onto Vero (African green monkey kidney) and primary *Pteropus alecto* kidney (PaKi) cell monolayers. We observed no viral cytopathic effects (CPE) after 7 days; however, the Vero tissue culture supernatant (TCSN) from 1 sample (BO13) tested positive when we employed generic reverse transcription PCR primers for paramyxovirus and henipavirus/morbillivirus (*12*). Sequencing of PCR products revealed a novel henipavirus sequence. Further passage of this virus in Vero cells yielded no CPE, and the virus did not replicate. However, when we inoculated TCSN from Vero cells onto PaKi cells, we observed replication and CPE. We then propagated a working stock in Vero cells, resulting in viral CPE demonstrating small syncytia, cell fusion, and rounded up cells (Appendix Figure, https://wwwnc.cdc.gov/EID/article/31/9/25-0470-App1.pdf). We designated the novel virus Salt Gully virus (SGV) based on the collection location.

Author affiliations: Commonwealth Scientific and Industrial Research Organisation, Health and Biosecurity, Geelong, Victoria, Australia (J. Barr, S. Caruso, S.J. Edwards, S. Todd, I. Smith, M. Tachedjian, G. Crameri, G.A. Marsh); Duke University-National University of Singapore Medical School, Singapore (L-F. Wang)

DOI: http://doi.org/10.3201/eid3109.250470

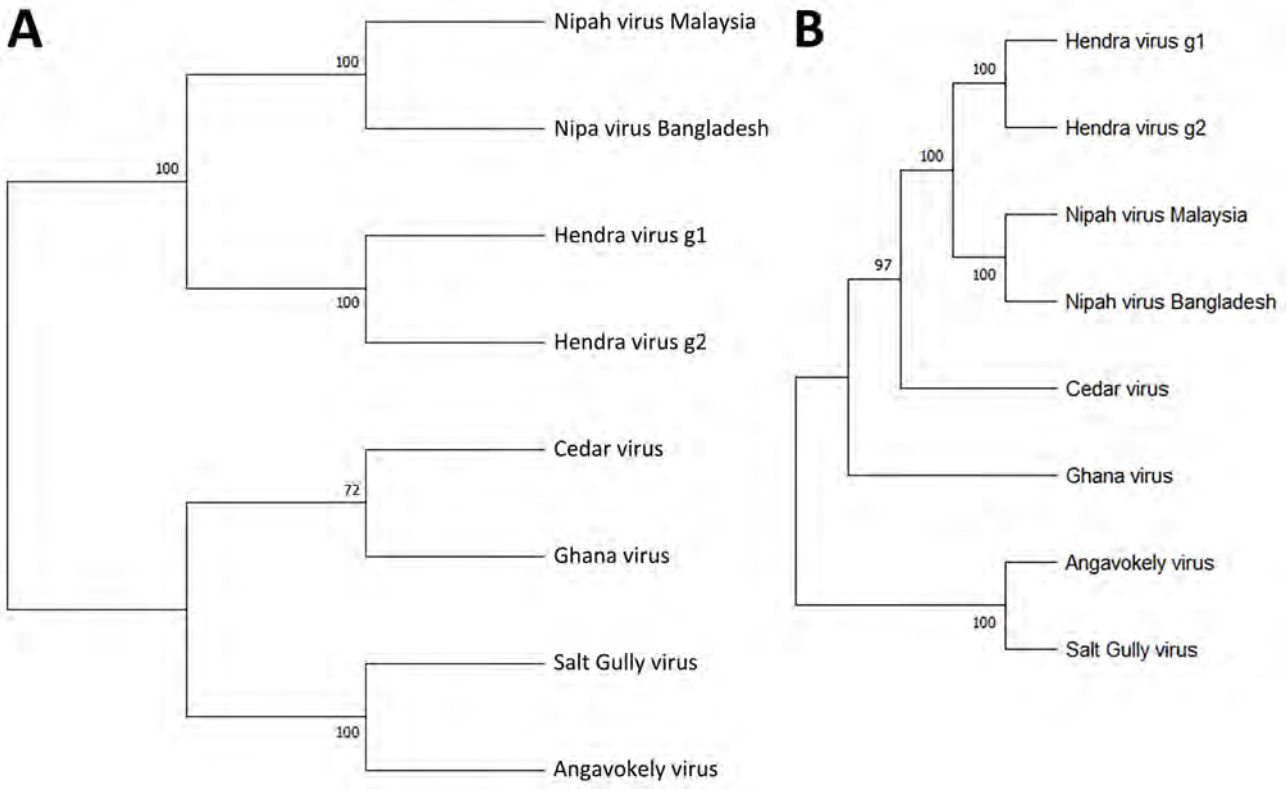

Figure 1. Phylogenetic analysis of members of the genus *Henipavirus* from a study investigating a novel henipavirus, Salt Gully virus, isolated from pteropid bats, Australia**.** A) We aligned complete L protein amino acid sequences by using ClustalW (https://www.genome.jp/tools-bin/clustalw) and inferred evolutionary history by using the maximum-likelihood method and the Jones-Taylor-Thornton matrix-based model. B) We aligned complete virus genome sequences by Muscle software and inferred evolutionary history by using the maximum-likelihood method and general time reversible plus gamma plus invariate sites model. Bootstrap support values (1,000 replicates) are shown next to each branching node. Evolutionary analyses were conducted in MEGA11 (https://www.megasoftware.net).

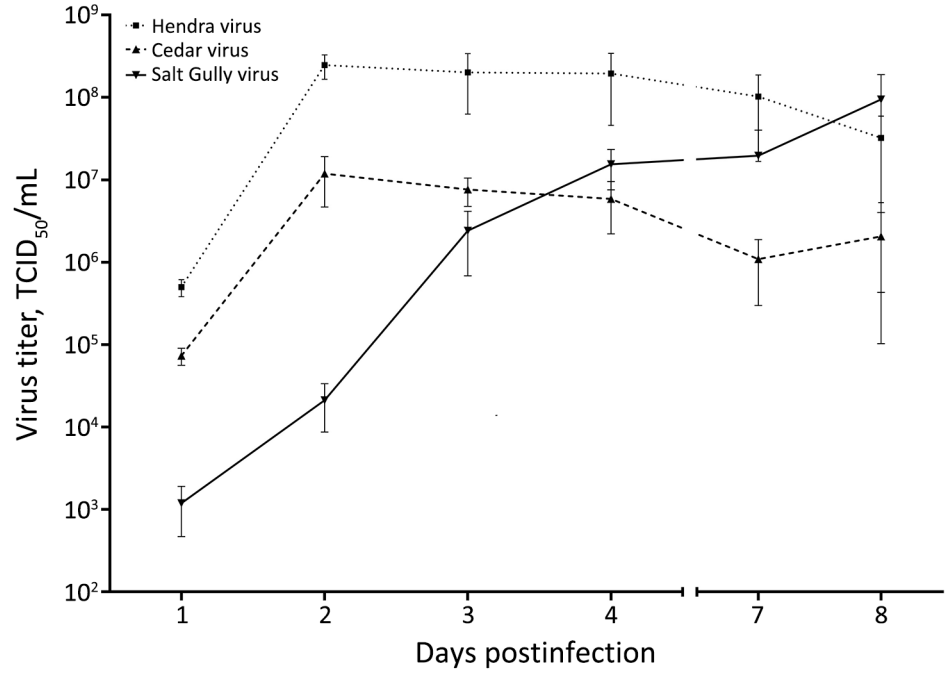

Figure 2. Growth of Salt Gully virus in Vero cells compared with Hendra virus and Cedar virus from study investigating a novel henipavirus, Salt Gully virus, isolated from pteropid bats, Australia**.** Vero cell monolayers were infected with each virus at a multiplicity of infection of 0.01 in triplicate, and tissue culture supernatant was collected until day 8 for $TCID_{50}$ assay to determine the viral titer. Error bars indicate the standard deviation of the mean between replicates. $TCID_{50}$, 50% tissue culture infectious dose.

Table. Growth of viruses in 5 mammalian cell lines 3 days postinfection in study of novel henipavirus, Salt Gully virus, isolated from pteropid bats, Australia*

Virus	% Cell monolayer infected				
	Vero	PaKi	HeLa	EFK	PK15a
Salt Gully virus	20–50	20–50	<20	0	0
Cedar virus	>50	>50	>50	0	>50
Hendra virus	100	20–50	100	20–50	<20

*Cell types: Vero, African green monkey kidney; PaKi, Pteropus alecto kidney; HeLa, human epithelial; EFK, equine fetal kidney; PK15a, porcine kidney.

Next-generation sequencing of RNA extracted from TCSN on the Illumina platform (https://www.illumina.com), followed by genome assembly and analysis, revealed a large, complete genome of 19,884 nt (GenBank accession no. PV233879), adhering to the rule of 6 for paramyxoviruses (*13*). This genome included 6 distinct open reading frames that encoded 6 proteins: nucleocapsid (N), phosphoprotein (P), matrix (M), fusion (F), glycoprotein (G), and RNA polymerase (L). In addition, an alternative start codon within the P gene indicated the presence of a 7th open reading frame and a C protein, consistent with other henipavirus genomes. Whole-genome nucleotide alignment with other known henipaviruses showed that SGV shared 38% identity with HeV and NiV, 37% identity with Angavokely virus (AngV), and 35% identity with CedV and Ghana virus. We determined SGV to be phylogenetically most closely related to AngV (Figure 1).

Investigating species tropism and growth kinetics, we found that SGV infected Vero, pteropid bat, and human cell lines, showing varying levels of CPE by 3 dpi. We observed no viral CPE in porcine or primary equine cell lines by 7 dpi. HeV replicated in all 5 cell lines, and CedV replicated in all except equine (Table). Initially, SGV displayed delayed replication in Vero cells; however, SGV reached maximum viral titer by 8 dpi at a titer comparable to HeV and CedV, which peaked by 2 dpi and then declined (Figure 2).

We used human epithelial (HeLa)-USU cells and recombinant HeLa-USU cell lines expressing ephrin-B2 or ephrin-B3 to assess SGV receptor usage. We observed viral CPE in HeLa cells expressing ephrin-B2 and ephrin-B3 for HeV and in ephrin-B2-expressing HeLa cells for CedV after 2 dpi. HeV and CedV did not infect HeLa-USU cells, as shown previously (*14*). In contrast, SGV caused CPE in all 3 HeLa cell lines after 5 dpi, indicating usage of an unknown receptor that is neither ephrin-B2 nor ephrin-B3 (Figure 3).

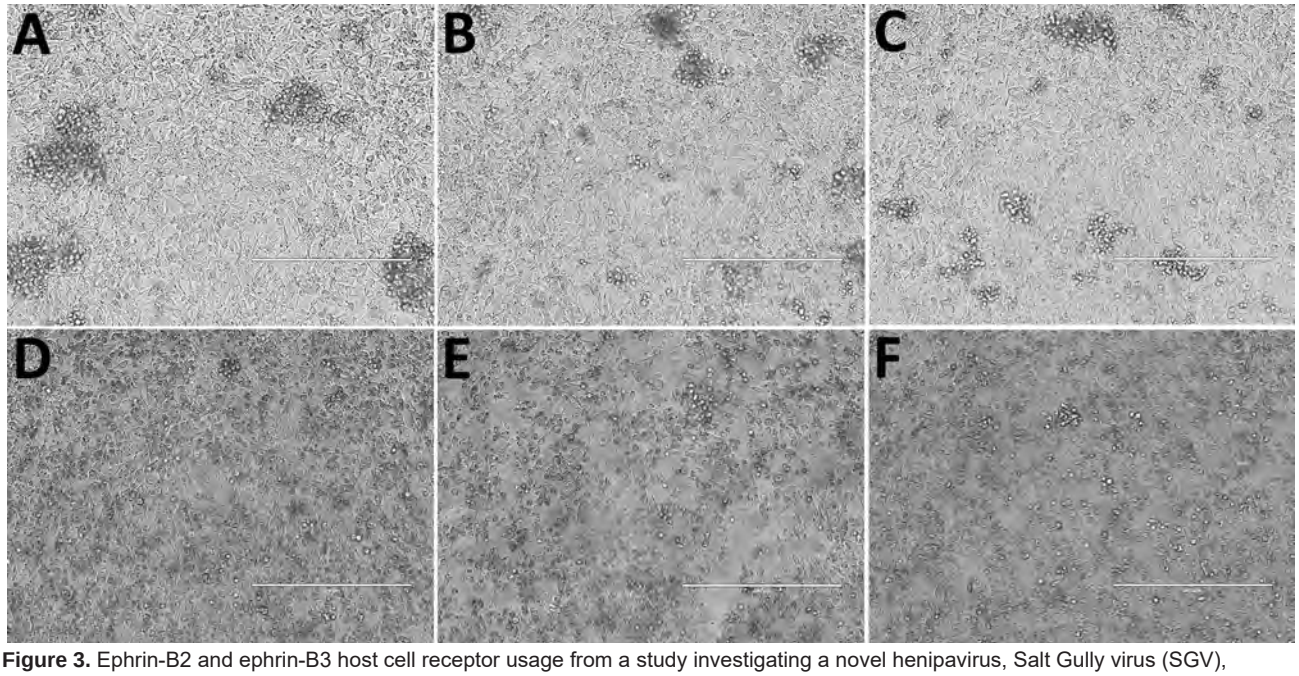

Figure 3. Ephrin-B2 and ephrin-B3 host cell receptor usage from a study investigating a novel henipavirus, Salt Gully virus (SGV), isolated from pteropid bats, Australia. Three cell lines—HeLa-USU, recombinant HeLa-USU expressing ephrin-B2, and HeLa-USU expressing ephrin-B3—were inoculated with SGV and observed daily for viral cytopathic effects (CPE). CPE was seen in all 3 cell lines by 5 dpi, indicating that SGV does not use ephrin-B2 or ephrin-B3 as a host cell receptor. A) Uninfected HeLa-USU cells; B) uninfected HeLa-USU cells expressing ephrin-B2; C) uninfected HeLa-USU cells expressing ephrin-B3; D) SGV-infected HeLa-USU cells; E) SGV-infected HeLa-USU ephrin-B2 cells; and F) SGV-infected HeLa-USU ephrin-B3 cells. Scale bars indicate 400um.

Conclusions

We detected SGV in bat urine samples collected in Australia in 2011 and successfully isolated the virus using pteropid bat cell lines. Initially, the CPE of inoculated Vero cells was minimal, requiring passage in pteropid kidney cells to achieve efficient virus replication. Despite the identification of multiple new henipa-like viruses in pteropid bats and small mammals globally, viral isolation is largely unsuccessful and remains a technical challenge. In our study, employing primary cell lines derived from the relevant species resulted in virus isolation.

Full-length genome sequencing of SGV revealed a genome organization consistent with other known henipaviruses, with all predicted henipavirus protein ORFs identified. Whole-genome alignments comparing SGV to other henipaviruses revealed 35%–38% identity at a nucleotide level. Of interest, phylogenetic analysis of the genome clusters SGV with AngV, a henipavirus that was detected in fruit bats (*Eidolon dupreanum*) in Madagascar in 2022 (*15*).

We assessed the ability for SGV to infect various mammalian cell lines in vitro, including Vero, PaKi, HeLa, equine fetal kidney, and porcine kidney cells. SGV's notable ability to infect human cells underscores its potential for human infection. Unlike HeV, which infected all 5 cell lines, SGV did not cause CPE in porcine or equine cells. SGV could grow to high titer in Vero cells, albeit slower than HeV. Collectively, these results indicate SGV may not have the broad species tropism of pathogenic henipaviruses but could pose a human risk.

Ephrin-B2 and ephrin-B3 are host cell receptors for HeV and NiV (*14*), and the sequence conservation of those ligands across many species supports the broad species tropism of classical henipaviruses. The HeLa-USU cell line we used has been shown to lack expression of ephrin-B2 and ephrin-B3 and was used to determine the functional host cell receptor for CedV. In our study, SGV infected all 3 HeLa-USU cell lines, demonstrating that SGV cell entry is not reliant on ephrin-B2 or ephrin-B3, suggesting SGV uses a yet unidentified host cell receptor. In comparison, research has shown the glycoprotein G of Ghana virus could bind to ephrin-B2 (but not ephrin-B3), whereas predicted structure-based alignments suggest AngV is unlikely to use ephrin receptors for host cell entry (*15*). Further characterization is required to determine the functional host cell receptor for SGV and accurately assess pathogenicity in other species.

In summary, we identified, isolated, and characterized a novel henipavirus from pteropid bats in Australia. Amid the increasing discovery of novel henipa-like viruses in new locations and species, SGV is a true henipavirus and phylogenetically clusters with other bat henipaviruses. However, this virus's pathogenicity remains unknown, making the susceptibility of human and animal populations in Australia uncertain.

Acknowledgments

We acknowledge Hume Field and team for assisting with urine collection from underneath pteropid bat colonies, James Gilkerson for providing the primary equine fetal kidney cell line used in this study, Christopher Broder for providing the HeLa-USU cell line used to study ephrin usage, and Kyle Catalan and Kim Blasdell for technical help with full-length sequencing.

About the Author

Ms Barr is an experimental scientist at the CSIRO Australian Centre for Disease Preparedness in Geelong, Victoria, Australia. Her research interests include zoonotic batborne viruses, virus discovery, viruses requiring high-containment, and serologic assays.

References

1. Rima B, Balkema-Buschmann A, Dundon WG, Duprex P, Easton A, Fouchier R, et al.; ICTV Report Consortium. ICTV virus taxonomy profile: *Paramyxoviridae.* J Gen Virol. 2019;100:1593–4. https://doi.org/10.1099/jgv.0.001328
2. Murray K, Selleck P, Hooper P, Hyatt A, Gould A, Gleeson L, et al. A morbillivirus that caused fatal disease in horses and humans. Science. 1995;268:94–7. https://doi.org/10.1126/science.7701348
3. Chua KB, Bellini WJ, Rota PA, Harcourt BH, Tamin A, Lam SK, et al. Nipah virus: a recently emergent deadly paramyxovirus. Science. 2000;288:1432–5. https://doi.org/10.1126/science.288.5470.1432
4. Middleton D, Pallister J, Klein R, Feng YR, Haining J, Arkinstall R, et al. Hendra virus vaccine, a One Health approach to protecting horse, human, and environmental health. Emerg Infect Dis. 2014;20:372–9. https://doi.org/10.3201/eid2003.131159
5. Queensland Government. Summary of Hendra virus incidents in horses. 2022 [cited 2025 Jul 23] https://www.business.qld.gov.au/industries/service-industries-professionals/service-industries/veterinary-surgeons/guidelines-hendra/incident-summary
6. New South Wales Government. Summary of human cases of Hendra virus infection. 2022 [cited 2025 Jul 23] https://www.health.nsw.gov.au/Infectious/controlguideline/Pages/hendra-case-summary.aspx
7. Marsh GA, de Jong C, Barr JA, Tachedjian M, Smith C, Middleton D, et al. Cedar virus: a novel henipavirus isolated from Australian bats. PLoS Pathog. 2012;8:e1002836. https://doi.org/10.1371/journal.ppat.1002836
8. Wu Z, Yang L, Yang F, Ren X, Jiang J, Dong J, et al. Novel henipa-like virus, Mojiang paramyxovirus, in rats, China, 2012. Emerg Infect Dis. 2014;20:1064–6. https://doi.org/10.3201/eid2006.131022
9. Vanmechelen B, Meurs S, Horemans M, Loosen A, Joly Maes T, Laenen L, et al. The characterization of multiple

novel paramyxoviruses highlights the diverse nature of the subfamily *Orthoparamyxovirinae*. Virus Evol. 2022;8:veac061. https://doi.org/10.1093/ve/veac061
10. Lee SH, Kim K, Kim J, No JS, Park K, Budhathoki S, et al. Discovery and genetic characterization of novel paramyxoviruses related to the genus *Henipavirus* in *Crocidura* species in the Republic of Korea. Viruses. 2021;13:2020. https://doi.org/10.3390/v13102020
11. Caruso S, Edwards SJ. Recently emerged novel Henipa-like viruses: shining a spotlight on the shrew. Viruses. 2023;15:2407. https://doi.org/10.3390/v15122407
12. Tong S, Chern SWW, Li Y, Pallansch MA, Anderson LJ. Sensitive and broadly reactive reverse transcription-PCR assays to detect novel paramyxoviruses. J Clin Microbiol. 2008;46:2652–8. https://doi.org/10.1128/JCM.00192-08
13. Kolakofsky D, Pelet T, Garcin D, Hausmann S, Curran J, Roux L. Paramyxovirus RNA synthesis and the requirement for hexamer genome length: the rule of six revisited. J Virol. 1998;72:891–9. https://doi.org/10.1128/JVI.72.2.891-899.1998
14. Bonaparte MI, Dimitrov AS, Bossart KN, Crameri G, Mungall BA, Bishop KA, et al. Ephrin-B2 ligand is a functional receptor for Hendra virus and Nipah virus. Proc Natl Acad Sci U S A. 2005;102:10652–7. https://doi.org/10.1073/pnas.0504887102
15. Madera S, Kistler A, Ranaivoson HC, Ahyong V, Andrianiaina A, Andry S, et al. Discovery and genomic characterization of a novel henipavirus, Angavokely virus, from fruit bats in Madagascar. J Virol. 2022;96:e0092122. https://doi.org/10.1128/jvi.00921-22

Address for correspondence: Jennifer Barr, CSIRO ACDP, 5 Portarlington Rd, East Geelong, VIC 3220, Australia; email: jennifer.barr@csiro.au

Modeling Case Burden and Duration of Sudan Ebola Virus Disease Outbreak in Uganda, 2022

Donal Bisanzio, Henry Kyobe Bosa, Barnabas Bakamutumaho, Carolyne Nasimiyu, Diana Atwine, Daniel Kyabayinze, Charles Olaro, Robert F. Breiman, M. Kariuki Njenga, Henry Mwebesa, Jane Ruth Aceng, Richard Reithinger

In 2022, a Sudan Ebola virus outbreak was confirmed in Uganda. Within 1 month of the outbreak's onset, we developed an individual-based modeling platform to estimate the unfolding outbreak's burden of cases and deaths, as well as its duration, using different scenarios. Modeled projections were within the range of observed cases.

Ebola virus disease (EVD) is a severe, often fatal illness affecting humans and primates (*1*). In the past 4 decades, 36 EVD outbreaks have occurred across 11 countries, resulting in >15,000 deaths (*2*). With case-fatality rates that can reach >65%, EVD is among the most lethal viral hemorrhagic fevers.

On September 20, 2022, an outbreak of Sudan Ebola virus (SUDV; *Orthoebolavirus sudanense*) in south-central Mubende District, Uganda, was confirmed by the Uganda Ministry of Health (MOH) (*3*,*4*); cases rapidly spread to 8 nearby districts. By mid-October, concerns within the MOH and the international community about the potential magnitude of the outbreak accelerated when a treatment-seeking infected person traveled to the highly populated capital city, Kampala; many new cases were linked to that patient (*5*), who eventually died. Because no effective treatment or vaccine existed against SUDV (*6*), the MOH's response to mitigate the outbreak relied on nonpharmaceutical interventions (NPIs), including aggressive case isolation and contact tracing; safe burials; hygiene promotion; social and behavior change; and lockdowns. NPIs were applied on the basis of successful experiences from previous EVD outbreaks in sub-Saharan Africa and built upon the prevailing COVID-19 pandemic response infrastructure (*7*). The aim of this study was to develop—during the first month after the outbreak started—a methodological approach to rapidly predict the epidemic curve and burden of the SUDV outbreak, depending on the timing and intensity of the interventions by local health officials.

Author affiliations: RTI International, Washington, DC, USA (D. Bisanzio, R. Reithinger); Ministry of Health, Kampala, Uganda (H.K. Bosa, B. Bakamutumaho, D. Atwine, D. Kyabayinze, C. Olaro, H. Mwebesa, J.R. Aceng); Washington State University, Pullman, Washington, USA (C. Nasimiyu, M.K. Njenga); Emory University, Atlanta, Georgia, USA (R.F. Breiman)

DOI: https://doi.org/10.3201/eid3109.241545

The Study

We modified a well-characterized individual-based model (IBM) framework, previously used to estimate disease burden for COVID-19 (*8*), mpox (*9*), and Ebola (*10*), for the purposes of the SUDV outbreak (IBM-SUDV; Appendix, https://wwwnc.cdc.gov/EID/article/31/9/24-1545-App1.pdf). Unlike ordinal differential equation models or other IBMs previously published for Ebola (*11*), IBM-SUDV included the geographic distribution and movement of the Uganda population, as well as a contact network representing population interactions at local and regional levels, using available demographic data and accounting for heterogeneity in interactions among age groups. IBM-SUDV included uptake and impact of NPIs, simulating the response to the 2022 SUDV outbreak in Uganda, such as contact tracing, case isolation, safe burial, and use of personal protective equipment (PPE). We modeled timing of intervention deployment and response heterogeneity to estimate the outbreak's case burden, deaths, and duration.

We modeled SUDV transmission using the classical susceptible→exposed→infectious→recovered compartmental model structure (*8*–*10*). The transition from one status to another was a function of pathogen characteristics (e.g., probability of effective transmission per close contact, incubation period, infectious period, and fatality rate) and

Table. Comparison of predictions obtained from modeling case burden and duration of Sudan Ebola virus disease outbreak in Uganda, 2022*

Scenarios	No. cases (95% CrI)	No. deaths (95% CrI)	Epidemic duration (95% CrI)
2022 Ebola outbreak†	164	77	16.5 wk
Individual-based Uganda model‡			
Baseline	193 (131–277)	81 (55–124)	22 wk (14–25 wk)
Delayed response	778 (665–901)	303 (259–351)	24 wk (20–28 wk)
Out-of-control	13,537 (9,376–19,919)	5,279 (3,656–7,768)	24 mo (22–27 mo)

*CrI, credible interval.
†Reported burden and duration.
‡Predicted burden and duration.

interaction among persons (only for susceptible to infectious). For all persons, we determined parameter values for treatment-seeking behavior, hospitalization, fatality, and burial by using either published data or estimates. This model represented the baseline scenario. We then compared the baseline scenario to 2 hypothetical scenarios: a delayed outbreak response scenario, which assumed a 5-month delay in reaching the coverage and uptake of the 2022 SUDV outbreak NPI response; and an out-of-control outbreak scenario, which assumed a 5-month delay in having NPIs in place, as well as a mean 50% contact tracing and isolation rate (i.e., similar to what was observed in the early phase of the 2014–2016 West Africa Ebola outbreak).

For each scenario, we completed 1,000 simulations with a time horizon of 150 weeks each. For each scenario, we estimated the median number of cases, hospitalizations, and deaths, as well as the outbreak's median duration. The outbreak's duration was determined from the occurrence of the first case to the time at which zero cases were observed 42 days after the last infection event. For each outcome, we calculated a 95% credible interval (CrI) using the adjusted bootstrap percentile approach (*12*).

We compiled and visualized the predicted epidemic curve for each of the 3 scenarios (Table; Figure). With NPIs implemented, the baseline scenario estimated a median number of 193 (95% CrI 131–277) cases and 81 (95% CrI 55–124) deaths; the outbreak's median duration was 22 (95% CrI 14–25) weeks (Figure, panel A). The delayed outbreak response scenario estimated 778 (95% CrI 665–901) cases and 303 (95% CrI 259–351) deaths, and the outbreak's median duration extended to 24 (95% CrI 20–28) weeks (Figure, panel B). The out-of-control outbreak scenario estimated 13,537 (95% CrI 9,376–19,919) cases, 5,279 (95% CrI 3,656–7,768) deaths, and a median outbreak duration of 24 (95% CrI 22–27) months (Figure, panel C). The IBM-SUDV's modeled projections were completed on November 1, 2022, and shared with the Uganda MOH on November 11, 2022.

Before 2022, Uganda had reported 6 EVD outbreaks (*2*). Of the reported outbreaks, 4 were caused by SUDV (2000, 2011, and 2012 [n = 2]), 1 was caused by Bundibugyo virus (*O. bundibugyoense*; 2007), and 1 was caused by Zaire Ebola virus (*O. zairense*; 2019). Those outbreaks' median number of cases was 8.5 (range 1–425) and median deaths was 4 (range 1–224); in total, the outbreaks resulted in 596 cases and 273 deaths (*2*).

For the 2022 SUDV outbreak, the actions of the MOH swiftly halted virus circulation in all affected districts (*5*,*13*). Ebola treatment units (ETUs) were activated at Mubende and Fort Portal Regional Referral Hospitals on September 20, 2022, and symptomatic contacts were evacuated directly to ETUs for testing. Entebbe Regional Referral Hospital activated its

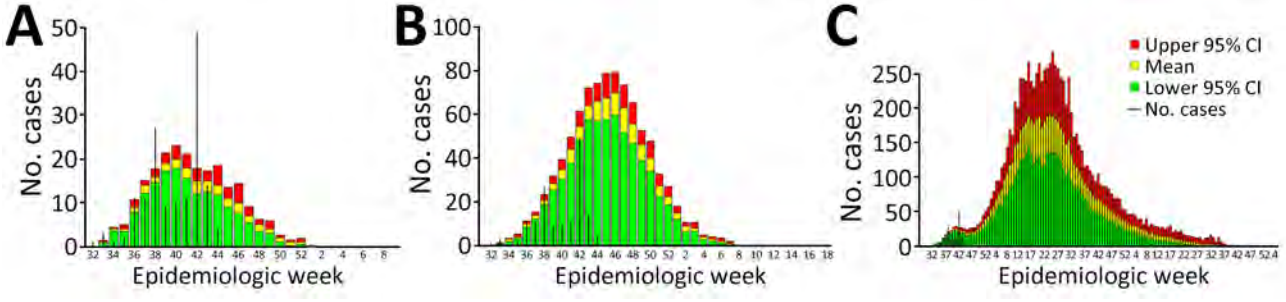

Figure. Predicted individual-based model epidemic curves compared with actual epidemic data for study modeling case burden and duration of Sudan Ebola virus (SUDV) disease outbreak in Uganda, 2022. A) Baseline scenario, simulating the actual response to the outbreak, including timing of nonpharmaceutical interventions (NPIs; i.e., contact tracing, isolation, personal protective equipment). B) Delayed outbreak response scenario, which assumed a 5-month delay in reaching the NPI coverage and uptake of the 2022 SUDV outbreak. C) Out-of-control scenario, which assumed a 5-month delay in having NPIs in place, as well as a mean 50% contact tracing and isolation rate. Black bars indicate actual numbers of cases reported during the outbreak.

ETU on October 6, 2022, and Mulago National Referral Hospital's ETU was activated on October 15. Early in the outbreak, most cases were healthcare-associated rather than household-associated; cases resulting from burial or vertical or sexual transmission were rare (*13*). The 2022 SUDV outbreak lasted 69 days and caused 164 cases and 77 deaths (*3*). The mean age of case-patients was 28 years, and the highest case-fatality rates were observed among children <10 years of age (75%) and adults 40–49 years of age (61.5%). Uganda's MOH officially declared the outbreak's end on January 11, 2023, sixty days after the last infection event.

Conclusions

During the 2022 SUDV outbreak in Uganda, within 1 month of the first case being confirmed, we developed the IBM-SUDV to model the burden and duration of the outbreak. The outbreak's reported numbers of cases and deaths (164 cases and 77 death reported vs. 193 [95% CrI 131–277] cases and 81 [95% CrI 55–124] deaths modeled), as well as the average duration (16.5 weeks reported vs. 22 [95% CrI 14–25] weeks modeled), were within the ranges of our baseline scenario. Delayed outbreak and out-of-control outbreak scenarios would have resulted in a substantially greater outbreak burden and duration, similar to the 2014–2016 EVD outbreak across Guinea, Liberia, and Sierra Leone (i.e., 28,600 cases and 11,325 deaths). The model highlighted the importance of a rapid response to effectively control the outbreak, which ultimately occurred (*5*,*13*). After we shared model results with MOH in early November, the MOH intensified NPI implementation, particularly contact isolation and an unprecedented lockdown of 2 hotspot districts. Further IBM-SUDV modeling is being discussed with the MOH, including to determine SUDV transmission dynamics more accurately, using actual 2022 SUDV outbreak clinical, epidemiologic, and operational response data (e.g., from individual cases and contact tracing) (*4*,*5*,*14*), as well as estimate the effectiveness of changing various NPI parameters, additional NPIs, and available therapeutic options (e.g., vaccine).

In summary, our model estimated that the MOH's prompt response to this outbreak averted up to 13,000 cases and 5,000 deaths. The effective response was likely aided by Uganda's prior experience responding to EVD outbreaks (*3*), a national disaster preparedness and management policy (https://faolex.fao.org/docs/pdf/uga171437.pdf), a public health emergency operations center and relevant task forces (*15*), external partner coordination, and infrastructure and resources built during the COVID-19 pandemic (*7*).

Acknowledgments

We thank 2 anonymous reviewers for their constructive comments during the manuscript review process.

Funding for this work was provided by the US National Institute of Allergy and Infectious Disease/National Institutes of Health, grant no. U01AI51378 to the Center for Research in Emerging Infectious Diseases Coordinating Center (D.B., R.R.) and grant no. U01AI151799 to the Centre for Research in Emerging Infectious Diseases–East and Central Africa (C.N., R.F.B., M.K.N.).

About the Author

Dr. Bisanzio is a senior epidemiologist at RTI International. His primary research interests are the prevention, control, and surveillance of vectorborne, zoonotic, and emerging infectious diseases.

References

1. Biedenkopf N, Bukreyev A, Chandran K, Di Paola N, Formenty PBH, Griffiths A, et al. Renaming of genera *Ebolavirus* and *Marburgvirus* to *Orthoebolavirus* and *Orthomarburgvirus*, respectively, and introduction of binomial species names within family Filoviridae. Arch Virol. 2023;168:220. https://doi.org/10.1007/ s00705-023-05834-2
2. Rugarabamu S, Mboera L, Rweyemamu M, Mwanyika G, Lutwama J, Paweska J, et al. Forty-two years of responding to Ebola virus outbreaks in sub-Saharan Africa: a review. BMJ Glob Health. 2020;5:e001955. https://doi.org/10.1136/bmjgh-2019-001955
3. Aceng JR, Bosa HK, Kamara N, Atwine D, Mwebesa H, Nyika H, et al. Continental concerted efforts to control the seventh outbreak of Ebola virus disease in Uganda: the first 90 days of the response. J Public Health Afr. 2023;14:2735. https://doi.org/10.4081/jphia.2023.2735
4. Kiggundu T, Ario AR, Kadobera D, Kwesiga B, Migisha R, Makumbi I, et al.; Uganda Ebola Response Team. Notes from the field: outbreak of Ebola virus disease caused by Sudan ebolavirus—Uganda, August–October 2022. MMWR Morb Mortal Wkly Rep. 2022;71:1457–9. https://doi.org/10.15585/mmwr.mm7145a5
5. Komakech A, Whitmer S, Izudi J, Kizito C, Ninsiima M, Ahirirwe SR, et al. Sudan virus disease super-spreading, Uganda, 2022. BMC Infect Dis. 2024;24:520. https://doi.org/10.1186/s12879-024-09391-0
6. Ibrahim SK, Ndwandwe DE, Thomas K, Sigfrid L, Norton A. Sudan virus disease outbreak in Uganda: urgent research gaps. BMJ Glob Health. 2022;7:e010982. https://doi.org/10.1136/bmjgh-2022-010982
7. Kyobe Bosa H, Njenga MK, Wayengera M, Kirenga B, Muttamba W, Dawa J, et al. Leveraging the structures of the COVID-19 pandemic response for successful control of Ebola in Uganda. Nat Med. 2023;29:1892–3. https://doi.org/10.1038/s41591-023-02395-4
8. Bisanzio D, Reithinger R, Alqunaibet A, Almudarra S, Alsukait RF, Dong D, et al. Estimating the effect of non-pharmaceutical interventions to mitigate COVID-19 spread in Saudi Arabia. BMC Med. 2022;20:51. https://doi.org/10.1186/s12916-022-02232-4
9. Bisanzio D, Reithinger R. Projected burden and duration of the 2022 monkeypox outbreaks in non-endemic countries.

Lancet Microbe. 2022;3:e643. https://doi.org/10.1016/S2666-5247(22)00183-5
10. Bisanzio D, Davis AE, Talbird SE, Van Effelterre T, Metz L, Gaudig M, et al. Targeted preventive vaccination campaigns to reduce Ebola outbreaks: an individual-based modeling study. Vaccine. 2023;41:684–93. https://doi.org/10.1016/j.vaccine.2022.11.036
11. Nash RK, Bhatia S, Morgenstern C, Doohan P, Jorgensen D, McCain K, et al.; Pathogen Epidemiology Review Group. Ebola virus disease mathematical models and epidemiological parameters: a systematic review. Lancet Infect Dis. 2024;24:e762–73. https://doi.org/10.1016/S1473-3099(24)00374-8
12. Dikta G, Scheer M. Bootstrap methods: with applications in R. Berlin: Springer Nature; 2021.
13. Kabami Z, Ario AR, Harris JR, Ninsiima M, Ahirirwe SR, Ocero JRA, et al.; Uganda Ebola Response Team. Ebola disease outbreak caused by the Sudan virus in Uganda, 2022: a descriptive epidemiological study. Lancet Glob Health. 2024;12:e1684–92. https://doi.org/10.1016/S2214-109X(24)00260-2
14. Wanyana MW, Akunzirwe R, King P, Atuhaire I, Zavuga R, Lubwama B, et al. Performance and impact of contact tracing in the Sudan virus outbreak in Uganda, September 2022–January 2023. Int J Infect Dis. 2024;141:106959. https://doi.org/10.1016/j.ijid.2024.02.002
15. Kayiwa J, Homsy J, Nelson LJ, Ocom F, Kasule JN, Wetaka MM, et al. Establishing a public health emergency operations center in an outbreak-prone country: lessons learned in Uganda, January 2014 to December 2021. Health Secur. 2022;20:394–407. https://doi.org/10.1089/hs.2022.0048

Address for correspondence: Richard Reithinger, RTI International, 701 13th St, Ste 750, Washington, DC 20005-3967, USA; email: rreithinger@yahoo.co.uk

Detection of Rat Lungworm (*Angiostrongylus cantonensis*) in Rats and Gastropods, Italy

Divakaran Pandian,[1] Anna Šipková,[1] Stefano Scarcelli,[1] Giovanni Sgroi, Jana Kačmaříková, Francesco Buono, Elisa Castaldo, Nicola D'Alessio, Barbora Červená, Vincenzo Veneziano, David Modrý

The emerging zoonotic nematode *Angiostrongylus cantonensis* causes severe neural angiostrongyliasis in both humans and animals. The parasite has been reported in Spain. We detected *A. cantonensis* in rats and gastropods from the Campania region, southern Italy, demonstrating its broad distribution on the southern coast of Europe.

The rat lungworm, *Angiostrongylus cantonensis*, a neurotropic zoonotic parasite, is receiving increasing attention because of its potential to cause severe neurologic disease in humans and animals (*1*). This rat lungworm has an indirect life cycle involving rats (mainly *Rattus* spp.) as definitive hosts, mollusks as intermediate hosts, and different paratenic and transient hosts such as frogs, lizards, and crustaceans (*2*). Infection in humans usually occurs by accidental ingestion of infective third-stage larvae (L3) found in raw or undercooked snails or paratenic hosts or by contact with L3-contaminated water or products (*3*). Identified in China in 1935, *A. cantonensis* has since become endemic in Southeast Asia, East Asia, North and South America, and selected Pacific and Caribbean islands, where most human cases of neuroangiostrongyliasis occur; >7,000 human cases have been recorded worldwide (*4*).

In the past 2 decades, the geographic range of *A. cantonensis* lungworms has increased in Europe, and they have been detected in the Canary Islands (Tenerife, Spain) (*5*), in the Balearic Islands (Mallorca, Spain) (*6*), and most recently in mainland Spain (Valencia) (*7*), indicating a continued spread in the Mediterranean basin. Although human cases remain rare in Europe and have been associated with travel to well-established endemic regions, such as Southeast Asia and the Caribbean Islands (*8*), the subtropical climate and historically active maritime trade in Naples, Italy, provide favorable conditions for the spread of *A. cantonensis* to human and animal hosts. We investigated *Rattus* spp. rats and snail populations in periurban and rural areas of the Campania region of southern Italy to determine whether the *A. cantonensis* lungworm has spread to this region along the Mediterranean Coast of Europe.

The Study

We obtained a total of 32 frozen rat specimens, 10 *R. rattus* and 22 *R. norvegicus*, from a pest control company operating in metropolitan Naples and its surroundings. We conducted an initial sampling phase randomly across various locations. After we detected *A. cantonensis* lungworm in rats, we conducted a second sampling, during which we collected 352 gastropods from locations where infected rats were collected and from nearby areas selected at random. In total, we sampled rodent and gastropod samples from 15 locations during January–November 2024 (Figure 1; Appendix 1, https://wwwnc.cdc.gov/EID/article/31/9/25-0648-App1.xlsx).

We necropsied rats at the Experimental Zooprophylactic Institute of Southern Italy in Naples. We isolated the heart and lungs and inspected them

Author affiliations: Czech University of Life Sciences, Prague, Czech Republic (D. Pandian, D. Modrý); Masaryk University, Faculty of Science, Brno, Czech Republic (A. Šipková, D. Modrý); University of Naples Federico II, Naples, Italy (S. Scarcelli, F. Buono, E. Castaldo, V. Veneziano); Experimental Zooprophylactic Institute of Southern Italy, Portici, Italy (G. Sgroi, N. D'Alessio); University of Veterinary Sciences Brno, Brno, (J. Kačmaříková, B. Červená); Institute of Vertebrate Biology, Czech Academy of Sciences, Brno (J. Kačmaříková, B. Červená); Biology Center of Czech Academy of Sciences, Institute of Parasitology, České Budějovice, Czech Republic (D. Modrý)

DOI: https://doi.org/10.3201/eid3109.250648

[1]These first authors contributed equally to this article.

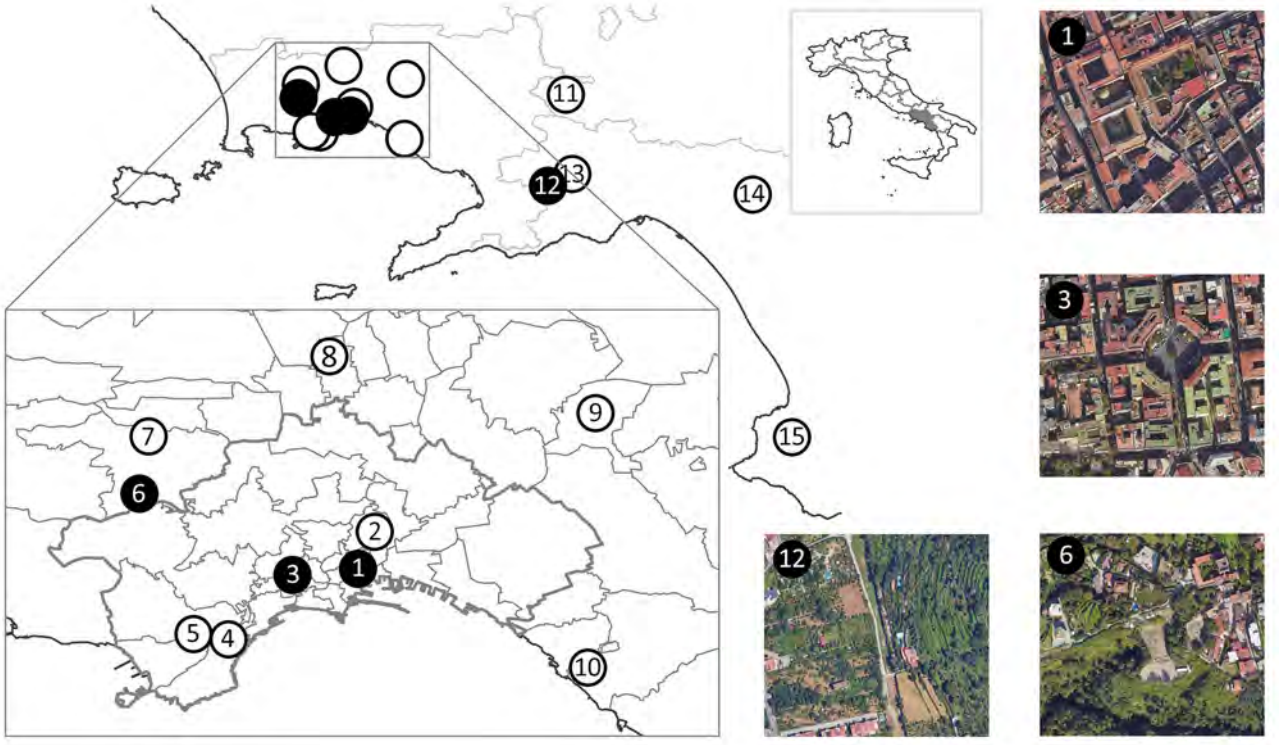

Figure 1. Sampling locations used for detection of rat lungworm (*Angiostrongylus cantonensis*) in rats and gastropods, Italy. Solid black circles indicate sites from which *A. cantonensis*–positive samples were collected, white circles indicate *A. cantonensis*–negative sites; numbering corresponds to numbers in the Table. Inset at top shows region of Italy in which sampling was conducted (gray area); inset at bottom shows detailed sampling areas within Naples; outer satellite images show areas with *A. cantonensis*–positive samples. Detailed information on locations, including geospatial positioning coordinates, are available in Appendix 1 Table (https://wwwnc.cdc.gov/EID/article/31/9/25-0648-App1.xlsx). Map images created by using Google Maps (https://www.google.com/maps), Maxar Technologies (https://www.maxar.com), and Airbus (https://www.airbus.com).

for adult *Angiostrongylus* spp. worms, characterized by the distinctive barber pole appearance in female nematodes; we preserved isolated worms in 96% ethanol. We froze tissue samples from the brain, heart, kidneys, liver, lungs, and spleen of rats for molecular analysis. We confirmed rat species on the basis of DNA extracted from spleen samples by using the Nucleic Acid Extraction Kit (Magnetic Bead Method) (Zybio, https://www.zybio.com), followed by amplification of the mitochondrial

Table. Summary of rat and gastropod samples positive for rat lungworm (*Angiostrongylus cantonensis*), Italy

Location		Rats		Gastropods		GenBank
no.	Municipality (quarter)	No. positive/total no.	Haplotype	No. positive/total no.	Haplotype	accession no.
1	Naples (Porto)	1/1	NAP1	0/15	–	PV425925
2	Naples (San Carlo all'Arena)	0/1	–	0/61	–	–
3	Naples (Vomero)	1/3	NAP2	0/0	–	PV425926
4	Naples (Posillipo)	0/2	–	0/0	–	–
5	Naples (Fuorigrotta)	0/1	–	0/0	–	–
6	Naples (Camaldoli)	11/13	NAP1	7/73	NAP1	PV425925
7	Marano di Napoli	0/0	–	0/25	–	–
8	Casandrino	0/1	–	0/0	–	–
9	Casalnuovo di Napoli	0/0	–	0/12	–	–
10	Ercolano	0/1	–	0/0	–	–
11	Lauro	0/0	–	0/25	–	–
12	Corbara	0/4	–	1/76	†	–
13	Nocera Inferiore	0/0	–	0/51	–	–
14	Giffoni Valle Piana	0/0	–	0/14	–	–
15	Laureana Cilento	0/5	–	0/0	–	–

*Location numbers correspond to numbers in Figure 1. Detailed information on species and georeferenced data on sampled locations provided in Appendix 1 Table (https://wwwnc.cdc.gov/EID/article/31/9/25-0648-App1.xlsx). –, no positive samples.
†Failed sequencing.

cytochrome b gene (Appendix 2, https://wwwnc.cdc.gov/EID/article/31/9/25-0648-App2.pdf). We detected *A. cantonensis* nematodes in 13 (40.6%) of 32 rats collected from 3 locations, with a mean of 7 (range 1–24) worms per rat (Table; Figure 1; Appendix 1).

Molecular analysis confirmed *A. cantonensis* nematodes in 12 positive rats, and we subsequently sequenced 69 adult worms. We extracted DNA from those adult worms by using the DNeasy Blood & Tissue Kit (QIAGEN, https://www.qiagen.com), and we amplified the complete cytochrome c oxidase subunit 1 (*CO1*) gene (Appendix 2). The obtained sequences revealed 2 distinct haplotypes (NAP1 and NAP2), differing by 2 single-nucleotide polymorphisms (SNPs) at positions 1092 and 1481 of the *CO1* gene; the SNP at position 1481 resulted in a different amino acid. In a maximum-likelihood phylogenetic tree (Figure 2), both haplotypes clustered within clade II sensu, as previously defined (*9*), alongside other sequences from Europe, except for 1 (GenBank accession no. PP468354; 215 bp) from Valencia that

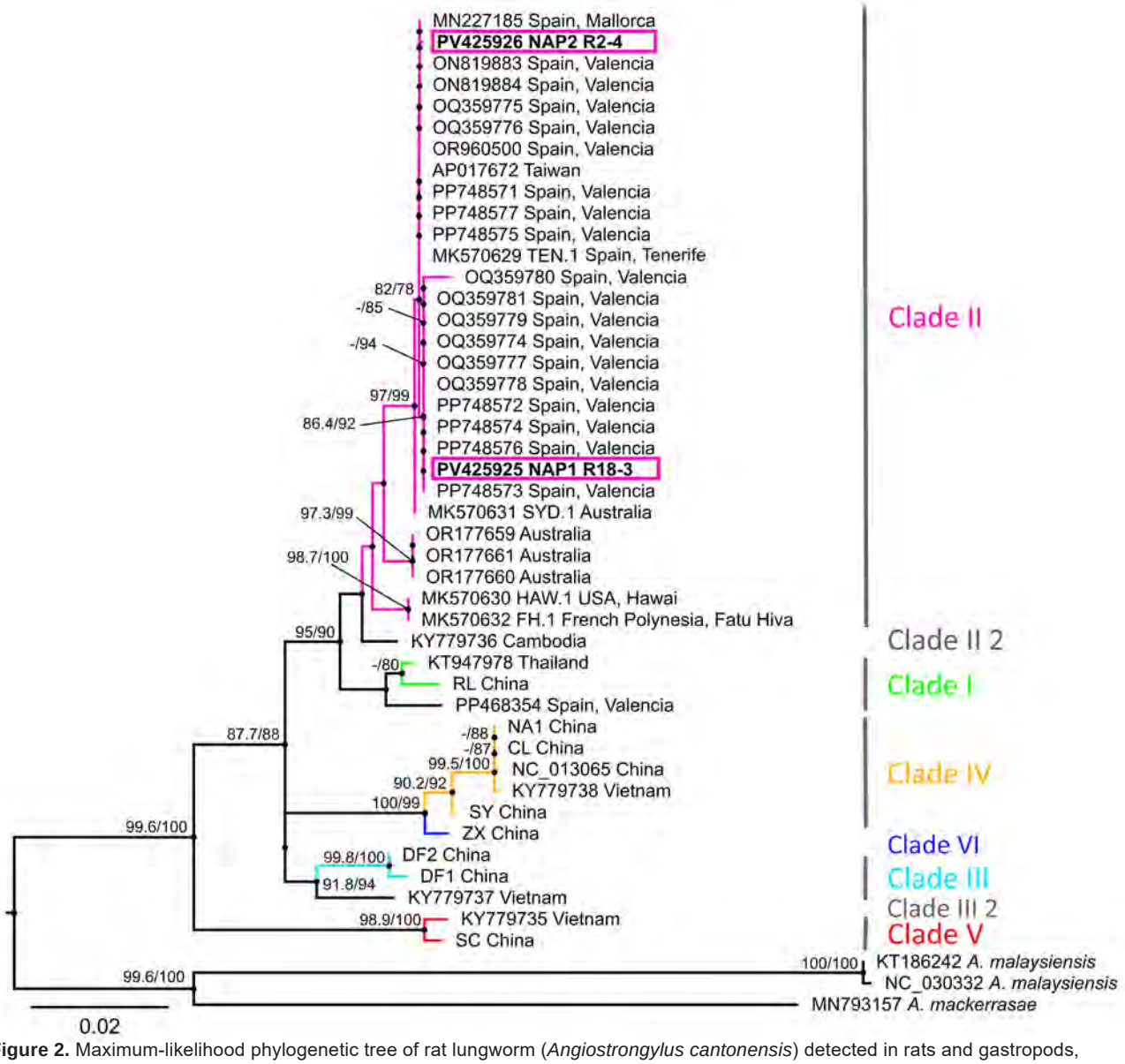

Figure 2. Maximum-likelihood phylogenetic tree of rat lungworm (*Angiostrongylus cantonensis*) detected in rats and gastropods, Italy. Tree is based on cytochrome c oxidase subunit 1 gene (1,578 bp) and partial sequences (215–561 bp) calculated by a Tamura-Nei plus model in IQ-TREE (http://www.iqtree.org) (*9*). Labeling of the clades follows previous studies (*10*). Sequences are labeled by GenBank accession numbers, where available, and locality of origin is indicated. Pink boxes indicate the 2 unique sequences from this study. Numbers at nodes indicate percentage SH-aLRT/ultrafast bootstrap support. Only values >75 are shown. Scale bar indicates nucleotide substitutions per site.

clustered in a separate clade, a sister to clade I, differing from all other sequences from Europe in 3 SNPs. Compared with the TEN.1 isolate (GenBank accession no. MK570629) from Tenerife, Spain, each haplotype from Italy differed by a single SNP: NAP1, detected in Naples (Porto) and Marano di Napoli, differed at position 1092; and NAP2, detected in Naples (Vomero), differed at position 1481. The 394-bp sequence from Mallorca, Spain (GenBank accession no. MN227185), was identical to NAP2. Among the Valencia isolates, 10 sequences were identical to NAP1, 3 were identical to NAP2, and the rest differed in 1, 2, or 3 SNPs from the other sequences from Italy.

Collected gastropods were identified to species level by a trained malacologist on the basis of morphological criteria. Molecular identification was performed on juvenile and shell-less specimens lacking distinct morphological characteristics. DNA was extracted from muscle tissue using the same protocol used for rat spleen samples, with an extended overnight prelysis phase at 56°C, optimized for the L3 stage of *A. cantonensis*. Molecular identification was made on the basis of sequences of the mitochondrial 16S rRNA gene (Appendix 2). We detected *A. cantonensis* worms by using a species-specific quantitative PCR on DNA isolated from gastropod tissue (*11*). Of the 352 gastropods examined, 8 (2.3%) gastropods from 2 localities tested positive for *A. cantonensis* DNA (Figure 1, Table; Appendix 1). We successfully obtained 6 *CO1* gene fragment sequences from the 8 positive gastropods (Appendix 2), and compared those with sequences from adult *A. cantonensis* lungworms from rats in this study. All sequences belonged to the NAP1 haplotype.

Conclusions

We provide robust evidence that the *A. cantonensis* rat lungworm is in the central Mediterranean region in the Naples area of Italy. Circulation of this zoonotic nematode in the highly populated Naples metropolitan area is concerning because of its ability to cause severe neurologic and ocular disorders in humans. Because Naples has an environment ideal for *A. cantonensis* transmission to the human population, enhanced awareness is needed among healthcare practitioners and diagnostic protocols should be revised and applied locally in the differential diagnosis of meningoencephalitis cases (*12*). In addition, considering reported clinical cases in domestic animals and in wildlife in known endemic foci (*13*–*15*), veterinary practitioners in the Naples area should be alerted.

Acknowledgments

We thank Petr Janoš for preparing the map of localities studied. We also thank Radovan Coufal and Veronika Horsáková for their assistance with the morphologic and molecular identification of gastropod specimens.

This study was supported by the Czech Science Foundation, grant no. 22-26136S. The work of Divakaran Pandian was supported by the Erasmus+ mobility program, and Anna Šipková was supported by Specific Research and Support of Student Projects (no. MUNI/A/1762/2024).

About the Author

Mr. Pandian is a doctoral student at the Department of Veterinary Sciences of Czech University of Life Sciences Prague. His research interests include all aspects of emergence and circulation of *Angiostrongylus cantonensis* in endemic and newly formed foci.

References

1. Morgan ER, Modry D, Paredes-Esquivel C, Foronda P, Traversa D. Angiostrongylosis in animals and humans in Europe. Pathogens. 2021;10:1236. https://doi.org/10.3390/pathogens10101236
2. Alicata JE. Biology and distribution of the rat lungworm, *Angiostrongylus cantonensis*, and its relationship to eosinophilic meningoencephalitis and other neurological disorders of man and animals. Adv Parasitol. 1965;3:223–48. https://doi.org/10.1016/S0065-308X(08)60366-8
3. Cowie RH. Biology, systematics, life cycle, and distribution of *Angiostrongylus cantonensis*, the cause of rat lungworm disease. Hawaii J Med Public Health. 2013;72(Suppl 2):6–9.
4. Turck HC, Fox MT, Cowie RH. Paratenic hosts of *Angiostrongylus cantonensis* and their relation to human neuroangiostrongyliasis globally. One Health. 2022; 15:100426. https://doi.org/10.1016/j.onehlt.2022.100426
5. Foronda P, López-González M, Miquel J, Torres J, Segovia M, Abreu-Acosta N, et al. Finding of *Parastrongylus cantonensis* (Chen, 1935) in *Rattus rattus* in Tenerife, Canary Islands (Spain). Acta Trop. 2010;114:123–7. https://doi.org/10.1016/j.actatropica.2010.02.004
6. Paredes-Esquivel C, Sola J, Delgado-Serra S, Puig Riera M, Negre N, Miranda MÁ, et al. *Angiostrongylus cantonensis* in North African hedgehogs as vertebrate hosts, Mallorca, Spain, October 2018. Euro Surveill. 2019; 24:33. https://doi.org/10.2807/1560-7917.ES.2019.24.33.1900489
7. Galán-Puchades MT, Gómez-Samblás M, Osuna A, Sáez-Durán S, Bueno-Marí R, Fuentes MV. Update on the first finding of the rat lungworm, *Angiostrongylus cantonensis*, in *Rattus* spp. in continental Europe, Valencia, Spain, 2022. Pathogens. 2023;12:4. https://doi.org/10.3390/pathogens12040567
8. Federspiel F, Skovmand S, Skarphedinsson S. Eosinophilic meningitis due to *Angiostrongylus cantonensis* in Europe. Int J Infect Dis. 2020;93:28–39. https://doi.org/10.1016/j.ijid.2020.01.012
9. Trifinopoulos J, Nguyen LT, von Haeseler A, Minh BQ. W-IQ-TREE: a fast online phylogenetic tool for maximum

likelihood analysis. Nucleic Acids Res. 2016;44:W232–5. https://doi.org/10.1093/nar/gkw256
10. Tian X, Chen S, Duan L, Qian Y, Li H, Lv S. The global spread pattern of rat lungworm based on mitochondrial genetics. Pathogens. 2023;12:13. https://doi.org/10.3390/pathogens12060788
11. Anettová L, Baláž V, Coufal R, Horsák M, Izquierdo-Rodriguez E, Šipková A, et al. Lizards as sentinels for the distribution of *Angiostrongylus cantonensis*. Epidemiol Infect. 2024;152:e168. https://doi.org/10.1017/S0950268824000931
12. Ansdell V, Kramer KJ, McMillan JK, Gosnell WL, Murphy GS, Meyer BC, et al. Guidelines for the diagnosis and treatment of neuroangiostrongyliasis: updated recommendations. Parasitology. 2021;148:227–33. https://doi.org/10.1017/S0031182020001262
13. Garijo-Toledo M, Alarcón-Elbal PM, Montero E, Bravo-Barriga D, Sansano-Maestre J, Ahuir-Baraja AE, et al. Mortality associated with *Angiostrongylus cantonensis* in non-human primates in Europe. Int J Parasitol. 2025;55:427–34. https://doi.org/10.1016/j.ijpara.2025.04.002
14. Odani J, Sox E, Coleman W, Jha R, Malik R. First documented cases of canine neuroangiostrongyliasis due to *Angiostrongylus cantonensis* in Hawaii. J Am Anim Hosp Assoc. 2021;57:42–6. https://doi.org/10.5326/JAAHA-MS-6989
15. Cowie RH, Malik R, Morgan ER. Comparative biology of parasitic nematodes in the genus *Angiostrongylus* and related genera. Adv Parasitol. 2023;121:65–197. https://doi.org/10.1016/bs.apar.2023.05.003

Address for correspondence: David Modrý, Department of Veterinary Sciences, Faculty of Agrobiology, Food and Natural Resources, Czech University of Life Sciences, Kamýcká 129, 16500 Prague, Czech Republic; email: modry@af.czu.cz

Emergence of Autochthonous *Leishmania* (*Mundinia*) *martiniquensis* Infections in Horses, Czech Republic and Austria, 2019–2023

David Modrý, Edmund K. Hainisch, Hans-Peter Fuehrer, Edwin Kniha, Maria Sophia Unterköfler, Jovana Sádlová, Petr Jahn, Kristína Řeháková, Kamil Sedlák, Jan Votýpka

We report 4 cases of equine cutaneous leishmaniasis caused by *Leishmania martiniquensis* in Czech Republic and Austria, outside the known endemic range of leishmaniases. The parasite should be considered as a potential cause of cutaneous lesions in horses; the risk for zoonotic transmission to immunocompromised humans is anticipated throughout central Europe.

Leishmaniasis is a relatively rare equine disease caused by several *Leishmania* spp. protozoan parasites. In Mediterranean Europe, clinical leishmaniasis in animals (mainly domestic carnivores) and humans is primarily caused by *L. infantum*. In areas endemic for *L. infantum*, sporadic cases of leishmaniosis in horses have also been reported, typically manifesting as ulcerating cutaneous nodules (*1*). During 2002–2010, cases of leishmaniosis were reported in horses (*2*) and cattle (*3*) in areas north of the Alps, which are considered nonendemic because of the low abundance of *L. infantum* vectors. Those sporadic cases were initially attributed to *L. siamensis* but were later reclassified as *L. martiniquensis* (*4*).

L. martiniquensis, a member of the subgenus *Mundinia*, is a zoonotic species originally described from a human visceral case in the Caribbean (*5*). *L. martiniquensis* parasites have wide distribution, spanning ≥3 continents, overlapping with other *Leishmania* species in many areas, including Europe (*6*). However, the full host range and epidemiology remain unclear. The distribution of cases outside the range of *Phlebotomus*/*Lutzomyia* sand flies supported by recent experimental studies and field surveys in Thailand suggest the involvement of biting midges (*Culicoides* spp., Ceratopogonidae) in transmission (*7*–*9*).

Approximately a decade after cases of *L. martiniquenis* infection were reported in Germany and Switzerland, we present 4 independent cases of cutaneous leishmaniosis in horses outside the known range of leishmaniasis in Europe. Our report includes a phylogenetic analysis of the detected isolates and results of a pilot serologic examination.

The Study

L. martiniquensis was identified in 4 sport horses during 2019–2023 (Table). Case 1 (identified in May 2019) was in a 4-year-old Akchal-Teke mare admitted to the veterinary clinic of the University of Veterinary Sciences in Brno, Czech Republic. The mare had several small nodules (3–10 mm) on the left upper eyelid; the largest was localized near the medial canthus, measuring ≈1 cm in diameter. The mare lived in north Moravia and had been imported from Ukraine 2 years previously without any obvious lesions. Equine sarcoid was suspected on the basis of clinical examination, and bovine papillomavirus type 1 was detected by PCR in the skin smear. Case 2 (identified in May

Author affiliations: Masaryk University, Brno, Czech Republic (D. Modrý); Czech University of Life Sciences, Prague, Czech Republic (D. Modrý); Biology Centre of Czech Academy of Sciences, České Budějovice, Czech Republic (D. Modrý, J. Votýpka); University of Veterinary Medicine, Vienna, Austria (E. K. Hainisch, H.-P. Fuehrer, M.S. Unterköfler); Medical University of Vienna, Vienna (E. Kniha); Charles University, Prague (J. Sádlová, J. Votýpka); University of Veterinary Sciences Brno, Brno (P. Jahn, K. Řeháková); State Veterinary Institute Prague, Prague (K. Sedlák)

DOI: https://doi.org/10.3201/eid3109.250254

Table. Overview of detected cases of autochthonous *Leishmania* (*Mundinia*) *martiniquensis* infections in horses, Czech Republic and Austria, 2019–2023*

Case no.	Geographic origin and time of first diagnostics	Lesion localization	Methods of leishmania detection
1	Olomouc district, Czech Republic, May 2019	Periorbitally above the left eye	Cytology, cultivation, ITS1 PCR
2	Pardubice district, Czech Republic, May 2021	Periorbitally under the right eye	Cytology, cultivation, ITS1 PCR
3	Styria, Graz-Umgebung district, Austria, May 2021	Lower eyelid	Cytology, histology, ITS1 and 18SrDNA PCR
4	Ústí nad Labem district, Czech Republic, Jan 2023	Periorbitally around left canthus and on conjunctiva of the left eye	Cytology, ITS1 PCR

*ITS, internal transcribed spacer.

2021) was in a 5-year-old Kladruber mare from a large stud farm that was admitted to the clinic with a group of small nodules (5–15 mm) located unilaterally on the facial area near to the lower eyelid. Case 3 was in a 5-year-old Fjord mare seen in May 2021 by veterinarians at the Equine Clinic of the Veterinary University (Vienna, Austria) with nodular lesions on the lower eyelid, chest, and udder; *Leishmania* was detected in the eyelid and udder lesions and bovine papillomavirus was detected in all 3 lesions. Case 4 was in a 12-year-old gelding living in the northwestern Czech Republic, first seen by the veterinarian in January 2023 for lesions on the left facial area. The clinical manifestation was very similar to those seen in cases 1–3. Again, the lesions were initially suspected to be sarcoid tumors, but the surface eventually exulcerated into an open wound. With supportive treatment, the lesion resolved over a period of 15 months; follow-up at 27 months showed no recurrence of lesions.

We obtained bioptic samples from cutaneous lesions using a fine needle aspiration biopsy (FNAB) for cases 1, 2, and 4 or as impression smears for case 3. We conducted routine microscopic evaluation of the FNAB material after Diff-Quick staining. Examination of the smears revealed intracytoplasmic *Leishmania* amastigotes in cells tentatively identified as neutrophiles (Figure 1). We cultured material obtained by FNAB from periorbital lesions (cases 1, 2, and 4) at 23°C on rabbit blood agar SNB-9 supplemented with fetal bovine serum, RPMI-1640, Schneider's medium, and antibiotics; we then cryopreserved a single strain. Conventional PCR targeting the *Leishmania* internal transcribed spacer 1 (*10*) performed on clinical material revealed identical sequences in all 4 cases with 100% identity to other GenBank sequences of *L. martiniquensis* worldwide but only 99.5% concordance with previous cases in Germany and Switzerland (Figure 2).

Antibodies to *Leishmania* were detected by an indirect fluorescent antibody test using glass slides coated with promastigote *L. infantum* (VMRD, https://www.vmrd.com) and antihorse IgG (whole molecule) FITC conjugate (Sigma Aldrich, https://

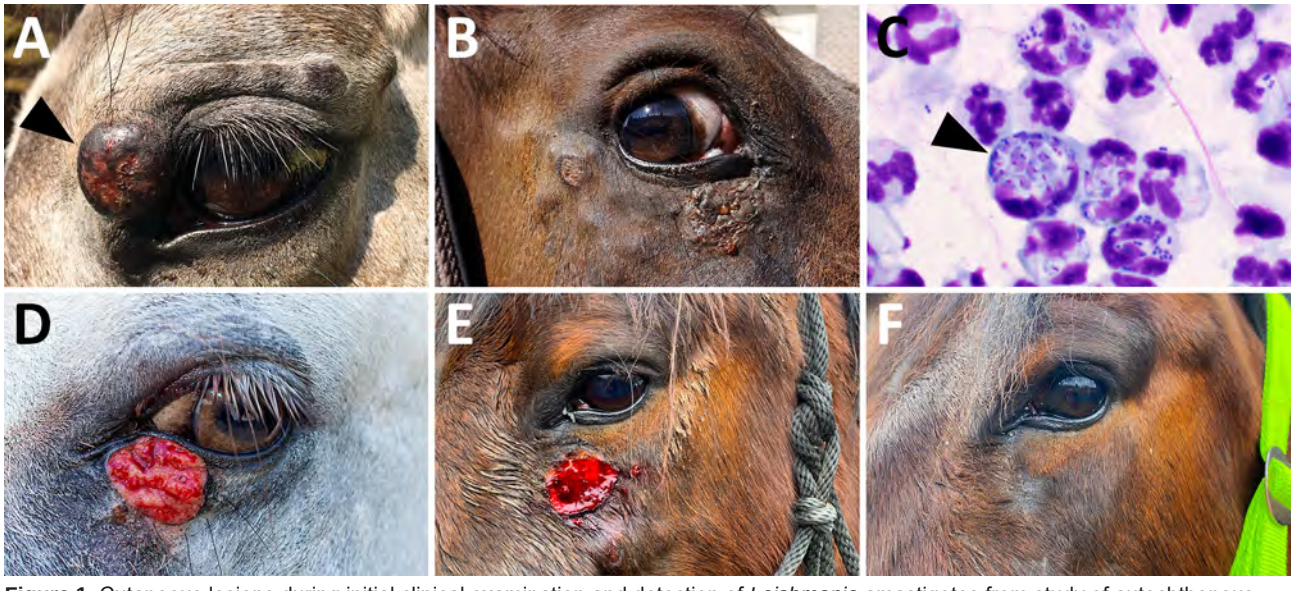

Figure 1. Cutaneous lesions during initial clinical examination and detection of *Leishmania* amastigotes from study of autochthonous *Leishmania* (*Mundinia*) *martiniquensis* infections in horses, Czech Republic and Austria, 2019–2023. A) Periorbital nodular lesions from case 1 (*L. martiniquensis* was cultured from a fine needle aspiration biopsy of the largest lesion, indicated by arrowhead); B) periorbital lesions in case 2; C) *Leishmania* amastigotes (indicated by arrowhead) in a stained smear from sample from case 1; D) lower eyelid lesion in case 3 (image by Christian Bernkopf); E) facial lesions in case 4 at the time of *Leishmania* detection; F) photograph of case 4 horse showing no recurrence 27 months later.

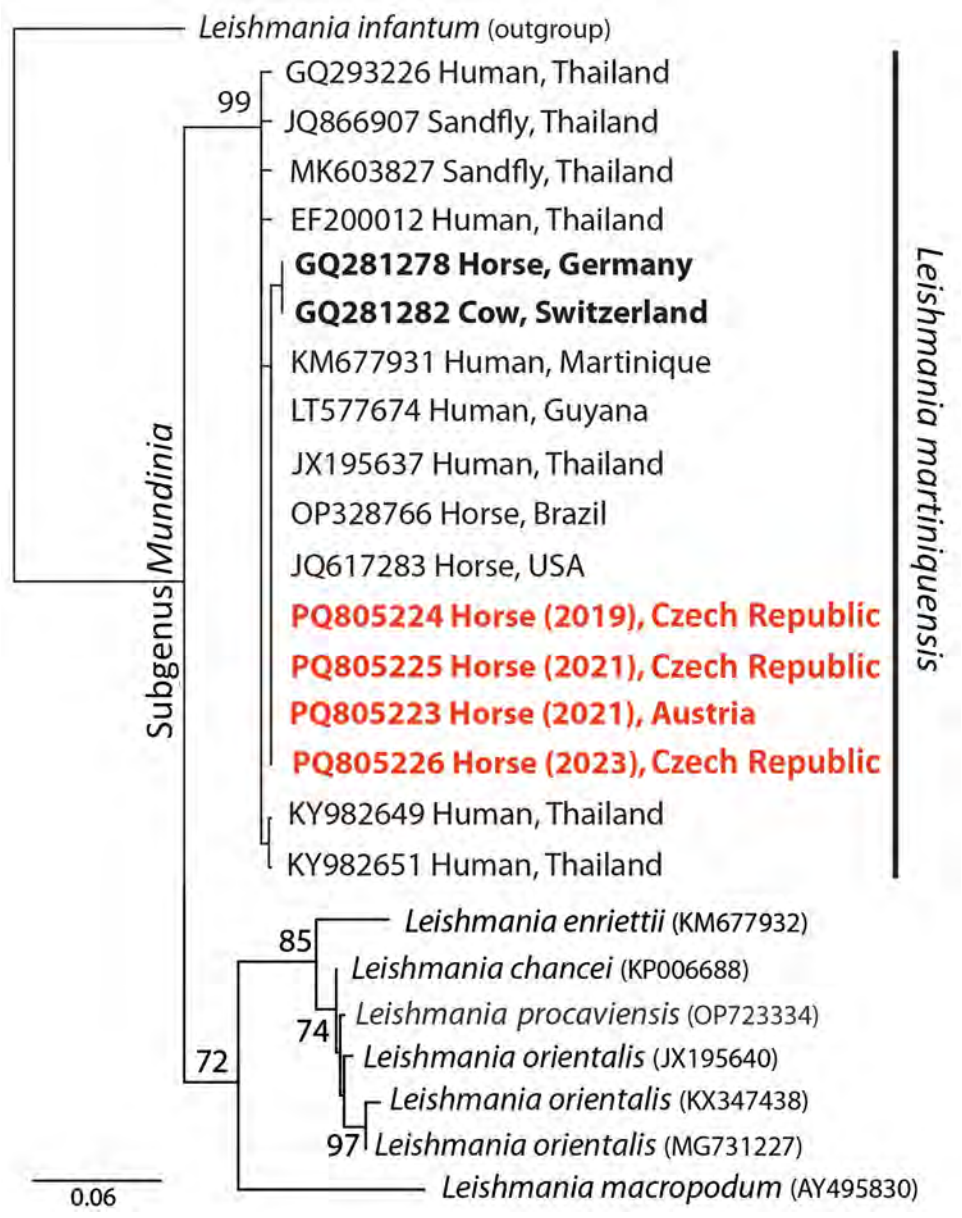

Figure 2. Phylogenetic analysis of isolates from study of autochthonous *Leishmania* (*Mundinia*) *martiniquensis* infections in horses, Czech Republic and Austria, 2019–2023. Analysis of the internal transcribed spacer 1 sequences was conducted using a maximum-likelihood tree with *L. infantum* as an outgroup; GenBank accession numbers precede the host and locality description. Red bold text indicates cases from this study. Black bold text indicates previous cases from Europe. Node support values were derived through bootstrapping with 1,000 replicates. Scale bar indicates number of nucleotide substitutions per site.

www.sigmaaldrich.com). We diluted serum samples in a 2-fold series starting with a 1:50 base dilution and used positive and negative control serum samples. We considered a titer ≥50 positive. We found antibodies to *Leishmania* at titers of 50 (cases 1, 2, and 3) and 100 (case 4).

Conclusions

We report 4 equine cases of *L. martiniquensis* infection outside the known range of the typical leishmaniasis caused by *L. infantum* in Europe, detected >12 years after the last published *L. martiniquensis* cases in Germany (*2*) and Switzerland (*3*). The cases occurred over a period of >3 years with no proven link between them and were also geographically dispersed across central Europe, suggesting that horses play a nonnegligible role as reservoir hosts throughout the range of *L. martiniquensis*. The symptomatology of *L. martiniquensis* cases in horses is strikingly uniform. In all 4 newly described cases, infection was diagnosed as cutaneous lesions near the eyes or in the facial area, resembling previous instances in which 7 of 10 cases were reported as lesions on the head (*2*,*11*,*12*).

All 4 cases were initially suspected to be sarcoid, a common skin tumor in horses caused by bovine papillomaviruses types 1, 2, and 13. Of note, in 2 cases (case 1 and 3) bovine papillomavirus types 1

and 2 were detected by PCR in lesions with *Leishmania* but also in lesions without the parasite. This association between sarcoid-like lesions and *Leishmania* infection is very suggestive. We therefore believe that the sarcoid may be attractive to blood-sucking insects (including biting midges, the potential vectors of *Mundinia*), thus opening the window for parasite infection. Additional cases of *L. martiniquensis* infection could possibly be underreported because of misdiagnosis and treatment as sarcoid or masked by a true sarcoid. Also, cases of cutaneous leishmaniosis in herbivores diagnosed in Europe should always be evaluated for the possibility of being caused by *L. martiniquensis*, even in areas in which *L. infantum* is endemic (*13*), particularly in the absence of sand flies.

The serologic response to *L. martiniquensis* remains poorly understood. A single case of cutaneous leishmaniasis in a cow revealed a robust antibody response (*3*). More recently, Carbonara et al. (*13*) reported low antibody titers in equids, including those with skin lesions or asymptomatic infections. Consistent with those observations, our findings confirm that horses with mild skin lesions exhibit only a limited antibody response. Nevertheless, serologic testing during active infection could serve as a valuable diagnostic tool.

The presence of biting midges is ubiquitous in Europe (*14*), and the equine population is in daily contact with them during active season. The occurrence of 4 independent cases of equine leishmaniosis caused by *L. martiniquensis* suggests its endemic status and circulation in Central Europe. The extent of distribution of this kinetoplastid in the equine population and other hosts in Europe remains speculative, as does its transmission biology. Given its zoonotic potential, this pathogen should be widely investigated in cases of equine skin lesions using a combination of cytology and PCR followed by sequencing. Similarly, possible *L. martiniquensis* infection should be anticipated in suspected visceral and cutaneous cases of human leishmaniasis, including patients without a history of travel to endemic areas.

Acknowledgments

We thank the field veterinarians and horse owners for their assistance in sampling and information collecting.

About the Author

Dr. Modrý is professor of infectious diseases of the Faculty of Science of Masaryk University in Brno and in the Department of Veterinary Sciences of the Czech University for Life Science in Prague. His interests revolve around the transmission of infectious diseases at the livestock–wildlife–humans interface, parasites as a part of biological invasions, One Health, and conservation medicine.

References

1. Gama A, Elias J, Ribeiro AJ, Alegria N, Schallig HD, Silva F, et al. Cutaneous leishmaniosis in a horse from northern Portugal. Vet Parasitol. 2014;200:189–92. https://doi.org/10.1016/j.vetpar.2013.12.005
2. Müller N, Welle M, Lobsiger L, Stoffel MH, Boghenbor KK, Hilbe M, et al. Occurrence of *Leishmania* sp. in cutaneous lesions of horses in Central Europe. Vet Parasitol. 2009; 166:346–51. https://doi.org/10.1016/j.vetpar.2009.09.001
3. Lobsiger L, Müller N, Schweizer T, Frey CF, Wiederkehr D, Zumkehr B, et al. An autochthonous case of cutaneous bovine leishmaniasis in Switzerland. Vet Parasitol. 2010;169:408–14. https://doi.org/10.1016/j.vetpar.2010.01.022
4. Sereno D. *Leishmania* (*Mundinia*) spp.: from description to emergence as new human and animal *Leishmania* pathogens. New Microbes New Infect. 2019;30:100540. https://doi.org/10.1016/j.nmni.2019.100540
5. Desbois N, Pratlong F, Quist D, Dedet JP. *Leishmania* (*Leishmania*) *martiniquensis* n. sp. (Kinetoplastida: Trypanosomatidae), description of the parasite responsible for cutaneous leishmaniasis in Martinique Island (French West Indies). Parasite. 2014;21:12. https://doi.org/10.1051/parasite/2014011
6. Kniha E, Aspöck H, Auer H, Walochnik J. *Leishmania* infections and *Leishmania* species in central Europe. Wien Tierärztl Monat–Vet Med Austria. 2023;110.
7. Bečvář T, Vojtková B, Siriyasatien P, Votýpka J, Modrý D, Jahn P, et al. Experimental transmission of *Leishmania* (*Mundinia*) parasites by biting midges (Diptera: Ceratopogonidae). PLoS Pathog. 2021;17:e1009654. https://doi.org/10.1371/journal.ppat.1009654
8. Kaewmee S, Mano C, Phanitchakun T, Ampol R, Yasanga T, Pattanawong U, et al. Natural infection with *Leishmania* (*Mundinia*) *martiniquensis* supports *Culicoides peregrinus* (Diptera: Ceratopogonidae) as a potential vector of leishmaniasis and characterization of a *Crithidia* sp. isolated from the midges. Front Microbiol. 2023;14:1235254. https://doi.org/10.3389/fmicb.2023.1235254
9. Sunantaraporn S, Thepparat A, Phumee A, Sor-Suwan S, Boonserm R, Bellis G, et al. *Culicoides* Latreille (Diptera: Ceratopogonidae) as potential vectors for *Leishmania martiniquensis* and *Trypanosoma* sp. in northern Thailand. PLoS Negl Trop Dis. 2021;15:e0010014. https://doi.org/10.1371/journal.pntd.0010014
10. Schönian G, Nasereddin A, Dinse N, Schweynoch C, Schallig HDFH, Presber W, et al. PCR diagnosis and characterization of *Leishmania* in local and imported clinical samples. Diagn Microbiol Infect Dis. 2003;47:349–58. https://doi.org/10.1016/S0732-8893(03)00093-2
11. Reuss SM, Dunbar MD, Calderwood Mays MB, Owen JL, Mallicote MF, Archer LL, et al. Autochthonous *Leishmania siamensis* in horse, Florida, USA. Emerg Infect Dis. 2012;18:1545–7. https://doi.org/10.3201/eid1809.120184
12. Mendes AAV Junior, Filgueira CPB, Miranda LFC, de Almeida AB, Cantanhêde LM, Fagundes A, et al. First report of *Leishmania* (*Mundinia*) *martiniquensis* in South American territory and confirmation of *Leishbunyavirus* infecting this parasite in a mare. Mem Inst Oswaldo Cruz. 2023;118:e220220. https://doi.org/10.1590/0074-02760220220

13. Carbonara M, Mendoza-Roldan JA, Bezerra-Santos MA, de Abreu Teles PP, Lia RP, Locantore F, et al. *Leishmania* spp. in equids and their potential vectors in endemic areas of canine leishmaniasis. PLoS Negl Trop Dis. 2024;18:e0012290. https://doi.org/10.1371/journal.pntd.0012290
14. Cuéllar AC, Kjær LJ, Baum A, Stockmarr A, Skovgard H, Nielsen SA, et al. Modelling the monthly abundance of *Culicoides* biting midges in nine European countries using Random Forests machine learning. Parasit Vectors. 2020;13:194. https://doi.org/10.1186/s13071-020-04053-x

Address for correspondence: David Modrý, Department of Veterinary Sciences, Faculty of Agrobiology, Food and Natural Resources, Czech University of Life Sciences Prague, Kamýcká 129, 165 21 Prague, Czech Republic; email: modry@af.czu.cz

Imported Malaria and Congenital Acquisition in Infant, Portugal, 2024

Inês Lopes, Joana Dias, Edvaldo Das Neves, Maria Morais, Ana Santos-Reis, Ana M. Garcia, Luis Varandas,[1] Dinora Lopes[1]

Plasmodium falciparum infection was diagnosed in a 3-month-old baby in Portugal by optical microscopy. The mother had had malaria in Angola 13 months earlier, before she emigrated to Portugal. She remained asymptomatic throughout and after pregnancy. We confirmed the diagnosis of an imported malaria case and congenital transmission using molecular techniques.

Imported malaria cases in Europe from sub-Saharan Africa countries can manifest with very low parasite densities and asymptomatic infections. Those infections can pose a public health threat, given the potential for onward transmission in areas with competent vectors and suitable conditions (*1*–*3*).

Congenital malaria in infants is rare because the placenta acts as an effective barrier preventing the transfer of malaria parasites from maternal to fetal circulatory system; transmission during labor is the most likely mechanism (*4*). Ultrasensitive molecular diagnostic tools detect infections in settings with low parasite density (*5*,*6*). Congenital malaria is not universally defined. Some authors define it as the presence of asexual forms of malaria parasites in an infant's cord blood or peripheral blood during the first week of life, regardless of clinical symptoms (*4*,*7*). Others require the presence of parasites in the newborn's peripheral blood on the first day of life for diagnosis (*4*,*7*). However, a timely diagnosis can be missed if a patient has no suggestive symptoms or clinical or travel history that prompt an early assessment. We report *Plasmodium falciparum* infection in a 3-month-old baby in Portugal.

Author affiliations: Global Health and Tropical Medicine, Associate Laboratory in Translation and Innovation Towards Global Health, Instituto de Higiene e Medicina Tropical, Universidade NOVA de Lisboa, Lisbon, Portugal (I. Lopes, E. Das Neves, A. Santos-Reis, L. Varandas, D. Lopes); Unidade Local de Saúde São José, Lisbon (J. Dias); Hospital of Vila Franca de Xira, Vila Franca de Xira, Portugal (M. Morais); Unidade Local de Saúde São José EPE Centro de Investigação, Lisbon (A.M. Garcia, L. Varandas)

DOI: https://doi.org/10.3201/eid3109.250536

The Study

A 3-month-old female infant was brought to a pediatric emergency department of Vila Franca de Xira Hospital (Vila Franca Xira, Portugal) with a 2-day history of fever and splenomegaly; maximum axillary temperature was 38.6°C. Initial laboratory tests revealed a hemoglobin level of 10.9 g/dL (reference threshold is 11.0 g/L for children 6–59 months of age), a leukocyte count of 10,500/mm^3 (2,040/mm^3 neutrophils and 5,970/mm^3 lymphocytes) (reference ranges 7,300–16,600/mm^3 for leukocytes, 1,500–6,900/mm^3 for neutrophils, and 3,400–9,400/mm^3 for lymphocytes), platelet count of 66,000/mm^3 (reference range 180,000–440,000/mm^3), and C-reactive protein level of 53.4 mg/L (reference range <10 mg/L). A peripheral blood smear revealed *P. falciparum* trophozoites; parasite count was estimated at 4.6%. Further investigation of family history revealed that the infant was born via cesarean delivery; infant and mother were discharged from hospital without any concerns. The infant had no history of traveling abroad, but her mother had moved to Portugal from Angola 13 months earlier. The mother had received artemether/lumefantrine treatment for *P. falciparum* infection in Angola 1 week before relocating to Portugal.

Because our findings were consistent with a suspected case of congenital malaria, we obtained samples from the mother and infant for molecular testing. We collected samples from the infant, with written consent from her mother, from the neonatal Guthrie card with blood collected via heel prick at the fourth day of life, during initial hospital admission, and at a

[1]These authors contributed equally to this article.

Table 1. PCR amplification of *Plasmodium* spp. in study of malaria in mother and infant, Portugal*

Target	Primers	Assay type	Amplification conditions
18ssrRNA			
Plasmodium sp.	1st PCR reaction: rPLU forward primer, 5′-CTTGTTGTTGCCTTAAACTTC-3′; rPLU reverse primer, 5′-TTAAAATTGTTGCAGTTAAAACG-3′	Nested PCR	1× PCR master mix,† T1 Thermocycler–Biometic: 1 cycle, 95°C, 3 min); 30 cycles, 94°C, 1 min; 58°C, 1 min; 72°C, 1 min
P. falciparum	Nested PCR: Pf forward primer, 5′-TTAAACTGGTTTGGGAAAACCAAATATATT-3′; Pf reverse primer, 5′-ACACAATGAACTCAATCATGACTACCCGTC-3′ (Singh et al. [*8*])		1× PCR master mix,† 1 cycle, 95°C, 3 min; 35 cycles, 94°C, 1 min; 58°C, 1 min; 72°C, 1 min
*var*ATS	Forward primer, 5′-CCCATACACAACCAAYTGGA-3′; reverse primer, 5′-TTCGCACATATCTCTATGTCTATCT-3′; probe, 5′-6-FAM-TRTTCCATAAATGGT-NFQ-MGB-3′ (Hofmann et al. [*6*])	qPCR	1× TaqMan Gene Expression Mastermix,† 0.8 μM of each primer, 0.4 μM of probe; CFX96 Real-Time PCR Detection System‡: 1 cycle, 50°C, 2 min; 95°C 10 min; 45 cycles, 95°C, 15 sec; 55°C, 1 min
		dPCR	5x Absolute Q DNA Digital PCR Mastermix;§ Absolute Q Digital PCR§: 1 cycle, 50°C, 2 min; 95°C 10 min; 45 cycles, 95°C, 15 sec; 55°C, 1 min

*dPCR, digital PCR; qPCR, quantitative PCR.
†Thermo Fisher Scientific, https://www.thermofisher.com.
‡Bio-Rad Laboratories, https://www.bio-rad.com.
§Thermo Fisher, https://www.thermofisher.com.

follow-up appointment, at which we also took a sample from the mother. Maternal thick and thin blood smears did not reveal any malarial parasites; a rapid diagnostic test for malaria returned negative results.

We performed total DNA extraction using a QIAamp DNA Mini Kit (QIAGEN, http://www.qiagen.com) on dried blood spots on Whatman filter paper. We tested samples by endpoint nested PCR, as described by Singh (*8*). We performed molecular assays (Table 1) to assess parasite density, using standard curves prepared with 10-fold dilutions of DNA obtained from the *P. falciparum* 3D7 clone; result range was 10^4 to 10^{-1} parasites/μL (Figure 1). We applied high-sensitivity quantitative PCR (qPCR) targeting the multicopy telomeric *var* genes to estimate the densities of the parasite. We performed digital PCR to confirm and compare results (Figure 2) (*5*).

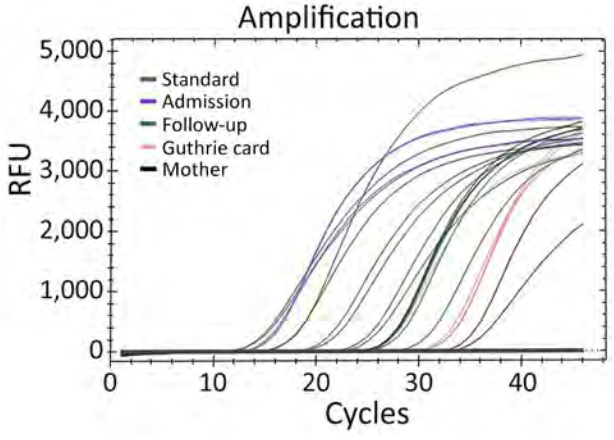

Figure 1. Quantitative PCR amplification of samples from infant and mother in study of congenital malaria, Portugal. We obtained results from arithmetic average values of triplicate results. Additional curves represent standard results obtained by serial dilution to determine parasite quantification. Results were 0.07 parasites/μL from infant's Guthrie card sample 4 days after birth; 1,178.13 parasites/μL from sample taken at hospital admission; 21.99 parasites/μL from sample taken at follow-up appointment; 0.03 parasites/μL from sample taken from the mother at follow-up appointment. RFU, relative fluorescence unit.

Conclusions

This case highlights 2 key aspects for a better understanding of *P. falciparum* transmission: the role of imported, low-density asymptomatic cases as reservoirs and their potential contribution to congenital transmission. In Europe, ≈8,000 cases of imported malaria are reported annually (*2*); imported cases are mainly *P. falciparum* infections. Those populations can become a parasite reservoir that can pose significant risk to public health. Migrants may also display mild symptoms or be asymptomatic, often with submicroscopic parasitemia (*2*), which may be attributed to immunity acquired while residing in malaria-endemic regions (*9*). Such low levels of parasitemia can only be detected through sensitive molecular methods (*10*), such as qPCR-based techniques; we obtained the positive test result from this patient by nested PCR in the sample taken at hospital admission, when she was experiencing symptoms and parasitemia. In Portugal, there are potentially malaria-receptive areas and also a vector with some degree of competence (*3*).

In non–malaria-endemic settings, availability of diagnostic tools varies by healthcare setting (Table 2). Nevertheless, clinicians should recognize the likelihood of congenital malaria and refer blood samples from suspected cases for testing.

var genes are known for their role in antigenic variation, enabling *P. falciparum* to evade the host immune response. The high copy number of *var* genes can enhance the sensitivity of detection methods. For instance, the use of multicopy subtelomeric targets has been shown to improve the detection of low-density infections that might otherwise be missed using standard assays such as *18ssRNA* PCR (*6*). In our study, we established an accurate diagnosis for the mother through *pfvarATS* qPCR, which detected 0.03 parasites/µL, and digital PCR (dPCR), which detected 0.5 parasites/µL. Without the mother's diagnosis, the child's infection would have likely gone undetected and untreated. We have not established whether transmission to the infant was transplacental or from direct contact with maternal blood during labor. In most pregnancies resulting in congenital malaria, the mother's infection tends to be symptomatic (*11*); malaria can also be diagnosed after uncomplicated asymptomatic pregnancies (*11*).

For our study, we defined congenital malaria as outlined in Oluput-Oluput (*12*) as the direct infection of an infant with malaria parasites from the mother before or during birth. Although all clinical indicators were consistent with congenital malaria, we pursued confirmation by detecting and quantifying parasite DNA in the Guthrie card sample taken on day 4 after birth. Both qPCR and dPCR confirmed the presence of *P. falciparum* parasites in the infant's peripheral blood, with very low parasite densities (0.07 parasites/µL by qPCR and 0.49 parasites/µL by dPCR). Those findings align with the parasitemia levels observed in the mother, further supporting the likelihood of vertical transmission.

The delayed onset of symptoms in the infant can be attributed to several factors: the transfer of maternal antibodies through transplacental transfer and breastfeeding (*13*), low iron levels, and reduced erythropoiesis in newborns that do not favor *Plasmodium* spp. growth (*14*). Parasitemia might increase as maternal antibodies decline (*15*). In this case, the onset of symptoms occurred later than the previously reported median age, making the diagnosis more challenging (*7*). Furthermore, the nonspecific clinical signs of congenital malaria can be difficult to distinguish from other causes of sepsis (*4*). Our study highlights the importance of considering congenital malaria in the differential diagnosis of febrile infants born to mothers who have lived in malaria-endemic areas (*7*). We also emphasize the need for thorough analysis of blood smears in sepsis cases, particularly when thrombocytopenia is present (*12*).

In conclusion, this case underscores the utility of ultrasensitive detection targets and methods such as *pfvartATS* qPCR and dPCR for detecting submicroscopic malaria infections, particularly in asymptomatic migrant populations or populations at higher risk such as pregnant women and infants. Our findings emphasize the public health risk of overlooking hidden parasite reservoirs, which could hinder effective malaria control and prevention efforts in vulnerable groups.

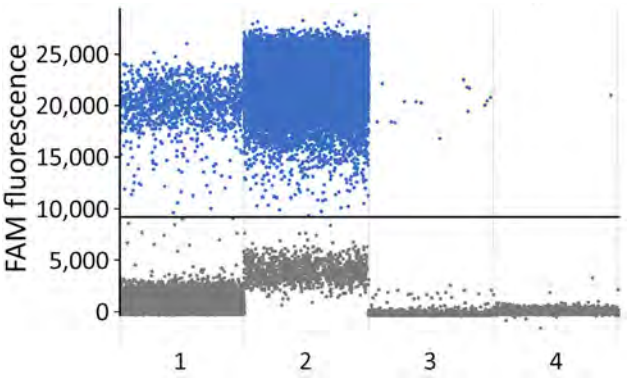

Figure 2. Digital PCR results from samples from infant and mother in study of congenital malaria, Portugal. We obtained results from arithmetic average values (parasite/µL) of triplicate results. Results indicate the number of positive droplets in each sample: 1, taken from infant's Guthrie card on day 4 after birth, 0.49 parasites/µL; 2, taken from infant at hospital admission, 30,000 parasites/µL; 3, taken from infant at follow-up appointment, 599.8 parasites/µL; and 4, taken from mother at follow-up, 0.5 parasites/µL. FAM, fluorescein amidite.

Table 2. Diagnostic tools for *Plasmodium falciparum* detection in study of malaria in mother and infant, Portugal*

Diagnostic method	Limit of detection, parasites/µL	Level of care	Observations
Microscopy, thick smear	50–100	Secondary	Operator-dependent; limited sensitivity for low-density parasitemia
Rapid diagnostic test	100–200	Primary	Limited sensitivity for low-density parasitemia
Nested PCR, 18S rRNA target	1–5	Secondary/tertiary	Moderate sensitivity but may still miss low-density infections in neonates and mothers
qPCR, pfvarATS target	0.03	Tertiary	Multicopy gene enhances detection
dPCR pfvarATS target	≤0.01	Tertiary	Highest sensitivity, suitable for confirmatory diagnosis

*Sources: Dong et al. (*5*); Hofmann et al. (*6*); Singh et al. (*8*). dPCR, digital PCR; qPCR, quantitative PCR.

Acknowledgments

We thank the patient's mother for consenting to the publication of these results. We thank Rui Batista, Gonçalo Carvalho, and Sara Mateus for their invaluable technical support during the digital PCR experiments and analysis workflow.

Fundação para a Ciência e a Tecnologia supported this work (GHTM—UID/04413/2020 and LA-REAL–LA/P/0117/2020).

About the Author

Dr. Lopes is a senior technician at the Global Health and Tropical Medicine Research Centre, Instituto de Higiene e Medicina Tropical, NOVA University Lisbon. Her primary research and teaching interests are malaria and other neglected tropical diseases, focusing on development and capacity-building in tropical disease diagnostics and public health, mainly in Portuguese-speaking countries in Africa.

References

1. Corbacho-Loarte MD, Crespillo-Andújar C, Chamorro-Tojeiro S, Norman F, Pérez-Molina JA, Martín O, et al. Screening of imported malaria infection in asymptomatic migrants from sub-Saharan Africa: a retrospective analysis of a 2010–2019 cohort. Travel Med Infect Dis. 2022;49:102411. https://doi.org/10.1016/j.tmaid.2022.102411
2. Pousibet-Puerto J, Lozano-Serrano AB, Soriano-Pérez MJ, Vázquez-Villegas J, Giménez-López MJ, Cabeza-Barrera MI, et al. Migration-associated malaria from Africa in southern Spain. Parasit Vectors. 2021;14:240. https://doi.org/10.1186/s13071-021-04727-0
3. Gomes E, Capinha C, Rocha J, Sousa C. Mapping risk of malaria transmission in mainland Portugal using a mathematical modelling approach. PLoS One. 2016;11:e0164788. https://doi.org/10.1371/journal.pone.0164788
4. Bilal JA, Malik EE, Al-Nafeesah A, Adam I. Global prevalence of congenital malaria: a systematic review and meta-analysis. Eur J Obstet Gynecol Reprod Biol. 2020;252:534–42. https://doi.org/10.1016/j.ejogrb.2020.06.025
5. Dong L, Li W, Xu Q, Gu J, Kang Z, Chen J, et al. A rapid multiplex assay of human malaria parasites by digital PCR. Clin Chim Acta. 2023;539:70–8. https://doi.org/10.1016/j.cca.2022.12.001
6. Hofmann N, Mwingira F, Shekalaghe S, Robinson LJ, Mueller I, Felger I. Ultra-sensitive detection of *Plasmodium falciparum* by amplification of multi-copy subtelomeric targets. PLoS Med. 2015;12:e1001788. https://doi.org/10.1371/journal.pmed.1001788
7. Prior AR, Prata F, Mouzinho A, Marques JG. Congenital malaria in a European country. BMJ Case Rep. 2012;2012:bcr2012007310. https://doi.org/10.1136/bcr-2012-007310
8. Singh B, Bobogare A, Cox-Singh J, Snounou G, Abdullah MS, Rahman HA. A genus- and species-specific nested polymerase chain reaction malaria detection assay for epidemiologic studies. Am J Trop Med Hyg. 1999;60:687–92. https://doi.org/10.4269/ajtmh.1999.60.687
9. Cirera L, Sacoor C, Meremikwu M, Ranaivo L, Manun'Ebo MF, Arikpo D, et al. The economic costs of malaria in pregnancy: evidence from four sub-Saharan countries. Gates Open Res. 2023;7:47. https://doi.org/10.12688/gatesopenres.14375.2
10. Omer S, Khalil E, Ali H, Sharief A. Submicroscopic and multiple *plasmodium falciparum* infections in pregnant Sudanese women. N Am J Med Sci. 2011;3:137–41. https://doi.org/10.4297/najms.2011.3137
11. Morven S. Edwards. Fungal and protozoal infections. In: Fanaroff AA, Martin RJ, editors. Neonatal-perinatal medicine: diseases of the fetus and infant. 7th ed. St. Louis: Mosby; 2002. p. 751–752.
12. Olupot-Olupot P, Eregu EIE, Naizuli K, Ikiror J, Acom L, Burgoine K. Neonatal and congenital malaria: a case series in malaria endemic eastern Uganda. Malar J. 2018;17:171. https://doi.org/10.1186/s12936-018-2327-0
13. Natama HM, Moncunill G, Vidal M, Rouamba T, Aguilar R, Santano R, et al. Associations between prenatal malaria exposure, maternal antibodies at birth, and malaria susceptibility during the first year of life in Burkina Faso. Infect Immun. 2023;91:e0026823. https://doi.org/10.1128/iai.00268-23
14. Severe malaria. Trop Med Int Health. 2014;19:7–131. https://doi.org/10.1111/tmi.12313_2
15. Stassijns J, Van den Boogaard W, Pannus P, Nkunzimana A, Rosanas-Urgell A. Prevalence and diagnostics of congenital malaria in rural Burundi, a cross-sectional study. Malar J. 2016:15;443–6. https://doi.org/10.1186/s12936-016-1478-0

Address for correspondence: Dinora Lopes, Universidade Nova de Lisboa, Instituto de Higiene e Medicina Tropical, UEI Tropical Clinic, Science and Community Support Service (SACC), Rua da Junqueira, 100 Lisbon, Lisbon 1349 008 Portugal; email: dinora.lopes@ihmt.unl.pt

Apicoplast [ā’-pik-ō-plast]

Hari Shankar, Michal Shahar, Anat Florentin

The apicoplast is a unique organelle found in obligatory unicellular parasites called Apicomplexa due to a distinguished complex in their apex (top). The phylum Apicomplexa includes human pathogens, such as *Plasmodium* spp. that cause malaria and *Toxoplasma* spp. that cause toxoplasmosis, and prevalent veterinary parasites, such as *Babesia* and *Eimeria* spp.

The apicoplast was first identified in *Toxoplasma* parasites as a relict nonphotosynthetic chloroplast, a plastid, which is a term derived from the Greek *plastos*, meaning molded. The biological, evolutionary, and clinical consequences of that discovery were immediately apparent, and it was given the name apicoplast, a fusion of Apicomplexa and plastid. The name hints at the organelle’s unique evolutionary past. It was formed via secondary endosymbiosis, in which a unicellular protist engulfed another unicellular red alga and its chloroplast. Most Apicomplexan parasites retained that endosymbiont for metabolic purposes but lost all photosynthetic abilities. Few, like the genera of *Cryptosporidium*, lost the entire organelle. Of note, certain nonparasitic organisms related to Apicomplexa, like *Chromera*, still live as marine phototrophs, due to their photosynthetic plastid.

Regardless of photosynthesis, these plastids share similar metabolic pathways, have a small circular remnant genome, and are engulfed by no less than 4 distinct membranes (Figure). Perhaps more than anything, these membranes tell the evolutionary story of the apicoplast; much like a Russian Matryoshka doll, one organism is nested within another.

This work was supported by the Israel Science Foundation (ISF) under The Joint Canada-Israel Health Research Program (grant No. 3000/22 to A.F.). A.F. is supported by The Abisch-Frenkel Faculty Development Lectureship.

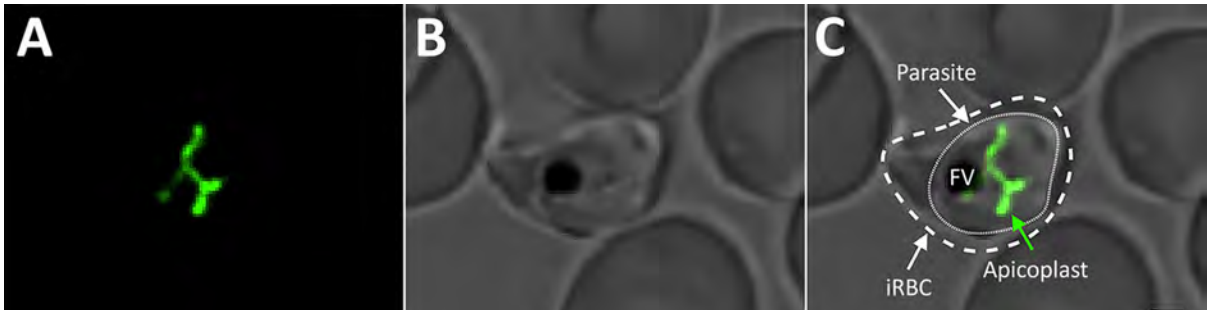

Figure. Visualization of the apicoplast organelle inside a malaria parasite. Microscopy image of a *Plasmodium falciparum* transgenic parasite expressing a green fluorescent protein (GFP) fused to a transit peptide, which marks the apicoplast. A) Apicoplast visualized through targeted GFP; B) bright field showing *P. falciparum* parasite in human RBC; C) merged image of GFP and bright field. Outer dashed line depicts the membrane of the iRBC. Inner dashed line depicts the cell membrane of the intraerythrocytic parasite. The intricate green structure is the apicoplast in its elongated phase during the last hours of the intraerythrocytic cell cycle. FV appears as a black sac-like structure. Image taken using a confocal microscope; scale bar indicates 1.25 μm. FV, food vacuole; iRBC, infected red blood cell.

Sources

1. Fichera ME, Roos DS. A plastid organelle as a drug target in apicomplexan parasites. Nature. 1997;390:407–9. https://doi.org/10.1038/37132
2. Janouškovec J, Horák A, Oborník M, Lukes J, Keeling PJ. A common red algal origin of the apicomplexan, dinoflagellate, and heterokont plastids. Proc Natl Acad Sci U S A. 2010;107:10949–54. https://doi.org/10.1073/pnas.1003335107
3. Köhler S, Delwiche CF, Denny PW, Tilney LG, Webster P, Wilson RJ, et al. A plastid of probable green algal origin in Apicomplexan parasites. Science. 1997;275:1485–9. https://doi.org/10.1126/science.275.5305.1485
4. McFadden GI, Reith ME, Munholland J, Lang-Unnasch N. Plastid in human parasites. Nature. 1996;381:482. https://doi.org/10.1038/381482a0
5. Wilson RJ, Denny PW, Preiser PR, Rangachari K, Roberts K, Roy A, et al. Complete gene map of the plastid-like DNA of the malaria parasite *Plasmodium falciparum*. J Mol Biol. 1996;261:155–72. https://doi.org/10.1006/jmbi.1996.0449

Author affiliations: Indian Council of Medical Research, New Delhi, India (H. Shankar); The Kuvin Center for the Study of Infectious and Tropical Diseases and Department of Microbiology and Molecular Genetics, Faculty of Medicine, The Hebrew University of Jerusalem, Jerusalem, Israel (H. Shankar, M. Sahar, A. Florentin)

Address for correspondence: Anat Florentin, The Kuvin Center for the Study of Infectious and Tropical Diseases, Department of Microbiology and Molecular Genetics, Faculty of Medicine, The Hebrew University of Jerusalem, PO Box 12271, Jerusalem 91120, Israel; email: anat.florentin@mail.huji.ac.il

DOI: https://doi.org/10.3201/eid3109.241446

Monkeypox Virus Clade IIa Infections, Liberia, 2023–2024

Dougbeh Chris Nyan,[1] Irina Maljkovic Berry,[1] Bode I. Shobayo, Monika Mehta, Gabriella Worwa, Shawn Hirsch, Sarah E. Klim, Fahn Taweh, Kalilu S. Donzo, B.M. Freeman, Alberta B. Corvah, Francis Jaryan, Julius S.M. Gilayeneh, Ian Crozier, Courtney Renken, Laura McNay, J. Soka Moses, Jens H. Kuhn, Lisa E. Hensley, Sara E. Zufan

Author affiliations: National Public Health Institute of Liberia, Monrovia, Liberia (D.C. Nyan, B.I. Shobayo, F. Taweh, K.S. Donzo, B.M. Freeman, A.B. Corvah, F. Jaryan, J.S.M. Gilayeneh, J.S. Moses); National Institutes of Health, Frederick, Maryland, USA (I. Maljkovic Berry, M. Mehta, G. Worwa, S. Hirsch, S.E. Klim, J.H. Kuhn, S.E. Zufan); Clinical Monitoring Research Program Directorate, Frederick National Laboratory for Cancer Research, Frederick (I. Crozier); National Institutes of Health, Bethesda, Maryland, USA (C. Renken, L. McNay); US Department of Agriculture, Manhattan, Kansas, USA (L.E. Hensley)

DOI: https://doi.org/10.3201/eid3109.250271

We performed monkeypox virus genome sequencing on clinical samples from Liberia, yielding 5 clade IIa genomes. Our analysis found no evidence of sustained human-to-human transmission, suggesting independent zoonotic spillovers from a diverse viral lineage. Public health officials should continue monitoring and sequencing efforts to identify emerging monkeypox virus lineages.

Monkeypox virus (MPXV; Poxviridae: *Orthopoxvirus monkeypox*) isolates cluster into 2 major clades, I and II, and each has subclades a and b (*1*,*2*). Clades Ia and IIa, primarily circulating in Equatorial Africa, generally cause zoonotic spillovers, whereas specific lineages of clades Ib and IIb from the 2024 outbreak in Central Africa have been associated with sustained human-to-human transmission (*3*,*4*). Clade I typically causes more severe disease and higher case-fatality rates than clade II, and the 2024 outbreaks in Democratic Republic of the Congo showed lower case-fatality rates for clade Ia and less-severe clade Ib infections (*5*). Those clade Ib–driven outbreaks nonetheless include severe cases, underscoring the need to elucidate genetic determinants of virulence within and between MPXV lineages.

During December 2023–August 2024, we collected 41 clinical samples (lesion swabs, crusts, whole blood, and serum) from 21 persons in Liberia suspected to have mpox. We recorded epidemiologic and clinical data on a standardized form based on the Integrated Disease Surveillance and Response Technical Guidelines (https://www.who.int/publications/i/item/WHO-AF-WHE-CPI-05-2019#:~:text=The%20third%20edition%20of%20the%20Integrated%20Disease%20Surveillance,and%20the%20U.S.%20Agency%20for%20International%20Development%20%28USAID%29). In August 2024, an mpox outbreak caused by clade Ib MPXV was declared a public health emergency of international concern (*6*), whereas clade IIb continued to circulate globally. Diagnostic testing at the National Public Health Institute of Liberia National Reference Laboratory (https://nphil.gov.lr) used an MPXV real-time PCR (Liferiver Bio-Tech Corp., http://www.liferiverbiotech.com) for initial virus detection and confirmation (Table) (*7*).

To determine which MPXV clades were circulating in Liberia, the National Public Health Institute of Liberia partnered with the Integrated Research Facility at Fort Detrick (IRF-Frederick) to perform genomic sequencing. That collaboration aimed to identify previously undetected MPXV strains and possible co-infections to inform public health measures and clinical management.

We transferred 41 inactivated specimens from 21 patients to IRF-Frederick, which extracted nucleic acids by using a MagMAX Viral/Pathogen Nucleic Acid Isolation Kit (Thermo Fisher Scientific, https://www.thermofisher.com) on a KingFisher Flex system (Thermo Fisher Scientific). We prepared sequencing libraries by using the DNA Prep with Enrichment kit with 10- to 49-ng input (Illumina, https://www.illumina.com) and enriched the libraries by using the Comprehensive Viral Research Panel (Twist Biosciences, https://www.twistbioscience.com). We prepared the libraries by using unique dual indices (IDT for Illumina UDIs, Set A; Illumina) followed by precapture pooling assembled in 6-plex with up to 500 ng per library. After capture, we pooled all libraries equimolarly and loaded the libraries on a single NextSeq 1000/2000 P1 XLEAP-SBS 300-cycle flow cell (2 × 150 bp; Illumina). This enrichment-based metagenomic sequencing approach enabled detection of MPXV and other viral DNA pathogens present in the samples.

We analyzed sequencing reads with EsViritu version 0.2.3 (https://github.com/cmmr/EsViritu) to identify viruses and quantify viral genomes. We further processed MPXV reads by using the nf-core/viralrecon pipeline version 2.6.0 (https://nf-co.re/viralrecon/2.6.0/) and aligned the reads to

[1]These first authors contributed equally to this article.

Table. Patient and sample characteristics from suspected mpox cases in monkeypox virus clade IIa infections, Liberia, 2023–2024*

Sample ID	Age, y/sex	Location	Symptom onset date	Sample collection date	Liferiver MPXV result	Liferiver MPXV (FAM) Ct
LIB-MPV24-001	22/F	Nimba	2023 Dec 28	2024 Jan 9	+	36.74
LIB-MPV24-007	5/M	Sinoe	2024 Feb 8	2024 Feb 12	+	27.92
LIB-MPV24-014	30/M	Nimba	2024 Mar 8	2024 Mar 12	+	37.06
LIB-MPV24-015	39/F	Nimba	2024 Mar 10	2024 Mar 11	+	37.56
LIB-MPV24-027	24/F	Grand Kru	2024 May 2	2024 May 6	+	37.63
LIB-MPV24-037	7/M	Nimba	2024 Jun 26	2024 Jun 4	+	34.27
LIB-MPV24-054	7/F	Sinoe	2024 Aug 20	2024 Aug 24	+	29.98
LIB-MPV24-069	2/M	Lofa	2024 Aug 27	2024 Aug 29	+	30.33
LIB-MPV24-087	27/F	Sinoe	2024 Sep 4	2024 Sep 5	+	26.44
LIB-MPV24-107	6/M	River Gee	2024 Aug 17	2024 Sep 7	+	36.8
LIB-MPV24-114	20/M	Bong	2024 Sep 3	2024 Sep 11	–	38.5
LIB-MPV24-116	16/M	Bong	2024 Sep 4	2024 Sep 11	–	Undetermined
LIB-MPV24-117	12/M	Lofa	2024 Sep 3	2024 Sep 9	–	Undetermined
LIB-MPV24-118	16/F	Grand Gedeh	2024 Aug 25	2024 Sep 10	–	Undetermined
LIB-MPV24-119	56/M	Montserrado	2024 Sep 10	2024 Sep 13	–	Undetermined
LIB-MPV24-123	29/M	Bong	2024 Sep 3	2024 Sep 14	–	Undetermined
LIB-MPV24-136	28/M	Montserrado	2024 Aug 31	2024 Sep 16	–	Undetermined
LIB-MPV24-141	23/M	Sinoe	2024 Sep 10	2024 Sep 13	–	Undetermined
LIB-MPV24-142	17/F	Grand Gedeh	2024 Aug 24	2024 Sep 14	–	Undetermined
LIB-MPV24-143	58/F	Grand Kru	2024 Aug 30	2024 Sep 13	–	Undetermined
LIB-MPV24-144	1/M	Sinoe	2024 Sep 10	2024 Sep 13	–	Undetermined

*Sample IDs in italics yielded near complete genomes (>98%), and sample IDs in bold met the threshold for detectable MPXV reads, defined as >1 read per kilobase of the MPXV reference genome per 1 million filtered reads. Of the 5 PCR-positive samples reported by the National Public Health Institute of Liberia that did not yield sequences, 3 had undetectable MPXV reads and insufficient DNA input (<10 ng), and 2 had detectable reads but lacked sufficient coverage for consensus genome generation. +, positive; –, negative; Ct, cycle threshold; FAM, fluorescein; MPXV, monkeypox virus.

a reference MPXV strain rom GenBank (accession no. KJ642613.1).

Overall, we detected MPXV DNA in 10 patients and varicella zoster virus (VZV) in 10 patients, including 2 cases of possible MPXV–VZV co-infection (Appendix Figure 1, https://wwwnc.cdc.gov/EID/article/31/9/25-0271-App1.pdf). We also detected partial genomes of Epstein-Barr virus (Herpesviridae: *Lymphocryptovirus humangamma 4*), hepatitis B virus (Hepadnaviridae: *Orthohepadnavirus hominoidei*), and torque teno mini virus 8 (Anelloviridae: *Betatorquevirus homini 8*). Detection of multiple viral pathogens, including VZV and MPXV within the same time frame, reinforces the value of broad metagenomic approaches for diagnosing lesions of unknown etiology, particularly when clinical manifestations overlap.

We assembled 5 near-complete (>98%) MPXV genomes; Nextclade (https://docs.nextstrain.org/projects/nextclade/en/stable/index.html) analysis confirmed that all belonged to clade IIa. We deposited all sequences in GenBank (accession nos. PV122071–5). To determine whether those MPXV cases arose from zoonotic spillover or ongoing human-to-human transmission, we analyzed phylogenetic relationships, mutation rates, and apolipoprotein B mRNA editing enzyme, catalytic subunit 3G (APOBEC3)–mediated editing patterns (Figure; Appendix Figure 2). Maximum-likelihood analysis and APOBEC3 ancestral reconstruction using squirrel version 1.0.11 (https://github.com/aineniamh/squirrel) showed limited APOBEC3-mediated editing (6/61 internal single-nucleotide polymorphisms [9.8%]). By contrast, clade IIb viruses from the 2022 global outbreak exhibited extensive APOBEC3-driven hypermutation (*8*).

Next, by using a fixed local clock model in BEAST version 1.10.5 (https://beast.community), we estimated a mean evolutionary rate of 1.96×10^{-6} substitutions/site/year (95% highest posterior probability 7.61×10^{-7} to 3.92×10^{-6}) for the clade IIa sequences. That rate is ≈15-fold lower than the APOBEC3-driven rates reported for 2022 clade IIb strains (*9*), further indicating that those infections reflect spillover events rather than sustained human-to-human transmission.

Finally, because MPXV diversity is largely shaped by geographic separation rather than time (*10*), the distinct phylogenetic clustering of cases from Sinoe County versus those from Nimba County (Appendix Figure 2) also supports independent zoonotic spillover events rather than a single transmission chain. However, inference is limited by the small number of available sequences.

In conclusion, this study contributes MPXV genomes from Liberia, addressing a multidecade absence of genomic data from human cases in western Africa. Continued monitoring and sequencing efforts are essential for identifying emerging virus lineages, informing targeted public health interventions, and guiding clinical management strategies to address the varied presentations associated with different MPXV clades.

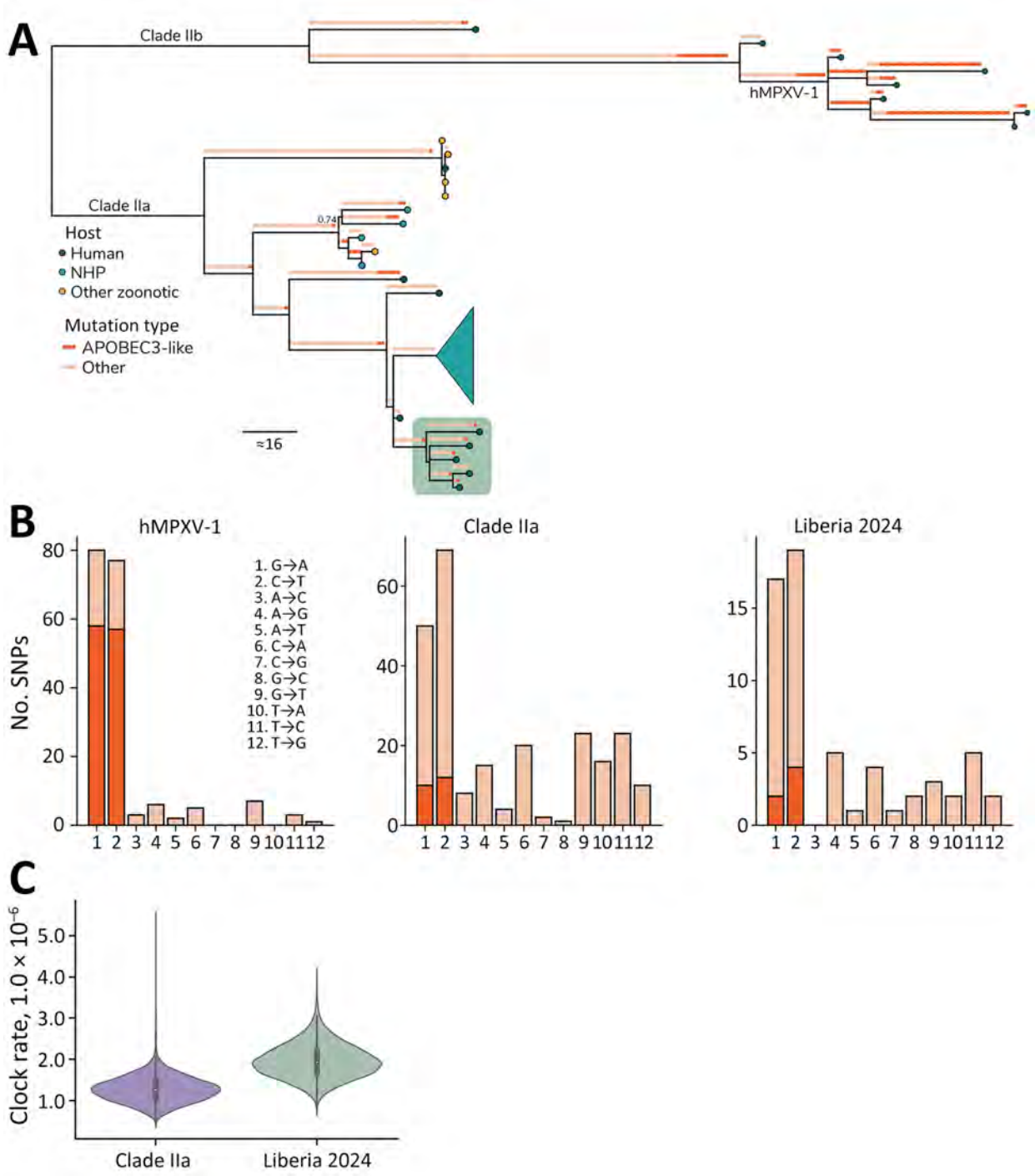

Figure. Sequencing characteristics of monkeypox virus clade IIa infections, Liberia, 2023–2024. A) Ancestral state reconstruction of the clade II phylogeny comparing the 5 new sequences against all publicly available clade IIa genomes (n = 27) and a subset of clade IIb sequences for context (n = 7), including hMPXV-1. Mutations are annotated along each branch with circles colored by whether it is an APOBEC3-like signature (TC→TT and GA→AA; dark orange) or whether it is another mutation type (light orange). Branch tips show circles colored by host (human, dark blue; NHP, turquoise; other, yellow). The sequences generated from this study are displayed in the green box. A large clade from Côte d'Ivoire NHPs is collapsed (turquoise funnel). Ultrafast bootstrap support is indicated only at nodes for which support <0.75. B) Number of APOBEC3-like SNPs of all mutations for subclade hMPXV-1, prior clade IIa sequences, and the new clade IIa found in Liberia. C) Comparison of the evolutionary clock rate of the prior clade IIa and new Liberian clade IIa sequences estimated under the local clock model. APOBEC3, apolipoprotein B mRNA editing enzyme catalytic subunit 3; hMPXV-1, sustained human monkeypox virus outbreak; NHP, nonhuman primate; SNP, single-nucleotide polymorphism.

Acknowledgments

We thank Anya Crane for critically editing the manuscript and Jiro Wada for preparing figures. We also thank the Ministry of Health Liberia County Health Teams and National Public Health Institute of Liberia research and laboratory team members for their support in collection and transport of samples, as well as support with information about the mpox cases.

This study was approved under the public health sample collection policy of the Government of Liberia and received a nonhuman subject determination by the National Institutes of Health (NIH; IRF-Frederick project no. 2024-015), as defined by National Institutes of Health Policy Manual 3014-204. This work was supported in part through a Laulima Government Solutions, LLC, prime contract with the National Institute of Allergy and Infectious Diseases (NIAID), NIH (contract no. HHSN272201800013C). I.M.B., M.M., G.W., S.H., S.E.K., and S.E.Z. performed this work as employees of Laulima Government Solutions, LLC. J.H.K. performed this work as an employee of Tunnell Government Services, a subcontractor of Laulima Government Solutions, LLC (contract no. HHSN272201800013C). This work was also supported in part with federal funds from the National Cancer Institute (NCI), NIH (contract no. 75N910D00024, task order no. 75N91019F00130). I.C. was supported by the Clinical Monitoring Research Program Directorate, Frederick National Lab for Cancer Research, sponsored by NCI. This work was also supported in part with federal funds from an Oak Ridge Institute for Science and Education (ORISE) postdoctoral research fellowship program through and agreement with NIAID. S.E.Z. also performed this work as a postdoctoral fellow under the ORISE program.

About the Author

Dr. Nyan is director-general of the National Public Health Institute of Liberia in 2024. He specializes in infectious disease diagnostics and innovation and biomedical and clinical research. Dr. Berry is employed by Laulima Government Solutions and serves as study director and the clinical studies support team lead at the National Institutes of Health, National Institute of Allergies and Infectious Diseases, Division of Clinical Research, Biosafety Level 4 facility, the integrated research facility at Fort Detrick, Frederick, Maryland, USA. Her research interests include evaluation of medical countermeasures, outbreak response and surveillance initiatives, and high-consequence and emerging or reemerging pathogens in high- and low-resource settings.

References

1. Happi C, Adetifa I, Mbala P, Njouom R, Nakoune E, Happi A, et al. Urgent need for a non-discriminatory and non-stigmatizing nomenclature for monkeypox virus. PLoS Biol. 2022;20:e3001769. https://doi.org/10.1371/journal.pbio.3001769
2. Likos AM, Sammons SA, Olson VA, Frace AM, Li Y, Olsen-Rasmussen M, et al. A tale of two clades: monkeypox viruses. J Gen Virol. 2005;86:2661–72. https://doi.org/10.1099/vir.0.81215-0
3. Masirika LM, Udahemuka JC, Schuele L, Ndishimye P, Otani S, Mbiribindi JB, et al. Ongoing mpox outbreak in Kamituga, South Kivu province, associated with monkeypox virus of a novel Clade I sub-lineage, Democratic Republic of the Congo, 2024. Euro Surveill. 2024;29:2400106. https://doi.org/10.2807/1560-7917.ES.2024.29.11.2400106
4. Mauldin MR, McCollum AM, Nakazawa YJ, Mandra A, Whitehouse ER, Davidson W, et al. Exportation of monkeypox virus from the African continent. J Infect Dis. 2022;225:1367–76. https://doi.org/10.1093/infdis/jiaa559
5. Levy V, Branzuela A, Hsieh K, Getabecha S, Berumen R III, Saadeh K, et al.; Clade I Mpox Response Team. First clade Ib monkeypox virus infection reported in the Americas–California, November 2024. MMWR Morb Mortal Wkly Rep. 2025;74:44–9. https://doi.org/10.15585/mmwr.mm7404a1
6. World Health Organization. WHO director-general declares mpox outbreak a public health emergency of international concern [cited 2025 Jan 6]. https://www.who.int/news/item/14-08-2024-who-director-general-declares-mpox-outbreak-a-public-health-emergency-of-international-concern
7. Schuele L, Masirika LM, Udahemuka JC, Siangoli FB, Mbiribindi JB, Ndishimye P, et al.; GREATLIFE MPOX Group. Real-time PCR assay to detect the novel clade Ib monkeypox virus, September 2023 to May 2024. Euro Surveill. 2024;29:2400486. https://doi.org/10.2807/1560-7917.ES.2024.29.32.2400486
8. Patrono LV, Pléh K, Samuni L, Ulrich M, Röthemeier C, Sachse A, et al. Monkeypox virus emergence in wild chimpanzees reveals distinct clinical outcomes and viral diversity. Nat Microbiol. 2020;5:955–65. https://doi.org/10.1038/s41564-020-0706-0
9. Gigante CM, Korber B, Seabolt MH, Wilkins K, Davidson W, Rao AK, et al. Multiple lineages of monkeypox virus detected in the United States, 2021–2022. Science. 2022;378:560–5. https://doi.org/10.1126/science.add4153
10. Forni D, Molteni C, Cagliani R, Sironi M. Geographic structuring and divergence time frame of monkeypox virus in the endemic region. J Infect Dis. 2023;227:742–51. https://doi.org/10.1093/infdis/jiac298

Address for correspondence: Sara E. Zufan, National Institutes of Health, 8200 Research Plaza, Fort Detrick, Frederick, MD 21702, USA; email: sara.zufan@nih.gov

Detection of Rat Lungworms in Invasive Mollusks, Georgia, USA, 2024

Tyler J. Achatz, Caley H. Chun, Maggie A. Young, Jim Page, Matthew Rowe, Caroline Cooper, Laura Wenk, Vasyl V. Tkach

Author affiliations: Middle Georgia State University, Macon, Georgia, USA (T.J. Achatz, C.H. Chun, M.A. Young); Georgia Department of Natural Resources, Atlanta, Georgia, USA (J. Page, M. Rowe, C. Cooper, L. Wenk); University of North Dakota, Grand Forks, North Dakota, USA (V.V. Tkach)

DOI: https://doi.org/10.3201/eid3109.250133

The rat lungworm, *Angiostrongylus cantonensis*, is an invasive, zoonotic parasite that can cause severe disease in humans. We collected *A. cantonensis* larvae from 2 host species, invasive apple and mystery snails, from bodies of water in Georgia, USA. Recreational water users should avoid ingesting potentially infected hosts, aquatic vegetation, and water.

The rat lungworm, *Angiostrongylus cantonensis* (Nematoda: Angiostrongylidae), is an invasive human pathogen in many countries, including the United States. This nematode naturally parasitizes rodents (*1*–*3*); a variety of gastropod mollusks, typically terrestrial gastropods, act as intermediate hosts. However, aquatic and semiaquatic mollusks, such as invasive apple snails (*Pomacea* spp.) and mystery snails (*Cipangopaludina* spp.), have been reported as intermediate hosts (*4*,*5*). Freshwater crustaceans, amphibians, reptiles, and flatworms might serve as paratenic hosts (*1*–*4*). Infective third-stage level (L3) nematode larvae can also be found on vegetation exposed to infected snails (*1*). When L3 larvae are ingested by rats, the larvae migrate through vasculature, reaching the central nervous system, and later develop into adults in the pulmonary arteries. In humans, accidental ingestion of rat lungworm can cause severe pathology, including meningitis, or death when L3 larvae migrate to the central nervous system (*6*).

Rat lungworms are native to Southeast Asia but have spread worldwide (*4*); the parasite was first reported in the United States in Hawaii in 1960 (*2*). It was not detected again until 1986 in Louisiana. Recent years have seen a geographic expansion of this parasite: 2013 in Florida, Mississippi, and Texas; 2014 in Alabama and California; 2015 in Oklahoma; 2019 in South Carolina; and 2019–2022 in Georgia (*2*,*4*,*5*,*7*–*9*). Despite the broad geographic distribution of rat lungworm, few cases of human angiostrongyliasis have been detected in the United States (*8*). We collected 2 rat lungworm host species, invasive apple snails (*Pomacea maculata*) and mystery snails (*Cipangopaludina japonica*), in bodies of water in Georgia and tested them for *A. cantonensis* larvae.

We collected the snails from 8 water bodies in 7 counties during May–October 2024 (Table; Figure). We sampled 430 apple snails (Camden, Chatham, and Dougherty Counties) and 2,562 mystery snails (Cherokee, Greene, Hall, and Jasper Counties) and screened them for nematodes (Appendix, https://wwwnc.cdc.gov/EID/article/31/9/25-0133-App1.pdf). A total of 14 snails (5 mystery snails, 9 apple snails) were infected with rat lungworm. No variation was detected among *cox*1 sequences from the nematodes. BLAST analysis (https://blast.ncbi.nlm.nih.gov) showed a 100% match to *A. cantonensis* parasites previously collected in Atlanta (*9*). Among sites sampled for mystery snails, we detected rat lungworm from Lake Lanier (Hall County; prevalence 18.0/1,000 snails) and the Ocmulgee River (Jasper County; prevalence 6.3/1,000 snails), whereas mystery snails from Lakes Allatoona (Cherokee County) and Oconee (Greene County) were not infected. Apple snails taken from ponds and marshes in Kingsland (prevalence 189.2/1,000 snails) and St. Marys (prevalence 8.5/1,000 snails), both in Camden County, and from Pipemakers Canal (Chatham County; prevalence 4.5/1,000 snails), were infected with rat lungworm, but those from Lake Chehaw (Dougherty County) were not infected (Table).

Table. Prevalence of rat lungworm (*Angiostrongylus cantonensis*) in invasive apple snails (*Pomacea maculata*) and mystery snails (*Cipangopaludina japonica*), Georgia, USA*

Location	County	GPS coordinates	Snail type	No. infected/ no. screened	Prevalence, infections/1,000 snails
Lake Allatoona	Cherokee	34°07′58.1″N, 84°37′46.5″W	Mystery	0/1,371	0
Lake Lanier	Hall	34°17′35.0″N, 83°56′17.6″W	Mystery	2/111	18
Lake Oconee	Greene	33°30′16.5″N, 83°16′58.0″W	Mystery	0/607	0
Ocmulgee River	Jasper	33°19′07.4″N, 83°50′32.6″W	Mystery	3/473	6.3
Kingsland	Camden	30°47′17.0″N, 81°38′46.0″W	Apple	7/37	189.2
Lake Chehaw	Dougherty	31°36′37.2″N, 84°06′56.3″W	Apple	0/55	0
Pipemakers Canal	Chatham	32°06′21.0″N, 81°11′43.0″W	Apple	1/221	4.5
St. Marys	Camden	30°47′07″N, 81°35′25.0″W	Apple	1/117	8.5

*GPS, global positioning satellite.

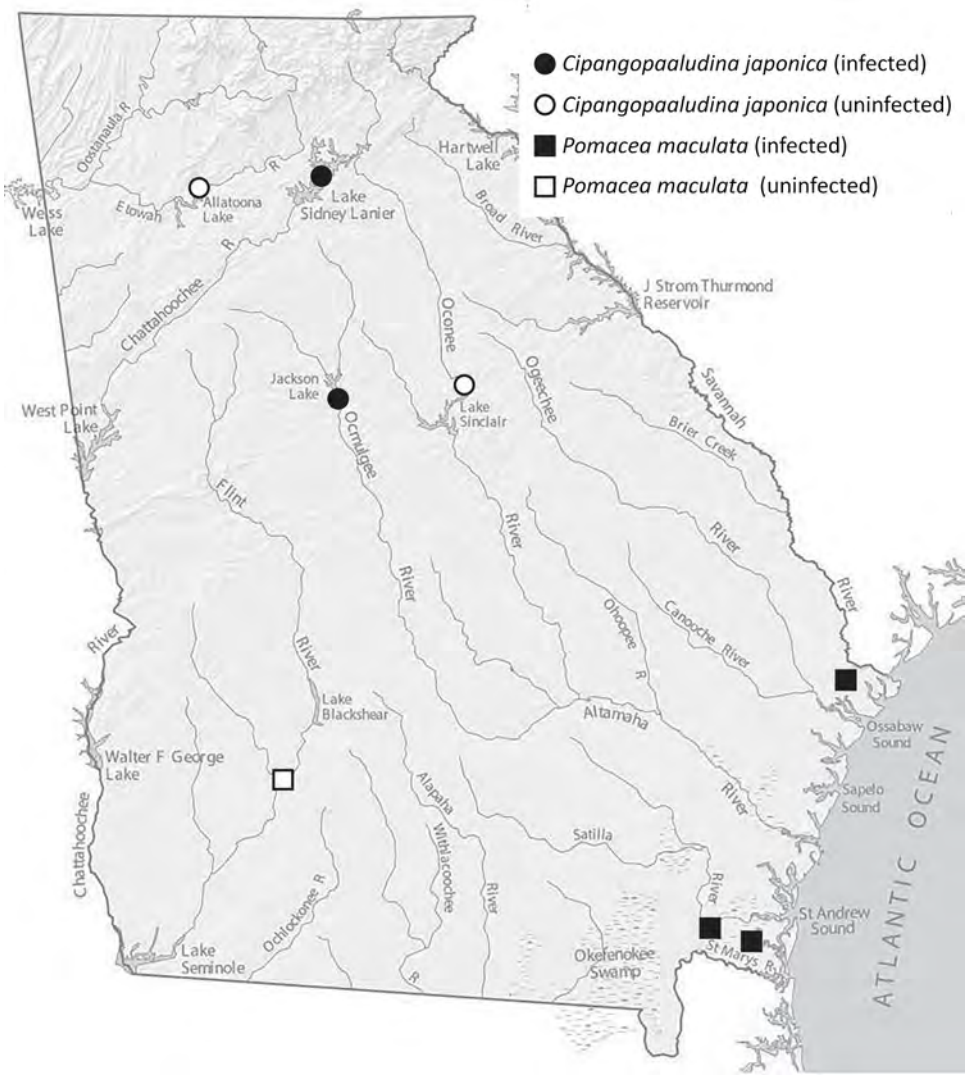

Figure. Sites where invasive apple snails (*Pomacea maculata*) and mystery snails (*Cipangopaludina japonica*) were collected and screened for rat lungworm (*Angiostrongylus cantonensis*), Georgia, USA.

Despite our broad sampling of snails, we detected low overall prevalence of rat lungworm.

Apple snails were first reported in Georgia in 1974 but not reported again until 2005 (*10*). The early records of the snails were limited to southern Georgia, but in 2013, apple snails were reported in Rockdale County in north central Georgia (*10*). In the early 2020s, apple snails began to be reported more frequently in the central and northern parts of the state, including in and around the Atlanta metropolitan area (*10*). Mystery snails are a more recent introduction to Georgia; they were first reported in the state in 2013 from the Atlanta metropolitan area (Clayton and Fulton Counties) (*10*). Reports of mystery snails throughout the state have become increasingly frequent in recent years (*10*). We anticipate that future sampling of these snails statewide will show a general trend of increasing prevalence as the invasive snail populations become more established and widespread.

Humans can be infected with rat lungworm by ingesting the molluscan intermediate host or the paratenic host (e.g., crustaceans) or by swallowing infective (L3) larvae, which are found on vegetation (*1*–*3*). Apple snails are commonly consumed in some communities in the United States, including Georgia (C.H. Chun, J. Page, M. Rowe, pers. observ.). However, risk of contracting rat lungworm infection is low. Thoroughly cooking the infected snail or paratenic host kills the nematodes and prevents infection; however, accidental exposure through ingesting contaminated vegetation poses a greater human health risk (*1*). Prior studies have suggested potential human infection through contaminated drinking water (*3*).

In conclusion, whereas public health decisions related to this parasite should be left to the Centers

for Disease Control and Prevention and the Georgia Department of Public Health, we encourage efforts to educate recreational water users to avoid ingesting potentially infected hosts, aquatic vegetation, and water. Long-term management and monitoring of the invasive snail and rodent populations are needed to help minimize the potential spread of rat lungworm and human infection risk in Georgia.

Acknowledgments

We thank Anakela Escobar and the Region 1 fisheries staff (Georgia Department of Natural Resources) for providing mystery snails from Lake Allatoona. We are also grateful to Sarah A. Orlofske (University of Wisconsin – Stephens Point) and Robert A. Newman (University of North Dakota) for their assistance with data analysis.

This work was supported by the University System of Georgia Stem Initiative IV and Center for Middle Georgia Studies.

About the Author

Dr. Achatz is a professor in the Department of Natural Sciences at Middle Georgia State University, Macon, Georgia, USA. His research focuses on parasite taxonomy and systematics as well as disease ecology related to parasitic organisms.

References

1. Ewers EC, Anisowicz SK. The potential danger of eating wild lettuce: a brief review of human rat lungworm infection. Hawaii J Med Public Health. 2014;73(Suppl 2):28–32.
2. Niebuhr CN, Jarvi SI, Siers SR. A review of rat lungworm infection and recent data on its definitive hosts in Hawaii. Hum Wildl Interact. 2019;13:238–49.
3. Cowie RH. Pathways for transmission of angiostrongyliasis and the risk of disease associated with them. Hawaii J Med Public Health. 2013;72(Suppl 2):70–4.
4. Qvarnstrom Y, Bishop HS, da Silva AJ. Detection of rat lungworm in intermediate, definitive, and paratenic hosts obtained from environmental sources. Hawaii J Med Public Health. 2013;72(Suppl 2):63–9.
5. Underwood EB, Walker MJ, Darden TL, Kingsley-Smith PR. Frequency of occurrence of the rat lungworm parasite in the invasive island apple snail in South Carolina, USA. J Aquat Anim Health. 2019;31:168–72. https://doi.org/10.1002/aah.10063
6. Jarvi S, Prociv P. *Angiostrongylus cantonensis* and neuroangiostrongyliasis (rat lungworm disease): 2020. Parasitology. 2021;148:129–32. https://doi.org/10.1017/S003118202000236X
7. Burns RE, Bicknese EJ, Qvarnstrom Y, DeLeon-Carnes M, Drew CP, Gardiner CH, et al. Cerebral *Angiostrongylus cantonensis* infection in a captive African pygmy falcon (*Polihierax semitorquatus*) in southern California. J Vet Diagn Invest. 2014;26:695–8. https://doi.org/10.1177/1040638714544499
8. Al Hammoud R, Nayes SL, Murphy JR, Heresi GP, Butler IJ, Pérez N. *Angiostrongylus cantonensis* meningitis and myelitis, Texas, USA. Emerg Infect Dis. 2017;23:1037–8. https://doi.org/10.3201/eid2306.161683
9. Gottdenker NL, Nascimento Ramos RA, Hakimi H, McHale B, Rivera S, Miller BM, et al. *Angiostrongylus cantonensis* infection in brown rats (*Rattus norvegicus*), Atlanta, Georgia, USA, 2019–2022. Emerg Infect Dis. 2023;29:2167–70. https://doi.org/10.3201/eid2910.230706
10. US Geological Survey. Nonindigenous aquatic species [cited 2025 Jan 8]. https://nas.er.usgs.gov

Address for correspondence: Tyler J. Achatz, Middle Georgia State University, 100 University Pkwy, Jones Bldg, Rm 372, Macon, GA 31206, USA; email: tyler.achatz@mga.edu

Characterization of Emerging Human *Dirofilaria repens* Infections, Estonia, 2023

Kalev Nõupuu, Maare Mõtsküla, Riina Pulges, Mikk Pauklin, Urmas Saarma

Author affiliations: Tartu University Hospital, Tartu, Estonia (K. Nõupuu, R. Pulges, M. Pauklin); Estonian University of Life Sciences, Tartu (M. Mõtsküla); University of Tartu, Tartu (U. Saarma).

DOI: https://doi.org/10.3201/eid3109.241890

Mosquitoborne diseases are a growing threat to public health worldwide. Human dirofilariasis, caused by the nematode *Dirofilaria repens* and transmitted by mosquitoes from various genera, has recently expanded into new areas of Europe. In this article, we report molecularly confirmed autochthonous human *D. repens* infections in Estonia.

Human dirofilariasis, caused by nematodes of the genus *Dirofilaria*, is a mosquitoborne parasitosis with growing public health importance. In Europe, the main causative species is *D. repens*, and infections with *D. immitis* are less frequent. Mosquitoes play a crucial role in the transmission of infectious larvae, and suitable species span various mosquito genera, including *Aedes*, *Anopheles*, and *Culex* (*1*). The definitive hosts of *D. repens* nematodes are domestic and

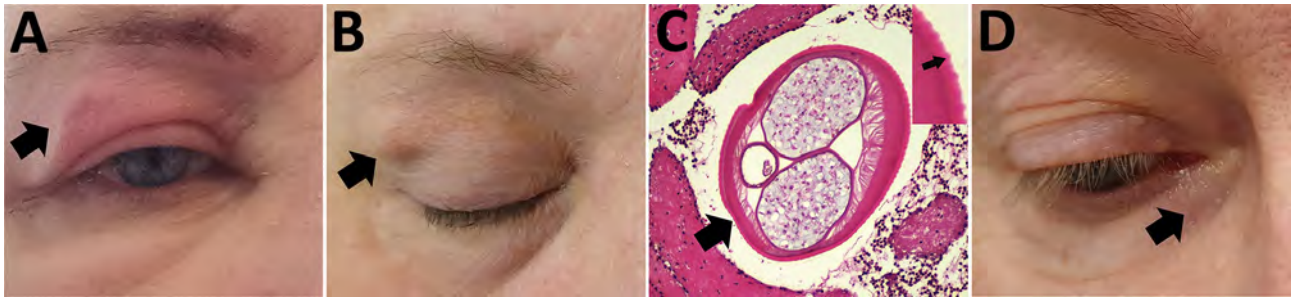

Figure 1. Autochthonous *Dirofilaria repens* infections in 2 women, Estonia, 2023. A–C) Case-patient 1, showing a painful subcutaneous lesion with edema on her right eyelid (A; black arrow). Two months later, the edema resolved, but a 1.5 cm subcutaneous nodule persisted (B; black arrow). Histopathologic examination of the removed nodule confirmed *Dirofilaria* spp. (C; larger black arrow); distinctive transverse striations on the cuticle with average distance of 12 μm between the peaks suggested *D. repens* (inset; small black arrow). Hematoxylin and eosin stain; original magnification ×100. The diameter of the parasite was 390 × 529 μm. D) Case-patient 2, showing a subcutaneous nodule under the right lower eyelid (black arrow).

wild carnivores. Humans are considered accidental hosts, in whom the parasitic larvae typically develop into a nonfertile stage. Although most human cases are subclinical, *D. repens* infection might occasionally result in subcutaneous swelling with subsequent development of subcutaneous nodular lesions. The clinical manifestations can include a mobile mass within the conjunctiva (*2*) and can lead to irreversible ocular damage (*3*). In rare cases, microfilaremia has been described (*3*,*4*). The distribution of *D. repens* nematodes includes countries in Europe, Africa, Middle East, Asia, and South America (*1*). In Europe, the parasite has recently spread north, and cases of human dirofilariasis caused by *D. repens* infection have emerged in Lithuania, Latvia, and Finland (*5*,*6*). *D. repens* nematodes have been reported in dogs in Estonia (*7*,*8*). Here, we describe 2 molecularly confirmed human *D. repens* infection cases from Estonia.

In February 2023, a 46-year-old woman in Estonia with no travel history abroad was referred to a neurology service for investigation of recurrent headache and painful facial subcutaneous nodular lesions with accompanying edema. The patient described a 1.5–2 cm palpable lesion that remained at the same location for 1–2 days before disappearing and reappearing elsewhere. Her symptoms persisted for 1 month, during which she observed nodules and edema on her upper (Figure 1, panel A) and lower eyelids, forehead, lips, and scalp. Two months later, a permanent 1.5 cm subcutaneous nodule developed in her right upper eyelid (Figure 1, panel B), and the patient was referred to an ophthalmologist. We surgically removed the nodule and sent it for histopathologic examination. The parasite in the nodule was confirmed as *Dirofilaria* spp. (Figure 1, panel C). After the removal of the parasite, her symptoms resolved and did not recur.

In February 2023, a 77-year-old woman in Estonia with no travel history abroad was referred to an ophthalmologist because of a nodular lesion under the right lower eyelid (Figure 1, panel D). The patient reported an episode of a mild, painful swelling that preceded the formation of the lesion. The oval lesion (1 × 1.5 cm) was located nasally under the right lower eyelid next to the orbital rim, was not painful and was freely movable, and was not adhered to the orbital rim or lacrimal sac. Initially, we recommended conservative observation; however, over the next 5 months, the lesion grew, and mild edema reappeared. Because of a clinical suspicion of a tumor, we surgically excised the lesion. The specimen was submitted for a histopathologic examination, which identified *Dirofilaria* spp.

No treatment guidelines for human *D. repens* infection have been established; however, surgical removal of the parasite is usually sufficient, and pharmacologic treatment is rarely necessary (*3*). After the removal of the encapsulated parasite in the 2 cases described, the symptoms resolved. No systemic treatment was applied. Additional data for both human cases are provided (Appendix, http://wwwnc.cdc.gov/EID/article/31/9/24-1890-App1.pdf).

We conducted molecular genetic analysis for species identification and phylogenetic inference on samples collected from both patients (Appendix). We submitted sequences to GenBank (accession nos. PQ608665, PQ608666, and PQ608671). We conducted species identification on the basis of the 331 bp sequence by using homology search with nucleotide BLAST (https://blast.ncbi.nlm.nih.gov) and identified both pathogens as *D. repens* nematodes. On the basis of the longer fragment of *cox1* (570 bp), we built a phylogenetic network that comprised the human isolate *In2* from Estonia and 38 highly homologous sequences from GenBank (Figure 2). In that network, the human isolate *In2* from Estonia formed a unique haplotype 1, suggesting low-level divergence from

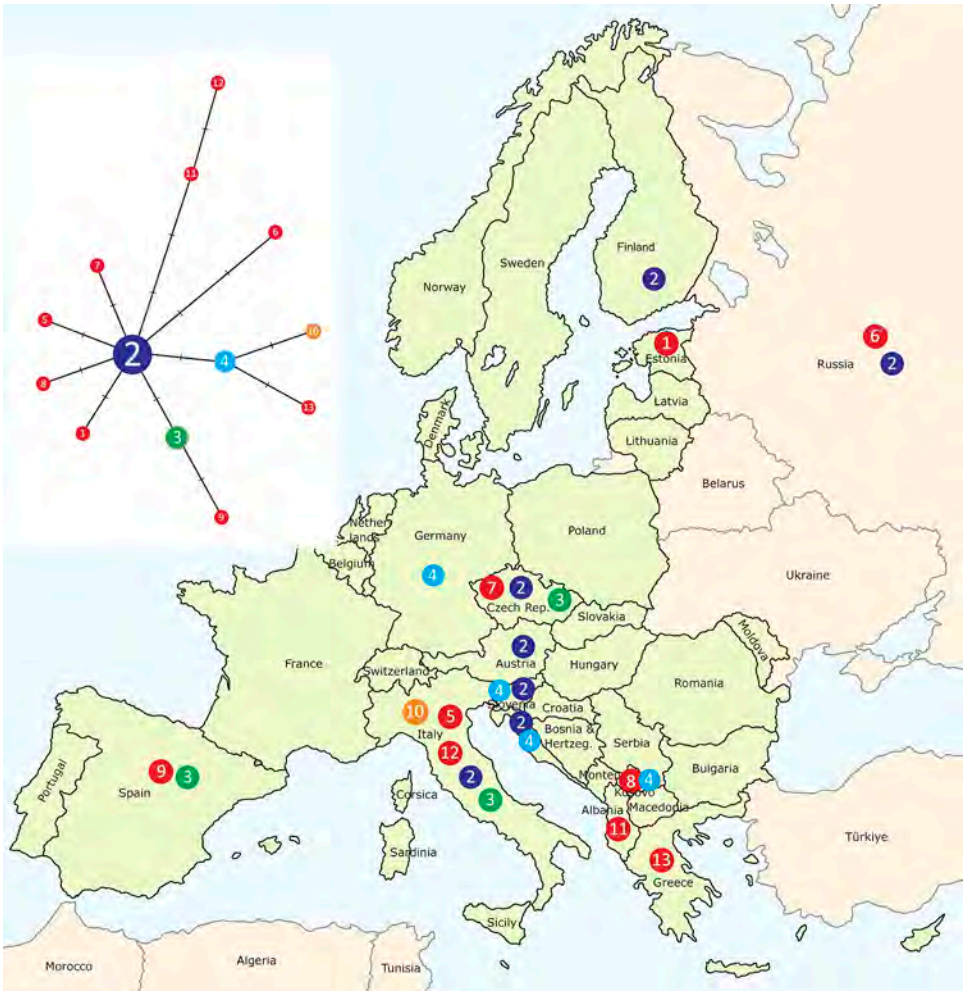

Figure 2. Distribution map of emerging *Dirofilaria repens* haplotypes (n = 13) in Europe, including samples from Estonia, 2023. Haplotypes were derived from the median joining network analysis (left), illustrating relationships of *D. repens* isolates (n = 39) from Estonia and other countries. We established relationships on the basis of partial mtDNA *cox1* gene sequence variation (570 bp). The circled number is the haplotype identification number. Red circles represent haplotypes with unique sequences. Haplotypes represented by ≥2 are in different colors. Each crossed bar equates to a single-nucleotide polymorphism differentiating the haplotypes. Of note, the human isolate *In2* from Estonia has a unique haplotype 1, which is closely related to the central haplotype 2, reported previously in *D. repens* isolates from humans, dogs, and mosquitoes in various countries (Appendix Table 2, https://wwwnc.cdc.gov/EID/article/31/9/24-1890-App1.pdf). mtDNA, mitochondrial DNA.

the central haplotype 2. Of note, *D. repens* is genetically closest to a newly described species, *D. asiatica* (*9*) (Appendix).

We report 2 autochthonous human *D. repens* infections in Estonia, highlighting the importance of recognizing this emerging threat. The geographic distribution of *D. repens* may have expanded because of climate change, enabling the parasite and its vectors to adapt in colder regions and spread the infection northward (*3*,*8*). Therefore, it is necessary to increase the awareness of the parasite among healthcare professionals working in Estonia. In both of these cases, the diagnosis was delayed, and several unnecessary tests were conducted because of a lack of knowledge about dirofilariasis. The common nodular lesions in the facial region might mimic tumors, granulomas, or cysts (*10*). Because no commercially available tests are available to diagnose *D. repens* infection from blood samples, molecular analysis of the parasite is essential for diagnosis (*3*).

Acknowledgments

We thank Mikk Tooming for his technical assistance and Sander Lupp for the histopathologic analysis.

This research was financed by the Estonian Ministry of Education and Research (grant nos. PRG1209 and TK215 to U.S.).

About the Author

Dr. Nõupuu is working as a senior ophthalmologist and eye surgeon in the Eye Clinic of Tartu University Hospital. His primary research interests are eye diseases, including those caused by zoonotic parasites.

References

1. Perles L, Dantas-Torres F, Krücken J, Morchón R, Walochnik J, Otranto D. Zoonotic dirofilariases: one, no one, or more than one parasite. Trends Parasitol. 2024;40:257–70. https://doi.org/10.1016/j.pt.2023.12.007
2. Redón-Soriano M, Blasco A, Gomila B, González-Sánchez M, Simón F, Esteban JG. Subconjunctival human dirofilariasis by

Dirofilaria repens in the Mediterranean Basin. Am J Ophthalmol Case Rep. 2022;26:101570. https://doi.org/10.1016/j.ajoc.2022.101570
3. Capelli G, Genchi C, Baneth G, Bourdeau P, Brianti E, Cardoso L, et al. Recent advances on *Dirofilaria repens* in dogs and humans in Europe. Parasit Vectors. 2018;11:663. https://doi.org/10.1186/s13071-018-3205-x
4. Potters I, Vanfraechem G, Bottieau E. *Dirofilaria repens* Nematode infection with microfilaremia in traveler returning to Belgium from Senegal. Emerg Infect Dis. 2018;24:1761–3. https://doi.org/10.3201/eid2409.180462
5. Pietikäinen R, Nordling S, Jokiranta S, Saari S, Heikkinen P, Gardiner C, et al. *Dirofilaria repens* transmission in southeastern Finland. Parasit Vectors. 2017;10:561. https://doi.org/10.1186/s13071-017-2499-4
6. Deksne G, Davidson RK, Buchmann K, Kärssin A, Kirjušina M, Gavarāne I, et al. Parasites in the changing world—ten timely examples from the Nordic-Baltic region. Parasite Epidemiol Control. 2020;10:e00150. https://doi.org/10.1016/j.parepi.2020.e00150
7. Jokelainen P, Mõtsküla PF, Heikkinen P, Ülevaino E, Oksanen A, Lassen B. *Dirofilaria repens* microfilaremia in three dogs in Estonia. Vector Borne Zoonotic Dis. 2016;16:136–8. https://doi.org/10.1089/vbz.2015.1833
8. Alsarraf M, Levytska V, Mierzejewska EJ, Poliukhovych V, Rodo A, Alsarraf M, et al. Emerging risk of *Dirofilaria* spp. infection in Northeastern Europe: high prevalence of *Dirofilaria repens* in sled dog kennels from the Baltic countries. Sci Rep. 2021;11:1068. https://doi.org/10.1038/s41598-020-80208-1
9. Colella V, Young ND, Manzanell R, Atapattu U, Sumanam SB, Huggins LG, et al. *Dirofilaria asiatica* sp. nov. (Spirurida: Onchocercidae)—defined using a combined morphological-molecular approach. Int J Parasitol. 2025;55:461–74. https://doi.org/10.1016/j.ijpara.2025.04.006
10. Simón F, Siles-Lucas M, Morchón R, González-Miguel J, Mellado I, Carretón E, et al. Human and animal dirofilariasis: the emergence of a zoonotic mosaic. Clin Microbiol Rev. 2012;25:507–44. https://doi.org/10.1128/CMR.00012-12

Address for correspondence: Urmas Saarma, Department of Zoology, Institute of Ecology and Earth Sciences, University of Tartu, J. Liivi 2, 50409 Tartu, Estonia; email: urmas.saarma@ut.ee

Zoonotic Rat Lungworm *Angiostrongylus cantonensis* in Black Rats, Houston, Texas, 2024

Daniela A. Sierra, Tiana L. Sanders, Erin E. Edwards, Christine M. Molter, Guilherme G. Verocai

Author affiliations: Texas A&M University College of Veterinary Medicine and Biomedical Sciences, College Station, Texas, USA (D.A. Sierra, T.L. Sanders, G.G. Verocai); Texas A&M Veterinary Medicinal Diagnostic Laboratory, College Station (E.E. Edwards); Houston Zoo, Houston, Texas, USA (C.M. Molter)

DOI: http://doi.org/10.3201/eid3109.251710

The *Angiostrongylus cantonensis* rat lungworm is a zoonotic nematode that infects several rat species. This nematode causes eosinophilic meningitis and meningoencephalitis in humans and other accidental hosts. We found a 20% prevalence of *A. cantonensis* lungworms in black rats from a zoo facility in Houston, Texas, USA.

The *Angiostrongylus cantonensis* rat lungworm (Strongylida: Metastrongyloidea) is a widely distributed zoonotic parasitic nematode (*1*). This nematode has an indirect life cycle, requiring a rodent definitive host and a gastropod intermediate host (*2*). The cycle begins when a rat within the genus *Rattus* ingests a gastropod intermediate host infected with third-stage larvae (L3). L3 penetrate the intestinal wall, migrate to the brain, molt twice, and then migrate to the right ventricle and pulmonary arteries, where they develop into adults. Within pulmonary arteries, adults reproduce sexually and female worms lay eggs, which hatch into first-stage larvae (L1) that are subsequently coughed up and swallowed. L1 travel through the gastrointestinal tract and are passed in the feces. L1 then reenters the gastropod either orally or by actively penetrating its foot. L1 molt twice within the gastropod host to develop into infective L3. The L3 may be ingested by paratenic hosts, remaining dormant but infective.

Accidental hosts, including humans, can become infected through ingestion, deliberately or accidentally, of infected gastropods, paratenic hosts, or L3 (*1*). In those hosts, *A. cantonensis* infection causes eosinophilic meningitis or meningoencephalitis (i.e., neural angiostrongyliasis). Disease in humans is characterized by nonspecific neurologic signs such as neck pain and stiffness and sensitivity

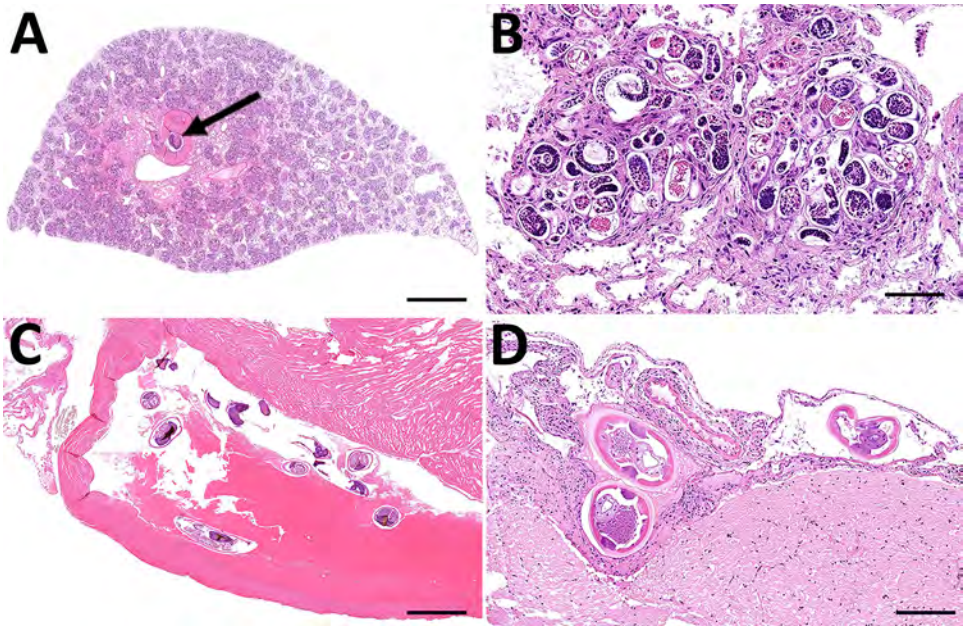

Figure 1. Histopathology of *Angiostrongylus cantonensis* rat lungworm infection in metropolitan black rats, Houston, Texas, 2024. A) Severe pulmonary consolidation due to verminous pneumonia. Adult nematode is visible within a large artery (arrow). Scale bar = 1.5 mm. B) Higher magnification of lung with numerous *A. cantonensis* larvae and eggs surrounded by granulomatous inflammation. Scale bar = 80 µm. C) Multiple adult *A. cantonensis* nematodes in right ventricle of the heart. Scale bar = 1.5 mm. D) Mild lymphoplasmacytic meningitis with cross sections of *A. cantonensis* nematodes. Scale bar = 300 µm.

to touch and light and may be severe or fatal, particularly without timely or effective intervention (*3*). The first human case of eosinophilic meningitis caused by *A. cantonensis* in the United States occurred in Hawaii (*4*). In addition to travel-related cases (*1*), autochthonous cases of *A. cantonensis* in humans and captive and free-ranging wildlife in the United States have occurred in Alabama, Louisiana, Oklahoma, Mississippi, Florida, Texas, Tennessee, and Georgia (*1*,*4*–*8*).

Finding only a few reported cases of rat lungworm infection in humans and nonhuman primates in Texas (*6*,*9*), and noting a lack of research investigating rodent definitive hosts in the state, we investigated the prevalence of *A. cantonensis* lungworms in rodents captured from a zoo located in the metropolitan area of Houston, Texas, USA. We confirmed autochthonous *A. cantonensis* infections in black rats (*Rattus rattus*) through necropsy, gross and histopathological evaluation, microscopy of nematode specimens, and molecular testing as described previously (*5*) (Appendix, Appendix Table, https://wwwnc.cdc.gov/EID/article/31/9/25-1710-App1.pdf).

During March−June 2024, we collected rodents at the Houston Zoo in Harris County, Texas (29.7158° N; 95.3903° W). Of the rats examined, we found 15 (20%) of 75 to be infected with *A. cantonensis* worms. The average number of nematodes per rat was 26.6 (range 2–108. We traced infected rats to groups collected during April−June (Appendix Figure). Of the 15 rats histologically confirmed as infected, 11 showed verminous pneumonia with high larval and egg loads, 11 had cross-sections of adults within pulmonary vessels or the right heart ventricle, and 2 had meningitis due to parasitic larval migration (Figure 1). In 13 of the 15 infected rats, we found eggs or larvae with the characteristic dorsal-spined L1 in the lung sediment. We found no larvae in the 2 remaining rats, coincidentally the 2 with meningitis, compatible with prepatent infections. Histologic examination revealed eosinophilic meningitis in the brain tissue, caused by *A. cantonensis* larvae, which we inferred to be L3, L4, or L5 on the basis of infection progression (Figure 1, panel D). We noted adult specimens and larvae in the pulmonary arteries in association with severe, chronic granulomatous pneumonia.

Our molecular analysis confirmed the identity of each specimen as *A. cantonensis*. The sequences obtained were 100% identical to each other (Figure 2). We submitted 28 sequences that were 190-bp to GenBank (accession nos. PQ556202–29). A 20% prevalence of in the wild black rat population indicates that this parasite is well established at the zoo. We theorize that the parasite is also likely established in the city of Houston and Harris County, the third most populous county in the United States. Studies reported similar prevalence of the nematode in Florida (22.8%) (*7*) and notably higher prevalence in Louisiana (38%) (*8*) and eastern Hawaii Island (93.9%) (*10*). Our results suggest the need for a temporally and geographically broader study to assess parasite distribution and epidemiology in Texas.

The established *A. cantonensis* cycle within this metropolitan area highlights the risk of zoonotic exposure to humans. In addition, *A. cantonensis*

lungworms may be an emerging threat to conservation of threatened or endangered captive animals housed in zoos in endemic areas. The loss of a single animal can have a massive impact on the genetic pool. Therefore, establishment of this nematode in the area imparts greater risk for those endangered species (*6*). The sequences we generated were 100% identical to haplotype 17a, previously found in Louisiana and Georgia (*5*,*8*). This finding suggests that, after introduction and establishment, *A. cantonensis* lungworms have possibly spread across the southeastern United States. Our study highlights the importance of statewide or countrywide surveys to determine the full geographic distribution of *A. cantonensis* lungworms to inform strategies to mitigate the threat to both human and animal health.

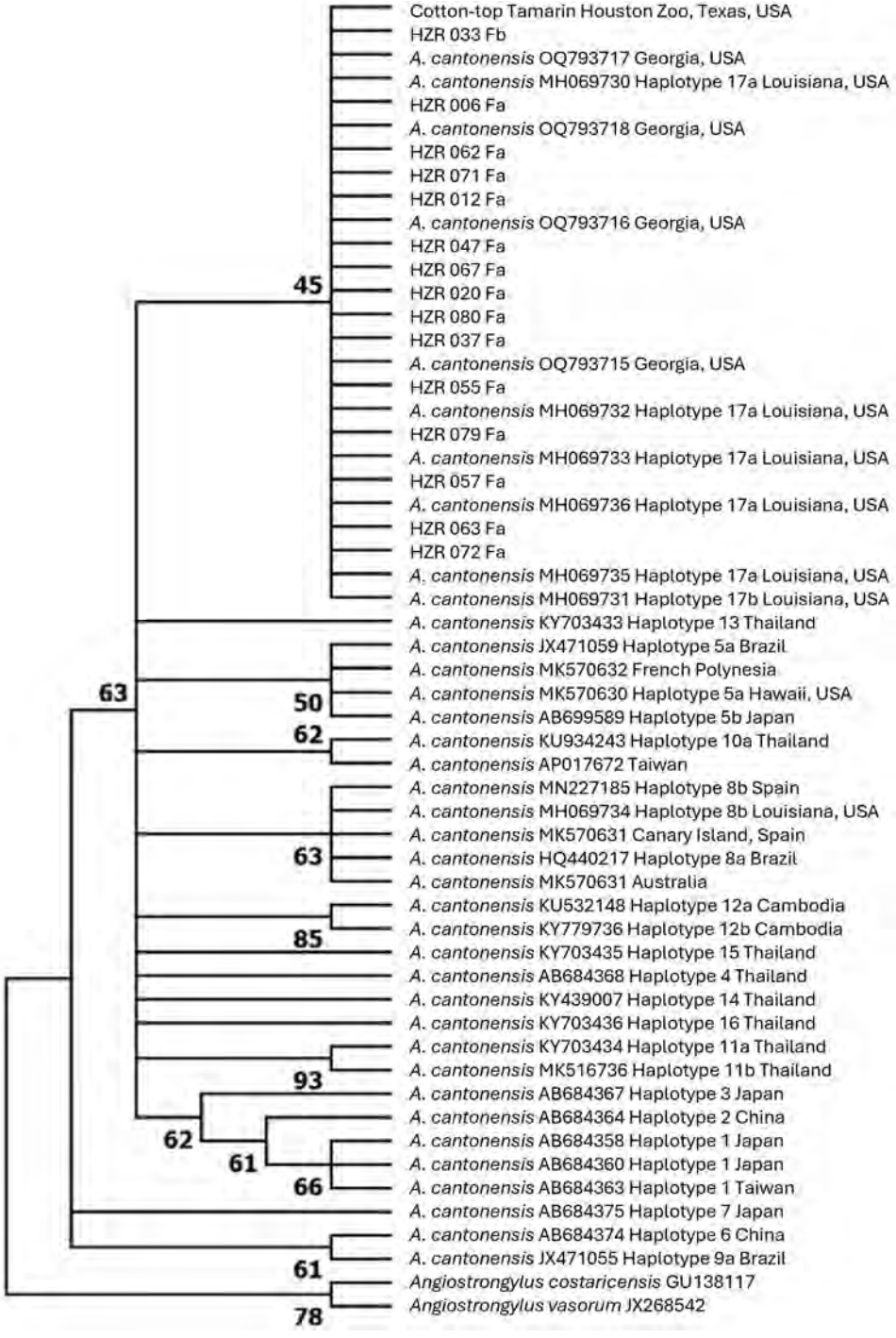

Figure 2. Maximum-likelihood phylogenetic tree (1,000 bootstrap replicates) from study of zoonotic rat lungworm *Angiostrongylus cantonensis* in black rats, Houston, Texas, 2024. Tree depicts the phylogenetic relationships of *A. cantonensis* sequences generated from samples in this study and representative sequences of *A. cantonensis* haplotypes from the United States and globally. Sequences generated in the study are labeled HZR and were deposited into GenBank (accession nos. PQ556202–29). Reference sequences are identified by GenBank accession number and location.

D.A.S. was supported by the Boehringer Ingelheim Veterinary Scholars Program through the Veterinary Medical Scientist Research Training Program at the Texas A&M University College of Veterinary Medicine and Biomedical Sciences.

About the Author

Ms. Sierra is a DVM student at Texas A&M University College of Veterinary Medicine and Biomedical Sciences and has a strong interest in zoologic medicine.

References

1. Cowie RH, Ansdell V, Panosian Dunavan C, Rollins RL. Neuroangiostrongyliasis: global spread of an emerging tropical disease. Am J Trop Med Hyg. 2022;107:1166–72. https://doi.org/10.4269/ajtmh.22-0360
2. da Silva AJ, Morassutti AL. *Angiostrongylus* spp. (Nematoda; Metastrongyloidea) of global public health importance. Res Vet Sci. 2021;135:397–403. https://doi.org/10.1016/j.rvsc.2020.10.023
3. Ansdell V, Kramer KJ, McMillan JK, Gosnell WL, Murphy GS, Meyer BC, et al. Guidelines for the diagnosis and treatment of neuroangiostrongyliasis: updated recommendations. Parasitology. 2021;148:227–33. https://doi.org/10.1017/S0031182020001262
4. Flerlage T, Qvarnstrom Y, Noh J, Devincenzo JP, Madni A, Bagga B, et al. *Angiostrongylus cantonensis* eosinophilic meningitis in an infant, Tennessee, USA. Emerg Infect Dis. 2017;23:1756–8. https://doi.org/10.3201/eid2310.170978
5. Gottdenker NL, Nascimento Ramos RA, Hakimi H, McHale B, Rivera S, Miller BM, et al. *Angiostrongylus cantonensis* infection in brown rats (*Rattus norvegicus*), Atlanta, Georgia, USA, 2019–2022. Emerg Infect Dis. 2023;29:2167–70. https://doi.org/10.3201/eid2910.230706
6. Edwards EE, Borst MM, Lewis BC, Gomez G, Flanagan JP. *Angiostrongylus cantonensis* central nervous system infection in captive callitrichids in Texas. Vet Parasitol Reg Stud Reports. 2020;19:100363. https://doi.org/10.1016/j.vprsr.2019.100363
7. Stockdale Walden HD, Slapcinsky JD, Roff S, Mendieta Calle J, Diaz Goodwin Z, Stern J, et al. Geographic distribution of *Angiostrongylus cantonensis* in wild rats (*Rattus rattus*) and terrestrial snails in Florida, USA. PLoS One. 2017;12:e0177910. https://doi.org/10.1371/journal.pone.0177910
8. Rael RC, Peterson AC, Ghersi-Chavez B, Riegel C, Lesen AE, Blum MJ. Rat lungworm infection in rodents across post-Katrina New Orleans, Louisiana, USA. Emerg Infect Dis. 2018;24:2176–83. https://doi.org/10.3201/eid2412.180056
9. Foster CE, Nicholson EG, Chun AC, Gharfeh M, Anvari S, Seeborg FO, et al. *Angiostrongylus cantonensis* infection: a cause of fever of unknown origin in pediatric patients. Clin Infect Dis. 2016;63:1475–8. https://doi.org/10.1093/cid/ciw606
10. Jarvi SI, Quarta S, Jacquier S, Howe K, Bicakci D, Dasalla C, et al. High prevalence of *Angiostrongylus cantonensis* (rat lungworm) on eastern Hawai'i Island: a closer look at life cycle traits and patterns of infection in wild rats (*Rattus* spp.). PLoS One. 2017;12:e0189458. https://doi.org/10.1371/journal.pone.0189458

Address for correspondence: Guilherme G. Verocai, Department of Veterinary Pathobiology, Texas A&M Veterinary Medicine & Biomedical Sciences, 4467 TAMU, College Station, TX 77843-4467, USA; email: gverocai@cvm.tamu.edu

Human Babesiosis Caused by *Babesia venatorum*, Russia, 2024

Olga P. Zelya, Irina V. Kukina, Ludmila S. Karan, Elena A. Krasilovskaya, Vadim V. Garin

Author affiliations: First Moscow State Medical University (Sechenov University), Moscow, Russia (O.P. Zelya, I.V. Kukina, V.V. Garin); Research Center of Neurology, Moscow (L.S. Karan); Centre for Strategic Planning of the Federal Medical and Biological Agency, Moscow (L.S. Karan); Sayanogorsk Interdistrict Hospital, Sayanogorsk, Russia (E.A. Krasilovskaya)

DOI: http://doi.org/10.3201/eid3109.250319

We report a case of acute babesiosis in a splenectomized 63-year-old man in Siberia, Russia. We confirmed the causative agent, *Babesia venatorum*, by PCR. Our study demonstrated a change in the structure of the parasite population, from single parasite invasion of erythrocytes to multioccupancy, without an increase in parasitemia level.

Babesiosis is an emerging tickborne infection caused by intraerythrocytic protozoa. To date, researchers have described more than 50 cases of babesiosis in humans in Europe, almost always fulminant in splenectomized patients and typically attributed to *Babesia divergens*. Some recent reports also describe several cases of human infection with *B. venatorum*, associated with milder infections than those caused by *B. divergens* (*1*). Researchers have also described sporadic cases of babesiosis caused by infection with *Babesia microti* and *B. divergens* in Asia-Pacific regions (*2*,*3*), but the practically asymptomatic course of the human infection with *B. venatorum* is more common (*4*). Although reports have noted detection of *Babesia* spp. DNA in *Ixodes persulcatus* ticks in Siberia (*5*), cases of human infections have yet to be reported in that region of Russia.

We report the case of a 63-year-old man who resided in a forested, mountainous area of Khakassia, East Siberia, Russia, and had undergone splenectomy. On September 30, 2024, the man sought treatment for an influenza-like syndrome with signs and symptoms that included a fever of 38°C, severe general weakness, darkening of urine, a decrease in diuresis, jaundice, dyspnea, and stomachache. Attending physicians admitted the patient to the hospital on October 2, 2024 (Table). The patient reported no awareness of a tick bite and had received no blood products in the previous 3 months.

Table. Characteristics of case-patient in study of human babesiosis caused by *Babesia venatorum*, Russia, 2024*

Tests performed	Results by date						Reference range
	Oct 3	Oct 7	Oct 10	Oct 14	Oct 22	Nov 8	
Hematologic parameters							
Hemoglobin, g/dL	11.2	9.3	11.6	11.6	12.0	15.5	11.7–18.0
Hematocrit, %	32.0	27.0	34.8	32.7	36.1	46.8	35–52
Erythrocytes, $\times 10^{12}$ cells/L	3.48	3.01	3.96	3.51	3.85	5.1	3.8–6.1
RBCN, L	10:100	4:100	7:100	NA	NA	NA	0:100
Platelets, $\times 10^{9}$/L	21	127	154	346	230	217	150–450
Leukocytes, $\times 10^{9}$ cells/L	4.8	8.3	7.8	5.7	9.1	10.4	4–11
Parasitemia level, %†	2.43	2.91	1.56	0	0	0	0
Biochemistry							
Alanine aminotransferase, U/L	7.4	22.0	NA	21.0	16.0	NA	≤40
Aspartate aminotransferase, U/L	27.0	67.0	NA	25.0	30.0	NA	≤40
Total bilirubin, µmol/L	84.9	38.1	NA	11.8	9.0	NA	3.1–16.9
C-reactive protein, mg/L	1.3	0.7	NA	1.6	4.0	NA	0–0.5
Urea, µmol/L	na	7.5	NA	3.3	6.0	NA	2.5–8.3
Creatinine, mcM/L	97.0	91.0	NA	111.0	107.0	NA	53–106
Glucose, µmol/L	25.6	14.6	NA	8.4	7.5	NA	3.3–5.5
Total protein, g/L	56.0	55.0	NA	68.5	93.0	NA	62–81

*NA, not available; RBCN, red blood cell normoblasts.
†Percentage of erythrocytes that were infected.

Blood smears obtained on hospital admission tested positive for *Plasmodium* spp. However, because the patient reported no recent travel to malaria-endemic areas, we sent the blood samples for retesting at Sechenov University (Moscow, Russia), where results confirmed babesiosis. We then examined the blood smears after Romanovsky-Giemsa staining, noting the paired forms diverging at a wide angle (≤180°), which is characteristic of both *B. divergens* and *B. venatorum* (Appendix Figure 1, https://wwwnc.cdc.gov/EID/article/31/9/25-0319-App1.pdf).

We screened DNA samples extracted from the blood smears for *B. divergens*, *B. microti*, and *B. venatorum* by PCR, using methods described previously (*6*). We partially sequenced the 18S rRNA gene (1,112 bp; GenBank accession no. PV086113) (*5*). We aligned, compared, and analyzed the resulting nucleotide sequences and reference sequences downloaded from GenBank by using MEGA X (*7*). We also reconstructed a phylogenetic tree (Appendix Figure 2). Using forward and reverse primers form 18S RNA of *Babesia* spp. from Europe, we were able to detect only *B. venatorum* DNA.

We started etiotropic treatment for the patient 3 days from the time we initially detected intraerythrocytic parasites and identified the causative agent as *Babesia* spp. The patient responded to therapy (clindamycin and quinine sulfate), and by day 9 of treatment, parasites were no longer detectable with microscopy (Table). We noted that the ratio of erythrocytes invaded by ≥1 trophozoite changed as the infection progressed. Four days after symptom onset, single trophozoites and pairs (figure 8 pattern) predominated. On the 8th day of infection, with the same level of parasitemia, almost half of the infected erythrocytes contained ≥4 trophozoites (Figure). Parasites continued to divide intensively but did not leave the host cell. Prior research has noted multiple parasites present in individual erythrocytes during fulminant infections in humans (*8*) and in heavily infected in vitro cultures (*9*). Results of such studies suggests that multioccupancy of trophozoites in the erythrocyte

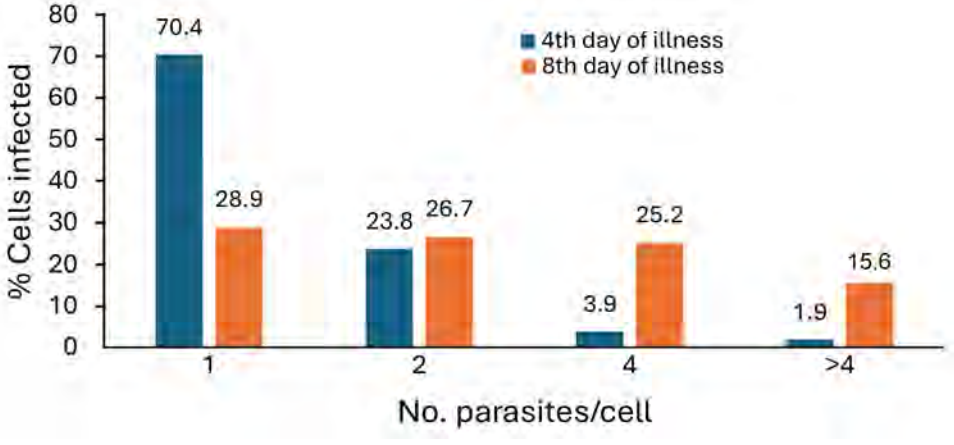

Figure. Dynamics of the parasite population in erythrocytes in case-patient in study of human babesiosis caused by *Babesia venatorum*, Russia, 2024. As the infection progressed with constant parasitemia (<3%), 4 main populations of infected red blood cells were seen: 1 parasite, 2 parasites, 4 parasites, and >4 multioccupancy (>4 parasites).

prevents a sharp increase in parasitemia and helps to preserve the parasite population in the host (*9*). However, the phenomenon we observed occurred at both high (>23%) and low (<3%) parasitemia.

Our study of this unique case of human babesiosis in Siberia, Russia, provides molecular evidence that the etiologic agent was *B. venatorum*. Prior research noted the Asia variant of *B. venatorum* in asymptomatic persons from China (*4*). *B. divergens* infection in splenectomized humans could lead to death, even with timely treatment (*1*). However, the similar course and positive outcome of babesiosis in our patient resembled those in cases previously reported in Europe (*1*), suggesting that the causative agent of the disease was *B. venatorum*, which we confirmed by PCR.

Our patient resided in a village located in a forested area, which is a natural habitat for ticks. The man's work involved staying in the forest, again increasing his risk for tick bites. The fact that the patient did not notice a tick bite is not unusual. Only 50% to 70% of patients with tickborne diseases recall being bitten by a tick (*2*). Considering the ability of *B. venatorum* to be transmitted transovarially and transstadially within *I. persulcatus* ticks, it is possible for a person to become infected through the bite of a tick nymph, which is smaller and less noticeable than the adult (*10*).

In conclusion, our case study revealed the potential risk of *B. venatorum* infection for persons living in Siberia, Russia. Clinicians should be aware that infection can occur as an influenza-like illness and may go unnoticed in immunocompetent persons.

Acknowledgment

We are deeply grateful to Svetlana L. Lukovenko for her collaboration in preparing and sending us blood products (thick and thin blood films) with intraerythrocytic protozoa.

About the Author

Dr. Zelya is a parasitologist working as an assistant professor at Martsinovsky Institute of Medical Parasitology, Tropical and Vector-Borne Diseases, Sechenov University, Moscow, Russia. Her primary research interests are centered on laboratory diagnostics and epidemiology of parasitic diseases.

References

1. Hildebrandt A, Zintl A, Montero E, Hunfeld K-P, Gray J. Human babesiosis in Europe. Pathogens. 2021;10:1165. https://doi.org/10.3390/pathogens10091165
2. Zhou X, Xia S, Huang JL, Tambo E, Zhuge HX, Zhou XN. Human babesiosis, an emerging tick-borne disease in the People's Republic of China. Parasit Vectors. 2014;7:509. https://doi.org/10.1186/s13071-014-0509-3
3. Kumar A, O'Bryan J, Krause PJ. The global emergence of human babesiosis. Pathogens. 2021;10:1447. https://doi.org/10.3390/pathogens10111447
4. Jiang JF, Zheng YC, Jiang RR, Li H, Huo QB, Jiang BG, et al. Epidemiological, clinical, and laboratory characteristics of 48 cases of "*Babesia venatorum*" infection in China: a descriptive study. Lancet Infect Dis. 2015;15:196–203. https://doi.org/10.1016/S1473-3099(14)71046-1
5. Rar VA, Epikhina TI, Livanova NN, Panov VV. Genetic diversity of Babesia in *Ixodes persulcatus* and small mammals from North Ural and West Siberia, Russia. Parasitology. 2011;138:175–82. https://doi.org/10.1017/S0031182010001162
6. Michelet L, Delannoy S, Devillers E, Umhang G, Aspan A, Juremalm M, et al. High-throughput screening of tick-borne pathogens in Europe. Front Cell Infect Microbiol. 2014;4:103. https://doi.org/10.3389/fcimb.2014.00103
7. Kumar S, Stecher G, Li M, Knyaz C, Tamura K. MEGA X: Molecular evolutionary genetics analysis across computing platforms. Mol Biol Evol. 2018;35:1547–9. https://doi.org/10.1093/molbev/msy096
8. Kukina IV, Zelya OP. Extraordinary high level of propagation of *Babesia divergens* in severe human babesiosis. Parasitology. 2022;149:1160–3. https://doi.org/10.1017/S0031182022000439
9. Lobo CA, Cursino-Santos JR, Singh M, Rodriguez M. *Babesia divergens*: a drive to survive. Pathogens. 2019;8:95. https://doi.org/10.3390/pathogens8030095
10. Bonnet S, Brisseau N, Hermouet A, Jouglin M, Chauvin A. Experimental in vitro transmission of *Babesia* sp. (EU1) by *Ixodes ricinus*. Vet Res. 2009;40:21. https://doi.org/10.1051/vetres/2009004

Address for correspondence: Olga P. Zelya, Martsinovsky Institute of Medical Parasitology, Tropical and Vector-Borne Diseases, Sechenov University, Malaya Pirogovskaya st., 20-1, Moscow 119435, Russia; email: zelya_o@mail.ru

Linezolid and Meropenem for *Nocardia otitidiscaviarum* Actinomycetoma, India

Kabir Sardana, Savitha Sharath, Soumya Sachdeva, Shukla Das, Gargi Rai, Praveen Kumar Singh

Author affiliations: Atal Bihari Vajpayee Institute of Medical Sciences and Research Institute and Dr Ram Manohar Lohia Hospital, New Delhi, India (K. Sardana, S. Sharath, S. Sachdeva); University College of Medical Sciences and Guru Teg Bahadur Hospital, New Delhi (S. Das, G. Rai, P.K. Singh)

DOI: https://doi.org/10.3201/eid3109.250514

Treatment of actinomycotic mycetoma with joint involvement is challenging. We present a patient in India with actinomycotic mycetoma who reached complete cure and remission after linezolid and meropenem treatment with a 2-year posttreatment follow-up. Clinicians should use novel drug regimens based on subspecies variations of *Nocardia* and regional drug susceptibility patterns to guide therapy.

Actinomycotic mycetoma presents as a triad of symptoms: painless swelling, discharging sinuses, and presence of grains. *Nocardia brasiliensis* is commonly implicated (*1*). Although varied drugs and regimens have been tried, regional variations in antimicrobial drug sensitivities and species should guide therapy (*2*). We detail the clinical course of a refractory case caused by *N. otitidiscaviarum* infection in a patient in which complete clinical and radiologic remission was achieved with a combination regimen of linezolid and meropenem co-administered with trimethoprim/sulfamethoxazole. We also examine the role of penems on the basis of existing data.

In 2019, we saw a 30-year-old man for painless swelling and multiple pus-discharging sinuses in his right knee for 2 years, which was preceded by trauma from a road traffic accident. Actinomycotic mycetoma was diagnosed and treated with trimethoprim/sulfamethoxazole and dapsone for 6 months, which led to remission for 1 year before recurrence. The patient declined amikacin injections and was treated with trimethoprim/sulfamethoxazole (160 mg/800 mg 2×/d) and faropenem (300 mg) for 6 months, which resulted in complete resolution. Recurrence occurred within 10 months of stopping therapy.

On examination, multiple nodules with overlying sinuses and scanty seropurulent discharge were apparent on the anterior aspect of right knee (Figure 1, panel A). Ultrasonography of the right knee showed a characteristic dot-in-circle sign (Appendix Figure 1, https://wwwnc.cdc.gov/EID/article/31/9/25-0514-App1.pdf) that was confirmed by magnetic resonance imaging. A deep incisional skin biopsy specimen from the nodule revealed epidermal hyperkeratosis, parakeratosis, neutrophil exudate, and irregular acanthosis with multiple small grains in superficial dermis rimmed by dense neutrophilic infiltrate, suggestive of Splendore-Hoeppli phenomenon.

The biopsy specimen collected from the nodule on the right knee revealed the presence of gram-positive, thin, branching filaments, suggestive of actinomycetes. Modified Ziehl-Neelsen stain (using 1% sulphuric acid) showed acid-fast, thin, branching, beaded, filamentous bacilli. Blood agar showed growth of colonies 2–3 mm in size after 72 hours of aerobic incubation that appeared dry, convex, white, and adherent to the medium (Figure 2). On Sabouraud dextrose agar, the colonies were dry and yellowish-orange in color. Subculture and microscopy

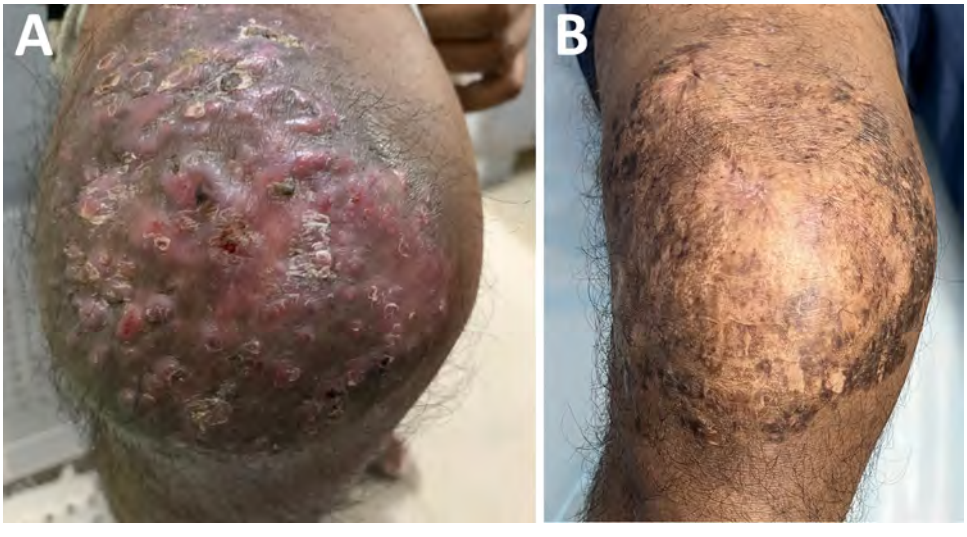

Figure 1. Anterior right knee of patient treated with linezolid and meropenem for *Nocardia otitidiscaviarum* actinomycetoma, India. A) Multiple nodules with overlying sinuses over right knee. B) Near-complete resolution with subsidence of sinuses and nodules leaving behind scarring after 2 months of treatment with a 21-day cycle of linezolid and meropenem combined with trimethoprim/sulfamethoxazole.

Figure 2. Tissue culture from patient treated with linezolid and meropenem for *Nocardia otitidiscaviarum* actinomycetoma, India. Blood agar culture shows growth of dry, convex, white colonies that are adherent to the medium. Original magnification ×200.

reevealed a branching gram-positive rod, and *Nocardia* was confirmed.

Sequencing using PCR displayed >99% similarity with *N. otitidiscaviarum* sequences deposited in GenBank (accession nos. NR_041874.1, KM678016.1, and OQ034626.1) by using BLAST (https://blast.ncbi.nlm.nih.gov) (Appendix). A sensitivity assay using a Sensititre Rapid Growing Mycobacteria RAPMYCOI Plate (Thermo Fisher Scientific, https://www.thermofisher.com) showed sensitivity to sulfamethoxazole, ciprofloxacin, moxifloxacin, cefoxitin, amikacin, doxycycline, linezolid, imipenem, tobramycin, and ceftriaxone.

A 21-day cycle of intravenous linezolid (600 mg 2×/d) and meropenem (500 mg 3×/d), along with trimethoprim/sulfamethoxazole (160 mg/800 mg 2×/d) led to a decrease in discharge within 3 weeks and substantial clinical improvement within 2 months of treatment. (Figure 1, panel B). Trimethoprim/sulfamethoxazole was continued at the same dose for another 10 months and stopped. Residual disease was treated with another cycle of linezolid and meropenem after 10 months. The patient tolerated therapy well and was in remission for 24 months after stopping treatment.

Actinomycotic mycetoma is primarily caused by *Nocardia*, *Streptomyces*, and *Actinomadura* species, and the highest incidence is reported in India, Asia, Pakistan, and Yemen (*1*). Of the various *Nocardia* species, *N. otitidiscaviarum* is rarely reported, predominantly affecting immunocompromised hosts (*3*), and is an uncommon and unreported cause of mycetoma. A previous study with DNA sequencing of 441 *Nocardia* species reported *N. otitidiscaviarum* in 5.9% of samples (*4*). Although there are reports of nocardiosis caused by that species (*4*), actinomycotic mycetoma has not been reported. The existing drug regimens entail cyclical administration and long durations of therapy, and our aim was to explore the use of penems as monotherapy or in combination to treat actinomycotic mycetoma (*2*,*5*,*6*), but no previous study has used a combination with linezolid.

We tried to avoid the use of amikacin because of its side effects. One the basis of sensitivity patterns and previous data (*7*), we used a combination of linezolid and meropenem. Although the sensitivity analysis was tested for imipenem, in vitro studies have shown higher activity of meropenem compared with imipenem against *Nocardia* and reflect its clinical efficacy (*8*). Linezolid has also shown in vitro activity against *Actinomadurae* spp. and *Nocardia* spp. in refractory actinomycotic mycetoma (*9*).

The refractory nature and recurrences in this case could be a consequence of *N. otitidiscaviarum* spp. infection, which is an uncommon cause of actinomycotic mycetoma. The rapid response and long-term remissions make the described regimen suitable and saves inpatient admission costs and repeated admissions that are needed for other regimens (*10*). Thus, it is useful to collate existent sensitivity data with regional antimicrobial sensitivity for a logical combination regimen, and more data on that combination can determine its widespread applicability in mycetoma caused by *Nocardia* spp. Clinicians should use advances in drug regimens according to subspecies variations of *Nocardia* and regional antibiotic drug susceptibility patterns to guide therapy.

About the Author

Dr. Sardana is director professor and head of the dermatology department at Atal Bihari Vajpayee Institute of Medical Sciences and Dr Ram Manohar Lohia hospital. His research interests include infectious diseases, acne, systemic drugs, and the immunopathogenesis of dermatologic disorders.

References

1. Reis CMS, Reis-Filho EGM. Mycetomas: an epidemiological, etiological, clinical, laboratory and therapeutic review. An Bras Dermatol. 2018;93:8–18. https://doi.org/10.1590/abd1806-4841.20187075
2. Sardana K, Chugh S. Newer therapeutic modalities for actinomycetoma by *Nocardia* species. Int J Dermatol. 2018;57:e64–5. https://doi.org/10.1111/ijd.14073

3. Barry M, AlShehri S, Alguhani A, Barry M, Alhijji A, Binkhamis K, et al. A fatal case of disseminated nocardiosis due to *Nocardia otitidiscaviarum* resistant to trimethoprim-sulfamethoxazole: case report and literature review. Ann Clin Microbiol Antimicrob. 2022;21:17. https://doi.org/10.1186/s12941-022-00511-9
4. Wang H, Zhu Y, Cui Q, Wu W, Li G, Chen D, et al. Epidemiology and antimicrobial resistance profiles of the *Nocardia* species in China, 2009 to 2021. Microbiol Spectr. 2022;10:e0156021. https://doi.org/10.1128/spectrum.01560-21
5. Ameen M, Arenas R, Vásquez del Mercado E, Fernández R, Torres E, Zacarias R. Efficacy of imipenem therapy for *Nocardia actinomycetomas* refractory to sulfonamides. J Am Acad Dermatol. 2010;62:239–46. https://doi.org/10.1016/j.jaad.2009.06.043
6. Ameen M, Vargas F, Arenas R, del Mercado EV. Successful treatment of *Nocardia actinomycetoma* with meropenem and amikacin combination therapy. Int J Dermatol. 2011;50:443–5. https://doi.org/10.1111/j.1365-4632.2010.04748.x
7. Zhao P, Zhang X, Du P, Li G, Li L, Li Z. Susceptibility profiles of *Nocardia* spp. to antimicrobial and antituberculotic agents detected by a microplate Alamar Blue assay. Sci Rep. 2017;7:43660. https://doi.org/10.1038/srep43660
8. Lai CC, Tan CK, Lin SH, Liao CH, Chou CH, Hsu HL, et al. Comparative in vitro activities of nemonoxacin, doripenem, tigecycline and 16 other antimicrobials against *Nocardia brasiliensis, Nocardia asteroides* and unusual *Nocardia* species. J Antimicrob Chemother. 2009;64:73–8. https://doi.org/10.1093/jac/dkp144
9. Sardana K, Sachdeva S. A combination of trimethoprim/sulfamethoxazole with linezolid is useful for actinomycotic mycetoma: a summary of the existing data and the rationale of combination therapy. Indian J Dermatol Venereol Leprol. 2022;88:212–3. https://doi.org/10.25259/IJDVL_539_2021
10. Verma P, Jha A. Mycetoma: reviewing a neglected disease. Clin Exp Dermatol. 2019;44:123–9. 10.1111/ced.13642

Address for correspondence: Kabir Sardana, Atal Bihari Vajpayee Institute of Medical Sciences and Research Institute and Dr Ram Manohar Lohia Hospital, Rm 167, OPD Bldg, New Delhi 110001, India; email: article.sardana@gmail.com

Subarachnoid Neurocysticercosis Caused by Larval-Stage *Taenia crassiceps* Tapeworm, Slovenia

Barbara Šoba, Sandra Kolar, Albin Gačnik, Manca Radež, Timotej Petrijan, Jana Rejc Marko

Author affiliations: University of Ljubljana, Ljubljana, Slovenia (B. Šoba, M. Radež); University Medical Centre Maribor, Maribor, Slovenia (S. Kolar, A. Gačnik, T. Petrijan, J. Rejc Marko)

DOI: https://doi.org/10.3201/eid3109.250014

We present a case of subarachnoid neurocysticercosis caused by *Taenia crassiceps* in an elderly woman in Slovenia with no underlying disease or immunosuppressive treatment. The parasite was identified by 12S rDNA PCR and sequencing. Despite prolonged therapy with albendazole and praziquantel, the disease recurred after treatment was discontinued.

Human neurocysticercosis is a severe infection of the central nervous system, generally caused by larvae of the tapeworm *Taenia solium* and, rarely, by other *Taenia* species, such as *T. crassiceps*. So far, 2 cases of *T. crassiceps* neurocysticercosis have been reported in humans (*1*,*2*).

The adult *T. crassiceps* is an intestinal parasite of carnivores, mainly foxes; small mammals, such as rodents, serve as natural intermediate hosts for cyst-like larvae that proliferate by budding in their body cavities or subcutaneous tissues, leading to massive infections. Humans can become accidental intermediate hosts by ingesting parasite eggs excreted in the definitive hosts' feces or by contamination of open wounds with eggs, as suspected in subcutaneous infections (*3*). In addition to neural and subcutaneous infections, infestation of eyes, muscle tissue, and tendons has been reported in humans (*1*,*3*). We describe a case of *T. crassiceps* infection in an elderly patient with meningitis and progressive deterioration of neurologic symptoms diagnosed by a combination of serologic and molecular methods.

Neurologic symptoms developed in a 74-year-old woman from northeastern Slovenia with no underlying diseases in December 2022. Symptoms worsened and led to gait ataxia; tetraparesis, which was markedly left-sided; urinary incontinence; and cognitive decline within a year.

Lumbar puncture (LP) performed in May 2023 confirmed aseptic meningitis. Cerebrospinal fluid

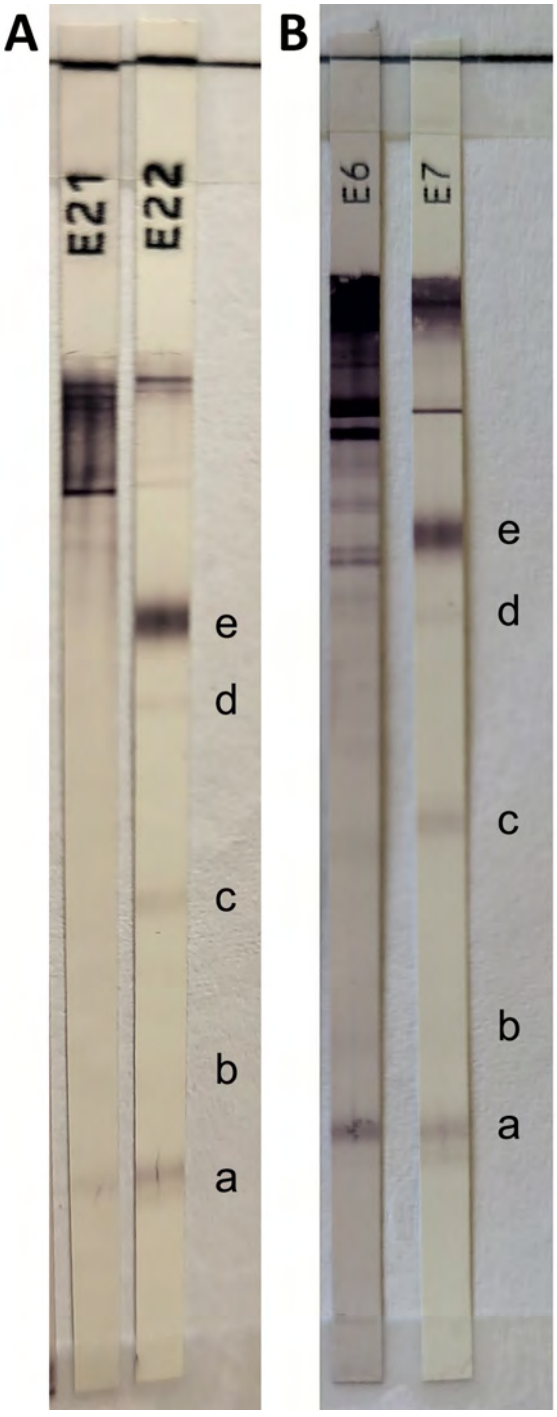

Figure 1. Equivocal results of Cysticercosis Western blot IgG (LDBIO Diagnostics, https://ldbiodiagnostics.com) assay in study of subarachnoid neurocysticercosis caused by larval-stage *Taenia crassiceps* tapeworm, Slovenia. Results of patient's serum (A) and cerebrospinal fluid (B) samples show 6–8 kDa band and a weak 12 kDa band. Cysticercosis-specific bands are 6–8 kDa (a), 12 kDa (b), 23–26 kDa (c), 39 kDa (d), and 50–55 kDa (e). The presence of ≥2 well-defined bands among the 5 mentioned is indicative of neurocysticercosis. E21, patient's serum; E6, patient's cerebrospinal fluid; E7 and E22, positive controls.

(CSF) showed elevated protein levels (0.72 g/L; reference range 0.15–0.45 g/L). Glucose (2.8 mmol/L; reference range 2.5–3.9 mmol/L) and glucose ratio between CSF and serum (0.44; reference >0.31) were unremarkable. Pleocytosis was present with a total leukocyte count of 108 × 10^6 (reference <5 × 10^6) cells/L. Analysis of CSF sediment revealed 1% neutrophils, 75% lymphocytes and 3% plasma cells, 9% monocytes, and 12% eosinophils. Intrathecal synthesis of IgG (163.9 mg/L), IgM (5.0 mg/L), and IgA (5.7 mg/L) was confirmed. Results of blood tests, including a differential blood count, were unremarkable.

Magnetic resonance imaging (MRI) of the brain revealed an enlarged ventricular system that was more pronounced on the right side without changes in the brain parenchyma. Follow-up LPs confirmed the persistence of pleocytosis in the CNS. Extensive microbiological analyses of CSF and blood samples for infectious agents (Appendix, https://wwwnc.cdc.gov/EID/article/31/9/25-0014-App1.pdf) and tests for autoimmune and paraneoplastic encephalitis were repeatedly negative, with the exception of serologic testing of blood and CSF samples for *T. solium* IgG, which was equivocal (Figure 1). Because this result was suspicious for neurocysticercosis, we tested CSF using cestode-specific PCR amplifying the mitochondrial 12S rRNA gene (*4*); the result was positive. After sequencing and BLAST analysis (https://blast.ncbi.nlm.nih.gov/Blast.cgi) of the 242-bp amplicon obtained (Gen Bank accession no. PQ764695), the sequence showed 100% homology with *T. crassiceps*.

MRI of the brain with contrast performed in March 2024 showed changes consistent with a subarachnoid form of neurocysticercosis (Figure 2). Results of investigations to identify additional foci of cysticercosis, including MRI of the spinal cord, were unremarkable.

We initiated dual therapy for neurocysticercosis with albendazole (800 mg/d) and praziquantel (2,400 mg/d), along with dexamethasone (6 mg/d) to prevent inflammation, in April 2024. Dexamethasone was administered for 4 weeks and praziquantel with albendazole for 85 days. After 85 days of therapy, subsequent CSF PCRs were negative. Praziquantel was discontinued, and treatment with albendazole was continued for a further 80 days. An LP performed 10 days after discontinuation of treatment showed no signs of meningitis. One month later, eosinophilic meningitis was again confirmed with a total leukocyte count of 20 × 10^6 cells/L in CSF, of which 27% were eosinophils in the sediment, and PCR was again positive. The patient was restarted on dexamethasone, albendazole, and praziquantel for 2 weeks in November 2024, after

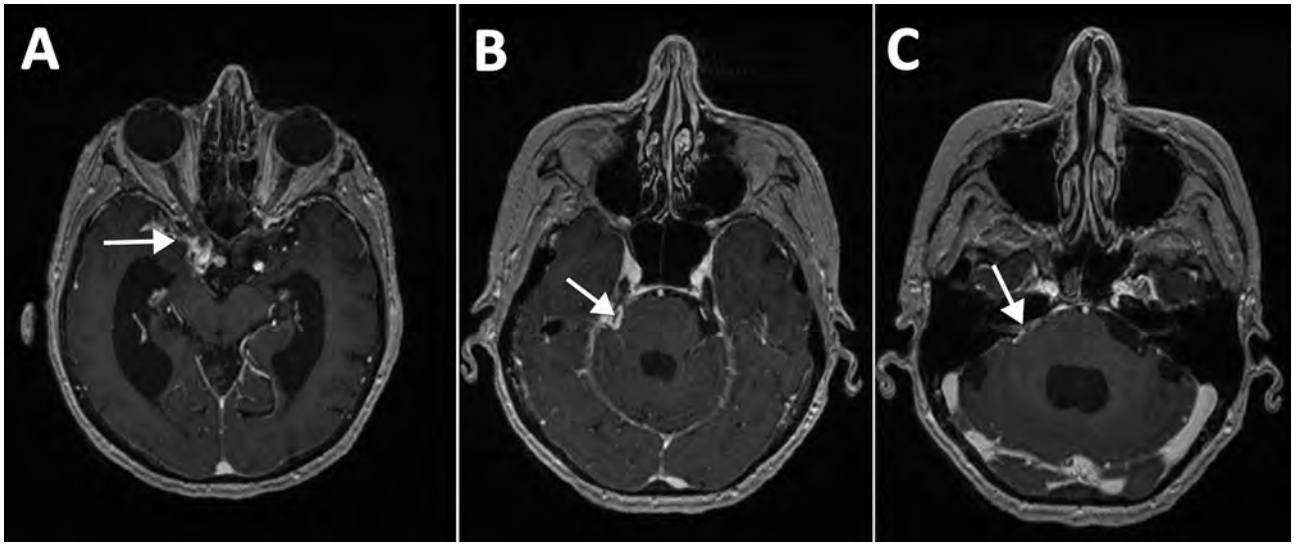

Figure 2. Magnetic resonance imaging of the brain in study of subarachnoid neurocysticercosis caused by larval-stage *Taenia crassiceps* tapeworm, Slovenia. Imaging shows pathological signal enhancement at the site of inflammation after contrast administration (white arrows) and a dilated ventricular system (hydrocephalus) as a result of impaired cerebrospinal fluid drainage in the right basal cisterns (A), right parapontine basal cistern (B), and right pontocerebellar angle (C).

which she continued treatment with albendazole. At least 1 year of albendazole treatment was planned and, in case of recurrence, lifelong therapy.

The patient's cognitive status improved substantially after treatment, but spastic tetraparesis did not. She was no longer able to care for herself and moved into a nursing home.

Human *T. crassiceps* infections are rare; 16 cases have been reported during 1973–2023, mostly in immunocompromised but also in immunocompetent persons (*1*–*3*,*5*–*9*). Although our patient had no underlying conditions, her age might have led to immunosenescence, increasing her susceptibility to infection.

Laboratory diagnosis of *T. crassiceps* cysticercosis is challenging, especially when no clinical material is available for parasitological and pathological evaluation, as in our patient who had subarachnoid neurocysticercosis. The cystic appearance of the larvae was not visible on MRI, which differs from 2 other described cases of the parenchymal form of the disease (*1*,*2*). Equivocal or weak positive results of serologic tests for other helminthiases might indicate a possible infection (*1*,*8*,*9*). In fact, the initial suspicion of cysticercosis in this patient arose from equivocal blood and CSF *T. solium* serologic testing.

The source of this patient's infection is unknown, but she owned a dog, as did several other reported case-patients (*1*,*5*,*7*,*8*). Increased recreational activity in wildlife areas raises risk for *T. crassiceps* infection in domestic carnivores, making regular canid deworming essential to prevent infections in humans.

Acknowledgments

We thank the patient and her family for consenting to publication of this case report.

This study was partly supported by funding from the Slovenian Research and Innovation Agency (grant no. P3-0083).

About the Author

Dr. Šoba is head of the Laboratory of Parasitology at the Institute of Microbiology and Immunology at the Faculty of Medicine, University of Ljubljana, Slovenia. Her primary research interests are diagnostics, epidemiology, and clinical significance of human parasites and their molecular typing.

References

1. Ntoukas V, Tappe D, Pfütze D, Simon M, Holzmann T. Cerebellar cysticercosis caused by larval *Taenia crassiceps* tapeworm in immunocompetent woman, Germany. Emerg Infect Dis. 2013;19:2008–11.
2. Floß N, Dolff S, Junker A, Blau T, Rauschenbach L, Sure U, et al. Cerebral *Taenia crassiceps* larvae infection in a 71-year-old immunocompetent male. Infection. 2023;51:277–81.
3. Deplazes P, Eichenberger RM, Grimm F. Wildlife-transmitted *Taenia* and *Versteria* cysticercosis and coenurosis in humans and other primates. Int J Parasitol Parasites Wildl. 2019;9:342–58.
4. Roelfsema JH, Nozari N, Pinelli E, Kortbeek LM. Novel PCRs for differential diagnosis of cestodes. Exp Parasitol. 2016;161:20–6.
5. Goesseringer N, Lindenblatt N, Mihic-Probst D, Grimm F, Giovanoli P. *Taenia crassiceps* upper limb fasciitis in a patient with untreated acquired immunodeficiency syndrome and

chronic hepatitis C infection—the role of surgical debridement. J Plast Reconstr Aesthet Surg. 2011;64:e174–6.
6. Heldwein K, Biedermann HG, Hamperl WD, Bretzel G, Löscher T, Laregina D, et al. Subcutaneous *Taenia crassiceps* infection in a patient with non-Hodgkin's lymphoma. Am J Trop Med Hyg. 2006;75:108–11.
7. Roesel C, Welter S, Stamatis G, Theegarten D, Tappe D. Management of a chest-wall soft-tissue tumor caused by an infection with the larval tapeworm pathogen *Taenia crassiceps*. Am J Trop Med Hyg. 2014;91:541–3.
8. Schmid S, Grimm F, Huber M, Beck B, Custer P, Bode B. *Taenia crassiceps* infection—an unusual presentation of a tapeworm diagnosed by FNA cytology and PCR. Cytopathology. 2014;25:340–1.
9. Tappe D, Berkholz J, Mahlke U, Lobeck H, Nagel T, Haeupler A, et al. Molecular identification of zoonotic tissue-invasive tapeworm larvae other than *Taenia solium* in suspected human cysticercosis cases. J Clin Microbiol. 2016;54:172–4.

Address for correspondence: Barbara Šoba, Institute of Microbiology and Immunology, Faculty of Medicine, University of Ljubljana, Zaloška 4, 1000 Ljubljana, Slovenia; email: barbara.soba@mf.uni-lj.si

Pediatric Case Report and Overview of Autochthonous Tick-Borne Encephalitis, Belgium

Justine De Langhe, Jo Sourbron, Robbe Van Herreweghe, Marjan van Esbroeck, Koen Vercauteren, Tessa de Block, Jasmine Coppens, Daan Jansen, Dorien Van den Bossche, Veerle Staelens, Sarah De Schryver, Jos Van Acker

Author affiliations: Ghent University Hospital, Ghent, Belgium (J. De Langhe); Ghent University Faculty of Medicine and Health Sciences, Ghent (J. De Langhe, R. Van Herreweghe); University Hospital KU Leuven, Leuven, Belgium (J. Sourbron); Ghent University Hospital Center for Medical Genetics, Ghent (J. Sourbron); Institute of Tropical Medicine Antwerp, Antwerp, Belgium (M. van Esbroeck, K. Vercauteren, T. de Block, J. Coppens, D. Jansen, D. Van den Bossche); AZ Sint-Lucas Gent, Ghent (V. Staelens, S. De Schryver, J. Van Acker)

DOI: https://doi.org/10.3201/eid3109.250093

Prevalence of tick-borne encephalitis (TBE) is increasing in much of Europe. In May 2024, an autochthonous pediatric case of TBE was diagnosed in a 6-year-old girl in Belgium. Clinicians should recognize the symptoms and signs of TBE infections and consider this disease in patients with unexplained neurologic symptoms, regardless of travel history.

Tick-borne encephalitis (TBE) is a disease of the central nervous system (CNS) caused by TBE virus (TBEV). TBEV is endemic in regions from Europe to the Far East, where ixodid ticks act as vectors (*1*–*3*). TBEV has 3 main subtypes: European, Siberian, and Far Eastern (*2*–*4*).

Since 1973, TBE incidence has increased by nearly 400% in Europe, excluding Portugal and Belgium. TBE is mainly transmitted from late spring to early autumn, and spread is linked to global warming (*1*–*3*). TBEV infection can also occur by consumption of unpasteurized milk products from infected livestock (*1*,*3*).

Clinical course and outcomes vary by TBEV subtype. The European subtype often causes a biphasic illness. Up to 10% of TBE patients develop pareses from myelitis, and the mortality rate is 0.5%–2%. Symptoms begin 8 days after tick bite (incubation range 4–28 days) with a nonspecific febrile illness (viremic phase), which resolves before potentially progressing to CNS inflammation 2–8 days later (neurotrophic phase). Neurologic symptoms include meningitis and meningoencephalitis, typically lasting 7–10 days (*1*,*3*). Preventive measures are essential, because no effective treatment exists (*1*).

According to the literature available through August 2024, in Belgium, 8 nonautochthonous (*5*) and 3 autochthonous (*6*) TBE cases had occurred in adults. We report an autochthonous pediatric TBE case in Belgium and compare that case to the 3 autochthonous TBE cases in adults.

A 6-year-old girl was brought for care with a 6-day history of fever, diarrhea, and myalgia. She had returned from Thailand 3 weeks earlier and engaged in several outdoor activities after her return to Belgium. A clinical examination did not identify a cause for the fever. Blood tests showed mild thrombocytopenia, leukopenia, and elevated creatine kinase (CK) (Table). An infectious serology search focused on common infections in Thailand. Results of testing of a urine sample and nasopharyngeal swab specimen were negative. A stool sample showed the presence of *Salmonella enterica* serovar Bareilly and *Campylobacter jejuni*; azithromycin was initiated for 3 days. During her 5-day hospital stay, the patient showed clinical improvement, and her fever resolved.

Table. Details of autochthonous tick-borne encephalitis cases in a child compared with 3 previous cases in adults, Belgium*

Characteristic	Patient no. from 2021 report (*6*)			Case report from 2024 (this study)
	1	2	3	
Age of onset, y/sex	48/F	59/M	58/M	6/F
Tick bite†	2 weeks before symptom onset	2 weeks before symptom onset	Multiple tick bites in the weeks before symptom onset	No observed tick bite, but increased outdoor activities
Likely site of tick bite, postal code (province)‡	Oostkamp, 8020 (West Flanders)	Lille, 2275 (Antwerp)	Wanze, 4520 (Liège)	Evergem, 9940 (East Flanders)
Signs/symptoms				
During first (viremic) phase	Myalgia, fever	Fever, fatigue, myalgia, headache	Dyspnea, cough, fever	Recurrent fever, diarrhea, anorexia, arthralgia (ankles, hands and wrists), myalgia, ophthalmalgia, cervicalgia
During second (neurotrophic) phase	Asthenia, tremor, drowsiness, fever, peripheral facial palsy, brachial weakness, nuchal rigidity	Fever, fatigue, myalgia, headache, paraparesis, signs of meningitis, severe motor polyradiculitis	Recurrent fever, severe and persistent headaches, weakness, diarrhea, anorexia	Spiking fever, photophobia, vomiting, agitated behavior, fatigue, myalgia, arthralgia, diarrhea
At follow-up (time)	Weakness of right arm, loss of cognitive function, inability to concentrate, fatigue, tremor (≈2 mo)	Improved motor skills 9 mo after hospitalization (wheelchair at discharge) (9 mo)	Occasional headaches, otherwise recovered (≈2 mo)	No residual symptoms (6 mo)
Sample type (no. days after symptom onset)	Serum (5), CSF (6)	Serum (20), CSF (18)	Serum (2), serum (18)	Serum (5), serum (17), CSF (17), serum (19), serum (26)
Flavivirus IFA serum (no. days after symptom onset)	Serum (5): IgM, TBEV+; IgG, TBEV+	Serum (20): IgM, TBEV+; IgG, TBEV+	Serum (2): IgM, TBEV–; IgG, TBEV–. Serum (18): IgM, TBEV+; IgG, TBEV+	Serum (5): IgM, TBEV–; IgG, TBEV–. Serum (17): IgM, TBEV+ (>1/80); IgG, TBEV+ (>1/80). Serum (26): IgM, TBEV+ (>1/80); IgG, TBEV+ (>1/80)
Flavivirus IFA CSF (days after symptom onset)	CSF (6): IgM, TBEV+; IgG, TBEV+	CSF (18): IgM, TBEV+; IgG, TBEV+	ND	CSF (17): IgM, TBEV+; IgG, ND (sample too small for both Ig types)
$PRNT_{90}$ titer (no. days after symptom onset)	Serum (5): 1:25; CSF (6): ND	Serum (20): 1:60; CSF (18): ND	Serum (2): ND; serum (18): 1:194	Serum (26): 1:204
rRT-PCR (no. days after symptom onset)	Serum (5): ND; CSF (6): ND	Serum (20): ND; CSF (18): ND	Serum (2): +; serum (18): ND	Serum (5): + (Ct 36.27); serum (17): ND; CSF (17): ND; serum (19): ND; serum (26): ND
TBEV RNA sequencing (serum)	ND	ND	ND	European subtype TBEV

*Additional case characteristics are provided in Appendix Table 2 (https://wwwnc.cdc.gov/EID/article/31/9/25-0093-App1.pdf). CSF, cerebrospinal fluid; Ct, cycle threshold; IFA, indirect fluorescent antibody; ND, not determined; $PRNT_{90}$, 90% plaque reduction neutralization test; rRT-PCR, real-time reverse transcription PCR; TBEV, tick-borne encephalitis virus; +, present/positive; –, absent/negative.
†Early removal of the tick might not prevent encephalitis (*4*). Approximately 30% of cases occur without a reported tick bite (*2*,*4*).
‡Locations show no clear proximity (Appendix Figure 3).

Four days after discharge, the girl was readmitted because of recurrent fever for 1 day and arthralgia. Additional blood results showed no anomalies. On day 4 of readmission, meningeal signs appeared, and blood tests showed leukocytosis. Extensive imaging showed no anomalies. A lumbar puncture showed cerebral spinal fluid (CSF) leukocytosis, prompting intravenous cefotaxime. Extensive serology testing was performed. After 7 days of intravenous cefotaxime treatment, TBEV IgM was detected in CSF. The patient, whose symptoms resolved, was discharged. Follow-up consultations indicated favorable recovery without residual symptoms. A brain magnetic resonance imaging scan showed no cerebral injuries.

We compared the clinical course of this patient to those of the 3 previous autochthonous TBEV cases in Belgium (Table). We noted no geographic links between those 3 cases and the pediatric case we report. In all cases, a biphasic course was observed. In 2 of the previous cases, long-term neurologic sequelae were documented several months postinfection; however, we did not observe such sequelae in our case. In cases with persistent neurological deficits, paresis was already evident during the neurotrophic phase, consistent with the 10% of TBE patients who develop paresis as a result of myelitis.

We observed a biphasic course, observed in 75% of TBE cases (*1*–*3*), in this patient. Serum CK levels were

also elevated (*4*). Some TBE patients have myalgia/myositis, and up to one third have elevated serum CK levels (*7*), yet the clinical relevance is still unclear. After the patient had a symptom-free interval, fever recurred, and meningitis was confirmed. TBEV IgM was detected in serum and CSF. Testing for Japanese encephalitis was initiated because of the patient's travel history; TBEV testing was included in that panel.

Given the incubation range of 4–28 (median 8) days (*2*,*3*), we cannot exclude possible TBEV infection in Thailand. However, no TBE cases have been reported in Thailand (*8*). Moreover, sequencing of the TBEV RNA from a serum sample identified the European subtype, suggesting infection acquired in Europe (Appendix, https://wwwnc.cdc.gov/EID/article/31/9/25-0093-App1.pdf). Although no tick bite was reported for this patient, her increased outdoor activities posed a substantial risk; tick bites go unnoticed in about one third of TBE cases (*3*).

A rare transmission route of TBEV (1% of all cases) is through consuming unpasteurized milk from infected livestock (*9*). This patient consumed unpasteurized cow's milk >2 weeks before symptoms appeared; however, the Federal Agency for Food Chain Safety in Belgium investigated the identified producer's milk and found no TBEV RNA.

Of note, the patient's dog had recently been euthanized because of a suspected stroke. Neurologic signs such as ataxia, plegia/paresis, cranial nerve deficits, and seizures have been described in TBEV-infected dogs (*10*). However, postmortem investigations were not performed because the animal was cremated.

Because most (70%–98%) TBEV infections are asymptomatic, prevalence of TBEV infections is presumably underestimated (*4*,*6*). Clinicians should recognize the signs and symptoms of TBEV infection and consider TBE in patients with unexplained neurologic symptoms, particularly a biphasic course (*2*).

Acknowledgments

We thank the patient and their parents for participating in our study, sharing their medical histories, and allowing us to publish these data. We thank Sandra Coppens and Kadrie Ramadan for their technical support.

All authors made substantial contributions to the conception and design of the study; data acquisition, analysis, and interpretation; and drafting of the article.

J.S. served as a consultant or speaker for UCB and Bright Minds Biosciences and as a member of the medical advisory board for UCB.

About the Author

Ms. De Langhe is a pediatrician in training at the University of Ghent.

References

1. Palyga-Bysiecka I, Kręcisz B, Szczepańska B. Clinical course and neurological sequels after tick-borne encephalitis in children—case report. Ann Agric Environ Med. 2022;29:162–7. https://doi.org/10.26444/aaem/133206
2. Riccardi N, Antonello RM, Luzzati R, Zajkowska J, Di Bella S, Giacobbe DR. Tick-borne encephalitis in Europe: a brief update on epidemiology, diagnosis, prevention, and treatment. Eur J Intern Med. 2019;62:1–6.
3. Lindquist L, Vapalahti O. Tick-borne encephalitis. Lancet. 2008;371:1861–71.
4. Cesaroni CA, Frattini D, Lecis M, Bonvicini F, Bartolomeo D, Rizzi S, et al. Tick-borne encephalitis in a 6-year-old patient: a case report. Neurohospitalist. 2024;14:64–8.
5. National Reference Center for TBEV. Tick-borne encephalitis virus, List of confirmed human cases of acute TBE, 2012–2017. Antwerp: The Center; 2017.
6. Stoefs A, Heyndrickx L, De Winter J, Coeckelbergh E, Willekens B, Alonso-Jiménez A, et al. Autochthonous cases of tick-borne encephalitis, Belgium, 2020. Emerg Infect Dis. 2021;27:2179–82. https://doi.org/10.3201/eid2708.211175
7. Bogovič P, Lotrič-Furlan S, Ogrinc K, Avšič Županc T, Korva M, Kastrin A, et al. Elevated levels of serum muscle enzymes in the initial phase of tick-borne encephalitis. Infect Dis (Lond). 2024;56:504–9. https://doi.org/10.1080/23744235.2024.2335349
8. Raksakoon C, Potiwat R. Current arboviral threats and their potential vectors in Thailand. Pathogens. 2021;10:80. https://doi.org/10.3390/pathogens10010080
9. Buczek AM, Buczek W, Buczek A, Wysokińska-Miszczuk J. Food-borne transmission of tick-borne encephalitis virus—spread, consequences, and prophylaxis. Int J Environ Res Public Health. 2022;19:1812. https://doi.org/10.3390/ijerph19031812
10. Kleeb C, Golini L, Beckmann K, Torgerson P, Steffen F. Canine tick-borne encephalitis: clinical features, survival rate and neurological sequelae: a retrospective study of 54 cases (1999–2016). Front Vet Sci. 2021;8:782044. https://doi.org/10.3389/fvets.2021.782044

Address for correspondence: Jos Van Acker, Laboratory of Microbiology, AZ Sint-Lucas Gent, Groenebriel 1, 9000 Gent, Belgium; email: Jos.VanAcker@azstlucas.be

New World Screwworm Infestation in Wild Mountain Tapirs, Central Andes Mountains, Colombia

Juan Camilo Cepeda-Duque, Leidy Johana Cano-González, Gerardo Elejalde, Juan Camilo Mantilla, Diego Álvarez-Arellano, Julio Cesar Gómez-Salazar, Victoria Rodríguez, Diego J. Lizcano, Jesús Alfredo Cortés-Vecino, Álvaro A. Faccini-Martínez, Thiago Fernandes Martins, Jacob Owens, Jordan Davis-Powell, Liza Dadone, Carlos Galvis, Budhan S. Pukazhenthi, Juliana Vélez

Authors affiliations: Tiger Cats Conservation Initiative, Dosquebradas, Colombia (J.C. Cepeda-Duque); Organización Ambiental Chinampa, Pereira, Colombia (J.C. Cepeda-Duque, L.J. Cano-González, J.C. Mantilla); International Union for Conservation of Nature and Natural Resources Species Survival Commission, Tapir Specialist Group, Gland, Switzerland (J.C. Cepeda-Duque, V. Rodríguez, D.J. Lizcano, J. Owens, J. Davis-Powell, L. Dadone, C. Galvis, B.S. Pukazhenthi, J. Vélez); Laboratorio de Entomología, Corporación Universitaria de Santa Rosa de Cabal, Santa Rosa de Cabal, Colombia (G. Elejalde, D. Álvarez-Arellano); Corporación Autónoma Regional de Risaralda, Pereira (J.C. Gómez-Salazar); Wildlife Conservation Society, Colombia, Cali, Colombia (D.J. Lizcano); Laboratorio de Parasitología Veterinaria, Facultad de Medicina Veterinaria y de Zootecnia, Universidad Nacional de Colombia, Bogota, Colombia (J.A. Cortés-Vecino); Hospital Militar Central, Bogota (Á.A. Faccini-Martínez); Universidad Militar Nueva Granada, Bogota (Á.A. Faccini-Martínez); Faculdade de Medicina Veterinária e Zootecnia, Universidade de São Paulo, Sao Paulo, Brazil (T.F. Martins); Los Angeles Zoo & Botanical Gardens, Los Angeles, California, USA (J. Owens, J. Davis-Powell); Giraffe Veterinary Services, Colorado Springs, Colorado, USA (L. Dadone); Fundación Zoológica de Cali, Cali (C. Galvis); Smithsonian's National Zoo and Conservation Biology Institute, Front Royal, Virginia, USA (B.S. Pukazhenthi); Center for Conservation Biology, Stanford University, Stanford, California, USA (J. Vélez); The Natural Capital Project, Stanford University, Stanford (J. Vélez)

DOI: https://doi.org/10.3201/eid3109.250339

We describe New World screwworm (Cochliomyia hominivorax) infestation in 2 injured mountain tapirs (Tapirus pinchaque) from a protected area in the Central Andes, Colombia. Screwworms were not a known threat to mountain tapirs. Community outreach is needed to raise awareness on effects of this parasite on humans, domestic animals, and wildlife.

The New World screwworm (NWS) (*Cochliomyia hominivorax*) is an obligate parasite that requires a living host for larval development (*1*). NWS is endemic in countries in the Caribbean region and in South America, and cases have spread north to Central America (https://www.aphis.usda.gov/livestock-poultry-disease/cattle/ticks/screwworm). Thus, risk for re-introduction of NWS from South America to NWS-free areas in Central and North America is constant (*2*). Because of its substantial effects on livestock, wildlife, and human health, NWS infection is reportable in Colombia (*1*,*3*). However, reports of this parasite affecting the mountain tapir (*Tapirus pinchaque*), an endangered species on the International Union for Conservation of Nature Red List (https://www.iucnredlist.org), have only been anecdotal. Here, we describe 2 cases of myiasis caused by NWS infestation in mountain tapirs in a protected area of the Central Andes of Colombia.

We collected NWS larvae from 2 adult mountain tapirs, 1 female on October 19, 2024, and 1 male on January 28, 2025, in Ucumari Regional Natural Park (4°42′14″N, 75°32′14″W) at an altitude of 2,097 meters. Both tapirs had deep, 8–10-cm long wounds with exposed muscles in their hindquarters, consistent with myiasis caused by NWS larvae feeding on living tissues (Figure 1). Neither tapir received prior treatment or was subsequently monitored, making determination of the cause or progression of their injuries impossible. To collect larvae, the local environmental authority, Corporación Autónoma Regional de Risaralda, chemically restrained the female tapir, but the male tapir exhibited docile behavior in its interactions with the local community and did not require restraint.

We collected 2 larvae directly from the female tapir's wound with tweezers and placed larvae in a box until they pupated; after 12 days, they emerged as adult flies (both male) (Appendix Figure 1, https://wwwnc.cdc.gov/EID/article/31/9/25-0339-App1.pdf), which we photographed then stored in 96% ethyl alcohol. We collected 20 larvae from the male tapir and stored larvae in 70% ethyl alcohol. We also photographed phenotypic traits of maggots from the male tapir to enable taxonomic identification and confirm NWS (Figure 2) (*4*).

Our assessment of wild mammals in the area that have potential to host NWS indicated that other threatened species are also at risk, including the clouded tiger-cat (*Leopardus pardinoides*), little red brocket (*Mazama rufina*), northern pudu (*Pudela mephistophiles*), Andean bear (*Tremarctos ornatus*), mountain coati (*Nasuella olivacea*), and Andean squirrel

(*Leptosciurus pucheranii*) (Appendix Figure 2). NWS infestations have been documented in several threatened neotropical mammals in the Caribbean and the Americas, including the giant armadillo (*Prionodon maximus*), maned wolf (*Chrysoscyon brachyurus*), jaguar (*Panthera onca*), giant anteater (*Myrmecophaga tridactyla*), lowland tapir (*Tapirus terrestris*), and giant otter (*Pteronura brasiliensis*) (Appendix Table). Humans and domestic animals are also at risk for NWS infestation.

Although often overlooked, myiasis has been linked to severe population declines in wild ungulates, raising conservation concerns for species with low reproductive rates and population sizes, such as mountain tapirs (*5*). For instance, in October 2016, NWS myiasis led to the loss of 14% of the total Key deer (*Odocoileus virginianus clavium*) population in Florida in the United States (*2*). In addition, myiasis resulted in mortality rates of white-tailed deer fawns (*O. v. texanus*) that ranged from 25% to 80% across different regions of the United States (*6*). The proximity of livestock has been associated with NWS outbreaks, and climate change could contribute to expansion of NWS into new areas (*7*).

Factors associated with the emergence of NWS in mountain tapirs remain unclear. Although livestock production in the local area is minimal, contact between livestock and tapirs might exist. Free-ranging dogs, known carriers of NWS (*3*), also have been documented negatively interacting with mountain tapirs (*5*). In addition, intraspecific aggression among tapirs and prolonged use of radio collars also can cause wounds promoting myiasis development, as observed in collared peccaries (*Pecari tajacu*) (*8*) and lowland tapirs (*9*). The parasite also affects humans, and a case of umbilical myiasis was reported in a 7-day-old infant in La Virginia, Risaralda, Colombia, in 2020 (*10*).

To mitigate the threat from NWS, Colombia should consider implementing a biological control

Figure 1. Myiasis in cases of New World screwworm infestation in wild mountain tapirs, Central Andes Mountains, Colombia. Myiasis and active larvae can be seen in large, 8–10-cm wounds on left side of adult male tapir (A, C) and on right hindquarters of adult female tapir (B, D). Both tapirs were in the Ucumari Regional Natural Park, Risaralda, Colombia. We retrieved 2 larvae from the female tapir's wound and placed in a box until they pupated; after 12 days they emerged as adults (both male) (Appendix Figure 1, https://wwwnc.cdc.gov/EID/article/31/9/25-0339-App1.pdf), which we stored in 96% ethyl alcohol. We collected 20 larvae from the male tapir and stored in 70% ethyl alcohol.

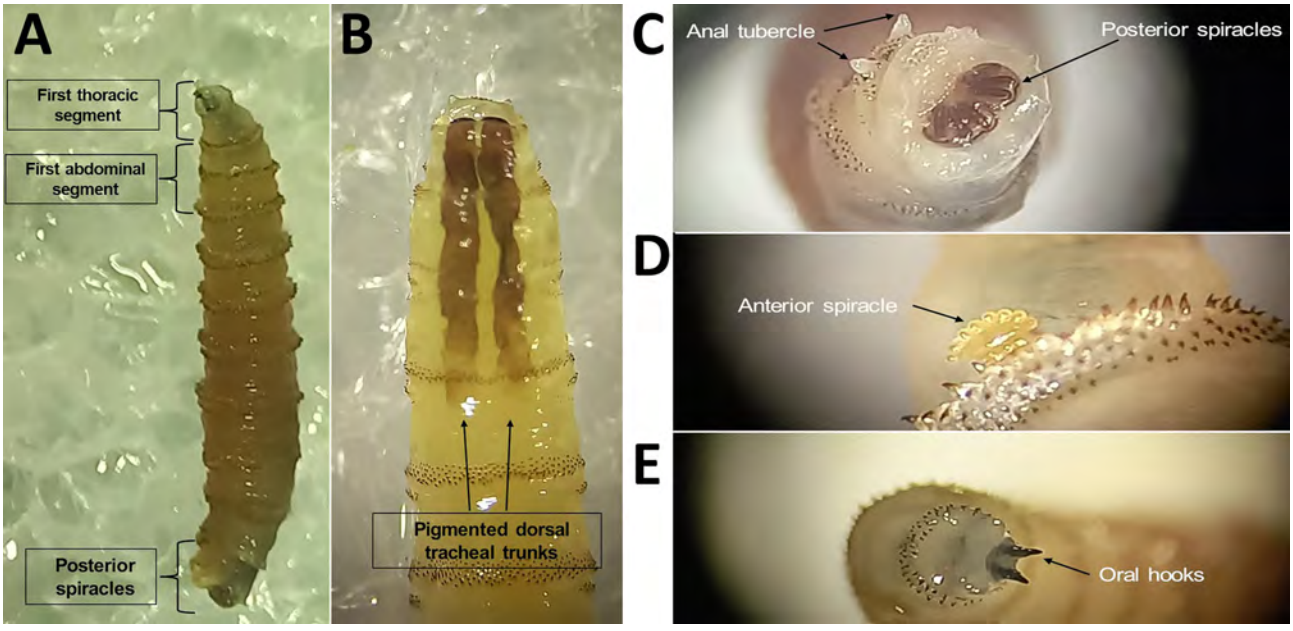

Figure 2. *Cochlyiomia hominivorax* larvae collected from a case of New World screwworm infestation in wild mountain tapir, Central Andes Mountains, Colombia. The larvae were collected from a male tapir and depict features used for taxonomic identification. A) Full larva, showing morphologic features; original magnification ×5. B) First thoracic section, demonstrating pigmented dorsal tracheal trunks; original magnification ×10. C) Posterior spiracles and anal tubercle; original magnification ×25. D) Anterior spiracle; original magnification ×25. E) Oral hooks from first thoracic segment; original magnification ×25. Photographs were taken at the Laboratorio de Parasitología Veterinaria, Universidad Nacional de Colombia, by using an SZX12 stereomicroscope (Olympus, https://www.olympus-lifescience.com).

program using the sterile insect technique, similar to eradication efforts in North and Central America (*1*). Implementing such a program in Colombia would require studies to assess technical, political (intergovernmental cooperation), economic (cost-sharing), and environmental feasibility. Integrated control measures at smaller scales could help reduce NWS populations to nonthreatening levels (*1*). Threat mitigation strategies should include medical care for infested wildlife and community outreach to raise awareness about the effects of the parasite on humans, domestic animals, and wildlife.

Acknowledgments

We appreciate the efforts of the staff from the Corporación Autónoma Regional de Risaralda for the medical assistance provided to the injured mountain tapirs in Ucumari Regional Natural Park. Special thanks to Laboratorio de Parasitología Veterinaria of the Universidad Nacional de Colombia for the parasitology procedures.

This manuscript is part of the work performed by the Mountain Tapir Task Force, an alliance integrated by multiple parties at local, regional, and international levels to protect mountain tapirs in the landscape. Written consent to study and mitigate threats for mountain tapirs was obtained by the environmental authority, the Corporación Autónoma Regional de Risaralda (CARDER). No experiments on animals were conducted in this study. All procedures described in this manuscript were carried out based on clinical decisions and to address animal health and welfare concerns. All interventions and larvae collection were conducted and authorized by the Corporación Autónoma Regional de Risaralda (CARDER), the local environmental authority, in accordance with local laws and regulations. Screwworm fly larvae and adults were deposited in the Laboratorio de Parasitología Veterinaria of the Universidad Nacional de Colombia (sample nos. LPV-19747 and LPV-19902).

About the Author

Mr. Cepeda-Duque is a wildlife conservation biologist from the Colombian Andes. He is member of the International Union for Conservation of Nature and Natural Resources Species Survival Commission Tapir Specialist Group. His research interests focus on the ecology and conservation of mammals in the tropical Andes.

References

1. Scott MJ, Concha C, Welch JB, Phillips PL, Skoda SR. Review of research advances in the screwworm eradication program over the past 25 years. Entomol Exp Appl. 2017;164:226–36. https://doi.org/10.1111/eea.12607
2. Parker ID, Lopez RR, Silvy NJ, Pierce BL, Watts KG, Myers EP, et al. Florida Key deer abundance and recovery

following New World screwworm infestation. Southeast Nat. 2020;19:179–91.
3. Muñoz AAF, Caceres AFB, León JCP. First report of myiasis in dogs caused by *Cochliomyia hominivorax* (Coquerel 1858) in Colombia. Vet Parasitol Reg Stud Reports. 2020;19:100356. https://doi.org/10.1016/j.vprsr.2019.100356
4. World Organisation for Animal Health. Chapter 3.1.14: New World screwworm (*Cochliomyia hominivorax*) and Old World screwworm (*Chrysomya bezziana*). In: WOAH terrestrial 2019. Paris: The Organisation; 2019. p. 1–10.
5. Cepeda-Duque JC, Arango-Correa E, Frimodt-Møller C, Lizcano DJ. Howling shadows: first report of domestic dog attacks on globally threatened mountain tapirs in high Andean cloud forests of Colombia. Neotropical Biolog Conserv. 2024;19:25–33. https://doi.org/10.3897/neotropical.19.e117437
6. Marburger RG, Thomas JW. A die-off in white-tailed deer of the Central Mineral Region of Texas. J Wildl Manage. 1965;29:706–16. https://doi.org/10.2307/3798546
7. Maxwell MJ, Subia J, Abrego J, Garabed R, Xiao N, Toribio RE. Temporal and spatial analysis of the New World screwworm (*Cochliomyia hominivorax*) in Darien and Embera, Panama (2001–2011). Transbound Emerg Dis. 2017;64:899–905. https://doi.org/10.1111/tbed.12457
8. Medri I, Mourão G. Male-male aggression in free-ranging collared peccaries, *Pecari tajacu* (Artiodactyla, Tayassuidae), from Brazilian Pantanal. Current Ethology. 2016;15:24–9.
9. Quse V, Fernandes-Santos RC. Manual of veterinary medicine for tapers, 2nd edition [in Portuguese]. Gland (Switzerland): International Union for Conservation of Nature Species Survival Commission Tapir Specialist Group; 2014.
10. Ruiz-Zapata JD, Figueroa-Gutiérrez LM, Mesa-Franco JA, Moreno-Gutierrez PA. Umbilical myiasis by *Cochliomyia hominivorax* in an infant in Colombia. Front Med (Lausanne). 2020;6:292. https://doi.org/10.3389/fmed.2019.00292

Address for correspondence: Juliana Vélez, The Natural Capital Project, Stanford University, 27 Campus Dr, Bass Biology Bldg 123, Stanford, CA 94305, USA; email: velez063@stanford.edu or julianavelezgomez@gmail.com

COMMENT LETTER

Nosocomial Transmission of *Plasmodium falciparum* Malaria, Spain, 2024

Jesús L. Gómez Perales, Antonio García Mendoza, M. Teresa Gutiérrez Amares

Author affiliations: Puerta del Mar Hospital, Cádiz, Spain (J.L. Gómez Perales, M.T. Gutierrez Amares); Torrecárdenas, Almería, Spain (A. García Mendoza).

DOI: https://doi.org/10.3201/eid3109.250920

To the Editor: We wish to express our concerns regarding the recent Research Letter by Liroa Romero et al. (*1*). The authors' identification of the lead shield as the transmission source is inferred from the exclusion of other routes, procedural sequence, parasitemia in the previous patient, and genotypic similarity. The absence of demonstrated contamination of the equipment means this finding remains indirect. An unaddressed alternative route could include contamination through blood on gloves if gloves are not changed between patients (*2*).

Nevertheless, assuming their hypothesis is correct, the authors propose a transmission mechanism supported by a video (https://youtu.be/2OW9g2tiBjc). However, this video appears to depict a deviation from current good radiopharmacy practice guidelines (*3*). Specifically, inserting an unsealed syringe—without a sterile needle or Luer-lock cap—into the lead shield poses a serious contamination risk (*4*). Furthermore, the video omits critical earlier and later procedural steps that are essential for fully identifying potential cross-contamination points. To illustrate the complete process in line with good radiopharmacy and best injection practices (*5*), we have prepared an explanatory video (https://youtu.be/5wGFH6GGe8M). The risk for blood contamination arises after administration, when the needle is discarded and the unsealed syringe is withdrawn from the shield. Therefore, the contents of the syringe with the next dose would only be exposed at the same late stage, after the contents have already been injected. Cross-contamination before injection would be plausible only if an unsealed syringe were inserted into an already contaminated shield before the injection itself, as depicted in the authors' video.

We contend that strict aseptic technique, rather than equipment disinfection alone, is paramount to preventing such incidents. Adopting the authors' reasoning would imply that each nuclear medicine department would need to stock several lead shields equivalent to their maximum daily dose capacity, which presents serious logistical challenges in routine clinical settings.

References

1. Liroa Romero MF, Ruiz Pérez de Pipaón M, Navarro Amuedo MD, Rubio Muñoz JM, Jiménez-Hoyuela JM, Cisneros JM. Nosocomial transmission of *Plasmodium falciparum* malaria, Spain, 2024. Emerg Infect Dis. 2025;31:1250–3.
2. Pittet D, Allegranzi B, Sax H, Dharan S, Pessoa-Silva CL, Donaldson L, et al.; WHO Global Patient Safety Challenge, World Alliance for Patient Safety. Evidence-based model for hand transmission during patient care and the role of improved practices. Lancet Infect Dis. 2006;6:641–52.
3. Gillings N, Hjelstuen O, Ballinger J, Behe M, Decristoforo C, Elsinga P, et al. Guideline on current good radiopharmacy practice (cGRPP) for the small-scale preparation of radiopharmaceuticals. EJNMMI Radiopharm Chem. 2021;6:8.
4. Centers for Disease Control and Prevention. Injection safety: guidelines for safe injection practices in healthcare settings [cited 2025 Jun 18]. https://www.cdc.gov/injectionsafety
5. World Health Organization. WHO best practices for injections and related procedures toolkit [cited 2025 Jun 19]. https://apps.who.int/iris/handle/10665/44298

Address for correspondence: Jesús L. Gómez Perales, Nuclear Medicine, Puerta del Mar Hospital, Ana de Viya, 21. 11009 Cádiz, Spain; email: jesusl.gomez.sspa@juntadeandalucia.es

Manuel F. Liroa Romero, Maite Ruiz Pérez de Pipaón, Maria D. Navarro Amuedo, Jose M. Rubio Muñoz, Jose M. Jiménez-Hoyuela, Jose M. Cisneros

Author affiliations: University of Seville, Seville, Spain (M.F. Liroa Romero, M. Ruiz Pérez de Pipaón, M.D. Navarro Amuedo, J.M. Jiménez-Hoyuela, J.M. Cisneros); Hospital Universitario Virgen del Rocío, Seville (M.F. Liroa Romero, M. Ruiz Pérez de Pipaón, M.D. Navarro Amuedo, J.M. Jiménez-Hoyuela, J.M. Cisneros); CIBERINFEC Instituto de Salud Carlos III, Madrid, Spain (J.M. Rubio Muñoz, J.M. Cisneros)

DOI: https://doi.org/10.3201/eid3109.251210

In Response: We appreciate the opportunity to respond to the letter from Dr. Perales (*1*) regarding our article on a case of nosocomial transmission of *Plasmodium falciparum* during a thyroid scintigraphy (*2*). The author of the letter proposes as an alternative mechanism the nosocomial transmission of the parasite by contact with blood on gloves not changed between patients. We respectfully disagree because the mechanism he proposes lacks scientific basis; no evidence of malaria transmission by such contact has been documented. On the contrary, nosocomial transmission of *P. falciparum* by parenteral route is well demonstrated, through blood transfusions, transplants (*3*), or invasive medical procedures involving exposure to contaminated blood (*3*), as occurred in our case (*2*).

References

1. Gómez Perales JL, García Mendoza A, Gutiérrez Amares MT. Nosocomial transmission of Plasmodium falciparum malaria, Spain, 2024. Emerg Infect Dis. 2025;31:1874–1875
2. Romero MFL, de Pipaón MRP, Amuedo MDN, Rubio Muñoz JM, Jiménez-Hoyuela JM, Cisneros JM. Nosocomial transmission of Plasmodium falciparum malaria, Spain, 2024. Emerg Infect Dis. 2025;31:1250–3.
3. ISCIII-Vigilancia en Salud Pública-RENAVE. ISCIII portal web [cited 2025 Aug 3]. https://www.isciii.es/servicios/vigilancia-salud-publica-renave

Address for correspondence: Jose M. Cisneros, Hospital Virgen del Rocío, Manuel Siurot Ave, s/n. 41013 Sevilla, Spain; email: jmcisnerosh@gmail.com

Giulio Aristide Sartorio (1860–1932), ***Malaria***, official title ***Dum Romae consulitur, morbos imperat*** **(1883)**. Oil on canvas. 125 cm × 223 cm. Museo Nacional de Bellas Artes, Buenos Aires, Argentina. Public domain digital image from Wikipedia Commons.

While Man Deliberates, Malaria Rules

David O. Freedman

This month's cover of *Emerging Infectious Diseases* shows the 1883 painting by Italian artist Giulio Aristide Sartorio (1860–1932) that is commonly known as *Malaria* but officially is titled *Dum Romae consulitur, morbos imperat* (*While Rome Deliberates, the Disease Rules*, an ancient Roman proverb). Portraying the devastating human suffering of the disease, the painting depicts life and death in the Pontine Marshes (Agro Pontino), a quadrangular area of now former marshland in the Lazio Region of central Italy, extending along the coast southeast of Rome.

Sartorio, a notable Italian artist of his time, was a leader of the opposition to the prevailing artistic norms of the Royal Academy, whose proponents he believed were too focused on idealized forms and superficial techniques. Symbolists like Sartorio believed that art could convey deeper, more profound truths by using symbols to represent emotions, ideas, and spiritual experiences. Sartorio produced sophisticated depictions of animals, as well as war paintings, landscapes of the Roman countryside, and the places he visited in Latin America and the East.

Sartorio attended the Institute of Fine Arts beginning in 1876, and commercial success came quickly. In 1883, he debuted *Malaria* at the International Exhibition of Fine Arts in Rome. The dramatic powerful tones and colors and his skill as a daring draftsman, inspired by 17th Century realism, impressed the critics. *Malaria* was purchased in 1885 by a private collector and donated to the Museo Nacional de Bellas Artes in Buenos Aires, Argentina, sometime before 1910. In 1905, Sartorio returned to the theme and exhibited *Marsh Fever*, a very similar malaria-themed painting; its current location is unknown.

Author affiliation: University of Alabama at Birmingham, Birmingham, Alabama, USA

DOI: https://doi.org/10.3201/eid3109.AC3109

Malaria portrays the devastating effects of the disease, highlighting the human suffering and environmental conditions of the late 1800s in Symbolist terms. The grim reality of life in the marshy, malaria-ridden Roman campagna shows Sartorio's skill in capturing social realist themes with a poignant, almost photographic clarity. Social realism draws attention to the real sociopolitical conditions of the working class as a means to critique the power structures behind these conditions. This work signaled his early engagement with contemporary life, exposed the government's inaction as a public political protest, even as he was mastering the historical and mythological subjects favored by the Academy.

Sartorio treated the subject of a devastated mother kneeling beside her son's corpse with a crude and violent realism. The painting is an ambiguous, still firmly Symbolist, vision of the relationship between death and beauty, reinforced by the scene's setting in a deserted marsh. The landscape bathed in the light of twilight is a modern reinterpretation of the traditional theme of the pietà, that is, depictions of Mary holding the crucified body of Christ.

Historically, over the centuries since Roman Empire times, the Pontine Marshes have been subject to extensive and expensive periodic land reclamation work. The part of the marsh above sea level needs to be successfully and sustainably drained by channels, so that the highly fertile agricultural land is reclaimed. Whenever the channels are not maintained, the swamp reappears, and mosquito populations explode (Figure). Sartorio, therefore, participated in the debate on the cost–benefit of reclamation of the Pontine Marshes by seeking the symbolic reality of humanistic attitudes, which were disappearing from societal norms.

Malaria in the Agro Pontino, present since ancient times, prevented the expansion of Rome to the south. For example, in 1928, during the malaria season, 80% of those having spent 1 night in the marsh became infected. The region had <1,000 inhabitants for a coastal region of >700 km^2. The settling of the area could provide a new province for Italy and enable settlement that could prevent emigration of 200,000 Italians.

Under Benito Mussolini in the 1930s, the problem was nearly solved by placing dikes and pumping out that portion of the marsh that lay below sea level, but constant maintenance was required. The project reached a peak in 1933 with 124,000 men employed. However, in 1943, just before the Allies landed at the beachhead on the Pontine Marshes for the Battle of Anzio, malaria had returned to the Agro Pontino; quinine and other medicines were in short supply, at the same time infected veterans were returning from the Balkans. In an act interpreted by some as intentional biologic warfare, the Germans flooded the marshes once again. In early 1944, the Battle of Anzio left the marsh in a state of devastation; nearly everything Mussolini had accomplished was reversed. The marshes were full of brackish water, the channels filled in; the mosquitos were flourishing, and malaria was on the rise. Fortunately, the major structures for water control survived, and in a few years, the Agro Pontino was restored. The last of the malaria was conquered in the 1950s with the aid of DDT, and Italy was declared malaria-free by the World Health Organization in 1970. Still, receptive mosquito vectors remain in Italy (and in Greece) and nonsustained autochthonous cases secondary to introduced cases in entering travelers have continued to occur every few years.

In the United States, indigenous transmission of malaria was eliminated in 1951, although ≈2,000 annual malaria cases are imported from malaria-endemic areas. In 2023, nine locally transmitted cases were contracted by US residents who had not recently

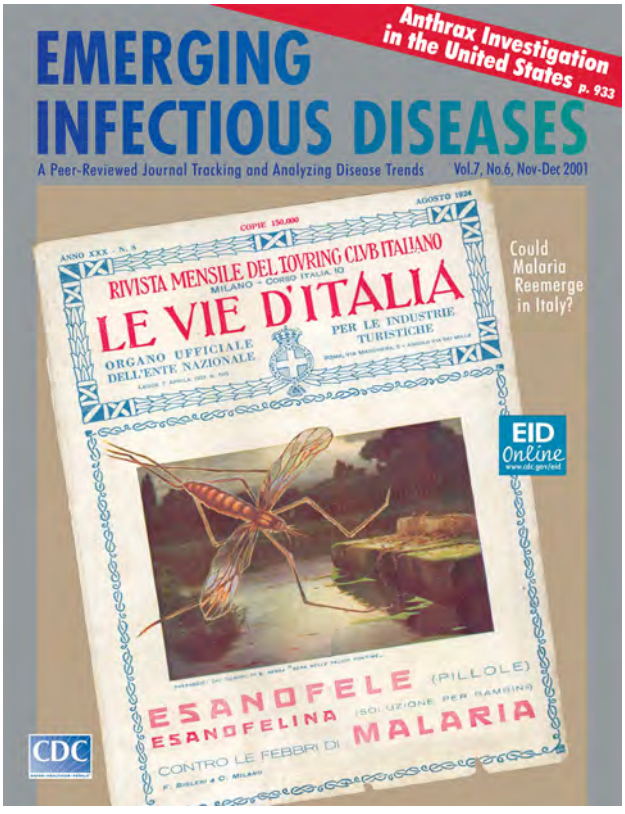

Figure. This issue is not the first time the Pontine Marshes of Italy have graced the cover of *Emerging Infectious Diseases*. This 1924 magazine cover from the Touring Club of Milan was featured in the journal's last bimonthly issue in 2001. Original image provided courtesy of Dr. Guido Sabatinelli.

traveled to endemic areas. Seven cases were recorded in Florida, and 1 each in Texas and Maryland, the result of widespread presence of the *Anopheles* mosquito vector throughout the nonmountainous United States.

The tragedy of malarial childhood death still occurs >400,000 times every year throughout malaria-endemic countries. Since 2022, the World Health Organization has approved 2 separate safe and novel vaccines for infants that are imperfect but can cut those deaths by 30%–50%. Continued need for global support for procurement and implementation programs to achieve vaccination goals remains a priority.

Bibliography

1. Romi R. Cover of Le Vie d'Italia magazine from 1924. Emerg Infect Dis. 2001;7:1073. https://doi.org/10.3201/eid0706.000000
2. Bietoletti S. Commentary on the painting *Malaria* [in Spanish]. Museo Nacional de Bellas Artes, Buenos Aires, Argentina [cited 2025 Jul 24]. https://www.bellasartes.gob.ar/coleccion/obra/5529
3. Kalu MC. When Italy dumped the Nazis for the Allies, the consequence was completely unexpected: malaria. War History Online. 2019 Jan 15 [cited 2025 Jul 24]. https://www.warhistoryonline.com/instant-articles/when-italy-dumped-the-nazis.html
4. Courtney AP, Boyanton BL Jr, Strebeck PV, Blount K, Ledford S, Ridpath AD, et al. Arkansas Locally Acquired Mosquito-Transmitted Malaria Response Team. Locally acquired (autochthonous) mosquito-transmitted *Plasmodium vivax* malaria—Saline County, Arkansas, September 2023. MMWR Morb Mortal Wkly Rep. 2024;73:646–9. https://doi.org/10.15585/mmwr.mm7342a2
5. World Health Organization. World malaria report 2024: addressing inequity in the global malaria response. Geneva: The Organization; 2024.

Address for correspondence: David O. Freedman, University of Alabama at Birmingham, 1720 2nd Ave S, Birmingham, AL 35294-2170, USA; email: dfreedman@uabmc.edu

EMERGING INFECTIOUS DISEASES®

Upcoming Issue • Fungal Infections

- Spotted Fever Group Rickettsioses among Hospitalized Patients and Circulation of *Rickettsia* in Ticks, Kazakhstan, 2019
- Reptile Exposure among Human Salmonellosis Cases and *Salmonella* Serotypes Isolated from Reptiles, Ontario, Canada, 2015–2022
- Recent Systemic Antifungal Exposure and Nonsusceptible *Candida* in Hospitalized Patients, South Africa, 2012–2017
- Comparative Epidemiology of *Salmonella* Paratyphi A and *Salmonella* Typhi Causing Enteric Fever, Bangladesh, 2018–2020
- Prolonged Monkeypox Virus Infections, California, USA, May 2022–August 2024
- Differences in COVID-19 Fatality Rates among Ethnic Groups, Hawaii, USA, 2020–2022
- Effects of Human Seasonal Influenza Vaccines on Highly Pathogenic Avian Influenza A(H5N1) Clade 2.3.4.4b Virus Infection in Ferrets
- Antimicrobial-Resistant Clonal Complex 11 *Neisseria meningitidis*–Associated Urethritis Cluster, Thailand
- Genomic Investigation of Increased Gonococcal Infections, Minnesota, USA, 2024
- *Escherichia coli* ST131:H22 in Parrots from Illegal Pet Trade, Brazil, 2024
- *Angiostrongylus cantonensis* in Definitive and Intermediate Hosts, Madagascar, 2023
- Detection of Mpox in Wastewater Solids at Wastewater Treatment Plants, United States
- Hypervirulent *Klebsiella pneumoniae* as a cause of lethal pneumocephalus in Europe
- Emergence and Polyclonal Dissemination of bla_{NDM-7}–Carrying InX3 Plasmid in *Enterobacter cloacae* Complex, France, 2021–2023
- Detection of Extended-Spectrum β-lactamase–Producing *Klebsiella pneumoniae* in Human and Food Samples, Switzerland, 2018–2019
- Disseminated Blastomycosis Mimicking Tuberculosis, China
- Cutaneous Coccidioidomycosis Mimicking Rosacea in Immunosuppressed Patient, Arizona, USA, 2024

Complete list of articles in the October issue at https://wwwnc.cdc.gov/eid/#issue-326

Earning CME Credit

To obtain credit, you should first read the journal article. After reading the article, you should be able to answer the following, related, multiple-choice questions. To complete the questions (with a minimum 75% passing score) and earn continuing medical education (CME) credit, please go to http://www.medscape.org/journal/eid. Credit cannot be obtained for tests completed on paper, although you may use the worksheet below to keep a record of your answers.

You must be a registered user on http://www.medscape.org. If you are not registered on http://www.medscape.org, please click on the "Register" link on the right hand side of the website.

Only one answer is correct for each question. Once you successfully answer all post-test questions, you will be able to view and/or print your certificate. For questions regarding this activity, contact the accredited provider, CME@medscape.net. For technical assistance, contact CME@medscape.net. American Medical Association's Physician's Recognition Award (AMA PRA) credits are accepted in the US as evidence of participation in CME activities. For further information on this award, please go to https://www.ama-assn.org. The AMA has determined that physicians not licensed in the US who participate in this CME activity are eligible for *AMA PRA Category 1 Credits*™. Through agreements that the AMA has made with agencies in some countries, AMA PRA credit may be acceptable as evidence of participation in CME activities. If you are not licensed in the US, please complete the questions online, print the AMA PRA CME credit certificate, and present ions online, print the AMA PRA CME credit certificate, and present it to your national medical association for review.

Article Title

Severe Group A *Streptococcus* Infection among Children, France, 2022–2024

CME Questions

1. Which of the following statements regarding the initial presentation and management of children with group A *Streptococcus* (GAS) infections in the current study is most accurate?

A. Nearly half of patients had a history of immunocompromise
B. The majority of patients required admission to the intensive care unit (ICU)
C. The most common presentation of GAS infection involved the ear-nose-throat
D. Less than 10% of patients required surgical intervention

2. Which of the following statements regarding bacterial testing for GAS in the current study is most accurate?

A. Nearly 80% of rapid antigen testing samples of the throat were positive for GAS
B. Polymerase chain reaction (PCR) testing for GAS achieved higher positivity rates compared with GAS culture
C. PCR testing for GAS achieved similar positivity rates compared with GAS culture
D. GAS testing of pleural effusion samples was unreliable

3. What was the most common emm type isolated in the current study of GAS infections among children?

A. *emm4*
B. *emm12*
C. *emm87*
D. *emm1*

4. Which of the following variables was most associated with a higher risk for major sequelae or death associated with GAS infection in the current study?

A. Pulmonary GAS infection
B. Female sex
C. Viral infection preceding infection with GAS
D. Treatment with corticosteroids

Earning CME Credit

To obtain credit, you should first read the journal article. After reading the article, you should be able to answer the following, related, multiple-choice questions. To complete the questions (with a minimum 75% passing score) and earn continuing medical education (CME) credit, please go to http://www.medscape.org/journal/eid. Credit cannot be obtained for tests completed on paper, although you may use the worksheet below to keep a record of your answers.

You must be a registered user on http://www.medscape.org. If you are not registered on http://www.medscape.org, please click on the "Register" link on the right hand side of the website.

Only one answer is correct for each question. Once you successfully answer all post-test questions, you will be able to view and/or print your certificate. For questions regarding this activity, contact the accredited provider, CME@medscape.net. For technical assistance, contact CME@medscape.net. American Medical Association's Physician's Recognition Award (AMA PRA) credits are accepted in the US as evidence of participation in CME activities. For further information on this award, please go to https://www.ama-assn.org. The AMA has determined that physicians not licensed in the US who participate in this CME activity are eligible for *AMA PRA Category 1 Credits*™. Through agreements that the AMA has made with agencies in some countries, AMA PRA credit may be acceptable as evidence of participation in CME activities. If you are not licensed in the US, please complete the questions online, print the AMA PRA CME credit certificate, and present it to your national medical association for review.

Article Title

Rickettsioses as Underrecognized Cause of Hospitalization for Febrile Illness, Uganda

CME Questions

1. Which of the following statements regarding rickettsial disease characteristics in sub-Saharan Africa is most accurate?

A. Nearly all patients have an eschar
B. The presence of leukopenia separates rickettsial disease vs other febrile infections
C. The presence of transaminitis separates rickettsial disease vs other febrile infections
D. Serologic testing for acute rickettsial disease has poor clinical utility

2. What was the sensitivity and specificity of serum ribosomal RNA (rRNA) reverse-transcriptase polymerase chain reaction (RT-PCR) for rickettsial disease in the current study?

A. Sensitivity: 95%; specificity: 98%
B. Sensitivity: 75%; specificity: 91%
C. Sensitivity: 64%; specificity: 78%
D. Sensitivity: 57%; specificity: 82%

3. How did PCR testing for rickettsial rRNA compare with testing for messenger RNA (mRNA) in the current study?

A. PCR testing for rRNA was similarly accurate compared with testing for mRNA
B. PCR testing for rRNA was more sensitive compared with testing for mRNA
C. PCR testing for rRNA was less sensitive compared with testing for mRNA
D. PCR testing for rRNA was far less sensitive and specific compared with testing for mRNA

4. Which of the following characteristics of cases of rickettsial disease in the current study is most accurate?

A. No patients with rickettsial disease received a tetracycline drug
B. Rash was present in nearly 70% of patients
C. Rickettsial disease was associated with more severe illness compared with other febrile illnesses
D. No patients with rickettsial disease died

Emerging Infectious Diseases
Photo Quiz Articles

Volume 14, Number 9
September 2008

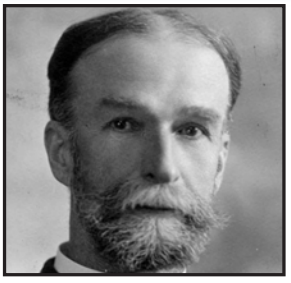

Volume 14, Number 12
December 2008

Volume 15, Number 9
September 2009

Volume 15, Number 10
October 2009

Volume 16, Number 6
June 2010

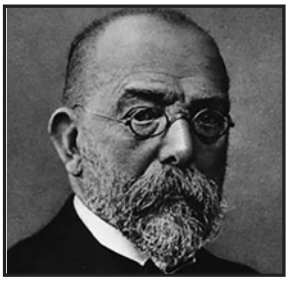

Volume 17, Number 3
March 2011

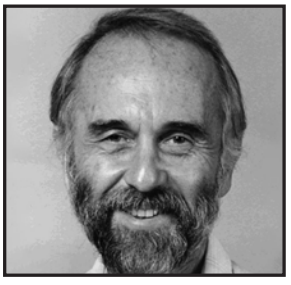

Volume 17, Number 12
December 2011

Volume 19, Number 4
April 2013

Volume 20, Number 5
May 2014

Volume 21, Number 9
September 2015

Volume 22, Number 8
August 2016

Volume 28, Number 3
March 2022

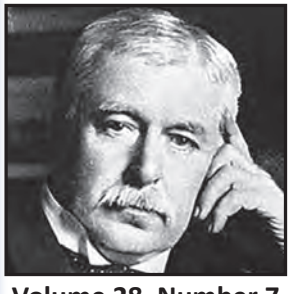

Volume 28, Number 7
July 2022

Click on the link below to read about the people behind the science.

https://bit.ly/3LN02tr

See requirements for submitting a photo quiz to EID.

https://bit.ly/3VUPqfj

EID Journal